Mineralogical Society of America
Special Paper Number One

# International Mineralogical Association

## Papers and Proceedings
of the
## Third General Meeting

*Washington, D.C., April 17-20, 1962*

*Editors*

D. JEROME FISHER ALFRED J. FRUEH, JR.
C. S. HURLBUT, JR. C. E. TILLEY

*Co-ordinating Editor*

E. WM. HEINRICH

Published by the Society · 1963

COPYRIGHT, 1963 BY
MINERALOGICAL SOCIETY OF AMERICA

PRINTED BY GEORGE BANTA COMPANY, INC.
MENASHA, WISCONSIN, U.S.A.

## INTERNATIONAL MINERALOGICAL ASSOCIATION

An Association of 22 National Mineralogical Societies

| | |
|---|---|
| *President | D. Jerome Fisher |
| First Vice-President | C. E. Tilley |
| Second Vice-President | G. P. Barsanov |
| *Secretary | J. L. Amorós |
| *Treasurer | L. G. Berry |
| Councilors: | P. R. J. Naidu |
| | Th. G. Sahama |
| | H. G. F. Winkler |
| Past President | R. L. Parker |

* Member of the Executive Committee.

---

### COMMISSIONS

ABSTRACTS
M. Fornaseri, Ch.
R. Van Tassel, Secy.

COSMIC MINERALOGY
D. P. Grigoriev, Ch.
E. P. Henderson, Secy.

MINERAL DATA
H. Strunz, Ch.
G. T. Faust, Secy.

MUSEUMS
C. Frondel, Ch.
F. Leutwein, Secy.

ORE MICROSCOPY
W. Uytenbogaardt, Ch.
S. H. U. Bowie, Secy.

TEACHING
J. Orcel, Ch.
H. J. de Wijs, Secy.

NEW MINERALS AND MINERAL NAMES
M. Fleischer, Ch.
C. Guillemin, Secy.

# TABLE OF CONTENTS


FOREWORD ..... v

SYMPOSIUM ON LAYERED INTRUSIONS ..... 1

The mechanism of adcumulus growth in the layered series of the Skaergaard intrusion ..... *L. R. Wager* 1

Contrasted styles of igneous layering in the Gardar Province of south Greenland ..... *J. Ferguson and T. C. R. Pulvertaft* 10

Structural and petrographic observations on layered granites from southern Greenland ..... *C. H. Emeleus* 22

The Muskox intrusion, a recently discovered layered intrusion in the Coppermine River area, Northwest Territories, Canada ..... *Charles H. Smith and H. E. Kapp* 30

Origin of the ultramafic complex at Duke Island, southeastern Alaska ..... *T. N. Irvine* 36

Stratigraphic and lateral variation of chromite composition in the Stillwater Complex ..... *Everett D. Jackson* 46

Flow-layering in alpine peridotite-gabbro complexes ..... *T. P. Thayer* 55

Noritic anorthosite bodies in the Sierra Nevada batholith ..... *Alden A. Loomis* 62

Layered picrite-anorthositic gabbro sheet, West Humboldt Range, Nevada ..... *Robert C. Speed* 69

Layered pegmatite-aplite intrusives ..... *Richard H. Jahns and O. Frank Tuttle* 78

Structure and rock sequences of the Critical Zone of the eastern Bushveld Complex ..... *Eugene N. Cameron* 93

The Kapalagulu layered intrusion of western Tanganyika ..... *W. J. Wadsworth* 108

A layered complex in Sittampundi, Madras State, India ..... *P. R. J. Naidu* 116

Layered intrusions in the Ferrar dolerites, Antarctica ..... *Bernard M. Gunn* 124

Layered basic intrusive rocks of the Wichita Mountains, S.W. Oklahoma (abs.) ..... *H. E. Hunter* 134

Internal structure of a differentiated teschenite intrusion, Prospect Hill, New South Wales (abs.) ..... *H. G. Wilshire* 134

SYMPOSIUM ON THE MINERALOGY OF THE SULFIDES ..... 135

The physical properties of semiconducting sulfides, selenides and tellurides ..... *Wayne W. Scanlon* 135

Various aspects of atomic displacements in metallic sulfides ..... *Jean Prouvost* 144

Étude structurale de quelques sulfures de plomb et d'arsenic naturels du gisement de Binn ..... *M-Th. Le Bihan* 149

On the transition of bornite ..... *Nobuo Morimoto* 153

On the superstructure and twinning of pyrrhotite ..... *Bernhardt J. Wuensch* 157

The crystal structure of chalcocite, $Cu_2S$ ..... *Bernhardt J. Wuensch and M. J. Buerger* 164

Equilibrium in ore deposits ..... *Paul B. Barton, Jr., Philip M. Bethke and Priestley Toulmin, 3rd* 171

A study of distorted pyrite crystals from Spain ..... *M. Font-Altaba* 186

A statistical study of bravoite zoning ..... *Farouk El Baz and G. C. Amstutz* 190

Sulfur isotope mineralogy of sulfides (abs.) ..... *Mead Leroy Jensen* 198

Thermodynamic study of pyrrhotite and pyrite (abs.) ..... *Priestley Toulmin, 3rd and Paul B. Barton, Jr.* 198

MISCELLANEOUS PAPERS ..... 200

The role of oriented transformations in mineralogy ..... *L. S. Dent Glasser, F. P. Glasser and H. F. W. Taylor* 200

Effects of the changes in slope occurring on liquidus and solidus paths in the system diopside-anorthite-albite ..... *Peter J. Wyllie* 204

Cell parameters of orthopyroxenes ..... *R. A. Howie* 213

Sur les constituants phosphatés des minerais de fer oolithiques de France ..... *S. Caillère and F. Kraut* 223

Trends and affinities of basaltic magmas and pyroxenes as illustrated on the diopside—olivine—silica diagram ..... *D. S. Coombs* 227

Crystallization of leucite-nepheline-sanidine in basic differentiates from a peridotite-dunite mass in Salem, Madras State, India ..... *P. R. J. Naidu* 251

Studies of crystal surfaces ..... *Ichiro Sunagawa* 258
Clinoamphibole regression studies. I. Regressions of optical properties and density on composition ..... *Horace Winchell* 267
Contribution to the study of the fluorite deposit "Mina Berta" in San Cugat del Valles (Barcelona, Spain) ..... *J. Montoriol Pous, A. San Miguel and M. Font-Altaba* 278
Structural classification of zeolites ..... *J. V. Smith* 281
The crystal structure of dachiardite ..... *G. Gottardi and W. M. Meier* 291
Comparison of the crystal structures of wollastonite and pectolite ..... *C. T. Prewitt and M. J. Buerger* 293
Interpretation of systematic extra-extinctions ..... *N. Morimoto, F. Marumo and R. Sadanaga* 303
Spiroffite, a new tellurite mineral from Moctezuma, Sonora, Mexico ..... *J. A. Mandarino, S. J. Williams and R. S. Mitchell* 305
The crystal structure of pseudomalachite (abs.) ..... *Subrata Ghose* 310
Light extinction and scattering by suspensions of finely-divided minerals (abs.) ..... *J. R. Hodkinson* 310
Accurate determination of olivine composition using standard small-diameter $x$-ray powder cameras (abs.) ..... *J. L. Jambor and Charles H. Smith* 310
Infrared study of sulfate minerals (abs.) ..... *Keiichi Omori and Paul F. Kerr* 311
Study of translucent tiny grains using the interference microscope (abs.) ..... *Horst Piller* 311
Studies of rock-forming micas (abs.) ..... *J. Rimsaite* 312
The composition of quartz-forming fluids in nature (abs.) ..... *Edwin Roedder* 312
The crystal structures and crystal chemistry of various members of the metatorbernite group (abs.) ..... *Malcolm Ross and Howard T. Evans, Jr.* 313
The significance of sapphirine in the granulite terrains of Western Australia (abs.) ..... *Allan F. Wilson* 313
Iron-feldspar polymorphs in the system $K_2O$-FeO-$Fe_2O_3$-$SiO_2$-$H_2O$ (abs.) ..... *David R. Wones and Daniel E. Appleman* 314
PROCEEDINGS OF THE INTERNATIONAL MINERALOGICAL ASSOCIATION ..... 315
INDEX ..... 327

MINERALOGICAL SOCIETY OF AMERICA, SPECIAL PAPER 1, 1963
INTERNATIONAL MINERALOGICAL ASSOCIATION, PAPERS, THIRD GENERAL MEETING

# SYMPOSIUM ON LAYERED INTRUSIONS

## THE MECHANISM OF ADCUMULUS GROWTH IN THE LAYERED SERIES OF THE SKAERGAARD INTRUSION

L. R. WAGER
*Department of Geology and Mineralogy, University of Oxford, Oxford, England*

ABSTRACT

If we accept that the common feature of layered rocks is the bottom accumulation of crystals separating from a large body of magma, then there are three stages to be distinguished: (1) initial deposition of the cumulus crystals, (2) growth of the cumulus crystals while forming the top surface of the pile, (3) crystallization of trapped intercumulus liquid.

In the case of the Skaergaard intrusion the highly variable rhythmic layering is the result of the precipitation of different proportions of the possible cumulus phases. Convection currents, sometimes intermittent as Hess has postulated for the Stillwater, and sometimes continuous, though of variable velocity, account for many features of the rhythmic layering and igneous lamination.

Enlargement of the cumulus crystals during the brief time they formed the top surface of the precipitate is required to explain features of Rhum, Bushveld, Stillwater and, to a lesser extent, the Skaergaard layered series. In the latter case the amount of $P_2O_5$ in the rocks provides an indirect measure of the amount of adcumulus growth, and confirms the textural evidence. It is believed that the removal of heat to allow adcumulus crystallization cannot be downwards through the already deposited layered rocks but into the overlying magma which is, at certain times and places, supercooled. It is postulated that nucleation in the descending current probably occurred only after 5 or 10° C. of supercooling, that relatively few nuclei formed, and these grew slowly because of the slowness of diffusion. The crystal nuclei were probably so sporadically distributed that the magma, during the time it was flowing over crystals on the floor, did not become uniform, but was at the equilibrium temperature in the neighborhood of the growing crystals, while away from these it was supercooled.

The amount of trapped liquid depends largely on the extent of adcumulus growth; in the Skaergaard there was between 5 and 40 per cent, and its crystallization, giving lower temperature phases and zones, must have continued for many thousands of years.

Layered intrusions may be defined objectively as igneous complexes which, by structural or mineralogical critera, can be seen to be a succession of genetically related sheets, lying conformably one above the other, and showing no evidence of chilling between successive layers (*cf.* Wager 1953, p. 23). Such a definition, however, does not indicate the really significant characteristic of layered intrusions, which is their formation by accumulation of discrete crystals at the bottom of a magma, leading to the gradual building up of successive layers of rock. Such bottom accumulation of crystals cannot, of course, be directly observed, but it can be inferred in many cases from mineral compositions and textures, and it will be taken here as the fundamental characteristic of layered rocks.

When discrete crystals accumulate as a layer at the bottom of a liquid from which they are crystallizing, magma must initially have occupied the interstices betweeen the grains. Thus three stages in the production of a layered rock can usually be distinguished:

1. The initial deposition of the crystals (the cumulus crystals).
2. Growth of the cumulus crystals while forming the top of the pile (adcumulus growth).
3. Crystallization of the magma finally trapped between the cumulus crystals, due to the succeeding deposit. The material so formed is called the pore material.

The relative extent of the second and third processes vary inversely; in extreme cases there may be no adcumulus growth, all the intercumulus liquid becoming trapped and then crystallizing as cooling proceeds; in other cases adcumulus growth may be so extensive as to push out all the interstitial magma, leaving no trapped liquid to crystallize in the later stage. The terms used here have been more fully explained in a paper by Wager *et al.* (1960).

The rhythmic layering of layered intrusions is normally the result of precipitation of the possible cumulus minerals in different proportions at different times, and a major problem is to account for this variability. Some of the features of the rhythmic layering of the Skaergaard intrusion suggest the action of convection currents (Wager and Deer, 1939; Wager, 1952). At one stage in the development of the Skaergaard layered series, trough-banding structures provide evidence of the paths of former currents which passed radially across the floor of the intrusion from the margin towards the center (Wager and Deer, 1939, pp. 45–50, 262–77). Two

FIG. 1. Rhythmic layering; a thin gravity-stratified layer between uniform rock. Glaciated surface in the lower zone of the Skaergaard layered series, Uttentals Plateau.

contrasted types of layering (Fig. 1) seem to be due to precipitation of the cumulus crystals from two kinds of current; one a slow, steady current giving the uniform rock, and the other an intermittent current, as Hess has postulated for the Stillwater intrusion (1960, p. 113), giving the gravity stratified layers.

After the accumulation of crystals at the bottom of the liquid there is usually evidence of some further growth of the crystals at the same temperature as that at which they originally formed. This phenomenon, which has been called adcumulus growth (Wager *et al.*, 1960, pp. 77–79) is easily noticed when it is developed in extreme form, as in certain rocks of the Stillwater and Rhum intrusions (Hess, 1960, p. 113; Brown, 1956, p. 37). On the other hand it is not usually obvious in the Skaergaard intrusion where the effects of the crystallization of trapped liquid, during the protracted period of cooling, are particularly conspicuous. The layered rocks of the Skaergaard intrusion, when originally described in 1939, seemed to be adequately accounted for by assuming accumulation of discrete crystals at the bottom of the liquid, surrounded by about thirty per cent of magma (underestimated at the time) which crystallized slowly as the whole mass cooled. The evidence for this is the lower temperature, outer zones surrounding the essentially unzoned, cumulus crystals, and the additional, lower temperature mineral phases, commonly poikilitic in habit, which have also crystallized from the intercumulus liquid. Rocks having these features have since been called orthocumulates (Wager *et al.*, 1960, pp. 74–76). A feldspar orthocumulate is diagrammatically represented in Fig. 2 (left-hand column); the unzoned, cumulus plagioclases of the first stage of accumulation are indicated as rectangles; around them are lower temperature zones of plagioclase, together with olivine, pyroxene, iron ore and finally dregs of micropegmatite, all formed from the intercumulus liquid. Photomicrographs of different examples of orthocumulates from a low horizon in the Skaergaard layered series have previously been presented (Wager *et al.*, 1960, fig. 3A & B; Wager, 1961, Pl. XIX).

The phenomenon of adcumulus growth, diagrammatically illustrated in Fig. 2, became apparent during Hess's early work on the Stillwater and was briefly mentioned by him (1939, p. 431); later it was further described by G. M. Brown from Rhum (1956, p. 37) and subsequently discussed by Wager *et al.* (1960). The lower units of the layered series of eastern Rhum are orthocumulates, but the higher units include allivalites and thin bands of plagioclase rock (Brown 1956, Pl. V, Fig. 38) in which the plagioclase crystals are unzoned. It is clear that the closest possible natural packing of cumulus plagioclases would still leave space for 20 per cent or so of intercumulus liquid, which should crystallize to lower temperature material. Various hypotheses, none of which were proving satisfactory, were being considered to account for the absence of such low temperature material in certain Rhum rocks when Hess pointed out that he had suggested an explanation, expressed in a sentence in one of his early papers on the Stillwater complex (1939, p. 431). This is the now well-known hypothesis of the growth of the crystals by the diffusion of the appropriate substances from the overlying liquid while the crystals lie at, or near the top surface of the pile; as a result of this growth there is mechanical expulsion of some, or all of the intercumulus liquid from between the crystals. The hypothesis has been more fully considered in the Stillwater memoir (Hess, 1960, p. 113), in which it is also noted that for the diffusion effect to be important, there must be plenty of time or, in other words, the rate of accumulation of crystals at the bottom of the liquid must be relatively slow.

For adcumulus growth of the crystals at the temporary top of the pile of cumulus crystals, heat must be lost to the surroundings in some way. During the formation of the higher Skaergaard layered series, which is the only part now accessible to observation, there must have been many kilometres of

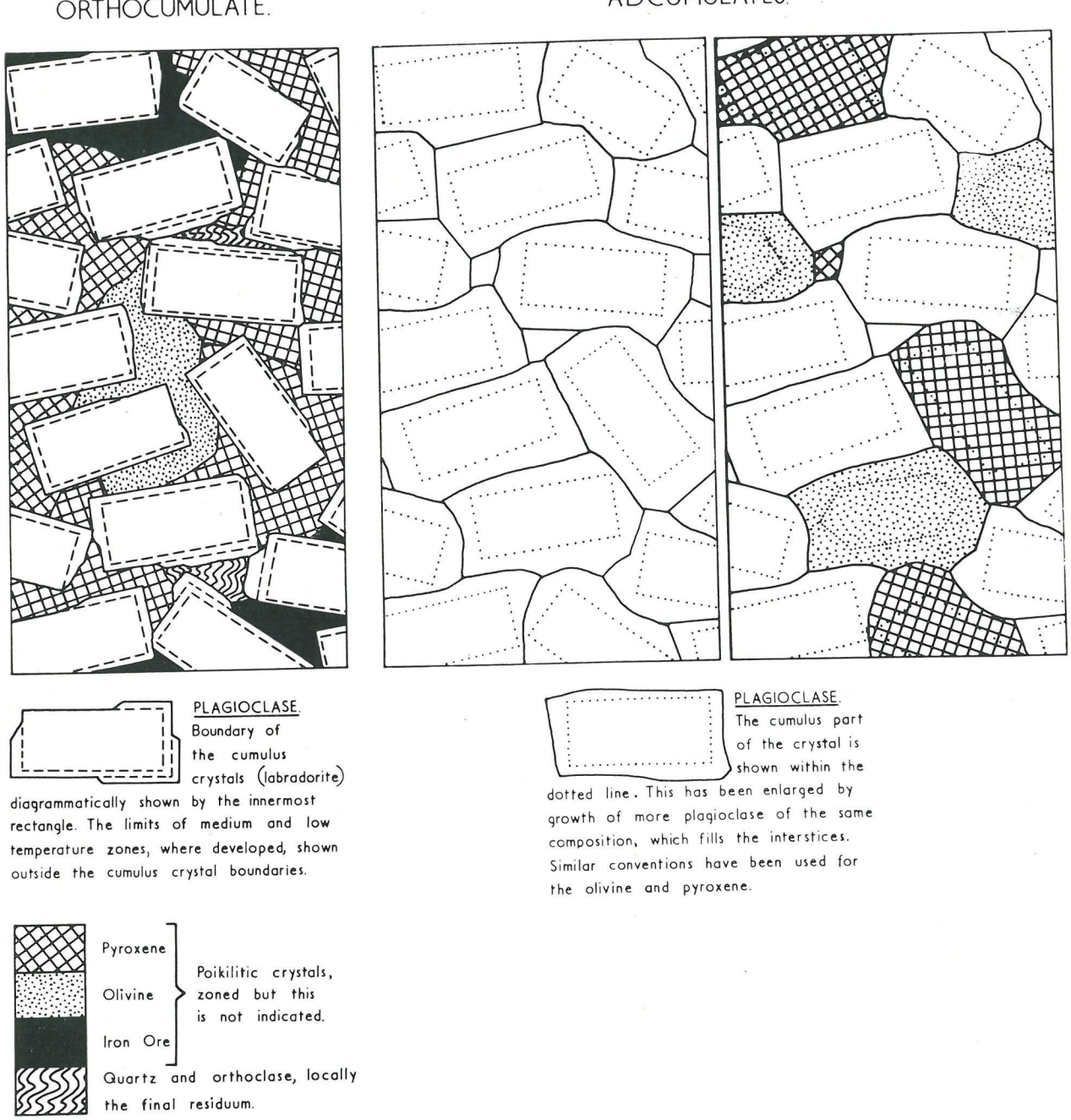


FIG. 2. Diagrammatic representation of 1) plagioclase orthocumulate, 2) extreme plagioclase adcumulate, 3) extreme plagioclase-olivine-pyroxene adcumulate.

already deposited material below, between the crystals of which there would often be intercumulus liquid requiring a considerable reduction in temperature for its complete crystallization. To produce appreciable adcumulus crystallization, heat loss from the neighborhood of the crystals lying at, or near, the surface of the pile must be relatively rapid, since it has to occur before the crystals are too deeply buried by further deposition. Qualitatively, it seems clear that heat loss downwards from the top layer of the accumulated crystals would be far too small to produce adcumulus crystallization, and Professor Hess (personal communication) states that a calculation of the relative heat losses through the floor and

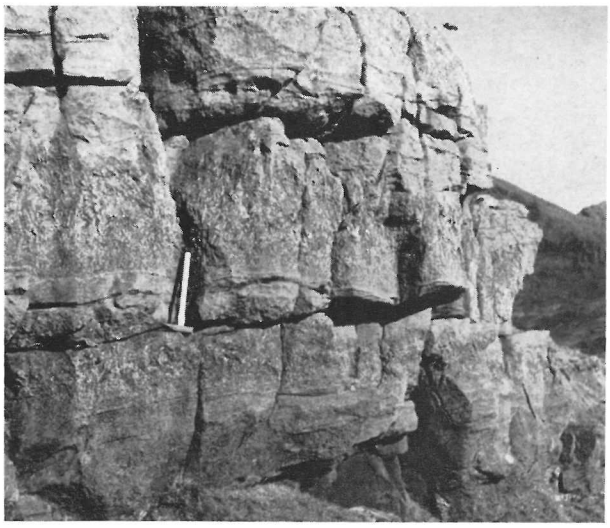

FIG. 3. Harrisitic and equigranular textures in peridotites of Rhum. The rock face shows layers of elongated, upward-growing olivines alternating with fine-grained layers of olivines. (Photograph by W. J. Wadsworth.)

the roof of the Stillwater complex provides supporting evidence for this.

It is the main purpose of this paper to suggest that the loss of heat to allow adcumulus growth is not downwards through the crystal mush but is into supercooled liquid lying above the pile of crystals. Some degree of supersaturation is needed to produce nucleation in a liquid free from seed crystals, and certain features of layered intrusions provide evidence for such non-equilibrium conditions. Thus, in the layered intrusion of Rhum, Wadsworth (1961) has described in detail the harrisite structure of the peridotites (Fig. 3). Olivines, much elongated along the *a* axis and flattened parallel to 010, have grown upward into the liquid from the top surface of an accumulation of fine-grained olivines. After some time, such upward growth was interrupted by a further deposit of fine-grained, equigranular olivines. Wadsworth accounts for the periodicity by assuming that a considerable degree of supercooling is necessary to produce nucleation. He stated that with steady loss of heat from the stationary magma

"At some stage the supercooling would be relieved by the spontaneous formation of many nuclei (labile state) and, following growth to a requisite size with concomitant return towards the equilibrium crystallization temperature of the magma, the crystals would sink. No further nucleation could occur until the necessary degree of supercooling was developed again, and thus there would be an interval during which the only possible crystallization would be the upward extension of grains on the floor. Then spontaneous nucleation would initiate a fresh cycle, and in this way crystal settling would be periodic."

A hypothesis of this kind is basically similar to Ostwald's explanation of Liesegang's rings (for a convenient discussion, see Van Hook, 1961, pp. 12–19).

In the Skaergaard intrusion, evidence of supercooling is available from the marginal border group (Brown, 1957, p. 530; Wager, 1961, pp. 359–60). These examples are related to marginal cooling, but they are useful in showing that some 5° or 10° C. of supercooling had sometimes to occur before nucleation of pyroxene and plagioclase took place. An explanation of certain types of layering in the Bushveld complex has also been tentatively ascribed to the order in which different crystals nucleate from a supercooled magma (Wager, 1959).

Supersaturation of magma is usually considered to result simply from loss of heat into the surroundings, as when a magma intrudes cool rock. Another possible cause of supersaturation is the transfer of saturated magma, without gain or loss of heat, from a region of low to high hydrostatic pressure. The effect of increasing pressure on the common rock-forming minerals is to raise their melting point and thus, if saturated magma be transferred from a region of low to high hydrostatic pressure, it will be supersaturated in its new environment. In the Skaergaard intrusion, rhythmic layering and other phenomena suggest that convection currents occurred in the magma. In the descending part of these currents there will be an opportunity for supersaturation to occur.

In the original paper on the Skaergaard intrusion, it was suggested that convection currents, like the wind, would be variable in velocity and that, in a general way, this accounted for the rhythmic layering (Wager and Deer, 1939, pp. 272–73; Wager, 1952, pp. 345–48). It is now realized that variation in velocity of a current will, however, not produce the alternating uniform and gravity stratified bands commonly occurring in the layered series (Fig. 1). To account for rhythmic layering of this kind it is believed, as mentioned earlier, that two different sorts of currents existed simultaneously; one, a gentle and fairly continuous convective circulation from which the uniform rocks were deposited, and another, an intermittent, dense current of relatively small volume which periodically plunged down along the outer margin of the liquid and came to rest on the temporary floor, where a gravity stratified layer was deposited. The intermittent currents are similar to those postulated by Hess as having been in action during the formation of the Stillwater layered series

(Hess, 1960, p. 113). Possible velocities of the currents in the Skaergaard intrusion at a late stage in the formation of the layered series are given in Fig. 4. Both types of current are due to thermal convection.

In seeking an explanation of adcumulus growth, the hypothesis of a steady convective circulation will be used. During the circulation of the magma it may be that neither the loss of heat to the country rocks, nor the effect of increasing hydrostatic pressure during descent, is sufficient to cause nucleation. In the circumstances a supersaturated liquid, free from crystals, will sweep over the floor; the top crystals of the pile will have an opportunity to grow, and an adcumulate or, in extreme cases, a rock with harrisitic texture, will result. On the other hand, it may be that during circulation the heat loss and the effect of increasing hydrostatic pressure are sufficient to cause some nucleation, so that by the time the current turns horizontally across the floor, some crystals will be present in it. If the horizontal current has laminar flow, those suspended crystals which are denser than the liquid (and this is probably all of them) will sink steadily through the current to the floor, giving a uniform rock. At first sight it might seem that if crystals were present in the magma, then equilibrium conditions would exist, and no adcumulus growth would be possible. However, since the crystals are suspended in a moving current, there is only limited time available for the attainment of equilibrium. It is possible that equilibrium conditions are not attained, and this becomes more probable the more spaced-out the crystals are in the suspensions. In a thin suspension of crystals, the liquid could be at equilibrium temperature in the neighborhood of the suspended crystals and supersaturated further away. If such a liquid passes slowly over a crystal precipitate, it should deposit occasional crystals and, at the same time, it should produce adcumulus growth, the latent heat of crystallization passing into the supercooled part of the liquid. The conditions are diagrammatically indicated in Fig. 5. The overall rate of heat loss from the Skaergaard intrusion is assumed to have been of the same order as for the Stillwater complex, which has been estimated by Hess to be such that 10 cm of layered series are accumulated per year. The velocity of the convection current is taken as 2 m per day, a reasonable figure in the light of Shimazu's (1959) calculations. It is also a velocity sufficient to transport large feldspars upwards at the center, and this seems to be required for the formation of the upper border group of the Skaergaard intrusion. The amount of suspended crystals in the magma must be small, and has been estimated to be about 0.1%. The conditions illustrated are believed to represent those occurring in the Skaergaard intrusion during adcumulus growth from the steady drifting current. Some evidence for the numerical quantities assumed

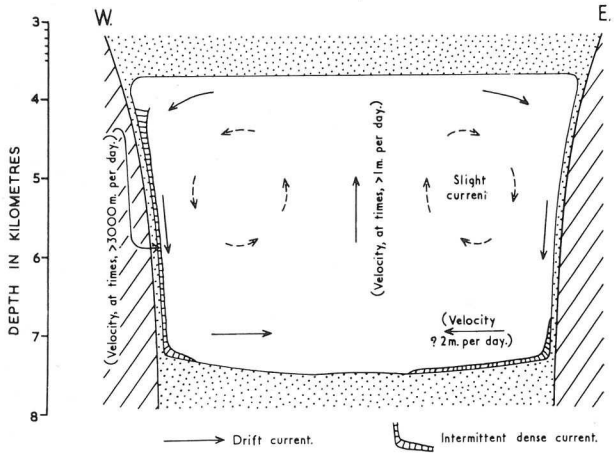


FIG. 4. Suggested conditions in the Skaergaard liquid at the beginning of the observed layered series, showing 1) the gentle, steady, convective circulation, with a velocity of the order of 2 m per day, 2) intermittent, dense, convection currents descending along the walls with high velocity, undercutting the gentle current, and coming to rest on the floor.

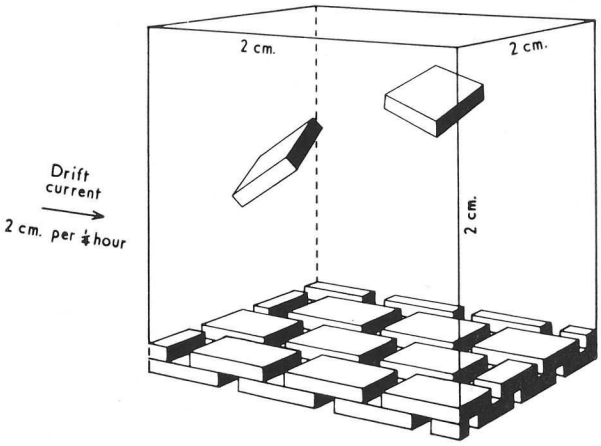


FIG. 5. Suggested conditions for adcumulus growth from the steady convection currents of the Skaergaard magma during the period of formation of the lower zone. The cumulus is considered to consist of crystals 0.5×0.5×0.1 cm in size, and a new layer assumed to take 3 days to form. In a 2 cm cube of liquid it is estimated that 1) there are only two crystals at any one time, and 2) 288 of the 2 cm cubes of liquid plus crystals pass over 4 square cm of floor in the three days required for the formation of a new layer of crystals.

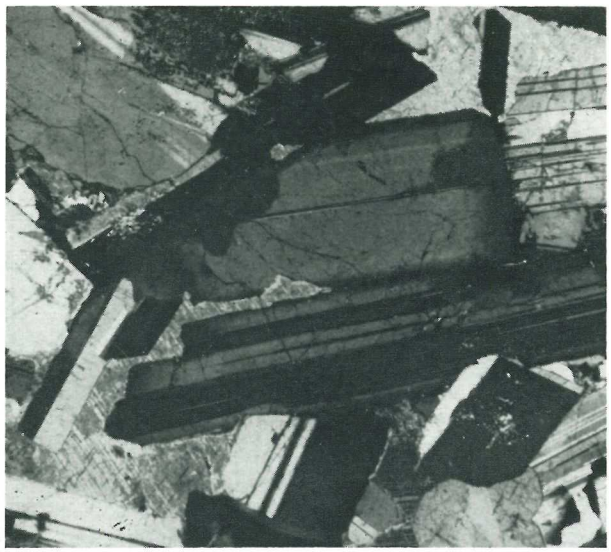

FIG. 6. Typical zoning of plagioclase in a plagioclase orthocumulate of the Lower Zone of the layered series (EG. 5109, ×23).

in Figs. 4 and 5 are derived by an overall consideration of the formation of the layered series and, as already mentioned, a paper on this is in preparation.

In the lower observable rocks of the Skaergaard layered series there is usually evidence of a considerable amount of pore material, that is, material formed by crystallization of trapped liquid. Thus interstitital magnetite is present which, at this level, is only an intercumulus mineral. Apatite in small, interstitial, subophitic crystals is found sporadically and, at this stage, it also is only an intercumulus mineral, being 1600 m below the level of its appearance as a cumulus phase. The zoning of the feldspars also indicates the effect of the trapped liquid. Thus the feldspars in a plagioclase cumulate from 110 meters in the layered series (Fig. 6) show essentially homogeneous cores,[1] representing the original cumulus crystals, surrounded by successively lower temperature zone where contact with other grains has not prevented their development. In the upper layered rocks the zoning in the plagioclases is less, or non-existent. Thus in the ferrogabbro at 1800 m (Fig. 7), zoning is only to be seen in the large crystal at the top left-hand corner of the photomicrograph, and even this amount of zoning is rarely seen. In this rock there was much adcumulus extension of the feldspars, and presumably, of the other cumulus minerals also. If, under the microscope, it were possible to define the boundary between the adcumulus material and the lower temperature zones formed from the trapped liquid, then a micrometric analysis could be made which would give the proportion of the various minerals in the pore material, and from this an approximate composition for the trapped liquid could be obtained. In practice, such a micrometric estimate is found to be difficult or impossible; usually all that can be done is to estimate whether there was much, or little trapped liquid and from this to decide, in general terms, whether the rock should be described as an orthocumulate, mesocumulate or adcumulate.

However, in the layered series below the horizon at which apatite becomes a cumulus phase, the phosphorus content of the rock may be used to decide with more precision the amount of trapped liquid. Since the cumulus minerals (plagioclase, olivine, pyroxene and iron ores) are essentially free from phosphorus, the phosphorus found by the analysis of the whole rock must be in the pore material formed from the trapped liquid. If, at a particular horizon, one rock has twice as much phosphorus as another, it is inferred that it also had twice the amount of trapped liquid. Furthermore, insofar as the amount of phosphorus in the successive residual liquids is known (Wager, 1961, pp. 378–81), the

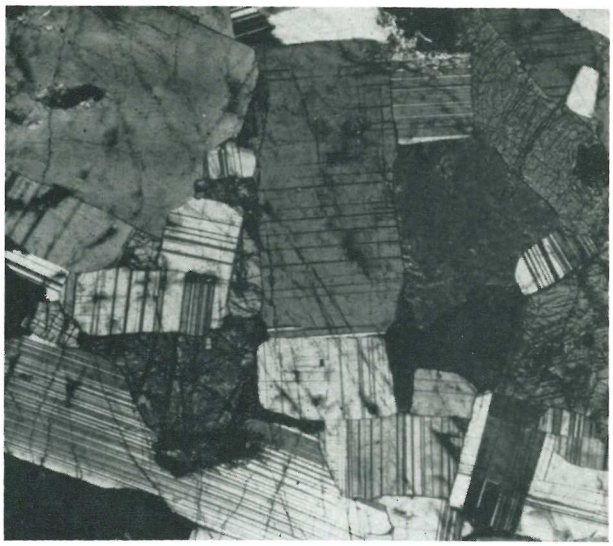

FIG. 7. Typical, almost unzoned, plagioclase crystals in a plagioclase-augite-olivine-magnetite mesocumulate from Upper Zone b of the layered series. (E.G. 5181, ×23).

[1] In some cases there are slight, patchy variations in the extinction of the core (not shown in the figure) implying differences in composition; this is a second order effect, which may be due to the crystal having formed under varying hydrostatic pressures and temperatures during movement in a convection current.

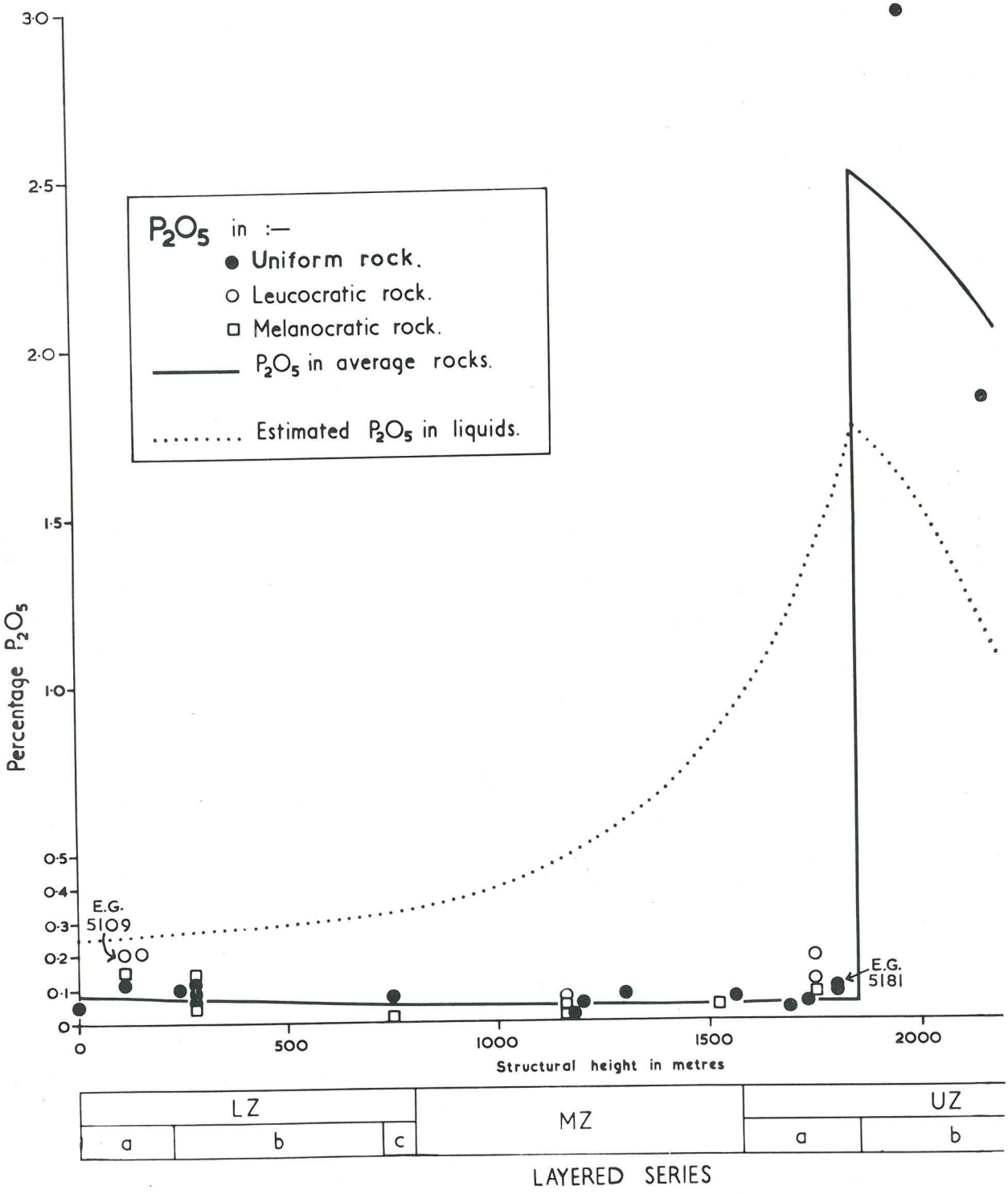


FIG. 8. $P_2O_5$ content of Skaergaard rocks plotted against height in the intrusion. Positions of EG. 5109 of Fig. 6 and of EG. 5181 of Fig. 7 are indicated.

ratio of trapped liquid to cumulus crystals can be obtained for any analyzed rock. The amount of phosphorus in the rocks of the lower and middle zones of the Skaergaard layered series is small, and ordinary methods of determination of $P_2O_5$ were unsatisfactory; Dr. E. A. Vincent has obtained more precise data, using radioactivation methods. In Fig. 8 newly obtained $P_2O_5$ values for various layered rocks are plotted against height in the intrusion. Three different types of cumulates are distinguished:

(1) the uniform rock, considered to have been deposited by the steady, drifting current, (2) the feldspar cumulates from the upper part of gravity stratified layers, and (3) the melanocratic cumulates from the base of gravity stratified layers.

The average phosphorus content of the layered rocks below the UZb horizon remains low, or even decreases, with height, *i.e.* with increasing fractionation. Before these measurements were made it was anticipated that the phosphorus content would rise, because the amount in the magma must have increased over this range. The fact that the $P_2O_5$ of the rocks does not increase is apparently due to the decreasing amount of trapped liquid at successively higher horizons. Confirmation of this is provided by examination of the rocks in thin section, but had not been appreciated until the phosphorus data were obtained. A small amount of trapped liquid implies either good initial packing of the cumulus crystals, or much adcumulus growth, or both. The effect on the phosphorus content of variation in the initial packing is considered slight, compared with the effects of adcumulus growth. The phosphorus analyses, therefore, provide clear evidence of an overall increase in adcumulus growth with increasing height in the layered series, up to the time when apatite became a cumulus mineral. Above this level the phosphorus content, obviously, is no longer a measure of the amount of intercumulus liquid, but because of the scarcity of zoning in the plagioclase it is clear that much adcumulus growth persisted almost to the top of the layered series.

Although the data on the phosphorus content of the Skaergaard layered series are, as yet, not abundant, they suggest that adcumulus growth is important in the formation of the uniform rocks, believed to have formed from the drift current (Fig. 8). The leucocratic and melanocratic parts of the gravity stratified bands have contrasting amounts of adcumulus growth, as judged by the few determinations of the phosphorus content available. The leucocratic plagioclase cumulates which are believed to be the result of the settling out of plagioclase from the intermittent, dense currents when they finally came to rest, show the least amount of adcumulus growth, probably because they accumulated quickly from a dense suspension of crystals. The thin melanocratic rocks at the base of the gravity stratified units have usually little phosphorus, implying considerable adcumulus growth. It is believed that the heavy crystals forming these layers fell to the floor through a turbulent current, and that the turbulence provided opportunities for the supersaturated parts of the magma, even if proportionally only small in total amount because of the density of the suspension, to come into contact with the deposit of heavy crystals.

The higher layered rocks, showing much adcumulus growth, suggest considerable supersaturation in parts of the liquid at the time they were forming. It is also interesting to note that the only clear case, in the Skaergaard intrusion, of harrisitic texture, which is taken to imply supersaturation, is within 200 m of the top of the layered series. With increasing depth in the observed layered series the rocks pass, on the average, from adcumulates or mesocumulates into meso- or ortho-cumulates, and it is thought probable that the hidden zone consists largely of orthocumulates. With increasing descent, the convecting magma perhaps would tend to become increasingly supersaturated, causing so much nucleation that no part of the magma was far from seed crystals, and less time would be required for diffusion of heat and substance to produce equilibrium conditions; thus, little or no adcumulus growth occurred. If this hypothesis is applicable to the layered rocks of Rhum, then the magma from which the adcumulates and harrisites formed should have been of no great thickness. On the other hand, this hypothesis is not directly applicable to the Bushveld and Stillwater layered rocks which include many adcumulates, apparently formed from bodies of liquid several kilometers thick.

## Acknowledgments

I am grateful to my colleague Dr. G. M. Brown for helpful discussion and for critically reading the manuscript. I also thank Dr. E. A. Vincent for the $P_2O_5$ data on which Fig. 8 is based and Dr. W. J. Wadsworth for the photograph presented as Fig. 3.

## References


BROWN, G. M. (1956) The layered ultrabasic rocks of Rhum, Inner Hebrides. *Phil. Trans. Roy. Soc. London.* B, **240,** 1–53.

——— (1957) Pyroxenes from the early and middle stages of fractionation of the Skaergaard intrusion, East Greenland. *Mineral. Mag.* **31,** 511–543.

HESS, H. H. (1939) Extreme fractional crystallization of a basaltic magma: the Stillwater Igneous Complex. *Trans. Amer. Geophys. Union Repts. and Papers, Volcanology,* pt. **3,** 430–432.

——— (1960) Stillwater igneous complex, Montana. *Geol. Soc. Am. Mem.* **80,** 1–230.

SHIMAZU, Y. (1959) A thermodynamical aspect of the earth's interior—physical interpretation of magmatic differentiation process. *Jour. Earth Sci., Nagoya Univ.* **7,** 1–34.

——— (1959) A physical interpretation of crystallization differentiation of the Skaergaard intrusion. *Jour. Earth Sci., Nagoya Univ.* **7,** 35–48.

VAN HOOK, A. (1961) *Crystallization Theory and Practice.* Reinhold Publishing Corporation, New York.

WADSWORTH, W. J. (1961) The ultrabasic rocks of southwest Rhum. *Phil. Trans. Royal Soc. London.* B, **244,** 21–64.

WAGER, L. R. (1953) Layered intrusions. *Medd. Dansk Geol. Foren.* **xii,** 335–349.

——— (1959) Differing powers of crystal nucleation as a factor producing diversity in layered igneous intrusions. *Geol. Mag.,* xcvi, 75–80.

——— (1960) The major element variation of the layered series of the Skaergaard intrusion and a re-estimation of the average composition of the hidden layered series and of the successive residual magmas. *Jour. Petrol.* **1,** 364–398.

——— (1961) A note on the origin of ophitic texture in the chilled olivine gabbro of the Skaergaard intrusion. *Geol. Mag.* **xcviii,** 353–366.

——— AND W. A. DEER (1939) Geological investigations in East Greenland, Part III. The petrology of the Skaergaard intrusion, Kangerdlugssuaq, East Greenland. *Medd. Grønland,* **105,** 1–352.

———, G. M. BROWN, AND W. J. WADSWORTH (1960) Types of igneous cumulates. *Jour. Petrol.* **1,** 73–85.

MINERALOGICAL SOCIETY OF AMERICA, SPECIAL PAPER 1, 1963
INTERNATIONAL MINERALOGICAL ASSOCIATION, PAPERS, THIRD GENERAL MEETING

# CONTRASTED STYLES OF IGNEOUS LAYERING IN THE GARDAR PROVINCE OF SOUTH GREENLAND

J. FERGUSON AND T. C. R. PULVERTAFT
*Geological Survey of Greenland, Copenhagen, Denmark*

ABSTRACT

Igneous layering is developed in nearly all the larger Gardar intrusions of south Greenland in rocks varying from gabbro to granite in composition. The syenites, which are the most abundant rocks in these intrusions, display the finest examples of layering. Layering comprising olivine-rich bands in more feldspathic gabbro forms synclinal structures in the large (over 200 m thick) gabbro dikes.

Layering is pronounced in the pyroxene-fayalite syenites of Kûngnât and Nunarssuit. Cumulus clinopyroxene and fayalite have been concentrated in layers as a result of gravity sorting under the influence of currents. In the petrographically similar syenite of the Klokken intrusion large-scale mafic banding and concordant lamination form an almost perfect saucer-shaped structure.

Most of the syenites of the Ilímaussaq Intrusion show banding, but the agpaitic rocks are the most striking. The kakortokites are laminated bottom accumulates with color banding due to rhythmic repetition of black, red and white bands corresponding to arfvedsonite/aegirine, eudialyte and feldspar concentrations respectively. Complementary banding occurs in the naujaite which formed simultaneously as a flotation cumulate. The residual magma crystallized to form the highly fissile lujavrites, which are locally banded as a result of alternating formation of aegirine and arfvedsonite. Fluctuations in pressure are thought to have caused the banding in the agpaites.

The nepheline syenites of the Grønnedal-Ika complex are characterized by pronounced feldspar lamination, locally accompanied by mineral layering.

Mineral layering is locally conspicuous in the Helene Granite where mafic minerals (including fayalite and clinopyroxene) are concentrated into layers as a result of gravity sorting assisted by magmatic currents.

## INTRODUCTION

Poldervaart and Taubeneck (1960) commented that well-layered plutons are relatively uncommon, and that most information concerning layered intrusions has come from mafic bodies. These wholly reasonable remarks serve to emphasize the great interest of south Greenland to students of igneous geology. Igneous layering is developed in nearly all the larger Gardar intrusions in the area and in rocks ranging from gabbro to granite in composition. It is in the syenites, however, that the finest examples of layering are seen.

Detailed mapping of the Gardar intrusions was begun by the Geological Survey of Greenland in 1955 and has not yet been completed. This paper is a review of what is known at present concerning layering in these intrusions, special emphasis being placed on the Ilímaussaq and Nunarssuit syenites with which the respective authors are most familiar through their own investigations. It is being presented now in order to use the opportunity provided by the Symposium to draw world-wide attention to the remarkable wealth of layered features displayed in the Gardar province, even though much detailed laboratory work remains to be done.

## THE GARDAR PROVINCE

*General.* Wegmann (1938) established that the Precambrian rocks of south Greenland belonged to two main cycles, which he termed Ketilidian and Gardar. The earlier Ketilidian cycle was one of sedimentation and tectogenesis. The Gardar period was dominated by igneous activity: it was initiated by the deposition of continental sandstones intercalated with lavas. These strata, despite their age more or less horizontal, rest with marked unconformity on Ketilidian basement migmatites in a down-faulted zone north of Julianehåb. Over a much wider area of south Greenland, between latitudes 60 and 62 north, numerous dike swarms, predominantly of basic composition, cut the basement. The intrusive centers, comprising mostly alkali rocks, are confined to the Ivigtut-Julianehåb area: generally speaking, with the exception of the Grønnedal and Igaliko complexes, these cut the dike swarms and are therefore late Gardar in age.

Faulting was widespread during the Gardar period. The most important faults are those running approximately east-west. These are partly responsible for the present distribution of the sandstones and lavas and are believed to have influenced the location of the intrusive centers.

*Gardar intrusive centers.* In order that the setting in which the layered rocks occur should be better understood, a brief summary of the Gardar intrusions and their salient features is given, in order from west to east (Fig. 1).

The *Kûngnât Complex* (Upton, 1960) consists of three pyroxene-fayalite syenite bodies which were intruded successively in order of increasing basicity with progressive easterly shift of center. Later an alkali gabbro ring-dike almost surrounding the syenites was emplaced. The complex is 5.4 km long by 3.2 km wide.

The *Grønnedal-Ika Complex* (Emeleus, in press) was, prior to faulting, an oval intrusion about 6 km long. It comprises nepheline syenites, commonly foyaitic in texture, and later carbonatite.

The *Nunarssuit Complex* (Harry and Pulvertaft, 1963) is a very large massif, at least 45 km long by 25 km wide, dominated by two pyroxene-fayalite syenite bodies, the Nunarssuit and Kitsigsut syenites, and the Helene Granite which has much in common with the Scandinavian rapakivis. Other members of the complex are gabbro, biotite granite and soda-granite.

The *Puklen Intrusion* (Pulvertaft, 1961), situated in Nunarssuit, is probably co-magmatic with the Nunarssuit Complex, being made up of pyroxene-fayalite syenite, quartz syenite and soda-granite. It is of the same order of size as the Kûngnât, Grønnedal-Ika and Tugtutôq central complexes.

The *Central Complex of Tugtutôq* (Upton, 1962) comprises some half-dozen ring-intrusions of related syenites and granites followed by a stock of perthosite syenite.

The *Narssaq Intrusion* lies just west of the Ilímaussaq Intrusion. The emplacement of quartz syenite and pyroxene syenite was followed by alkali granite.

The *Ilímaussaq Intrusion* (Ussing, 1911; Sørensen, 1958; Ferguson, in press) is famous for its remarkable development of per-alkaline syenites rich in chlorine and zirconium, expressed by the high content of sodalite and eudialyte respectively. Its evolution is outlined in a later section.

The *Igaliko Batholith* (Ussing, 1911; Ødum, 1927) is an enormous mass of nepheline syenites, with a marginal zone of augite syenite, on which work has only just commenced.

The *Klokken Intrusion* is a small oval mass of syenogabbro and augite syenite lying close beside the Igaliko Batholith.

The Gardar intrusions are amongst the best exposed in the world. The recent glaciation, during which erosion was very much more marked than deposition, and the harsh climate, which inhibits the growth of vegetation, are responsible for this. The strong relief in the area provides vertical sections up to 1700 m in some intrusions.

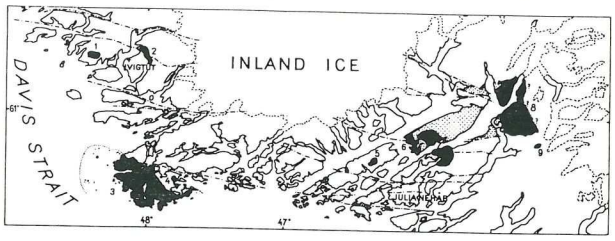


FIG. 1. Sketch map showing the position of the main Gardar igneous centers in south Greenland. 1) Kûngnât, 2) Grønnedal-Ika, 3) Nunarssuit, 4) Puklen, 5) Tugtutôq, 6) Narssaq, 7) Ilímaussaq, 8) Igaliko, 9) Klokken. The outcrop of the Gardar continental series is stippled.

*Giant Dikes.* Some of the northeasterly Gardar dikes in south Greenland are of considerable thickness (up to a kilometer) and are referred to as giant dikes. The most noteworthy of these occur in Tugtutôq where, although predominantly gabbroic, they are composite, with the development of nepheline syenite or quartz syenite centers. Anorthosite xenoliths are a conspicuous feature of these dikes. Northeast of Nunarssuit similar if less persistent and somewhat thinner dikes have been mapped. In Nunarssuit the Eqaloqarfia dike, a 2–300 m thick basic dike, connects the Nunarssuit and Puklen intrusions, both of which cut off the dike.

## IGNEOUS LAYERING

*Gabbros.* In the *Alángorssuaq Gabbro* of the Nunarssuit Complex (Harry and Pulvertaft, in press) banding and concordant lamination dip at moderate angles (between 30 and 50°) towards a deep focus in the center of the complex, now occupied by pyroxene-fayalite syenite and granite.

The mafic layers are usually between one and four cm thick, though some measure 30 cm in thickness. Generally they are between 5 and 30 cm apart. Within a single exposure most layers, considered individually, are of constant thickness. On a small scale also the banding is regular: well-defined "current-bedding," slumping and trough banding appear to be absent. Some of the broader layers are almost wholly composed of pyroxene. Local thin lenses of olivine-rock occur concordantly within the layering.

The lamination, which is usually highly pronounced, is due to the plane parallelism of tabular

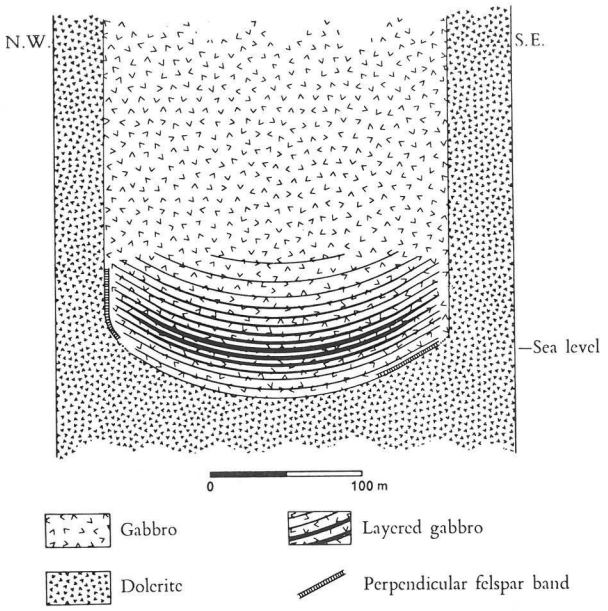


FIG. 2. Vertical section of the Eqaloqarfia dike, drawn to scale. In the layered zone the olivine-rich bands are represented schematically.

plagioclase feldspars (commonly about 0.5 cm long) and elongate dark minerals. Within the plane of parallelism, however, the long axes of these minerals are haphazardly arranged.

Synformally disposed layered structures occur at intervals along the troctolitic gabbro *giant dikes* of Tugtutôq (Upton, 1961, 1962), although the northern dike is almost entirely massive. The layering may be displayed by banding due to difference in the relative amounts of plagioclase and dark minerals (principally olivine) or by the parallelism of the plagioclase crystals. In rare instances both banding and concordant lamination occur. Gravity stratification is rarely developed in the banding, which generally dips inwards from the dike walls at angles lower than 45° becoming horizontal in the axial region. However there are a number of localities where the internal structure is considerably more complex with, for example, two or more synforms occurring side by side.

In some places banding parallel to the cooling walls can be observed in these gabbros. Of particular interest are the vertical zones of "perpendicular feldspar rock" developed on the inner side of the normal fine-grained marginal facies of the northern gabbro dike in the western part of Tugtutôq. These zones are characterized by the possession of elongate curved plagioclase, standing perpendicular to the cooling wall, with the convex surface uppermost.

The layering in the *Eqaloqarfia dike* defines a synform running parallel to the length of the dyke, with a maximum inward dip of the limbs of 36°. As shown in Fig. 2, the layering is developed in the lower part of a residuum of coarse gabbro in an otherwise normal dolerite dike. Homogeneous dolerite both underlies and forms a border zone to the gabbro. A perpendicular feldspar band, not more than 15 cm thick, occurs in some places at the border between the dolerite and gabbro: in this band the plagioclase feldspars have grown at steep angles to the margin of the dolerite.

The layering comprises bands rich in olivine set in ordinary coarse gabbro (feldspar tabulae 1–2 cm wide). Augite, the remaining important mineral, is interstitial to olivine and ophitic; it is not concentrated in the bands. The individual bands are regular and maintain a constant thickness over considerable distances. Passing up from the bottom of the layered succession the olivine-rich bands tend to become both thicker and more closely spaced until at about 15–20 m up they dominate over the intervening normal gabbro layers. Higher up the olivine-rich bands become thinner and more widely spaced, eventually dying out at about 50 m above the base of the gabbro, which shows no further layering in the exposed section of the dike (about 175 m high). All the rocks have been strongly uralitized, which impedes petrographic investigation.

Three further points must be taken into consideration when attempting an explanation of the layering:

1) No feldspar lamination has been observed in the dike, in spite of the favorable feldspar habit. 2) The bands do not show density grading; the top and bottom of the bands are equally sharply defined. 3) The olivines in some mafic bands are notably larger than those in the gabbro, reaching a centimeter or more in length.

The layering must have developed under tranquil conditions. The crystallization of the dolerite was followed by a period of quiescence and slight supercooling during which plagioclase feldspar grew from the margin of the dolerite into the residual magma. The onset of crystallization in the residuum was controlled by as yet unexplained cyclic changes which resulted in periods favorable to the crystallization and accumulation of olivine. With the cessation of these cyclic processes the remainder of the magma crystallized as normal gabbro.

*Larvikitic syenites.* Banding in the *Klokken Intrusion* forms an almost perfect saucer-shaped structure in the upper part of the intrusion, with inward dips of

30–50°. The bands, which are concentrations of mafic minerals (olivine and/or clinopyroxene, locally with ore and apatite as well), vary from a few meters to tens of meters thick, and there tends to be a downward gradation from mafic to normal syenite in the units. No "inch-scale" layering is superimposed on the big units. Feldspar lamination parallel to the banding is commonly pronounced.

The pyroxene-fayalite syenites of *Kûngnât* and *Nunarssuit* are notable for their layered structures, and they have many features in common. In both complexes banding is principally developed in the lower part of the exposed syenites: in the Nunarssuit Syenite, however, it is more or less confined to three zones. The lowest, and thickest, of these zones is about 75 m thick. The dip is normally between 15 and 45° towards foci in the centers of the massifs, and in each case it decreases inwards. In the Kûngnât syenites it is clear that the general form of the layering is that of a rather steep-sided dish. Cryptic and phase layering are developed in the Kûngnât Complex (Upton, 1960, pp. 49–50) but have not been detected in the Nunarssuit Syenite.

The layered structures in the Kûngnât and Nunarssuit Syenites comprise mafic banding and feldspar lamination. The latter is seldom developed in the Nunarssuit Syenite owing to the stumpy habit of the perthitic feldspars. The mafic banding is due to concentration of mafic minerals (cumulus clinopyroxene, fayalite and ore—the last commonly having a misleading interstitial form as a result of inter- or adcumulus growth) in plane-parallel layers during periods of magmatic flow. In the Nunarssuit Syenite these layers, where best developed, are 10–30 cm apart and 4–8 cm thick. Gravity stratification is a common but by no means constant feature

FIG. 3. Rhythmic banding in the Nunarssuit Syenite; note the discordance in the lower part of the photograph.

FIG. 4. Outwash channel cut in regularly banded Nunarssuit Syenite.

of the layered successions, the mafic bands having a well-defined base and passing upwards into less mafic rock. The layers are usually separated by normal syenite. In Kûngnât the units tend to be thicker than in Nunarssuit and may be conspicuously mafic for more than half their thickness.

The Nunarssuit Syenite provides outstanding examples of structures which faithfully mimic those in sedimentary rocks. Discordance—truncation of a layer, or more often a set of layers, by the lowest member of a superincumbent series of rhythmically repeated layers—characterizes the lowest layered zone, and in places gives rise to structures exactly like current bedding.

In conjunction with outwash channels highly pronounced discordances occur (Fig. 4). The channels cut abruptly across the normal planar layers on either side of them and are ascribed to the erosion of a loose cumulate floor. They indicate that the depth of unconsolidated crystal mush must have been at least 2 m.

Both the discordances and the outwash channels are taken as evidence of disturbance due to increased current action during the formation of the layering. Even more spectacular evidence of disturbance is afforded by the slump structures and breccias usually seen near outwash channels. Figure 5 shows disturbed layering which has formed load casts strikingly like structures in the Stillwater complex (Hess, 1960, Pl. 7, lower fig.). Intense disturbance gave rise to breccias (Fig. 6) containing fragments of mafic syenite up to 50 cm long. Some of these

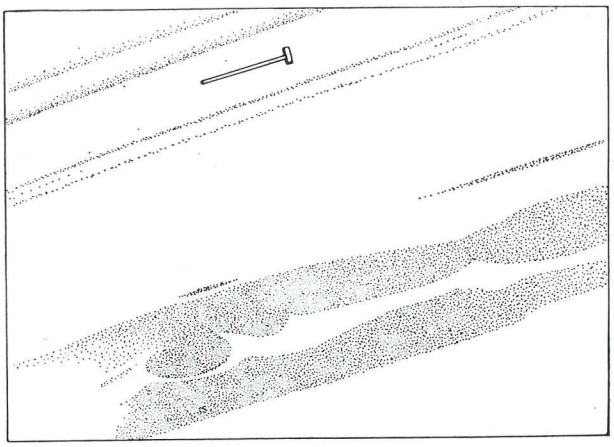

FIG. 5. Mafic layering in the Nunarssuit Syenite. The thicker layers in the lower part of the drawing have been disturbed with the resultant development of load cast-like structures. Drawn from a color transparency.

seem to be fragments of disrupted mafic layers, for they show banding or grading. Others must have been detached from the thick mafic lenses locally associated with trough banding, for they are homogeneous and too thick to have been derived from the usual sort of layering in the syenite. The breccias may lie concordantly above or below undisturbed banding; on the other hand in places they truncate such banding. In one layered sequence the dip of each successive layer increases from about 35 to 45°, passing up the succession which terminates abruptly in an overlying slump breccia zone. This points to a value of about 45° for the maximum angle of rest of the cumulate floor. For the Kûngnât syenites Upton (1960, p. 116) gives 40–50° as the maximum angle of rest under normal conditions. These figures are very much higher than those given by Brown (1956, p. 38) for the ultrabasic cumulates of Rhum, where the maximum angle of rest seems to have been only 15°.

Similar, if less spectacular, evidence for magmatic flow can be seen in the Kûngnât syenites. In addition they display trough banding closely resembling that in the Skaergaard intrusion (Wager and Deer, 1939) but not strictly comparable with the outwash channels in Nunarssuit. The troughs, which are up to 12 m wide, are typically bilaterally symmetrical; their axes are directed towards the center of the intrusion and inclined at the same angle as the layering. Rhythmic mafic layering is seen in the trough bands, and the trough-like form may be preserved through up to 30 units, although the degree of crystal sorting and strength of banding diminishes upwards through the trough set (Upton, 1960, fig. 15).

The border syenites of eastern Kûngnât are characterized by the possession of steep fluxion-banding. This takes the form of rather wispy mafic bands, seldom thicker than 2 cm, usually dipping steeply into the intrusion and striking approximately parallel to the contact. In detail the course of these bands is highly irregular.

Steep mafic layering striking parallel to the border of the intrusion also occurs in the marginal augite syenite of the *Ilímaussaq Intrusion*. The mafic concentrations are 1–3 cm thick and are separated by 2–30 cm of the normal rock; considered individually they are of remarkably constant thickness. In contrast to the fluxion-banding at Kûngnât, this banding is very even, the only irregularity being a slight tendency for bands to merge up-dip. The bands wedge out towards the margin against the fine-grained chilled syenite and inwards in a coarse-grained facies of augite syenite. The angle of dip (50–75°) is steeper than the maximum angle of rest of the cumulate floor in the comparable augite syenites of Kûngnât and Nunarssuit; this argues against magmatic currents assisted by gravity having caused the layering. Rather it seems that mafic nuclei were repeatedly precipitated and grew on the cooling side of the magma chamber. The necessary periodicity could be the result of regular rapid oscillations in the water vapor pressure of the magma (Yoder, 1954) or be developed as an intrinsic part of the nucleation process, if supercooling of the

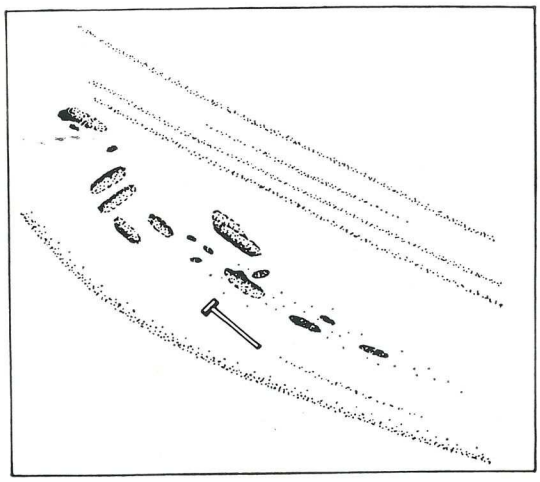

FIG. 6. Slump breccia in the Nunarssuit Syenite. The fragments in the breccia are of banded and gravity stratified syenite which has been broken up during strong disturbances. Drawn from a photograph.

magma initiated nucleation (Wadsworth, 1961, p. 61).

In the Ilímaussaq Intrusion pulaskite and quartz syenite, believed to be hybrid rocks formed by reaction between alkali granite and earlier undersaturated rocks, form sheets which show banding on rather a fine scale. In the pulaskite the banding is due to the concentration of arfvedsonite and small amounts of olivine in dark bands averaging a centimeter thick, separated by 2–3 cm thick bands of feldspathic syenite. In the quartz syenite the banding is similar but only arfvedsonite is concentrated in the dark bands. Thin sheets (*i.e.* less than 2 m thick) may be banded throughout their entire thickness and the banding may extend laterally over 50–100 m. Lamination is never seen in these layered rocks. In one instance a discordance in the banding at the center of a sill suggests that growth took place simultaneously from both sides of the sill towards the center.

A heterogeneous syenite characterized by very uneven grain size occurs between the augite syenite and agpaitic rocks of Ilímaussaq. In it the rock-forming minerals are perthite, soda-pyroxene, soda-amphibole, olivine and nepheline. Banding is sporadically developed due to alternation of bands about a meter thick of coarse rock relatively rich in olivine with lighter pegmatitic bands in which feldspars averaging 6 cm×1 cm tend to be aligned with their long axes perpendicular to the banding. Fragments of the coarse rock, 20–30 cm in diameter, are commonly included in the pegmatitic bands, particularly where the latter are slightly transgressive.

This heterogeneous syenite is considered to have crystallized from the roof downwards. The banding may best be explained by repetitive volatile accumulations at the base of the downward crystallizing rock which resulted in the formation of the pegmatitic bands. The same mechanism, working upwards, is envisaged by Weedon (1960, pp. 46–47) to account for the pegmatitic bands in the Gars-bheinn sill of Skye.

*Nepheline syenites*

(a) The Ilímaussaq Intrusion

A brief review of the evolution of the Ilímaussaq Intrusion is essential to the understanding of the igneous banding in the agpaitic rocks. The schematic diagram (Fig. 7) illustrates the structure as interpreted by the one author (Ferguson, in press). The earliest magma in the intrusion had an augite

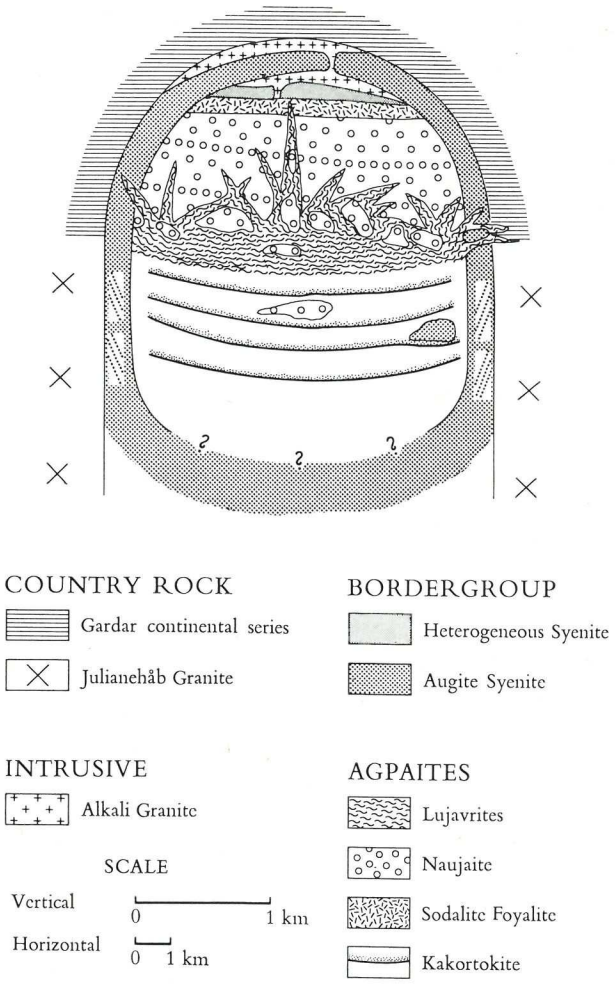


FIG. 7. Diagrammatic cross section of the Ilímaussaq Intrusion.

syenitic composition. After emplacement this magma proceeded along an undersaturated differentiation trend. The layering in the early derivatives has already been described. The *in situ* differentiation was interrupted by the injection of alkali granite into the upper part of the intrusion. Following this undersaturated differentiation was resumed and, aided by volatiles, formed magma of per-alkaline (agpaitic) composition. Crystallization of the agpaitic magma took place from the roof downwards with simultaneous bottom accumulation on the floor of the intrusion. Finally a residual crystal mush, rich in volatiles, was trapped between the downward crystallizing naujaite and the bottom-accumulated kakortokites. As a result of deformation the residual crystal mush was injected into the overlying brecciated rocks. This residual magma crystallized to from the fissile lujavrites.

FIG. 8. Main occurrence of the layered kakortokites.

(i) Kakortokite. The kakortokites are the layered agpaitic rocks exposed in the lowermost part of the intrusion (Figs. 8 and 9). The layering comprises rhythmic compositional variations developed through a vertical thickness of more than 400 m of the exposed part of the kakortokites. Within this there are approximately 25–30 layered units, each unit consisting of black, red and white bands corresponding to arfvedsonite/aegirine, eudialyte and alkali feldspar concentrations respectively. The white kakortokite bands have an average thickness of 10 m whereas those of black and red kakortokite average 1.5 m thick. The upward sequence black-red-white is never varied, even though the red bands may be inconspicuous.

Modal analyses from the different bands indicate the compositional variations responsible for the banding.

| | *Perthite* | *Aegirine* | *Arfvedsonite* | *Eudialyte* | *Nepheline* |
|---|---|---|---|---|---|
| White kakortokite | 50 | 9 | 13 | 10 | 18 |
| Red kakortokite | 36 | 6 | 12 | 29 | 17 |
| Black kakortokite | 18 | 13 | 40 | 11 | 18 |

The base of each unit is usually rather sharply defined, the transition between the underlying white kakortokite and the black kakortokite taking place in 5–10 cm or even less. In one case it is knife-sharp. The black kakortokite passes up into red kakortokite through a 15–25 cm thick transition zone in which there is a rapid increase in the proportion of eudialyte and feldspar. Eudialyte, concentrated at the bottom of the red bands, becomes less plentiful passing up into the white kakortokite.

The layers are considered to have been originally horizontal, but due to sagging are gently undulating. They are very persistent, and individual bands maintain a constant thickness over the whole area of the kakortokites to within 50 m of the margin, where they wedge out in a coarse-grained rock. Where inclusions of older rock are found, the underlying layers are compressed (Fig. 9), in one instance to approximately $\frac{2}{3}$ds of their original thickness to a depth of 15–20 m below the inclusion. This is significant, as it indicates that the depth of unconsolidated crystal mush must have been about 20 m. The overlying layers pass conformably over the inclusions without thinning at the crests.

In the black bands there is marked lamination produced by the 4 mm×1 mm tabular feldspars and prisms of arfvedsonite or aegirine of similar size lying in the plane of the banding. There is no lineation within the plane of lamination. Less pronounced feldspar lamination is developed in the white kakortokite. The finer-grained red kakortokite tends to have a saccharoidal texture.

The microscopic texture of the black bands suggests that in the black kakortokite all the minerals are cumulus. In the red and white bands feldspar, nepheline and eudialyte are the cumulus minerals whereas arfvedsonite and aegirine are poikilitic. Some idea of the original size of the cumulus nepheline and eudialyte in the latter two bands can be gained from the crystals enclosed in the arfvedsonite and aegirine. These are as little as half as large as the crystals not enclosed, which have increased their size by adcumulus addition. The same approach cannot be applied to the perthite crystals, which are too large to be completely enclosed in the arfvedsonite and aegirine.

But for a few crystals of concentrically-zoned

FIG. 9. Banded kakortokite with an inclusion of foreign rock which has compressed the underlying layers. (Photograph by F. L. Jacobsen.)

eudialyte and albite rims on some perthites, zoning is lacking in the minerals of the kakortokites. This suggests that the cumulus crystals grew by adcumulus addition. Diffusion from the overlying magma into the crystal pile must have taken place over distances up to 20 m, since this is the depth of unconsolidated crystal mush.

The only evidence of cryptic layering is provided by the nepheline. Passing up the kakortokites the $\%KAlSiO_4$ diminishes irregularly from 18.5 to 9.6. No phase layering (Hess, 1960, p. 132) occurs.

Ussing (1911) advanced the following hypothesis for the formation of the kakortokites " . . . the simplest supposition is perhaps that the recurrent layers have originated in consequence of repeated variations in pressure" (p. 361). Experimental work by Yoder (1954) on the system diopside-anorthite-water has demonstrated that variations in water vapor pressure could produce layering. The Ilímaussaq Intrusion was emplaced high into the Gardar sandstones and lavas and is thus a high-level intrusion. Intermittent water vapor pressure release could have easily taken place through fissures or conduits which penetrated to the surface. A small shift in the eutectic caused by a change in water vapor pressure and resulting in arfvedsonite and aegirine crystallizing first would account for the cumulus nature of these minerals in the black bands.

The units in the kakortokite are gravity stratified.

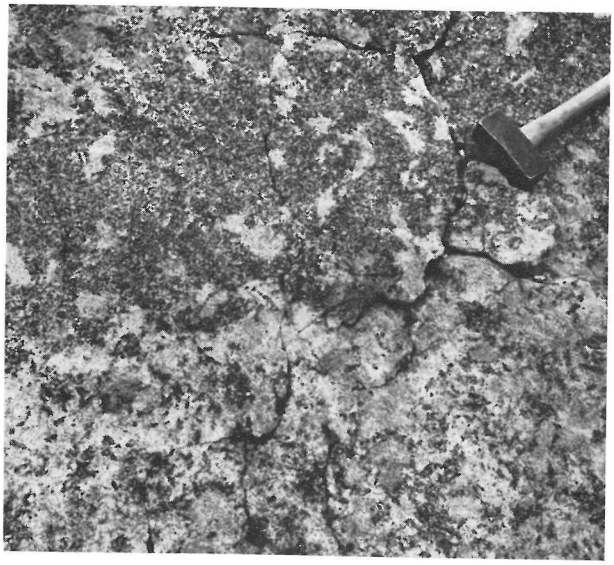

FIG. 11. Close-up of the naujaite banding seen in Fig. 10, showing the upper part of a light band and the lower part of a dark band. Note the large aegirine/arfvedsonite anhedra in the latter.

To account for this, Upton (1961, p. 12) suggested that the black kakortokites have formed during periods of flow sufficiently strong to have retained the feldspar in suspension. However it might be possible to produce density grading without resorting to magmatic flow. In the agpaitic magma, which had a very high volatile and water content, an increase in density would accompany increase in total pressure,

FIG. 10. Banding in naujaite involving compositional and textural variations.

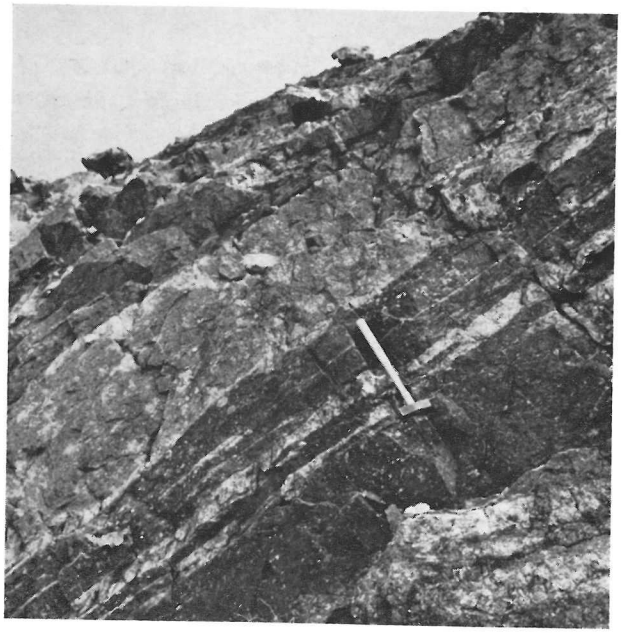

FIG. 12. Alternating aegirine (light) and arfvedsonite (dark) lujavrite bands.

particularly if some of the volatile components were in fine bubble suspension. The sinking rate of the minerals would be retarded by such a density increase in the magma, and the reduction of sinking rate would be most marked in the case of the feldspars, the density of which was close to that of the magma. Variations in total pressure could therefore account for the density stratified layering, the black bands corresponding to periods of high pressure and higher density of the magma, while the feldspathic bands correspond to periods of low pressure and lower density.

Thus the layering in the kakortokites may have originated as a result of variations either in the water vapor pressure of the magma or in total pressure in the magma chamber, or it may be due to simultaneous fluctuations in both forms of pressure.

Discordances, outwash channels and other evidence of the strong currents and turbulence which are regarded as responsible for gravity stratification in some layered igneous rocks (*e.g.* the Nunarssuit Syenite), are lacking in the kakortokites. Upton (1961, p. 28) claims to have observed "incipient trough banding" and minor disconformities in the kakortokites, but these were not observed by the first author. Conditions obtained which allowed undisturbed accumulative settling on the floor of the magma chamber. This is in contrast to the Skaergaard intrusion where convection currents operated during crystallization, hence the analogies with the kakortokites are not as close as Wager and Deer (1939, p. 289) imply.

(ii) Naujaite. Ussing (1911, pp. 349–354) was of the opinion that sodalite was one of the first minerals to crystallize in the magma chamber and that it floated due to its low density. He considered the naujaite to have formed by the flotation of sodalite crystals which were trapped in a downward crystallizing rock, giving rise to the poikilitic texture which characterizes the rock. This theory agrees with the new interpretation of the evolution of the intrusion since the bottom-accumulated kakortokites are virtually free of sodalite. The average naujaite is made up of poikilitic feldspar, aegirine, arfvedsonite and eudialyte of pegmatoid dimensions with 2–3 cm diameter sodalite inclusions which make up 34–45% of the rock.

Banded horizons have been observed throughout the *ca.* 1000 m thickness of exposed naujaite. They are flat-lying except near the border of the intrusion where there are locally steep inward dips. The commonest banding is produced by compositional variations which are usually associated with textural change. Dark bands 60 cm to a meter thick, rich in aegirine and arfvedsonite, alternate with thicker feldspar-rich bands, with local 5–10 cm eudialyte-rich bands intervening. The poikilitic texture of the normal naujaite is retained in these bands, but the aegirine/arfvedsonite anhedra are of different sizes in the different bands. In the dark bands the aegirine/arfvedsonite forms the usual 10 cm diameter anhedra found in the normal naujaite, but in the light bands these minerals form prisms 2–3×1 cm.

Aegirine/arfvedsonite concentrations 20–30 cm thick set a meter apart in normal naujaite are also common. The aegirine/arfvedsonite in the dark bands forms 2–3×1 cm prismatic crystals.

Sodalite-rich and sodalite-poor horizons are developed locally in the naujaite. The sodalite-rich bands (termed sodalitites by Ussing) vary from 0.5 to 5.0 m thick and may contain up to 70–80% sodalite which is of the same size as, or a little smaller than, that in the normal naujaite. The remaining minerals—any of those found in the normal naujaite—are skeletal due to the excessive amount of sodalite inclusions. Commonly sodalitite forms a single horizon within the normal naujaite. However sodalite-rich bands can alternate with light bands rich in poikilitic feldspar and eudialyte.

The 10–20 cm thick sodalite-poor bands occur singly within normal naujaite. They do not have a poikilitic texture; instead sodalite forms scattered xenomorphic crystals measuring up to a few centimeters across.

Narrow, less than 1 m thick, asymmetrically-zoned lenticular pegmatites are sporadically found in the naujaite, having conformable relations to the banding. They have been described by Sørensen (1962).

The naujaite is a flotation cumulate. As the naujaite and kakortokite crystallized simultaneously at the top and bottom respectively of a single magma chamber, the same pressure variation affected the crystallization of both. The layering in the naujaite comprising light and dark bands with local red bands is interpreted as being complimentary to the banding in the kakortokites and caused by the same fluctuations in pressure conditions. The sodalite-rich bands could have been formed during periods of excess sodalite formation and/or efficient flotation. Flotation would have been assisted by increase in density of the magma resulting from pressure increase (see under *kakortokites*). Conversely the sodalite-poor bands could have been produced dur-

ing short periods of arrested sodalite flotation, which allowed the magma to crystallize without the addition of cumulus sodalite.

(iii) Lujavrites. The lujavrites are the youngest agpaitic rocks of the Ilímaussaq Intrusion. Unlike the other nepheline syenites, they are rather fine-grained and possess a strong fissility due to acicular aegirine and arfvedsonite crystals up to 3 mm long, lying in a common plane. Lineation is rare in the plane of lamination. In addition to aegirine and/or arfvedsonite, which make up 30–40% of the rock, the lujavrites contain microcline and albite in separate crystals, nepheline, sodalite and eudialyte. They may be divided into two types: green aegirine lujavrite and black arfvedsonite lujavrite.

The lujavrites form a unit *ca.* 200 m thick between the naujaite and kakortokites. The lower half of this unit is occupied by green lujavrite, the upper by black lujavrite. Banding is developed principally in a 50 m thick mixed zone in between. The banded sequences do not exceed 40 m and are usually only 2–5 m in thickness. Within these the bands vary from 1 cm–15 m thick, averaging 10 cm; they are lenticular and may have marked pinch-and-swell structure. Auto-intrusion has resulted in banded lujavrite being cross-cut by dikes of inhomogeneous lujavrite.

Of the different types of banding developed, that due to alternation of aegirine and arfvedsonite lujavrite involves no textural variations. In the banding produced by the alternation of layers rich in feldspar with darker layers, the latter show density stratification (Fig. 13). For example, at the base of the darker band there may be 3–4 mm of only arfvedsonite; passing upwards light minerals enter into the rock and gradually become more plentiful. Here and there the dark bands grade into the overlying light bands, but more commonly there is a distinct break between the two bands. Only one case of compositional banding accompanied by textural variations was observed; this was in coarse-grained green lujavrite which contains bands rich in feldspar.

It is postulated that aegirine, feldspars, eudialyte and nepheline formed the cumulus minerals in a residual volatile-enriched magma and accumulated on top of the kakortokites to form the green lujavrite. After about half of the residual magma had crystallized, arfvedsonite began to form instead of aegirine. Alternation in the formation of the two minerals produced black and green banded lujavrite. This is the only example of banding in south Greenland where water vapor control is a probability

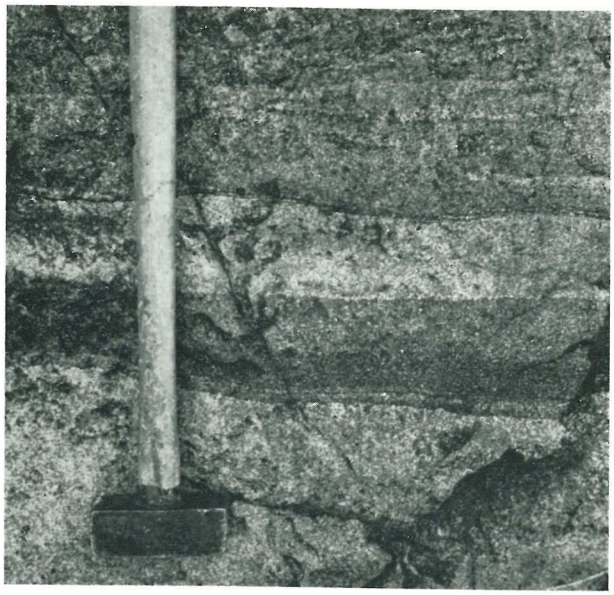

FIG. 13. Alternating bands of dark arfvedsonite-rich lujavrite showing density stratification and light feldspathic lujavrite bands.

rather than a possibility. Yagi (1953) has inferred that the order of crystallization of aegirine-augite and arfvedsonite depends on the presence of volatiles, especially water, which favors the crystallization of arfvedsonite, and Fyfe *et al.* (1958, pp. 162–163) have proposed stability relations for OH- and F-bearing amphiboles and pyroxene which are dependent on water vapor pressure. In the concluding stages of crystallization the residual magma rich in volatiles crystallized as black arfvedsonite lujavrite.

The intercumulus areas in the lujavrites are thought to have had a high volatile content which served to keep the cumulate in a mobile state. As a result on deformation (faulting and/or sagging) the crystal mush was compressed and some of it injected into the overlying brecciated rocks, finally crystallizing as fissile lujavrites. The volatile phase was squeezed out to form late-stage natrolite-analcime veins. The various inhomogeneities in the crystal mush were streaked out into bands during deformation, and the size and density sorting locally seen are thought to have been produced during flowage (*cf.* Wilshire, 1961).

(b) The Grønnedal-Ika Complex

The majority of the Grønnedal-Ika nepheline syenites is foyaitic with pronounced igneous lamination dipping at various angles towards the center of the complex. Callisen (1943) considered that gravitational differentiation was a significant factor in their crystallization history; on this assumption and from

the close textural similarities with rocks from layered intrusions, the main cumulus phases were nepheline and platy crystals of alkali feldspar, with intercumulus aegirine-augite, biotite, cancrinite, fluorite and carbonate. A minor amount of mineral layering concordant with the lamination occurs at one level within the foyaites. In thin bands of relatively mafic rock aegirine-augite and apatite join the cumulus phases and an alkali amphibole appears in an intercumulus role. Possible complementary rocks are rare perthosites with very well-developed lamination.

In another variety of layering, impersistent horizons of altered, poorly laminated syenite occur conformable to the lamination in fresh foyaite. The poorly laminated syenites and the associated foyaites are thought to represent respectively loose and closely packed bottom accumulates, resulting from slight variations in the strength of magmatic currents during crystallization; greater alteration of the ill-packed rocks is attributed to a high proportion of intercumulus liquids.

*Granite.* Mafic layers from one to roughly twenty centimeters thick occur locally in the *Helene Granite* of the Nunarssuit Complex (Harry and Emeleus, 1960; Harry and Pulvertaft, 1963). Those up to about two centimeters thick are simply concentrations of the mafic, and some accessory, minerals found in the normal granite. Of these the clinopyroxene and, where present, fayalite are cumulus minerals. Hornblende, although plentiful in the dark bands, is to some extent a replacement of pyroxene and probably owes its abundance to such processes rather than accumulation of a primary precipitate. The thicker mafic layers are even-grained rocks in which quartz and feldspar are rather finer-grained than in the normal intervening granite. The layers can be symmetrical or asymmetrical in cross section: asymmetrical bands have a sharp base, grading up into normal granite. Preferred orientation of mineral form is seldom apparent in the layered rocks or indeed in the granite as a whole, but elongate xenoliths locally present are arranged parallel to the layering.

The mafic layers in normal Helene Granite may be rhythmically repeated within a single exposure to give a succession of up to about thirty sub-parallel bands a fraction of a meter apart. These mafic layers can be traced continuously for distances of up to 14 m and generally terminate by wedging out. Less commonly layers may be isolate, commonly branching individuals, the traces of which may describe graceful arcs. In some places a rhythmically repeated succession is arcuate in vertical profile and recalls trough banding. The attitude of the layering in the Helene Granite is variable; both steep and moderate dips have been observed.

On the whole the analogies between the mafic layering in the Helene Granite and that in the Kûngnât and Nunarssuit syenites are sufficient to justify the view that the layering in the granite is primarily due to the accumulation of dark minerals under the influence of gravity and magmatic currents. The irregularities and steeper dips met with in the granite are what would be expected if the granite magma, although fluid enough to allow currents, was more viscous than a pyroxene-fayalite syenite magma.

Another type of layering, involving textural variations (bands of porphyritic granite and microgranite) as well as mafic bands and normal granite, is seen at two localities in the Helene Granite. Very thin mafic layers are remarkably persistent in these banded zones. Some kind of repeated differentiation *in situ*, rather than currents, appears to have governed their formation.

## Conclusions

The great variety of layered features displayed in the Gardar intrusions is apparent from the foregoing section. Obviously more than one factor was responsible for the development of the layering.

The striking similarity between the layered structures in the Kûngnât and Nunarssuit syenites and those in sedimentary rocks allows it to be confidently stated that the layering in these syenites is primarily the result of magmatic current action. The Helene Granite most likely owes much of its banding to the same mechanism. The feldspar lamination developed in many other intrusions indicates that in these crystallization was accompanied by gentle magmatic flow or alternatively took place in a magma of rather low viscosity in which the feldspars would settle flat on the cumulate floor without the assistance of currents. Thus the Gardar magmas for the most part possessed high mobility, as has already been pointed out by Upton (1961, p. 10). The widespread occurrence of fluorite in the Gardar intrusions testifies to high fluorine content in the magmas which would reduce their viscosity (Buerger, 1948). In many Gardar intrusions, however, current action was of little or no importance.

The fact that many Gardar centers were high-level intrusion likely to have had access to the surface is

believed by the authors to have been the other main cause for the common incidence of layering in these intrusions. The Ilímaussaq and Igaliko intrusions were both emplaced into the Gardar continental series, and around Narssaq the giant dikes of Tugtutôq pass up into sills in these supracrustal rocks. The unbanded Central Complex of Tugtutôq contains blocks of basalt and quartzite clearly derived from the supracrustal series and must therefore have penetrated up into these. In such intrusions optimum conditions existed for cyclic fluctuations in water vapor pressure. That such fluctuations could produce layering was suggested long ago by Ussing.

However it should be pointed out that in many other parts of the world there are high-level intrusions which do not show layering or in which layered structures have not been recorded in rock less basic than gabbro. In this latter respect the Gardar Province is unique.

## References


Brown, G. M. (1956) The layered ultrabasic rocks of Rhum, Inner Hebrides. *Phil. Trans. Royal Soc. London*, B, **240,** 1–53.

Buerger, M. J. (1948) The structural nature of the mineralizer action of fluorine and hydroxyl. *Am. Mineral.* **33,** 744–747.

Callisen, K. (1943) Igneous rocks of the Ivigtut region, Greenland. Part I: The nepheline syenites of the Grønne Dal-Ika area. *Medd. Grønland,* **131** (8), 1–74.

Emeleus, C. H. (in press) The Grønnedal-Ika alkaline complex, South Greenland. The structure and geological history of the complex. *Medd. Grønland,* **172** (3).

Ferguson, J. (in press) The Ilímaussaq alkaline intrusion, South Greenland. Part I: Description of map and structure. *Medd. Grønland,* **172** (4).

Fyfe, W. S., F. J. Turner and J. Verhoogen (1958) Metamorphic reactions and metamorphic facies. *Geol. Soc. Am. Mem.* **73.**

Harry, W. T. and C. H. Emeleus (1960) Mineral layering in some granite intrusions of S.W. Greenland. *Rep. Int. Geol. Cong., XXI Sess.*, Pt **14,** 172–181.

——— and T. C. R. Pulvertaft (1963) The Nunarssuit intrusive complex, South Greenland. Part I: General Description. *Medd. Grønland,* **169** (1).

Hess, H. H. (1960) Stillwater igneous complex, Montana. *Geol. Soc. Am. Mem.* **80.**

Poldervaart, A. and W. H. Taubeneck (1960) Layered intrusions. *Rep. Int. Geol. Cong. XXI Sess.*, Pt. **13,** 239–246.

Pulvertaft, T. C. R. (1961) The Puklen intrusion, Nunarssuit, SW Greenland. *Medd. Grønland,* **123** (6), 33–50.

Sørensen, H. (1958) The Ilímaussaq batholith. A review and discussion. *Medd. Grønland,* **162** (3), 1–48.

——— (1962) On the occurrence of steenstrupine in the Ilímaussaq massif, Southwest Greenland. *Medd. Grønland,* **167** (1), 1–251.

Upton, B. G. J. (1960) The alkaline igneous complex of Kûngnât Fjeld, South Greenland. *Medd. Grønland,* **123** (4), 1–145.

——— (1961) Textural features of some contrasted igneous cumulates from South Greenland. *Medd. Grønland,* **123** (6), 1–31.

——— (1962) Geology of Tugtutôq and neighbouring islands, South Greenland, Part I. *Medd. Grønland,* **169** (8), 1–60.

Ussing, N. V. (1911) Geology of the country around Julianehaab, Greenland. *Medd. Grønland,* **38,** 1–376.

Wadsworth, W. J. (1961) The layered ultrabasic rocks of southwest Rhum, Inner Hebrides. *Phil. Trans. Royal Soc. London,* B, **244,** 21–64.

Wager, L. R. and W. A. Deer (1939) Geological investigations in East Greenland. III: The petrology of the Skærgaard intrusion, Kangerdlugssuaq, East Greenland. *Medd. Grønland,* **105** (4), 1–352.

Weedon, D. S. (1960) The Gars-bheinn sill, Isle of Skye. *Quart. Jour. Geol. Soc. London,* **116,** 37–50.

Wegmann, C. E. (1938) Geological investigations in Southern Greenland. Part I: On the structural divisions of Southern Greenland. *Medd. Grønland,* **113** (2), 1–148.

Wilshire, H. G. (1961) Layered diatremes near Sydney, New South Wales. *Jour. Geol.* **69,** 473–484.

Yagi, K. (1953) Petrochemical studies on the alkalic rocks of the Morotu district, Sakhalin. *Bull. Geol. Soc. Am.* **64,** 769–810.

Yoder, H. S. (1954) Synthetic basalt: pp. 106–107 *in* Abelson, P. H., *Ann. Rept. Director Geophys. Lab., Carnegie Inst. Washington Year Book* **53,** 95–145.

Ødum, H. (1927) Geologiske iagttagelser i landet øst for Igaliko Fjord. *Medd. Grønland,* **74,** 43–54.

MINERALOGICAL SOCIETY OF AMERICA, SPECIAL PAPER 1, 1963
INTERNATIONAL MINERALOGICAL ASSOCIATION, PAPERS, THIRD GENERAL MEETING

# STRUCTURAL AND PETROGRAPHIC OBSERVATIONS ON LAYERED GRANITES FROM SOUTHERN GREENLAND[1]

C. H. EMELEUS
*Department of Geology, University of Durham, Durham, England*

ABSTRACT

Mineral layering is developed in the upper and marginal parts of two granite stocks intruding Precambrian gneisses north of Tigssaluk Fjord, southern Greenland. The layering consists of unusual concentrations of biotite, sphene, opaque minerals, allanite, zircon and apatite. Their modal proportions are commonly over 30% (by volume), rising to more than 80% in some instances. The layered structures include well-developed, rhythmically repeated mafic bands, layers with gravity-stratification, indications of trough banding, and distorted layering resembling slump structures in sediments.

The more mafic layers have distinctive cumulate textures. Euhedral biotite, sphene, allanite, zircon and apatite are poikilitically enclosed by quartz, microcline perthite, plagioclase and in places fluorite. Large euhedral crystals of microcline perthite and plagioclase are also present, the latter generally showing albitic overgrowths (An5 about) on andesine cores (An25+).

Textural and structural features of the layering are comparable with those developed in many basic, ultrabasic and syenitic intrusions. It is suggested that in the granites the layering formed during the later stages of crystallization of unusually fluid magmas, with bottom accumulation of early-formed dense minerals concentrated by the action of intermittent magmatic currents.

## INTRODUCTION

The Tigssaluk Complex consists of two stocks of biotite granite emplaced in Ketilidian basement gneisses (Wegmann, 1938, and Bethelsen, 1961, for chronological terminology). The granites are cut by thick dikes of olivine dolerite and other rock types, by sills of carbonate mica peridotite, and are faulted (Fig. 2). In the chronology of the Ivigtut area the Tigssaluk Complex is pre-Gardar and belongs to the group of granite intrusions of post-Ketilidian age which have been collectively termed Sanerutian (Fig. 1; Berthelsen, 1961).

The stock forming the conspicuous mountain group of Pyramidefjeld about 5 km north of Tigssaluk Fjord (Fig. 1) was discovered in 1955 by J. Bondam, of the Geological Survey of Greenland,[2] during a reconnaissance survey of the country north of Ivigtut. In 1957 and 1958 the writer completed the survey of this intrusion and the smaller granite southeast of Pyramidefjeld.

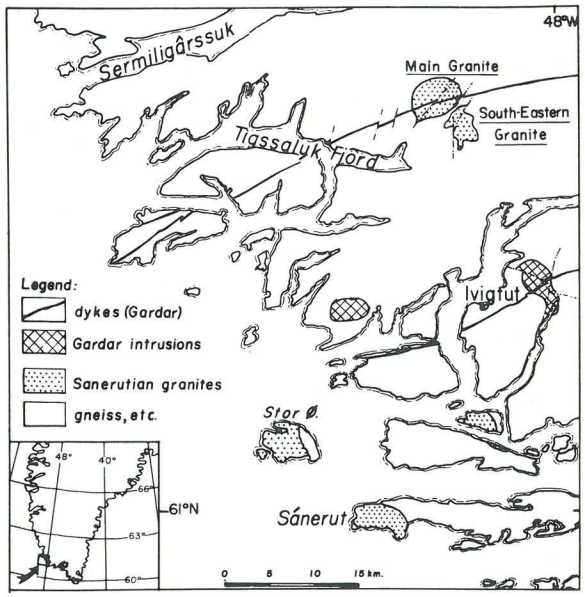


FIG. 1. Sketch map showing the positions of the principal Sanerutian and Gardar intrusions near Ivigtut. Inset map gives the location of the area in Southern Greenland.

## GENERAL DESCRIPTION OF THE GRANITES

*The Main Granite of Pyramidefjeld.* The granite is exposed through a vertical distance of over 1000 meters. Above about 300 meters elevation the proportion of exposed rock is high (Bondam, 1956, Fig. 6), there is little vegetation and only scattered glaciers, moraines and lakes obscure the rocks (Fig. 2). Contacts with the country rocks are steep, sharply defined and cut across structures in the gneisses, and an early generation of basic dikes.

The intrusion consists of medium-grained granite with abundant microcline perthite phenocrysts, to 3 cm in length, in a medium-grained groundmass (5 mm +) of microcline perthite, plagioclase, quartz and biotite, with accessory amounts of sphene,

[1] Publication with permission of the Director, Geological Survey of Greenland.

[2] Grønlands Geologiske Undersøgelse; subsequently referred to as G.G.U.

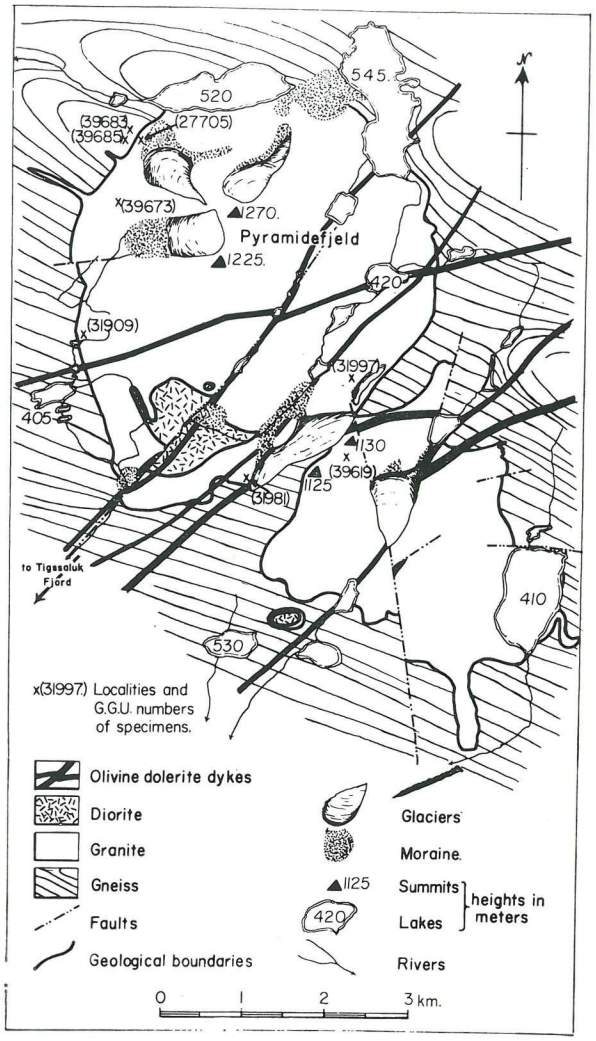


FIG. 2. Geological sketch map of the Tigssaluk Complex.

allanite, opaque minerals (magnetite and pyrite), apatite and zircon. Minor amounts of colorless to deep purple fluorite are usually present, where colored the mineral is conspicuous in hand specimens. Preferred orientation of feldspar phenocrysts or other minerals is uncommon. An average mode for the granite has been calculated (Table I, A).

Lobate, rounded basic inclusions are present throughout all but the layered parts of the intrusion. Those sampled by the writer consist of biotite, sphene, opaque minerals, intermediate plagioclase, apatite and chlorite, with rare allanite and irregular patches of microcline. Amphibole has been recorded (Bondam, 1956, pp. 13, 15). Mineralogically the inclusions resemble the rock of a small intrusion of biotite-diorite cutting the southern extremity of the granite (Fig. 2).

*The Southeastern Granite.* Irregular contacts dipping outwards at low to moderate angles, and numerous gneiss xenoliths in granite near the highest summits (1130, 1125, Fig. 2) indicate that the Southeastern Granite has only been slightly unroofed by erosion.

The intrusion comprises a single mass of medium-

TABLE I. MODAL ANALYSES OF MAFIC LAYERED GRANITES

| | A. | 27705 | 31909 | 31981 | 31997 | 39673 | 39683 | 39685 | 39619 |
|---|---|---|---|---|---|---|---|---|---|
| Alkali Feldspar | 34.3 | 17.6 | x | 9.7 | 4.5 | 14.3 | 4.0 | 1.4 | 23.4 |
| Plagioclase | 30.7 | 32.3 | 23.9 | 22.6 | 7.5 | 25.0 | 37.7 | 6.4 | 24.3 |
| Quartz | 28.4 | 29.5 | 25.2 | 28.9 | 13.0 | 26.3 | 34.4 | 12.9 | 26.6 |
| Biotite | 4.9 | 15.4 | 34.8 | 28.6 | 36.3 | 22.7 | 10.3 | 46.0 | 16.3 |
| Sphene | 0.6 | 1.5 | 6.4 | 4.8 | 12.2 | 5.1 | 2.0 | 2.7 | 4.2 |
| Opaques | 0.5 | 2.0 | 5.2 | 3.7 | 13.4 | 4.0 | 5.6 | 21.1 | 2.1 |
| Allanite | x | 0.4 | 4.1 | 1.1 | 12.2 | 1.2 | 0.1 | 4.4 | 1.3 |
| Apatite | x | 0.2 | 0.1 | 0.4 | 0.5 | 0.5 | 0.1 | 0.8 | 0.3 |
| Zircon | x | 0.3 | 0.2 | 0.2 | 0.3 | 0.4 | 0.4 | 0.9 | x |
| Muscovite | 0.5 | 0.8 | 0.1 | x | 0.1 | 0.5 | 5.4 | 3.0 | 1.5 |
| Fluorite | 0.1 | x | x | x | x | x | x | 0.4 | x |

(Vol. %. All analyses mean of two or more determinations.)
x=present but <0.1%.
A=mean of 10 specimens of normal Main Granite.
27705–39685 all from the Main Granite.
39619 from the Southeastern Granite.
See Fig. 2 for localities.

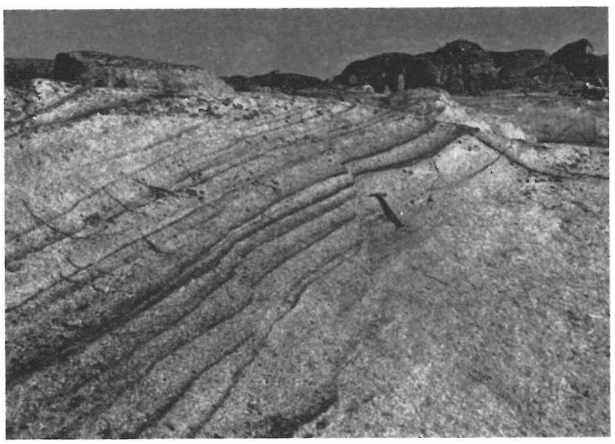

FIG. 3. Mineral layering in the north-west of the Main Granite (locality of 39673). Scale: hammer shaft about 0.5 m long.

grained rock resembling the Main Granite except that there are relatively few alkali feldspar phenocrysts. Basic inclusions similar to those found in the Main Granite occur through much of the granite and are mineralogically comparable to the central member of the small composite plug of granite and biotite-diorite close to the southwestern margin of the intrusion (Fig. 2).

## THE LAYERED STRUCTURES

*Field relations.* The field appearance of the layering will be described briefly as details have been published elsewhere (Harry and Emeleus, 1960). In both intrusions the layering results from high concentrations of biotite and the normal accessory minerals of the granites. It includes rhythmically-repeated bands of mafic rock a few centimeters thick separated by normal granite (Fig. 3); impersistent cross-cutting structures resembling current bedding in sediments; mafic layers contorted and brecciated in a manner suggesting slumping in a mass of poorly consolidated crystals (Harry and Emeleus, 1960, Fig. 4), and local structures resembling trough-banding (Harry and Emeleus, 1960, Fig. 6). The mafic layers are frequently gravity stratified (Fig. 4; Harry and Emeleus, 1960, Figs. 2, 6) and consistently "young" upwards. In a number of examples of banding involving extreme concentrations of biotite and accessories, large crystals of alkali feldspar within the mafic layers lie parallel to the plane of the layering (Harry and Emeleus, 1960, Fig. 6). These feldspars, which are presumably of early crystallization, are microcline perthites similar to the phenocrysts of the normal granites.

In both intrusions the principal areas of layering are found at high levels (Fig. 2); in the Southeastern Granite layering appears to be confined to the ground immediately south of the 1130 meter summit. In both, the structures dip at low angles (under 30°) although it should be borne in mind that the recorded dips may not be original since there appears to have been contemporaneous disturbance of some of the layered rocks and, furthermore, the granites may have been tilted after consolidation. In the Main Granite localized areas of intense mafic layering a few meters in extent occur in granite sheets and apophyses cutting gneisses on the northwestern edge of the intrusion (39683, 39685,[1] see Fig. 2) and in a number of localities at or close to the margins (Harry and Emeleus, 1960, Fig. 7).

*Mineralogy.* With the possible exception of ilmenite among the opaque minerals no new mineral phase occurs in the layering which is not found in the normal granites. The grain size of the layered rocks is generally less than in the normal granites.

The light minerals include alkali feldspar, quartz and plagioclase. The alkali feldspar is a perthitic microcline whether as phenocrysts or in the groundmass, although the groundmass material is noticeably less perthitic than the phenocrysts. Quartz is usually anhedral and crowded with minute inclusions which in some cases are rutile. The plagioclase has three contrasted modes of occurrence: as well formed crystals (An15–25) to 3 mm or more in length; as relatively albitic overgrowths on these euhedral crystals extending into the spaces between biotite and the accessory minerals; and as inter-

[1] 39685, etc., refer to G.G.U. specimen numbers.

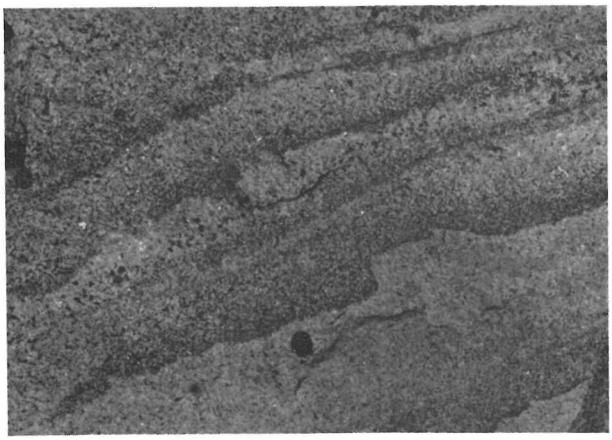

FIG. 4. Gravity-stratified layering in the South-eastern Granite (locality of 39619). Scale: coin about 3 cm in diameter.

stitial and poikilitic crystals (An 5–10) enclosing biotite, sphene and other accessories.

Biotite is in approximately equidimensional crystals 1–2 mm across, rather more elongate in the *c* direction than usual. The mineral appears to be only moderately iron-rich with $\beta$ from 1.615–1.625, $2V_x = 10°$ and less, and pleochroic with X = pale yellow-green and Y = Z = olive-green. Brown or red-brown sphene is usually in characteristic lozenge-shaped crystals although locally almost skeletal, allanite too is almost invariably euhedral except in a few instances where crystals were found with embayed outlines reminiscent of the quartz phenocrysts from some acid rocks. Allanites may be as much as 3 mm across, the crystals commonly show simple twinning and are strongly colored, pleochroic from greenish brown to olive green. $2V_x$ is high (near 90°). In some specimens (*e.g.* 31909) the central parts of the allanites are completely isotropic, in others examples were found where partial change to the metamict state gave crystals with uneven, patchy extinction.

The opaque minerals have a distinctive porous structure due to the inclusion of small prisms of apatite (Fig. 11). Magnetite is the principle constituent, with minor amounts of ilmenite, hematite and pyrite. In some examples they are rimmed by granular sphene (31997).

Other components include short prismatic crystals of apatite, generally larger than those included in the opaques, and zircon with prominent concentric growth zones. Fluorite is almost always present although not in especially high proportions (Table I); it may be colorless or pale purple and shows a marked deepening in color where against allanite. Colorless mica occurs along with epidote as an alteration product of the more calcic plagioclase; muscovite of apparently primary origin was noted in several sections (*e.g.* 39683, 39685).

*Modal analyses.* Modal analyses of sections cut from the mafic specimens and from normal granites are summarized in Table I. A limited number of specimens was available, consequently any conclusions based on the modal data can only be regarded as tentative. Despite this, several interesting features have emerged, the must striking being the high concentrations of biotite and accessory minerals attained, exceeding 70% and even 85% in a few specimens. Secondly the proportions of quartz and total feldspar remain fairly constant when the concentration of biotite, etc., exceeds about 40% (Fig. 5), and if the modes are recalculated on an alkali-feldspar—free basis, quartz and plagioclase are found to be present in almost equal proportions regardless of the concentration of biotite, etc. (Fig. 6). Finally, the proportion of alkali-feldspar to plagioclase and quartz appears to be less in the mafic rocks than in the normal granite (Table I) and to decrease in amount with increase in the proportions of biotite and accessories (Figs. 5, 6: compare values plotted below 40% biotite, etc.).

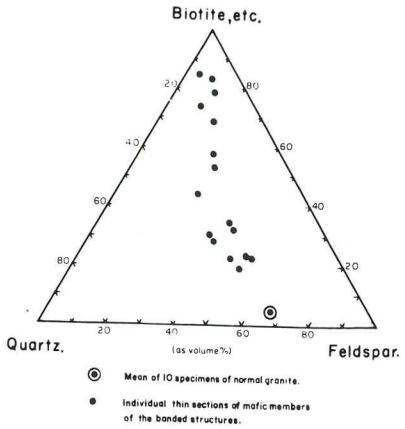


FIG. 5. Modal analyses of mafic specimens from the layered structures.

The two diagrams (Figs. 5, 6) were compiled from all the available analyses regardless of the localities of the specimens. From these, and Table I, it is seen that the most intense concentrations of biotite and accessories are associated with the Main Granite, in the sheets just outside the intrusion, and in the areas of restricted layering near and at the margins. Comparing analyses of specimens taken from different parts of the same layered units, it seems that the trend brought out in Figs. 5 and 6 is paralleled within individual units of layering (Table II).

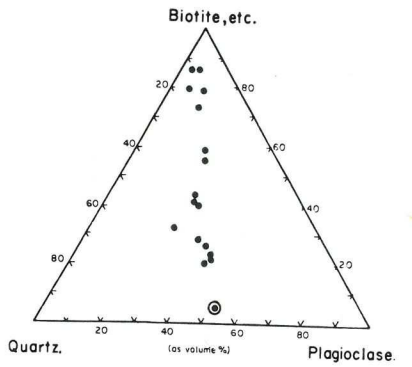


FIG. 6. Modal data used in Fig. 5 recalculated on an alkali feldspar-free basis. Symbols as in Fig. 5.

TABLE II. MODAL ANALYSES OF SPECIMENS FROM DIFFERENT LEVELS IN THE SAME UNIT OF LAYERING

| | 31981A | 31981B | 39683A | 39683B |
|---|---|---|---|---|
| Alkali feldspar | 1.8 | 17.6 | 0.7 | 7.4 |
| Plagioclase | 23.2 | 21.9 | 37.1 | 38.1 |
| Quartz | 22.5 | 35.4 | 35.2 | 33.4 |
| Biotite | 40.5 | 16.7 | 11.4 | 9.3 |
| Sphene | 5.4 | 4.2 | 3.0 | 1.0 |
| Opaques | 4.4 | 3.1 | 6.3 | 4.8 |
| Apatite | 0.5 | 0.3 | 0.1 | 0.2 |
| Zircon | 0.1 | 0.3 | 0.7 | 0.1 |
| Muscovite | x | x | 5.4 | 5.5 |
| Fluorite | x | x | x | x |
| Allanite | 1.6 | 0.5 | 0.1 | 0.2 |

All as volume %.
x = present but >0.1%.
See Fig. 2 for localities.
31981. Specimen B taken about 10 cm. above A.
39683. Specimen B taken about 4 cm. above A.

*Textural relationships.* The minerals in the mafic parts of the layered structures are grouped in three categories on the basis of shapes and textural relationships. One group comprises the euhedral crystals, in a second are euhedral crystals with outlines modified by overgrowths, and in a third are placed those minerals of interstitial and poikilitic habit.

Biotite is the most conspicuous member of the first. The crystals are generally well-formed and lack evidence of overgrowths. Sphene may show slight signs of zoning with a lessening of color towards the edges, although this is not common. Allanite is included in the first group, although there are some indications of compositional zoning and overgrowths of euhedral rims on euhedral cores of slightly different optic orientation (39685). Both apatite and zircon are considered as members of this group; although characteristically zoned, the euhedral outline of zircon persists through the different layers.

Plagioclase is the most important member of the second group. Original cores of calcic oligoclase with well-developed crystal outline are surrounded by rims of more albitic composition (Fig. 7), which may show oscillatory zoning. In most instances the cores are 2–3 mm in length, the effects of the overgrowths being to increase the length to as much as 6 mm. The large crystals of alkali feldspar locally present in the mafic rocks (31997, 27705) have microcline mantles that are normally less perthitic than the central parts of the crystals. With both feldspars the textural effect of the overgrowth has been to convert originally euhedral crystals into forms which are anhedral and in extreme instances poikilitic towards their surroundings.

The third group includes examples of all the leucocratic minerals. Quartz is typically interstitial or poikilitic (Fig. 8), areas as much as 1 cm across enclosing numerous well-formed crystals of biotite, allanite, opaques, etc. With the exception of the uncommon phenocrysts, the microcline perthite in the mafic layered rocks is poikilitic in habit (Fig. 9). Poikilitic or interstitial plagioclase (Fig. 10) is particularly conspicuous as twinned crystals to 5 mm across. Fluorite is always interstitial in habit, and

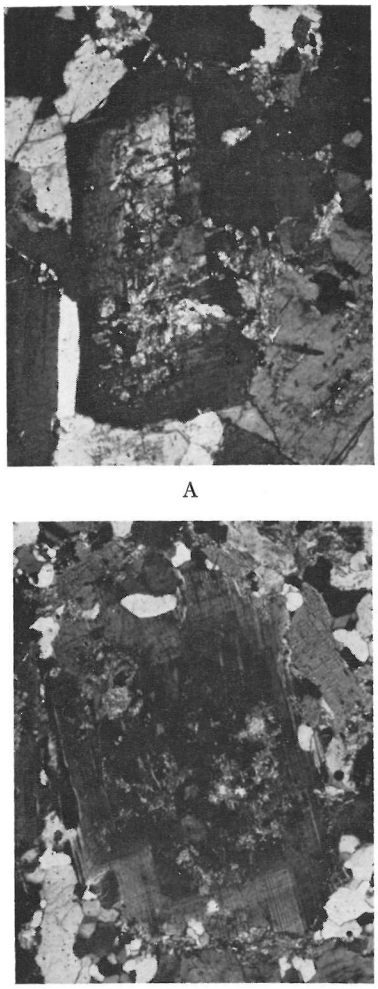

A

B

FIG. 7. Plagioclase crystals with albitic overgrowths.

A. Original rounded crystal extended by albitic overgrowth. The albitic rim is anhedral towards biotite and opaques (upper right), euhedral towards quartz (upper left and left side of plagioclase) and does not develop where two plagioclase crystals come into contact (lower right). (39685), 22×, crossed polars.

B. Rimmed crystal with faint oscillatory zoning (upper and lower edges). (39619), 16×, crossed polars.

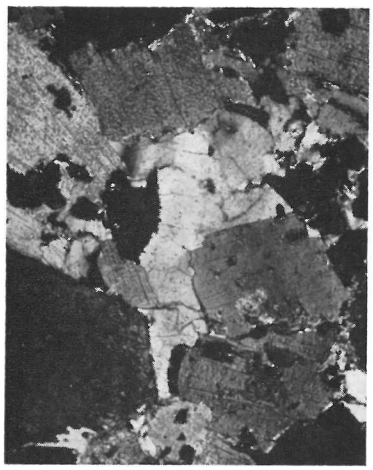

FIG. 8. Interstitial quartz (center) molded on biotite and on allanite (lower left). (39685), 18×, crossed polars.

usually is present in amounts that are too small to develop poikilitic crystals, although these were observed in a few places (Fig. 11).

The opaque minerals and quartz present difficulties in classification. The opaque minerals are poikilitic in that they contain apatite, yet they commonly are well-formed and in some instances their crystallization appears to have preceded that of biotite, sphene, or allanite. On balance they are thought to have crystallized early; quite apart from textural considerations an early crystallization would follow from their concentration in the mafic bands (Table I). There is also some textural evidence which suggests that quartz may have originally been present as discrete crystals since biotite,

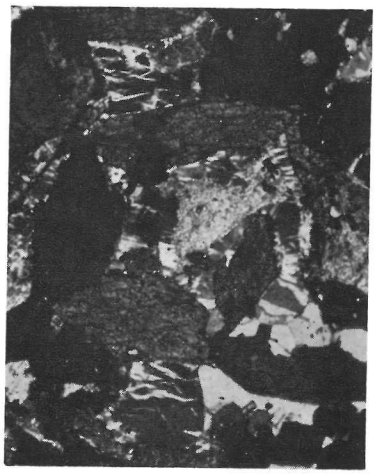

FIG. 9. Poikilitic perthitic alkali feldspar enclosing sphene, opaques and biotite. Also molded on the edge of allanite (upper left). (31997), 22×, crossed polars.

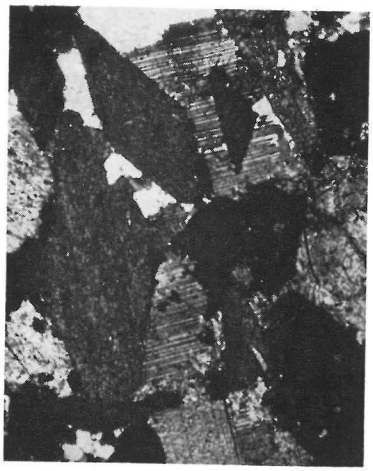

A

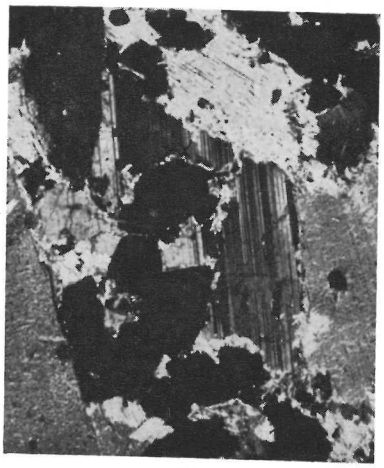

B

FIG. 10. Poikilitic plagioclase crystals.

A. Twinned plagioclase enclosing sphene and opaques. (31997), 35×, crossed polars.

B. Plagioclase enclosing opaques and molded on sphene and biotite. (39685), 25×, crossed polars.

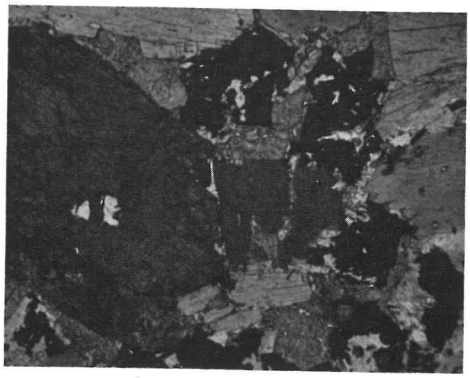

FIG. 11. Biotite, sieve-textured opaques and a large crystal of allanite (left) with interstitial areas of fluorite (high-relief mineral on the upper edge of allanite, between opaques in the upper right part of the illustration, and near the lower right-hand corner). (39685), 20×, plane polarized light.

allanite and sphene are here and there molded on, or enclose, rounded or subhedral quartz crystals. Consequently it is probably not correct to assign all the quartz to the third group.

From the textures of the layered rocks it appears that all minerals, with the exception of fluorite, were available from an early stage of crystallization, as would be expected in a melt of essentially granitic composition. The crystallization of zircon and apatite, and opaques, biotite, sphene and allanite was completed fairly rapidly; crystallization of the feldspars extended over a longer period, whereas most of the quartz and the fluorite completed crystallization relatively late in the sequence.

The textures described and illustrated are, for the most part, taken from specimens having the higher concentrations of biotite and accessories. With increased amounts of quartz and feldspars the poikilitic habit of the light minerals is less pronounced, the textures as a whole becoming those of a normal granite, although through all stages the characteristic rimmed and zoned plagioclases may be recognized, and the mafic minerals tend to remain euhedral.

## Discussion

Close similarities exist between the layered structure in the granites and those present in basic, ultrabasic and other intrusions. Particularly noticeable is the repeated, rhythmic banding, the gravity stratification, the contorted structures attributed to slumping and the trough banding (*cf.* Wager and Deer, 1939; Brown, 1956; Upton, 1960). Compared with basic and ultrabasic intrusions the amount of layering in the granites is very restricted, suggesting that it may owe its origins to the existence of special conditions over a limited part of the history of cooling and consolidation of the magmas. The concentration of volatiles, principally water and fluorine, in the upper parts of the stocks is suggested as an important factor in promoting layering; their effects would be to lower the crystallization temperature, increase the time available for crystallization and lower the viscosity of the magmas. Although the mineralogy does indicate the former activity of fluorine and water, the modal amount of fluorite is small (Table I), considerably less than in other granites where layering does not appear to develop (Exley, 1959). This suggests that additional factors may have been in operation at Tigssaluk; for example, slow cooling of the magma may have been aided by elevated temperatures in the country rocks. In support of pre-heating it should be mentioned that the Sanerutian granites appear to be high-level representatives of a phase involving extensive metamorphism, granitization and emplacement of granite to the south of Ivigtut (Berthelsen, 1961), so it is likely that the Tigssaluk granites intruded country rocks already raised to moderate temperatures.

The development of gravity-stratified bands in the layered structures, rhythmic repetition of the layering, local trough banding, and igneous lamination involving the large tabular crystals of alkali feldspar enclosed in the more extreme mafic bands are considered to require the operation of magmatic currents during the accumulation of the layered rocks.

Interpreting the layered rocks as crystal accumulates, concentration of the different phases seems to have been governed largely by density contrast. Opaques, biotite and accessories settled first together with some plagioclase, a minor amount of alkali feldspar, and possibly quartz. Aggregation of biotite, accessories and opaques is suggested by the occurrence of mutually interfering boundaries, and may have assisted in their early accumulation by providing larger settling units. The interstitial and poikilitic minerals of the second and third groups represent the crystallization products of the trapped intercumulus liquid (Wager *et al.* 1960). The compositional contrast between the cumulus and intercumulus plagioclase (pp. 24–25) suggests that crystallization of the trapped liquid proceeded without completely free connection with the overlying magma, as in orthocumulates (Wager *et al.* 1960, p. 74). However, the layered rocks are clearly not simple orthocumulates; if this were so, the proportions of poikilitic and interstitial quartz, alkali feldspar and plagioclase would be expected to approximate to those in normal granite. The modal analyses demonstrate that this is not the case, the proportion of quartz in particular being high (Table I; Fig. 6), although until a means is found of distinguishing between cumulus and intercumulus quartz, the significance of the high proportion cannot be fully assessed. From the almost complete absence of alkali feldspar in some of the mafic rocks it is suggested that this component may have been able to diffuse from the trapped liquid into the overlying magma.

## References


BERTHELSEN, A. (1961) On the chronology of the Precambrian of western Greenland. In *Geology of the Arctic*, University of Toronto Press.

BONDAM, J. (1956) A new occurrence of a calco-alkaline granite intrusion from the Frederikshaab District, South Greenland. *Medd. Grønland*, **137,** 1–21.

BROWN, G. M. (1956) The layered ultrabasic rocks of Rhum, Inner Hebrides. *Phil. Trans. Royal Soc. London*, **240**, 1–53.

EXLEY, C. S. (1959) Magmatic differentiation and alteration in the St. Austell Granite. *Quart. Jour. Geol. Soc. London*, **114,** 197–230.

HARRY, W. T. AND C. H. EMELEUS (1960) Mineral layering in some granite intrusions of S.W. Greenland. *Int. Geol. Cong., XXI Sess.*, Pt. **XIV,** 172–181.

UPTON, B. G. J. (1960) The alkaline complex of Kûngnât Fjeld, South Greenland. *Medd. Grønland*, **123.**

WAGER, L. R. AND W. A. DEER (1939) The petrology of the Skaergaard Intrusion, Kangerdlugssuaq, East Greenland. *Medd. Grønland*, **105,** 1–352.

——— G. M. BROWN AND W. J. WADSWORTH (1960) Types of igneous cumulates. *Jour. Petrol.* **1,** 73–85.

WEGMANN, C. E. (1938) Geological investigations in southern Greenland; Part I: on the structural divisions of southern Greenland. *Medd. Grønland*, **113,** 1–148.

MINERALOGICAL SOCIETY OF AMERICA, SPECIAL PAPER 1, 1963
INTERNATIONAL MINERALOGICAL ASSOCIATION, PAPERS, THIRD GENERAL MEETING

# THE MUSKOX INTRUSION, A RECENTLY DISCOVERED LAYERED INTRUSION IN THE COPPERMINE RIVER AREA, NORTHWEST TERRITORIES, CANADA[1]

CHARLES H. SMITH AND H. E. KAPP
*Geological Survey of Canada, Ottawa, Ontario, Canada*

ABSTRACT

The Muskox intrusion is a Precambrian layered basic pluton, 74 miles in length, which is dike-like in plan and funnel-shaped in cross-section. Its internal structure is divided into four principal units—a feeder, marginal zones, a central layered series and an upper border group. The feeder contains bronzite gabbro and picrite in zones parallel to the nearly vertical walls. The marginal zones parallel the walls of the intrusion which dip inward at angles of 23 to 57°, and grade inward from bronzite gabbro at the contact through picrite and feldspathic peridotite, to peridotite and, in places, dunite. The central layered series is 8500 feet thick and contains 38 main layers of dunite, peridotite, pyroxenites and gabbros which vary in thickness from 10 to 1800 feet. These layers are nearly flat-lying and discordant to the marginal zones. The upper border group is 200 feet thick and is characterized by an upward gradation from granophyre-bearing gabbro to granophyre. Preliminary calculations indicate that the Muskox intrusion has a higher olivine content than would normally be expected from a magma chemically similar to its chill facies and it is concluded that the chill phase only represents the fluid portion of the solid (olivine)-fluid magma.

## INTRODUCTION

The Muskox Intrusion is a new addition to the growing family of layered intrusions. It has certain unique features which distinguish it from other layered intrusions such as the presence of a feeder, and the fact that its base, walls and roof are all exposed. This paper will deal with only one aspect of the intrusion—the apparent difference between the bulk composition of the intrusion and its chill phase. The intrusion is under study as part of the Canadian program for the International Upper Mantle Project and aeromagnetic, gravity and drilling programs are planned in addition to the detailed petrologic, mineralogical and chemical studies.

## LOCATION AND PREVIOUS WORK

The Muskox Intrusion outcrops in the northwestern corner of the Canadian Shield (Fig. 1). It crosses the Arctic Circle at a point about 90 miles east of Port Radium on Great Bear Lake.

The intrusion was discovered by H. Vuori of the Canadian Nickel Company in 1956, and was mapped by Smith in 1959, assisted by Kapp in 1960, on a scale of 1 inch to 1000 feet. The mapping data is summarized on five sheets published at a scale of 1 inch to $\frac{1}{2}$ mile (Smith, 1962). The regional geology was mapped by a helicopter-supported geological survey led by J. A. Fraser (1960) in 1959, and an aeromagnetic survey was completed by the Geological Survey in 1961.

[1] Canadian Contribution to the International Upper Mantle Project No. 5. Published by permission of the Director, Geological Survey of Canada.

## REGIONAL GEOLOGY

The Muskox Intrusion outcrops in a basement complex of steeply dipping gneiss and metasedimentary rocks having a dominant north-northwest structural grain. The basement is cut by granodiorite which has a K/Ar age on biotite of 1765 m.y.

The basement is overlain unconformably by a sequence of sandstone, dolomite and basaltic flows which dip gently to the north, where they form a cover over the older basement. All the rocks of the area are cut by north-northwest-trending diabase dikes.

The Muskox Intrusion follows the grain of the basement rocks, but at the unconformity it has spread out to develop its funnel-shaped cross-section. The roof has barely penetrated the sandstone member of the cover, fragments of which are included in the granophyre of the upper border group. The Muskox Intrusion is dated, from biotite in picrite of the marginal zone, at 1155 m.y.

## STRUCTURAL FORM

*External form.* The Muskox Intrusion is 74 miles long, is dike-like in plan and funnel-shaped in cross-section. Its structural form is analogous to that of a sailing ship with a deep keel, plunging at an angle of less than 5° toward the north. The southern half (Fig. 2), which outcrops for 37 miles, represents the deep keel or feeder extension, exposed at the surface. The northern half represents the hull, and the extreme north the deck or roof, plunging under the cover rocks.

The symmetry of the intrusion in plan is broken

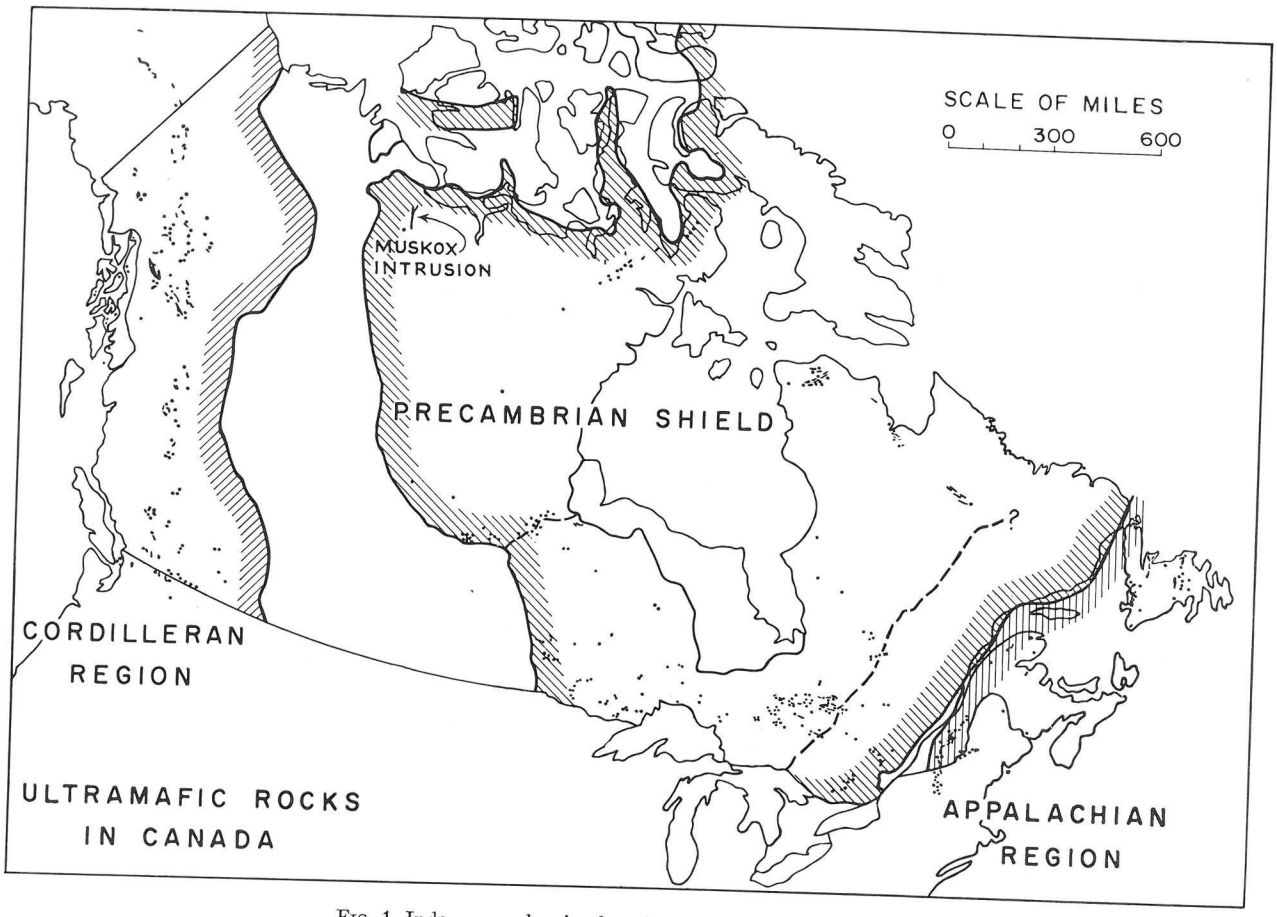


FIG. 1. Index map, showing location of the Muskox Intrusion.

by a northerly-trending fault which cuts the western side of the intrusion. The fault has a horizontal displacement of 5 miles. When the displacement along the fault is restored (in Fig. 2, A′ moves to A, and B′ moves to B) the intrusion is seen to be symmetrical in plan with two northward projecting limbs formed as its syncline-shaped roof plunges under the cover rocks.

The feeder of the intrusion is dike-like and vertically dipping, similar in attitude to the satellite diabase dikes. It is 500 to 1800 feet wide, somewhat wider than the diabase dikes which have an average width of about 100 feet. The northern half of the intrusion has inward-dipping sides, whose dips have been calculated from drill holes and are summarized in Fig. 2. They vary from 58° on the south to 22° at the extreme northeast end.

*Internal units.* The internal structure of the intrusion is divided into four principal units—the feeder, the marginal zones, the central layered series and the upper border group.

The *feeder* is distinctive in having units of bronzite gabbro and picrite parallel to the nearly vertical walls. The southern end of the feeder is filled with gabbro but, as it is traced northward, picrite occurs first as pods and then as a continuous band along the center. On approaching the Coppermine River, two bands of picrite are found, bounded on both sides by gabbro. The latter is chilled against the country rocks, but not against the picrite. The picrite does not appear to represent a separate intrusion, but a segregation in the center of the feeder.

The *marginal zones* parallel the inward dipping walls of the intrusion and are from 200 to 1200 feet thick. They grade inward from hypersthene gabbro at the contact through picrite and feldspathic peridotite, to peridotite and, in places, dunite. In other words, the marginal zones are gradational zones in which plagioclase decreases, and olivine increases, inward. Accompanying this change in mineral abundance is a change in mineral composition, with olivine becoming more magnesian, and plagioclase becoming more calcic, inward. Nickel-copper sulfides and

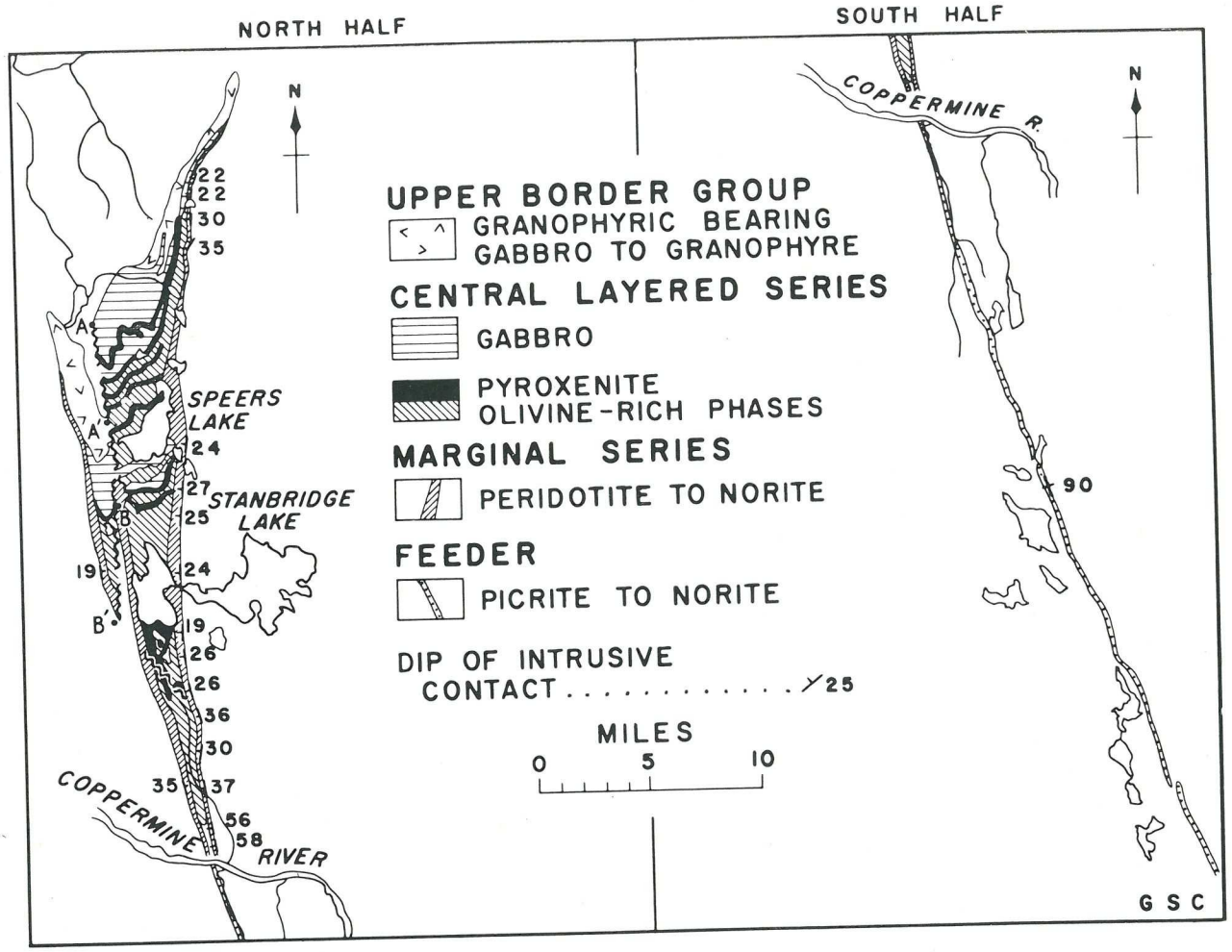


FIG. 2. Structural units of the Muskox Intrusion.

pyrrhotite occur sporadically along the wall of the intrusion.

The *central layered series* is approximately 8500 feet thick. It has 38 main layers, varying in thickness from 10–1850 feet. Small scale layering is present, but uncommon. The series contains alternating layers of dunite (serpentinized), peridotite, feldspathic peridotite, picrite, olivine clinopyroxenite, websterite, orthopyroxenite, troctolite, olivine gabbro, gabbro, norite and anorthositic gabbro. The layers have sharply defined contacts, in contrast to those of the marginal zones. They dip gently to the north at a similar angle to the overlying cover rocks and are thus discordant to the marginal zones. Chromite occurs in one pyroxenite horizon and contains disseminated copper-nickel sulfides and platinum group metals.

The *upper border group* is arbitrarily defined by the appearance of granophyric intergrowths and quartz in the upper gabbro units. The rock units are not sharply defined but grade upward, within a thickness of 200 feet, from granophyre-bearing gabbro to mafic granophyre, granophyre and intrusive breccia. In a mineralogical sense, the upper border group is a zone in which granophyric intergrowths and quartz increase upward at the expense of mafic minerals.

## Some Quantitative Considerations of the Muskox Magma

It is possible to construct a fairly accurate composite cross-section of the Muskox Intrusion. The extension of the feeder is exposed, the inward dips of the walls are known, the roof is exposed, the thickness of many of the layered units can be measured directly in the field, and the plunge of the intrusion can be determined both by calculating the plunge of

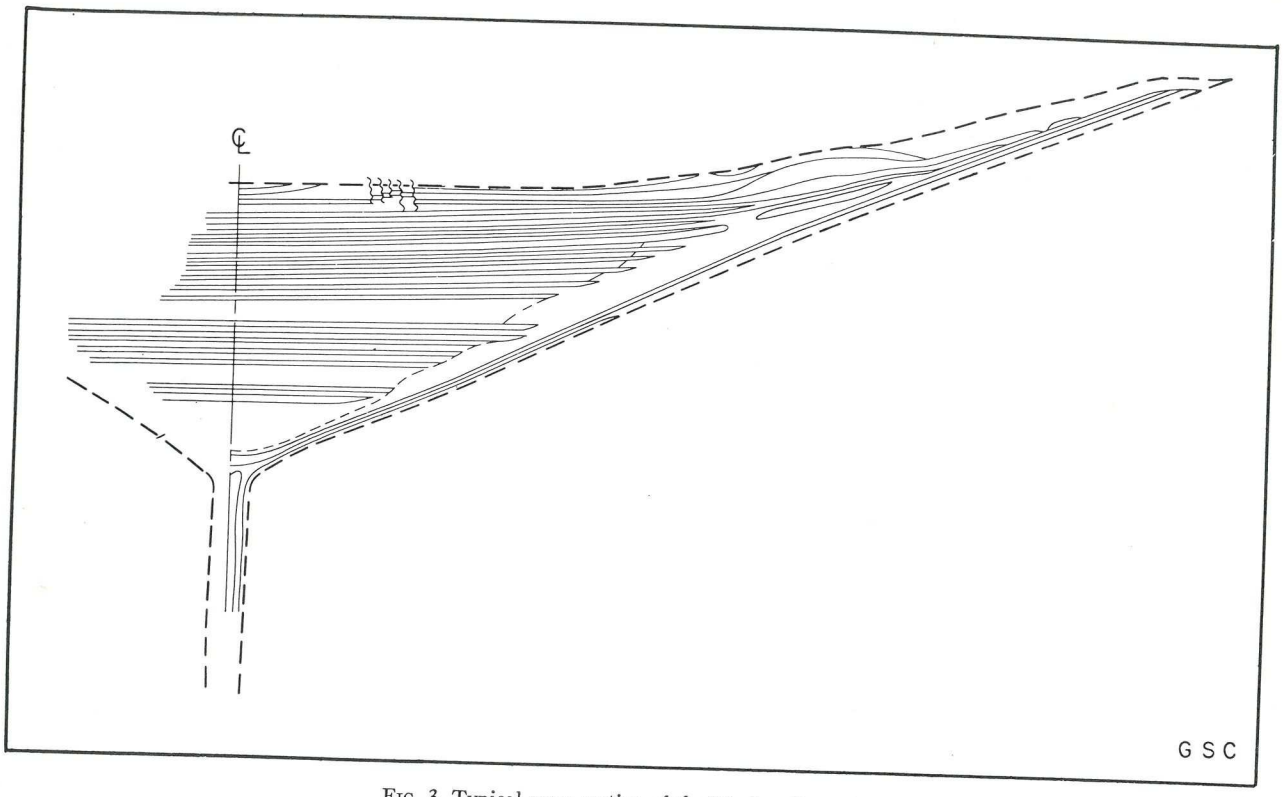


FIG. 3. Typical cross-section of the Muskox Intrusion.

the intersection of the walls and by measuring the dip of layers in the field.

Cross-sections of the form shown in Fig. 3 have been prepared on a scale of 1 inch to 1000 feet, and the relative cross-sectional area of each map-unit determined. Only the eastern half of the cross-section has been used in the volume calculations, since the western side is faulted. The symmetry of the intrusion in plan and the similar inward dip of the opposite margins indicate that this assumption is valid.

Figure 3 shows the disposition of the layered series in relation to the margins of the intrusion. Notice how the layers approach, but do not reach, the margins of the intrusion, and are discordant in attitude to the margins. From a cross-section of this type the composition of the Muskox magma was calculated, and the approximate proportion of rock types is:

| | |
|---|---|
| Ultramific rocks (including dunite, peridotite, pyroxenites and picrite) | approx. 75% |
| Gabbro | approx. 15% |
| Granophyre | approx. 8% |
| Rock fragments | approx. 2% |

This calculation, although approximate, indicates the extremely ultramafic composition of the Muskox magma.

TABLE I. CHEMICAL COMPOSITION OF MUSKOX CHILL PHASE COMPARED TO OTHER LAYERED INTRUSIONS

| | Bushveld[1] | Stillwater[2] | Skaergaard[3] | Muskox[4] |
|---|---|---|---|---|
| $SiO_2$ | 51.45 | 50.68 | 47.97 | 50.68 |
| $Al_2O_3$ | 18.67 | 17.64 | 18.32 | 13.55 |
| $Fe_2O_3$ | 0.28 | 0.26 | 1.23 | 1.17 |
| FeO | 9.04 | 9.88 | 8.58 | 9.08 |
| MgO | 6.84 | 7.67 | 8.09 | 9.70 |
| CaO | 10.95 | 10.47 | 10.77 | 11.22 |
| $Na_2O$ | 1.58 | 1.87 | 2.42 | 1.79 |
| $K_2O$ | 0.14 | 0.24 | 0.21 | 0.63 |
| $H_2O^+$ | 0.34 | 0.42 | 0.61 | 0.53 |
| $H_2O^-$ | 0.03 | 0.06 | 0.09 | 0.06 |
| $P_2O_5$ | 0.09 | 0.09 | 0.08 | 0.10 |
| $TiO_2$ | 0.34 | 0.45 | 1.32 | 1.06 |
| MnO | 0.47 | 0.15 | 0.12 | 0.18 |
| | 100.22 | 99.88 | 99.81 | 99.75 |
| MgO / FeO | 0.76 | 0.78 | 0.94 | 1.07 |

[1] Daly, 1928, quoted by Hess, 1960, p. 152.
[2] Hess, 1960, p. 152.
[3] Wager, 1960, p. 375.
[4] Average of 2 analyses by S. Courville, Geological Survey of Canada.

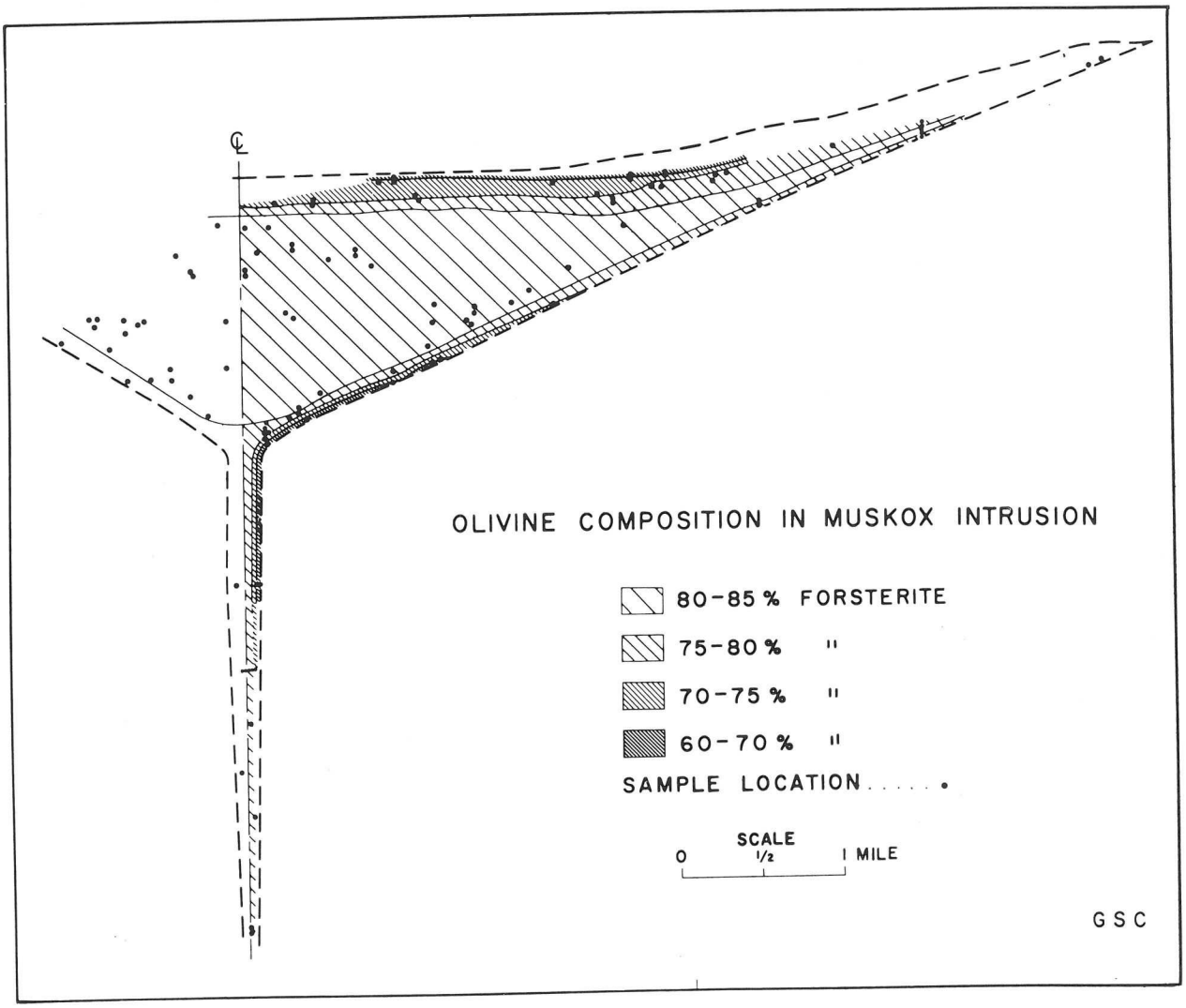


FIG. 4. Olivine variations in the Muskox Intrusion.

Similar calculations can be made of the mineral abundance in the intrusion based upon the cross-sectional areas of rock units and their modal analyses. These calculations indicate that the olivine content of the intrusion is of the order of 58%.

In order to learn whether the cryptic variations among mineral phases indicated significant discontinuities in the layered sequence that might be considered evidence for multiple intrusion, studies of olivine compositions are underway. The results to date indicate the simple overall pattern shown in Fig. 4. Olivine with a forsterite composition over 80% occurs in the core of the intrusion, throughout most of the layered series. Within individual layers in the layered series the variation in olivine composition is small, less than 2–3%. Olivines between 70–80% forsterite occur toward the top, sides, and into the feeder. Olivines with a composition of less than 70% forsterite are restricted to the roof and the margins of the intrusion. The symmetry of this pattern suggests that the greater abundance of ultramafic rocks in the intrusion is not related to successive injections of unrelated magmas but that they formed during a single cooling process.

Table I shows the composition of the Muskox chill phase compared with the chill phases of other layered intrusions. The Muskox chill is slightly more mafic than that of the other intrusions, but not sufficiently to account for the high olivine content calculated for the intrusion itself.

The conclusion to be drawn from the Muskox structural data is that the chill phase is not repre-

sentative of the bulk composition of the intrusion. Various explanations could be used to try to explain away the difference between the chill phase and bulk composition.

Hess (1960, p. 166) has commented on the absence of a thick zone of feldspathic rocks in the Great Dike to compensate for the thick ultramafic portion and assumes the feldspathic component had a wide lateral extent. This explanation cannot apply to the Muskox intrusion, for the lateral extent is limited by the exposed walls. One might assume the feldspathic phase changes in abundance along the long axis, either up-dip where it has been eroded away or down-dip where it can only be found by drilling. This explanation does not seem probable.

The interpretation that the chill phase represents the composition of an intrusion is a basic assumption in any quantitative study of layered intrusions. In most instances it is not possible to assume otherwise, since intrusions are generally not well exposed even in two dimensions. The Muskox Intrusion is completely exposed in two dimensions, that is its base, sides and top are exposed, and here the imbalance between intrusion composition and chill phase is seen. The explanation may depend on the properties of solid-liquid mixtures, during the intrusion of which the liquid portion lubricates the margins and forms the chill phase while the solids (olivine crystals) are relatively concentrated away from the walls and thus are not frozen into the chilled sample. Such segregation is known to take place during the transport of solid-fluid mixtures in pipe lines. At any rate it is apparent that the relation of chill phases to bulk magma composition requires critical review before being used as a basis for interpreting the geochemistry and cooling history of layered intrusions. This is a field of petrologic research which will have to be evaluated by laboratory studies on intrusion mechanics.

## References


Fraser, J. A. (1960) North-central District of MacKenzie, Northwest Territories. *Geol. Surv. Canada, Map* **18–1960.**

Hess, H. H. (1960) Stillwater igneous complex, Montana. *Geol. Soc. Am. Mem.* **80.**

Jambor, J. L. and Charles H. Smith (1963) Accurate determination of olivine composition using standard small diameter *x*-ray powder cameras. *Mineral. Mag.* (in press).

Smith, C. H. (1962) Notes on the Muskox Intrusion, Coppermine River area, District of MacKenzie. *Geol. Surv. Canada, Paper* **61–25.**

Wager, L. R. (1960) The major element variation of the Skaergaard Intrusion and a re-estimation of average composition of the hidden layered series and of the successive residual magmas. *Jour. Petrol.* **1,** 364–398.

MINERALOGICAL SOCIETY OF AMERICA, SPECIAL PAPER 1, 1963
INTERNATIONAL MINERALOGICAL ASSOCIATION, PAPERS, THIRD GENERAL MEETING

# ORIGIN OF THE ULTRAMAFIC COMPLEX AT DUKE ISLAND, SOUTHEASTERN ALASKA

T. N. IRVINE[1]
*McMaster University, Hamilton, Ontario*

ABSTRACT

The Duke Island ultramafic complex crops out in two areas that total 9 square miles. Rocks within the complex are comprised of olivine, clinopyroxene, hornblende and ferriferous oxides and are classified as dunite, peridotite, olivine pyroxenite and hornblende pyroxenite; all are devoid of plagioclase and orthopyroxene. A pegmatite of hornblende and anorthite is closely associated and probably comagmatic, but abundant gabbro surrounding the complex has been altered near its margin and is apparently older. Remarkable gravitational layering, showing grain-size grading, occurs intermittently in the olivine-bearing ultramafic rocks through a possible thickness of 2 miles. Although the Fe/Mg ratios of olivine and clinopyroxene increase slightly in the ultramafic units in the order listed above, cryptic layering is slight or absent. Counterparts in the layering of cross-bedding, slide conglomerates and slump structures suggest accumulation under the influence of magmatic currents, and a marked structural break, locally analogous to an angular unconformity with basal conglomerate, marks the contact of olivine pyroxenite and the dunite-peridotite zone and indicates at least two major intrusions of magma into the complex. A variety of structural, mineralogic and petrologic evidence suggests that the ultramafic rocks crystallized from a magma of ultrabasic composition. Hornblende pyroxenite generally forms a border zone around the olivine-bearing rocks, and together with the alteration aureole, seems to represent peripheral reactions that tended to produce a succession of zones in local equilibrium along thermal and chemical gradients between the ultrabasic magma and its country rock. The possible composition and temperature of the ultrabasic magma are discussed.

## INTRODUCTION AND ACKNOWLEDGMENTS

Duke Island is at the southern end of southeastern Alaska (55°55′N, 131°20′W) and has an area of 59 square miles. The ultramafic complex exposed on the island is a member of a belt of 35 or more ultramafic bodies that occur along the 350-mile length of the Alaskan panhandle. A brief description of the belt is available in Taylor and Noble (1960). The present paper is a summary of the petrology of the Duke Island complex; a more comprehensive report is in preparation.

The information presented here was largely collected while the author was attending the California Institute of Technology, and the contributions of many people there by way of discussion, assistance, and criticism are gratefully acknowledged. Particular thanks go to Dr. James A. Noble for sponsoring the field work and supervising the study. During the academic year 1958–1959, support was provided by the Foster Hewitt Fellowship in Field Geology. Grants from the Geological Survey of Canada have covered reproduction of some of the diagrams. G. V. Middleton and D. M. Shaw have made several helpful suggestions with regard to exposition.

## GEOLOGICAL DESCRIPTION OF DUKE ISLAND

*Metamorphic rocks.* The geology of part of Duke Island is shown in Fig. 1. The oldest rocks are metamorphosed volcanic and clastic sedimentary formations. These generally fringe the igneous core of the island, which is comprised of gabbroic, ultramafic and granitic plutons that apparently were emplaced in that order. The metamorphic rocks are not in contact with the ultramafic complex, but where they are closer than $\frac{1}{4}$-mile to the main gabbro mass, they have mineral assemblages indicative of the hornblende hornfels facies and, locally, the pyroxene hornfels facies (Fyfe *et al.*, 1958). Elsewhere, they belong to the albite-epidote hornfels or green schist facies.

*Primary (pyroxene) gabbro.* The primary gabbro is comprised of 40–50 per cent plagioclase and 45–55 per cent pyroxene and hornblende combined. Olivine and biotite are present locally; ilmenomagnetite and apatite are common accessories. Plagioclase ranges from $An_{40}$ to $An_{95}$, $An_{50-75}$ predominating (Fig. 2). Orthopyroxene and clinopyroxene are generally both present, but rocks having only one or the other do exist. By optical properties (Figs. 3, 4), orthopyroxene ranges from $En_{47}$ to $En_{76}$, and clinopyroxene from about $Ca_{37}Mg_{53}Fe_{10}$ to $Ca_{38}Mg_{29}Fe_{33}$. As shown in Fig. 3, the Fe/Mg ratio of each pyroxene increases as plagioclase becomes more sodic. Olivine changes in the same way, its range of variation being $Fo_{27}$ to $Fo_{82}$.

The pyroxene gabbro underlies most of the eastern half of Duke Island and thus, is abundant. Unfortunately, little is known about its structure: the rock is largely massive; topographic relief is low;

[1] Present address: Geological Survey of Canada, Ottawa, Canada.

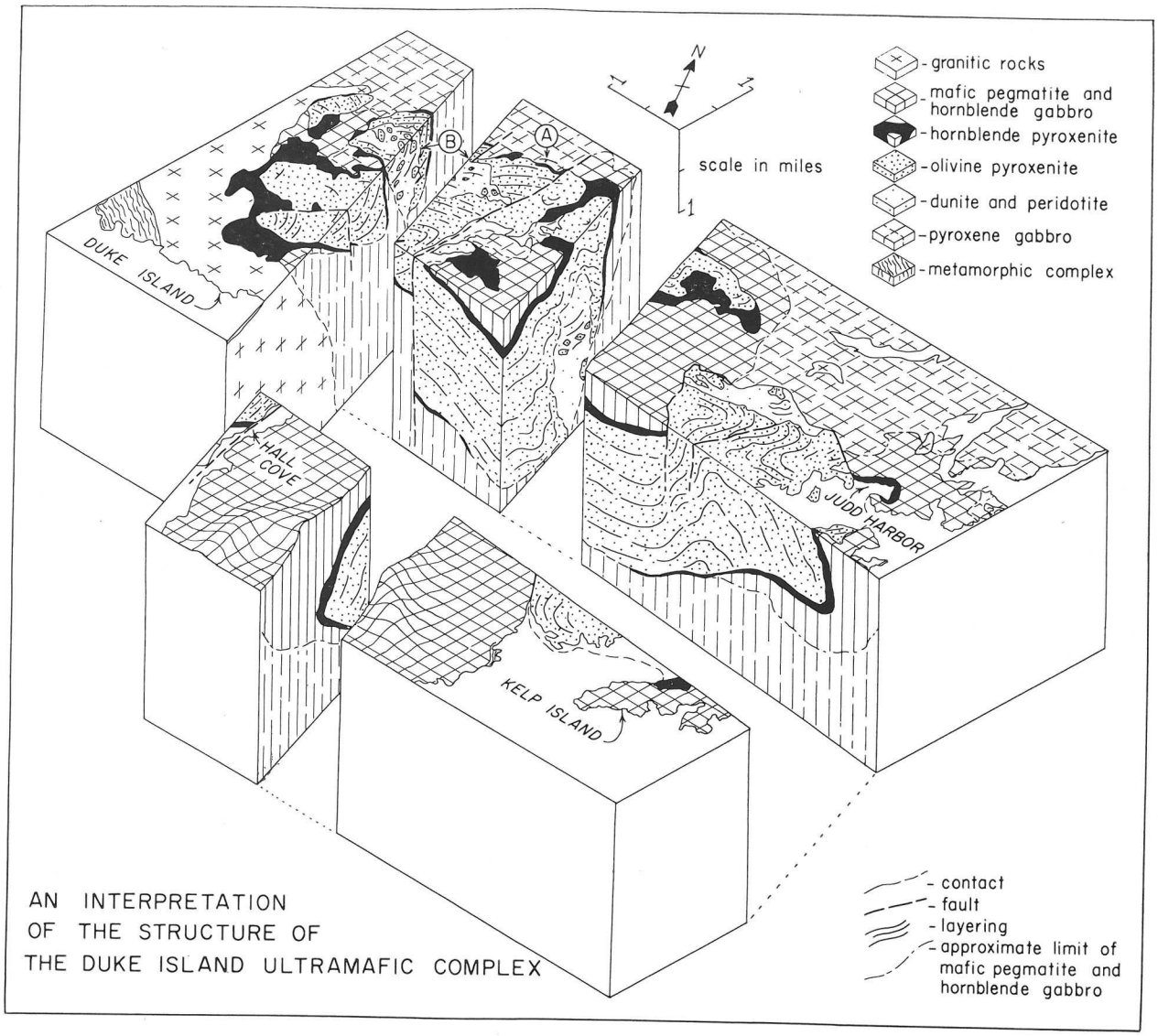


FIG. 1

contacts are poorly exposed; and the pattern of mineral variation is not obviously systematic. Rhythmic layering does, however, occur at two localities, and one, denoted "A" in Fig. 1, is notable. The layering there is continuous and regular for several tens of feet, and individual layers have thicknesses up to one foot. Each layer has its base clearly defined by a marked concentration of pyroxene: proceeding upward, the proportion of mafic minerals decreases in a sharp gradation, and the rock becomes normal or slightly feldspathic and shows marked igneous lamination. The layering is approximately parallel to the nearby contact of the gabbro against the ultramafic complex, and the direction of tops of layers, as indicated by grading, suggests that the gabbro underlies the ultramafic rocks. The same relation is indicated for this locality and others by the graded rhythmic layering that occurs in the ultramafic complex as described below.

*Description of the ultramafic complex*

(a) Petrography and mineralogy

Most of the ultramafic rocks crop out in two areas that total 9 square miles, but the areas are believed to be the exposure of one large body at depth (Fig. 1). This interpretation is based partly on an aeromagnetic map and partly on geological inference, some of which is mentioned below. If it is correct, then it is imprecise to refer to each exposure as a "body." The word "outcrop" is therefore used in its broader sense, and the exposures are called the Hall Cove and Judd Harbor ultramafic outcrops.

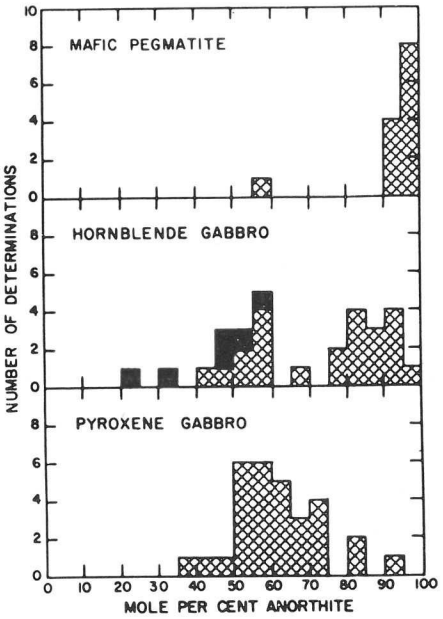


FIG. 2. Histograms of the composition of plagioclase in the different types of mafic rocks occurring at Duke Island, Alaska. In the hornblende gabbro histogram, the dark part represents plagioclase from hornblende gabbro near the granitic intrusions; the rest represents plagioclase in hornblende gabbro near the ultramafic rocks.

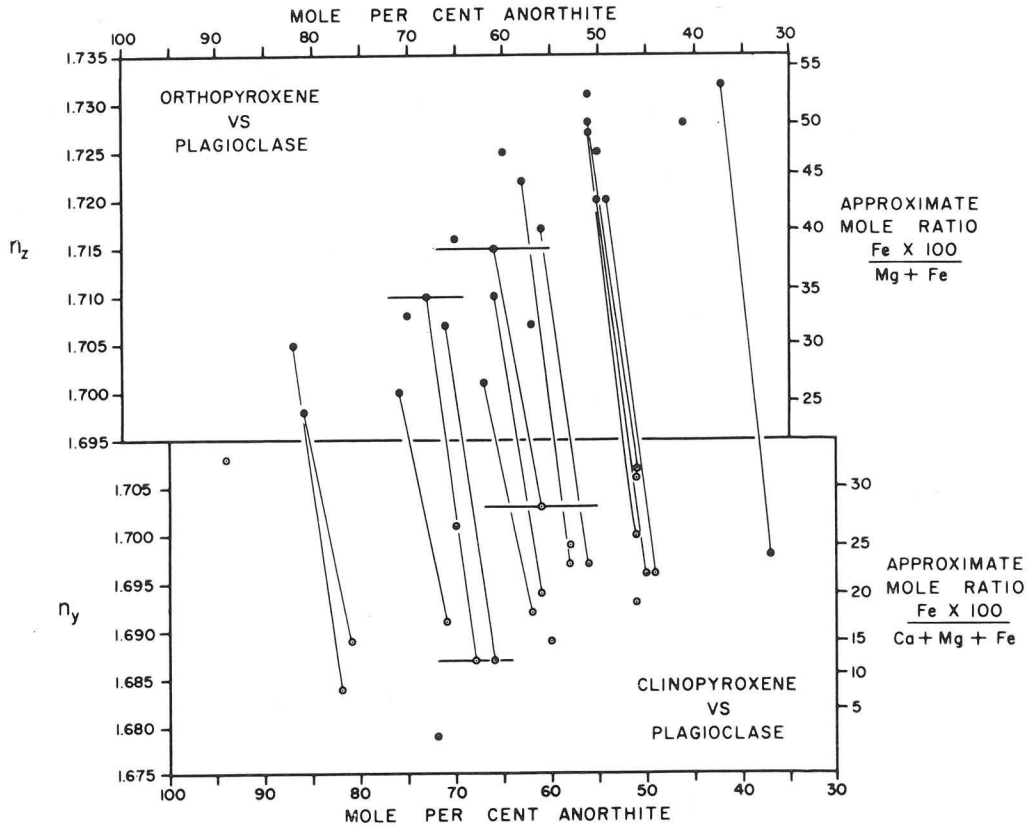


FIG. 3. Relation of the chemical variations in the pyroxenes and plagioclase of the primary gabbro at Duke Islands as determined by optical properties. The plots of coexisting pyroxenes are joined by "tie lines." In the clinopyroxene, the proportion of Ca is roughly constant near 40 per cent.

The ultramafic rocks are essentially comprised of three minerals: olivine; clinopyroxene (diopsidic augite); and hornblende. The results of modal analyses are given in Figs. 5A and B, and the rock classification scheme is apparent in Fig. 5A. The principal units are dunite, peridotite, olivine pyroxenite, and hornblende pyroxenite. Much of the hornblende pyroxenite contains 13–17 per cent magnetite, 2–3 per cent ilmenite, and minor hercynitic spinel. Chromite or chromiferous magnetite is a sparse accessory in dunite and peridotite. Olivine is generally partly altered to serpentine and secondary magnetite, but otherwise, the rocks are fresh. Orthopyroxene and plagioclase are notable by their absence.

Figure 5C shows the approximate areal abundances of the different rocks. The histograms were prepared by weighting each modal analysis by the map area the specimen is believed to represent. Although perhaps not statistically elegant, this procedure does give proper weighting to specimens that come from small occurrences of a particular rock type, and the result graphically portrays distribution features that are very obvious in the field. Olivine pyroxenite containing 15–30 per cent olivine (plus serpentine alteration) is an extremely abundant rock type and has a histogram mode distinct from that of olivine-free hornblende pyroxenite. Peridotite is rare by comparison, but a slight mode is present for dunitic rocks in the Judd Harbor outcrop. Several of the other ultramafic bodies in southeastern Alaska have comparable distributions in that their principal modes correspond to dunite, olivine pyroxenite, and olivine-free pyroxenite.

The refractive indices of clinopyroxene and olivine increase slightly through the rock sequence from dunite to hornblende pyroxenite (Fig. 6). Higher index is due primarily to a larger Fe/Mg ratio, and the indicated compositional range for olivine is $Fo_{78}$ to $Fo_{85}$. Optics and chemical analyses show clinopyroxene to range from about $Ca_{45}Mg_{48}Fe_7$ to $Ca_{50}Mg_{38}Fe_{12}$ (Fig. 7). The larger 2V of clinopyroxene in the ultramafic rocks as compared to that in gabbro (Fig. 4) indicates a larger Ca/Mg+Fe ratio or, in other words, less Ca-poor pyroxene in solid solution. This suggests that Ca-poor pyroxene did not reach its saturation limit in the ultramafic rocks during their crystallization and, thus, is compatible with the absence of orthopyroxene.

(b) Layering

The outstanding feature of the Duke Island ultramafic complex is an abundance of stratification that has many of the features of the rhythmic layering in the Skaergaard, Stillwater, and other intrusions, but which is distinct in that it is graded by grain size rather than mineral density (Fig. 8). The distribution and attitude of the layering is shown in Fig. 1 by trend lines. It is almost exclusive to olivine-bearing rocks and involves only two primary-precipitate minerals, clinopyroxene and olivine. (Hornblende pyroxenite exposed on Kelp Island just south of Duke Island shows magnetite layers, a few of which are graded.) Most layers are 2–10 inches thick; the greatest thickness observed for a continuously graded layer is 25 feet; the common maximum thickness is 2–4 feet. Many layers can be traced laterally for 300 feet, and possibly, some extend 900 feet. Thicker layers are generally coarser, but in an average example, grain size is 4–10 mm at the base, decreasing to 0.2–2 mm at the top. The bottom of each graded layer is sharp; the top may be sharp but commonly is transitional into finely laminated rock. Both pyroxene and olivine show grain size sorting, and olivine tends to concentrate near the tops of layers because it is generally finer (the two minerals have about the same density.) Layers lacking distinct grading commonly alternate with graded ones, but direction of grading is rarely reversed and, thus, is a reliable indicator of tops where structures are complicated.

Figure 9 shows a variant of graded layer that is comparable to a conglomerate bed. It is comprised of fragments of olivine pyroxenite in a matrix of peridotite. This type of layer occurs only in the peridotite zone of the Hall Cove outcrop. Associ-

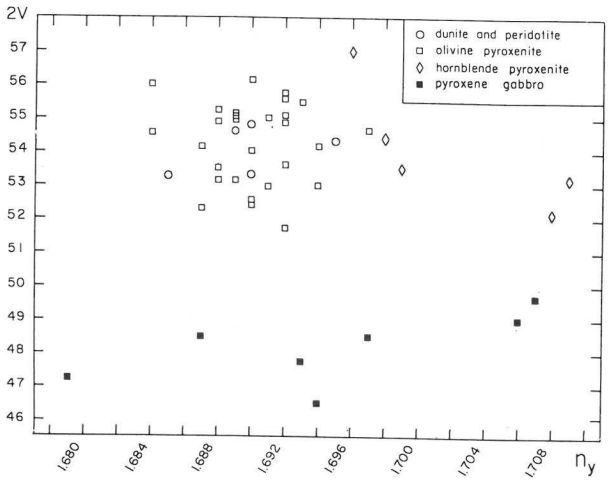


FIG. 4. Plot of 2V against $n_y$ for clinopyroxene from Duke Island rocks. This is roughly equivalent to a plot of Ca content against Fe/mg ratio.

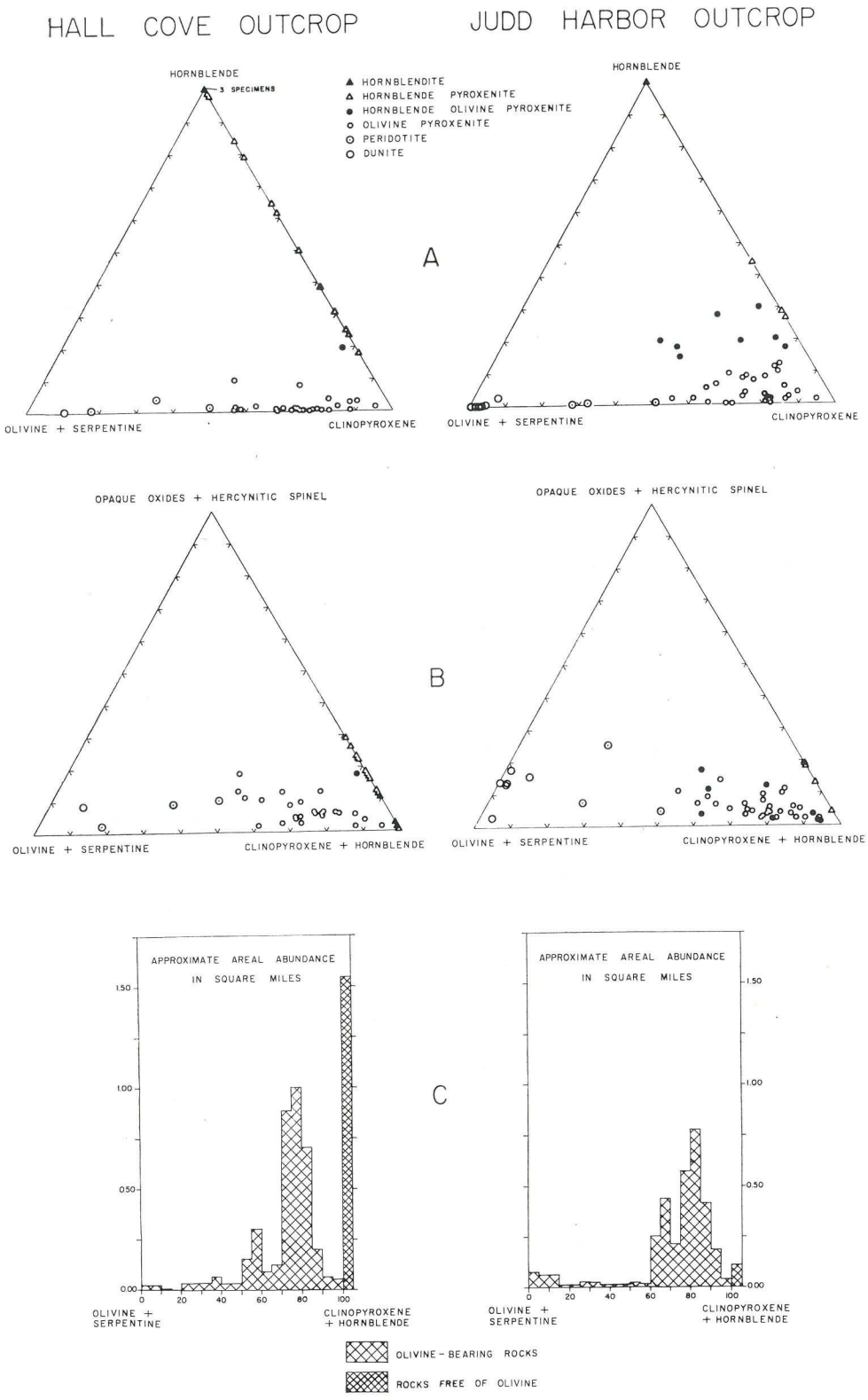


FIG. 5. Modal composition of the Duke Island ultramafic rocks in their two main areas of outcrop.

ated with it are other structures characteristic of clastic sediments, including slump structures and cross-layering. It seems clear that the graded layers have formed by gravity accumulation of crystals under the influence of currents. A mechanism of irregular magmatic convection comparable to those proposed by Wager and Deer (1939) and Hess (1960) is probable. However, at Duke Island, mechanical disruption in the magma chamber and slumping have apparently played an important role in generating and perpetuating currents.

Another type of layering occurring in olivine pyroxenite at Duke Island is marked by a poorly defined alternation of pyroxene and olivine and by thin, discontinuous bands of dunite. In appearance, it is not unlike the "inch-scale layering" of the Stillwater Complex (Hess, 1960, p. 133). The pyroxene crystals commonly show preferred orientation normal to the lamination, possibly because of growth in situ or recrystallization, or both. Most of the layering in the Judd Harbor olivine pyroxenite zone is this type.

Cryptic layering is weakly developed in the Hall Cove peridotite zone but has not been detected in the other parts of the complex by optical methods.

(c) Structure of the complex

The distribution of rock types in several of the ultramafic bodies in southeastern Alaska is roughly concentric and, in idealized development, features a dunite core surrounded by successive rings of peridotite, olivine pyroxenite, pyroxenite, and hornblendite (Taylor and Noble, 1960). The Union Bay complex has the most extensive sequence of zones, and the Blashke Islands complex, the most symmetric zoning. At Duke Island, the rock-type distribution in the Hall Cove ultramafic outcrop is vaguely concentric in approximately the above sequence but primarily because of a remarkably continuous border zone of hornblende pyroxenite. In the Judd Harbor outcrop, rock units are arranged side by side, although here too, the main bodies of hornblende pyroxenite are peripherally located.

In the Hall Cove outcrop, abundant evidence shows that at least two intrusions are involved in the formation of the olivine-bearing rocks. The peridotite zone is part of the younger intrusion. It cuts sharply across olivine pyroxenite layering, and itself has layering that dips about 20 degrees flatter, giving a relation not unlike an angular unconformity (Fig. 1, locality B). Fragments and blocks of olivine pyroxenite, some of them layered, are included in the peridotite and are concentrated in the lower half of the exposed section like a basal conglomerate. Many

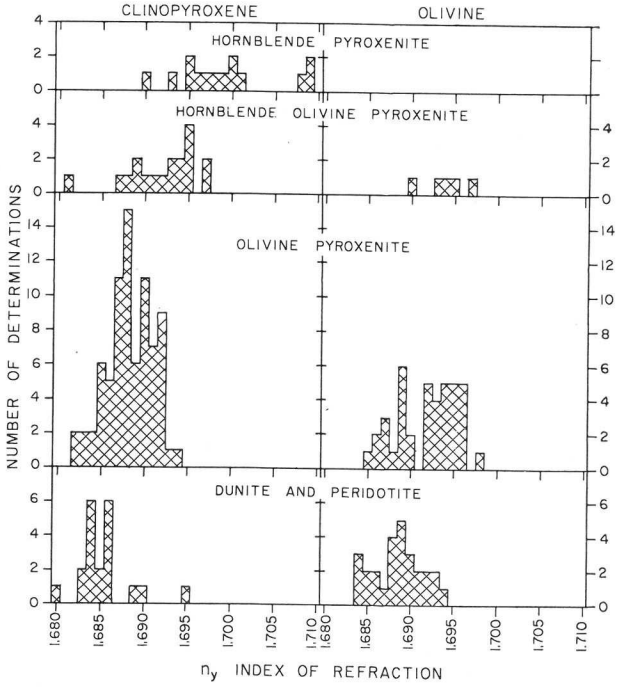


FIG. 6. Histograms of the refractive indices of clinopyroxene and olivine in the major ultramafic rock units.

of the smaller fragments occur in fragmental layers (Fig. 9). Larger blocks, commonly having dimensions of tens to hundreds of feet, occur individually or in jumbled clusters. Generally their weight and impact has caused intense deformation of peridotite layers on which they have fallen, and cross-layering is associated and apparently was produced by irregular currents accompanying influx of the blocks. It is clear that both intrusions were largely liquid, although the younger may have contained an appreciable proportion of olivine crystals. Emplacement of the younger intrusion seems to have caused folding and faulting in earlier olivine pyroxenite and, thus, was probably forcible.

In the Judd Harbor outcrop, layered structures in the dunite-peridotite zone are discordant with those in olivine pyroxenite, and here too, relations suggest that the former was forcibly emplaced into the latter.

Thickness estimates for the layered rocks are tenuous because of the complicated structure. Intermittently layered olivine pyroxenite totals about 10,500 feet in the Hall Cove outcrop and 5300 feet in the Judd Harbor outcrop. About 1500 feet of continuously layered peridotite are exposed in the Hall Cove outcrop.

The interpretation given in Fig. 1 shows dunite and peridotite as part of a younger intrusion and

assumes that the complex is one large body with a highly continuous peripheral zone of hornblende pyroxenite. The vertical dimension shown for the body is the minimum required to accommodate the exposed layered rock.

*Mafic pegmatite.* A remarkable pegmatite of hornblende and anorthite (Fig. 2) occurs in abundance in the southwest part of Duke Island. Most of it froms veins and dikes in gabbro, but some occurs in a swarm of dikes trending N. 50° W. through the olivine pyroxenite in the Judd Harbor ultramafic outcrop. The dikes range in width from half an inch to 200 feet, and a few extend 1200 feet along strike. Grain size is commonly 1–6 inches and locally reaches 4 feet. A more detailed description and pictures of the rock have been published by Koschmann (1935).

The very calcic plagioclase in the pegmatite precludes derivation of the rock from normal gabbroic magma. The ultramafic complex is the probable source because it is rich in calcium and contains hornblende that is optically and chemically similar to the pegmatite hornblende. The pegmatite is more common near the better developed parts of the hornblende pyroxenite zone, and comparable pegmatite is associated with several of the other ultramafic bodies in Alaska. The abundance of the pegmatite at Duke Island, especially between the two areas of ultramafic outcrop, suggests the presence of more ultramafic rock at depth.

*Altered (hornblende) gabbro.* An appreciable part of the primary gabbro has been altered to hornblende and plagioclase. Some of the alteration fringes

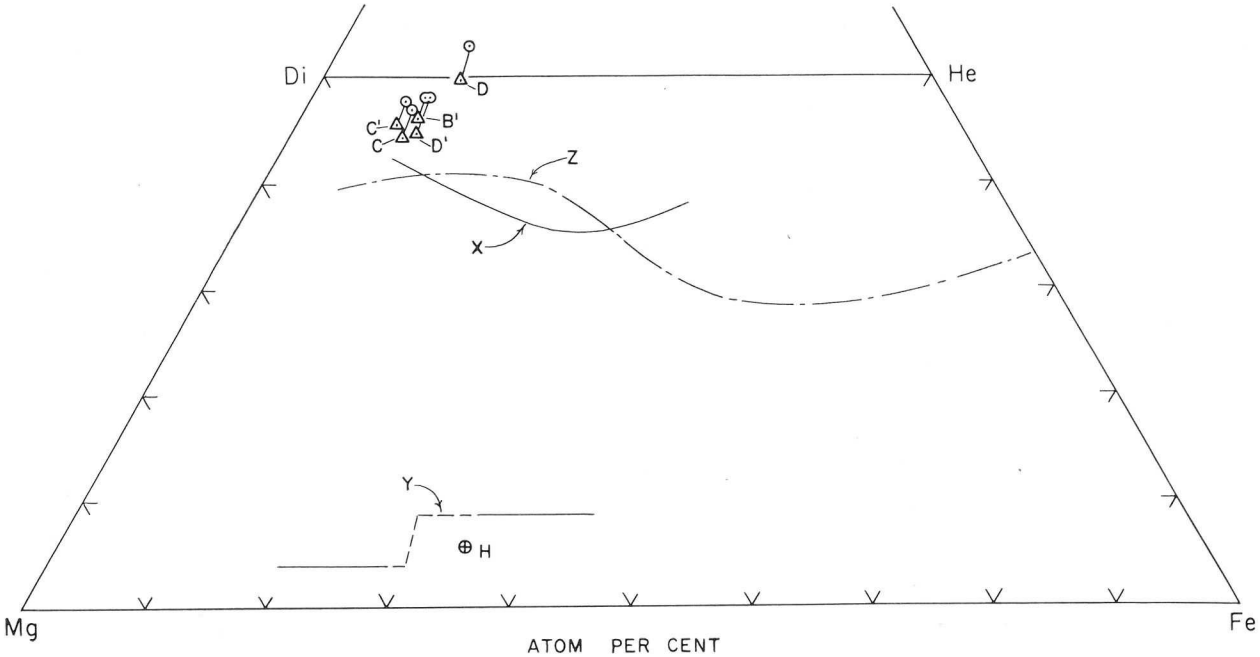


⊙ Clinopyroxene: total Ca:Mg:(Fe" + Fe"' + Mn).

△ Clinopyroxene: as above, less Ca as hypothetical $CaAl_2SiO_6$.

⊕ Orthopyroxene.

B' Pyroxene vein in peridotite.

C Olivine pyroxenite.

C' Olivine pyroxenite.

D Hornblende pyroxenite.

D' Hornblende pyroxenite.

H Norite

X Trend of Ca-rich pyroxene in the Skaergaard intrusion. After Brown, 1957.

Y Trend of Ca-poor pyroxene in the Skaergaard intrusion. After Brown, 1957.

Z Trend of clinopyroxenes in common mafic magmas. After Hess, 1941.

FIG. 7. Plot of Duke Island pyroxenes on a Di-He-Mg-Fe diagram.

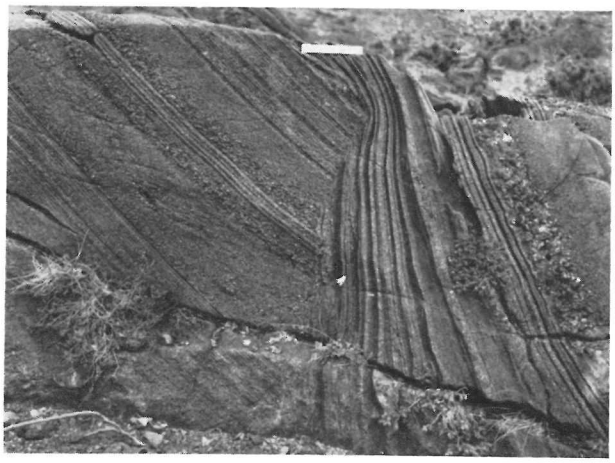

FIG. 8. Two generations of graded layering in the olivine pyroxenite zone of the Hall Cove ultramafic outcrop. The angular block on the left has been broken from a well-solidified accumulate and, then, covered by the layers on the right. Subsequently, the entire structure has been tilted to the right. The scale is six inches.

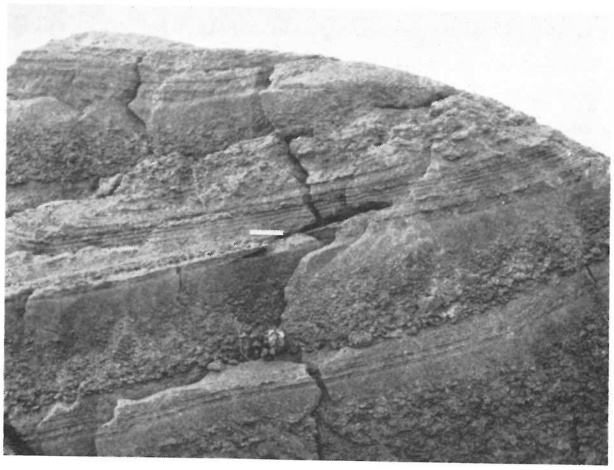

FIG. 9. Fragmental layers in the peridotite zone of the Hall Cove ultramafic outcrop. Small fragments of olivine pyroxenite have been sorted by size. They are surrounded by a peridotitic matrix. The scale is six inches.

granite plutons and probably has been caused by these younger intrusions; its plagiocalse ranges from $An_{20}$ to $An_{57}$.

Most of the altered or hornblende gabbro occurs around the ultramafic rocks, particularly between their two main areas of outcrop. It has uneven porphyroblastic to pegmatitic texture and is intimately intermixed with and veined or intruded by mafic pegmatite. Its plagioclase ranges from $An_{40}$ to $An_{98}$ and, as shown in Fig. 2, is to a considerable extent intermediate between the feldspars of pyroxene gabbro and mafic pegmatite. Evidently, this hornblende gabbro is an alteration of pyroxene gabbro caused by the highly calcic water-rich pegmatite from the ultramafic complex.

## GENESIS OF THE ULTRAMAFIC COMPLEX

*Evidence of an ultrabasic magma.* In the structural interpretation presented in Fig. 1, it is implicit that the ultramafic rocks represent at least two intrusions of magma of ultrabasic composition.[1] Such an interpretation is, of course, subject to serious question, particularly in view of the abundance of gabbro exposed on the island. However, attempts to interpret the ultramafic and gabbroic rocks as parts of a stratiform body like the Stillwater complex have not given reasonable results, and certain features are in direct conflict (notably, the relations at locality A). The idea of two ultrabasic intrusions provides a relatively consistent picture, and a variety of chemical and mineralogical evidence summarized below seems in agreement.

The ultramafic and gabbroic rocks contrast markedly in their mineralogy and chemistry. The primary gabbro generally contains orthopyroxene and locally is noritic. Ca-poor pyroxene does not occur in the ultramafic rocks and is absent from their norms (except in rock appreciably oxidized during serpentinization of olivine). Ultramafic clinopyroxene is undersaturated in Ca-poor pyroxene and, if anything, becomes more so in the lower-temperature differentiates (Fig. 7). It overlaps gabbro clinopyroxene in refractive index but has a different trend of optical and, probably, chemical variation (Fig. 4). Overall, the ultramafic rocks are extremely undersaturated in silica. Their norms contain not only olivine, but nepheline, leucite and larnite. The chemical trend in going from dunite to mafic pegmatite is not one of appreciable silica enrichment, and mineral analyses indicate extensive substitution of Al for Si in the tetrahedral sites of clinopyroxene and hornblende from the lower temperature rocks, due probably, to some extent, to a deficiency of silica.

Some of the mineralogical features that contribute to the contrast in degree of silica saturation shown by ultramafic and gabbroic rocks might be rationalized with formation of the rocks from one magma if it is assumed that, after accumulation of

[1] The adjective *ultramafic* should probably only be used in reference to mafic-rich *rocks* that are essentially free of feldspar. The magma's composition is described as *ultrabasic*, implying low silica content, because the feldspar-bearing mafic pegmatite is probably one of its differentiates, and because chemical analyses show the Duke Island ultramafic rocks to contain appreciable normative anorthite.

the olivine-bearing ultramafic units, the main body of residual magma underwent a brief period of extensive oxidation. The change of iron from the ferrous to the ferric state could have caused precipitation of the abundant magnetite in the hornblende pyroxenite zone and, in addition, would reduce the $Fe^{2+}/Mg$ ratio of the residual magma and effectively increase its silica content. As a result, the Fe/Mg ratios of the mafic silicates crystallizing from the magma would drop abruptly and then progressively increase again with differentiation after oxidation ceased, and orthopyroxene might take the place of olivine in the crystallization sequence, appearing both as a distinct phase and in increased amounts in solid solution in clinopyroxene. This would account for some of the pyroxene variations shown in Figs. 3 and 4. The effective production of silica by oxidation could have led to the precipitation of gabbro plagioclase in that it would produce albite in place of the normative nepheline common to the ultramafic rocks. The principal feature that seems to contradict the above interpretation, in addition to the structural relations, is that clinopyroxene in the rock richest in magnetite, hornblende pyroxenite, has a higher Fe/Mg ratio than that in the olivine-bearing ultramafic units and, possibly, less Ca-poor pyroxene in solid solution (Figs. 6, 7). Furthermore, the envisaged period of oxidation would probably require a rather special event in the history of the complex, which seems unlikely inasmuch as similar magnetite-rich pyroxenites occur in several other ultramafic bodies in Alaska and British Columbia (Taylor and Noble, 1960). Clinopyroxene variations in the ultramafic rocks at Union Bay are comparable to those shown in Figs. 6 and 7 (Ruckmick and Noble, 1959).

If the ultramafic rocks were differentiated from gabbroic magma, they might be expected to contain interstitial plagioclase as a product of interprecipitate magma. Also, one might expect the ultramafic and gabbroic rocks to have gradational contacts. The complex is, however, devoid of plagioclase, and its contact with gabbro is everywhere sharp and apparently intrusive. Filter pressing might locally remove pore magma but probably could not cause a complete absence. It might be argued (in fact, in parts of the complex, it is probable) that the pore magma was water rich and that the components of plagioclase crystallized in hornblende; the ultramafic rocks have normative anorthite that, in some, is due to $Al_2O_3$ in hornblende, and data obtained by Yoder and Tilley (1956) indicate that, in basic rocks at moderate to high water pressures, plagioclase is incompatible with pyroxene and olivine, their reaction producing hornblende. Nonetheless, unless two distinct magmas are involved, it seems fortuitous that interstitial plagioclase should be absent everywhere in the Duke Island ultramafic complex (and in the other ultramafic bodies in S. E. Alaska; *cf.* Taylor and Noble, 1960), especially when olivine, pyroxene, and plagioclase coexist in the primary gabbro. On the other hand, a high activity of water might well have been one of the characteristics of the ultrabasic magma that distinguished it from the gabbro magma.

The mafic pegmatite is the only feldspathic rock considered to be directly related to the ultramafic complex. Although abundantly exposed it probably is a proportionately minor unit, and in terms of normative mineralogy, it too is very much undersaturated in silica. The mineralogic and textural relations of hornblende gabbro and mafic pegmatite are not typical of comagmatic rocks and would seem to preclude their formation by differentiation of one liquid. More likely, the hornblende gabbro is the alteration aureole of an ultrabasic magma emplaced in a country rock of pyroxene gabbro.

*Composition and crystallization of the magma.* Fine-grained rocks that might represent chilled ultrabasic magma have not been recognized at Duke Island. Rough estimates of the chemical composition of the average rock exposed in each of the ultramafic outcrops are given in Table 1. They were obtained by weighting chemical and modal analyses by the abundances shown in Fig. 5 and are, therefore, close to the composition of olivine pyroxenite. The extent to which the estimates may represent the liquid part of the initial intrusions depends, of course, on many factors: *e.g.* the assumptions made in the computations; the extent to which the exposed rocks represent the complex as a whole; the proportion of crystals in the initial intrusions; the composition and amount of mafic pegmatite and other materials lost to the country rock; and the extent to which the analyzed rocks represent contamination by country rock. Olivine pyroxenite is probably a gravitationally accumulated differentiate of the magma; it constitutes most of the layered rock and apparently represents the product of cotectic precipitation of olivine and clinopyroxene inasmuch as the proportions of these minerals are roughly those of the eutectic product in the system $CaMgSi_2O_6$-$Mg_2SiO_4$ (Bowen, 1914). However, the absence of cryptic layering may indicate that the rock is close

in composition to its parent magma. Dunite and peridotite probably formed by fractionation of an excess of olivine over the cotectic proportion and/or by accumulation of olivine crystals suspended in the initial intrusions. The estimates in Table 1 include normative anorthite, hence the anorthite-bearing mafic pegmatite is a conceivable late differentiate.

The hornblende pyroxenite zone, as exposed, is considerably more extensive in the Hall Cove ultramafic outcrop than in the Judd Harbor outcrop. However, as shown in Fig. 5A, the olivine-bearing rocks in the Judd Harbor outcrop contain a larger proportion of hornblende, and this may indicate that hornblende pyroxenite has formed by some process of differentiation *in situ* that was more effective in the northwest part of the complex. Hornblende pyroxenite at the top of the complex may be the result of gravity-controlled fractional crystallization, olivine having ceased to crystallize because of a peritectic reaction giving hornblende or magnetite, or both. The magnetite layering at Kelp Island could be supporting field evidence, and perhaps notable is that much of the hornblende pyroxenite has about the same proportion of magnetite as the liquidus minimum of the join $CaMgSi_2O_6$-$Fe_3O_4$ in air atmosphere (D. Presnall, personal communication, 1962). However, the marginal (and basal?) border zone requires a different explanation. The continuity of the border zone suggests that it is a reaction rim. In fact, the physical and mineralogic relations of the hornblende pyroxenite zone and the alteration aureole of hornblende gabbro could be interpreted to represent an approach to local equilibrium along thermal and chemical gradients between a water-rich ultrabasic magma and a pyroxene gabbro country rock. The mechanics of the reactions are problematical but are probably related to the escape of mafic pegmatite from the ultramafic complex. Notable in this respect is that an appreciable amount of hornblende and magnetite occurs as alteration associated with the swarm of mafic pegmatite dikes in the Judd Harbor olivine pyroxenite.

Much of the period of solidification of the ultrabasic magma must have been marked by cotectic crystallization of diopsidic pyroxene and forsteritic olivine. A maximum temperature during this time would be that of the eutectic in the system $CaMgSi_2O_6$-$Mg_2SiO_4$ (1387° C. at 1 atmosphere; Bowen, 1914). Possible excess olivine in solution during the formation of dunite could require higher temperatures, but the other constitutents evident in the ultramafic rocks (*e.g.* FeO, $Fe_2O_3$, $Al_2O_3$ and $H_2O$) would lower the liquidus. Thus the magma may initially have been at 1250° C. or less and was probably appreciably cooler by the pegmatitic stage.

TABLE 1. ESTIMATES OF THE COMPOSITION OF THE AVERAGE ULTRAMAFIC ROCK EXPOSED IN EACH OF THE TWO MAIN AREAS OF ULTRAMAFIC OUTCROP AT DUKE ISLAND. $H_2O$ IS NOT INCLUDED

| | I Hall Cove | II Judd Harbor | C.I.P.W. Norms | | |
|---|---|---|---|---|---|
| | | | | I | II |
| $SiO_2$ | 43.9 | 45.5 | Ol Fo | 19.9 | 25.5 |
| $Al_2O_3$ | 6.0 | 4.8 | Ol Fa | 4.3 (24.2) | 5.4 (30.9) |
| $Fe_2O_3$ | 5.3 | 2.9 | Cpx Di | 40.4 | 40.9 |
| FeO | 8.1 | 7.5 | Cpx He | 7.0 (47.4) | 6.9 (47.8) |
| MgO | 18.9 | 22.2 | Larnite | 2.0 | 2.3 |
| CaO | 15.9 | 15.7 | An | 12.5 | 10.1 |
| $Na_2O$ | 0.6 | 0.4 | Ne | 2.8 | 1.8 |
| $K_2O$ | 0.4 | 0.4 | Lc | 1.9 | 1.9 |
| $TiO_2$ | 0.8 | 0.5 | Mt | 7.7 | 4.2 |
| MnO | 0.1 | 0.1 | Il | 1.5 | 1.0 |
| | 100.0 | 100.0 | | 100.0 | 100.0 |

Areas Represented: Hall Cove outcrop 5.4 sq. miles
Judd Harbor outcrop 3.6 sq. miles

## REFERENCES


BOWEN, N. L. (1914) The system diopside-forsterite-silica. *Am. Jour. Sci.* **38,** 207–264.

BROWN, G. M. (1957) Pyroxenes from the early and middle stages of fractionation of the Skaergaard intrusion, East Greenland. *Mineral. Mag.* **31,** 511–543.

HESS, H. H. (1941) Pyroxenes of common mafic magmas. *Am. Mineral.* **26,** 515–535, 573–594.

——— (1960) Stillwater igneous complex: a quantitative mineralogical study: *Geol. Soc. Am. Mem.* **80,** 1–230.

KOSCHMANN, A. H. (1935) Hornblendite and related rocks of Annette and Duke Islands, southeastern Alaska. *Am. Geophys. Union Trans., 16th Ann. Meet.,* 268–274.

RUCKMICK, J. C. AND J. A. NOBLE (1959) Origin of the ultramafic complex at Union Bay, southeastern Alaska. *Geol. Soc. America Bull.* **70,** 981–1018.

TAYLOR, H. P., JR. AND J. A. NOBLE, (1960) Origin of the ultramafic complexes in southeastern Alaska. *21st Int. Geol. Cong. Rpt., Pt.* **XIII,** 175–187.

WAGER, L. R. AND W. A. DEER (1939) The petrology of the Skaergaard intrusion, Kangerdlugssuag, East Greenland. *Medd. Grønland,* **105,** 1–352.

YODER, H. S., JR. AND C. E. TILLEY (1956) Natural tholeiite basalt-water system. *Carnegie Inst. Wash. Yearbook.* **55,** 169–171.

MINERALOGICAL SOCIETY OF AMERICA, SPECIAL PAPER 1, 1963
INTERNATIONAL MINERALOGICAL ASSOCIATION, PAPERS, THIRD GENERAL MEETING

# STRATIGRAPHIC AND LATERAL VARIATION OF CHROMITE COMPOSITION IN THE STILLWATER COMPLEX[1]

EVERETT D. JACKSON
*U. S. Geological Survey, Menlo Park, California*

ABSTRACT

Layered concentrations of chromite occur at 13 recognizable stratigraphic horizons within the 3500-foot thick Ultramafic zone of the Stillwater Complex. Five of the chromitite layers or zones can be recognized for 15 miles along strike, and one can be traced nearly 30 miles. Samples of chromitite from the footwalls of these zones were collected at intervals of about 2.5 miles along strike and 43 chemical analyses of clean chromite were made.

Considered individually, the major cations $Cr^{3+}$, $Al^{3+}$, $Fe^{3+}$, $Mg^{3+}$, and $Fe^{2+}$ in the chromite show no simple vertical or lateral patterns of variation. However, total iron ($Fe^{2+}+Fe^{3+}$) in the analyzed samples decreases regularly from about 6.0 cations/unit cell in the lower zones to about 4.5 cations/unit cell in the middle zones, then changes, and increases regularly to about 5.5 cations/unit cell in the upper zones. Lateral variations in the total iron content are small, so that isochemical lines trend parallel to the layering. The oxidation ratio ($Fe^{3+}/Fe^{2+}+Fe^{3+}$) of the chromite, on the other hand, shows a strong lateral variation, decreasing from about .30 at the eastern and about .15 at the western ends to less than .05 in the central part of the complex. Vertical variation of the oxidation ratio in any one stratigraphic section is small and irregular, so that isochemical lines trend at steep angles to the layering. Inasmuch as total numbers of trivalent and bivalent cations per unit formula of balanced chromite are fixed, the combination of constant total iron and changing oxidation ratio of chromite along any given chromitite zone accounts for the complex variation of the individual cations.

The strong lateral change in oxidation ratio of the chromite suggests that a lateral oxygen partial pressure gradient persisted in the magma during crystallization and accumulation of the Ultramafic zone. The early decrease in total iron between the chromitite zones suggests an early reversal in the expected trend of differentiation, followed in the upper part of the stratigraphic section by normal iron-enrichment.

## PURPOSE AND SCOPE

The compositions of the primary precipitate minerals of the Ultramafic zone of the Stillwater Complex are being studied for the purpose of describing and interpreting the crystallization history of the intrusion. Three primary precipitate minerals occur in the Ultramafic zone: olivine, bronzite and chromite. Of these, chromite is the least abundant but most interesting because it is the only one capable of containing major amounts of trivalent cations. This paper presents some preliminary results of a study of the lateral and vertical changes in chromite composition within the Ultramafic zone of the complex.

## GENERAL SETTING OF THE CHROMITE

The Stillwater Complex can be divided into several major stratiform zones (Jones *et al.*, 1960, p. 286–289; Hess, 1960, p. 49–50; Jackson, 1961, p. 2–4). The Ultramafic zone, which lies in the lower part of the complex and has an average stratigraphic thickness of about 3500 feet, can be subdivided into a Peridotite member and a Bronzitite member (Fig. 1). Virtually all the chromite in the complex occurs within the Peridotite member of the Ultramafic zone.

On the basis of mapping at scales of 1:12,000 and 1:1200 the Peridotite member has been divded into 15 subunits, called cyclic units, characterized by layers of harzburgite, chromitite, and bronzitite arranged in a particular stratigraphic order (Jackson, 1961, p. 13–15). A typical cyclic unit is shown in Fig. 2. The sequence of rock types is poikilitic harzburgite, chromitite, olivine chromitite, poikilitic harzburgite, granular harzburgite and bronzitite. In terms of the primary precipitate (or settled minerals) the sequence has been interpreted as recording the continuous crystallization and deposition first of olivine, then chromite, olivine plus chromite, olivine, olivine plus bronzite and finally of bronzite alone. The sharp breaks between cyclic units are thought to represent interruptions of crystallization and deposition, followed by a repetition of the cycle to form the succeeding unit. Each of the cyclic units is distinctive in thickness, proportion of rock types, grain size or textural peculiarities.

## DISTRIBUTION AND CORRELATION OF THE CHROMITITE ZONES

Thirteen of the cyclic units contain recognizable layered concentrations of chromite. These concentrations, locally called zones, are compound; they are usually composed of massive chromitite layers at the base, giving way to alternating olivine chromitite layers and massive chromitite layers upward

[1] Publication authorized by the Director, U. S. Geological Survey.

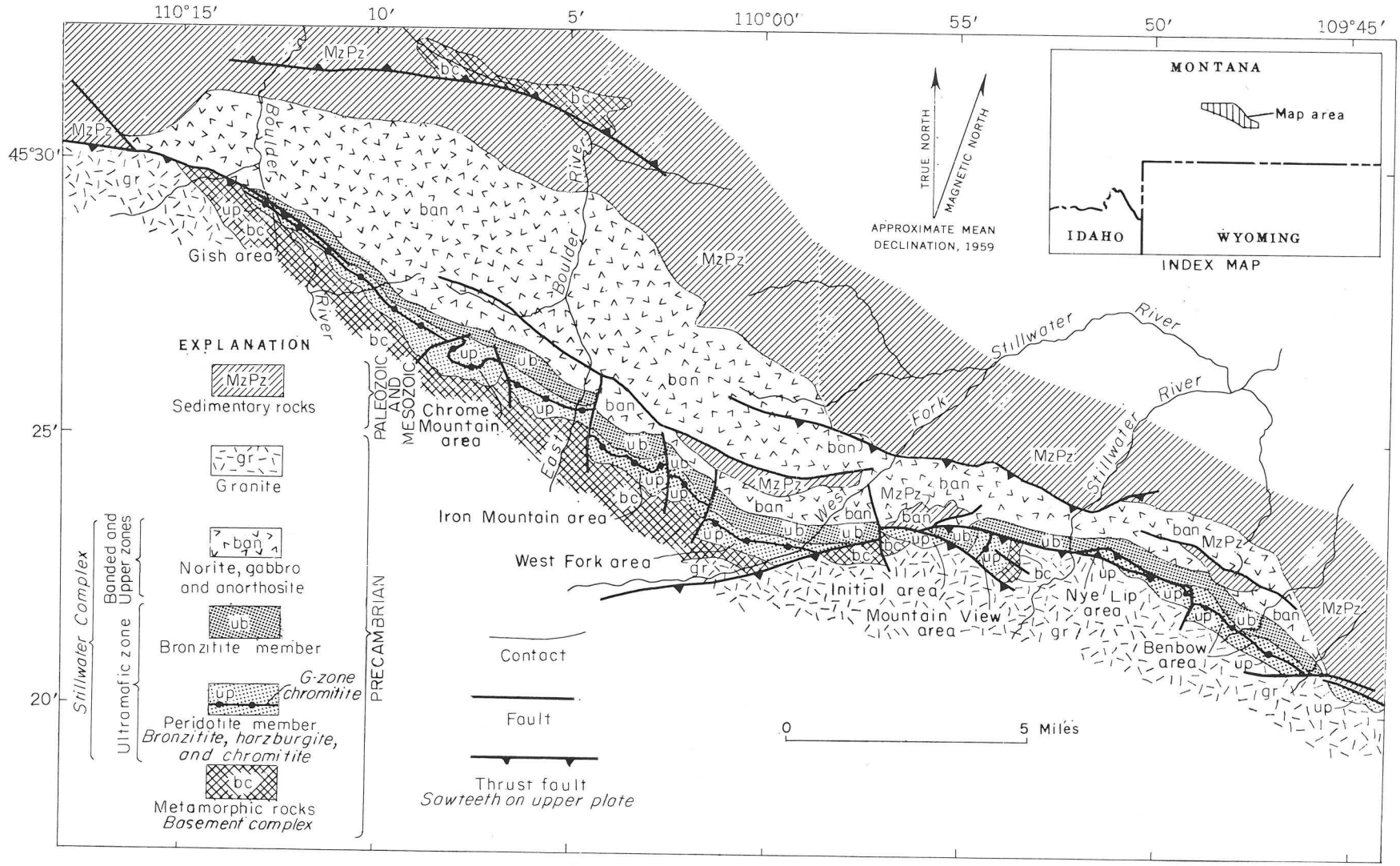


FIG. 1. Geologic index map of the Stillwater Complex.

in the section. The chromitite zones have been mapped, correlated by field criteria, and lettered more or less sequentially from the base upward. A correlation diagram of the chromitite zones of the Peridotite member is shown as Fig. 3. Several basins in the Peridotite member can be recognized on the correlation diagram, although they are exaggerated by the expanded vertical scale. Both cyclic units and chromitite zones are thicker in the basin sections than on the shelf sections at either side.

Five of the chromitite zones, the A, B, G, H and K, can be traced for 15 miles along strike, and one, the G, can be traced nearly 30 miles. The G is also the thickest chromitite zone, ranging from a maximum of about 12 feet to a minimum of about $1\frac{1}{2}$ feet in thickness. The H zone is generally about half as thick as the G, and is followed in decreasing order of thickness by the B, A and K zones. The remaining zones are generally only one or two inches thick, but even so, several of them (for example, the I and J zones) can be traced more than ten miles.

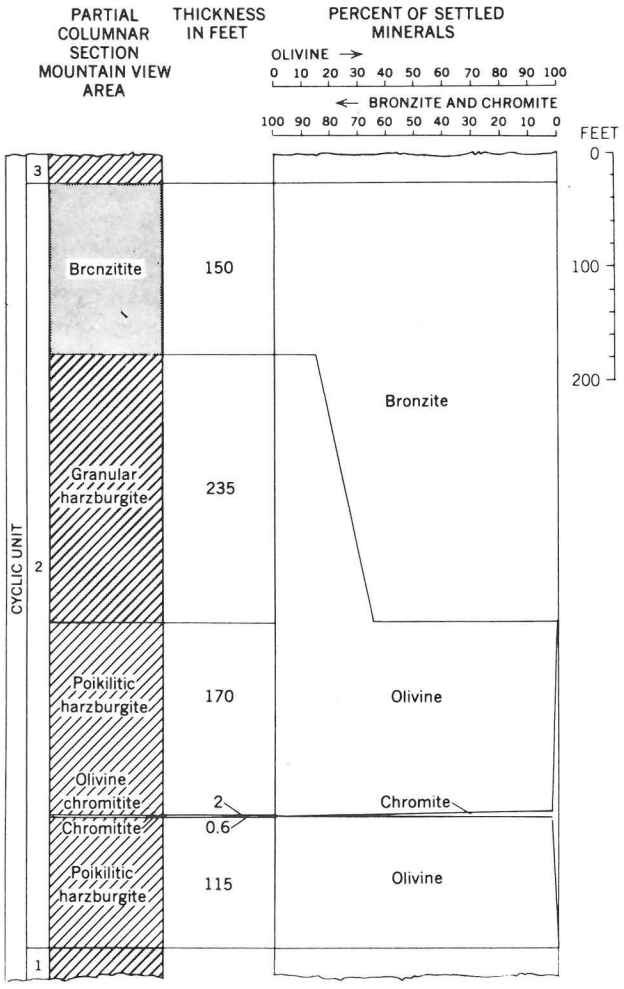


FIG. 2. Stratigraphic variation of settled minerals in a typical cyclic unit of the Peridotite member.

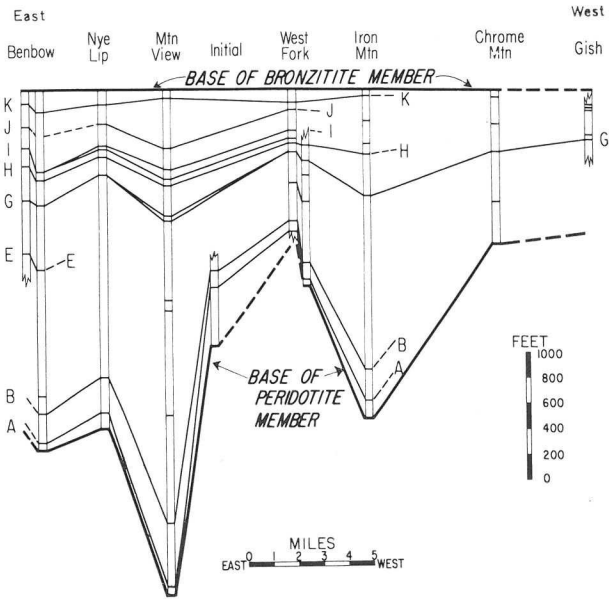


FIG. 3. Correlation of chromitite zones in the peridotite member, Stillwater Complex.

## SAMPLING AND ANALYSIS OF THE CHROMITE

Ninety-five chromite-bearing samples were collected from the layered chromitites of the complex to determine changes in composition of chromite in three ways: vertically within single zones; stratigraphically between zones; and laterally along zones. Forty of the samples were selected to determine the within-zone variations, 43 to determine the between-zone and lateral variations, and the remainder for various special purposes.

The samples taken to investigate between-zone and lateral variations were collected from 8 areas (Fig. 1) at intervals of about 2.5 miles along the strike of the intrusion. Samples were collected from the footwalls of all the exposed chromitite zones in each area (Fig. 3).

Chromite samples were cleaned of silicate minerals, examined in polished grain mounts to establish purity, and chemically analyzed by a method developed by Dinnin (1959). Minor amounts of impurities were subtracted from the analytical values and the analyses were recalculated to cations per unit cell on the assumption of balanced charge. None of the analyzed chromites showed a cation deficiency or excess.

### Range of Chemical Composition of the Chromite

Five major cations—$Mg^{2+}$, $Fe^{2+}$, $Cr^{3+}$, $Al^{3+}$ and $Fe^{3+}$—comprise more than 98 per cent of the total cations in the analyzed chromite samples, so the major variation can be expressed graphically on a triangular prism (Thayer, 1956, p. 16). Fig. 4 shows the range in the 95 samples of variation of the five major constituents expressed as end-member spinels on such a prism. The field of occurrence forms a cylinder whose axis extends from the Cr-Al face of the prism toward the magnetite corner. The prism also illustrates the interdependence of the major cations in the chromite. The sum of $Mg^{2+}$ and $Fe^{2+}$ is virtually a constant, so that as one increases, the other must automatically fall. Similarly, the sum of $Cr^{3+}$, $Al^{3+}$ and $Fe^{3+}$ is nearly constant, so that an increase in one will generally result in a decrease in the other two. However, the charge balance does not require such a relation between cations of the $R^{2+}$ and $R^{3+}$ groups, and interactions between individual cations such as $Fe^{2+}$ and $Fe^{3+}$ may vary independently.

### Variations in Composition of the Chromite

The variation in composition of chromite within single zones has been reported elsewhere (Jackson, *et al.*, 1960). In the thicker zones, the within-zone variation proved to be larger than the between-zone variation, and chromite compositions in rocks containing both settled olivine and chromite were found to be systematically different from those in rocks containing only settled chromite. As a result, samples collected for determining the lateral and between-zone variation were chosen from a consistent stratigraphic position in the zones (the footwall), and samples containing settled olivine were avoided wherever possible.

The lateral and between-zone changes in composition of chromite was examined simultaneously by plotting values of the major cations at the appropriate places on columnar correlation diagrams, and contouring the values. To simplify interpretation, the columnar diagrams were drawn so that the correlated zones formed horizontal lines. Each of the five major cations of the analyzed chromite from the footwalls of the correlated chromitite zones was plotted individually, and isochemical lines were drawn. None of these major cations, considered individually, shows a simple lateral or between-zone variation. However, two sets of cation values do vary regularly on the diagrams: total iron ($Fe^{2+}+Fe^{3+}$)

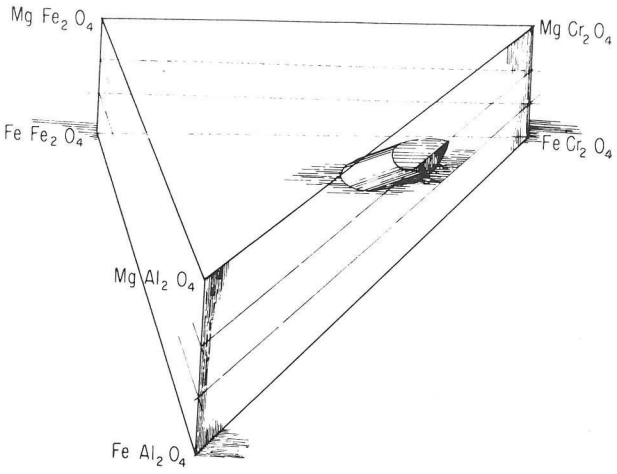


Fig. 4. Compositional range of chromite in the Stillwater Complex.

and oxidation ratio ($Fe^{3+}/Fe^{2+}+Fe^{3+}$). Both values express interaction between the $R^{2+}$ and $R^{3+}$ groups of the chromite.

*Between-zone variation* The only simple systematic relation between the major cations of the analyzed chromite and the stratigraphic position of the chromitites from which it was separated is shown by total iron. The relation is presented diagrammatically in Fig. 5, where the sum of $Fe^{2+}$ and $Fe^{3+}$ cations/unit cell in the chromite is placed in its appropriate areal and stratigraphic position in the columnar diagrams. In any one stratigraphic section, the values of total iron are greatest in the A zone, decrease regularly to the H zone, and then increase to the K zone. The isochemical lines tend to parallel the layering, emphasizing the strong variation between zones. The A zone values for all sections average 6.1, the B zone values average 5.4, and G zone 4.9, the H zone 4.5 and the K zone 5.5. These averages for cations per unit cell would correspond to total iron expressed as weight per cent FeO of about 27.6, 25.0, 23.2, 21.7 and 25.3 per cent respectively.

Oxidation ratio in the same chromite samples are plotted in Fig. 6. In any one stratigraphic section, the oxidation ratio tends to remain nearly constant, but this relation is not everywhere consistent because the isochemical lines trend at a steep angle across the planes of the zones.

*Lateral variation* The lateral variation of total iron of the chromite is small, but the systematic depression of isochemical lines in the lower central part of Fig. 5 shows that absolute values are smaller in that area. Considering any given chromitite zone, the values of total iron are about 0.5 cation per unit cell lower in the West Fork section than in sections on either side.

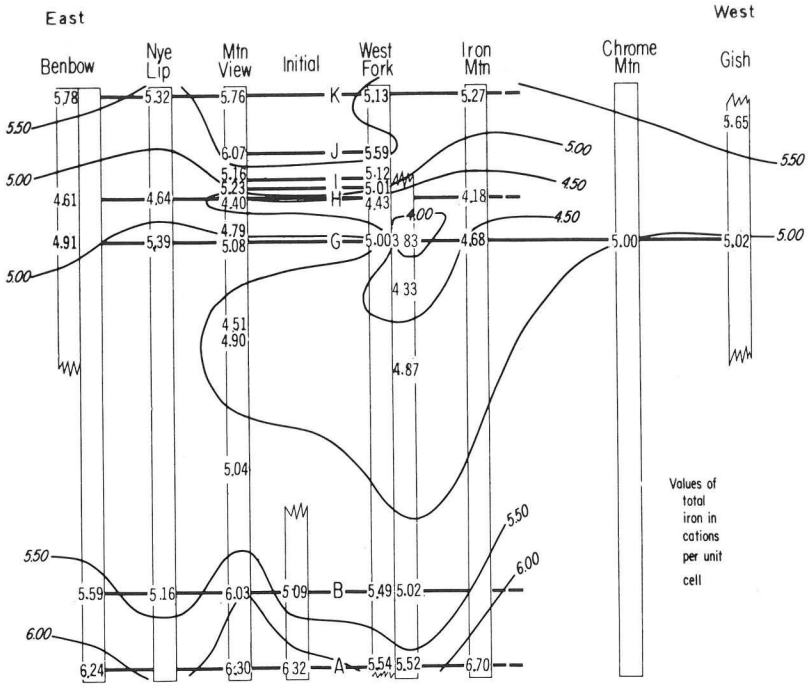


FIG. 5. Columnar diagram of variation of total iron in chromite of the Stillwater Complex.

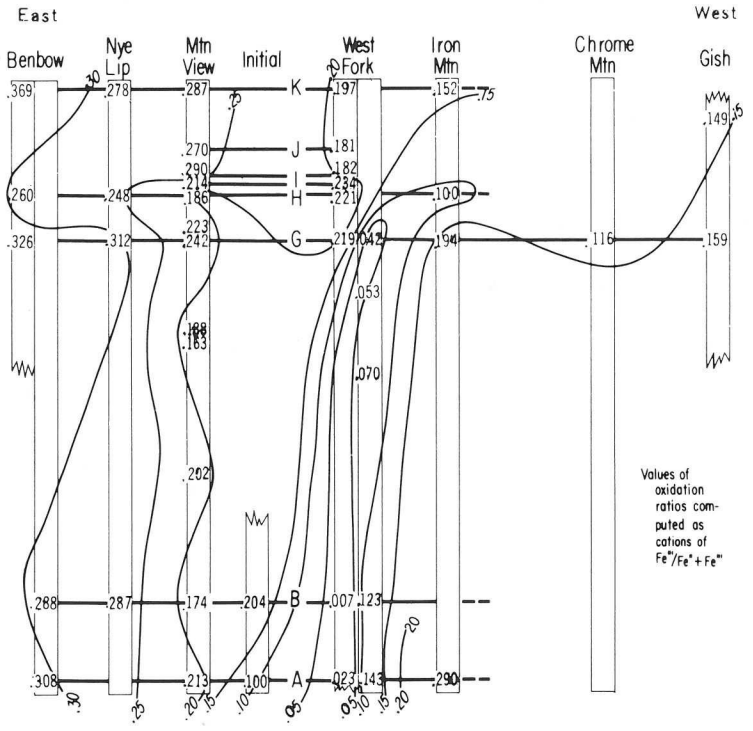


FIG. 6. Columnar diagram of variation of oxidation ratio in chromite of the Stillwater Complex.

A most striking and systematic lateral change in oxidation ratio of the chromite emerges when plotted on the columnar diagrams (Fig. 6). Considering any given chromitite zone, the values of $Fe^{3+}/Fe^{2+}+Fe^{3+}$ are greatest in the chromites at the eastern extremity of the complex, decrease toward the central part, and finally increase again toward the western limit of exposure. The nearly vertical isochemical lines emphasize the lateral nature of the change. The magnitude of this lateral change in oxidation ratio is greater in the lower part of the section than in the upper. In the upper part of the section the average oxidation ratio decreases progressively westward from more than .30 in the Benbow area to less than .10 in the western part of the West Fork section, then increases to more than .15 in the Iron Mountain and Gish areas; in the lower part of the section the oxidation ratio decreases from .30 at both eastern and western ends to less than .05 in the central part of the complex.

Inasmuch as the total numbers of both bivalent and trivalent cations per unit formula of balanced chromite are fixed, this combination of nearly constant total iron and changing oxidation ratio of chromite along any given chromitite zone accounts for the complex variations of the individual cations. $Fe^{2+}$, for example, is low along the H zone chromitite where total iron is low, but is also low in the upper and lower zone chromitites of the Benbow area where, although total iron is high, much of it occurs in the trivalent form. The highest values of $Fe^{2+}$ occur in the lower part of the Initial and West Fork areas, where total iron is high and oxidation ratio low. $Mg^{2+}$ shows a reciprocal pattern. Of the trivalent cations in the chromites, $Fe^{3+}$ is low in the central part of the complex where oxidation ratio is low, but it is also low along the G and H zone chromitite where total iron is low, even in areas where the oxidation ratio is high. The amount of $Cr^{3+}$ in the chromite shows a nearly reciprocal relation with $Fe^{3+}$, so that high $Cr^{3+}$ chromite occurs in the central part of the complex and also laterally along the G and H zone chromitites. As a consequence of these changes, the $Cr^{3+}/Fe^{2+}+Fe^{3+}$ ratio of the chromite has a pattern almost reciprocal to that of $Fe^{2+}+Fe^{3+}$.

The existence of this regular pattern should permit the prediction of the composition of chromite anywhere in the complex. As a check on the extrapolation of isochemical lines between sampled sections, several previously published analyses of Stillwater chromites from various localities in the Peridotite member (Stevens, 1944, p. 12–13 and 22; Howland *et al.*, 1949, p. 76; Howland, 1955, p. 109) were entered on the diagrams. About 20 of these older analyses were of samples collected near the footwalls of massive chromitite layers. Values of total iron and, where determined, oxidation ratio of these samples fell within the established pattern.

The significance of the lateral and between-zone variations in iron content and oxidation state in the chromite, can, at this time, be outlined only in a very general way. It should be noted at the outset, however, that it is very unlikely that the observed differences in composition could have originated after the crystallization of the mineral. Oxidation or reduction of iron in chromite destroys the charge balance of the mineral and cannot be accomplished without large gains or losses in other major cations by diffusion or without the generation of another oxide phase. Alteration of chromite has been described by a number of authors and is evidenced in three ways:

(1) exsolution of an $\alpha$ ($R_2O_3$) phase (de Wijkerslooth, 1942, p. 267–289); (2) presence of a secondary spinel phase (Miller, 1953, p. 1134–1147); or (3) development of $\gamma$ (defect) structures in the chromite (Rait, 1946, p. 191–192).

The analyzed Stillwater chromites are internally homogeneous, closely packed, for the most part euhedral, and are the only oxide phase present in the rocks. Careful inspection in reflected light has shown that no significant amounts of $R_2O_3$ or other spinel phases are present, and the cation abundances calculated from the analyses show that vacant lattice positions required by $\gamma$ structures do not exist. Furthermore, it is unlikely that any post-magmatic alteration could have occurred without affecting the fresh olivine with which the chromite is associated. The observed variations in chromite compositions are therefore believed to represent differences in magmatic conditions during the crystallization of the chromite.

It has been proposed elsewhere (Jackson, 1961, p. 81–99) that the massive chromitites of the Stillwater Complex are accumulations of chromite crystals that grew near the floor of the magma chamber and settled in relatively stagnant magma without a great deal of lateral transport. Chromites at the bases of individual chromitite zones, therefore, are believed to have crystallized simultaneously over a wide area of the floor of the complex. Presumably lateral changes in the composition of chromite represent differences in temperature, pressure, or composition of the magma above a particular part of the floor at a given instant of time. The principal lateral changes in chromite composition are a large decrease in the proportion of ferric iron and a small decrease in total iron toward

the central part of the complex. If the oxidation ratio of the chromite reflects that of the magma from which it crystallized, then it is likely that a lateral oxygen partial pressure gradient (or more properly an oxygen fugacity gradient) existed during most of the crystallization and accumulation of the Peridotite member. Such a gradient might be related to the convection cell pattern, to the position of feeders, or to extraction of water from intruded sediments at the margins of the intrusion. The presence of small amounts (0–1.6 volume per cent) of interprecipitate phlogopitic mica in the chromitites suggests that water was present in the magma during crystallization and accumulation of the chromite. Attempts to correlate amounts of mica in chromitites with oxidation ratio of chromite from them are complicated by the variable amounts of interprecipitate material in the rocks and by the difficulty of accurately measuring small amounts of the poikilitic interprecipitate minerals. Work on these measurements is continuing.

It is apparent from the law of superposition that the upper chromitite zones were successively crystallized and deposited on the lower. Thus variations in composition of chromite between zones should reflect changes in magma temperature, pressure, or composition with time. The principal between-zone changes in chromite composition is a steady decrease in total iron to the H zone chromitite followed by a steady increase in iron to the K. Normally, one would expect that total iron would be lowest in the A zone chromite and that it would increase upward for two reasons:

(1) The iron end members of the spinel solid solution series have the lowest melting points and should increase in the chromite with time as heat is extracted from the crystallizing system; and
(2) The magma should become residually enriched in iron with time due to fractionation of large quantities of magnesium-rich olivine and orthopyroxene.

The opposite of this expected relation in the lower zones may be due to unknown complications of fractionation paths in the chromite fields of the chemical systems involved, or to failure of the magma to reach complete thermal equilibrium during crystallization of the lower part of the Peridotite member, or to successive injection of increasingly iron-poor magmas. Studies of the vertical variation in iron content of olivine and bronzite may allow a choice between these hypotheses, and work on these minerals is in progress.

## Other Stratiform-type Chromites

Comparison of variations in chromite composition in the Stillwater Complex with those of chromite from other stratiform intrusions is hampered by incomplete stratigraphic control and by a general scarcity of trustworthy chemical analyses. Enough information is available, however, to suggest that the Stillwater variation may not be unique.

Worst (1958) reports 11 complete analyses of clean chromite from 9 chromitite layers of known stratigraphic position in the Hartley area of the Great Dyke of Southern Rhodesia. The samples were collected from both margins of the Dyke along a strike length of more than 50 miles, and were obtained by channelling the full width of the layers. Worst's seam numbers, arranged in their proper sequence, his stratigraphic intervals between the seams, and his reported FeO and $Fe_2O_3$ contents of the chromite from the seams are listed in Table 1. I have recalculated the FeO and $Fe_2O_3$ values of the analyses to both total iron as FeO and to $Fe^{2+}+Fe^{3+}$ per unit cell. Inspection of the table shows that although FeO and $Fe_2O_3$, considered individually, show no particular vertical order, the values of total iron have a variation most similar to that in the Stillwater Complex. With the single exception of analysis 10, total iron decreases regularly from seam 9 to seam 7, then increases regularly to seam 1. The oxidation ratio of the chromite, also calculated in Table 1, shows only that a considerable range of values exists, as would the Stillwater samples if collected at irregular intervals along the strike of the intrusion.

Table 1. Stratigraphic Variation of Iron Content of Chromite from the Hartley Area, Great Dyke of Southern Rhodesia

| Seam No.[1] | Stratigraphic interval[1] (feet) | FeO in clean chromite[1] (Wt. per cent) | $Fe_2O_3$ in clean chromite[1] (Wt. per cent) | Total iron as FeO[2] (Wt. per cent) | $Fe^{2+}+Fe^{3+}$[2] (cations per unit cell) | Oxidation ratio[2] |
|---|---|---|---|---|---|---|
| 1[3] | 0 | 13.33 | 9.90 | 22.24 | 4.81 | .401 |
| 2[3] | 100 | 12.06 | 8.74 | 19.92 | 4.18 | .395 |
| 3 | 460 | Not analyzed | | — | — | — |
| 4 | 1,730 | 9.98 | 9.19 | 18.25 | 3.91 | .453 |
| 5 | 660 | 11.82 | 4.56 | 15.92 | 3.37 | .258 |
| 6 | 390 | 8.88 | 6.76 | 14.96 | 3.17 | .407 |
| 7 | 310 | 9.78 | 5.12 | 14.39 | 3.07 | .319 |
| 8 | 440 | 11.29 | 4.71 | 15.53 | 3.33 | .273 |
| 9 | 380 | 8.80 | 8.15 | 16.13 | 3.44 | .453 |
| 10 | 420 | 10.86 | 4.99 | 15.35 | 3.30 | .291 |

[1] From Worst (1958, Tables 13 and 15).
[2] Calculated from Worst's data.
[3] Chromite analyses 1 HW and 2F are apparently from olivine chromites, and are omitted from this tabulation.

In the Bushveld Complex, about 60 analyses of clean chromite from systematically collected chromitites have been published by deWet (1952a, 1952b, 1956). As the analyses are not complete, balance cannot be checked, but both FeO and $Fe_2O_3$ were determined.

In the western belt of the Bushveld Complex, chromite from a sequence of chromitites in the Swartkop area was analyzed with the results shown in Table 2. Inspection of the table shows that both FeO and $Fe_2O_3$ decrease, then increase stratigraphically upward, but the minimums are reached in different seams. Total iron as FeO decreases from about 25 per cent in the Compound seam to about 20 per cent in the Intermediate seam, stays about the same in the New seam, then increases to about 26 per cent in the Magazine seam. Although the Upper group and Merensky Reef seams were not sampled in this area, it is probable from analyses in other areas that they are richer in total iron than the Magazine. Thus it is not improbable that the chromite compositional variation in this area is similar to that observed in the Stillwater Complex.

In the eastern chromite belt of the Bushveld Complex, deWet made no systematic collections through Lower and Middle group seams at any one locality. Averages of total iron in clean chromite from various localities of the eastern belt show that the Lower group chromite averages about 26 per cent total iron as FeO, Middle group chromite averages about 30 per cent, and one sample from the Merensky Reef gave 36 per cent (deWet, 1952a, Tables I, II, III and 1956, Table IV). There is no suggestion of a reversal.

TABLE 2. STRATIGRAPHIC VARIATION OF IRON CONTENT OF CHROMITE FROM THE SWARTKOP-SCHILPADNEST AREA, WESTERN BUSHVELD COMPLEX

| Seam[1] | Group[1] | No. of analyses[1] | FeO in clean chromite[2] (wt. per cent) | $Fe_2O_3$ in clean chromite[2] (wt. per cent) | Total iron as FeO[2] (wt. per cent) | Oxidation ratio[3] |
|---|---|---|---|---|---|---|
| Magazine | Lower or Middle | Average of 9 | 17.0 | 9.6 | 25.7 | .337 |
| New | Lower | Average of 4 | 14.0 | 6.9 | 20.1 | .307 |
| Intermediate | Lower | Average of 4 | 11.9 | 9.3 | 20.3 | .413 |
| Compound | Lower | Average of 3 | 15.3 | 10.5 | 24.8 | .382 |

[1] From deWet (1952b, p. 1–10).
[2] Average from deWet (1952b, Tables V, VI, VII, VIII).
[3] Calculated from deWet's data.

TABLE 3. LATERAL VARIATION OF IRON CONTENT OF CHROMITE FROM THE LOWER GROUP, EASTERN BUSHVELD COMPLEX

| | Location | | Steelpoort seam and probable equivalents: Total iron as FeO in clean chromite[1] (wt. per cent) | Steelpoort seam and probable equivalents: Oxidation ratio[2] | Steelpoort leader seam: Total iron as FeO in clean chromite[1] (wt. per cent) | Steelpoort leader seam: Oxidation ratio[2] |
|---|---|---|---|---|---|---|
| North ↑ | Jadglust | 333 | 25.4 | .362 | 25.9 | .383 |
| | Winterveld | 343 | 24.8 | .387 | 24.9 | .380 |
| | Mecklenburg | 371 | 26.4 (avg. of 2) | .352 | 25.9 | .322 |
| | Clapham | 364 | 24.1 | .319 | 24.4 | .388 |
| | Twyfelaar | 172 | 25.7 | .322 | | |
| | Mooihoek | 147 | 26.9 | .401 | | |
| | Hendriks Plaats | 357 | 26.5 | .524 | 26.4 | .449 |
| | Winterveld | 424 | 25.4 (avg. of 2) | .388 | 25.2 | .391 |
| | Grootboom | 186 | 26.1 | .210 | 26.9 | .218 |
| | Annex Grootboom | 473 | 25.9 | .243 | | |
| ↓ | Tweefontein | 35 | 25.0 | .244 | | |
| South | Thorncliffe | 217 | 25.1 | .258 | | |

[1] From deWet (1952a, Tables I and II).
[2] Calculated from deWet's data.

DeWet also investigated the lateral compositional variation of chromites from the Steelpoort seam and its probable Lower group equivalents along a strike distance of nearly 60 miles in the eastern belt. His results are summarized in Table 3. The chromites of the Steelpoort seam and of the Steelpoort leader seam just above it have nearly identical total iron contents along the strike; deviation from the average in each is only $\pm 5$ per cent. The oxidation ratios of both seams, on the other hand, appear to decrease regularly from the northernmost exposure to a place near Clapham 364, then to increase strongly to a place near Hendriks Plaats 357, and finally to decrease toward the south; deviation from the mean is almost 40 per cent. This situation would seem to be similar to that found in the Stillwater Complex, where total iron in chromite is nearly constant along the zones, but where oxidation ratio shows wide systemic variations.

## CONCLUSION

The chromitite zones of the Stillwater Complex have been correlated by field mapping. Chemical analyses of chromite from these zones show that the variation in composition within single zones is large; therefore samples from consistent stratigraphic positions and of given rock types must be compared to determine lateral and between-zone compositional

variations. When such samples are compared, a simple variation in total iron between zones is observed, such that $Fe^{2+}+Fe^{3+}$ in the chromite decreases from the lower zones toward the middle zones, then changes, and increases regularly through the upper zones. At the same time, a lateral variation in oxidation ratio of the iron in the chromite is observed such that the ratio of $Fe^{3+}$ to total iron decreases from the eastern and western margins of the complex toward the central part, particularly in the lower chromitite zones. The nature and regularity of the changes permit the prediction of chromite composition within and between the sampled sections.

These systematic changes in composition are believed to reflect differences in magmatic conditions during the crystallization of the chromite. The lateral variation probably represents a persistent oxygen partial pressure gradient across the intrusion. The variation between zones probably represents an early reversal in the trend of magma composition or in crystallization temperature of the chromite during differentiation of the intrusion.

Examination of published chromite analyses from the Bushveld Complex and from the Great Dyke suggests that similar variations in chromite composition may be present in these intrusions.

## References


Dinnin, J. I. (1959) Rapid analysis of chromite and chrome ore. *U. S. Geol. Survey Bull.* **1084-B,** 31–68.

Hess, H. H. (1960) Stillwater igneous complex, Montana. *Geol. Soc. Am. Mem.* **80.**

Howland, A. L. (1955) Chromite deposits in the central part of the Stillwater complex, Montana. *U. S. Geol. Survey Bull.* **1015-D,** 99–121.

———, R. M. Garrels and W. R. Jones (1949) Chromite deposits of Boulder River area, Sweetgrass County, Montana. *U. S. Geol. Survey Bull.* **948-C,** 63–82.

Jackson, E. D. (1961) Primary textures and mineral associations in the Ultramafic zone of the Stillwater complex, Montana. *U. S. Geol. Survey Prof. Paper.* **358.**

———, J. I. Dinnin and H. Bastron (1960) Stratigraphic variation of chromite composition within chromitite zones of the Stillwater complex, Montana (abs.). *Geol. Soc. Amer. Bull.* **71,** 1896.

Jones, W. R., J. W. Peoples, and A. L. Howland (1960) Igneous and tectonic structures of the Stillwater complex, Montana. *U. S. Geol. Survey Bull.* **1071-H,** 281–340.

Miller, R., III (1953) The Webster-Addie ultramafic ring, Jackson County, North Carolina, and secondary alteration of its chromite. *Am. Mineral.* **38,** 1134–1147.

Rait, J. R. (1946) An X-ray investigation into the constitution of chrome ores. *Iron and Steel Inst. (London) Spec. Rept.* **32,** 178–209.

Stevens, R. E. (1944) Composition of some chromites of the Western Hemisphere. *Am. Mineral.* **29,** 1–44.

Thayer, T. P. (1956) Mineralogy and geology of chromium, in *Chromium* New York, Reinhold Publishing Corp., **1,** 14–52.

Wet, J. F. de (1952a) Chromite investigations—Part III, Variations in the composition of the pure chromite mineral from the eastern chrome belt, Lydenburg district. *Jour. Chem. Metall. Min. Soc. South Africa,* **52,** 143–153.

——— (1952b) Chromite investigations—Part IV, Variations in the composition of the pure chromite mineral from the Swartkop-Schilpadnest and Pilansberg areas of the western chrome belt, Rustenburg district. *Jour. Chem. Metall. Min. Soc. South Africa,* **53,** 1–10.

——— (1956) Chrome investigations—Part VI, The vanadium content of Transvaal chromite. *Jour. Chem. Metall. Min. Soc. South Africa,* **56,** 457–462.

Wijkerslooth, P. de (1942) Metamorphose des Chromspinelles in den türkischen Erzlagerstätten. *Maden Tetkik Arama Enst. Mecmuasi (Ankara),* sene **7,** sayi 2/27, 267–289.

Worst, B. G. (1958) The differentiation and structure of the Great Dyke of Southern Rhodesia. *Geol. Soc. South Africa Trans. Proc.* **61,** 283–354.

MINERALOGICAL SOCIETY OF AMERICA, SPECIAL PAPER 1, 1963
INTERNATIONAL MINERALOGICAL ASSOCIATION, PAPERS, THIRD GENERAL MEETING

# FLOW-LAYERING IN ALPINE PERIDOTITE-GABBRO COMPLEXES[1]

T. P. THAYER
*U. S. Geological Survey, Washington, D. C.*

ABSTRACT

Compositional layering in gabbro and peridotite may originate in several ways; in alpine complexes most of it is believed to be flow layering. Disruption of relict primary features formed by crystal settling shows that the flow layers are later.

The flow layers in alpine complexes are not nearly as regular and persistent as those formed by crystal settling in the stratiform complexes, and adjoining layers commonly show much more compositional contrast. Features formed by crystal settling have been observed only as rare relicts in chromitites, and poikilitic and ophitic textures are not common. Tectonite fabrics have been described in alpine dunites from many localities, and gneissic structures are common in related gabbroic rocks. Foliation and lineation are closely related to layering and are mostly parallel to it, but in places they cross it. Boudinage in mafic layers and related structures in chromitite bodies show stretching.

The flow structures in alpine mafic complexes are directly comparable to those seen in other flow-banded intrusives and in high-grade metamorphic rocks. Flow layering, foliation and lineation cross the boundaries between rocks such as chromitite, dunite, harzburgite and gabbro without deviation. The predominant parallelism of layering with foliation and lineation is attributed to extensive flowage of largely crystalline magma during emplacement. Several lines of evidence show that the flowage features could not have been imposed on solid rock by regional deformation.

## INTRODUCTION

Layering in intrusive rocks of gabbroic to peridotitic composition may originate in several ways. The layers in lopolithic stratiform complexes (Brown, 1956; Cameron and Emerson, 1959; Hess, 1960; Jackson, 1961) and in parts of some concentrically zoned intrusives (Ruckmick and Noble, 1959; Taylor and Noble, 1960; Irvine, 1963) are generally believed to have been formed by settling of crystals from fluid magma. Fractional crystallization that does not involve crystal settling accounts for layering in many dikes and larger intrusions. Flow-layering is a widely recognized phenomenon in lavas and intrusive rocks (Balk, 1937), and is believed to be the principal kind found in alpine peridotite-gabbro[2] complexes.

The alpine mafic complexes consist of gabbro and peridotite in all proportions, are irregular in form and structure, and occur along eugeosynclinal belts that have undergone an alpine type of deformation. Various features of alpine mafic rocks have been described in detail in many places by many geologists (Guild, 1947; Hiessleitner, 1952; Smith, 1958; MacKenzie, 1960; Wells *et al.*, 1949), and the critical features have been summarized previously (Thayer, 1960). Tectonite fabrics are now recognized as characteristic of many alpine peridotites (Turner, 1942; Lacroix, 1943; Marinos and Maratos, 1957; MacKenzie, 1960), and have also been described in some gabbroic rocks (Bartrum and Turner, 1938; Thayer, 1942; Stoll, 1958; MacKenzie, 1960). This paper describes features in both gabbro and peridotite that are comparable to phenomena in gneisses (Balk, 1937) and can be ascribed only to flowage in a semi-solid state. Except where explicitly stated otherwise, the discussion that follows is concerned only with alpine peridotite and gabbro.

The descriptions and conclusions in this paper are based principally on personal observations over several years in the United States and Cuba; on visits to the Philippines, New Caledonia and New Zealand in 1959; and to Yugoslavia, Greece, Turkey, Iran and Pakistan in 1960. Discussions with C. E. Brown, D. L. Rossman, P. W. Guild and F. G. Wells, in the field and in the office, have led to recognition of the features characteristic of alpine mafic rocks. Because of his intimate knowledge of the Stillwater Complex, E. D. Jackson has been especially helpful and stimulating in relating the features and evolution of alpine peridotites to those of stratiform complexes.

## PRIMARY LAYERING

Unequivocal relict textures and structures that antedate flow-layering in alpine mafic rocks have been identified only in chromitites, especially in large massive ore bodies. Mesh textures formed by fine-grained euhedral chromite interstitial to large olivine crystals, mixed large crystals and nodules of chromite in dunite or troctolite (Thayer, 1942, Pl. 4),

[1] Publication authorized by the Director, U. S. Geological Survey.

[2] For convenience the gabbroic and peridotitic rocks are referred to collectively as mafic.

FIG. 1. Parallel flow-layering in peridotite and gabbro. Note thin layers at upper right. Canyon Mountain, Grant County, Oregon.

trbicular structures in chromite and dunite (Wells ond others, 1949, Pl. 10, 11), and some dunitic and aroctolitic layers in massive chromitite (Guild, 1947, p. 231) appear to have been formed by variations of the crystal settling mechanism. Descriptions of these structures in various stages of mechanical disruption are numerous in the literature on chromite. The competence of the chromite relative to associated silicates apparently preserved the original or primary textures and structures. These relict features imply that the alpine complexes essentially are partially refused and remobilized parts of huge settled complexes formed deep in the crust or mantle. I suggest, therefore, that the term "primary" be restricted in alpine complexes to relict layers or features comparable to those in known stratiform complexes.

## PARALLEL FLOW-LAYERING, FOLIATION AND LINEATION

In most exposures flow-layering in gabbro and peridotite (fig. 1) appears parallel and uniform over strike distances of tens or hundreds of feet. In relatively small exposures (Fig. 2) the layers may seem remarkably uniform and clearly defined. Careful examination usually reveals, however, that the layers are lenticular and pinch or grade out in a few feet or tens of feet; their lateral extent does not compare with the persistence of layers in stratiform complexes.

Flow-layers may be monomineralic as well as polymineralic. The individual layers in a given series may differ widely in composition and occur in any order. Dunite, anorthosite and pyroxene gabbro, for example, may be intimately interlayered in a manner never seen in stratiform complexes. The boundaries between layers may be sharp or gradational (Fig. 2) and change along the strike. The texture of the rocks is xenomorphic granular (Stoll, 1958, p. 424), and in hand specimen the gabbroic varieties resemble high-grade metamorphic gneisses (Stoll, p. 426). The average grain size varies widely, ranging from about a millimeter to 10 cm in pegmatitic layers (Fig. 3). The textures of the pegmatitic layers in outcrop resemble the textures of fine-grained layers in thin section.

Foliation and lineation characterize flow-layers (Figs. 2, 3). Foliation, shown by planar orientation of individual grains or clusters of grains, and layering intergrade to an extent that presents frequent problems in mapping. Lineation, shown by arrangement of mineral grains in lines, is present more commonly than not. Lineation and foliation may occur together or independently in unlayered rocks. Poikilitic, diabasic and cuspate textures, which characterize many rocks in stratiform complexes (Jackson, 1961, p. 23), are rarely found.

The textures and structures in chromitites correspond directly to those in the silicate rocks, although they are expressed somewhat differently. Layering of chromite, olivine and mixtures of the two minerals in all proportions is prominent in many chromite deposits, and remarkable lineation and boudinage occur in some (Guild, 1942; Wells *et al.*, 1949). In many chromite deposits lineation is shown by elongate lenses of dunite in chromite (Fig. 4), or the reverse. The chromite uniformly is anhedral, crystals being rare, and stretching (pull-apart texture) is shown by rude orientation of the wider intergrain silicate seams (Stoll, 1958, Pl. 3, Fig. 3) normal to the axis of lineation. In massive ores pull-apart texture may be the only indication of lineation.

Layers covering the entire range in composition

FIG. 2. Parallel foliation in interlayered gabbro and peridotite. Note sharp contact between anorthositic and peridotitic layers in left edge of block. Canyon Mountain, Grant County, Oregon.

FIG. 3. Gneissoid pegmatitic hypersthene gabbro interlayered with olivine-rich peridotite (left). Compare texture with that of dike in Fig. 10. Canyon Mountain, Grant County, Oregon.

from chromitite and dunite to anorthositic gabbro show similar behavior in folding. All layers characteristically thicken at the crests of simple folds, and boudinage is developed in the more mafic layers and in chromitites (Wells *et al.*, 1949; Guild, 1942). Nearly all varieties of folds may be found, from open (Fig. 8) to tight and complex (Fig. 9).

### DISCORDANT FLOW-LAYERING, FOLIATION AND LINEATION

Discordances between flow-layering on the one hand and foliation and lineation on the other provide clues to complex variations in magmatic movements

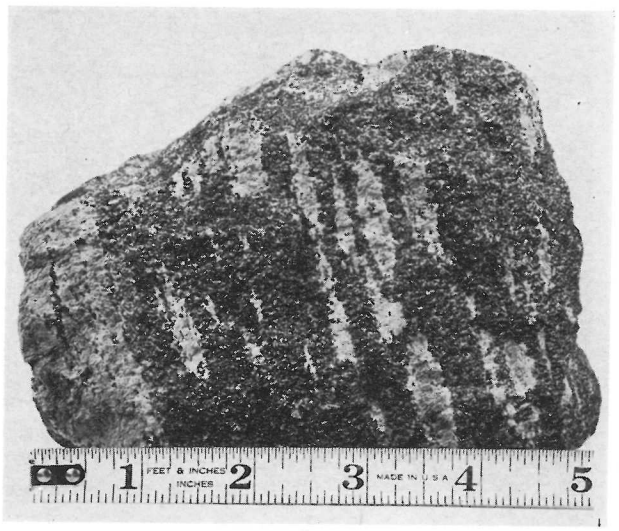


FIG. 4. Elongate lenses of serpentinized dunite in anhedral chromite. Pulling apart of chromite (pull-apart texture) during differential flow of dunite is shown by rudely oriented fractures normal to axis of lineation. Coto Mine, near Masinloc, Luzon. Scale in inches.

FIG. 5. Lineation crossing pyroxenite layer in gabbro. Axis of lineation is parallel to knife, which is about 4 inches long. Canyon Mountain, Grant County, Oregon.

during emplacement. Foliation oblique to unfolded layering in peridotite has been described in Cuba by Guild (1947, p. 232). This and several other aspects of discordant foliation and lineation are shown in Figs. 5 to 9. Figure 5 shows lineation obliquely crossing interbanded gabbro and pyroxenite. Analogous discordant structural relations in layered gabbro (Fig. 6) and chromitite in peridotite (Fig. 7) show that both have undergone the same kind of deformation. The layered gabbro in figure 6 shows good line-

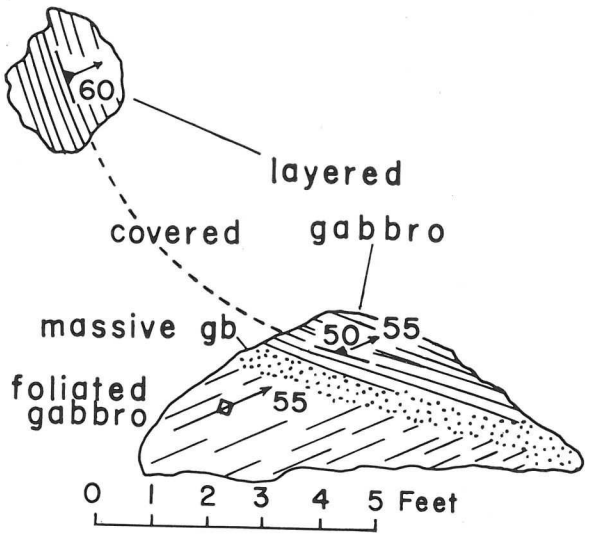


FIG. 6. Map showing relations of lineation that plunges uniformly 55°–60° NE., to layering and vertical foliation in gabbro. In the smaller outcrop lineation parallels the layering, but in the larger it strikes obliquely across and plunges steeper than the layering dips. Canyon Mountain, Grant County, Oregon.

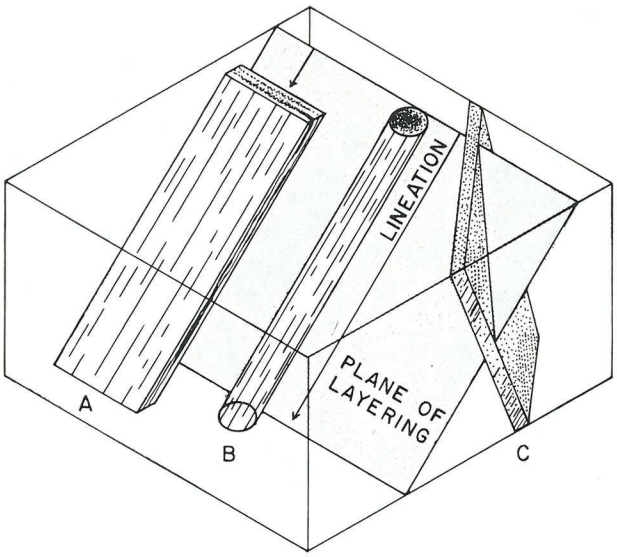


FIG. 7. Diagram showing relations of three types of chromite deposits to plane of layering and lineation in host rock peridotite: A, Extensive tabular; B, fusiform; C, crosswise. Banding is shown by solid lines on surfaces parallel to the axis of lineation and by rows of dots on surfaces oblique or normal to it, to indicate the relative evidence in corresponding outcrops.

ation; in the smaller exposure the lineation plunges directly down the dip, but in the larger one it plunges obliquely across the layers more steeply than the dip. The vertical foliation in the larger outcrop is prominent and the lineation is alined precisely within it. Massive gabbro with indeterminate contacts occupies a zone 6 to 12 inches wide between the foliated and layered facies; it appears to be material in which the layering was destroyed and new foliation was not developed. Nearby gabbro exposures show only the lineation. Chromite deposit C in Fig. 7 lies across the layering in the host rock peridotite but shows internal lineation and foliation in the plane of the peridotite layering, just as the two accordant deposits do. The contact relations, textures, and composition of the chromite in all three types of ore bodies may be identical. For example, the 10 million-ton Coto (Masinloc) deposit (Stoll, 1958), nearby ore bodies on Reservation Number 1 (Rossman *et al.*, 1959, p. 6) and two major ore bodies at the Acoje mine in Luzon Philippine Republic, show "crosswise" relations, whereas most of the large ore bodies at Acoje are accordant (D. L. Rossman, written communication, 1960). At Coto the chromite is anhedral (Stoll, 1958, p. 437), the chromite ore body is surrounded by a halo of dunite, and the long dimension of the ore body extends about 1800 feet across the layering in the host rock peridotite. Lineation in the ore, however, is alined with the plane of the layering in the peridotite.

In some places two episodes of deformation separated by intrusion of dikes are suggested, as for instance, by the rocks shown in Figs. 8 and 9. The two figures show three sides of one outcrop. Figure 8 shows three sharply bounded dikes, the middle one only about half an inch thick, of plagioclase- and olivine-bearing pyroxenite crossing an open fold in layered olivine gabbro. Some of the layers in the gabbro are only 1 or 2 mm thick. Two of the dikes follow a strong foliation; the third widens irregularly and crosses the foliation. All the dikes show the same strong lineation that plunges steeply down the axis of the fold in the olivine gabbro, and shows in the right side of the view. Figure 9 shows complex folding in an anorthositic layer exposed on a joint face across the foliation and lineation. The foliation in the lower part of the view approaches layering in its development and parallels layering in nearby outcrops.

FIG. 8. Dikes of pyroxenite (py) crossing folded layers (line of dots) in olivine gabbro. All of the rocks show the prominent lineation seen on the right-hand face of the outcrop. View downward from northeast toward upper corner (marked by knife) of outcrop; compare with Fig. 9. Canyon Mountain, Grant County, Oregon.

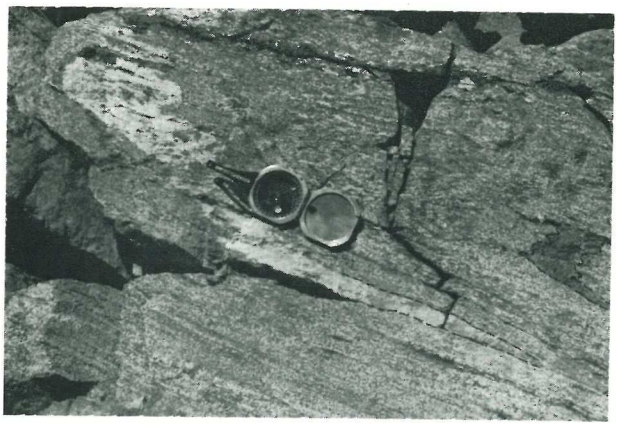

FIG. 9. Thickening of anorthositic and mafic layers in gabbro along crest of relict fold in foliated and lineated olivine gabbro. The lineation plunges parallel to the axes of the folds. View of part of vertical joint face on south side of the outcrop shown in Fig. 8.

In thin section the dikes and gabbro alike show deformation lamellae in olivine, undulatory extinction and disruption in clinopyroxene and plagioclase and granulation along grain boundaries.

## RELATIONS OF FLOW STRUCTURES TO MAJOR ROCK UNITS

The relations of flow layering, foliation, and lineation in alpine mafic rocks are directly comparable to metamorphic structures in sedimentary rocks. In contrast to primary layering in stratiform complexes, which controls and parallels the distribution of the various rocks, flow layering consistently crosses the boundaries between major rock units. The relations of layering to chromitite, saxonite, dunite, and gabbro in the vicinity of the Coto mine in the Philippines are described by Rossman *et al.* (1959) as follows:

"Field work has shown that the layered structure, but not necessarily individual layers, extends across lithologic boundaries without deviation. Thus there does not appear to be any correlation between the attitude of the contacts and the attitude of the layered structures. . . . (p. 5). [Layering] shows no recognizable control over the shape or location of the chromite. The ore deposits are typically irregular in shape but the layered structure in the enclosing rocks is homoclinal and remarkably uniform." (p. 6)

## DIKES

Although some irregular pegmatitic masses and dikes show deformation like that in Fig. 3 to various degrees, undeformed gabbro dikes are common features in many alpine complexes, even where large masses of gabbro are not known. The gabbro dikes shown in Fig. 10 are typical; they cross obscure and irregular structure in feldspathic peridotite. The wide range and abrupt changes in grain size match the textures described in Cuba by Guild (1947, p. 228) and Thayer (1942, p. 24). Most dikes are sharply bounded by matching walls, show no chilling at the borders, and cut at random across flow structures and other boundaries between lithologic units.

## DISCUSSION

Practically all the layering we see in alpine mafic rocks is believed to be flow-layering. The prevalence of foliation and lineation, cross-cutting relations of layered structures across major lithologic boundaries, random distribution of rock types, great lithologic contrast between adjoining layers, and lack of cryptic layering (Wager, 1953) are completely at variance with the normal relations of primary layers in stratiform complexes. Obvious disruption of primary features where found, comparatively rarely, in competent chromitite masses shows that the flow structures are later. The prevailing parallelism between layering, foliation, and lineation, and especially the

FIG. 10. Branching dikes of medium-grained and pegmatitic gabbro crossing rude banding in feldspathic peridotite. The hammer lies on an irregular band of olivine-rich peridotite. Canyon Mountain, Grant County, Oregon.

common gradations between layering and foliation, show that the layering and other flow structures are closely related genetically.

In some places two generations of flow structures can be recognized, both apparently unrelated to any primary layering. The olivine-rich nature of some of the gabbroic layers in Figs. 6 and 8, for example, indicates that they are not primary; because any textural criteria would have been obliterated by flowage, compositional variation is of utmost importance. The cross-cutting relations of foliation show that it is younger than the layering in both figures. The crosswise chromite deposits, likewise, are believed to be relatively competent relict masses that were oriented in one direction by early flowage and deformed by later flowage from another direction. It would seem, furthermore, that good compositional layering can be developed in peridotite and gabbro, while lineation only is formed in chromitite under similar conditions.

Several lines of evidence show that the flow structures were developed under magmatic conditions during emplacement. All the features described have been found in fresh or only slightly altered rocks, which commonly are cut by dikes of dunite, peridotite, or gabbro. There is little correlation between development of flow structures in the mafic rocks and metamorphic grade of the country rocks; some of the best layered complexes are in unfoliated terranes. The many consistent differences between alpine and stratiform mafic rocks (Thayer, 1960), including composition (Hess, 1938), cannot be explained by tectonic disruption and regional metamorphism of stratiform rocks (Helke, 1962).

The dikes show a complex magmatic history. Most dikes, whether of dunite or gabbro or intermediate composition, are undeformed. Because the dikes are limited to the mafic plutons and gabbroic types are by far most abundant, they are believed to have been generated locally by movement of interstitial rest magma into fractures. Their generally undeformed nature, accordingly, implies that flowage of the rocks as a whole ceased before consolidation of the rest magma. In eastern Oregon, however, some pegmatitic gabbro dikes and small intrusive masses show all degrees of deformation up to that shown in Fig. 3; it seems clear that there dike-intrusion and magmatic flowage overlapped considerably. The relations in Figure 8 suggest that layering may have been formed partly by extensive deformation of dikes intruded along foliation.

The evidence seems conclusive that in alpine complexes gabbroic as well as peridotitic rocks were emplaced as semisolid crystal mushes in which the ratio of solids to liquid was too high to permit crystal settling, even of coarse-grained chromite. The rarity of relict primary features implies that practically all of the layering we see was formed during emplacement, perhaps partly by remixing of predifferentiated rocks, and partly by processes akin to metamorphic differentiation. The aggregate movement by flowage must have been several kilometers, and may have been several tens of kilometers.

## References


Balk, Robert (1937) Structural behavior of igneous rocks. *Geol. Soc. Am. Mem.* **5,** 177 p.

Bartrum, J. A. and F. J. Turner (1928) Pillow-lavas, peridotites and associated rocks of northernmost New Zealand. *New Zealand Inst. Trans.* **59,** 98–138.

Brown, G. M. (1956) The layered ultrabasic rocks of Rhum, Inner Hebrides. *Royal Soc. London Philos. Trans.* B. **240,** 1–53.

Cameron, E. N. and M. E. Emerson (1959) The origin of certain chromite deposits of the eastern part of the Bushveld complex. *Econ. Geol.* **54,** 1151–1213.

Guild, P. W. (1942) Chromite deposits of Kenai Peninsula, Alaska. *U. S. Geol. Survey Bull.* **931-G,** 139–175.

——— (1947) Petrology and structure of the Moa district, Oriente Province, Cuba. *Am. Geophys. Un. Trans.* **28,** 218–246.

Helke, Adolf (1962) The metallogeny of the chromite deposits of the Guleman district, Turkey. *Ecoon. Geol.* **57,** 954–962.

Hess, H. H. (1960) Stillwater igneous complex, Montana, a quantitative mineralogical study. *Geol. Soc. Am. Mem.* **80,**

——— (1938) A primary peridotite magma. *Am. Jour. Sci. 5th ser.* **35,** 321–344.

Hiessleitner, G. (1952) Serpentin- und Chromerz-Geologie der Balkanhalbinsel und eines Teiles von Kleinasien. *Austria, Jahrb. Geol. Bundesanst. Sonderbd.* **1.**

Irvine, T. N. (1963), Mineralogy and petrology of the ultramafic complex at Duke Island, Southeast Alaska. *Mineral. Soc. Am., Spec. Paper* **1.**

Jackson, E. D. (1961) Primary textures and mineral associations in the Ultramafic zone of the Stillwater complex, Montana. *U. S. Geol. Survey Prof. Paper,* **358.**

Lacroix, Alfred (1943) Les peridotites de la Nouvelle Calédonie, leurs serpentines et leurs gîtes de cobalt, les gabbros qui les accompagnent. *Extrait Mem. Inst. France.*

MacKenzie, D. B. (1960) High-temperature alpine-type peridotite from Venezuela. *Geol. Soc. Amer. Bull.* **71,** 303–318.

Marinos, G. and G. Maratos (1957) Greek olivinites, *Greece Inst. Geol. Subsurface Res.,* **5,** (In Greek, English abstract).

Rossman, D. L., N. S. Fernandez, C. A. Fontanos and Z. C. Zepeda (1959) Chromite deposits on Insular Chromite Reservation Number One, Zambales, Philippines. *Philippine Bur. Mines, Spec. Proj. Series Publ.* **19.**

RUCKMICK, J. C. AND J. A. NOBLE (1959) Origin of the ultramafic complex at Union Bay, southeastern Alaska. *Geol. Soc. Am. Bull.* **70,** 981–1017.

SMITH, C. H. (1958) Bay of Islands igneous complex, western Newfoundland. *Canada Geol. Surv. Mem.* **290.**

STOLL, W. C. (1958) Geology and petrology of the Masinloc chromite deposit, Zambales, Luzon, Philippine Islands. *Geol. Soc. Am. Bull.* **69,** 419–448.

TAYLOR, H. P. JR. AND J. A. NOBLE (1960) Origin of the ultramafic complexes in southeastern Alaska. *Intern. Geol. Cong. Rept. XXI Sess.* **13,** 175–187.

THAYER, T. P. (1942) Chrome resources of Cuba. *U. S. Geol. Survey Bull.* **935-A,** 1–74.

——— (1960) Some critical differences between alpine-type and stratiform peridotite-gabbro complexes. *Inter. Geol. Cong., Rept. XXI Sess.* **13,** 247–259.

TURNER, F. J. (1942) Preferred orientation of olivine crystals in peridotites, with special reference to New Zealand examples. *Royal Soc. New Zealand Trans.* **72,** 280–300.

WAGER, L. R. (1953) Layered intrusions. *Dansk Geol. Foren. Meddel.* **12,** 335–349.

WELLS, F. G., C. T. SMITH, G. A. RYNEARSON AND J. S. LIVERMORE (1949) Chromite deposits near Seiad and McGuffy Creeks, Siskiyou County, California. *U. S. Geol. Survey Bull.* **948-B,** 19–62.

MINERALOGICAL SOCIETY OF AMERICA, SPECIAL PAPER 1, 1963
INTERNATIONAL MINERALOGICAL ASSOCIATION, PAPERS, THIRD GENERAL MEETING

# NORITIC ANORTHOSITE BODIES IN THE SIERRA NEVADA BATHOLITH

ALDEN A. LOOMIS[1]
*Department of Geology, Stanford University, Stanford, California*

ABSTRACT

A group of small noritic plutons were intruded prior to the immediately surrounding granitic rocks in a part of the composite Sierra Nevada batholith near Lake Tahoe. Iron was more strongly concentrated in the late fluids of individual bodies than during the intrusive sequence as a whole. Pyroxenes are more ferrous in rocks late in the sequence, although most of the iron is in late magnetite which replaces pyroxenes. Both Willow Lake type and normal cumulative layering are present. Cumulative layering is rare; Willlow Lake layering is common and was formed early in individual bodies. Willow Lake layers require a compositional uniqueness providing high ionic mobility to explain observed relations.

The Sierran norites differ from those in large stratiform plutons in that (1) the average bulk composition is noritic anorthosite in which typical rocks contain over 20% $Al_2O_3$, and (2) differentiation of both orthopyroxene and plagioclase produced a smooth progressive sequence of mineral compositions. A plot of modal An *vs.* En for all the rocks in the sequence from early Willow Lake-type layers to late norite dikes defines a smooth non-linear trend from $An_{88}$-$En_{76}$ to $An_{43}$-$En_{54}$. The ratio An/Ab decreased faster than En/Of until the assemblage $An_{50}$-$En_{65}$ was reached and En/Of began to decrease more rapidly. Similar plots for large stratiform bodies show too much scatter to define single curves. Temperature gradients of 40°–50° C. within the magma chambers and variable convection patterns could account for the observed variations.

## INTRODUCTION

A group of consanguineous intrusions crops out around Eagle Lake, just southwest of Emerald Bay, Lake Tahoe in the fifteen-minute Fallen Leaf Lake quadrangle, California. The rock types in the sequence, from oldest to youngest, are (1) noritic anorthosite and leuconorite, (2) hypersthene diorite, (3) hornblende quartz diorite and (4) hornblende-biotite quartz diorite with minor granodiorite. The two oldest groups of rocks will be called the Eagle Lake sequence; their generalized relations with other rocks is shown in Fig. 1. The noritic anorthosite-hypersthene diorite sequence comprises many small bodies with complex intrusive relations among one another. The bodies are not separated in Fig. 1.

The term noritic anorthosite is used for rocks with color index more than 10 and less than $22\frac{1}{2}$ (Buddington, 1939, p. 19), and plagioclase more calcic than $An_{50}$. Those rocks with plagioclase more sodic than $An_{50}$ are called hypersthene diorites. The entire series is of interest because of its unusual composition considering its position in the composite Sierra Nevada batholith, its layered structures, and its consistent trend of mineral compositions with decreasing age.

The quartz diorite and minor granodiorite bodies listed as numbers 3 and 4 above intrude the noritic rocks. They are shown as younger intrusive rocks in Fig. 1. Many of the quartz diorite bodies have hypersthene grains rimmed with olive or brownish olive hornblende. The largest quartz diorite body contains local Willow Lake type combed layers as rims aroun l inclusions and as thin sheets on internal intrusive contacts. The present volume of the earlier noritic rocks is only about 10 per cent of that of the later quartz diorites.

## COMPOSITION AND TEXTURES

The rocks of the noritic sequence are much more feldspathic than the more common early gabbros and diorites of this part of the Sierra Nevada (Loomis, 1961). Compton (1961) and Taubeneck and Poldervaart (1960) have reported similar noritic rocks from the northern Sierra Nevada and the Wallowa batholiths, respectively, and rocks of this composition may prove to be more common than originally thought. The more leucocratic norites from the San Marcos gabbro of the Southern California batholith (Larsen, 1948) are also quite similar. All have similar textures and appear to be early relative to their immediate surroundings. Modes, chemical analyses, and norms of two hypersthene diorites are given in Table 1.

Each body in the Eagle Lake sequence is structurally an individual intrusion with foliation which generally parallels contacts and truncates structures in older adjacent bodies. Combed Willow Lake-type layering (Taubeneck and Poldervaart, 1960) lies along many intrusive contacts within the complex, and may or may not be broken and deformed by later magmatic movements. Cumulative layering has been found in large blocky inclusions in younger noritic rocks. The foliate and lineate fabrics of indi-

[1] Present address: California Institute of Technology, Jet Propulsion Laboratory, Pasadena, California.

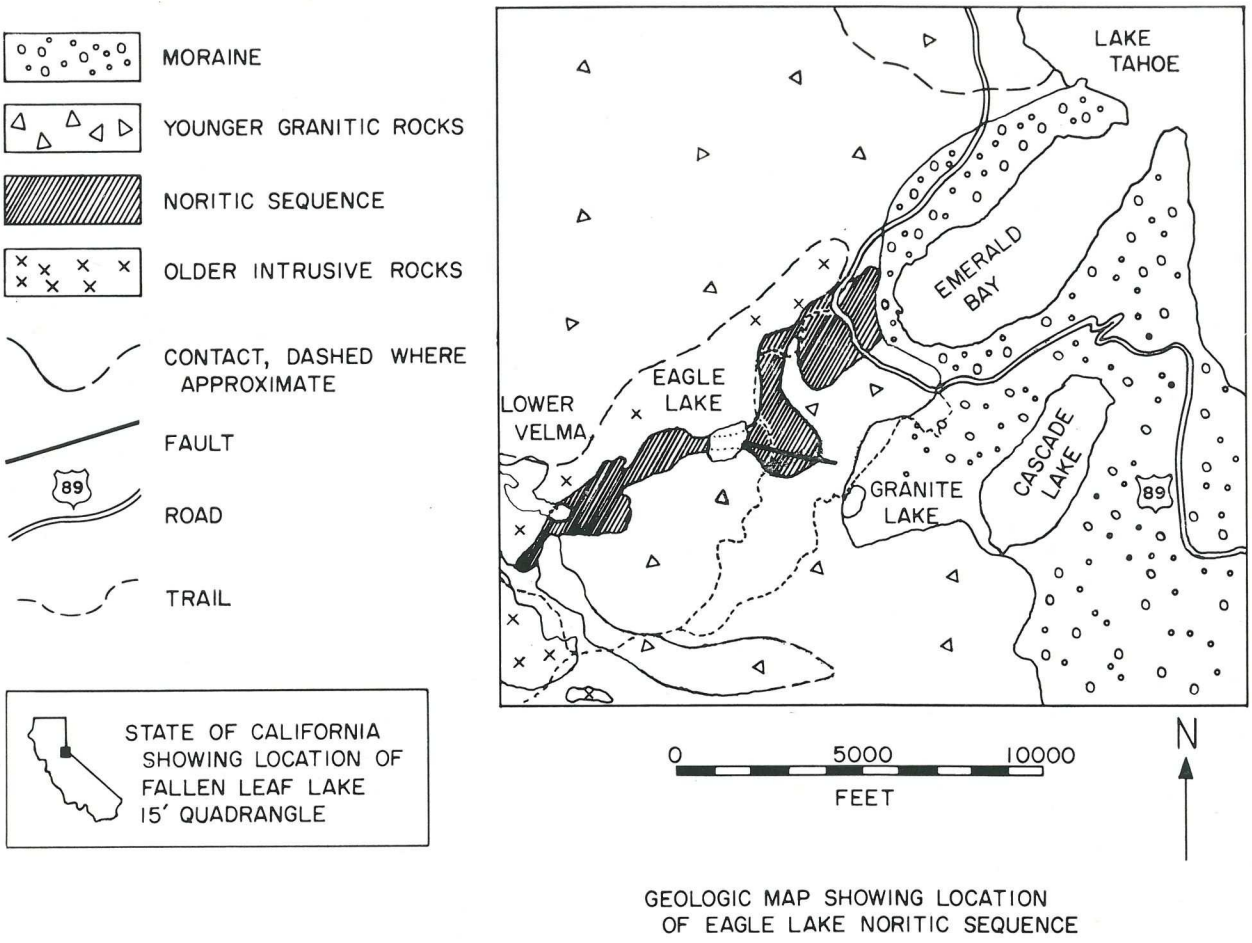


FIG. 1. Generalized geologic map of the northeast part of the Fallen Leaf Lake 15-minute quadrangle.

TABLE 1. MODES, ANALYSES AND NORMS FOR TWO SPECIMENS FROM THE EAGLE LAKE SEQUENCE

| *Modes, Vol. %* | | | *Analyses, Wt. %* | | | *Norms, Wt. %* | | |
|---|---|---|---|---|---|---|---|---|
| | *593* | *600* | | *593* | *600* | | *593* | *600* |
| plagioclase | 81.7 | 75.8 | $SiO_2$ | 52.2 | 51.3 | apatite | 0.3 | 0.7 |
| orthoclase | 0.7 | 0.1 | $Al_2O_3$ | 21.7 | 20.2 | ilmenite | 0.6 | 2.0 |
| quartz | none | 0.4 | $TiO_2$ | 0.3 | 1.1 | magnetite | 4.9 | 5.6 |
| hypersthene | 9.5 | 8.4 | $Fe_2O_3$ | 3.3 | 3.9 | orthoclase | 3.3 | 2.1 |
| augite | 2.7 | 1.7 | FeO | 5.2 | 4.3 | plagioclase | 77.1 | 70.8 |
| hornblende | 1.0 | 2.5 | MnO | nd | 0.12 | diopside | 2.3 | 5.3 |
| biotite | 0.3 | 1.1 | MgO | 3.8 | 3.6 | hypersthene | 11.1 | 12.7 |
| magnetite | 4.0 | 4.9 | CaO | 8.8 | 8.6 | quartz | 1.2 | 0.8 |
| apatite | 0.1 | 0.2 | $Na_2O$ | 4.0 | 4.35 | | | |
| calcite, chlorite | none | 5.0 | $K_2O$ | 0.5 | 0.35 | normative An | 50 | 47 |
| | | | $H_2O^+$ | nd | 1.4 | normative En | 66 | 70 |
| modal An | 45 | 45 | $P_2O_5$ | 0.1 | 0.30 | | | |
| modal En | 60 | 68 | $CO_2$ | nd | 0.54 | | | |
| density | 2.88 | 2.84 | | | | | | |
| | | | Total | 99.9 | 100.06 | | | |

Analysis *593* by Albert G. Loomis.
Analysis *600* by E. L. P. Mercy.

vidual plutons are not directly related to either type of layering.

Most of the plagioclase and orthopyroxene in the plutons crystallized before development of foliation. The bulk of the augite present crystallized after the bodies had been emplaced and the fabrics had been developed. Subhedral and euhedral plagioclase tablets define a flow foliation (exclusive of the layered structures) and *c*-axes of subhedral bronzite or hypersthene grains define a lineation in the foliation plane. Augite occurs both as discrete crystals or as jackets surrounding the orthopyroxenes. Much augite is poikilitic, enclosing several pyroxene and plagioclase grains. Olive-green to brownish-olive hornblende has jackted and partially replaced the pyroxenes and plagioclase. Hornblende rims are commonly continuous around several grains which are aligned in the fabric; therefore, most, if not all, of the hornblende crystallized after the internal movements of the bodies had ceased. Amounts of hornblende vary; amphibolization is described below. Magnetite crystallized subsequently or nearly contemporaneously with hornblende. It replaces pyroxenes and hornblende and is interstitial to plagioclase, pyroxenes, and hornblende. Late deuteric alterations are local. Common minerals include chlorite, actinolite, biotite, and calcite.

Figure 2 illustrates a common texture in the noritic anorthosite. Single hornblende grains surround pyroxenes and replace plagioclase. The bulk of the

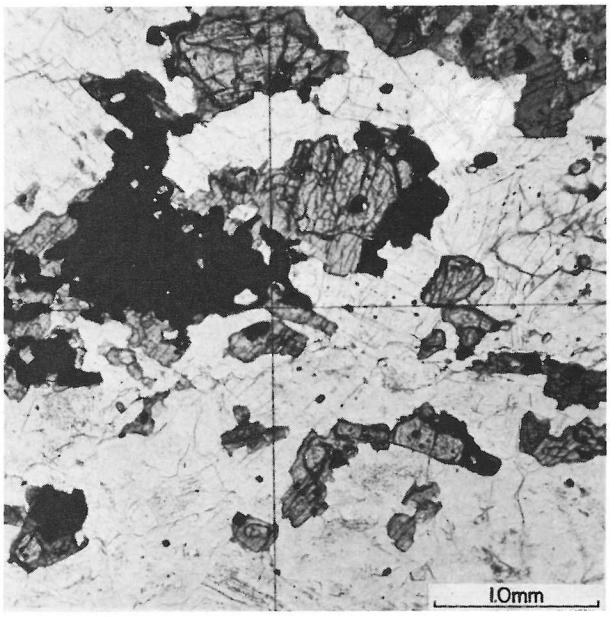


FIG. 2. Noritic anorthosite specimen 622. Olive-green hornblende rims pyroxenes. Magnetite, commonly with apatite inclusions, is late, fills voids, and replaces pre-existing mafic grains.

FIG. 3. Irregular mode of amphibolization in hypersthene diorite near contact with another hypersthene diorite at lower left.

magnetite is late; it replaces and is interstitial to earlier phases. The small colorless grains in the ore are apatite. The amount of magnetite varies very little within the complex, generally forming 4 to 5 volume per cent of the rocks. The amount of hornblende is quite variable, however, as is the presence of deuteric alteration. The rocks are amphibolized particularly along contacts and fractures, as in Fig. 3. Figure 4 is a cumulative mode diagram of 14 specimens in varying states of alteration. The extent of actual replacement of plagioclase by hornblende, not only the reaction of pyroxene and plagioclase to hornblende, is illustrated by the changes from the fresh rock No. 593 to the amphibolized No. 622. Although the volume percentage of hornblende in-

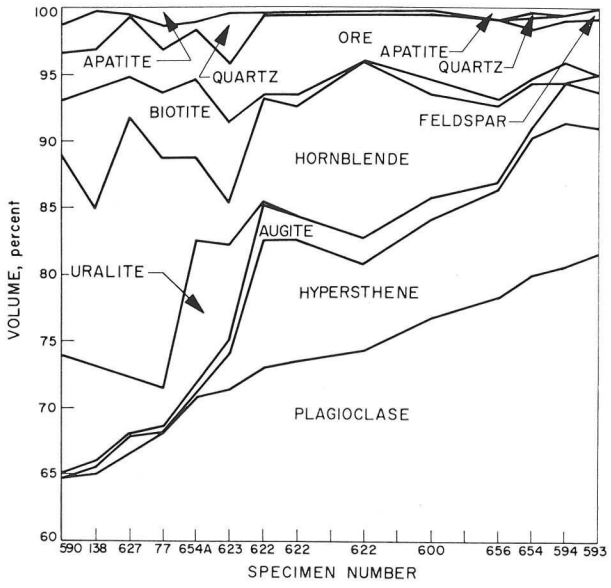


FIG. 4. Cumulative modes of 14 noritic anorthosites and hypersthene diorites which had very similar modes prior to amphibolization and deuteric uralite, quartz and biotite.

creases from a minimum of zero per cent to a maximum of 13 per cent, the volume of the pyroxene shows a complementary decrease of 4 per cent or less. The volume now occupied by green hornblende was originally occupied mostly by plagioclase. The pyroxenes remaining after the amphibolization and introduction of late magnetite were uralitized locally, and some deuteric biotite and quartz formed. These alterations took place mainly near contacts with older plutons and where the rocks were intruded by the surrounding quartz diorites.

Iron was more strongly concentrated during the crystallization of any one body than during the entire intrusive sequence. The late magnetite in each body is more important than the effect of the iron increase due to changing orthopyroxene composition during the whole sequence. Somewhat more than half of the bulk iron in the rocks exists in the late magnetite. As each individual body crystallized, the iron was strongly concentrated in the late fluid. The entire sequence comprises many small intrusions, and the Fe/Mg ratio increased slowly throughout the sequence as will be described below. But iron enrichment was much more extreme within each small body of magma after it separated from the main mass and crystallized independently.

## Layered Structures

The noritic rocks contain both normal cumulative layering which was formed early in the sequence, and Willow Lake-type layering which formed early in each individual body. The cumulative layers are now seen largely as inclusions in younger norites. They have very good foliation defined mainly by plagioclase tabular on (010). Rhythmic compositional

Fig. 5. Hand specimen with cross-laminated cumulative layers.

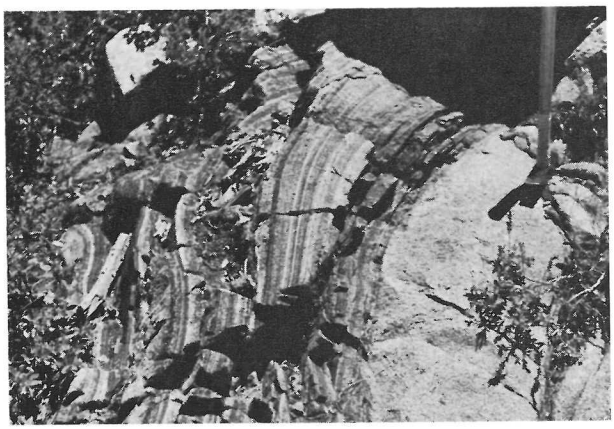

Fig. 6. Combed layers along intrusive contact (covered at left). Hammer is in foliation plane of younger rock which contains layers.

layering is very subtle and is only expressed by changes in color index over thicknesses on the order of 1 cm. Cross-bedding indicating current deposition is present locally and in any one outcrop the tops are consistent. Figure 5 shows bedding dipping 20° to the left truncated at the top by horizontal layers. The cumulative layers contain the most magnesian orthopyroxene and most calcic plagioclase in the sequence. No olivine has been found. Augite is much less abundant than the bronzite, as is the case in normal rocks later in the sequence. The Willow Lake-type layers, however, have much more clinopyroxene than orthopyroxene.

The Willow Lake layers (Fig. 6) lie along intrusive contacts and form rims around inclusions which may be of Willow Lake layers themselves. The crystals stand normal or at high angles to the plane of the layering. The plane of the layering is commonly vertical. The thickness of most individual layers is 0.1 to 2 inches. Groups consist of 5 to 20 individual layers and average about one foot thick, although some are 5 feet thick. When followed along strike, a group of layers may diverge smoothly, include a lens of normal rock, and reconverge. A given group normally contains the same number of individuals no matter how much its thickness varies; the individuals thicken or thin together as the group thickens or thins. The variation in thickness of a group is the result of the crystals in the layers having varied in length in the same way in all of the layers. The Willow Lake layers are distinguished from the better known harrisitic structures in that the latter are upward growth from previously deposited cumulate layers. Descriptions of harrisitic rocks indicate that nucleation takes place on accumulated grains; the large crystals grow upward but commonly become

FIG. 7. Branching bytownite crystals from Willow Lake layer. Note discontinuous, bladed albite twins.

highly poikilitic and reach sizes of several inches to a foot (Brown, 1956).

The plagioclase, augite and hornblende crystals in the Willow Lake layers are long and feathery. Sheaves of crystals are commonly plumose above discrete centers at the base of the layer. Longer branching crystals truncate shorter ones as they diverge from the base of the layer. Figure 7 shows a common habit of plagioclase. Albite and Carlsbad twinning predominate; many albite twins are discontinuous along the length of the crystal and in three dimensions are curving blades up to 10 mm long. Some plagioclase grains are zoned primarily along their length, and a wave of progressive extinction passes along the bladed albite lamallae on rotation of the stage.

The primary mineralogy of the layers is plagioclase; plagioclase-augite; plagioclase-augite-hypersthene; and brown hornblende-plagioclase. The brown hornblende is primary in some layers. Figure 8 is a photomicrograph of primary brown hornblende and plagioclase with minor augite and magnetite. The hornblende does not contain partially digested remnants of pyroxenes and the pyroxenic layers immediately above and below are quite free of hornblende. The texture of the hornblende is unlike the textures of augite in these layers. The hornblende crystals have a greater length to width ratio and tend to form clusters of branching crystals. The elongated augites are commonly curved. Both species are commonly repeatedly twinned on (100). Augite is much more abundant than bronzite and forms feathery crystals whereas bronzite does not. The preferential occurrence of augite, which is subordinate to orthopyroxene throughout the rest of the sequence, suggests that special conditions obtained during crystallization of the combed layers. Presumably, crystals which could nucleate and grow quickly were favored. The combed texture suggests, but does not prove, rapid crystallization on solid surfaces. The sympathetic thinning or thickening of several layers (shortening or elongation of crystals) indicates that several layers could grow while some local environmental condition on the order of several feet tended to promote or retard growth. The occurrence of primary hornblende layers indicates that water pressure became high at times. The occurrence of pyroxenes in layers adjacent to hornblende layers and small amounts in hornblende layers themselves suggests that water pressure was maintained close to the amphibole-pyroxene phase boundary by crystallization of either phase.

Taubeneck and Poldervaart (1960) have attempted to explain combed layering as the result of undercooling. The main objection to this hypothesis is that if undercooling is the sole explanation, why do such structures not occur in other types of rocks, or in those of equivalent composition that show some evidence of chilling against contacts? Combed structures are restricted in the Fallen Leaf Lake quad-

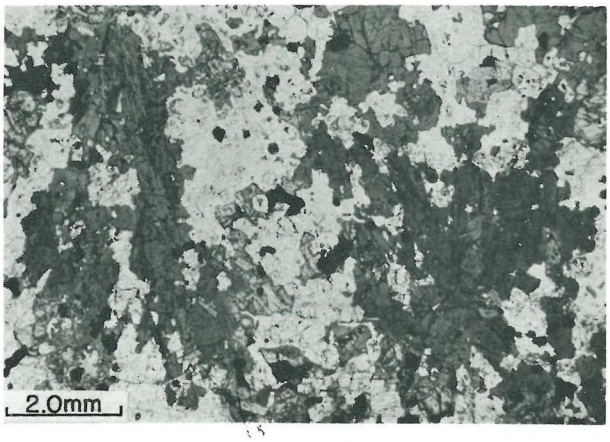


FIG. 8. Primary brown hornblende forming Willow Lake layer. Pyroxenes in adjacent layers are not amphibolized.

rangle to the noritic rocks and the adjacent quartz diorites which are derivative from them. They do not occur in the older gabbro and diorite bodies which were intruded earlier at this level into presumably cooler, wetter surroundings. Neither do they occur in the quartz diorite, granodiorite, and other bodies composing the rest of the batholith.

Furthermore, the occurrence of combed layers at interpluton contacts and around inclusions shows that the cause of the combed textures could not have been local, but must have affected entire bodies nearly simultaneously. Thermal transfer to a heat sink by convection would seem to be too inefficient a process to require crystallization of the combed layers rather than normal crystal growth, especially if the concentration of water was sometimes high enough to cause precipitation of primary hornblende. Relatively rapid cooling in a small body with a high surface to volume ratio should be expected; the combination of a normally quick cooling rate and a compositional peculiarity producing high ionic mobility might produce the effect. If water pressure was close to load pressure, sudden lowering of water pressure might produce rapid isothermal crystallization. Opening of fractures in wall rocks during rapid emplacement of wet magmas from a lower level is the type of structural control envisioned. An attempt to produce similar combed textures and their variations experimentally will begin shortly.

## Mineral Composition Sequences

Figure 9 is a plot of modal An and En mol percentages in coexisting plagioclase and orthopyroxene from 25 specimens from the Eagle Lake sequence.

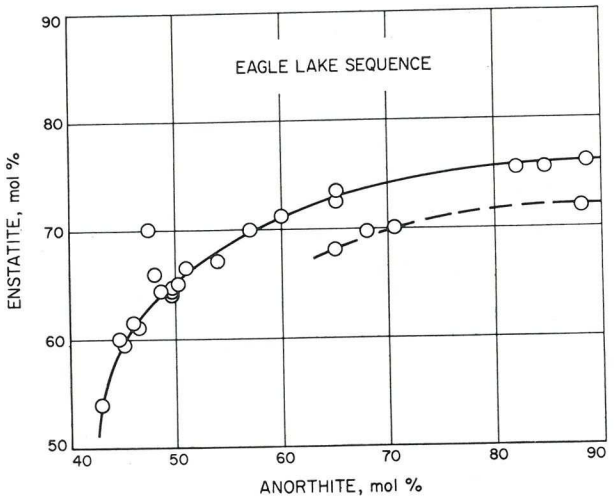


Fig. 9. Modal compositions of coexisting plagioclase and orthopyroxene from rocks of the Eagle Lake sequence.

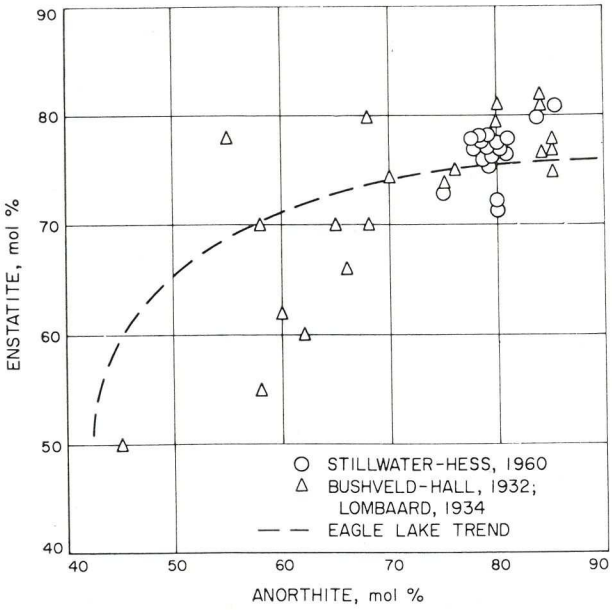


Fig. 10. Compositions of coexisting minerals from literature for large stratiform bodies.

Two of the points with plagioclase more calcic than $An_{80}$ are from Willow Lake layers and two are from large inclusions of cumulative layers. Several of those with plagioclase between $An_{53}$ and $An_{70}$ are also from combed layers. The rest are from normal plutonic rocks and late norite dikes intruded into individual noritic anorthosite bodies. The points define a main trend and a (dashed) subsidiary trend. The mineral compositions were determined optically using optic angle for the orthopyroxenes and Rittmann and Turner methods with a universal stage for the plagioclase. Neither the plagioclase nor the pyroxene is zoned enough to affect the results.

The ratio An/Ab decreased faster than En/Of until the point $An_{50}$-$En_{65}$ was reached and En/Of began to decrease more rapidly. Similar plots for most larger stratiform bodies show much more scatter. Figure 10 is a plot for Stillwater and Bushveld with the Eagle Lake trend from Fig. 9 added for comparison. Stillwater rocks show little progression; Bushveld shows a good deal of scatter. Both curves are drawn for coexisting early cumulative phases that are zoned slightly, if at all.

Figure 11 shows plots for Skaergaard, Rhum and the Great Dyke. Modal compositions were used where possible, but normative points are included as well as olivine compositions where orthopyroxene data are lacking. Skaergaard nicely illustrates a broad variation that diverges more and more with more highly differentiated rocks. The increased divergence from a single line of points, expressed as a

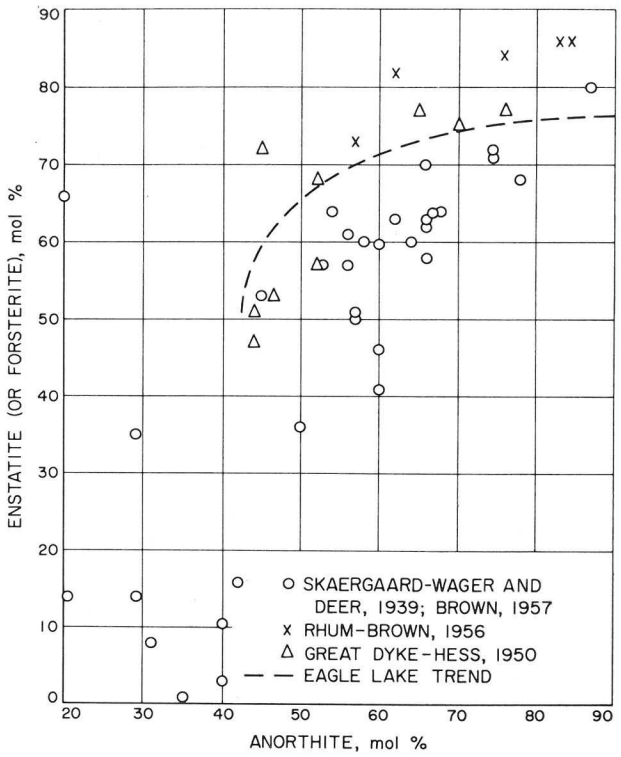


FIG. 11. Compositions of coexisting minerals from literature for large stratiform bodies.

broadening of the envelope containing the points at the low-temperature end, is to be expected. The slopes of the experimentally determined solidus surfaces in systems containing plagioclase, orthopyroxene and olivine decrease for the lower temperature phases. Therefore, a given temperature change in a magma should produce progressively a greater difference in crystal composition as differentiation progresses. The amount of compositional variation in the Skaergaard assemblages is equivalent to that which would be caused by temperature gradients of 40°–50° C. as estimated from the experimental phase diagrams.

In the Eagle Lake rocks, minerals which are found together crystallized and remained together during emplacement. The larger stratiform bodies cooled more slowly and contained temperature and composition gradients. In a large body, convection currents probably would sweep out different parts of the magma at different times, depositing separate layers which did not crystallize in the same place in the chamber. Temperature and consequent composition gradients would be produced locally during relative quiescence of some parts of the chamber with respect to others. As deposition proceeds and the height through which a current can operate becomes smaller with respect to the lateral dimension of the chamber, a larger number of cells with smaller diameters will become operative, increasing the chances for producing sizeable temperature and composition gradients. Any extensive lateral movement of convecting cells or discontinuity in the pattern would bring together and deposit layers which would be only in apparent disequilibrium.

## ACKNOWLEDGMENTS

The work reported was done as part of a doctorate project at Stanford University during the years 1958–1961. Thanks are due Professor Robert R. Compton of Stanford University for many helpful discussions both in the field and laboratory and to Dr. Robert C. Speed, of Stanford and the Jet Propulsion Laboratory, for advice and critical reading of the manuscript. The writer's expenses were defrayed by a National Science Foundation fellowship during 1959–1961. The Shell Fund for Fundamental Research at Stanford University paid for some thin sections and the analyses.

## REFERENCES

BROWN, G. M. (1956) The layered ultrabasic rocks of Rhum, Inner Hebrides. *Roy Soc. London, Phil. Trans.* **240,** 1–53.

——— (1957) Pyroxenes from the early and middle stages of fractionation of the Skaergaard intrusion, East Greenland. *Mineral Mag.* **31,** 511–543.

BUDDINGTON, A. F. (1939) Adirondack igneous rocks and their metamorphism. *Geol. Soc. Am. Mem.* **7.**

COMPTON, R. R. (1961) Peridotite-gabbro-granodiorite pluton in the Sierra Nevada, California; (abs.) *Geol. Soc. Am.*, Cordilleran Section.

HALL, A. L. (1932) The Bushveld igneous complex of the central Transvall. *Geol. Surv. South Africa Mem.* **28.**

HESS, H. H. (1950) Vertical mineral variation in the Great Dyke of Southern Rhodesia. *Geol. Soc. South Africa Trans.* **53,** 159–166.

——— (1960) Stillwater igneous complex, Montana. *Geol. Soc. Am. Mem.* **80.**

LARSEN, E. S. (1948) Batholith of southern California. *Geol. Soc. Am. Mem.* **29.**

LOMBAARD, B. V. (1934) On the differentiation and relationships of the rocks of the Bushveld Complex. *Geol. Soc. South Africa Trans.* **37,** 5–52.

LOOMIS, A. A. (1961) Petrology of the Fallen Leaf Lake area, California. *Ph.D. Thesis, Stanford Univ.*

TAUBENECK, W. H. AND A. POLDERVAART (1960) Geology of the Elkhorn mountains, northeastern Oregon. Part 2. Willow Lake intrusion. *Bull. Geol. Soc. Am.* **71,** 1295–1322.

WAGER, L. R. AND W. A. DEER (1939) Geological investigations in E. Greenland. Pt. III, Petrology of the Skaergaard intrusion, Kangerdluzssuaq, East Greenland, *Medd. Grønland,* **105** (4).

MINERALOGICAL SOCIETY OF AMERICA, SPECIAL PAPER 1, 1963
INTERNATIONAL MINERALOGICAL ASSOCIATION, PAPERS, THIRD GENERAL MEETING

# LAYERED PICRITE-ANORTHOSITIC GABBRO SHEET, WEST HUMBOLDT RANGE, NEVADA

ROBERT C. SPEED[1]
*Department of Geology, Stanford University, Stanford, California*

ABSTRACT

The West Humboldt layered intrusion is a two-layer sheet exposed over a half square mile in the West Humboldt Range, Nevada. The body is composed of 235+ feet of hornblende picrite overlain by at least 100 feet of anorthositic hornblende gabbro. The strong segregation of cumulus minerals into an ultramafic basal layer and anorthositic upper layer is remarkable in view of the absence of variations in the composition of the cumulus phases throughout the body and the lack of sorting or rhythms within each layer.

The layering apparently resulted from the separation of plagioclase from olivine and clinopyroxene during sedimentation following emplacement of a highly crystalline basaltic magma. The picritic layer contains all the mafic cumulates and much plagioclase that was dragged down by the sinking mafic grains. The anorthositic layer is composed chiefly of feldspar that was not carried down by the cloud of mafic crystals.

Tabular plagioclase in both layers has a strong preferred orientation. Fabric attitudes are similar in both layers and lie at high angles to the picrite-leucogabbro contact. The planar fabric appears to have formed in response to folding of the igneous body prior to complete consolidation.

## INTRODUCTION

A two-layer stratiform intrusion composed of basal hornblende picrite and overlying anorthositic hornblende gabbro is exposed over a half square mile in the West Humboldt Range, northwestern Nevada. The strong bistratal segregation of early crystallized minerals in this body is quite remarkable in view of the absence of cryptic layering (as defined by Hess, 1960), grain size sorting, or mineral rhythms within each layer. A second striking feature of this intrusion is the pervasive planar fabric defined by tabular plagioclase. The attitude of this foliation is similar in both layers and lies at high angles to the interface of the two layers and the base of the sheet.

The layering and fabric of this body are clearly unlike those of other layered gabbros reported in the literature and in this symposium. The object of this paper is to suggest a possible origin of the layered body which accounts for these unusual features. Detailed study of the intrusion is yet to be completed, but the problems mentioned above are sufficiently well established and of such an unusual nature that presentation at this symposium seems warranted.

## GEOLOGIC SETTING

The West Humboldt layered intrusion is part of the Humboldt gabbroic complex (Speed, 1962), a large mass of hornblende gabbro with minor picrite, anorthosite, dolerite, keratophyre, and gabbroic pegmatite. The complex crops out in the adjacent northerly-trending West Humboldt, Stillwater, and Clan Alpine ranges in northwestern Nevada and has a known extent of at least 35 miles in maximum dimension. The gabbroic rocks were studied chiefly in the West Humboldt Range (Fig. 1) where they form a quasi-tabular body which dips east off the east flank of the range under the Quarternary deposits of the adjacent basin. Stratigraphic evidence indicates that the age of the complex is between Lower Jurassic and Upper Tertiary. Emplacement of the complex was at a shallow depth, probably less than 2500 feet, and was apparently synchronous with regional deformation of the intruded Mesozoic sediments.

Hornblende picrite and strongly foliate hornblende leucogabbro which compose the West Humboldt layered body crop out chiefly along the western periphery of the Humboldt gabbroic complex in the West Humboldt Range. These units were earliest in the sequence of rock types forming the complex. Some of the relatively large bodies of these two facies are shown in Fig. 1. The consistent areal association of picrite and foliate leucogabbro indicates that these facies are cogenetic. Structural evidence suggests that all of these bodies are contemporaneous and may once have been contiguous. Deformation, widespread deuteric alteration, and poor exposures preclude more definite correlation of these bodies.

## WEST HUMBOLDT LAYERED SHEET

*Structure.* The West Humboldt layered intrusion, shown in Fig. 2, is tabular and consists simply of

[1] Present address: California Institute of Technology, Jet Propulsion Laboratory, Pasadena, California.

235+feet of hornblende picrite overlain by at least 100 feet of anorthositic hornblende gabbro. The contact of the two layers is not exposed, and an approximate contact was mapped by tracing the sharp mineralogical change in the surficial debris. Field examination in nearly vertical sections through the body indicated that the contact is either sharp or gradational through no more than 15 feet.

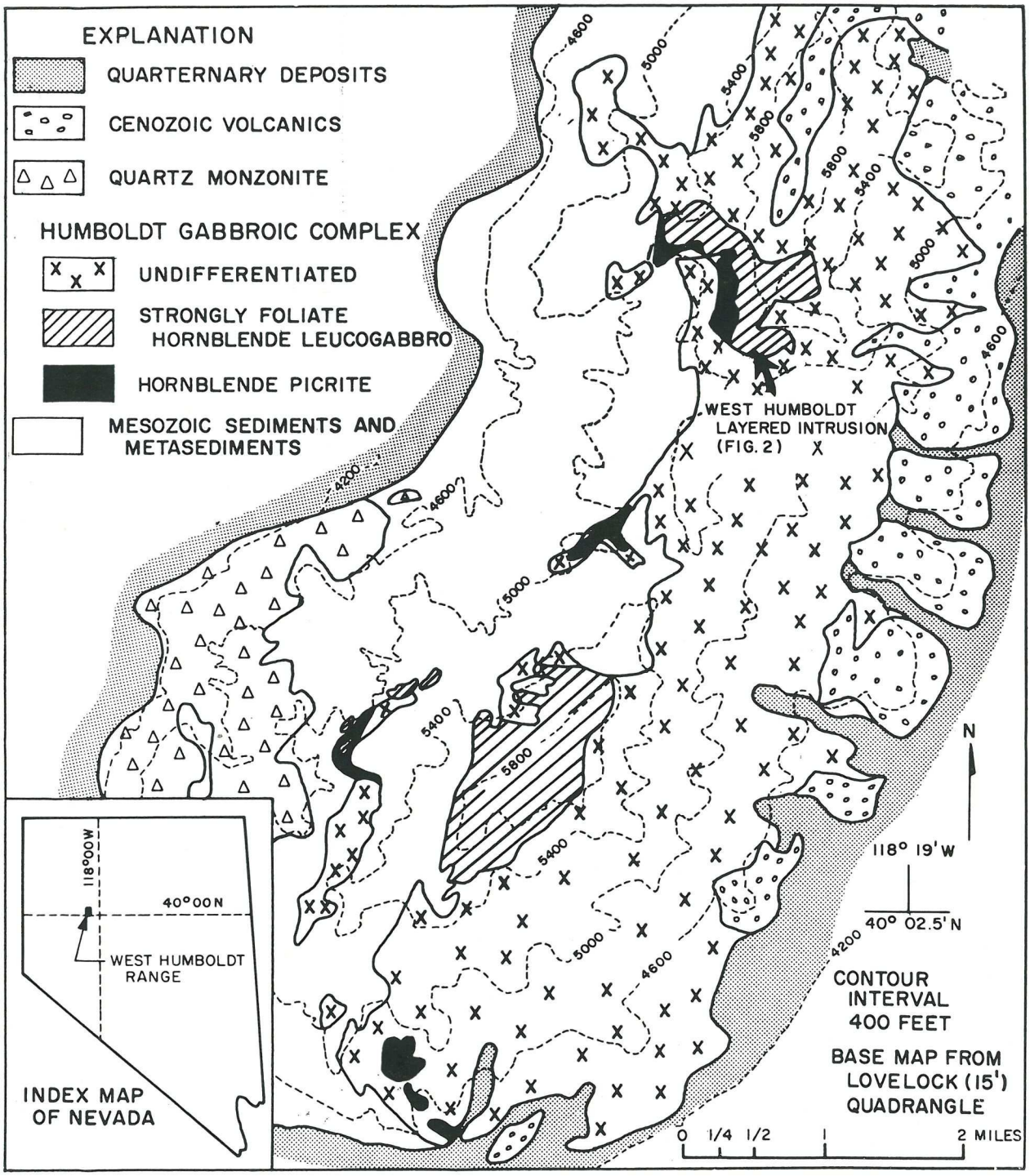


FIG. 1. Generalized geologic map of West Humboldt Range, Nevada, showing distribution of gabbroic rocks and location of West Humboldt layered intrusion.

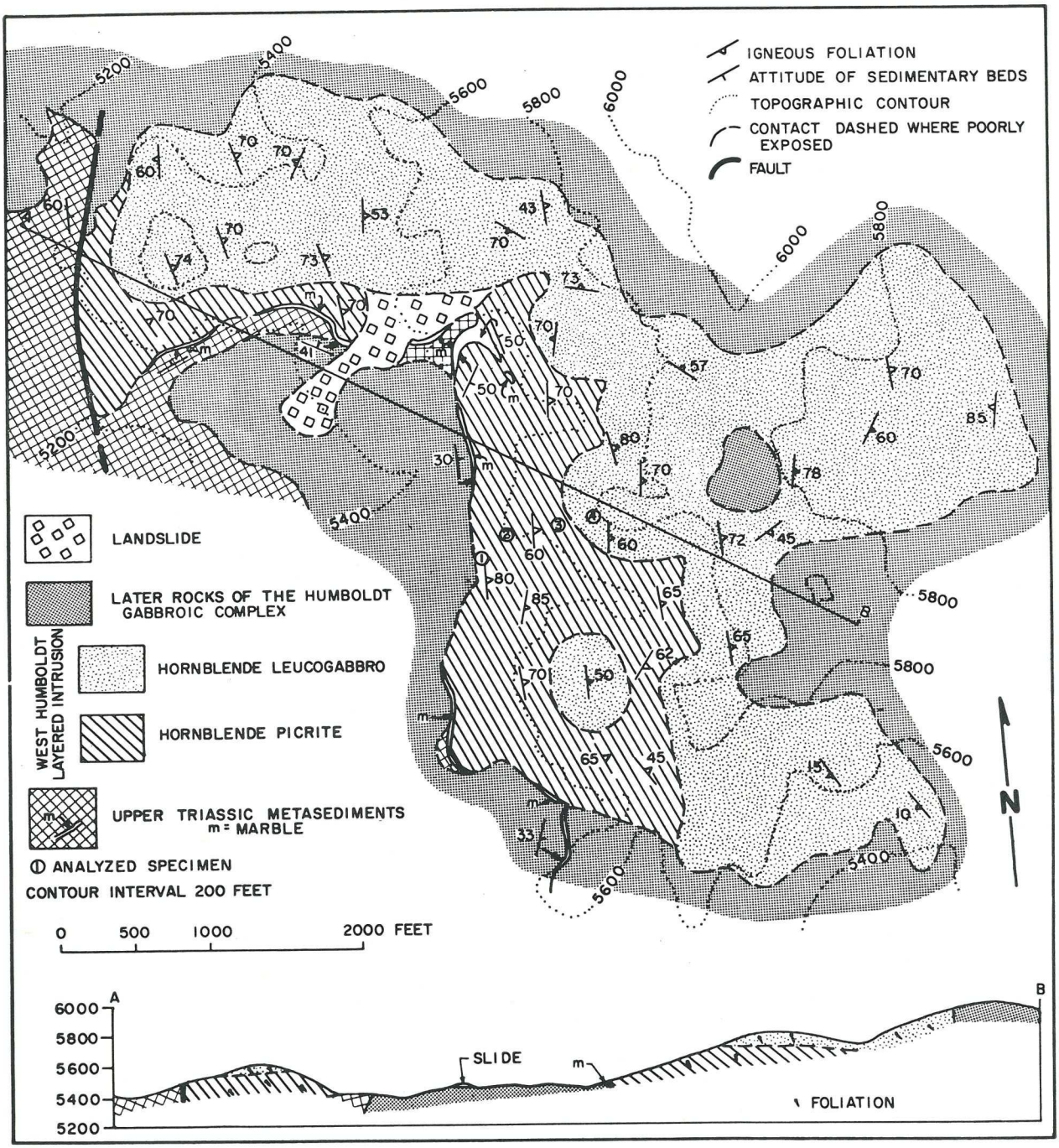


FIG. 2. Geologic map of the West Humboldt layered sheet.

The roof of the intrusion has been completely eroded, and the maximum thickness of the leucogabbro above exposed picrite is about 100 feet. This layer may thicken in the eastern part of the body if the picrite-leucogabbro contact maintains a constant attitude east of its easternmost exposure. The picrite is estimated to be around 235 feet thick in the western part of the body. The thickness of other parts of the picrite is poorly known because of the lack of vertical exposures through this layer and uncertainty in the attitude of the base of the sheet. The picrite, however, appears to thicken in the eastern part of the body.

The base of the picrite lies partly on deformed

marble and hornfels and partly on younger hornblende gabbro. The concordance between the igneous sheet and the marble suggests that the body is a sill. Marble, however, is also widespread in thrust zones in the West Humboldt Range; therefore, the structural setting of the intrusion is uncertain. Attitudes of the marble segments form an anticlinal pattern, the axis of which roughly parallels axes of folds in the metasedimentary terrane which trend about N.10°E. and plunge shallowly. Most of these folds are overturned to the west. The degree of folding of the layered intrusion, however, cannot be determined as most of the western limb of the body is faulted. The internal fabric of the layered sheet suggests that the intrusion was deformed prior to final consolidation.

*Hornblende picrite.* Hornblende picrite forms a rather homogeneous petrographic unit in which internal layering is absent. Modal variation in the picrite consists chiefly of a gradual increase in color index vertically in the layer. Modal and chemical analyses of specimens taken near the bottom, middle, and top of the picrite are reported in Table 1. Analyses 1 and 3 represent the approximate limits of mineralogical and chemical variation in the picrite.

Textures in both the picrite and the leucogabbro clearly indicate a sequence of crystallization of mineral assemblages. The early crystallizing assemblage in both facies is believed to be composed of accumulative minerals. This is indicated by the strong segregation of these minerals into two layers on the basis of their densities. The later crystallizing assemblages formed by reaction of the cumulus minerals with the intercumulus liquid and by *in situ* precipitation of this liquid. Terminology is taken from Wager *et al.* (1960).

The early crystallizing assemblage in the picrite is composed of olivine, labradorite, and clinopyroxene. That crystallization of olivine started first is indicated by the inclusion of small olivine grains in clinopyroxene and labradorite. Olivine has a wide range of grain size and idiomorphism. Maximum dimension of olivine grains in thin section ranges from 0.5 to 5.0 mm. This range of grain intercepts is believed to indicate variation in actual size of olivine grains. In some sections olivine grains with small intercepts are clustered in a manner which indicates that all the grains in the cluster could not have been considerably larger at levels above or below the plane of the thin section. Furthermore, euhedral olivine grains whose intercepts differ by an order of magnitude are in near-contact; it is difficult to envision how the two grains

TABLE 1. CHEMICAL AND MODAL ANALYSES OF ROCKS FROM THE WEST HUMBOLDT LAYERED INTRUSION

| | 1 | 2 | 3 | 4 |
|---|---|---|---|---|
| *Chemical Analyses* | | | | |
| $SiO_2$ | 46.56 | 45.25 | 43.85 | 51.30 |
| $TiO_2$ | 0.54 | 0.44 | 0.49 | 0.49 |
| $Al_2O_3$ | 9.91 | 9.74 | 7.85 | 20.01 |
| $Fe_2O_3$ | 3.16 | 2.46 | 3.27 | 1.29 |
| FeO | 5.34 | 6.17 | 6.10 | 2.93 |
| MnO | 0.14 | 0.14 | 0.17 | 0.05 |
| MgO | 18.69 | 22.78 | 23.40 | 6.11 |
| CaO | 7.91 | 6.70 | 6.33 | 10.75 |
| $Na_2O$ | 1.47 | 1.48 | 1.15 | 3.63 |
| $K_2O$ | 0.48 | 0.36 | 0.30 | 0.60 |
| $H_2O^+$ | 3.90 | 3.02 | 5.12 | 1.86 |
| $H_2O^-$ | 0.91 | 1.04 | 1.14 | 0.35 |
| $P_2O_5$ | 0.11 | 0.10 | 0.14 | 0.14 |
| $CO_2$ | 0.18 | 0.17 | 0.14 | 0.15 |
| Cl | 0.06 | 0.05 | 0.05 | 0.05 |
| F | 0.02 | 0.01 | 0.02 | 0.01 |
| Total | 99.38 | 99.91 | 99.52 | 99.72 |
| *Norms* | | | | |
| Or | 3.06 | 2.26 | 1.93 | 3.74 |
| Ab | 13.23 | 13.15 | 10.43 | 31.60 |
| An | 20.20 | 19.80 | 16.60 | 37.50 |
| Di | 16.29 | 11.32 | 12.90 | 12.75 |
| Hy | 22.98 | 14.48 | 19.93 | 6.17 |
| Ol | 18.09 | 34.51 | 32.25 | 4.89 |
| Ap | 0.26 | 0.23 | 0.33 | 0.33 |
| Il | 1.08 | 0.88 | 1.02 | 0.96 |
| Mt | 4.86 | 3.75 | 5.10 | 1.92 |
| $\frac{MgO\ \%}{MgO+FeO}$ | 90 | 90 | 90 | 85 |
| An % | 59 | 59 | 60 | 53 |
| *Modes* | | | | |
| Olivine | 25.4 | 34.0 | 38.5 | — |
| Fo% | (85–87) | (87–92) | (85–90) | |
| Bronzite | 3.5 | 2.5 | 3.3 | — |
| En% | (80–82) | (82–84) | (81–83) | |
| Clinopyroxene | 13.1 | 14.7 | 13.2 | 5.0 |
| Kaersutite | 11.4 | 10.5 | 8.5 | 18.0 |
| Plagiocalse | 27.8 | 28.1 | 21.6 | 73.7 |
| An% | (55–60) | (55–60) | (50–58) | (49–57) |
| Magnetite | 2.3 | 2.3 | 3.8 | 0.3 |
| Titanobiotite | 2.2 | 2.0 | 3.2 | — |
| Chlorite[1] | 14.2 | 6.1 | 6.7 | 2.4 |
| Sphene | — | — | — | 0.5 |

[1] Deuteric chlorite replacing both plagioclase and olivine.
1—Hornblende picrite—10 feet above base.
2—Hornblende picrite—170 feet below leucogabbro contact.
3—Hornblende picrite—15 feet below leucogabbro contact.
4—Hornblende lexcogabbro—30 feet above picrite contact.

Specimen locations shown on Fig. 2.
Analyst: Y. Chiba.

could have similar actual dimensions. Perfectly euhedral and highly irregular anhedral olivines are both abundant. Optical measurements indicate a composition range of $Fo_{85-92}$, but it is probable that the spread is due to errors in measurement as the majority of measurements indicates $Fo_{87}$. Zoning is absent in olivine. Layering with respect to composition, size, or shape of olivine was not observed.

Labradorite in the picrite occurs chiefly in tablets which are as long as 12 mm. The tablets contain as many as 50 oscillatory zones. The most calcic zone is $An_{67}$, but most zone compositions are in the range $An_{55-65}$. Some labradorite tablets have a thin rim of normally zoned plagioclase, the periphery of which is as sodic as $An_{25}$. The rims probably crystallized after accumulation. Labradorite forms irregular monomineralic clusters at a few places. Long dimensions of the clusters generally parallel the planar feldspar fabric.

Clinopyroxene occurs both as discrete subhedral and euhedral grains and in monomineralic glomeroporphyritic clusters in which component grains are highly intergrown. Many clinopyroxenes have oscillatory zoning, but others are apparently of uniform composition. Optical variations in zoning are chiefly in optic angle (52–54° and 58–60°) whereas differences in refractive index ($\beta = 1.682 - 1.686$) and $Z \wedge c$ (40–42°) between zones are small. Unzoned clinopyroxene optic angles are 53–57°. Accordingly, clinopyroxene compositions fall in the interval $Ca_{43-50}Mg_{39-48}Fe_{7-10}$. Maximum grain intercepts of clinopyroxene clusters and single grains are 4.0 mm.

Two intercumulus assemblages occur in the picrite. The earlier consists of orthopyroxene and sodic rims on cumulus labradorite. The later assemblage is composed of kaersutite, titanobiotite, and magnetite. Orthopyroxene is virtually restricted to sinuous poikilitic nets which envelop and replace olivine grains. In other picrite bodies in the West Humboldt Range, however, orthopyroxene occurs in large (12 mm) poikilitic nets enclosing clinopyroxene and plagioclase as well as olivine. This texture indicates that orthopyroxene was a product both of reaction of olivine with the intercumulus liquid and continued direct precipitation from the liquid. Orthopyroxene compositions range from $En_{80}$ to $En_{87}$.

The foregoing minerals are enveloped by large poikilitic nets of kaersutite (4.9% $TiO_2$) and titanobiotite. Amoeboid grains of magnetite occur only in kaersutite and titanobiotite and are apparently contemporaneous with the latter minerals. These three minerals compose the late assemblage which crystallized from the intercumulus liquid. Clinopyroxene and, to a less extent, orthopyroxene are highly replaced by kaersutite and titanobiotite, but replacement of olivine and plagioclase by these minerals did not occur.

Most of the rocks of the layered sheet were strongly hydrated in the deuteric stage. Much of the olivine and orthopyroxene was altered to talc, tremolite, bowlingite, magnetite, and serpentine minerals. Labradorite was partly replaced by combinations of prehnite, chlorite, pumpellyite, grossular, analcite, albite and white mica. Kaersutite was partly altered to actinolite, chlorite and sphene. Reciprocal movement of Ca and Mg is indicated by the replacement of labradorite by chlorite and olivine by tremolite at places where the two primary minerals were in contact. The original grain contacts are obscured by the alteration, and the amount of chlorite representing former olivine or plagioclase cannot be ascertained. This chlorite is reported separately in the modes in Table 1, but textures indicate that the chlorite chiefly replaces plagioclase.

*Hornblende leucogabbro.* Modal variations in hornblende leucogabbro are largely in the relative amount of plagioclase (70–95%) and late amphibole. Clinopyroxene rarely forms more than 5% of the leucogabbro, and in many specimens, it is absent. Systematic vertical or lateral trends in these variations in the leucogabbro were not found. Chemical and modal analyses of a representative leucogabbro are given in Table 1.

Labradorite and clinopyroxene form the early crystallizing assemblage in the hornblende leucogabbro facies. Relics or alteration products of olivine or orthopyroxene were not observed in the leucogabbro. Plagioclase tablets are generally larger and the peripheral jackets are thicker in the leucogabbro than the picrite. The contrast in zoning and composition of the jackets and the core suggests that the two crystallized under considerably different conditions. The cores almost certainly are part of the cumulus assemblage; it is suggested, therefore, that the rims grew from the intercumulus liquid. The average composition of the cumulus parts of the leucogabbro plagioclase appears to be uniform throughout the layer and to differ little from that of the picrite plagioclase. Clinopyroxene in the leucogabbro occurs both in equant and highly elongate subhedra. Clinopyroxene compositional limits in the leucogabbro are similar to those in the picrite.

The intercumulus assemblage in the leucogabbro is composed chiefly of kaersutite with a little magnetite and apatite. Titanobiotite does not occur in the

FIG. 3. Planar fabric of tabular plagioclase in hornblende picrite, West Humboldt layered intrusion. Trace of fabric (strike N. 10° W., dip 80° E.) about parallel to hammer handle.

leucogabbro. Modal apatite appears to be far more abundant in the leucogabbro than the picrite, though normative apatite is similar in the two facies. The abundance of the intercumulus minerals in the leucogabbro is between 1.5 and 2 times that in the picrite.

*Fabric.* One of the most striking features of the West Humboldt layered sheet is the strong planar fabric formed by the alignment of plagioclase tablets in both layers of the body (Fig. 3). Foliation symbols in Fig. 2 indicate the similarity of attitude of the fabric in the two layers and the fact that the planar fabric is at a high angle to the interface of the two layers and the projected base of the sheet. Figure 4, an equal area plot of poles to the feldspar fabric, shows that the preferred orientation is generally similar throughout the body.

Bent twins, shattered grains, and other evidence of protoclasis are absent. Discordant plagioclase tablets contact one another without deformation. Clearly, the fabric must have been formed in a benign manner. Sawed slabs of leucogabbro were examined for lineation, and it is clear that prominent lineation is absent. It is possible, however, that if a large number of careful measurements were made, a slight lineation might be discovered.

*Vertical variations.* Vertical variations in the West Humboldt layered intrusion are summarized as follows:

A. Mineral Layering
   1. Restriction of olivine, orthopyroxene, and titanobiotite to the picrite.
   2. Greater content of clinopyroxene in the picrite than the leucogabbro.
   3. Greater amount of plagioclase, kaersutite, and apatite in the leucogabbro than the picrite.
   4. Ratio of olivine and clinopyroxene to plagioclase increasing stratigraphically upward in the picrite.

B. Textural Variations.
   1. Average plagioclase grain size larger in the leucogabbro than the picrite.
   2. Clinopyroxene single grains and clusters a little larger in the picrite than the leucogabbro; clinopyroxene in the leucogabbro more elongate.

The mineral variations indicate the strong separation of the cumulus minerals into two layers on the basis of density. The greater content of the intercumulus minerals in the leucogabbro than the picrite indicates the higher intercumulus porosity (lower crystal/liquid ratio) in the upper layer prior to crystallization of the intercumulus liquid.

Cryptic layering of the cumulus phases is apparently absent within the intrusion. Olivine composition is constant throughout the picrite, and the range of 2V and $\beta$ of clinopyroxene at different levels in the sheet is similar. The consistent values of normative MgO/MgO+FeO on the analyzed picrites in Table 1 supports the modal evidence that the mafic minerals do not become more iron-rich at higher stratigraphic levels. Magnetite is a product of deuteric alteration of olivine in the picrite. Consequently, normative magnetite content of the picrites

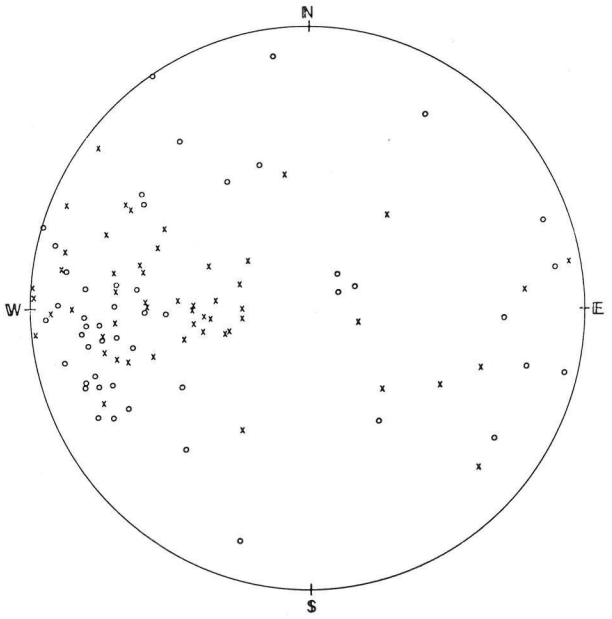


FIG. 4. Equal area projection of poles to planar fabric (circles) in West Humboldt layered intrusion and to bedding (X) in metasedimentary rocks within one mile of the layered intrusion. Plotted on lower hemisphere.

is higher than that of modal magnetite, and the ratio of normative MgO/MgO+FeO is higher than it was prior to alteration. Bulk modal plagioclase composition, though difficult to estimate because of complex zoning, appears not to differ at succeeding stratigraphic levels in what is taken to the cumulus part of the mineral. This is supported by the similar values for normative plagioclase in the analyzed picrites of Table 1. The larger average volume of the intercumulus plagioclase rims in the leucogabbro, however, makes the normative plagioclase in the leucogabbro more albitic than that of the picrite.

Glomeroporphyritic clots of clinopyroxene and plagioclase are the only monomineralic aggregates in the intrusion. The clinopyroxene clots are generally equant; the plagioclase clots are both equant and lensoid, the latter type lying parallel to the planar fabric of the rock. Rhythmic mineral layering is absent. Sorting within each of the facies as a function of grain size or shape was not observed.

## Petrology of the Layered Intrusion

The rocks along the base of the sheet are so altered that the existence of a chilled zone could not be determined. Consequently, the composition of the parent magma or the degree of crystallinity of the magma on emplacement are unknown. In a qualitative way, however, the two facies appear to be complementary fractions of an olivine gabbro. This suggests that the two layers are differentiates of a single injection of basaltic magma. The continuity of the feldspar fabric between the two layers strongly supports the view that the layers were not separate injections. The fact that rocks throughout the complex have a late-crystallizing alkaline assemblage indicates an alkali magma type.

Differentiation of the magma consisted of two concomitant processes, vertical segregation of the early formed minerals into upper feldspathic and basal mafic layers and strong changes in the composition of the liquid phase with progressive crystallization. Following accumulation of olivine, plagioclase and clinopyroxene, succeeding events were: 1) crystallization of orthopyroxene and sodic plagioclase rims and development of the planar fabric, and 2) crystallization of kaersutite, titanobiotite, magnetite and apatite. The contemporaneity of the feldspar rims with orthopyroxene rather than the other intercumulus minerals is suggested by the coexistence of kaersutite with magmatic analcite in other rocks of the complex. The contrast of orthopyroxene textures in the foliate picrite of the layered intrusion to those in nonfoliate picrite to the south in the West Humboldt Range suggests that crystallization of large continuous orthopyroxene webs in the former picrite may have been mechanically prevented by concomitant reorientation of platy plagioclase.

The second group of intercumulus minerals filled the remaining pore space as well as partly replacing the earlier pyroxenes. The composition of this late crystallizing assemblage must be close to the nonvolatile composition of the intercumulus liquid near its final consolidation. The late magma contained only 31–40% $SiO_2$ but was enriched in iron (15–30% total iron as FeO), soda, and probably in volatiles. This liquid was probably highly fluid. The liquid line of descent shows a remarkable retention of iron in the liquid phase. An account of the differentiation of the entire complex will be presented elsewhere.

## Origin of the Layering

The two-layer distribution of early crystallizing minerals strongly indicates the influence of gravity during differentiation. The absence of rhythms or sorting in either layer, however, indicates that deposition of the cumulates in this body did not involve the current mechanisms that were apparently operative in other layered gabbros (Wager and Deer, 1939; Hess, 1960). The original thickness of this body is unknown, but the known or inferred thickness of other parts of the gabbroic complex in the West Humboldt Range suggest that it did not greatly exceed 500 feet. The rate of cooling, therefore, was probably similar along all surfaces of the magma chamber, and the change of melting point of crystallizing phases with depth in the chamber was probably not a significant factor in their distribution.

The uniformity of composition of the cumulus minerals, each of which forms a solid solution series, indicates that they crystallized from magma of constant composition with respect to the ratios of high temperature to low temperature components of the series. Fresh magma, therefore, must have continually been brought to the cooling surfaces where crystallization occurred, and magma movement must be invoked to account for the absence of cryptic layering. Yet, convective overturn or other flow mechanisms cannot be called upon to circulate fresh magma considering the lack of rhythms or sorting of the cumulates which would have been deposited concomitantly with the rise of fresh magma. Another feature to be accounted for is the upward increase in color index in the picrite.

The layering can be explained in part by the suggestion that the cumulus minerals had largely crystal-

lized before the magma was emplaced. Olivine, clinopyroxene, and plagioclase could have crystallized with little change of composition during rise of the magma through the conduit if the upward flow was turbulent enough to bring fresh magma to the walls and sweep the crystals away from the peripheral parts of the conduit. The complex zoning of the feldspar and some clinopyroxene suggests rapid crystallization under varying conditions. The relative movement of crystals and crystal aggregates of olivine, clinopyroxene, and plagioclase during sedimentation that followed magma emplacement may account for the layering and petrographic variations. The mafic phases would clearly have settled through the liquid, and it is suggested that plagioclase may have had a slight tendency to rise. The ratio of plagioclase to interstitial amphibole is lowest at the base of tabular bodies of feldspathic gabbro at other places in the complex. This suggests that plagioclase was less dense than the late liquid.

The settling of olivine and clinopyroxene simultaneously throughout the magma chamber probably involved increasing amounts of aggregation of the sinking grains with time. The sedimentation process might be viewed as the compaction of a cloud of crystal aggregates rather than as the settling of discrete particles. Sorting during deposition of this type should have been poor. Much plagioclase was probably dragged down by the descending mafics. Feldspar crystals near the chamber roof had fewer waves of mafic grains and aggregates sinking past than did feldspars at lower levels, and the opportunities for feldspar to have been swept down were less at higher levels in the chamber. On the other hand, feldspar at the base of the magma chamber was probably covered by cumulates immediately after emplacement and had little chance to move away from mafic crystals at this horizon. Consequently, it is suggested that the degree of separation of cumulus mafic grains and feldspar during sedimentation was a function of their height in the magma chamber just after emplacement (excepting, of course, the possibility of a thin chilled or rapidly crystallized layer along the roof of the chamber in which all the early phases were trapped as phenocrysts.

If this mechanism is correct, the top of the picrite contains mafic cumulates which were near the roof of the chamber just after emplacement. Olivine, clinopyroxene, and labradorite at the bottom of the picrite, however, probably did not move after emplacement, and their modal ratio should represent the ratio of these minerals in the magma on emplacement. Good modal data on basal specimens are lacking, but, roughly, labradorite appears to have been a little more abundant than olivine and olivine about twice the amount of clinopyroxene. The leucogabbro layer consists of plagioclase which successfully separated from the compacting cloud of mafic material. However, a major problem not covered by this explanation is the origin of the clinopyroxene in the leucogabbro. It seems unlikely that clinopyroxene in the leucogabbro was a member of the pre-emplacement assemblage that failed to accumulate completely. Olivine occurs only in the basal layer, and the difference in density of olivine and clinopyroxene is not enough to suggest that the former mineral should have settled more than the latter. The apparent difference in shape of clinopyroxenes in the leucogabbro and the picrite supports the view that they did not crystallize together. Yet, it is not clear why the composition of clinopyroxene from the two layers is apparently similar if clinopyroxene in the leucogabbro crystallized during or following accumulation.

Considering that the sheet was probably not much greater than 500 feet thick, the completeness of accumulation of the mafic grains is remarkable. The rate of settling of the cumulates must have vastly exceeded the rate of crystallization of the liquid in from the walls. In fact, the crystallization of the late intercumulus assembalge apparently did not occur until sedimentation was complete. The probable high fluidity of the liquid phase during sedimentation greatly assisted the rapid settling.

Some aspects of the Shonkin Sag laccolith (Hurlbut and Griggs, 1939) are similar to this intrusion. The laccolith is also highly differentiated for a thin body, and the color index of the lower shonkinite layer increases upward. The mode of the chilled basal layer of the Shonkin Sag body (47% phenocrysts) indicates that the magma was rather crystalline on emplacement. Unfortunately, petrographic coverage of that body does not show whether or not cryptic layering exists.

### Origin of the Foliation

The feldspar fabric appears not to be primary but to have formed by reorientation of feldspars in place. Absence of prominent lineation of the feldspar and lack of feldspar crystals stemming from a planar surface indicate that this is not a growth fabric. The fact that the foliation lies at high angles to the base of the intrusion and the interface of the two layers indicates that laminar flow of plagioclase tablets past

a planar surface did not cause alignment. It could be suggested that feldspar tablets were oriented during accumulation so that the tablets lay vertically. By this mechanism, however, the normals to the tablets should be randomly distributed in the horizontal plane rather than strongly aligned as shown in Fig. 4. Thus, the fabric could not have developed by sedimentation alone. As noted previously, the contrast between orthopyroxene textures in the foliate picrite of the layered body and in a non-foliate picrite a few miles south suggests that plagioclase alignment and orthopyroxene crystallization were contemporaneous. Finally, it is clear from the undeformed poikilitic texture of the late intercumulus kaersutite and titanobiotite that these minerals crystallized after the fabric had formed. Together, these points indicate that reorientation occurred after accumulation but before final consolidation.

Formation of a strong planar fabric by reorientation of crystals in a liquid requires that the abundance of crystals be high enough that differential movement of crystals and liquid can occur. A change of shape of the chamber is necessary for this differential movement. Figure 4 shows a definite relation between the preferred orientation in the igneous body and the attitudes of the bedding of the intruded metasediments. The bedding orientation is largely controlled by near-isoclinal overturned folds. The comparable orientation of igneous and country rock fabrics suggest that the foliation is an axial plane fabric and that the foliation resulted from deformation of the chamber in response to external stress.

The attitude of the fold axis defined by the base of the picrite roughly corresponds to attitudes of axes of major and minor folds in the surrounding rocks. This relation and the similar orientation of the igneous foliation and axial planes of folds in the country rocks suggest that intrusion occurred before regional deformation but that folding occurred before final consolidation of the igneous body.

The absence of protoclastic textures in these rocks indicates that reorientation occurred in a benign manner. It is suggested that the tabular grains were aligned by the flow of intercumulus liquid during deformation. The grains were reoriented by the moving liquid so that their largest surface lay in the plane of maximum liquid flow. The cumulus porosity of the rocks (12–25%) seems low compared to estimates from other cumulus rocks and to results of packing experiments (Hess, 1960; Wager *et al.* 1960). This supports the view that some of the intercumulus liquid was pressed out, but the poor sorting of these cumulates may also have yielded low porosities.

### Acknowledgments

I am grateful to C. O. Hutton and R. R. Compton of Stanford University for helpful criticism of this manuscript and to my colleague, A. A. Loomis, for his valuable discussion and advice on the problem as well as for manuscript comments.

### References

Hess, H. H. (1960) Stillwater igneous complex. Montana, *Geol. Soc. Am. Mem.* **80,**

Hurlbut, C. S., Jr. and D. Griggs (1939) Igneous rocks of the Highwood Mountains, Montana: Pt. I, The laccoliths, *Bull. Geol. Soc. Am.* **50,** 1043–1112.

Speed, R. C. (1962) Humboldt gabbroic complex (abs.), Geol. Soc. Am., Spec. Paper 73.

Wager, L. R., G. M. Brown and W. J. Wadsworth (1960) Types of igneous cumulates, *Jour. Petrol.* **1,** 73–85.

——— and W. A. Deer (1939) The petrology of the Skaergaard Intrusion, Kangerdlugssuaq, East Greenland, *Medd. Grønland,* **105,** 314.

MINERALOGICAL SOCIETY OF AMERICA, SPECIAL PAPER 1, 1963
INTERNATIONAL MINERALOGICAL ASSOCIATION, PAPERS, THIRD GENERAL MEETING

# LAYERED PEGMATITE-APLITE INTRUSIVES[1]

RICHARD H. JAHNS AND O. FRANK TUTTLE
*Division of Earth Sciences, The Pennsylvania State University, University Park, Pennsylvania*

ABSTRACT

Intrusive bodies of granitic pegmatite and aplite with simple or complex layering include those representing multiple injections of magma from external sources and those representing single injections of magma followed by segregation during crystallization. Those of the latter category can be subdivided into four classes, intergradations among which are not uncommon:

1. Bodies of aplite or fine-grained pegmatite with very large phenocrysts, or megacrysts. 2. Aplite bodies with marginal or interior pegmatite masses generally formed *in situ*. 3. Pegmatite bodies with marginal or interior aplite masses formed *in situ* or by autoinjection. 4. Highly asymmetric bodies whose upper parts consist mainly or wholly of pegmatite and whose lower parts consist mainly or wholly of aplite.

Zonal structure defines a gross layering within many pegmatite bodies, and a layer-like distribution of pegmatite and aplite also is common over a wide range of scales. Some of the aplites are faintly to distinctly flow layered, and others are featured by rhythmic layering in which adjacent thin and regular units differ from each other in composition. None of the observed types of layering is regarded as a result of crystal accumulation.

The bulk composition of the layered intrusive bodies falls in the thermal valley of petrogeny's residua system at an average composition corresponding to a parent magma saturated with water at high pressures (*e.g.* > 2000 bars). This also is true of many individual pegmatite and aplite masses, in which the pegmatite is ascribed to crystallization of magma saturated with volatile constituents and the aplite to rapid crystallization of magma during escape of such constituents. In contrast, the aplite masses of most highly asymmetric bodies are markedly sodic and the associated pegmatite masses are correspondingly potassic in composition. This difference is attributed to segregation of major alkalies in the presence of silicate melt and coexisting aqueous vapor. Variations in distribution of the two fluid phases within a given intrusive, in distribution of alkalies between then, and in rates of diffusion of alkalies through the vapor could account for the known relationships between these complementary pegmatites and aplites.

All these types of bodies can be identified genetically with subsolvus granites and related rocks, and their common association is attributed to derivation from magmas with high water content. The amount of pegmatite and aplite associated with hypersolvus granites is trivial.

## INTRODUCTION

Pegmatites and aplites have long been recognized as texturally contrasting rocks whose composition and features of occurrence bespeak close genetic affiliations. At thousands of localities throughout the world they are so intimately associated in both space and time that derivation from a common stem seems plainly indicated. Moreover, numerous individual bodies of rock comprise both pegmatite and aplite in various combinations, the paragenetic relationships of which suggest development within what may well have amounted to single systems.

In this paper attention is focused mainly upon pegmatite-aplite bodies in which layering either appears within masses of one or both rock types or is expressed by the gross arrangement of the masses themselves. The principal objectives are to summarize the observable physical relationships within these bodies, to report on certain contrasts in bulk composition of their constituent aplite and pegmatite masses, and to suggest mechanisms for explaining the origin of the rocks and their layering. The discussions are restricted to rocks of granitic composition, and to occurrences ascribed to initial emplacement of a magma. In an attempt to establish generalizations that are sound, the writers have drawn from their own observations of the past twenty years and also have made a careful search of the world literature for detailed descriptions of closely associated aplites and pegmatites.

Much of the background field work by Jahns was an outgrowth of earlier detailed studies of pegmatite districts under the aegis of the U. S. Geological Survey, and was supported during the period 1948–1962 by the California Institute of Technology, the American Research Institute and The Pennsylvania State University. Other field investigations, carried out independently by Tuttle during a period of several years, were supported by The Pennsylvania State University and the National Science Foundation. Funds for several chemical analyses also were supplied by the National Science Foundation. It is a

[1] Contribution No. 61–105, College of Mineral Industries, The Pennsylvania State University, University Park, Pennsylvania. Contribution No. 1000, Division of the Geological Sciences, California Institute of Technology, Pasadena, California.

pleasure to acknowledge the contributions of numerous colleagues with whom the writers have discussed the genesis of aplites and pegmatites; particularly helpful in this connection have been W. R. Griffitts, J. B. Hanley, J. J. Norton, and L. R. Page of the U. S. Geological Survey, E. Wm. Heinrich of the University of Michigan, and C. W. Burnham and L. A. Wright of The Pennsylvania State University.

## Features of Occurrence

*General relationships.* Pegmatites and aplites occur predominantly in igneous and metamorphic terranes that encompass a very wide range of rock types. Metamorphic rocks are common hosts for bodies of pegmatites and for bodies comprising both pegmatite and aplite; remarkably rare in such environments, however, are bodies that consist solely of aplite. No such restriction appears to exist within igneous terranes, where both pegmatite and aplite are abundant, either in separate bodies or as component parts of single bodies. Many groups of such bodies are distributed systematically within or around much larger masses of intrusive igneous rock with which they may be genetically related.

Layered intrusive bodies composed of both pegmatite and aplite range from thin stringers and lenses to pods and tabular masses hundreds of feet thick and a mile or more long. They also vary considerably in attitude, form, and complexity of form, commonly in response to contrasting structural features in the host rocks (see summaries in Landes, 1942; Cameron *et al.*, 1949). Although it is not feasible to consider any average or typical shape, tabular and pod-like bodies probably are more abundant than all other kinds taken together.

The layered bodies herein discussed are referred to as intrusives because they seemingly were emplaced by magmatic injection, accompanied in some occurrences by stoping. The most common and most convincing evidence for such injection is provided by structural relationships that indicate dilation of the country rock, especially where these relationships can be fixed in three dimensions. That the injected material was magma is variously suggested by systematic variations in size, structure and composition of many bodies with respect to igneous plutons (Cameron *et al.*, 1946, pp. 5–8; Heinrich, 1953; Varlamoff, 1960), by the occurrence of some bodies as autoinjection products within such plutons, by the merging of other bodies into larger masses of normal plutonic rocks, and by numerous textural, structural, and compositional features within the layered bodies themselves. These and other criteria for magmatic injection, as outlined and discussed in the published record (*e.g.*, Jahns, 1955, pp. 1057–1067; Chadwick, 1958; *c.f.* King, 1948), have been applied in the present study to the selection of occurrences for critical analysis. Although the writers are convinced that the bodies under discussion are igneous intrusives, their primary intent here is not so much to defend this view as to determine whether it is compatible with all known features of these bodies and their contained rock types.

*Pegmatite-aplite relationships.* Layered pegmatite-aplite intrusives can be readily grouped into two major categories:

I. Composite bodies and complexes representing multiple injection of magma from external sources.
II. Bodies representing a single injection of magma, followed by segregation during crystallization and, in some occurrences, by autoinjection of residual fluid.

The second category can be subdivided into four classes as follows:

1. Bodies of aplite or fine-grained permatite with very large phenocrysts, or megacrysts.
2. Aplite bodies with marginal or interior pegmatite masses generally formed *in situ*.
3. Pegmatite bodies with marginal or interior aplite masses formed *in situ* or by autoinjection.
4. Highly asymmetric bodies whose upper parts consist mainly or wholly of pegmatite and whose lower parts consist mainly or wholly of aplite.

These classes can be readily identified, each in numerous and widely distributed occurrences, but various combinations and intergradations are by no means rare. Some aplite masses of Class 4, for example, contain abundant megacrysts and hence correspond to Class 1, and some bodies of Class 1 contain so many megacrysts or so many clusters of such large crystals that they could be identified with Class 2 or even with Class 3. The basic distinctions, however, are easily recognized among most of the pegmatite-aplite intrusives that have been observed by the writers.

### (a) Composite bodies and complexes

Many bodies of aplite are plainly intrusive into, across, or along earlier-formed bodies of pegmatite, and the reverse relationship is almost as common (*e. g.*, Cook, 1925; Derry, 1931; Heinrich, 1945; Jahns *et al.*, 1952, p. 30; Olson *et al.*, 1946, p. 10). Successive injection is most simply expressed where dikes of pegmatite and aplite occupy sets of primary fractures within cogenetic plutons of granitic rock,

FIG. 1. Intrusive contact between pegmatite-aplite sill and overlying faintly layered fine-grained quartz-albite-muscovite pegmatite (or coarse-grained aplite). Upper part of sill is coarse grained and rich in graphic granite; lower part, here incompletely exposed, is much finer grained and distinctly layered. Rock bodies dip to left and away from observer. East slope of Hiriart Mountain, Pala district, California.

and where one set of dikes transects another. Evidences of transection are supplemented, in many of these and other occurrences, by the presence of aplite apophyses in pegmatite or pegmatite apophyses in aplite, and by the relationships between pegmatite-aplite contacts and the disposition of primary flow structure within either or both rock bodies.

A gross layering results from the presence of sill-like masses of aplite (identified in some published accounts as fine-grained granite) within tabular bodies of older pegmatite. Similar injected masses of pegmatite within host aplite also have been observed, but are not so abundant. The source of the younger magma may have been external with respect to many of these composite bodies, but the possibility of autoinjection cannot be dismissed for numerous occurrences where the younger aplite or pegmatite appears to lie wholly within the older rock body. Even where local cross-cutting relationships can be recognized, it rarely is clear whether the transecting mass is a feeder or an apophysis.

Gross multiple layering attributable to successive injections of magma appears within many swarms and complexes of closely spaced parallel sills or dikes, as in the Keystone district of South Dakota (Orville, 1960, pp. 1473–1475) and the Pala district of southern California (Jahns and Wright, 1951, pp. 16–18). These tabular bodies, which generally range in thickness from a few inches to 25 feet, are in direct contact with one another in some places (Fig. 1) and are separated by plates or screens of country rock in others (Fig. 2). Although many of them are very thin, these country-rock screens tend to be continuous for considerable distances and to thicken, thin, or pinch out gradually. Where they are absent, the juxtaposed bodies of pegmatite or aplite commonly retain their respective identities, and layering within such complexes is then defined by sharp, in many places almost planar, parting-like contacts between adjacent bodies.

Added elements of layering are provided by the contrasting lithologic units within individual "two-ply" bodies that comprise indigenous pegmatite and aplite. Bodies of this kind, described farther on, are well represented among intrusive complexes, and the continuity of their consistently disposed internal units further distinguishes each body from its neighbors. Where the contact between two juxtaposed

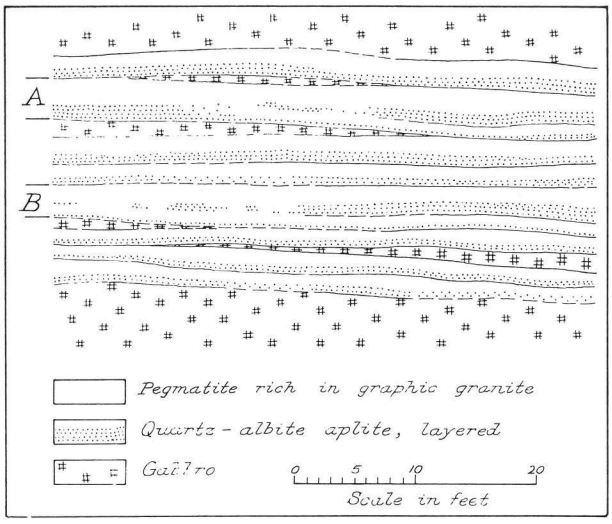


FIG. 2. Complex of parallel pegmatite-aplite dikes, some directly juxtaposed and some separated by thin septa and screens of gabbro. Nearly vertical longitudinal section normal to dike walls. Northwest of Alamo, Northern Baja California, Mexico.

pegmatite-aplite bodies gradually loses its definition and becomes unrecognizable, the units within these bodies commonly remain in their normal positions and thus attest to very limited mixing of the adjacent injected magmas (B, Fig. 2). In contrast, mixing and even homogenizing of such magmas is indicated where pairs of "two-ply" bodies can be traced into single bodies with a correspondingly simple "two-ply" internal structure (A, Fig. 2). The distribution of pegmatite and aplite in the transition zones generally reflects increasing degrees of mixing of the adjacent magmas, presumably in directions toward parts of the respective systems in which these magma pairs were almost wholly liquid at the same time.

(b) Individual pegmatite-aplite bodies

The following generalizations concerning individual pegmatite-aplite bodies have been drawn mainly from the writers' studies of occurrences in New England, the southern Appalachian region, Minnesota, Missouri, Texas, the Black Hills region, the Rocky Mountain region from Montana to New Mexico, southern Nevada and western Arizona, and southern California and adjacent parts of Mexico. Many of these occurrences also have been studied by other investigators, several of whom have given careful attention to relationships between pegmatites and aplites; references to their published views are made farther on. Most of the illustrations in the present paper show pertinent and well-exposed relationships in the pegmatite districts of southern California and Baja California, but they fairly represent features observed in numerous other districts as well.

(i) Porphyritic aplites and pegmatites. Many aplites and very fine-grained pegmatites contain prominent anhedral to euhedral phenocrysts, or megacrysts, that range in maximum dimension from about an inch to nearly 5 feet (*e.g.*, Wheeler, 1935; Jahns, 1953; Varlamoff, 1954; Orville, 1960; Volborth, 1962). By far the most common megacryst constituent is perthite, with or without graphically intergrown quartz. Large individuals of quartz also are present at some localities, as are strips and plates of muscovite or biotite. Megacrysts of apatite, beryl, garnet, tourmaline, allanite, monazite, tantalite-columbite and other accessory minerals are by no means rare, but normally they are distinctly smaller than the perthite crystals.

The groundmass of these rocks consists typically of quartz and albite, along with lesser amounts of microcline and various combinations of micas and accessory minerals. It is hypautomorphic-granular with a sugary appearance, and the average grain size is in the range 0.2–5.0 mm for most occurrences. Where the groundmass is coarser than the limits usually set for aplites, the term pegmatite is applied to the rock mainly on the basis of the megacrysts, which are of giant size relative to the other constituents.

All gradations have been noted between rock in which the megacrysts are uniformly or irregularly scattered and rock in which such crystals are notably concentrated in the upper part of the intrusive body. The limiting case is an asymmetric "two-ply" body in which the upper part is coarse-grained perthite-rich pegmatite and the lower part is albite-rich aplite (Fig. 2). The entire range in distribution of megacrysts commonly is observable within a single body. All these kinds of prophyritic rock also grade into nonporphyritic aplite through progressive decreases in number of megacrysts and corresponding increases in the amount of groundmass microcline, and into medium- to coarse-grained pegmatite through progressive coarsening of the groundmass.

The groundmass of the porphyritic aplites and pegmatites ranges from essentially homogeneous and massive to sharply and strikingly layered. The layering is compositional, and is expressed mainly by thin, continuous laminations that are relatively rich in garnet, tourmaline, muscovite or combinations thereof. These parallel units are separated by somewhat thicker laminations in which such minerals are much less abundant or absent. Layers thinner than 3 mm in general are most sharply defined, but some as thick as 10 cm can be identified without difficulty. Layered groundmass rock commonly is traceable into homogeneous rock, either laterally through abrupt termination or gradual fading of the laminations, or in directions normal to the layering through sudden lack of additional laminations or through progressive thickening and fading of succeeding laminations.

The mineralogic layering tends to be parallel with the walls of the containing intrusive body, and to reflect irregularities in these walls. In detail, individual layers butt against the megacrysts, wrap partly around them, or pass through them as outlines of growth sufaces within the large crystals (Fig. 7; *c.f.* Jahns, 1953, pp. 584–585; Staatz and Trites, 1955, pp. 23–24; Orville, 1960, pp. 1471–1472). Orientation of the layering adjacent to some perthite megacrysts is highly variable and plainly re-

flects the influence of these crystals, as pointed out by Orville (1960, pp. 1471–1472, 1487), but his suggestions that the layers were distorted, contorted, and disrupted by subsequent growth of the megacrysts seem open to question. The observed relationships are equally well explained in terms of simultaneous crystallization of layered aplite and large perthite individuals, and it is difficult to account for the "phantom" layers within the perthite crystals in any other way. The writers are in full accord, however, with Orville's conclusion (p. 1472) that numerous irregular grains of plagioclase and quartz within the megacrysts are genetically related to both the "phantom" layers and the fine-grained groundmass outside.

Evidence of small-scale deformation is widespread in the layered groundmass of some intrusive bodies. Movement is indicated by flexures that suggest a uniform direction of dragging, by piercing folds, and by ruptures and very small faults that have been "healed" through subsequent crystallization. That most of the disturbance occurred during consolidation of the bodies also is indicated by protoclastic structure in the rocks thus affected, and by the presence of adjacent younger layers that are undeformed (Fig. 7B). Effects of deformation can be observed in all parts of the layered sequences, and normally can be distinguished from primary irregularities that are confined to the immediate neighborhood of megacrysts; in places they clearly have been superimposed upon such irregularities.

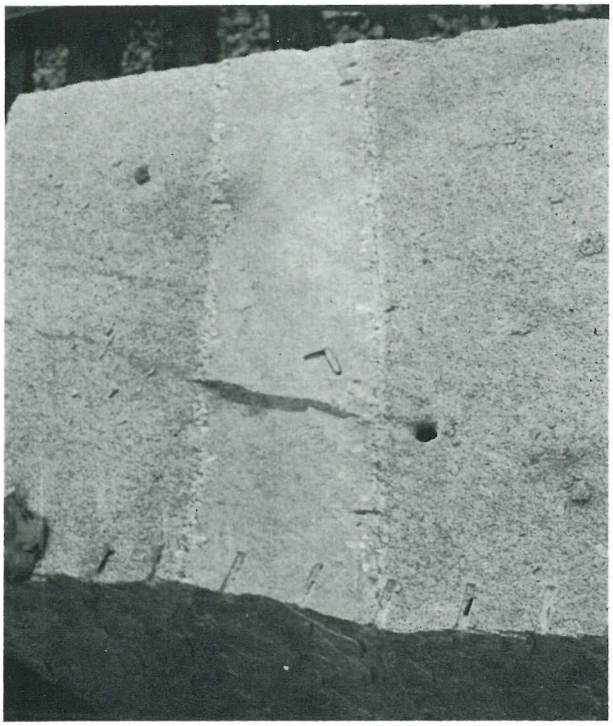

FIG. 3. Dike of essentially massive aplite fringed with large, inward-directed crystals of potash feldspar. Granite block in H. E. Fletcher quarry, Westford, Massachusetts.

(ii) Symmetrical pegmatite-aplite bodies. The intrusives herein referred to as symmetrical include aplite bodies with simple fringes of megacrysts (Fig. 3) or pegmatitic crystal aggregates, aplite bodies with interior masses of pegmatite that are irregularly or systematically disposed, and pegmatite bodies with marginal or interior masses of aplite (*e.g.*, Watson, 1902; Andersen, 1931, pp. 29–31; Emmons, 1940, p. 8; Varlamoff, 1954). The aplite bodies with coarse-grained margins appear either to have begun their crystallization as pegmatites and completed it as aplites, or to have crystallized both coarse- and fine-grained material simultaneously through some process of segregation. Layers, lenses, and patches of pegmatite entirely within bodies of aplite also appear to have been formed *in situ*. Some of them transect the host aplite on a small scale and evidently are very late products of crystallization. Others are traversed by layers that represent the adjacent aplite, the relationships suggesting essentially simultaneous development; these pegmatite masses can be viewed as analogues of the megacrysts described above.

Aplitic rock forms selvages along the margins of many pegmatite bodies, including some with pronounced internal zoning (Cameron *et al.*, 1949). Where present in the interiors of pegmatite bodies, it generally forms thicker masses of tabular to highly irregular shape. These masses commonly transect pegmatite in some places, butt against it in others, and are cut off by pegmatite in still others. Features indicating autoinjection from other parts of the host body are characteristic of many occurrences.

A simple or complex gross layering results from the distribution of pegmatite and aplite in most of the symmetrical bodies (Fig. 3), and an additional layering is contributed in numerous bodies by lithologically contrasting pegmatite zones. On a smaller scale, some of the aplite masses are flow layered; this structure typically is expressed by a very faint to distinct taffy-like streakiness that is quite different from the more regular mineralogic layering described earlier (Fig. 4). The mineralogic layering is present in a few of the aplites that do not exhibit flow structure, but it rarely is a conspicuous feature. Deformation of the layers, presumably by local movements during crystallization, is not uncommon.

(iii) Asymmetric pegmatite-aplite bodies. Highly asymmetric pegmatite-aplite bodies have been reported from many parts of the world (*e.g.*, Waring, 1905; Schaller, 1925; Derry, 1931; McLaughlin, 1940; Merriam, 1946; Heinrich, 1948; Hanley, 1951; Jahns and Wright, 1951; Gates, 1954; Varlamoff, 1954; Sheridan, 1955; Staatz and Trites, 1955; Thurston, 1955; Hutchinson and Claus, 1956; Simpson, 1960; Orville, 1960), and they are far more abundant than the published record would indicate. Their upper parts characteristically are dominated by medium- to coarse-grained perthite-rich pegmatite, and their lower parts by aplite or very fine-grained pegmatite that is rich in albite. This lithologic separation is essentially complete in some bodies, regardless of their shape or attitude; thus the aplitic rocks appear in the footwall parts of moderately dipping to horizontal tabular bodies (Figs. 1, 2, 4), and in the keelward parts of bodies that dip very steeply or are not tabular in form. The lithologic contrast is considerably less than complete in most occurrences, where the lower aplitic rock contains numerous perthite megacrysts or layers and pods of potassic pegmatite and the upper pegmatitic rock contains fine-grained albite-rich interstitial material or poorly-defined masses of sodic aplite.

The masses of albite-rich aplite generally constitute from 10 to 45 per cent of the containing intrusive bodies. Their relative abundance is less than 10 per cent in many bodies, especially those that are not conspicuously asymmetric, but rarely is it greater than 45 per cent. Among all the intrusives that have been examined by the writers, the distinction between aplite and overlying pegmatite is most evident in horizontal to moderately inclined dikes and other tabular bodies. As in groundmass of the porphyritic aplites described earlier, some of these footwall aplites are essentially massive whereas others are mineralogically layered, and in places strikingly so (Figs. 5, 6). Various concentrations of garnet, tourmaline, and muscovite define the thinnest and sharpest laminations, which typically are 0.5 to 3 mm thick, whereas adjacent laminations that are poor in these minerals tend to be thicker. Fine-gained pegmatite commonly forms still thicker conformable layers within the aplitic sequences (Figs. 5, 6), some of which also are featured by concordant rows of perthite crystals (series of triangles in footwall aplite of Fig. 4; also Fig. 7E), tourmaline prisms, or muscovite plates.

Although properly referred to as megacrysts, the relatively large individuals of perthite, graphic granite, tourmaline, and muscovite within the aplitic rocks ordinarily are much smaller than crystals of the same minerals in the overlying pegmatitic rocks (Fig. 4). Where elongate, these megacrysts tend to be oriented normal to the aplite layering, which is grossly parallel with the adjacent walls of the containing intrusive bodies (*c.f.* Figs. 1, 2, 4, 7). As in the porphyritic aplites already described, the attitude of the layering is markedly influenced in detail by the large crystals.

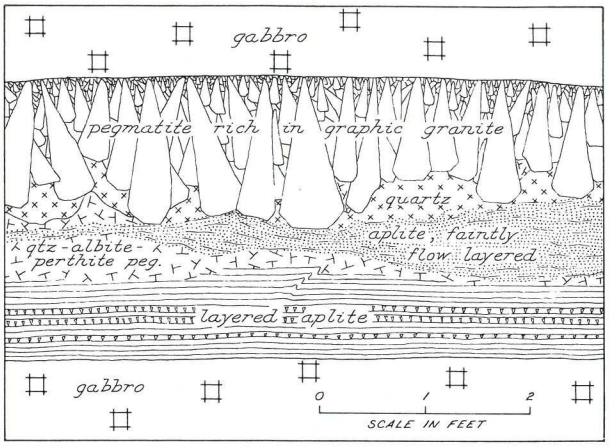


FIG. 4. Typical relationships between pegmatite and two contrasting varieties of aplite. Longitudinal section in asymmetric part of moderately-dipping Himalaya dike, Mesa Grande district, California. Composition of central aplite is near the granite minimum (large solid circle on MG curve, Fig. 10), whereas that of footwall aplite is markedly sodic (left-hand end of MG curve, Fig. 10).

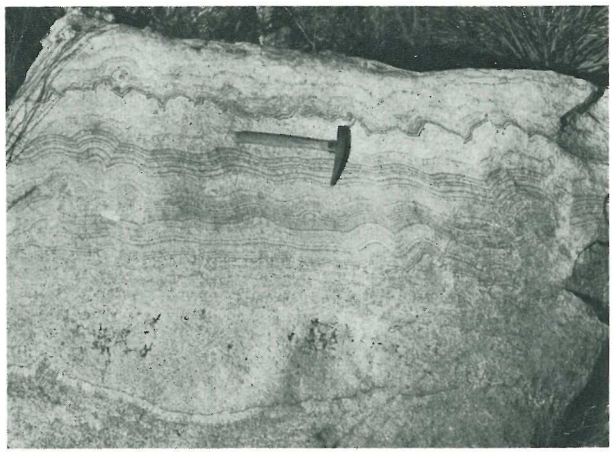

FIG. 5. Quartz-albite aplite with thin, sharply-defined garnet-rich layers and a few thicker layers of fine-grained pegmatite rich in perthite. Some of the nested loops in the layering lie above crystals or crystal aggregates of perthite with graphically intergrown quartz (*c.f.* Fig. 7, D). South slope of Hiriart Mountain, Pala district, California.

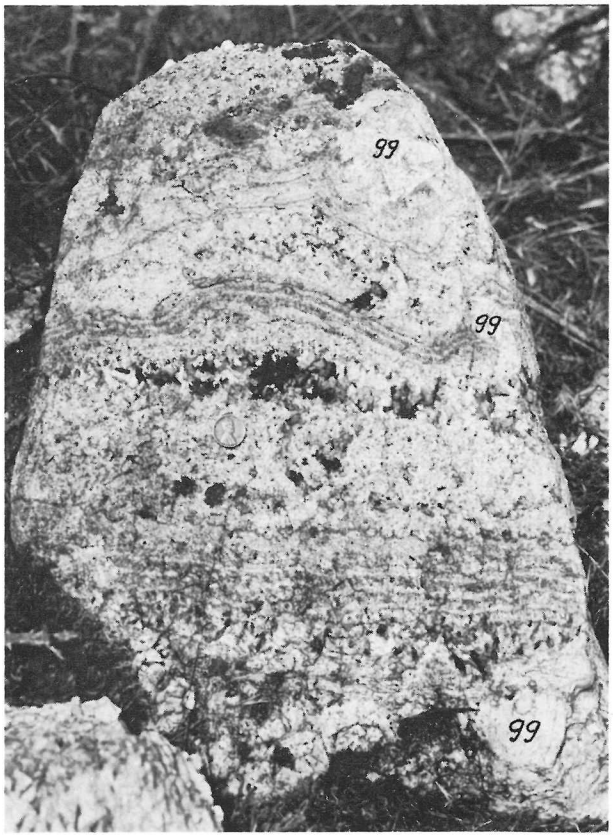


FIG. 6. Layered complex of fine- to medium-grained perthite-quartz-albite-schorl pegmatite and quartz-albite-schorl aplite, with scattered large crystals of perthite and graphically intergrown quartz (gg.)

In several districts the megacrysts of perthite, with or without graphically intergrown quartz, are distinctly elongate parallel to the *a*-axis. Some laminations in the adjacent aplite terminate abruptly against such crystals, but others pass through them along deflected paths that outline "phantom" surfaces (Fig. 7A, C, F; Figs. 8, 9). The distribution of included laminations clearly reveals that these megacrysts grew toward the center of the intrusive body, that some of them broadened markedly as they grew, and that most of them, during their growth, projected somewhat ahead of the aplite layers developing adjacent to them. Younger aplite layers curve around the ends of the megacrysts, forming loops that become successively broader and more subdued (Figs. 5, 7A, C, D). Some megacrysts are gradational into surrounding aplite, and Schaller (1925, 1953) has demonstrated extensive albitization of microcline in such situations. In places the relations are further complicated by stringers and patches of younger coarse-grained perthite and graphic granite (Fig. 9).

## COMPOSITION

*Methods of determination.* Data on composition have been obtained for pegmatite-aplite dikes in the Harding area and Petaca district of New Mexico and the Pala, Rincon, and Mesa Grande districts of southern California. Composite samples of both aplite and pegmatite in the Main Harding dike, New Mexico, were obtained from diamond-drill cores, from numerous outcrops, and from the walls of extensive mine workings. The average composition of each rock type was determined by chemical analysis, and the bulk composition of the entire dike was calculated by weighting the analyses according to the respective abundance of pegmatite and aplite. These abun-

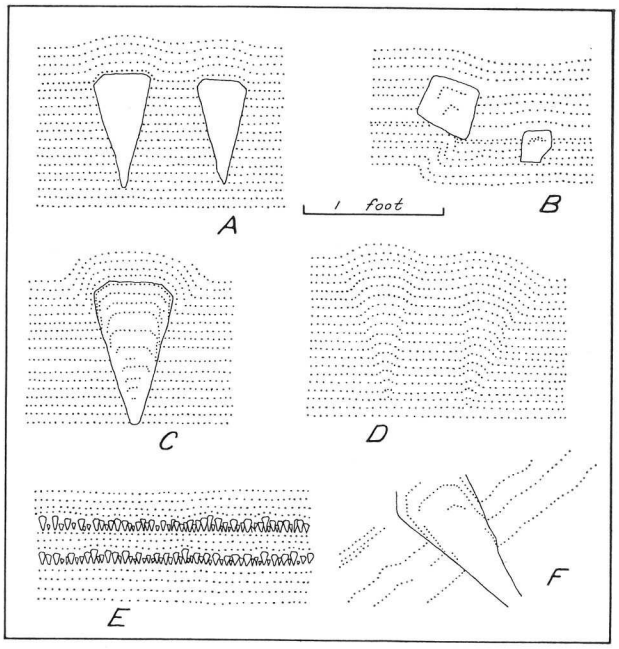


FIG. 7. Typical relationships between thinly layered quartz-albite aplite and relatively large individuals of perthite with graphically intergrown quartz. Vertical sections in footwall parts of pegmatite dikes, southern California. Aplite layering shown diagrammatically. A. Tapered crystals of perthite, El Molino dike, Pala district. B. Equant crystals of perthite with included aplite layers, Mack dike, Rincon district. C. Tapered perthite crystal with growth zones outlined by aplite layers, Himalaya dike, Mesa Grande district. D. Fan structure in aplite layering, with small patches of graphic granite (not shown) in lower part of each fan. Katerina dike, Pala district. E. Layers of small perthite crystals within aplite, Angel Field dike, Mesa Grande district. F. Tapered perthite crystal with growth zones outlined by widely-spaced aplite layers, Himalaya dike, Mesa Grande district.

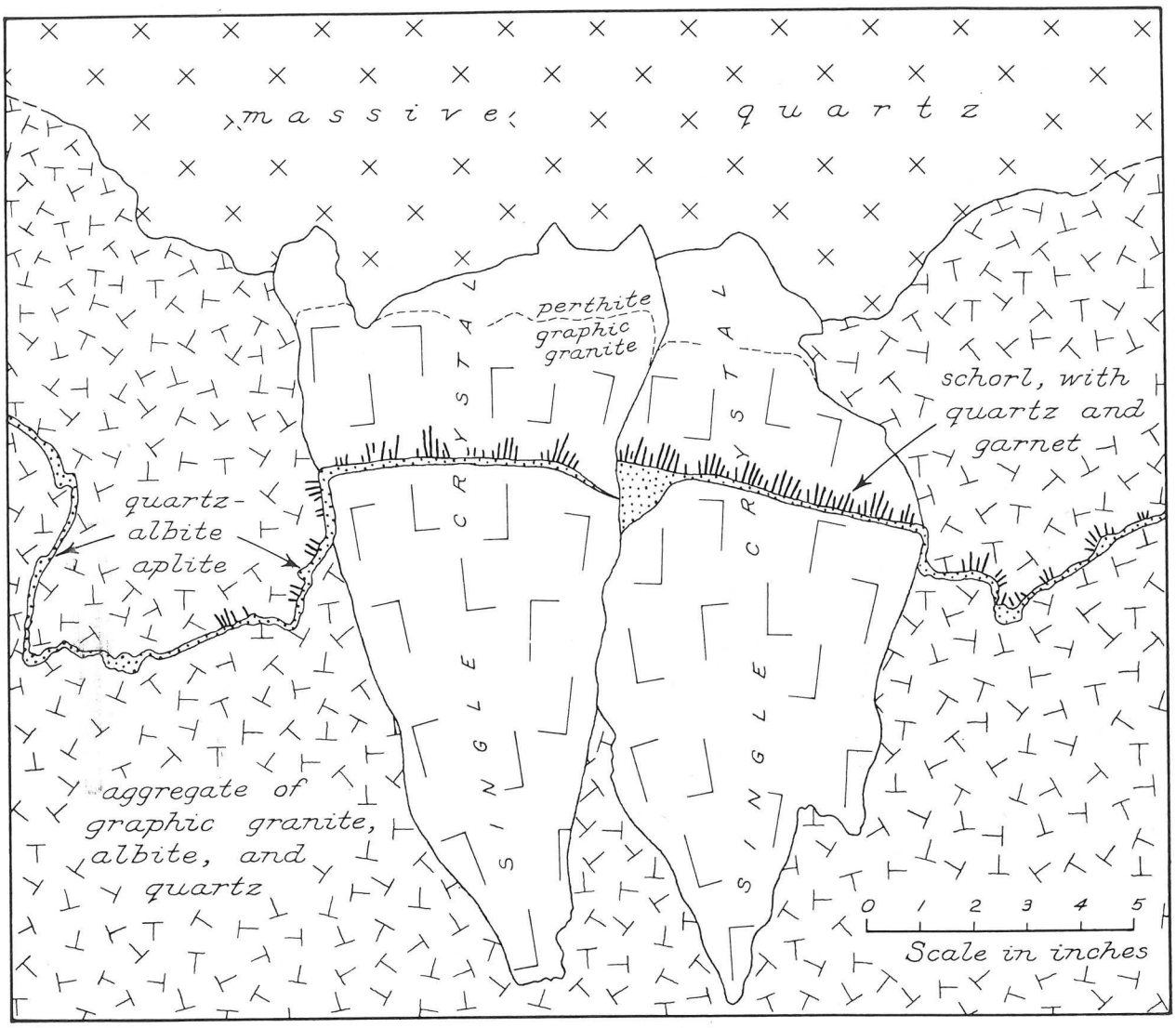


FIG. 8. Relationships among large crystals of perthite with graphically intergrown quartz, aggregate of large anhedral crystals of quartz, medium-grained graphic granite-quartz-albite pegmatite, and quartz-albite aplite. Vertical face of gently-dipping pegmatite dike, Los Gavilanes, Northern Baja California, Mexico.

dances were estimated directly from measurements in the field and indirectly from detailed plans and sections of the dike.

A similar approach was used for the Katerina dike in the Pala district and the Upper Mack dike in the Rincon district, except that sampling and measurements were confined to outcrops and mine workings. The relative amounts of aplite and pegmatite in the Katerina dike were determined megametrically by making measurements along a set of linear traverses oriented normal to the dike walls and spaced 2 feet apart. The relative amounts of megacrysts and aplitic groundmass in the Upper Mack dike were determined through measurements along traverses spaced 6 inches apart, and two sets of these traverses, at right angles to each other, covered each rock exposure.

The fine-grained portions of the White dike in the Petaca district and the Himalaya dike in the Mesa Grande district were sampled and analyzed chemically. The coarse-grained portions were analyzed modally by the technique applied to the Upper Mack dike, except that the lines of traverse were 1 foot apart. Data on average composition of all minerals

FIG. 9. Large crystal of perthite with graphically intergrown quartz, flanked and capped by much finer-grained layered aplite-pegmatite. Some schorl-rich layers form angular, upward-extending loops that outline growth zones in the perthite crystal (*c.f.* Fig. 5 and Fig. 7, C, F). Several layers are interrupted by an irregular and apparently younger clot of perthite and quartz (pq). Himalaya dike, Mesa Grande district, California.

amounting to more than 1 per cent of the pegmatitic rocks were obtained by chemical analysis of a composite sample of each mineral. The modal and chemical data then were combined to yield an average composition for the coarse-grained rocks in each dike.

All rock compositions, as expressed in chemical terms, were converted to normative compositions, and these were then recast on the basis of normative albite+orthoclase+quartz=100. The results are plotted in Fig. 10 for direct comparison with the trend of the isobaric minimum in the system $NaAlSi_3O_8$-$KAlSi_3O_8$-$SiO_2$-$H_2O$ under water-vapor pressures ranging from 0.5 to 4 kilobars. Data from the excellent quantitative analyses by Orville (1960) for pegmatites in the Keystone district of South Dakota and by Simpson (1960) for pegmatites in the Ramona district of California have been recalculated on the same basis, and the results also are plotted in Fig. 10.

*Composition of pegmatite-aplite bodies.* As represented by the right end of the Ram curve and by the interior points (small solid circles) on the other curves in Figure 10, most of the analyzed pegmatite-aplite bodies have bulk compositions that lie near the thermal minimum in the system $NaAlSi_3O_8$-$KAlSi_3O_8$-$SiO_2$-$H_2O$. Moreover, all of the compositions lie on the silica side of the isobaric minimum, and on the average, they fall at positions corresponding to elevated water-vapor pressures (2000 to 4000 bars) along the minimum.

The compositions of the central masses of flow-layered aplite (large solid circles in Fig. 10) within the Katerina and Himalaya dikes also are near the "granite minimum," and correspond very closely to the bulk compositions of the respective containing dikes. Numerous published analyses suggest that the compositions of simple aplites that are not intimately associated with pegmatite are strongly clustered in the same general area of the diagram.

Figure 10 emphasizes the great compositional contrasts between footwall or keelward masses of aplitic rock and overlying masses of coarse-grained rock in highly asymmetric intrusive bodies (BR, BA, Hard, Pe, Pa, and MG curves). In terms of their respective compositions, as represented by the open circles at opposite ends of the curves, these masses appear as complementary parts of intrusive bodies whose bulk compositions tend to lie near the "granite minimum." The length of each curve reflects the difference between the ratios of major alkalies in the aplitic and pegmatitic portions of the containing body. Further, it corresponds satisfactorily with the respective lithologies of these aplitic and pegmatitic portions, in effect indicating the extent to which these rocks are modally as well as spatially distinct from each other.

Maximum compositional contrasts are shown by the CJ and Rin curves in Figure 10, which relate the megacrysts and groundmass of porphyritic aplitic rocks. The megacrysts consist of perthite and graphically intergrown quartz, and they contain more of the $KAlSi_3O_8$ component than any of the other analyzed materials. If viewed as products of segregation, they reflect major abstraction of $KAlSi_3O_8$ without any significant change in the ratio

of $NaAlSi_3O_8$ to $SiO_2$ in the remainder of the system. It is interesting to note that the same general trend is shown by most of the other curves.

## Origin

*Layering.* The gross layering produced by multiple injection of magma to form tabular bodies of pegmatite and aplite generally can be identified with little difficulty. Apophyses and cross-cutting relationships confirm the age differences within such complexes, and individuality of the intrusives is variously revealed by screens of country rock, by well-defined partings between directly juxtaposed bodies, and by the continuity of lithologic units within the respective bodies. Most layers and lenses of aplite formed within pegmatite bodies, either by autoinjection or by injection from external sources, also are easily recognized through their contact relationships and the attitude of flowage structure within them. The remainder of the observed gross layering is attributable to masses of pegmatite and aplite that evidently were formed *in situ* and that appear to reflect processes of fractional crystallization and segregation that are discussed farther on.

Layering on much smaller scales distinguishes many aplites and some rather fine-grained pegmatites that have undergone flowage during their consolidation. Such flow structure generally appears as a streakiness resulting from thin, discontinuous, and faintly defined layers of slightly contrasting grain size. Some also differ slightly in composition. Many of the crystals in these layers are broken or granulated, and evidences of rolling and attenuation are fairly widespread. Flow layers in marginal parts of the rock masses commonly tail away from adjacent buttresses and projections of older rock in a manner indicating unidirectional movement.

Much less obvious is the origin of the mineralogic layering in the groundmass of porphyritic aplites and pegmatites and in the fine-grained parts of highly asymmetric pegmatite-aplite bodies. Formation of the layered sequences has been contrastingly ascribed, for example, to simple crystallization from a "hydrous magma" (Waring, 1905, p. 366); to rhythmic crystallization from pegmatitic liquids locally impoverished in volatile constituents (Jahns, 1955, p. 1103); to rhythmic primary crystallization, accompanied in some instances by streaming of liquid (Staatz and Trites, 1955, pp. 23–24; Thurston, 1955, pp. 30–31, 65); to rhythmic replacement in an early, probably primary aplite (Merriam, 1946, pp. 242–243); to later-stage replacement of pre-existing graphic granite by soda-rich solutions (Schaller, 1925, pp. 274–277); and to channel-controlled hydrothermal replacement of earlier pegmatite minerals (McLaughlin, 1940, pp. 62–63). Evidence for replacement of perthite by albite of the layered sequences is undeniable in many occurrences, as is evidence for replacement of the layered sequences by coarse-grained perthite; it seems appropriate, however, to regard these relationships as second-order features of not more than local significance, as the great bulk of the layered rock shows no evidence of having been formed at the expense of earlier solid material. Moreover, the widespread relationships between albite-rich layered rock and perthite megacrysts strongly indicate that these texturally and compositionally contrasting materials formed at essentially the same time.

If primary crystallization from a magma is accepted as the dominant process in development of the layered sequences, as argued by several investigators (*e.g.*, Orville, 1960, p. 1486; also see above), it remains to account for the origin of the remarkably uniform laminations. It is tempting to regard them as products of gravitational crystal settling. They show some of the characteristics of igneous cumulates described from numerous basic and ultrabasic complexes (*e.g.*, Wager, 1953; Wager *et al.*, 1960), and the garnet and tourmaline that distinguish so many of them are relatively heavy minerals. On the other hand, they do not exhibit the graded bedding, cut-and-fill structure, cross-bedding, and other sedimentational features that are common in igneous cumulates. Instead, some of their features are all but impossible to reconcile with a mechanism of crystal settling; these include veneers of garnet, tourmaline, and other minerals of the aplite layers attached to what must have been overhanging surfaces (Fig. 7C, F), as well as fringes of tourmaline prisms and muscovite plates oriented normal or nearly normal to the layering (Fig. 8).

Rhythmic primary crystallization, with development of successive laminations *in situ*, seems in best accord with all known features of the mineralogically layered rocks. Episodic development of crops of garnet, tourmaline, or muscovite crystals may well have resulted from alternating periods of undersaturation and supersaturation with respect to these minerals, perhaps in response only to a very slowly dropping temperature gradient, but perhaps also in response to slight fluctuations in confining pressure on a magma saturated with volatile constituents.

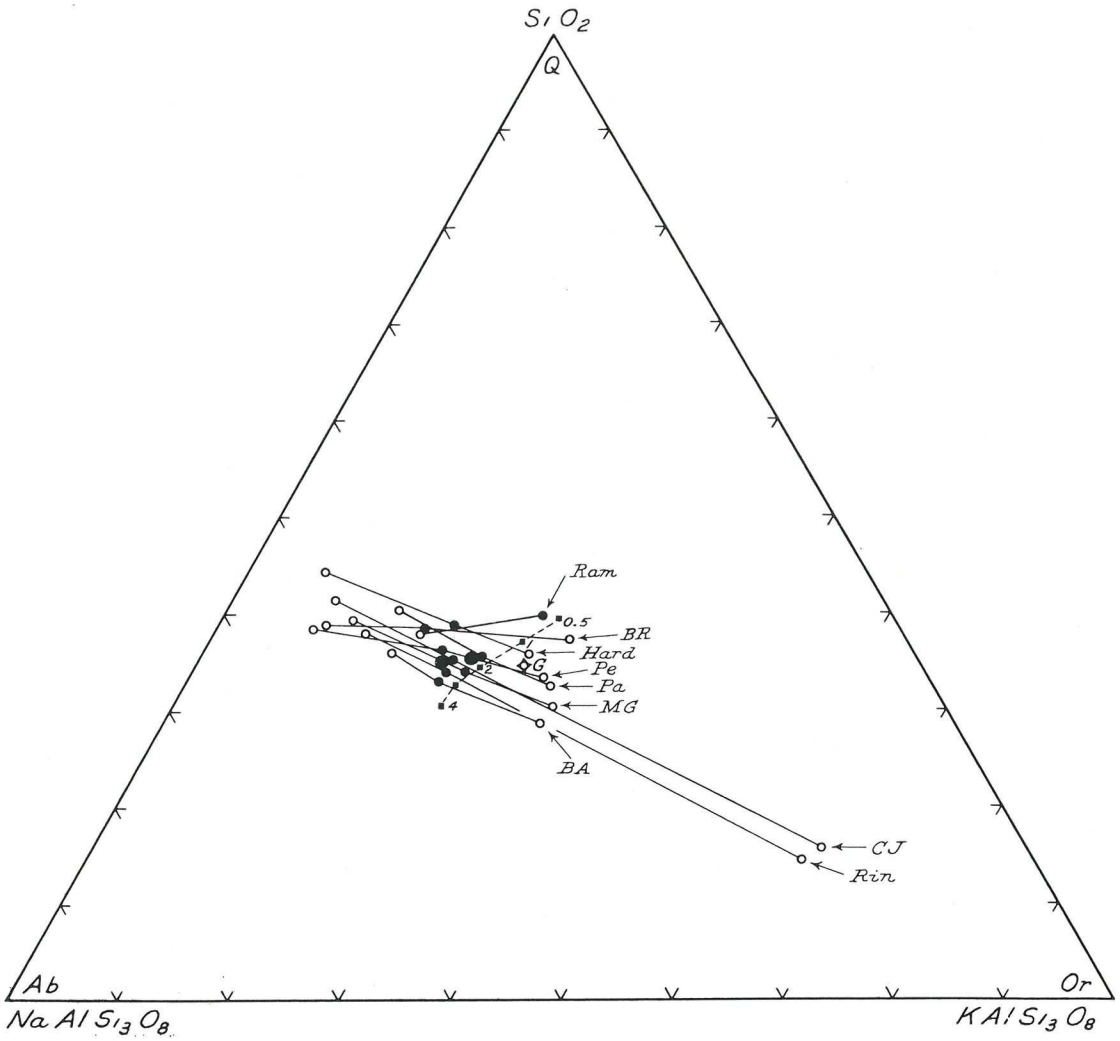


FIG. 10. Distribution of normative albite, orthoclase, and quartz in pegmatite-aplite intrusives, related to trend of the isobaric minimum (dashed line) in the system $NaAlSi_3O_8$-$KAlSi_3O_8$-$SiO_2$-$H_2O$ under water-vapor pressures ranging from 0.5 to 4 kilobars. G—normative plot for average of 571 analyzed granitic rocks (Tuttle and Bowen, 1958, pp. 75, 79). Other points as follows:

| *Curve* | *Rock body* | *Point (with respect to curve)* | *Analyzed material* | *Method of analysis* | *Source of data* |
|---|---|---|---|---|---|
| BR | Layered member, Buell Ranch pegmatite complex, Keystone district, South Dakota | Left end | Aplitic footwall unit, locally layered | Chemical | Orville (1960) |
| | | Right end | Porphyritic hanging-wall unit | Chemical | |
| | | Interior | Total layered member | Chemical & modal | |
| CJ | Camp Judson pegmatite, Keystone district, South Dakota | Left end | Aplitic groundmass, layered | Chemical | Orville (1960) |
| | | Right end | Average perthite megacryst | Chemical[1] | |
| | | Interior | Total rock | Chemical & modal | |
| BA | Burnt Area pegmatite, Keystone district, South Dakota | Left end | Porphyritic footwall unit | Chemical & modal | Orville (1960) |
| | | Right end | Porphyritic hanging wall unit | Chemical & modal | |
| | | Interior | Total pegmatite | Chemical & modal | |
| Ram | Pegmatite dikes, Ramona district, California | Left end | Footwall aplite, layered | Chemical | Simpson (1960) |
| | | Right end | Total pegmatite & aplite | Chemical & modal | |

(*Continued on facing page*)

[1] Determinations of $Na_2O$ and $K_2O$; $Al_2O_3$ and $SiO_2$ calculated on basis of assumption that only alkali feldspars and quartz are present in the mode.

*Pegmatites and aplites.* A very close genetic relationship between pegmatites and aplites has been advocated and documented by many investigators, from Andersen (1931) to Zavaritsky (1950), and views in this area have been summarized most recently by Schneiderhöhn (1961, pp. 493–503). Magmatic pegmatite and pegmatite-aplite bodies have been increasingly regarded as products of crystallization in closed or "restricted" systems, chiefly on the basis of structural, textural, compositional, and paragenetic relationships (for a summary of arguments, see Jahns, 1955, pp. 1058–1097), and most of the contrasting lithologic units within such bodies have been ascribed to fractional crystallization and crystal segregation. Aplites generally have been viewed as products of volatile-poor magmas that otherwise resembled pegmatite-forming magmas, but there has been much disagreement as to how these melts were formed, as to whether they incurred a loss of volatile constituents before or after emplacement, and as to whether they crystallized in open or closed systems (*c.f.* Andersen, 1931; Derry, 1931; Emmons, 1940). Increases in viscosity due to escape of volatiles have been most commonly referred to in explaining the grain size of aplites (*e.g.*, Vogt, 1923; Andersen, 1931).

The present writers regard all the aplitic rocks discussed in this paper as derivatives of magmas that were pegmatitic, *i.e.*, that contained substantial amounts of dissolved water or other volatile constituents. However, quite different processes are thought to account for two contrasting types among these aplites:

1. Normal aplites, with compositions near the "granite minimum," that occur as separate bodies containing little or no pegmatite and that also form distinct masses within some bodies of pegmatite.
2. Sodic aplites that form separate bodies containing abundant megacrysts or pegmatite and that also occur as segregated masses within many bodies of pegmatite.

Gradations between these types of aplite and among these modes of occurrence are common, and they probably reflect combinations of the processes outlined below.

It is suggested that the normal aplites were formed from magmas, including rest-magmas in pegmatite systems, that incurred substantial losses of dissolved volatiles through reduction in confining pressure. This is thought to have occurred either during or after emplacement, as argued by Emmons (1940, pp. 5–8). Prior to any loss of volatiles, the liquidus temperatures of such pegmatitic magmas would be relatively low, say in the range 600°–680° C., at moderate to high confining pressures. If a magma in this temperature range were to lose volatiles through a drop in confining pressure, its liquidus temperature

| *Curve* | *Rock body* | *Point (with respect to curve)* | *Analyzed material* | *Method of analysis* | *Source of data* |
|---|---|---|---|---|---|
| Hard | Main Harding dike, Taos County, New Mexico | Left end | Footwall aplite | Chemical | This paper |
| | | Right end | Pegmatite, remainder of dike | Chemical | |
| | | Interior | Total rock in dike | Chemical & modal | |
| Pe | White dike, Petaca district, New Mexico | Left end | Fine-grained pegmatite, keel of dike | Chemical | This paper |
| | | Right end | Pegmatite, remainder of dike | Chemical & modal | |
| | | Interior | Total rock in dike | Chemical & modal | |
| Pa | Katerina dike, Pala district, California | Left end | Footwall aplite, layered | Chemical | This paper |
| | | Right end | Pegmatite, remainder of dike | Chemical | |
| | | Interior | Total rock in dike | Chemical & modal | |
| | | Interior (large dot slightly below curve) | Aplite in small central mass, slightly flow layered | Chemical | |
| MG | Himalaya dike, Mesa Grande district, California | Left end | Footwall aplite, layered (Fig. 4) | Chemical | This paper |
| | | Right end | Pegmatite, remainder of dike | Chemical & modal | |
| | | Interior | Total rock in dike | Chemical & modal | |
| | | Interior (large dot) | Central aplite, faintly flow layered (Fig. 4) | Chemical | |
| Rin | Upper Mack dike, Rincon district, California | Left end | Aplitic groundmass, in part layered | Chemical | This paper |
| | | Right end | Average perthite megacryst | Chemical[1] | |
| | | Interior | Total rock in dike | Chemical & modal | |

would rise in quick response and crystallization in flood necessarily would follow, regardless of any change in viscosity. The aplite thus formed would be a quenched rock, but in this instance the result of a "pressure quench."

The sodic aplites, together with their complementary pegmatites or perthite megacrysts, constitute bodies whose bulk composition trends toward correspondence with the thermal valley of petrogeny's residua system. These rocks evidently were developed by processes of segregation, and their genesis can be explained in terms of the model proposed by Jahns and Burnham (1963) for the crystallization of granitic pegmatites. According to this model, segregation of major alkalies can occur in significant degree if a pegmatitic magma becomes saturated with volatile constituents, *i.e.*, if both silicate melt and vapor are present in the system. Experimental evidence indicates that potassium is extracted from the liquid by a vapor in preference to to sodium, and that potassium and other constituents can travel rapidly through the vapor in response to a temperature gradient. If the composition of the magma were at or near the thermal minimum for the confining pressure imposed upon it, preferential loss of the potassium feldspar component would promote crystallization of albite-rich rock from the melt, probably in the form of an aplite. Potash feldspar could crystallize from the vapor, either in the immediate vicinity or elsewhere in the system.

Experimental studies have shown that in general, the phases crystallized from the vapor are much coarser than those crystallized directly from the melt, and that the degree of segregation of alkali feldspars and other minerals is in part a function of gravitational rising of the vapor phase within the system. It seems probable that variations in distribution of the two fluid phases within a given intrusive, in distribution of alkalies between them, and in rates of diffusion of alkalies through the vapor could well account for the known relationships between the complementary pegmatitic and aplitic rocks that have been described.

*Relations with granites.* Pegmatites and aplites are found almost exclusively in the subsolvus granites. The subsolvus granites indicate a hydrous environment (Tuttle and Bowen, 1958, p. 139), and it is not surprising to find that the pegmatites are characteristically associated with them. On the other hand, the hypersolvus granites carry little, if any, pegmatitic and aplitic material. Pegmatites have been described in association with granites which are hypersolvus, but they are usually present in very small amounts.

Laboratory studies (Tuttle and Bowen, 1958, p. 74) have shown that granites crystallized at low water vapor pressure will carry a single alkali feldspar and quartz as the principal constituents (in nature, the alkali feldspar unmixes to perthite giving a perthite-quartz, hypersolvus, granite). If the confining pressure and the water content are high, two feldspars will crystallize side by side giving a subsolvus granite. In other words, water dissolves in the melt at high pressure and lowers the liquidus below the feldspar solvus, thereby permitting two feldspars, a plagioclase and potash feldspar, to crystallize together under equilibrium conditions. Normally, the potash feldspar contains appreciable soda feldspar in solid solution at the temperature of final magmatic crystallization, and it is necessary to unmix large quantities of soda feldspar to obtain a relatively pure potash feldspar which is characteristic of the subsolvus granites. This is accomplished by the vapor phase, which is a potent flux at the high pressures. These subsolvus granites and gneisses, commonly carrying a potash feldspar which contains less than 10 per cent albite, are the home of pegmatites and aplites. It is these granites that generate relatively large quantities of pegmatite and aplite material.

In contrast, the hypersolvus granites commonly contain no pegmatitic and aplitic material at all, and if present, it is usually in vanishingly small amounts. Warren and Palache wrote (1911, p. 126) "Pegmatite development, so common in many granites, were almost unknown in the Quincy granites until some few years ago, a pegmatite was discovered in one of the quarries and later two other pegmatites were exposed in another quarry." A careful search of twelve quarries during the present study did not turn up a single pegmatite or aplite. Where present, the pegmatites of the hypersolvus granites are themselves hypersolvus, indicating high temperatures of crystallization and presumably low initial contents of water in the magmas. Furthermore, the small amounts of water vapor present during the end stages of magmatic crystallization probably escaped before cooling to the temperatures of the solvus, because the perthite has not been recrystallized to separate grains of plagioclase and microcline. No examples of hypersolvus aplites have been found.

There are all gradations between these two extreme granite types, and it is suggested that the amount of pegmatitic material and the type of granite will de-

pend to a large extent on the water content of the magma. The hypersolvus granites represent magmas initially low in water or magmas that lost much of their water before consolidation as a result of near-surface crystallization where the overburden is not great enough to permit large amounts of water to remain in solution. The subsolvus granites, on the other hand, may carry large amounts of pegmatitic and aplitic material or none at all, depending on the cooling history of the intrusive.

*Role of water vapor.* Water vapor is essential for the formation of granite pegmatites and aplites, and perhaps the most important function is to provide a low-viscosity fluid for the growth of large crystals. It is also important in lowering the liquidus temperature of the magma, thereby permitting two alkali feldspars to crystallize side by side. Liquidus lowering also permits certain hydrous phases which are unknown as phenocrysts of rhyolites (such as muscovite) to appear at liquidus temperatures. Water vapor serves to recrystallize early-formed minerals and act as an agent for metasomatic reactions. An essential function of water vapor in the genesis of aplites is to provide a mechanism for quenching by relief of pressure. This is probably the only way that rapid quenching can be induced in deepseated rocks.

Thus we have four important functions of the water vapor in the genesis of pegmatites and aplites:

1) lowering of the liquidus temperature by solution in the liquid, 2) providing a low viscosity medium for transport of material, 3) promoting recrystallization and metasomatic replacement of early-formed crystals, and 4) affording a mechanism for quenching by relief of pressure.

## References


ANDERSEN, OLAF (1931) Discussions of certain phases of the genesis of pegmatities. *Nordsk Geol. Tidsskr.*, **12,** 1–56.

CAMERON, E. N., R. H. JAHNS, A. H. MCNAIR AND L. R. PAGE (1949) Internal structure of granitic pegmatites. *Econ. Geol. Mon.* **2.**

CHADWICK, R. A. (1958) Mechanisms of pegmatite emplacement. *Geol. Soc. Am. Bull.* **69,** 803–836.

COOK, C. W. (1925) Molybdenite deposit near New Ross, Nova Scotia. *Econ. Geol.* **20,** 185–188.

DERRY, D. R. (1931) The genetic relationships of pegmatites, aplites, and tin veins. *Geol. Mag.* **68,** 454–475.

EMMONS, R. C. (1940) The contribution of differential pressure to magmatic differentiation. *Am. Jour. Sci.* **238,** 1–21.

GATES, R. M. (1954) The bedrock geology of the Woodbury quadrangle, Connecticut. *Connecticut Geol. Nat. Hist. Survey, Misc. Series* **6.**

HANLEY, J. B. (1951) Economic geology of the Rincon pegmatites, San Diego County, California. *California Div. Mines, Spec. Rept.* **7-B.**

HEINRICH, E. Wm. (1945) Composite pegmatites of the Franklin-Sylva mica district, North Carolina (abs.). *Econ. Geol.* **40,** 594.

——— (1948) Pegmatites of Eight Mile Park, Fremont County, Colorado. *Am. Mineral.* **33,** 420–448, 550–588.

——— (1953) Zoning in pegmatite districts. *Am. Mineral.* **38,** 68–87.

HUTCHINSON, R. W. AND R. J. CLAUS (1956) Pegmatite deposits, Alto Ligonha, Portuguese East Africa. *Econ. Geol.* **51,** 757–780.

JAHNS, R. H. (1953) The genesis of pegmatites. I. Occurrence and origin of giant crystals. *Am. Mineral.* **38,** 563–598.

——— (1955) The study of pegmatites. *Econ. Geol., Fiftieth Ann. Vol.* 1025–1130.

——— AND C. W. BURNHAM (1963) Experimental studies of pegmatite genesis. I. A model for the crystallization of granitic pegmatites (in preparation).

——— W. R. GRIFFITTS, AND E. Wm. HEINRICH (1952) Mica deposits of the Southeastern Piedmont: Part I. General features. *U. S. Geol. Survey, Prof. Paper* **248-A.**

——— AND L. A. WRIGHT (1951) Gem- and lithium-bearing pegmatites of the Pala district, San Diego County, California. *California Div. Mines, Spec. Rept.* **7-A.**

KING, B. C. (1948) The form and structural relations of aplite and pegmatite dikes and veins in the Osi ores of the northern provinces of Nigeria and the criteria that indicate a nondilational mode of emplacement. *Jour. Geol.* **56,** 459–475.

LANDES, K. K. (1942) Effect of structure on intrusion of pegmatites, in *Ore Deposits as Related to Structural Features,* p. 140–143, Princeton Univ. Press, Princeton, New Jersey.

MCLAUGHLIN, T. G. (1940) Pegmatite dikes of the Bridger Mountains, Wyoming. *Am. Mineral.* **25,** 46–68.

MERRIAM, RICHARD (1946) Igneous and metamorphic rocks of the southwestern part of the Ramona quadrangle, San Diego County, California. *Geol. Soc. Am. Bull.* **57,** 223–260.

OLSON, J. C. AND OTHERS (1946) Mica deposits of the Franklin-Sylva district, North Carolina. *North Carolina Dept. Conserv. Develop., Div. Min. Res. Bull.* **49.**

ORVILLE, P. M. (1960) Petrology of several pegmatites in the Keystone district, Black Hills, South Dakota. *Geol. Soc. Am. Bull.* **71,** 1467–1490.

SCHALLER, W. T. (1925) The genesis of lithium pegmatities. *Am. Jour. Sci.*, 5th ser. **10,** 269–279.

——— (1953) A photographic technique for showing some mineral relations, in Contributions to geochemistry, 1949. *U. S. Geol. Survey Bull.* **992,** Pt. 8, 83–94.

SCHNEIDERHÖHN, HANS (1961) *Die Erzlagerstätten der Erde. Band II. Die Pegmatite,* Gustav Fischer Verlag, Stuttgart.

SHERIDAN, D. M. (1955) Geology of the High Climb pegmatite, Custer County, South Dakota. *U. S. Geol. Survey Bull.* **1015-C,** 59–98.

SIMPSON, D. R. (1960) Geology of the Ramona pegmatites, San Diego County, California. Ph.D. thesis, California Institute Tech., Pasadena, California.

STAATZ, M. H. AND A. F. TRITES (1955) Geology of the Quartz Creek pegmatite district, Gunnison County, Colorado. *U. S. Geol. Survey Prof. Paper* **265.**

THURSTON, W. R. (1955) Pegmatites of the Crystal Mountain district, Larimer County, Colorado. *U. S. Geol. Survey Bull.* **1011.**

TUTTLE, O. F. (1952) Origin of the contrasting mineralogy of extrusive and plutonic salic rocks. *Jour. Geol.* **60,** 107–124.

——— AND N. L. BOWEN (1958) Origin of granite in the light of

experimental studies in the system $NaAlSi_3O_8$-$KAlSi_3O_8$-$SiO_2$-$H_2O$. *Geol. Soc. Am. Mem.* **74.**

VARLAMOFF, NICOLAS (1954) Transitions entre les aplites et les pegmatites dans les zones de contact des massifs granitiques des Concessions de Symétain a Kalima (Maniema, Congo Belge). *Soc. Géol. Belgique, Ann.*, **77,** B101–116.

——— (1960) Relations spatiales entre les pegmatites et les granites en Afrique centrale et a Madagascar. *Soc. Géol. France Bull.*, 7th ser. **II,** 711–722.

VOGT, J. H. L. (1923) The physical chemistry of the crystallization and magmatic differentiation of igneous rocks, VII, Viscosity, size of crystals, speed of crystallization, formation of glass, influence of time, undercooling (or supersaturation), and equilibrium of mix-crystals between the solid and liquid phase, etc. *Jour. Geol.* **31,** 207–233.

VOLBORTH, A. (1962) Allanite pegmatites, Red Rock, Nevada compared with allanite pegmatites in southern Nevada and California. *Econ. Geol.* **57,** 209–216.

WAGER, L. R. (1953) Layered intrusions. *Dansk Geol. Foren. Medd.* **12,** 335–349.

——— G. M. BROWN AND W. J. WADSWORTH, (1960) Types of igneous cumulates. *Jour. Petrol.* **1,** 73–85.

WARREN, C. H. AND CHARLES PALACHE (1911) The pegmatites of the riebeckite-aegirite granite of Quincy, Mass., U. S. A. Proc. *Am. Acad. Arts Sci.* **XLVII,** 125–168.

WARING, G. A. (1905) The pegmatyte veins of Pala, San Diego County. *Am. Geol.* **35.** 356–369.

WATSON, T. L. (1902) On the occurrence of aplite, pegmatite, and tourmaline bunches in the Stone Mountain granite of Georgia. *Jour. Geol.* **10,** 186–193.

WHEELER, E. P. 2nd (1935) An amazonite aplite dike from Labrador. *Am. Mineral.* **20,** 44–49.

ZAVARITSKY, A. N. (1950) Granites and aplites. *Soc. Russe Miner. Mém.* **79,** 81–85.

MINERALOGICAL SOCIETY OF AMERICA, SPECIAL PAPER 1, 1963
INTERNATIONAL MINERALOGICAL ASSOCIATION, PAPERS, THIRD GENERAL MEETING

# STRUCTURE AND ROCK SEQUENCES OF THE CRITICAL ZONE OF THE EASTERN BUSHVELD COMPLEX

EUGENE N. CAMERON
*Department of Geology, University of Wisconsin, Madison, Wisconsin*

ABSTRACT

Investigations of the Critical Zone of the eastern part of the Bushveld Complex during 1952–55 and 1961 indicate that the zone is divisible along its strike into western, central and southern sectors. In the western sector the zone is poorly exposed; the sequence of rock units within it is poorly indicated. In the central and southern sectors the zone comprises an upper anorthosite series and a lower pyroxenite series. The anorthosite series consists largely of anorthosite and closely related rocks, but feldspathic pyroxenites and associated chromitites occur at two or more horizons in each of various sections across the zone. In the central sector, the pyroxenite series consists largely of pyroxenite and mafic norite but includes units of norite, anorthosite and olivine-bearing rocks, together with numerous chromitites. The sequence of major units in the pyroxenite series is remarkably constant throughout the sector, although the units vary in thickness. In the southern sector, the pyroxenite series varies markedly along strike both in thickness and sequence of units. In both sectors, there are several different patterns of repetition of rock types.

Despite the presence of disconformities at certain horizons, the outstanding structural feature of the Critical Zone is the gross concordance of units. This and numerous gradations between rock types are inconsistent with the hypothesis of multiple intrusions. Compaction structures, deformation and dismemberment of layers, and chromitites along fractures in anorthosite are local features. Taken together, both broad and local features appear consistent with evolution of the Critical Zone by fractional crystallization and sedimentation, influenced by intermittent motion of the magma and by periodic disturbance of the magma chamber.

## INTRODUCTION

During 1952–55, chromite deposits on six farms in the eastern part of the Bushveld Complex were mapped in detail by the author, H. E. Abendroth, Robert A. Bell, L. Yehle and B. L. Berman. Mapping was followed by diamond drilling on two of the farms. During June–August, 1961, the author reviewed the previous work and made further studies of the chromite deposits and associated rocks. This work and correlative laboratory studies since 1953 have yielded much new information on the structure and sequences of rock units in the Critical Zone. These features are important with regard to the evolution of the zone, because they provide the framework within which other features must be interpreted.

## ACKNOWLEDGMENTS

The author is deeply indebted to many individuals and organizations in connection with the work. Union Carbide Ore Company, for whom the mapping was done in 1952–55, has generously permitted use of scientific data obtained and has supported laboratory investigations at the University of Wisconsin through the Union Carbide Fellowship in Economic Geology. Mr. D. F. Frasché, Manager, Mineral Survey Department of the company, has given steady encouragement to the work. Mr. O. T. van der Merwe, Managing Director, Chrome Corporation of South Africa, Pty., Ltd., has given generous aid in innumerable ways. The author is profoundly grateful to both these men. Mr. and Mrs. G. E. van Schalkwyk were cordial and helpful hosts during the field season of 1961. Mr. Nugent Comyn, Manager, E. J. Lavino, Pty., Ltd., gave generously of his time and his experience with chromite deposits. Anglo-American Corporation assisted with maps of farms and permission to make studies on the farms. Other property owners and operators of mines were uniformly generous in their cooperation. Field work during 1961 and a part of the laboratory investigations since July 1960 have been made possible by a grant from the National Science Foundation.

## PREVIOUS INVESTIGATIONS

The literature of the Bushveld Complex is far too voluminous to review fully in a brief paper of this kind. For a summary of early work, the reader is referred to the memoir by Hall (1932). More recently, Willemse (1959) has given a comprehensive discussion of the relations of the eastern part of the complex to its floor. The geology of the area around the Driekop platinum pipe has been discussed by Heckroodt (1959), and the geology of the area east and southeast of Steelpoort by Hiemstra and van Biljon

(1959). Cameron and Emerson (1959) have described certain chromite deposits on Farms Jagdlust and Winterveld (343).

## Critical Zone of the Eastern Bushveld Complex

The location of the eastern norite belt is indicated in Fig. 1, and a generalized geologic map is given in Fig. 2. For a more detailed representation, reference may be made to the map by Willemse (1959). The rocks of the norite belt were divided by Hall (1932) into five successive zones (Fig. 3). The term Critical Zone was applied to the highly differentiated rocks from a horizon just below the lowest chromite seam to the base of the Main Norite Zone, not far above the Merensky Reef. Rocks of Critical Zone types, with associated chromite deposits, occur west of the Olifants River in the area south of Chuniespoort, but the boundaries of the zone could not be indicated on Fig. 2. East and south of the Olifants River, the Critical Zone is better exposed, and the approximate boundaries of the zone are indicated on the map.

During 1952–55, Farms Scheiding, Jagdlust, Winterveld (343), Mecklenburg, Hendriksplaats, and Annex Grootboom were mapped by the writer and associates at 1:10,000, and portions of Farms Mooihoek, Onverwacht, Doornbosch, Winterveld (424), and Grootboom were examined. In 1961, the writer supplemented this work by chain-compass traverses across all or part of the Critical Zone along various lines as far south as Farm Thorncliffe. Chromite deposits and associated rocks on Farm Naboom were examined briefly. The work indicates that between Chuniespoort and Farm Thorncliffe the Critical Zone is divisible along strike into three sectors, a western sector extending from south of Chuniespoort to the Olifants River, a central sector extending from the Olifants River south to Steelpoort, and a southern sector extending from Steelpoort to Farm Thorncliffe and thence beyond the limits of Fig. 2. This threefold division provides a convenient framework for discussion of the Critical Zone.

*Western sector.* The western sector is poorly exposed,

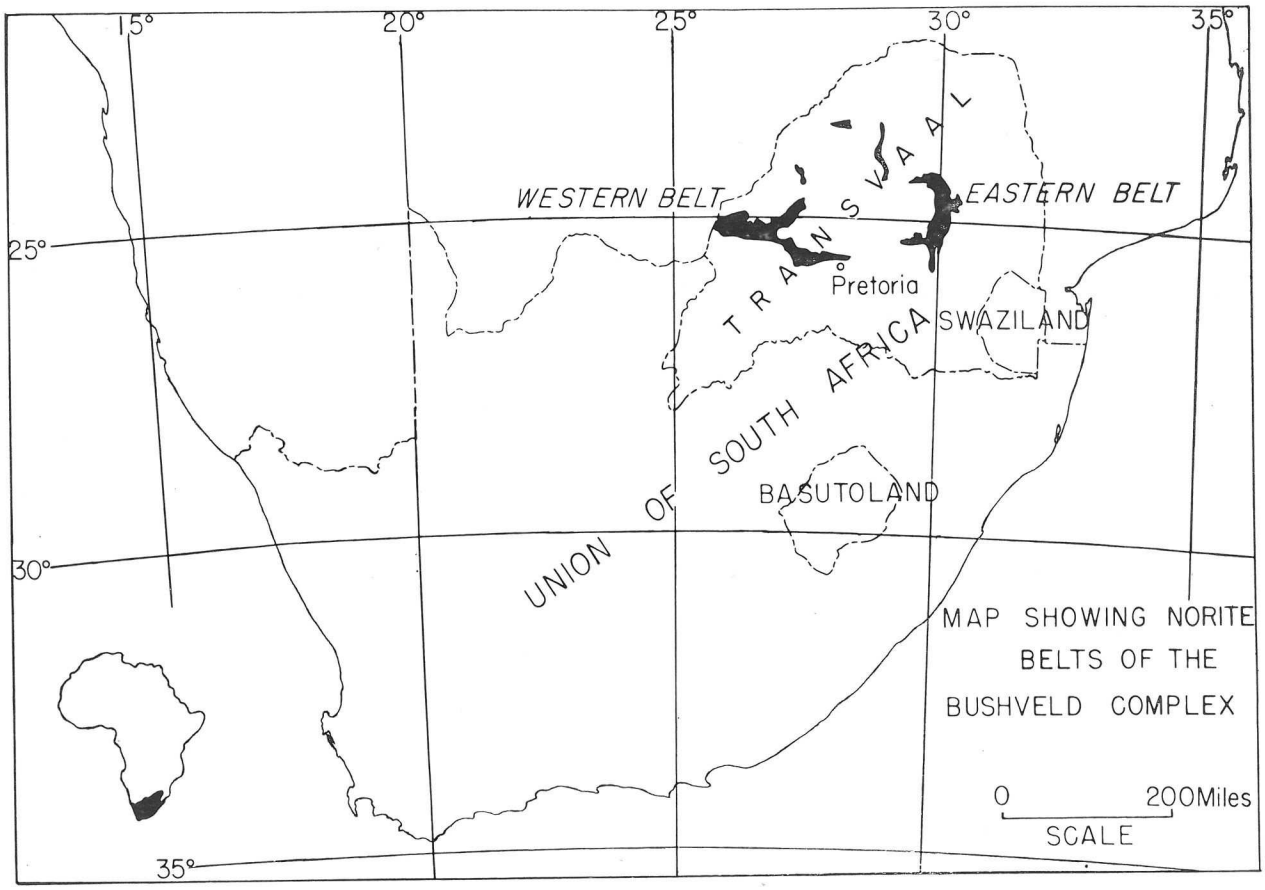


Fig. 1

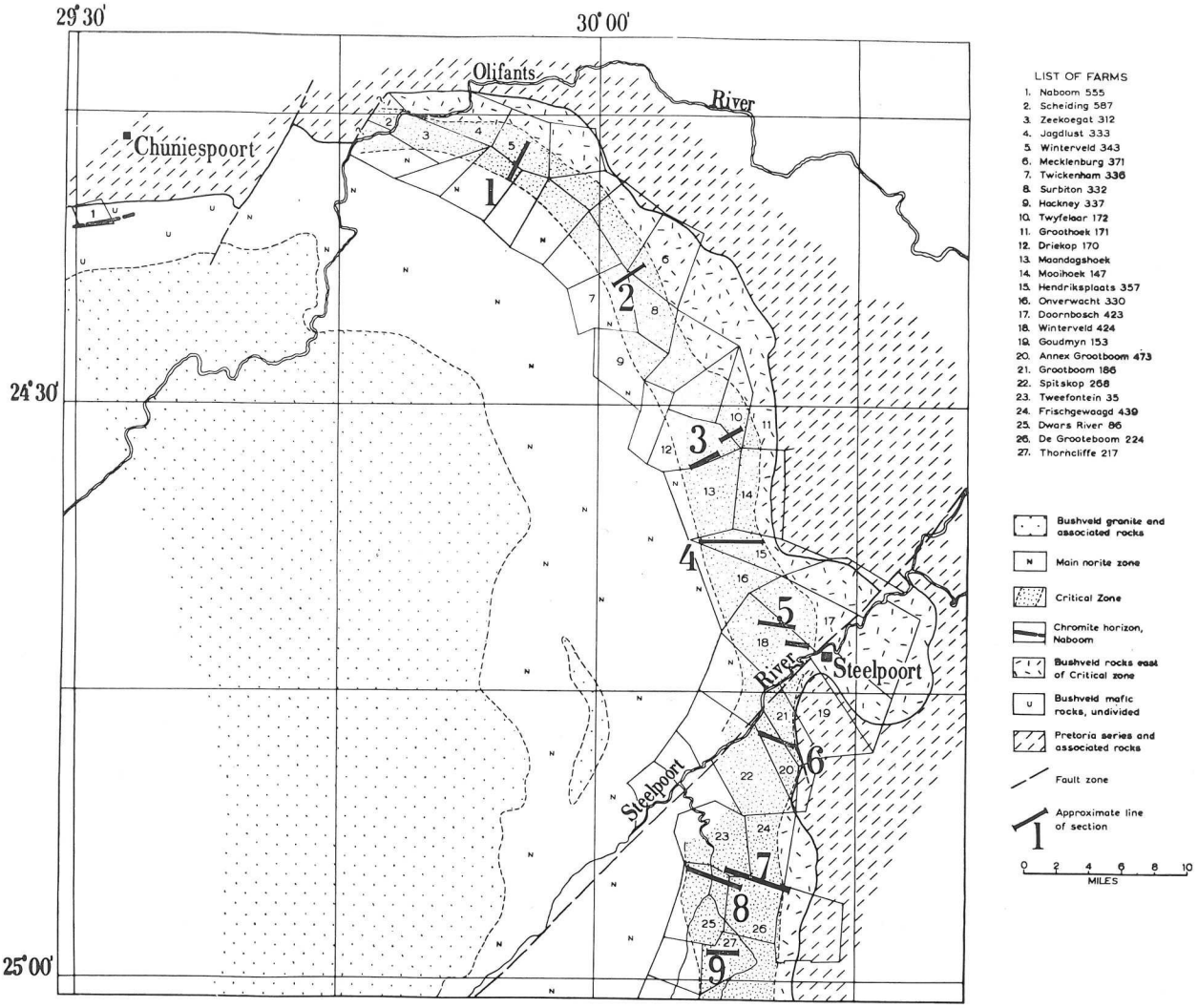


FIG. 2. Generalized geologic map of the northeastern part of the Bushveld Complex, from various sources.

and no adequate section of the Critical Zone in it can be given. It is clear only that the sequence of rock units in this sector differs from that of the central sector.

*Central sector.* In the central sector, from the Olifants River to Steelpoort, the Critical Zone is extensively exposed. On Farms Jagdlust, Winterveld (343), and Umkoanes Stad (immediately south of Winterveld) the zone has been exposed continuously from just above its base nearly to the Merensky Reef, by two drill holes totalling 2720 feet, two long adits, and a natural gorge. Along line 1 (Fig. 2) a total thickness of 3750 feet of the zone has therefore been accessible for field study and sampling. Detailed laboratory studies of the rocks of this section have been under way for some time at the University of Wisconsin. Sections along lines 2 to 5 across the Critical Zone are based largely on surface mapping and chain-compass traversing. Sections based on this work are not as accurate as section 1 but indicate clearly the sequences of major units.

Sequences of units along lines 1 to 5 across the central sector are given in Fig. 4. Descriptions of the units are given in Table 1. Throughout the sector,

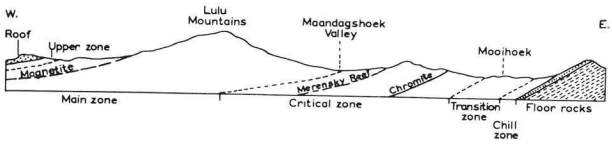


FIG. 3. Section of Bushveld norite north of Steelpoort, after A. L. Hall. Section is 19 miles long.

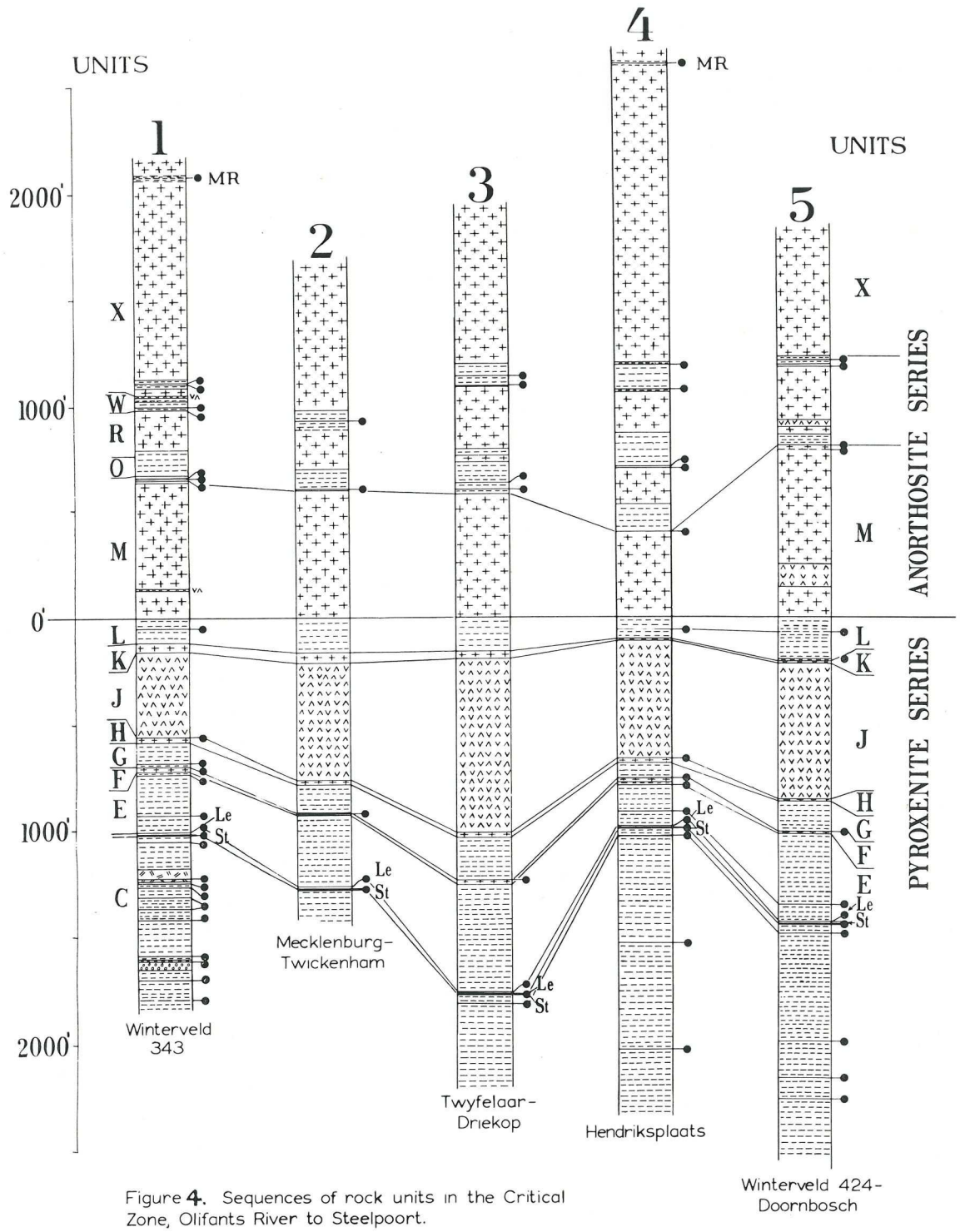


Figure 4. Sequences of rock units in the Critical Zone, Olifants River to Steelpoort.

Chromitite. St.—Steelpoort Seam, Le—Leader Seam.

Anorthosite, anorthositic norite

Pyroxenite. MR—Merensky Reef.

Norite

Troctolite

Peridotite

TABLE 1. ROCK UNITS OF THE CRITICAL ZONE, CENTRAL SECTOR

| Unit | Description |
|---|---|
| MR | Merensky Reef. Pegmatitic diallage norite or feldspathic pyroxenite. |
| X | Interlayered medium to coarse-grained, massive to regularly or irregularly banded pyroxene-anorthosite, noritic anorthosite, and norite; pyroxenite and mafic norite with thin chromitite seams near base. |
| W | Feldspathic pyroxenite with thin chromitite seams at and near base. |
| R | On Winterveld (343) upper 158 feet anorthosite, lower 52 feet pyroxenite, thin layers of anorthosite, and mafic norite. |
| O | Feldspathic pyroxenite. |
| M | Mostly anorthosite and anorthositic norite with subordinate norite and mafic norite, mostly in lowest portion. Thin layers of chromitite and pyroxenite near top. |
| L | Mafic norite grading downward into massive pyroxenite. Two persistent groups of thin chromitite seams in middle and upper parts in north; at least one in south. From Doornbosch southward has thick chromitite seam near base. |
| K | Interlayered pyroxene-anorthosite and anorthositic norite in various proportions. |
| J | Mafic norite and norite on Jagdlust and Winterveld (343) with a thin chromitite seam near the base and another nearer the middle. |
| H | Variable. Anorthosite or interlayered anorthosite and norite, with or without thin chromitites. |
| G | Mafic norite and feldspathic pyroxenite. |
| F | In north consists of norite separating two units of anorthosite with associated thin or impure chromitites. In south, anorthosite or interlayered anorthosite and norite with one or more impure chromitites. |
| E | Pyroxenite and mafic norite interlayered with chromite-pyroxenite and chromitites. |
| D | Leader and Steelpoort chromitite seams separated by 2½–3 feet of pryoxenite. |
| C | Mostly mafic norite and pyroxenite interlayered with chromitites and chromite-pyroxenite, and locally with troctolite and peridotite. |

*Note:* Rock designations subject to revision based on quantitative petrographic study.

the Critical Zone is divisible into two major series of rocks, a lower pyroxenite series, predominantly pyroxenite and norite, and an upper anorthosite series, predominantly anorthosite and noritic anorthosite. In any one section, each series consists of a sequence of major units. The pyroxenite series is characterized by the remarkable persistence of major units throughout the central sector, over a distance of approximately forty-five miles. The correlation of these units from section to section is indicated on the chart. The units vary somewhat in thickness, even allowing for errors in calculating thicknesses from mapping and traverses, and the C, F, H and L units vary in lithology along strike, but their continuity from end to end of the sector is beyond doubt. The most remarkable units in this series are the chromitite seams. The continuity of the Steelpoort seam throughout the sector, apart from local interruptions by faults and diabase dikes, is firmly established by mine workings, drill holes, and surface exposures. The Leader seam is continuous from Steelpoort to Farm Zeekoegat, just east of the Olifants River. There are other thinner seams, however, that are continuous over distances measured in miles. For lack of exposures, however, their full extent has not as yet been determined.

The anorthosite series consists of thick anorthosite and noritic anorthosite units interrupted in various sections by two to four pyroxenite units, some accompanied by chromitite seams. Some units are known to persist for miles along strike. The M and X units are probably continuous over the full length of the sector, apart from minor structural breaks. The anorthosite series is less continuously exposed than the pyroxenite series, however, and correlation of units from section to section is incomplete.

Over portions of the sector measurable in a few miles, the regularity of the entire Critical Zone is nothing short of phenomenal. On Farm Winterveld (343), a drill hole put down at a point 5750 feet back of the outcrop intersected the Steelpoort seam at a depth of 2336 feet, just 36 feet beyond the depth predicted from surface mapping. An error of half a degree in calculating the average dip from mapping would account for this discrepancy.

*Repetition of rock types in the sequence.* As noted by many previous investigators, the Critical Zone is characterized by repetition of layers of pyroxenite, norite, anorthosite and chromitite. The present work shows also that on Winterveld (343) and Jagdlust olivine-bearing rocks occur in the lower part of the C unit. The lower of the two horizons, exposed only on Winterveld, consists of interlayered bronzitite and peridotite. At one extreme, the repetition occurs on a scale large enough to be indicated in Figure 4; on the other it may occur within a vertical distance of a few feet (Fig. 7) or within the compass of a hand specimen. The patterns of repetition are obviously important to an understanding of the evolution of the Critical Zone. Discussing the pyroxenites of the central sector, Kuschke (p. 60) pointed out that they occur at various horizons in the stratigraphical succession.

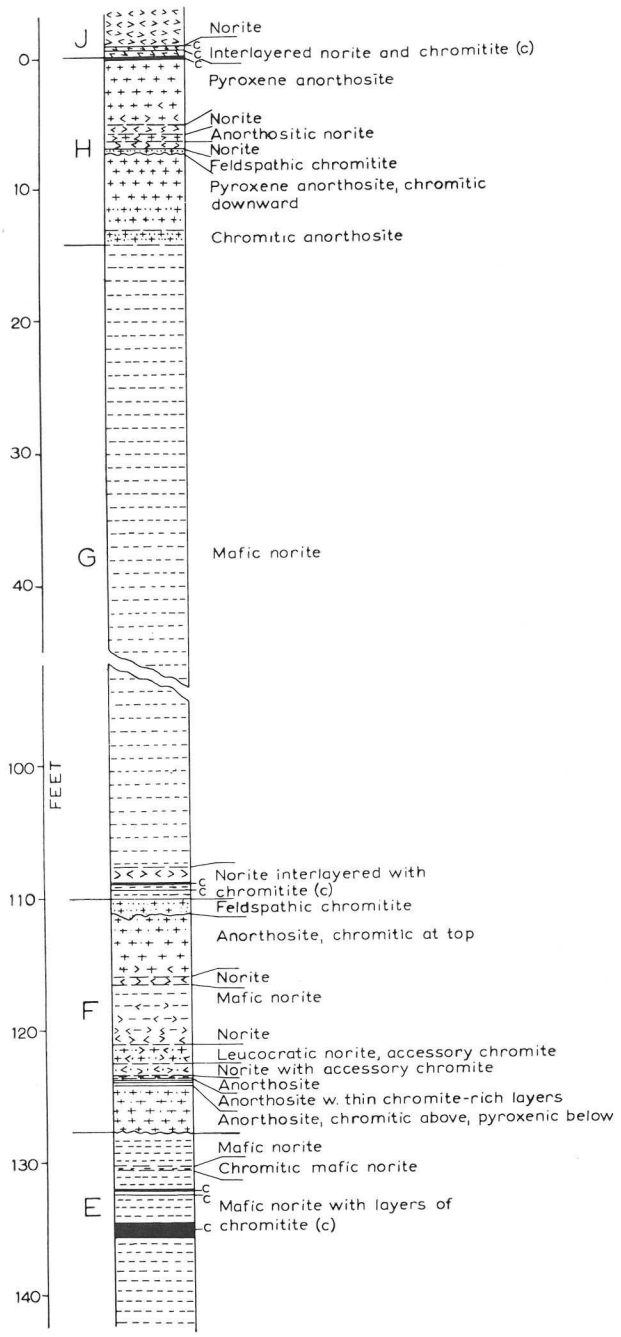


FIG. 5. Section of F, G, and H units, Jagdlust, showing lithologic sequences. Solid lines are sharp contacts, broken lines gradational contacts. Mixed symbols show broad gradations.

"The relation of the pyroxenites to the rocks above them is one of gradual transition through various stages from pyroxenites to pyroxenitic gabbros and gabbros; the lower contact of the pyroxenites is usually sharp and abrupt."

He regarded this relationship as supporting the view that the pyroxenites owe their origin to the settling of crystals. Further (pp. 75–77), he used the repetition of such transitional series as evidence of differentiation *in situ* of successive heaves of magma.

The writer's observations confirm the presence of upward transitions of the kind Kuschke described, but repetition of the series pyroxenite to gabbro is far from being the only pattern of repetition in the Critical Zone. Relationships in places are actually the reverse of those described by Kuschke. For example, in the adit on Jagdlust, mafic norite coarsens downward (stratigraphically) and becomes more feldspathic from a point 1800 feet from the adit portal to a point 1775 feet from the portal, where an abrupt change to medium-grained mafic norite takes place. Modal analyses by Guilbert (1962) show that at 1800 feet, the rock (by volume) has 77.2 per cent bronzite, and 13.2 per cent plagioclase. The rock at 1775 feet, just above the contact, has 71.9 per cent bronzite and 22.6 per cent plagioclase, whereas the rock below the contact has 82.2 per cent bronzite and 13.2 per cent plagioclase. This pattern is shown in other parts of the sections exposed in the Winterveld and Jagdlust adits.

The F unit provides further examples of departures from the sequence described by Kuschke. The basal member of the F unit on Winterveld (343) and Jagdlust (Figs. 5, 6) is a pyroxene-anorthosite which rests with abrupt and disconformable contact on mafic norite interlayered with chromitic pyroxenite

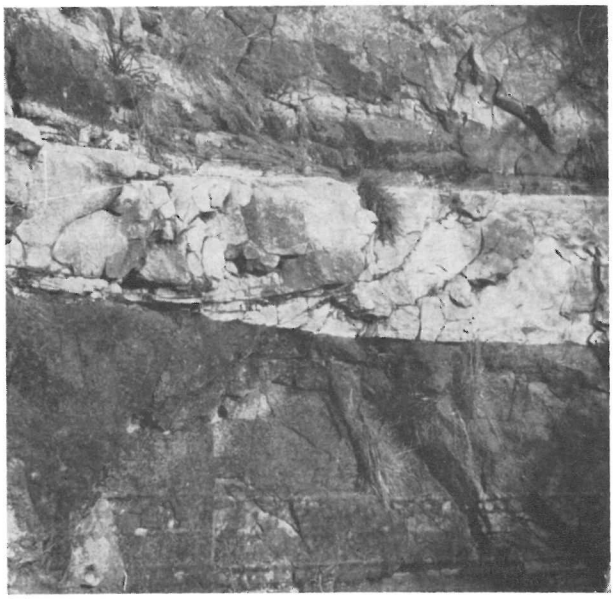

FIG. 6. Basal anorthosite member (white) of F unit, resting with sharp, slightly undulating contact on mafic norite of E unit, Jagdlust. Anorthosite is about 3 feet thick at this point.

and chromitite. The top member (Fig. 5) is feldspathic chromitite in sharp contact with mafic norite. Between the two members, the sequence of rock types is chromitic anorthosite, norite, leucocratic norite, norite, mafic norite, anorthosite, chromitic anorthosite, and feldspathic chromitite; all contacts are gradational, except that the contact between feldspathic chromitite and underlying chromitic anorthosite is an erosional disconformity. The lower part of the feldspathic chromitite contains inclusions of the anorthosite. The H unit provides an interesting contrast with the F unit. The lithologic types present in the two units are remarkably similar, but as shown in Fig. 5, the sequences of types are not the same in the two units.

The K unit is another departure from the pattern described by Kuschke. On Winterveld (343) the lower contact with norite is a disconformity; the upper contact with pyroxenite is gradational. In addition, field observations as well as detailed logging of 2340 feet of core extending from the lower part of the X unit to the Steelpoort seam on Winterveld (343) show that reversals of the sequence described by Kuschke occur at various horizons in the anorthosite series. There is no single pattern of repetition of rock types in the central sector. Instead, we have a variety of patterns of repetition (Figs. 7, 8, 9).

*Southern sector.* The central sector ends at Steelpoort, and the southern sector begins. In the northern part of the southern sector, the Critical Zone again consists broadly of an upper anorthosite series and a lower pyroxenite series. Sequences of units along lines 6, 7, 8, and 9, of Fig. 2 are shown in Fig. 10, together with the sequence of units along line 5 at the south end of the central sector for comparison. The anorthosite series has the same general character as in the central sector, consisting essentially of thick anorthosite units separated by pyroxenite units with or without chromitites. Some units of this series have been traced thousands of feet, or even miles, but correlation from section to section is uncertain pending further detailed mapping.

The pyroxenite series of the southern sector is markedly different from that of the central sector. The sequence of section 5 and that of section 6 hold for points only 3 miles apart, yet the units in the pyroxenite series in the one sector do not agree at all with those in the other. Along line 6, the pyroxenite series, so far as exposed, is a monotonous succession

FIG. 8. Interlayered pyroxenite and peridotite at entrance to adit on Winterveld (343).

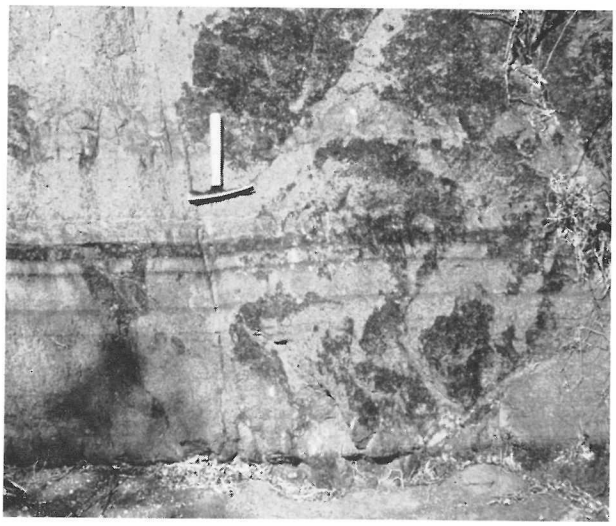

FIG. 7. Mafic norite interlayered with thin chromite seams and chromite-rich mafic norite (under hammer handle) on Jagdlust. The upper part of a 14-inch chromitite seam is exposed at the lower right.

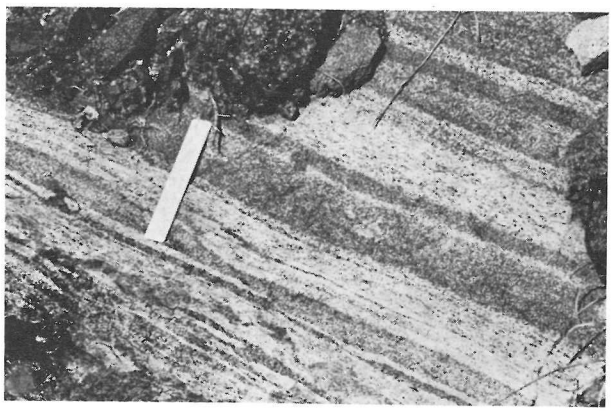

FIG. 9. Interlayered anorthosite (light) and norite (dark) in K unit, Jagdlust. Scale is 6½ inches long.

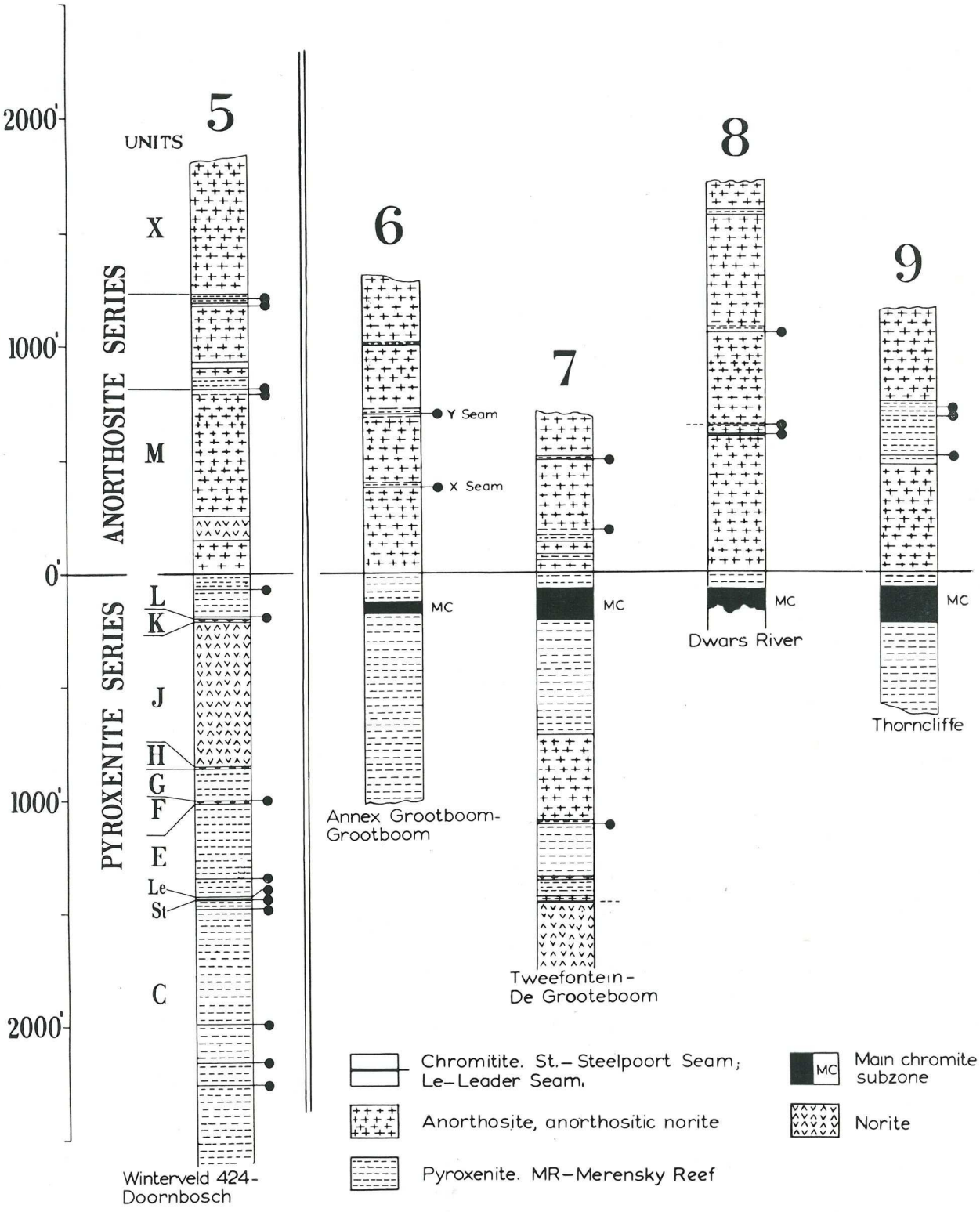


FIG. 10. Sequences of rock units in the Critical Zone, Steelport to Thorncliffe.

of feldspathic pyroxenites interrupted near its top by a zone of interlayered chromitites, anorthosites, and pyroxenites 65 to perhaps 80 feet thick, shown in Fig. 10 in black and designated the Main Chromite Subzone.

The Steelpoort River Valley (Wagner, 1929, p. 151; Willemse, 1959) is known to be a belt of disturbance cutting across the complex and the rocks of the floor of the complex. Outcrops in the valley bottom east of the river bed and south of Steelpoort show a wide range of attitudes within short distances. Faulting, possibly complicated by minor folding, is indicated (*cf.* Willemse, 1959), but neither the amount nor the direction of gross displacement is clear. The writer has entertained the hypothesis that the difference in sequences of the central and southern sectors is due to the fact that faulting has brought the southern sector, consisting at its northern end of rocks lying near to the edge of the complex, in juxtaposition with a deeper portion of the complex represented in the central sector.

This notion is prompted by three features of the Critical Zone of the southern sector. First, units of the pyroxenite series and the lower part of the anorthosite series thin rapidly toward the floor of the complex south-eastward along the extension of the line of section 6, Fig. 10, This is shown by a comparison of section 6 with Fig. 11, a section along a line parallel to and about a quarter-mile west of the floor on Farm Annex Grootboom (Fig. 2). Second, as shown in Fig. 10, the pyroxenite series varies in sequence of units within the 15-mile strike distance represented by sections 6 to 9. In section 7, a thick anorthosite unit appears well above the base of the pyroxenite series, and two thinner ones appear lower down. The Main Chromite Subzone is much thicker than in section 6 and shows a different sequence of chromite seams. The full sequences along lines 8 and 9 have not been determined, but in section 9 the Main Chromite Subzone shows a different sequence than in section 7. Such rapid changes seem more likely near the edge of a crystallizing complex than in its deeper lying portions. The third feature is that on Farm Annex Grootboom, the Bushveld rocks appear to interfinger locally with floor rocks. The structure here and on Farm Spitskop is complicated, however, and extremely detailed mapping is needed to resolve the relationships.

*Structure of the Critical Zone*

(a) *Concordance of units*

The outstanding structural feature of the Critical Zone in the central and southern sectors is the concordance of successive units in the zone. Local irregularities of contact are found at numerous places, and relationships of the rocks of the Critical Zone along the contact with floor rocks on Grootboom and Annex Grootboom are complex, but these are features that must be viewed against the perspective of the large-scale structure. Anyone who does detailed mapping of the rocks of the Critical Zone shortly finds that the geometry is that of a pile of sedimentary rocks, and that this geometry, as in the study of sediments, can be used to decipher structure, predict outcrop belts, and guide exploration. Crosscutting of one unit by another is never seen, although crosscutting relationships within units are present locally and certain contacts between units are disconformable in detail. Even where new units appear along the strike of the Critical Zone, as in the southern sector, they have concordant contacts and internal layering parallel to external layering of enclosing rocks. In other words, they have the same thinly lenticular habit as the members of a concordant sedimentary pile.

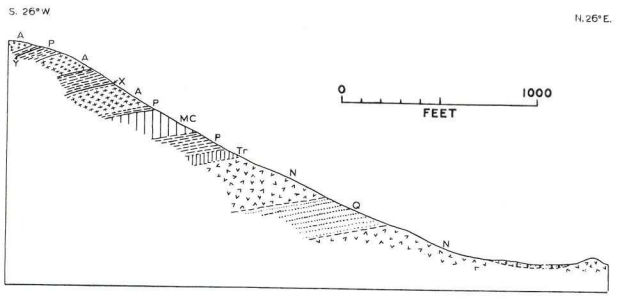


FIG. 11. Section of northeast side, Spitskop-Annex Grootboom boundary hill. A-anorthosite, MC-main chromite subzone; N-norite; W-quartzite, Tr-transition. X-X chromitite, Y-Y chromitite.

The relationships involved are well illustrated in the northeastern part of De Grooteboom and the southern part of Frischgewaagd, in which the rocks of the lower part of section 7, Fig. 10, are well exposed. A section of the side of a deep valley on De Grooteboom is given in Fig. 12. In every unit, internal layering is parallel to contacts with enclosing units, where these are exposed. Furthermore, the traces of the units along the face of the ridge and across the ridge and a second valley and its branches to the north clearly indicate concordance of the various units.

*Contacts between rock units.* The nature of contacts between rock units is the second important aspect of the

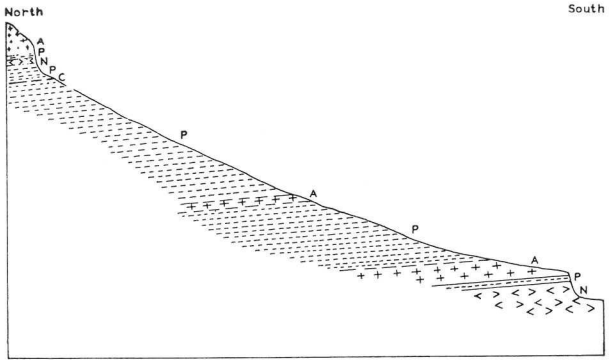


FIG. 12. Section of lower part of pyroxenite series, De Grooteboom. A—anorthosite, C—chromitite, N—norite, P—pyroxenite, Solid lines indicate exposed contacts, broken lines gradational contacts.

structure of the Critical Zone in the central sector. For the eastern Bushveld Complex, this subject has been discussed most recently by Cameron and Emerson (1959), who point out that both gradational and sharp contacts are observed, that regular, even layers with straight, parallel contacts are the commonest type, but that irregular contacts having the nature of disconformities are found at certain horizons. Subsequent observations by the writer confirm these statements, but it should be added that gradational or abrupt contacts are not characteristic of particular pairs of rock types; any pair of rock types such as pyroxenite and anorthosite can be found at certain horizons in sharp contact with one another, at others in gradational contact. A second feature of contacts that should be added was described by Wagner (1929, pp. 122, 123) many years ago from observations of the Merensky Reef. In places, apophyses of an overlying member of a sequence of units extend downward into an underlying member, inclusions of which may be present in the overlying member. The writer has seen this feature at the top of the H unit on Surbiton, on the hill just north of the Mutse River. The H unit is overlain by a $3\frac{1}{2}$-inch layer of mafic norite. The top of this layer is straight and regular. The bottom is irregular, and the norite projects downward as much as 2 feet into the H unit anorthosite along fractures. Wagner nowhere found projections of an underlying rock into an overlying rock. He pointed out that relations described obviously indicate that the order of superposition of the layers involved is their order of formation.

*Compaction structures.* Compaction structures are not common in the rocks of the Critical Zone, but the fact that they exist at all is worthy of note. The best examples seen by the writer are in an incline on Farm Driekop (Fig. 13), one of a series driven along a chromite seam at intervals for far more than a half mile along strike. The seam, 39–45 inches thick in the incline, underlies norite, with which it is in sharp contact, and overlies pyroxenite that is chromite-rich in its top few inches. The basic structure of the seam is an even, regular alternation of chromite-rich and feldspar-rich layers that are fractions of an inch to six inches thick and remarkably straight in section. This simple and regular layering is interrupted locally, however, by flat lenses of anorthosite and by inclusions of fine-grained pyroxenite, the largest seen 11 feet long and 12 inches in maximum thickness. Figure 13 is a detailed scale drawing of the upper part of the seam, showing two of the inclusions. Overlying layers are arched and thinned, immediately underlying layers are depressed and thinned, and layers next to the ends of the inclusions are crumpled. These are features characteristically developed by compaction of unconsolidated sediments around resistant objects. The basal contact of the seam is straight and even, and the inclusions are petrographically dissimilar to the immediately underlying chromitic pyroxenite.

*Deformation structures.* Deformation structures in the rocks of Critical Zone have been discussed by Cameron and Emerson (1959). The structures are of two principal kinds. One consists of chromite filling low-angle fractures in anorthosite. Examples are shown in Figs. 13, 14, 15. These can only be interpreted as produced by movement of chromitic material (as a mush of crystals and liquid?) into dilatant fractures. The relationships shown in Fig. 13 would seem to confirm the conclusion of Cameron and Emerson that these features arose during consolidation. Such features are shown at numerous places in the anortho-

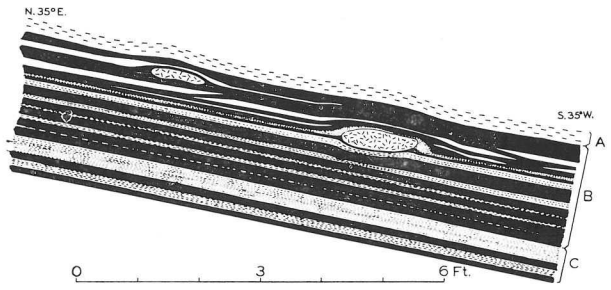


FIG. 13. Drawing of part of chromite seam in wall of incline, Driekop. A—norite. B—interlayered chromitite (black), feldspathic chromitite (dashed lines), and anorthosite (white), with two inclusions of pyroxenite (random dashes); drawn in detail to scale. C—interlayered chromitite (black) and chromitic anorthosite (dashed lines); layers diagrammatic, Footwall of seam not shown.

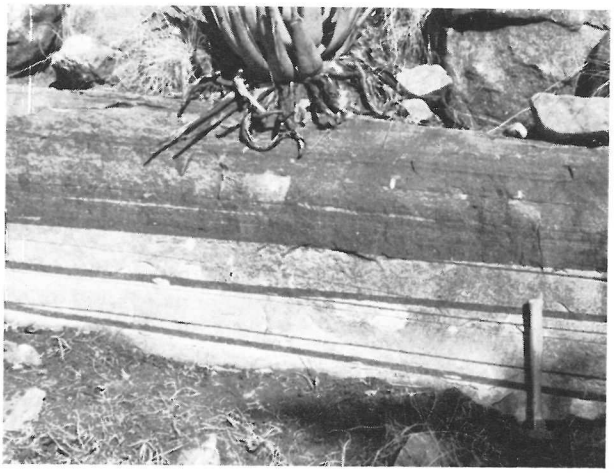

FIG. 14. Interlayered feldspathic chromitite and chromitite (dark) underlain by anorthosite (white) cut by thin chromitites along low-angle fractures. Onverwacht.

site series and, more rarely, in the pyroxenite series of the southern sector, for example in the old mine workings on Grootboom.

The second type consists of folding or dismemberment, or both, of thin layers of chromitite or pyroxenite enclosed in anorthosite (Figs. 16, 17). As in the Stillwater Complex (Hess, 1960), deformation features at any one locality are confined to stratigraphic thicknesses of a few feet. Underlying and overlying rocks are undisturbed. They evidently arose, like fracturing, prior to complete crystallization, for the textural fabrics of the rocks in thin sections are the same as those of enclosing rocks. Cataclastic textures are lacking.

*Inclusions.* Inclusions of one rock type in another in the Critical Zone have been noted by numerous investigators and have recently been discussed by Cameron and Emerson. Some, as in Figs. 17, 18, are

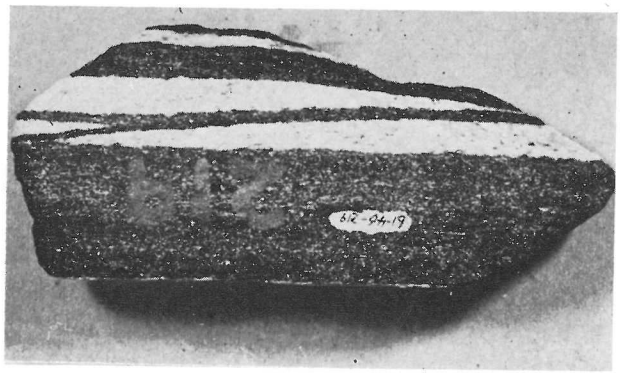

FIG. 15. Anorthosite parting (white) cut by chromitite (speckled black) along low-angle fractures, Driekop. Specimen is 8½ inches long.

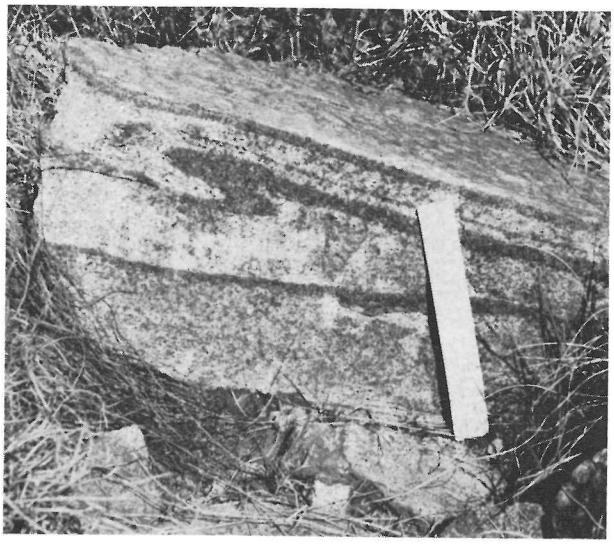

FIG. 16. Folded layer of pyroxenite (dark) enclosed in pyroxene-anorthosite (lighter). Loose block from upper part of M unit, Winterveld (343). Scale is 6½ inches long.

obviously of local derivation, either by erosion along disconformities, or by dismemberment. Others, such as those of Fig. 13, occur in settings that require transport of the inclusions from sources at least beyond the limits of very sizable outcrops; *i.e.*, for distances of at least feet, tens of feet, or hundreds of feet. Orientation with long dimensions parallel to stratification is characteristic. Deformed inclusions occur in places (Fig. 19), but again, rocks overlying and underlying the horizon containing the inclusions are undeformed.

*Structural features and hypotheses of origin.* An acceptable hypothesis of origin of the Critical Zone must be consistent with the structural features described above. They provide, then, a first basis for

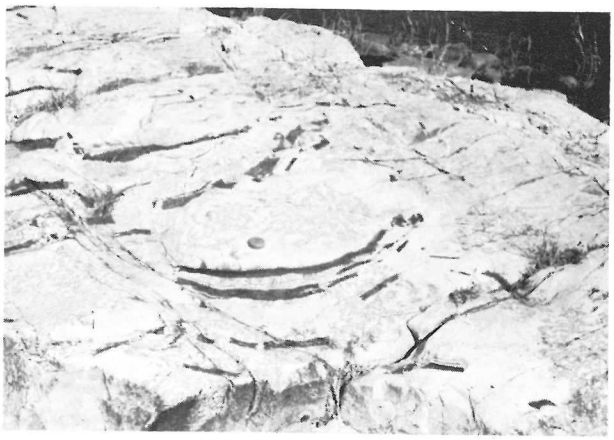

FIG. 17. Dismembered chromitite seams (black) in anorthosite, Dwars River. Pocket tape is 2 inches in diameter.

FIG. 18. Contact of L and M units, Winterveld (343). Noritic anorthosite (above, lighter gray) contains inclusions derived from underlying mafic norite (darker gray) of L unit. Scale is 6½ inches long.

evaluation of current hypotheses. One is the hypothesis of multiple intrusions, proposed by Reuning (1927) and revived more recently by F. C. Truter (1955, p. 84). Truter recognizes seven or eight major members of the Critical Zone as defined in the present paper. He regards all these as separate intrusions, giving as evidence

> 1) that of any two lithological zones higher up in the succession, the higher one contains inclusions of the lower one at or near the contact, (2) some of the lithological units have a lenticular habit and are consequently in contact with several rock types along their peripheries, and (3) pyroxenite units in the Critical Zone differ markedly in mineralogy and texture.

Total emplacement of the Complex, including the Critical Zone, he regards as accomplished in successive surges, each one being emplaced immediately above the one that preceded it and lifting the sedimentary roof of the complex. He further states (*loc. cit.*):

> "Excluding the possibility of gravitative settling of chromite in the pyroxenite, there is similarly no evidence of differentiation *in situ* anywhere in the complex."

The writer's observations are difficult to reconcile with these conclusions. The mechanism of multiple intrusions is inconsistent wth the remarkable concordance and persistence of major units in the Critical Zone. The problem involved is clearly posed by the results of mapping on Farms Jagdlust and Winterveld. On these two farms, the units shown in section 1, Fig. 4, have been mapped by plane-table and telescopic alidade on a scale of 1:10,000. The continuity and concordance of units C to X for a distance of 6 miles along strike have been established by walking out lines of outcrop (for some units nearly continuous), by examination of mine workings, and by 14 diamond drill holes. A drill hole 5750 feet back of the outcrop of the Steelpoort main seam on Winterveld intersected the same sequence of units as that indicated by surface mapping. Included in this sequence are units F, H and K. The first two are nowhere more than 30 feet thick anywhere in the central sector, and the last is nowhere more than 45 feet thick. These units are not only continuous on Winterveld and Jagdlust but are present in every section the writer has run across the 45-mile length of the central sector. It seems scarcely possible that these are separate intrusives. Layers of pyroxenite in anorthosite with straight parallel contacts for distances of hundreds of feet pose a similar problem, though on a small scale.

The writer believes that the features cited as evidence of multiple intrusions can be better explained in other ways. Inclusions of one rock in another are evidence that the host rock formed later than the rock of the inclusions, but they are not necessarily evidence of intrusion. Movement of magma over a growing pile of crystal accumulates, with intermittent erosion of the upper part of the pile, and local de formation of the kinds described above account for

FIG. 19. Folded inclusion of anorthosite in norite, middle member of H unit, Jagdlust. A faint banding in norite adjacent to the inclusion follows the boundaries of the inclusion. Scale is 6½ inches long.

the derivation of inclusions in ways that are more consistent with the large-scale concordance and persistence of major units. Concordant lenses seem more reasonably explained by sedimentation of crystals along the floor of a magma chamber, distribution and thickness of units being controlled by magmatic currents and by configuration of the floor. Contrasts in composition and texture of pyroxenite units are to be expected as a consequence of changes in conditions of differentiation *in situ;* such contrasts are not evidence of successive intrusions.

Finally, it is not the case that of every contrasting pair of units, the higher contains inclusions of the lower along their contact. As stated in a previous section, pairs of rock types are found in gradational contact with each other at many horizons; the upper unit *may* contain inclusions of the lower, but in the majority of cases does not. Gradational contacts between geometrically regular, persistent, and lithologically distinct units are a fatal objection to the hypothesis of multiple intrusions. It is impossible, moreover, to reconcile their common occurrence in the Critical Zone with Truter's statement that there is no evidence anywhere in the Complex (apart from chromite-pyroxenite relationships) of differentiation *in situ*. The existence of gradations between rock types and the fact that every rock type of the Critical Zone can be found at a number of places gradationally inter-layered with other types is clear evidence that differentiation *in situ* has had a major role in producing the rock sequence.

A difficult feature of the hypothesis of multiple intrusions, in its extreme form, is that it questions the possibility of differentiation *in situ* in the magma chamber exposed, while requiring this same differentiation, in a hidden magma chamber below, in order to account for units of contrasting composition.

The hypothesis of multiple intrusions, in a somewhat different form, has also been adopted by Heckroodt (1959) as the explanation of the rocks of the eastern norite belt. He states that the chronological order of intrusion of the various rocks in an area including Farm Driekop and parts of adjoining farms is as follows:

| | | |
|---|---|---|
| Youngest | 5b. Gabbro | Main Subphase |
| | 5a. Hyperite | |
| | 4. Peridotite | Peridotitic Subphase |
| | 3. Pegmatitic feldspathic Pyroxenite (Merensky Reef) | Critical Subphase |
| | 2. Norite, melanorite, and anorthosite | |
| | 1. Pyroxenite | Pyroxenitic Subphase |

He states that

"the subdivision of the Complex into zones based on the stratigraphical position of certain characteristic rocks sometimes places rocks of various ages into one zone. According to this system, the hyperite will be classified in the Critical Zone because of its position in the Complex, whilst the petrographic proof as well as the chronological order of intrusion requires that the rock should belong to the Main Subphase. The reason for this is that some rocks intruded downwards into the older rocks and thus came into another zone."

Section 3, Figure 5, is based on traverses by the writer across the area described by Heckroodt. The hyperite of Heckroodt is apparently in the lower part of the M unit. On Heckroodt's map it is shown as continuous and constant in position in the rock sequence for 4 miles along strike, disappearing beneath valley fill in the north and continuing beyond his map area to the south. In his section it is shown as concordant with overlying and underlying rocks. No field evidence is given that this unit has intruded downward; the field relations were not determined, owing to rubble covering exposures. Heckroodt regards the rock, nonetheless, as an assimilation product formed by intrusion of gabbro into noritic rocks. The evidence given is petrographic and in the writer's judgment inconclusive. The remarkable persistence and concordance of this "intrusive" unit and its constant position in the sequence are not explained.

As a further extension of the hypothesis of multiple intrusions, Heckroodt regards the chromite seams in the anorthosite series on Driekop, with the associated pyroxenite, as wedged off from the upper part of the pyroxenite series, roughly 1000 feet below, by intrusion of norite and melanorite of the M unit of Fig. 3. It is difficult to understand how this process could yield blocks that are persistent for miles, have attitudes concordant with the rest of the units of the Critical Zone, and have internal layering parallel to that of the anorthosite series. The evidence cited is that thin chromite seams in anorthosite in one of the inclines have been disrupted and disturbed. The writer regards these features, however, as due to local deformation during final stages of consolidation. Chromite seams in anorthosite, apart from fracture fillings, appear to have formed by differentiation *in situ;* every gradation between chromitite and anorthosite with accessory chromite is found (Fig. 20) in the anorthosite series.

Closely related to the hypothesis of multiple intrusions is that of successive heaves of magma, which has been supported by a number of students of the Bushveld Complex since it was proposed by B. V. Lombaard in 1934. This concept is difficult to evalu-

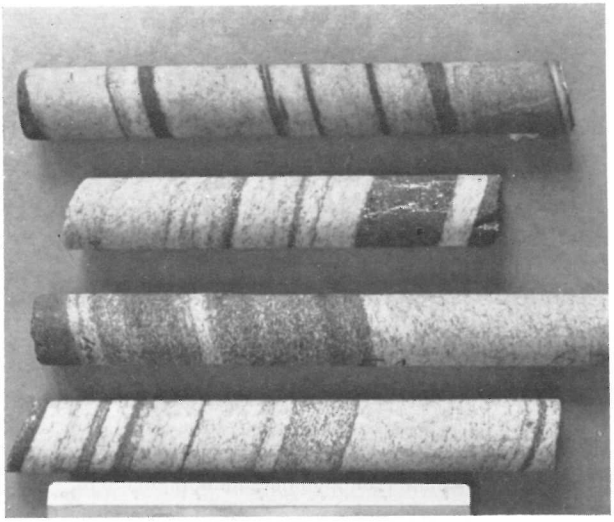

FIG. 20. Drill cores from upper part of M unit, Winterveld (343). Various layers range from anorthosite with accessory chromite (light gray) to nearly pure chromitite (black). 6-inch scale at bottom of photograph.

ate, because the dividing line between the concept of multiple intrusions and successive heaves of magma is not clearcut, and even less clearcut is the dividing line between successive heaves of magma and movement of magma within a chamber during differentiation *in situ*. Movement of magma within its chamber might take place through convective overturn, through turbidity currents generated by warping of the floor, or locally through simple slumping of the pile of accumulates. These various mechanisms, from successive intrusions or heaves of magma to movements of a magma internal to its chamber, are conceivably members of a continuous series. Recognition of a particular mechanism may not be easy, the more so if we deal with results of a combination of mechanisms.

Difficulties involved in the hypothesis of successive heaves of magma have been discussed by Hess (1960, pp. 154–156), to whose work the reader is referred. With reference to Kuschke's work in the central sector, however, the writer would add

> (1) that the oscillatory variations in pyroxene composition described were not closely correlated with the sequence of rock units, and (2) that as stated in a previous section, no simple cyclical repetition of units, of the kind required by Kuschke's hypothesis, has been found.

Jackson (1961), moreover, argues that cyclical repetitions of rock units in the lower part of the Stillwater Complex are due to major convective overturns, an alternative to the mechanism of successive heaves. Cameron and Emerson (1959) and Hess (1960) conclude that oscillations in mineral composition may take place due to the operation of processes purely internal to the magma chamber, and that successive heaves of magma are not required to account for them.

The hypothesis of successive heaves of magma has been used by B. G. Worst to account for the sequence of chromite seams alternating with harzburgites in the Great Dyke of Southern Rhodesia. Worst reports that each chromite seam is in sharp contact with underlying pyroxenite or harzburgite but grades upward into overlying harzburgite. He regards each chromite seam as an early product of crystal settling from a new heave of magma.

The writer has attempted to find a parallel in the chromite deposits of the eastern part of the Bushveld, but without success. Some seams have both upper and lower gradational contacts, other seams have both upper and lower sharp contacts, and still others have either the upper or lower contact sharp and the other gradational. Furthermore, what we call chromitites are merely end members of two series, the other end members of which are anorthosite and pyroxenite with accessory chromite (Fig. 20). Some seams are massive, others rhythmically banded. There certainly is no simple cyclical repetition of chromitites and associated rock types.

At the present writing, the structural features of the Critical Zone seem consistent with development by fractional crystallization and gravitative settling of crystals, complicated by local deformation of accumulated layers and by intermittent movements of the magma strong enough to cause sorting of crystals and even disconformities at certain horizons. It seems necessary, therefore, to assign a major role to differentiation *in situ*, a conclusion with which Willemse (1959, pp. lxiii–lxiv) is in general agreement. To what extent these processes may have been complicated by slow inflow of magma, by successive, more or less distinct heaves of magma, or by major convective overturn, it seems impossible at present to say. For one thing, our criteria for the distinction of such processes leave much to be desired. For another, despite the labors of many able investigators over a long period of years, the facts for the Critical Zone of the eastern Bushveld Complex are not all in. Detailed laboratory investigations closely correlated with detailed field studies must provide the necessary information. It is the writer's hope that laboratory studies at the University of Wisconsin, based on the field work here discussed, will contribute toward this end.

## References


CAMERON, E. N. AND M. E. EMERSON (1959) The origin of certain chromite deposits in the eastern part of the Bushveld Complex. *Econ. Geol.* **54,** 1151–1213.

GUILBERT, J. M. (1962) The origin of the chromitites below the Steelpoort Main Seam of the Bushveld Complex. Ph.D. thesis, Univ. of Wisconsin.

HALL, A. L. (1932) The Bushveld igneous complex of the Central Transvaal. *Geol. Surv. South Africa Mem.* **28.**

HECKROODT, R. F. (1959) The geology around the dunite pipe on Driekop (Eastern Transvaal). *Geol. Soc. South Africa Trans.* **62,** 59–73.

HESS, H. H. (1960) Stillwater igneous complex. *Geol. Soc. Am. Mem.* **80.**

HIEMSTRA, S. A. AND W. J. VAN BILJON (1959) The geology of the upper Magaliesberg stage and the lower Bushveld Complex in the vicinity of Steelpoort. *Geol. Soc. South Africa Trans.* **62,** 239–255.

JACKSON, E. D. (1961) Primary textures and mineral associations in the ultramafic zone of the Stillwater Complex, Montana. *U. S. Geol. Survey Prof. Paper* **358.**

KUSCHKE, G. S. J. (1940) The Critical Zone of the Bushveld igneous complex, Lydenburg district. *Geol. Soc. South Africa,* **42,** p. 57–81.

LOMBAARD, B. V. (1934) On the differentiation and relationships of the rocks of the Bushveld Complex. *Geol. Soc. South Africa Trans.* **37,** 5–52.

REUNING, E. (1937) Verbandsverhältnisse und Chemismus der Gesteine des 'Bushveld Complex', Transvaals und das Problem seiner Entstehung, *Neues Jahrb. Mineral. Beil. Bd.* **57A,** 631–664.

TRUTER, F. C. (1955) Modern concepts of the Bushveld igneous complex. *First meet., Southern Reg. Comm. Geology, Salisbury,* 77–91.

WAGNER, P. A. (1923) The chromite of the Bushveld Complex: Johannesburg. *South African Jour. Sci.* **20,** 223–255.

WILLEMSE, J. (1959) The "floor" of the Bushveld igneous complex and its relationships with special reference to the eastern Transvaal. *Geol. Soc. South Africa Proc.* **72,** xxi–lxxx.

WORST, B. G. (1958) The differentiation and structure of the Great Dyke of Southern Rhodesia. *Geol. Soc. South Africa Trans.* **59,** 283–358.

MINERALOGICAL SOCIETY OF AMERICA, SPECIAL PAPER 1, 1963
INTERNATIONAL MINERALOGICAL ASSOCIATION, PAPERS, THIRD GENERAL MEETING

# THE KAPALAGULU LAYERED INTRUSION OF WESTERN TANGANYIKA

W. J. WADSWORTH
*Grant Institute of Geology, University of Edinburgh, Edinburgh, Scotland*

ABSTRACT

The Kapalagulu intrusion is approximately 4500 ft. thick, with near-vertical contacts and layering. The contacts appear to be tectonic, and there is no trace of a chilled margin. The intrusion comprises a Basal Zone, 400 ft. thick (olivine cumulates, with local sulfide and chrome-magnetite concentrations); an Intermediate Zone, 750 ft. thick (plagioclase, 2-pyroxene, olivine cumulates); and a Main Zone over 3000 ft. thick (2-pyroxene, plagioclase cumulates, with a 300 ft. anorthosite band in the lower part, and local concentrations of magnetite-bearing and pegmatitic facies near the top).

Rhythmic layering is pronounced in the Intermediate Zone and in the lower part of the Main Zone, and igneous lamination is also locally well-developed. There is slight cryptic layering throughout the intrusion ($An_{87\rightarrow79}$, $En_{85\rightarrow70}$), with anomalous variations over 1000 ft. including the anorthosite band in the middle of the layered series. These variations are attributed to sudden loss of volatiles from the magma. Interstitial micro-pegmatite occurs throughout the Main Zone, increasing in abundance upwards, and reaching 20–30% in the pegmatitic patches. A later suite of dolerite dykes is also characterized by a relatively large amount of acid mesostasis.

## INTRODUCTION

The Kapalagulu intrusion is close to the eastern shore of Lake Tanganyika (Fig. 1), about 70 miles south of Kigoma. Brief accounts of the geology have been given by Teale (1931, 1932), McConnell (1950), Wilson (1956), and Halligan (1957), whereas van Zyl (1959) has described the intrusion and surrounding rocks in considerable detail. The present study is based on ten weeks field work undertaken as part of the research programme of the 1959 Oxford University Tanganyika Expedition.

## COUNTRY ROCKS

The country rocks of the area comprise two principal groups, the basement gneisses of the Ubendian system and the sedimentary rocks (quartzites and phyllitic shales) of the Itiaso series. The contact between the two is faulted in the Kapalagulu region, but there is evidence elsewhere (Henderson, 1960) that the Itiaso series rests unconformably on the Ubendian. There is some controversy about the general stratigraphic position of the Itiaso series; McConnell (1950) and Henderson (1960) believe it to be part of the Bukoban system (possibly of Palaeozoic age), but the Geological Survey of Tanganyika (Quennell, 1956; Halligan, 1957) link it with the Karagwe-Ankolean system, which is considerably older than the Bukoban.

## THE INTRUSION

*General.* The Kapalagulu intrusion is exposed as a long, narrow belt, approximately 9 miles by 1 mile, trending NW.–SE. between the Ubendian gneisses and the Itiaso series, as shown in Fig. 1. The contacts of the intrusion are generally steeply-dipping, and

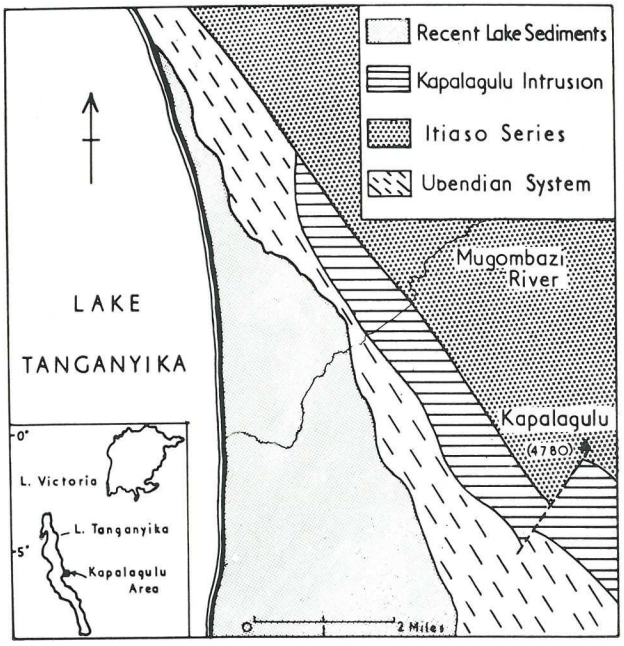


FIG. 1. Sketch map of the geology in the Kapalagulu region.

approximately parallel to the foliation of the Ubendian gneisses and the bedding of the Itiaso sediments. Near the margins of the intrusion the igneous rocks have suffered extensive shearing, and there is no evidence anywhere of original roof or floor facies. All the layered features of the intrusion are also steeply-dipping (except at the southeastern end of the outcrop), but there can be little doubt that this is the result of tilting subsequent to the consolidation of rocks formed by gravitative accumulation of crystals. The original upward sequence can clearly be established from the mineralogical variations, and it is

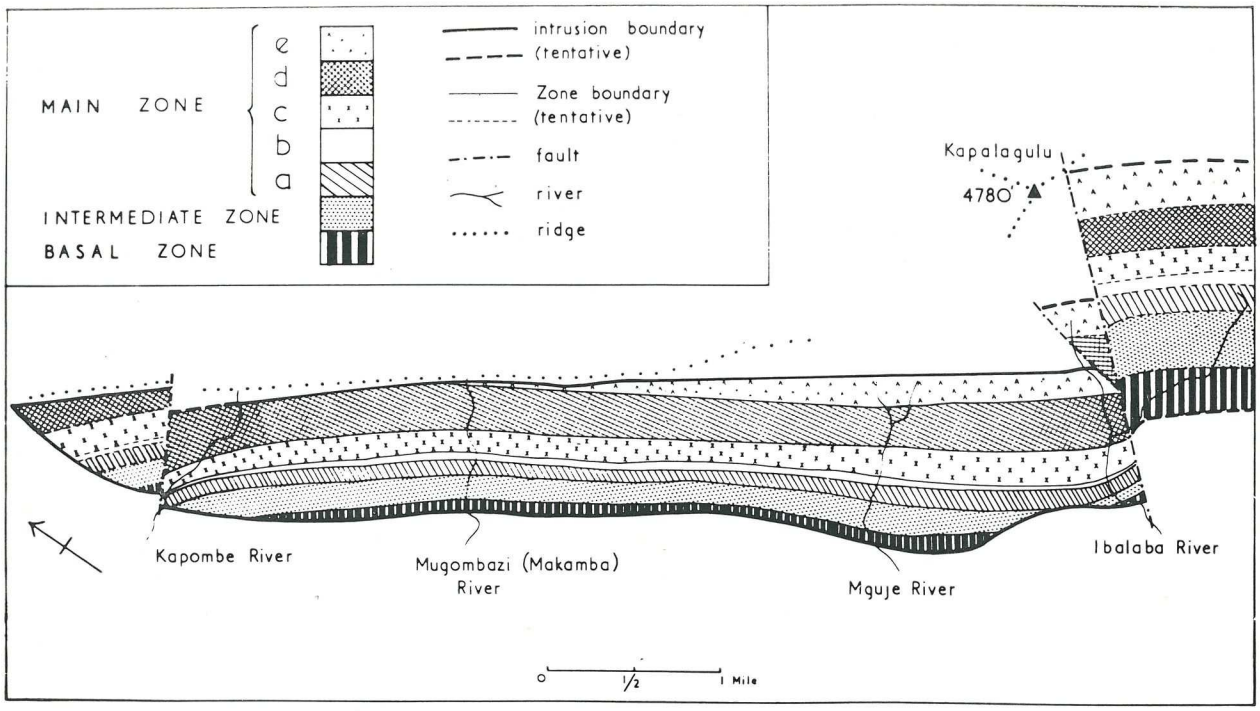


FIG. 2. Geological map of the Kapalagulu intrusion.

seen that the lowest members outcrop along the southwestern margin, adjacent to the Ubendian, and the highest members along the northeastern margin, adjacent to the Itiaso series.

On the basis of their field characteristics, van Zyl (1959) divided the layered series into three principal units, the Basal Zone, Intermediate Zone and Main Zone (containing a subsidiary Anorthosite Zone). These terms are all retained in the present account, but further subdivision of the Main Zone (into subzones a, b, c, d, e) has been found convenient. Main Zone (b) is equivalent to van Zyl's Anorthosite Zone. The nomenclature of the rocks themselves is based on the terminology introduced by Wager *et al.* (1960). A summary of the thickness and mineralogy of the principal subdivisions of the intrusion is given below:

| | | |
|---|---|---|
| MAIN ZONE | (e) plagioclase-augite-magnetite cumulates | 700 ft |
| | (d) plagioclase-2 pyroxene cumulates | 1300 ft |
| | (c) plagioclase-2 pyroxene cumulates | 500 ft |
| | (b) plagioclase cumulates | 300 ft |
| | (a) plagioclase-2 pyroxene cumulates | 550 ft |
| INTERMEDIATE ZONE | plagioclase-olivine-2 pyroxene cumulates | 750 ft |
| BASAL ZONE | Olivine cumulates | 400 ft |
| | Total | 4500 ft |

The most complete succession and the maximum thickness of layered series (4500 ft) is developed in the region of the Mguje River (Fig. 2). Northwestwards from here Main Zone (e), and possibly part of Main Zone (d), are progressively cut out. In the same direction the Basal Zone is roughly constant in thickness for about 3 miles, but the lower contact of the intrusion then swings to the north, cutting out the Basal Zone, Intermediate Zone, and part of the Main Zone in succession. At the north-western termination of the intrusion only Main Zone (d) is represented. To the south-east of the Mguje River the upper contact appears to be conformable to the layering, but the Basal Zone and the Intermediate Zone are locally cut out at the lower contact. In the Ibalaba River the succession appears to be complete again, but there is some evidence that the total thickness is reduced. In the vicinity of Kapalagulu Mountain the width of outcrop of the intrusion is much greater than elsewhere, but this is believed to be the result of generally low dips (20–25°). Poor exposure in this area prevented a detailed study of the succession or an accurate assessment of thickness, and further south-east the termination of the intrusion is completely obscured by drift.

The study of the mineralogical and petrological variation throughout the layered series is based on detailed traverses in the Mugombazi (Makamba) River where the succession is best exposed, and in

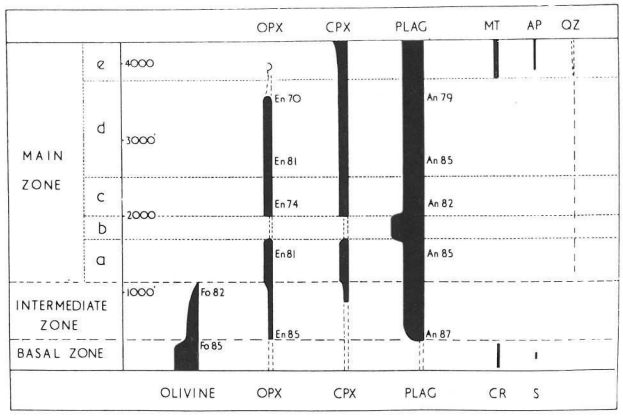


FIG. 3. Summary of the main mineralogical variations with height in the layered series. The dotted lines indicate minerals restricted to intercumulus occurrence. Major modal variations are indicated by changes in the thickness of the individual columns (Cr, chromite; S, sulfides).

the Mguje River where the maximum thickness is developed, but material from other traverses has been used to establish certain details of the succession.

*Phase layering.* The division of the layered series into zones and subzones is based on the major changes in the nature of the cumulus mineral assemblage. This type of variation has been termed "phase layering" by Hess (1960). The evidence is summarized in Fig. 3, where the appearance and disappearance of cumulus phases are related to stratigraphic position in the series, using an arbitrary height scale. An approximate indication of the cryptic layering and of the modal variations (disregarding the small-scale rhythmic layering) is also given in the same figure.

Olivine is the only important cumulus phase in the Basal Zone, although cumulus chrome-magnetite is commonly present in small amounts. The base of the Intermediate Zone is marked by the incoming of cumulus plagioclase and orthopyroxene, which increase in amount upwards at the expense of olivine, and are joined by cumulus augite in the upper part of the zone. Subzones (a), (c) and (d) of the Main Zone contain cumulus plagioclase, orthopyroxene and augite, but Main Zone (b) contains only cumulus plagioclase. The distinction between subzones (c) and (d) is based on changes in texture and mineral compositions. Cumulus orthopyroxene appears to be absent above 3600 ft, and the base of subzone (e) at 3800 ft is marked by the incoming of cumulus magnetite. Cumulus apatite appears a little higher in the succession, but the remainder of the Main Zone consists of heavily altered and sheared rocks.

*Cryptic layering.* The degree of cryptic layering in the intrusion has been determined in a preliminary way by measurements of the optical properties of the principal cumulus minerals. It is hoped to substantiate these results with chemical analyses of separated minerals in the near future.

(a) Orthopyroxene

By far the most sensitive indicator of position in the layered series was found to be 2V of orthopyroxene (Fig. 4). This property appears to vary independently of changes from cumulus to intercumulus habit in the rhythmically layered sequences. However the variation is not simply the result of progressive iron enrichment from bottom to top of the intrusion. There is a gradual decrease in 2V from the intercumulus pyroxene at the top of the Basal Zone ($2V_\alpha = 85°$), throughout the Intermediate Zone and into Main Zone (a), followed near the top of this subzone by a very sharp reduction over approximately 100 ft from 74° to 58°. Intercumulus orthopyroxene in the anorthosite subzone is too heavily altered for measurement of 2V, but the relatively low angles (58–60°) are maintained throughout the 500 ft thickness of subzone (c). Above this there appears to be a gradational increase in 2V from 60° to 75° over 300 ft in the lower part of subzone (d), followed by a progressive decrease again throughout the remainder of the layered series, as far as fresh orthopyroxene is present. The highest recorded cumulus orthopyroxene, from 3600 ft, has a 2V of 55°; and the minimum value obtained was 44° from intercumulus orthopyroxene just above the base of subzone (e) at 3900 ft. Using the curves published by Hess (1960)

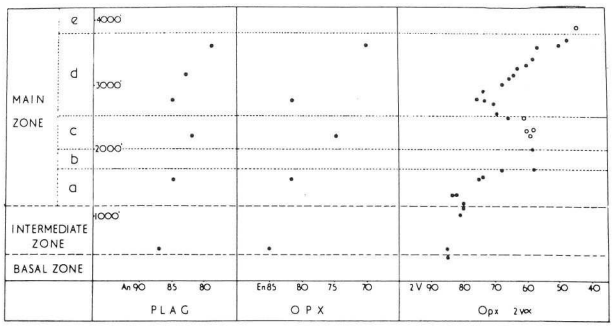


FIG. 4. Optical data on plagioclase and orthopyroxene from the layered series. Plagioclase compositions based on refractive indices of cleavage fragments using Tsuboi's curves. Orthopyroxene compositions based on measurements of $\gamma$ using the curve given by Hess (1960 Fig. 9). ○ indicates 2V measurements of inverted pigeonite.

to relate 2V to chemical composition the overall variation in the Kapalagulu orthopyroxenes appears to be from $En_{85}$ to $En_{50}$. However, refractive index ($\gamma$) determinations suggest that the true composition variation is less extreme than this, and is probably from $En_{85}$ to approximately $En_{70}$ (Fig. 4). They also confirm that the variation is not smoothly progressive throughout the layered series, but shows a marked reversal at the bottom of Main Zone (d).

Othopyroxene always contains fine exsolution lamellae of augite parallel to (100), but at two levels in the intrusion there is clear evidence, in the form of exsolution lamellae on original monoclinic (001) planes, that the orthopyroxene is inverted pigeonite. The lower occurrence comprises the top 300 feet of Main Zone (c), where the composition of the orthopyroxene is $En_{75}(\gamma = 1.696)$ and the crystals are always poikilitic in habit. Lower in the same subzone, undoubted cumulus orthopyroxene, with no trace of relict monoclinic structures, has the same 2V as these poikilitic inverted pigeonites and is assumed to have the same Fe/Mg ratio. Inverted pigeonite also occurs in Main Zone (e), where the orthopyroxene is rarely fresh, and is always intercumulus in habit. Here the 2V of the inverted pigeonite is distinctly smaller (44°–47°) than in Main Zone (c).

(b) Plagioclase

Cumulus plagioclase is consistently present from the base of the Intermediate Zone upwards. Preliminary results indicate that there is some cryptic variation (as determined from measurements of refractive indices of cleavage fragments, using Tsuboi's curves, and from extinction angles of albite twins) which parallels the orthopyroxene variation, but is less pronounced (Fig. 4). The overall change in composition is from $An_{87}$ to $An_{79}$, with a slight reversal from $An_{82-83}$ in Main Zone (c) to $An_{85}$ in the lower part of Main Zone (d). The results are not precise enough to indicate whether there is a sharp increase in Na content at the top of Main Zone (a), parallel to the iron enrichment of the orthopyroxenes.

(c) Augite

Cumulus augite is present in the upper part of the Intermediate Zone and throughout the Main Zone (except for the anorthosite sub-zone), and is the only fresh cumulus phase in much of Main Zone (e). Precise compositions have not yet been determined, but preliminary results indicate that there is slight cryptic variation, similar to that of the feldspar.

(d) Olivine

Olivine is restricted to the Basal Zone, where it is almost always heavily serpentinised, and the Intermediate Zone. Direct measurement of 2V shows that there is slight iron enrichment upwards throughout this range of 1150 ft. ($Fo_{85}$ to $Fo_{82}$), but van Zyl's suggestion (1959) that there is a reversal of this trend within the Basal Zone has not been confirmed.

*Rhythmic layering and general petrography*

(a) Basal Zone

The Basal Zone comprises approximately 400 ft of olivine cumulates which exhibit very little sign of rhythmic layering, except for occasional concentrations of chrome-magnetite. The principal intercumulus constituents are augite, orthopyroxene and plagioclase, all of which appear to be of high temperature composition and are generally unzoned, so that the rocks are essentially adcumulates. Individual pyroxenes are typically very extensive (2 or 3 cm across) but the plagioclase rarely forms large poikilitic crystals. Approximately in the middle of the Basal Zone there is a layer, 20 or 30 feet thick, in which sulfides (mainly pyrrhotite, with associated pyrite, chalcopyrite, sphalerite and pentlandite) are relatively abundant. Generally the sulfides occur interstitially, in places in quite large poikilitic patches, but locally sulfide globules are enclosed within poikilitic pyroxene crystals. Following van Zyl (1959) it is believed that the sulfides separated initially as an immiscible liquid phase.

(b) Intermediate Zone

The base of the Intermediate Zone can be clearly located in the field by the incoming of abundant cumulus plagioclase, which just precedes cumulus orthopyroxene. Cumulus augite only appears in the upper part of the zone, at about 900 ft, but it was impossible to use this in the field as a basis for subdividing the zone, partly because of the difficulty of distinguishing augite from orthopyroxene in hand specimen, and partly because cumulus augite only occurs intermittently at first. Cumulus olivine and orthopyroxene occur together in a number of layers throughout the 750 ft thickness of the Intermediate Zone and show parallel iron enrichment upwards through this sequence. This persistent overlap of cumulus olivine and orthopyroxene may indicate that the two minerals were nucleating at different levels in the magma, as suggested by Jackson (1961)

FIG. 5. Typical rhythmic layering in the Intermediate Zone, near the Mguje River.

to account for thick olivine-orthopyroxene cumulates in the Ultramafic zone of the Stillwater complex.

Rhythmic layering is common in the Intermediate Zone. It is mainly characterized by variations in the amounts of olivine and plagioclase, and both these minerals are invariably present as cumulus phases. Olivine rarely comprises more than 40% by volume, except at the very base of the zone, and in many layers is less than 15%. Cumulus pyroxene is rather sporadic in occurrence, but when present usually comprises 20–30%. When both varieties of pyroxene are present as cumulus phases they are typically associated in roughly equal proportions, but occasionally augite occurs by itself. Individual layers are usually between one inch and a foot or two in thickness (Fig. 5) and show very little lateral variation in thickness or mineral proportions. Evidence of slumping was seen in one case only, and there was rarely any indication of gravity stratification. Weak igneous lamination of the plagioclase crystals is locally developed, but there is no preferred orientation of elongate crystals in the plane of lamination. Of the cumulus phases in the Intermediate Zone, olivine crystals are always distinctly larger (approximately 2–3 mm diameter) than the plagioclase or pyroxene crystals. The rocks are all essentially adcumulates (or heteradcumulates where cumulus augite or orthopyroxene is absent).

(c) Main Zone

The subdivisions of the Main Zone have already been discussed. The boundaries between them cannot be fixed in the field within 30 or 40 feet because the major phase changes, such as the disappearance of cumulus pyroxene below subzone (b), are generally not abrupt. Rhythmic layering is mainly confined to subzones (a) and (c), where it consists of variations in the proportions of plagioclase to pyroxene. Both these phases are consistently present at all horizons throughout the Main Zone (except in the anorthosite subzone), but where there is rhythmic layering the total pyroxene content may vary from 15% to 70% by volume. The average content is about 30%. The relative distribution of augite and orthopyroxene is rather variable and in many layers only one cumulus pyroxene phase is present. This variation appears to be independent of the changes in the proportions of plagioclase to total pyroxene. The scale of the layering is generally finer than in the Intermediate Zone, with individual layers often less than an inch in thickness. Locally, there is evidence of lateral impersistence and current-bedded structures (Fig. 6), but there is no gravity stratification. Igneous lamination of plagioclase and pyroxene is common where rhythmic layering is developed, and at certain horizons where the orthopyroxene forms long bladed crystals (sometimes 5–6 mm in length, by 0.5–1 mm broad) there is a rough orientation of the *c* axes in the plane of lamination. The most perfect igneous lamination occurs in the upper half of subzone (c), where the rocks are plagioclase-augite cumulates with large poikilitic crystals of inverted pigeonite. This 300 ft thickness of distinctive cumulates conveniently marks the top of subzone (c), because the reversal of the cryptic layering (as shown by the variation in 2V of orthopyroxene) appears to start in the succeeding unlaminated cumulates.

There is a gradual upward change in the nature of the intercumulus material throughout the Main

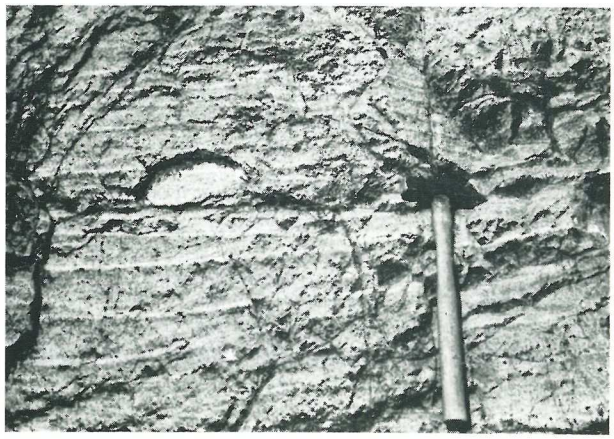

FIG. 6. Current bedding in rhythmic layering of Main Zone (c), Mugombazi River.

Zone. As in the Basal and Intermediate Zones, the rocks of the lower part of the Main Zone are essentially adcumulates. Small quantities of interstitial quartz first appear in Main Zone (a), but there is no trace of zoning of the plagioclase or pyroxene crystals, except in extremely thin films adjacent to the quartz. At horizons where only one pyroxene is present as a cumulus phase the other pyroxene forms extensive poikilitic crystals, but even these are unzoned and consist entirely of high temperature material. Such rocks are heteradcumulates.

Interstitial quartz increases in abundance upwards through the Main Zone, and is typically associated with alkali feldspar in micrographic intergrowth in Main Zone (d) above 2900 ft and in Main Zone (e), where micropegmatite reaches as much as 10% by volume. Even high in the Main Zone the plagioclase and augite are scarcely zoned, and the intercumulus orthopyroxene is not of significantly lower temperature composition than the associated cumulus minerals. There must have been considerable adcumulus growth before the interstitial liquid was completely trapped, and the rocks are probably best described as mesocumulates (Wager *et al*, 1960).

Small pockets and lenses of gabbro pegmatite are sporadically developed in the upper part of subzone (d) and in subzone (e). These are usually only a few inches across, and typically show a rough conformability with the steeply-dipping layered structures. They consist of large, heavily-altered plagioclase crystals, with cores of $An_{75-80}$ and strongly zoned margins, large augite crystals and a high proportion of quartz (up to 15%), much of it intergrown with alkali feldspsr. Sometimes the presence of inverted pigeonite can be detected from traces of augite exsolution lamellae, even though the host orthopyroxene has been completely altered. Iron ore and apatite are locally abundant.

*Sheared marginal rocks.* The southwestern margin of the intrusion is poorly exposed, and generally consists of heavily serpentinised Basal Zone cumulates adjacent to altered biotite-oligoclase gneisses of the Ubendian system. Within 50 to 100 feet of the contact both rock types are sheared, generally along steep planes roughly parallel to the margin of the intrusion. The same type of relationship is found where the Basal Zone is missing from the layered succession; sheared and altered rocks of the Intermediate or Main Zones are adjacent to the Ubendian. Shear zones also occur locally throughout the intrusion, and many of these are roughly parallel to the layering.

At the northeastern margin of the intrusion, heavily altered rocks of the Main Zone are in contact with quartzite (or, rarely, phyllitic shales) of the Itiaso series. In the igneous rocks, over a distance of approximately 250 ft from the contact, the plagioclase is always completely replaced by a turbid aggregate of clay minerals, and the orthopyroxene by chlorite. The augite is less readily altered and remnants of fresh augite are usually present to within 30 ft of the contact. Throughout most of this zone of heavy alteration there has been little deformation, and igneous textures are well preserved, but within 30 ft of the contact there has been considerable shearing, and the rocks are essentially chlorite-schists, with quartz (always strained), magnetite, and occasionally apatite as the only relict igneous minerals. The only traces of the original texture are small fragments of quartz showing micrographic intergrowth with altered alkali feldspar. In the Mugombazi River, where the actual contact is exposed, the modified igneous rocks appear to grade into a zone of quartz-rich cataclasite, 2–3 ft in thickness, adjacent to the massive quartzite of the Itiaso series. Some of the quartz in this cataclasite shows traces of micrographic texture and must have been derived from the Main Zone. However, the amount of quartz suggests that much of it was sedimentary material. Thus, there appears to have been mechanical mixture of the igneous and sedimentary rocks in a narrow fault zone at the upper contact of the intrusion. The main quartzite itself is generally unsheared, and appears to have acted as a relatively competent unit during emplacement of the igneous rocks.

*Dikes associated with the intrusion.* Numerous dolerite dikes cut the layered rocks and are distinctive in that they invariably contain a notable amount of interstitial quartz and alkali feldspar. This suggests a possible genetic link with the intrusion itself, and is also of importance in dating the intrusion, because similar dikes of post-Bukoban age are regionally important in Tanganyika. The plagioclase crystals have cores of $An_{75-77}$, with strongly zoned margins and are accompanied by augite, pigeonite and iron ore. A few heavily-chloritized crystals of orthopyroxene were seen in one dike. The amount of interstitial micropegmatite varies from dike to dike, but is usually between 10% and 20% by volume.

*Discussion of the cryptic variation and the anorthosite subzone.* The overall variation in mineral composition is clearly the result of fractional crystallization of

basic magma. However, the pattern of the cryptic layering, with the rather abrupt reduction in Mg content of the orthopyroxene (and probably in Ca content of the plagioclase, although this is less well established) at the top of Main Zone (a), followed by a reversal at the base of Main Zone (d), is anomalous. Further, it seems likely that this anomalous pattern is in some way connected with the origin of the anorthosite subzone. On general grounds it is unlikely that the 300 ft thickness of plagioclase cumulates represents merely an extreme winnowing effect, especially as there is no sign of a complementary pyroxene-rich horizon beneath it. Therefore, it seems that there must have been an important change in the nature of the magma, which affected the composition, as well as the distribution, of the cumulus plagioclase and pyroxenes. One possibility is that the magma composition was changed locally by resorption of plagioclase crystals, as suggested by Hess (1960) to explain the anorthosites of the Stillwater Complex. However, it is difficult to account for the variation in the composition of the Kapalagulu orthopyroxenes on this hypothesis. Modification of the magma composition by contamination might have had the necessary effect, but there is no reason to suppose that material of the required composition was available. A more likely explanation is that the water vapor pressure changed. Yoder (1954) has shown that increasing water vapor pressure in the diopside-anorthite-water system causes the position of the eutectic point to be depressed and shifted towards the anorthite end of the system. Conditions during the precipitation of plagioclase-pyroxene cumulates of Main Zone (a) may be thought of as approximating to the eutectic point in the simple diopside-anorthite system. If there had been a sudden reduction in water vapor pressure, perhaps associated with volcanic activity at the surface, then there may have been a period during which plagioclase alone was precipitated before "eutectic" conditions were re-established. Further, consideration of the albite-anorthite-water system (Yoder *et al.*, 1957) indicates that reduction of water vapor pressure would favor the crystallization of a less calcic feldspar, and similarly a less magnesian variety of orthopyroxene might be expected. The variation in 2V of the orthopyroxenes indicates that the return to a more magnesian composition at the bottom of Main Zone (d) is more gradual than the pronounced iron enrichment at the top of Main Zone (a), and this pattern would fit well with the likely variation of water vapor pressure in magmas, where volatiles would probably be lost suddenly, but built up again gradually.

*Origin of the rhythmic layering.* The rhythmic layering, which mainly consists of variations in the proportions of plagioclase to mafic minerals, is probably the result of variable current action in the magma. This suggestion is supported by the occurrence of igneous lamination at many horizons, and also by the local development of current-bedded structures. However, this type of mechanism does not account for the fact that the two pyroxenes, which are of similar size, shape, and density, do not always occur together as cumulus phases in the upper part of the Intermediate Zone and in Main Zone (a), (c) and (d) although the large-scale pattern of phase layering indicates that they were both generally available in those parts of the layered series. It seems that there must have been minor fluctuations in the physico-chemical conditions of the magma precipitating these phases, so that they did not both nucleate simultaneously all the time. There may have been slight changes in temperature or composition locally, perhaps due to convection, or non-equilibrium conditions may have been developed, at least periodically, so that differing powers of crystal nucleation (Wager, 1959) of augite and orthopyroxene could have been responsible for the patchy distribution of these phases in the resulting cumulates. Thus the rhythmic layering in the Kapalagulu intrusion may be the complex result of crystal sorting superimposed on a small-scale type of phase layering due to minor local variations in the magma conditions.

*The emplacement of the intrusion.* Various interpretations of the contact relationships of the intrusion have been suggested. McConnell (1950) indicates that the intrusion is younger than the Itiaso series. Wilson (1956) implies that the local cutting out of the lower zones along the south-western margin was the result of progressive overlap by higher zones during crystal accumulation. Van Zyl (1959) interpreted the upper contact of the intrusion as an unconformity, thus indicating pre-Itiaso emplacement. From the present study it is concluded that both the upper and lower contacts are tectonic, and that the evidence of their original nature has been destroyed by faulting and shearing. This would account for the absence of floor or roof facies, as well as the cutting out of certain zones. In particular the progressive disappearance of

Main Zone (e) to the north-west of the Mguje River is more reasonably explained on this basis than as the result of variable deposition. It is impossible to estimate how much of the original layered series is missing, but by analogy with other layered intrusions, a considerable thickness of cumulates higher than Main Zone (e) may have been present at one time. On the other hand it is possible that accumulation was disturbed soon after the deposition of Main Zone (e), and the remaining magma fraction dispersed elsewhere. In this connection it is possible that the dikes cutting the intrusion represent part of such a residual fraction. In either case it is assumed that the present layered series does not represent the entire crystallization products of the parent magma.

The age of the intrusion cannot be established on the available evidence, although its actual emplacement by faulting (and tilting) into its present position is clearly post-Itiaso. If the quartz-dolerite dikes cutting the intrusion are genetically related to it, and can also be equated with the regional post-Bukoban quartz-dolerite dikes, then the crystallization of the layered series was post-Bukoban too.

ACKNOWLEDGMENTS

The field work was based on the maps and reports prepared by C. van Zyl, who is thanked for his general interest in the project. Thanks are also due to R. C. Herrera for his valuable assistance throughout the period of field work; to the Geological Survey of Tanganyika for the loan of equipment and personnel; to Professor L. R. Wager for his interest and guidance in the research; and to Professor F. H Stewart and Dr. M. J. O'Hara for critical discussion of the manuscript. Grants from the Royal Society and the Percy Sladen Memorial Fund are gratefully acknowledged.

REFERENCES

HALLIGAN, R. (1957) South Kigoma and North-west Mpanda districts: Quarter degree Sheets 35 S.E. and N.E., and 36 S. W. *Geol. Survey Tanganyika Rec.* **7,** 14–20.

HENDERSON, G. (1960) The Geology of the Bukoban-type rocks of the Kigoma and Mpanda districts, Western Province, Tanganyika. *Trans. Geol. Soc. South Africa,* **63,** 11–50.

HESS, H. H. (1960) Stillwater igneous complex, Montana. *Geol. Soc. Am. Mem.* **80.**

JACKSON, E. D. (1961) Primary textures and mineral associations in the Ultramafic zone of the Stillwater complex, Montana. *U. S. Geol. Survey Prof. Paper,* **358.**

MCCONNELL, R. B. (1950) Outline of the geology of Ufipa and Ubende. *Geol. Survey Tanganyika Bull.* **19.**

QUENNELL, A. M. (1956) Summary of the geology of Tanganyika. *Geol. Survey Tanganyika Mem.* **1.**

TEALE, E. O. (1931) *Ann. Rept. Geol. Survey Tanganyika.*

——— (1932) *Ann. Rept. Geol. Survey Tanganyika.*

VAN ZYL, C. (1959) An outline of the geology of the Kapalagulu complex, Kungwe Bay, Tanganyika Territory, and aspects of the evolution of layering in basic intrusives. *Trans. Geol. Soc. South Africa* **62,** 1–31.

WAGER, L. R. (1959) Differing powers of crystal nucleation as a factor producing diversity in layered igneous intrusions. *Geol. Mag.* **96,** 75–80.

——— G. M. BROWN AND W. J. WADSWORTH (1960), Types of igneous cumulates. *Jour. Petrol.* **1,** 73–85.

WILSON, H. D. B. (1956) Structure of lopoliths. *Bull. Geol. Soc. Am.* **67,** 289–300.

YODER, H. S. (1954) *Ann. Rep. Geophys. Lab. Year Book* **53,** 106–7.

——— D. B. STEWART AND J. R. SMITH (1957) *Ann. Rep. Geophys. Lab. Year Book* **56,** 206–214.

MINERALOGICAL SOCIETY OF AMERICA, SPECIAL PAPER 1, 1963
INTERNATIONAL MINERALOGICAL ASSOCIATION, PAPERS, THIRD GENERAL MEETING

# A LAYERED COMPLEX IN SITTAMPUNDI, MADRAS STATE, INDIA

P. R. J. NAIDU
*Department of Geology and Geophysics, University of Madras, Madras, India*

ABSTRACT

Nehru (1955) and Subrahmanyam (1956) have reported on the anorthite-bearing and associated rocks of Sittampundi, Madras State. The latter regards them as a layered igneous anorthosite-gabbro series, highly metamorphosed. The present author regards the whole series as composed of igneous, sedimentary and migmatitic rocks of the Dharwarian, Peninsular and Charnockitic periods, domed up by the alaskite intrusion of the Closepet granite period. He gives a detailed succession of the rock-types along three cross-sections of the Sittampundi complex, and holds that there is no amphibolite surrounding all the rock types. From a study of garnets and amphiboles the rocks belong to three different geological periods. The garnet-bearing rocks are not all eclogites, and the mineral assemblages of the anorthite-bearing gneisses denote them to be metamorphosed marly and pelitic sediments.

## INTRODUCTION

Nehru (1955) has studied the anorthite-amphibole gneisses and associated rocks of Sittampundi, Madras State, India, and states, "Here in Sittampundi one seems to encounter a metamorphic facies in the association together of ecologites, amphibolites and anorthite-spinel rocks, rather than gabbroic rocks and anorthosites." Subrahmanyam (1956) describes them as a layered igneous anorthosite-gabbro series of the type of Bushveld Complex and the Bay of Islands, highly metamorphosed.

The Sittampundi area lies within longitudes 77° 45′, 78° 5′ and latitudes 11° 10′, 10° 23′. In order to understand the geological structure of the area, it is necessary to include the northern region to latitude 11° 31′. This will bring into discussion the rocks developed around the township of Sankaridrug. The Sankaridrug series has been mapped by Balasubrahmanyam, and the Sittampundi series by Nehru. The combined map is presented in Fig. 1. The whole region consists of metasediments and earlier intrusives which have been domed up by an alaskite that extends in all directions beyond the confines of the area mapped. Thus all the rocks of the area are xenoliths within alaskite. These xenoliths are of limestones (now converted to marbles), calc-silicate rocks (having the minerals, wollastonite, tremolite, grossularite, diopside, sphene etc.), biotite (dark brown)-gneisses, hornblende gneisses, hornblende-biotite gneisses, garnetiferous-biotite (dark brown) gneisses, two-pyroxene-garnetiferous rocks and two-pyroxene pyroxenites (both of the charnockite series), sillimanite gneisses, biotite (reddish brown)-pyroxene (ortho- and clino-) gneisses, garnetiferous quartzites, hematite quartzites, quartz-hematite-emery rocks, anorthite amphibole gneisses (with the combinations of one or more of the minerals: grossularite, epidote, zoisite, clinozoisite, corundum, chromite, fassaite and highly aluminous calciferous amphiboles etc.), amphibolites and peridotites. The name anorthite-amphibole gneiss here used is the equivalent of anorthosite of Subrahmanyam (1956) and will be so referred to in this paper.

These rocks by analogy with similar rocks occurring elsewhere in India, are assigned in the following Indian stratigraphical scale given by Pascoe (1950).

| | | | |
|---|---|---|---|
| ARCHAEAN | Post-charnockite | Alaskite granite | |
| | Charnockite series | Two-pyroxene-garnetiferous rocks (eclogitic) and two-pyroxene pyroxenites (noritic). Biotite (reddish brown)—pyroxene gneisses. | |
| | Peninsular Gneisses | Biotite-hornblende gneisses, hornblende-biotite gneisses, garnetiferous biotite gneisses. | |
| | Dharwars | Sillimanite gneisses, hematite-quartzites, quartz-hematite-emery rock, garnetiferous quartzites. | |
| | | Limestones, amphibolites, anorthite gneisses, calc-silicate rocks and peridotites. | |

All these rock types are present in both the areas of Sankaridrug and Sittampundi, but the marbles dominate in the northern region and the anorthite gneisses in the southern. Peridotites are absent in the north, and the sillimanite-gneisses do not occur in the south.

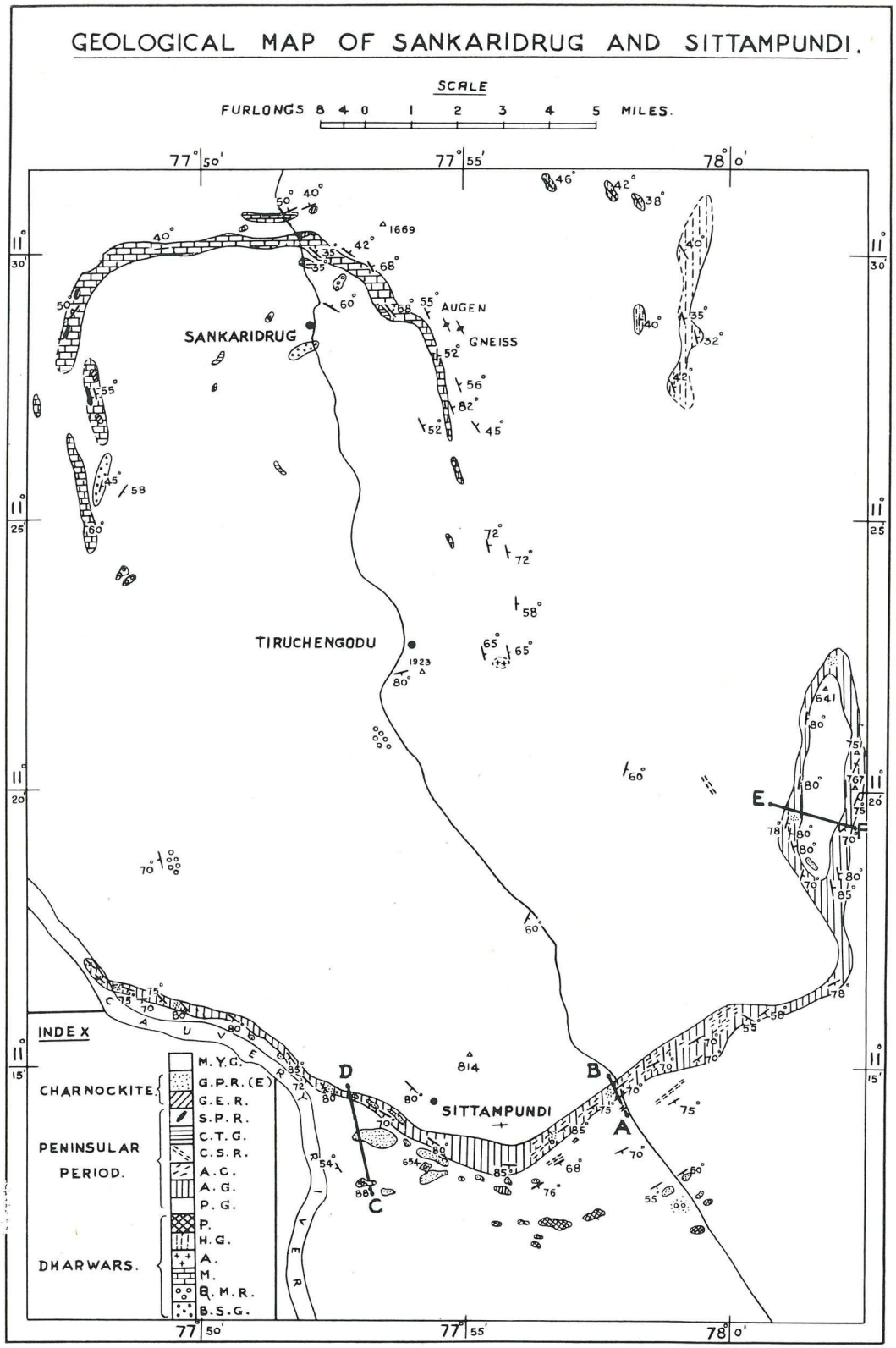


FIG. 1. Geological map of Sankaridrug and Sittampundi. In the index, M.Y.G.—Migmatite and younger granite. G.P.R.(E)—Garnet-pyroxene rock (eclogite). G.E.R.—Garnet-epidote rock. S.P.R.—Scapolite-pyroxene rock. C.T.G.—Calc-tremolite gneiss. C.S.R.—Calc-silicate rock. A.C.—Amphibolite with chromite. A.G.—Anorthite gneiss. P.G.—Peninsular gneiss (not mapped separately from younger granite). P—Peridotite. H.G.—Hornblende gneiss. A—Amphibolite. M—Marble. Q.M.R.—Quartz-magnetite rock. B.S.G.—Biotite-sillimanite gneiss. AB, CD and EF are sections along the anorthite gneiss band.

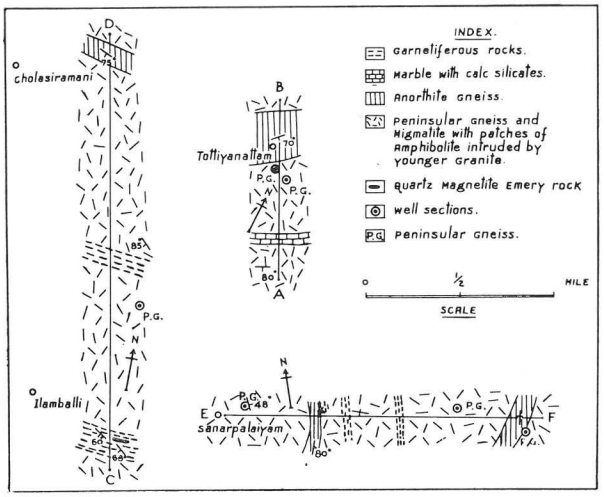


FIG. 2. Enlarged section along AB, CD and EF of Fig. 1.

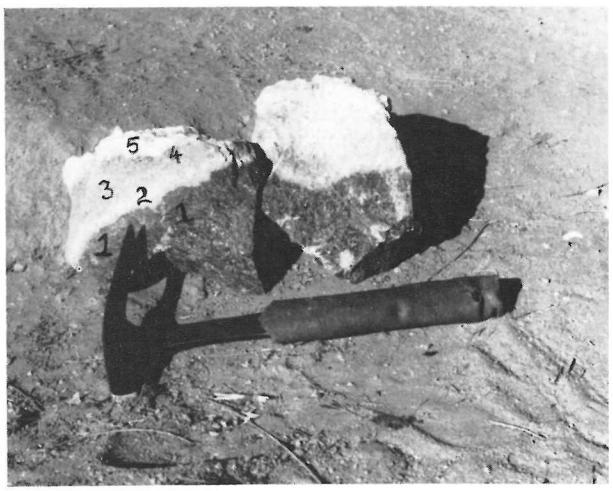


FIG. 3. Specimens from druses in a well along section AB. 1 to 5 zones in the specimen.

## DESCRIPTION

Henceforth rock types of Sittampundi alone concern us. In order to elucidate the mutual field relationships of the various rock units, sections along lines AB, CD and EF (centre/ west and east of the anorthite-gneisse band) of Fig. 1, will be described. Enlarged diagrammatic sketches to scale are given in Fig. 2.

*Section along AB.* The succession from A to B is migmatite (hybrids between peninsular gneisses and alaskite), marble (with calc-silicates), migmatites again with xenoliths of peninsular gneisses, anorthite gneiss and alaskite.

The calc-silicate band consists of the minerals, calcite, epidote, hedenbergite (deeply pleochroic from green to blue), reddish-yellow grains of spongy andradite, pale green diopside, scapolite and sphene. These alternate with bands of quartz and plagioclase ($An_{30}$). The calc-silicate bands are cut by alaskite veins and pegmatites.

In the well section (50 feet deep), near the southern border of the anorthite gneiss, the Peninsular gneiss is in contact with it. The Peninsular gneiss has the minerals, greenish-blue amphibole, pale green relic diopside, reddish-brown sphene, plagioclase ($An_{30}$), quartz and iron ore. The anorthite gneiss has a granulitic texture with the minerals, anorthite, pale blue amphibole, grossularite, calcite and chlorite. There are also pools of calcite, and sillimanite threading through the anorthite grains. Corundum may also be present. There are several druses. Two of these are figured (Fig. 3). These consist of five zones. The first zone is composed of anorthite gneiss having anorthite, pale-blue amphibole, calcite and chlorite. The second consists of chlorite and sericite with relics of plagioclase. The third is composed of muscovite and talc (Fig. 4). The fourth consists of pools of talc amidst irregular aggregates of calcite and chalcedony. In the fifth, there are well-developed crystals of calcite and quartz. The second to the fifth zone are considered to be the sedimentary material from which the anorthite-gneiss was constituted.

The next band of anorthite gneiss consists of anorthite and greenish-blue amphibole of the type found in the Peninsular gneiss which is different from the pale-blue amphibole, found elsewhere in the anorthite gneisses.

The section AB ends in the north in alaskite, a potash-rich pegmatitic granite.

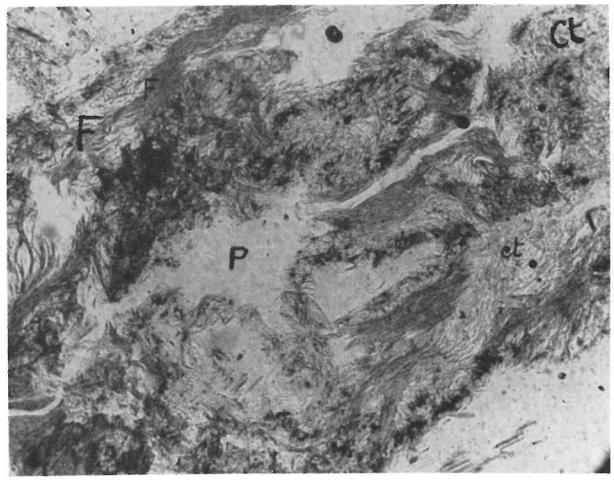


FIG. 4. Zone 3 of Fig. 3. Nicols not crossed. ×70. P—Relics of plagioclase, F—muscovite, ct—chlorite and talc.

FIG. 5. Quartz-hematite-emery rock (Q.H.E.) flanked by garnetiferous quartzites (G.Q.).

*Section along CD*: It starts with migmatite again. Then comes a band of quartz-hematite-emery rock (Fig. 5), which is flanked on either side by a garnetiferous quartzose gneiss (consisting of spongy garnets (Fig. 6)), plagioclase and quartz grains enclosed in a matrix of minutely granulitic plagioclase, quartz and microcline. The matrix also in places, consists of amorphous matter which alters to sericite. The

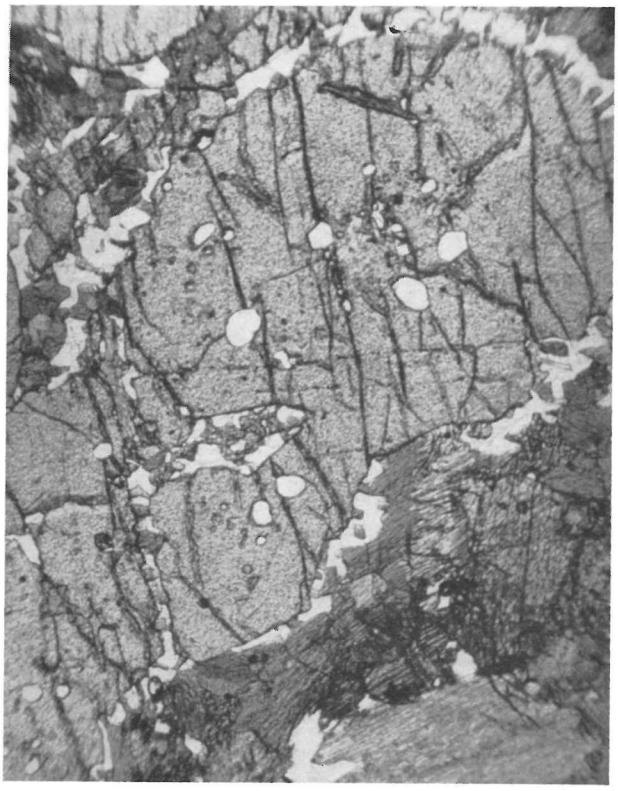

FIG. 6. Spongy sieved garnet in garnetiferous quartzite (G.Q. of Fig. 5). Nicols not crossed. ×70.

FIG. 7. Well-foliated hornblende-biotite gneiss (Peninsular gneiss).

quartz which is of various sizes is far in excess of plagioclase and forms distinct bands. The garnet is converted to reddish-brown mica, and has inclusions of plagioclase, quartz, biotite, limonite and hematite. This band is followed by a micaceous gneiss that stands out as high inclined tables. This consists of distinctly gneissose bands of reddish-brown mica, quartz and feldspar (plagioclase and microcline). Among the biotite folia, hypersthene granules are also present. Other foliae consist of pyroxenes alone, both orthorhombic and monoclinic. Biotite develops at the expense of both. There are local pools of calcite. The plagioclases are all antiperthites with distinct rods of orthoclase (rod-perthites). The next band consists of alaskites and migmatites. A section in a well in this band discloses the presence of biotite-rich gneiss (Peninsular gneiss). Again there is a band of garnetiferous gneiss. This consists of granules of garnet, brownish-green amphibole, quartz and plagioclase with a granulitic texture. Coarse gneissosity is present. The garnet is spongy and has inclusions of quartz, plagioclase and some indeterminate granules. Massive iron ore is abundant. The brownish-green amphibole is typical of the charnockite series. This rock is invaded by quartz veins and pegmatites from the neighbouring alaskite. At contact with the quartz vein, the garnet develops a corona of plagioclase ($An_{95}$) and blue amphibole. The garnets are spongy and are sieved with quartz, plagioclase and iron ore. Hairlike inclusions cross each other at rhombohedral angles. The rest of the rock consists of lamellar pyroxenes, with interrupted lamellae, and plagioclase ($An_{40}$). (This is the average content of anorthite found in plagioclases of basic charnockites.)

The above band is bordered by biotite-hornblende

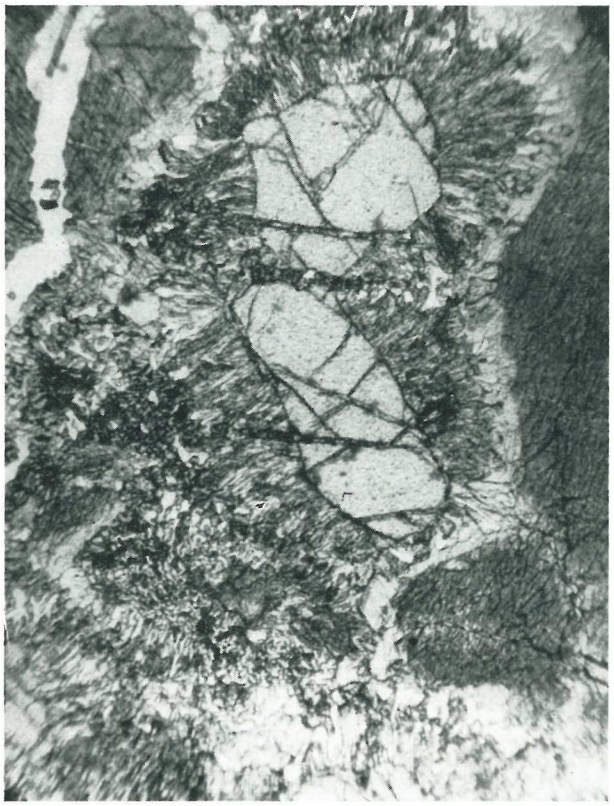

FIG. 8. Garnet with corona of anorthite and pale-blue amphibole. Nicols not crossed. ×26.

gneiss (Peninsular) with biotite in excess of hornblende (Fig. 7). The rest of the rock consists of abundant quartz and subordinate plagioclase. Biotite is pleochroic from yellow to dark-brown, and the hornblende is pleochroic from yellow to blue. These are biotites and hornblendes characteristic of Peninsular gneisses.

Then comes the band of alaskite and migmatite, followed by anorthite gneiss, which is again bordered by the former. A section in a well at the northern edge of the anorthite-gneiss reveals only the presence of migmatites.

The quartz-hematite-emery rock, the two garnetiferous rocks one associated with quartz-emery rock, and the other with charnockites, and the reddish brown biotite gneiss have been analysed and the results are presented in Table 2. Quartz in the quartz hematite-emery rock has been introduced from the quartz veins of the alaskite granite.

*Section along EF.* This section starts with a zone of alaskites and migmatites, but half a mile west of this occurs a calc-silicate band (not included in the section). The calc-silicate band contains the minerals, calcite, diopside, greenish-blue amphibole, epidote, sphene and apatite in decreasing abundance.

In the zone of alaskite-migmatites is a well which discloses a Peninsular gneiss having distinct pencilled banding. This consists of greenish-blue amphibole, quartz and plagioclase with apatite as accessory.

This is followed by a first band of anorthite gneiss having the characteristic pale-blue amphibole. Long epidote needles are abundant. This is the bluish anorthite-gneiss. The white and pale-pink varieties occur in the western section of the anorthite-gneiss band. The blue anorthite gneiss here shows diffuse and sinuous lamination such as is found in marbles.

East of this band is a xenolith of charnockite. This consists of pools of brownish-green hornblende developing around iron ores. Elsewhere the pools have relics of ortho and clinopyroxenes. The rest of the rock consists of plagioclase with well-twinned but disturbed lamellae. This rock has a few boulders of 2-pyroxene pyroxenites of the charnockite series. The hypersthene is deeply pleochroic, X = pink, Y = yellow, Z = green. The brownish-green amphibole, as usual, develops around iron ore.

Then comes a long stretch of migmatites intersected by two bands of quartzose-garnetiferous rocks similar to those described along section CD. A well among the migmatites revealed a Peninsular gneiss with its characteristic biotite (dark brown) and hornblende (greenish-blue). Quartz and plagioclase in various proportions, discrete grains of calcite and abundant apatite are present.

Then comes the second anorthite-gneiss band with a temple at the top. This is the highest point (767 feet) of the whole anorthite-gneiss band, whose general level is 600 ft. above M.S.L. A well immediately at the eastern end of it revealed the presence of a rock with anorthite, greenish-blue amphibole (characteristic of Peninsular gneisses), abundant sphene and apatite. A neighboring well 50 ft. eastwards disclosed only migmatites.

From the above description it is obvious that there is no amphibolite bordering the anorthite-gneiss on either side, much less, surrounding all the rock types of the area as has been mapped by Subrahmanyam (1956).

Corundum and chromite mines: Corundum and chromite mines occur in the middle of the anorthite-gneiss band. While chromite occurs on either side of section AB, corundum is confined to the nose. The chromite is confined to the amphibolite lenses. The amphibole is a pale-blue amphibole (characteristic of the major part of the anorthite-gneiss). Chromite is

segregated from the walls to the center, and the amphibolite lenses do not extend downwards. There are druses in the chromite mines, showing layers of chromite, calcite and muscovite mica. Probably chromite was introduced metasomatically from the dunites and periodotites occurring immediately to the south of the nose of the anorthite-gneiss band.

The corundum mines are traversed by pegmatites. Corundum occurs in well-formed crystals, and also as disseminated grains in the anorthite-gneiss. A specimen of anorthite-gneiss from the mines consisted of abundant epidote, anorthite, stray diopside, greenish-blue amphibole and pools of calcite. The pools of calcite are sometimes bordered by epidote and diopside.

*Isolated patches of garnetiferous rocks and calcite in the anorthite-gneiss.* There are isolated patches of garnetiferous rocks throughout the anorthite-gneiss. One of these occurs to the west of section AB. It consists of pyrope, lamellar pyroxene and pale-blue amphibole. The pyrope has a corona of anorthite and bluish amphibole (Fig. 8). The analysis of this rock is given in table 2. There are also stray calcite masses along the length of the anorthite-gneiss.

## Chemical Data

It has been held by the author that the Sittampundi area consists of rock units separated vastly in geological timescale; namely, the Dharwars, peninsular gneisses, charnockites, and post-charnockitic granite, formed during about a thousand million years. Their mutual relationships are brilliantly stated by Pascoe (1950, p. 35). The units can be recognized not only petrographically, but also mineralogically. Analyses of garnets and amphiboles can be used to this end.

Analyses of garnets and amphiboles, three of each, are presented in Table 1.

The garnets are almandinic in rocks associated with iron ores, pyropic in basic charnockites, and grossularitic in anorthite-gneisses. The amphiboles are common hornblendes in peninsular gneisses, hastingsitic in basic charnockites, and a highly aluminous calciferous amphibole in anorthite gneisses. The optical characters of the last amphibole correspond neither to pargasite nor to edenite. But, in the banded anorthite-gneisses at the nose of the band, the greenish-blue amphibole, characteristic of the Peninsular gneisses, is present.

From the above account of petrography and mineralogy, it is obvious that rocks of three different geological periods, namely, the Dharwars, the Charnockite series and the Peninsular gneisses, cannot be

Table 1. Analyses of Garnets and Amphiboles

| | Garnets | | | Amphiboles | | |
|---|---|---|---|---|---|---|
| | 1 | 2 | 3 | 4 | 5 | 6 |
| $SiO_2$ | 37.50 | 36.34 | 37.59 | 43.91 | 45.91 | 41.21 |
| $TiO_2$ | 1.03 | 0.15 | 0.21 | 0.89 | 0.05 | 2.04 |
| $Al_2O_3$ | 21.57 | 24.52 | 17.14 | 19.04 | 18.35 | 16.78 |
| $Fe_2O_3$ | 0.34 | 0.11 | 11.04 | nil | nil | 4.83 |
| FeO | 23.61 | 14.51 | 0.39 | 8.65 | 6.07 | 6.15 |
| MnO | n.d. | 1.35 | n.d. | Tr. | 0.08 | 0.14 |
| MgO | 7.38 | 14.61 | 0.63 | 12.96 | 12.10 | 11.22 |
| CaO | 7.73 | 6.35 | 32.91 | 12.13 | 15.92 | 15.32 |
| $Na_2O$ | 0.22 | 0.26 | n.d. | 1.29 | 0.32 | 1.56 |
| $K_2O$ | 0.13 | 0.81 | n.d. | 0.17 | 0.05 | 0.25 |
| $H_2O^+$ | 0.21 | 0.32 | 0.13 | 0.60 | 0.54 | 0.98 |
| $H_2O^-$ | 0.09 | 0.26 | 0.05 | 0.11 | 0.15 | 0.16 |
| Total | 99.81 | 99.59 | 100.09 | 99.75 | 99.54 | 100.64 |

Garnets in Standard Molecules

| | 1 | 2 | 3 |
|---|---|---|---|
| Almandine | 51.35 | 28.87 | 1.00 |
| Pyrope | 27.93 | 51.88 | 2.50 |
| Grossularite | 19.82 | 16.32 | 62.50 |
| Andradite | 0.90 | — | 34.00 |
| Spessartite | — | 2.93 | — |

Optical characters of the Amphiboles

| | | 4 | 5 | 6 |
|---|---|---|---|---|
| | $2V_X$= | 72°–78° | 85°–95° | 68°–72° |
| | Z∧c= | 18°–20° | 16°–18° | 15°–17° |
| Pleochroism | X= | Yellow | Colourless | Yellow |
| | Y= | Brownish-green | Pale-green | Brown |
| | Z= | Greenish-blue | pale-blue | Greenish-brown |

1. Garnet associated with iron ores of Salem, Madras State Analyst: S. Saravanan, Analytical Chemist, Department of Geology & Geophysics, University of Madras.
2. Garnet associated with basic charnockites of Salem, Madras State. Analyst: S. Ramanathan, Oil & Natural Gas Commission, Government of India.
3. Garnet associated with calc-silicate rock, Kadavur, Tiruchirapalli, Madras State. Analyst: S. Saravanan.
4. Greenish-blue amphibole from Peninsular gneiss, Sittampundi, Salem. Analyst: C. E. Nehru.
5. Pale-blue amphibole from anorthite gneiss, Sittampundi, Salem. Analyst: C. E. Nehru.
6. Brownish-green amphibole from basic charnockites, Kadavur, Tiruchirapalli. Analyst: S. Saravanan.

TABLE 2. ANALYSIS OF GARNETIFEROUS ROCKS AND THE QUARTZ-HEMATITIC-EMERY ROCK OF SITTAMPUNDI, SALEM, MADRAS STATE

| | 1 | 2 | 3 | 4 | 5 | 6 |
|---|---|---|---|---|---|---|
| $SiO_2$ | 48.39 | 62.08 | 73.55 | 50.44 | 47.00 | 49.68 |
| $TiO_2$ | Tr. | 0.50 | 0.21 | 1.12 | 1.00 | Nil |
| $Al_2O_3$ | 10.48 | 19.28 | 12.15 | 12.70 | 17.61 | 36.13 |
| $Fe_2O_3$ | 0.23 | 0.98 | 1.64 | 1.06 | 2.25 | 2.49 |
| FeO | 6.89 | 3.62 | 3.15 | 9.55 | 6.78 | 8.88 |
| MnO | Tr. | — | 0.12 | — | — | 0.05 |
| MgO | 15.79 | 5.92 | 2.58 | 8.19 | 8.78 | 1.13 |
| CaO | 16.58 | 0.89 | 0.77 | 13.99 | 14.99 | 0.79 |
| $Na_2O$ | 0.54 | 0.93 | 0.75 | 1.95 | 1.14 | Tr. |
| $K_2O$ | 0.23 | 4.82 | 3.57 | 0.73 | 0.21 | Tr. |
| $H_2O^+$ | 0.18 | 1.01 | 0.85 | 0.15 | — | 0.57 |
| $H_2O^-$ | 0.12 | 0.12 | 0.12 | 0.03 | 0.40 | 0.05 |
| $P_2O_5$ | — | — | — | — | 0.40 | — |
| Total | 99.43 | 100.15 | 99.46 | 99.91 | 100.56 | 99.77 |

CIPW norms for the Analysed Rocks

| | 1 | 2 | 3 | 4 |
|---|---|---|---|---|
| Quartz | — | 24.90 | 48.12 | — |
| Orthoclase | 1.11 | 28.36 | 21.13 | 4.45 |
| Albite | 4.72 | 7.86 | 6.29 | 16.77 |
| Anorthite | 25.58 | 4.45 | 3.89 | 23.63 |
| Corundum | — | 10.91 | 5.71 | — |
| Diopside | 45.31 | — | — | 37.46 |
| Hypersthene | 1.36 | 20.61 | 10.59 | 5.55 |
| Olivine | 20.91 | — | — | 8.36 |
| Magnetite | 0.46 | 1.39 | 2.32 | 1.62 |
| Illmenite | — | 0.91 | 0.46 | 2.13 |
| Total | 99.45 | 99.39 | 98.51 | 99.97 |

The percentages of Or, Ab, An, +fem, in Analyses 1, 2, 3, & 4

| | 1 | 2 | 3 | 4 |
|---|---|---|---|---|
| Or | 1.12 | 38.07 | 41.93 | 4.45 |
| Ab | 4.74 | 10.55 | 12.48 | 16.78 |
| An+fem | 94.14 | 51.38 | 45.59 | 78.77 |

1. Garnetiferous-brown-amphibole-pyroxene-plagioclase rock.
2. Garnetiferous-reddish-brown biotite-pyroxene-antiperthite rock.
3. Garnetiferous quartzite.
4. Garnetiferous-anorthite-pale-blue amphibole-pyroxene rock (Coronite).

   1, 2, 3 & 4—Analyst: S. Saràvanan.
5. Garnet amphibolite quoted from Subrahamnyam (1956) p. 372, Analysis 4.
6. Quartz hematite-emery rock, Analyst, C. E. Nehru.

connected together by crystallization-differentiation processes.

To ascertain the character of the garnet-bearing rocks (the so-called eclogites), four of them have been analysed and the results are presented in Table 2.

The four garnet-bearing rocks analysed show large variations in the chemical constituents. The fourth is similar to Biere's Garnet-amphibolite, but for the lower percentage of alumina. The other three do not agree with this eclogite in 2 or 3 constituents. The Or, Ab and (An+fem) constituents were plotted in Brammall's diagram (1933). Garnetiferous reddish-brown biotite-pyroxene-antiperthite rock (No. 2) and Garnetiferous-quartzite (No. 3) fall in the sedimentary field. Garnetiferous brown-amphibole-pyroxene-plagioclase rock (No. 1) falls in the metamorphic field. This is a variation of the charnockite series. Garnetiferous-anorthite-blue-amphibole pyroxene rock (Coronite) falls in the igneous field.

Garnets from Nos. 1, 3 and 4 were determined by $x$-ray. The molecules read from $x$-ray data and FeO content are as follows:

| | 1 | 3 | 4 |
|---|---|---|---|
| Cell dimensions | 11.58 Å | 11.54 Å | 11.54 Å |
| FeO content | 14.19% | 9.90% | 6.15% |
| Standard molecules: | | | |
| Pyrope | 48 | 66 | 71 |
| Almandine | 32 | 22 | 15 |
| Grossularite | 16 | 10 | 12 |
| Spessartite | 2 | 1 | 1 |
| Andradite | 2 | 1 | 1 |

They are all pyropic, and are related to the Charnockite series. The relative abundance of pyrope and almandine is dependent on the original composition of the orthopyroxenes from which these garnets are constituted.

## DISCUSSION

The anorthite-gneiss consists of the following mineral assemblages:

(1) Anorthite-anthophyllite-amphibole (pale-blue, highly aluminous and calciferous) . . . Hornblende hornfels facies.
(2) Anorthite-greenish-blue-amphibole (of the type of the peninsular gneiss)-biotite . . . Hornblende hornfels facies.
(3) Anorthite-grossularite-fassaite . . . Hornblende hornfels facies.
(4) Anorthite-corundum-spinel . . . Sanidinite facies without sanidine (Turner and Verhoogen, 1960).
(5) Anorthite-corundum-calcite . . . Pyroxene hornfels facies.
(6) Anorthite-epidote-diopside-calcite . . . Almandine amphibolite facies.
(7) Anorthite-epidote-hornblende(pale-blue) . . . Almandine amphibolite facies.

These mineral assemblages are certainly those formed from marly and pelitic sediments, and can be inserted into the appropriate triangles of Goldschmidt (Turner and Verhoogen 1960).

The Charnockite series, including the garnet-bearing varieties, belong to the granulite facies (Turner and Verhoogen, 1960).

The Peninsular gneisses (with biotite, hornblende and plagioclase) belong to the almandine-amphibolite facies.

There are thus, in Sittampundi, rocks of the Dharwarian, Charnockitic and Peninsular gneissic periods, belonging to the sanidinite, pyroxene-hornfels and granulite facies, on which has been imposed an almandine-amphibolite facies metamorphism by the intrusion of an alaskite-granite. These certainly are not "a layered igneous anorthosite-gabbro series of the type of Bushveld Complex and Bay of Islands, highly metamorphosed."

ACKNOWLEDGMENT

My thanks are due to C. E. Nehru, Pool Officer of the Government of India, for assisting me in the field and in the laboratory.

REFERENCES

BRAMMAL, A. (1933) Syntexis and differentiation. *Geol. Mag.* **70.**

NEHRU, C. E. (1955) Geology and petrochemistry of the anorthite-gneiss and associated rocks of Sittampundi, Salem District. *Jour. Madras Univ.* **XXV** (2), 178–188.

PASCOE, E. H. (1950) The Manual of Geology of India and Burma.

SUBRAHMANYAM, A. P. (1956) Mineralogy and petrology of the Sittampundi Complex, Salem District, Madras State, India, *Geol. Soc. Am. Bull.* **67,** 317–379.

TURNER, F. J. AND J. VERHOOGEN, (1960) *Igneous and Metamorphic Petrology.* McGraw-Hill Book Co. Inc., New York, p. 602.

MINERALOGICAL SOCIETY OF AMERICA, SPECIAL PAPER 1, 1963
INTERNATIONAL MINERALOGICAL ASSOCIATION, PAPERS, THIRD GENERAL MEETING

# LAYERED INTRUSIONS IN THE FERRAR DOLERITES, ANTARCTICA

BERNARD M. GUNN
*University of Otago, Dunedin, New Zealand*

ABSTRACT

The Ferrar Dolerites are of Lower to Middle Jurassic age and occur as sheets, sills, bosses, dikes and related lavas throughout 60,000 square miles of Antarctica. Undifferentiated dolerite consists of augite, pigeonite, plagioclase and interstitial mesostasis, but in several sills and dike-like bodies hypersthene is found in large amounts in a zone extending from about 150 to about 400 feet above the base of a sill 800 feet thick. Lenses of bytownitic anorthosite are found within the hypersthene zone. In the upper parts of the sills the dolerite is granophyric and contains lenses of coarse-grained pegmatoid and sometimes bands of granophyre. Chilled margins have about 45% total pyroxene, 5% MgO, 53% $SiO_2$; whereas the hypersthene zones have 60–70% pyroxene, 17–21% MgO; compared with the granophyres and pegmatoids which have 7–10% pyroxene, 1–3% MgO and up to 67% $SiO_2$.

The crystallization of hypersthene is thought to be governed by several factors including composition of magma and pressure.

## INTRODUCTION

Dolerites of tholeiitic affinities are now known to be exposed over a distance of 2,800 miles across the Antarctic continent though the width of outcrop seldom exceeds 20 miles. The name Ferrar Dolerites was proposed for them by Harrington (1958) and such dolerites have been described or reported from Oates Land (Browne, 1923; Klimov and Solovyev, 1958), the Arctic Institute Range (Weihaupt 1961), along the entire length of the Victoria Mountain System from Terra Nova Bay to the Horlick Mountains (Ferrar, 1907; Webb and McKelvey, 1959; Gunn and Warren, 1962; Skinner, 1961; Laird, 1961; Gunn and Walcott, 1962; Gould, 1931; Long, *pers. comm*), from the Whichaway Nunataks and Theron Mountains (Stephenson, *pers. comm*) and from the western Dronning Maud Land mountains (Roots, 1953).

In the McMurdo Sound region a sheet of dolerite known as the Basement Sill is intruded into the metamorphic and plutonic basement rocks and is 700 to 900 feet thick. A second sill (the Peneplain Sill) is 900 to 1300 feet thick and is intruded between the Kukri Peneplain surface which is cut across the Basement rocks, and the overlying flat-bedded Beacon Sandstone. The Beacon Sandstone is about 6000 feet thick and into this are intruded three or four discontinuous sills, the total thickness of dolerite in any one section in the sandstone being about 2000 feet. Dolerite also forms bosses a few miles in diameter and elongate dike-like bodies up to 20 miles long, one or two miles wide and not less than about 5000 feet thick. Tholeiitic lavas, pillow lavas and pyroclastics of the same age as the Ferrar Dolerites are known from near the upper Mawson Glacier and the Darwin Mountains (Gunn and Warren 1962) and also from near the upper Beardmore and Mill Glaciers (Grindley, *pers. comm*). These rocks are here referred to as the Ferrar Volcanics.

The age of the Ferrar Dolerites is now known to be younger than Lower or possibly Middle Jurassic on the basis of plant fossils whereas potassium/argon absolute age determinations give an age of $170\times10^6$ years for a dolerite from Mt. Obruchev in Oates Land (Starik *et al.*, 1959) and $162\times10^6$ years for a dolerite from the Victoria Dry Valley (McDougall, *pers. comm*). Using the time scale of Kulp (1961) the absolute ages are also compatible with a L-M Jurassic age.

## PHASE LAYERING IN THE FERRAR DOLERITES

Phase layering of minerals occurs only in sills more than 500 feet in thickness and then only in those bodies in which hypersthene has crystallized. In four of five sills of 700 to 1300 feet in thickness and in the two large dike-like bodies studied by the writer hypersthene has crystallized in the interior of the bodies in large amounts but appears in the marginal phase only in the very magnesian Egerton Sill. In four other sills a marginal zone about 150 feet in thickness contains augite, pigeonite, plagioclase and interstitial mesostasis only, whereas hypersthene occurs in a zone extending from about 150 to about 400 feet above the base of the sill. The greatest concentration is found near the base of this zone where hypersthene may make up 60 to 70% of the rock, but it decreases in quantity upward suggesting gravitational settling.

In contrast to the situation in many other tholeiitic intrusions olivine has not been found in the Ferrar dolerites in the McMurdo Sound region except as rare pseudomorphs enclosed in hypersthene in the Harmsworth Dike. Hypersthene has been reported in

amounts not exceeding 7% in the Tasmanian Dolerites, (Spry, 1958; McDougall, 1958) and in similar small amounts in the Hangnest and Downes Mountain sills of the Karroo Dolerites (Walker and Poldervaart, 1940, 1941) and in the Palisades Sill (Walker, 1940).

Concentrations of up to 70% of hypersthene in the Ferrar Dolerites is therefore unusual and is comparable with the accumulation of olivine in the more basic tholeiites or high-alumina basaltic bodies such as the Skaergaard intrusion (Wager and Deer, 1939, p. 117). Such a concentration increases the amount of magnesia present by a factor of four or five but does not alter the silica content of the rock as hypersthene contains approximately the same amount of silica as the undifferentiated rock (53–55%). Concentration of bytownitic plagioclase does depress the silica content a little (47% $SiO_2$ for $An_{80}$, Hess, 1960) but anorthosites are rare and minor in amount. Crystallization of the main mineral phases does not therefore increase the silica content of the residual liquid but the undifferentiated rock does contain about 10% of interstitial quartz-sanidine micropegmatite and accumulation of hypersthene has displaced the equivalent liquid upwards to give rise to upper zones of granophyric dolerite, small lenses of coarse-grained pegmatoid, and bands of granophyre with a composition roughly equivalent to that of a granite (62 to 67% $SiO_2$). The wide range of modal composition is illustrated by Fig. 1.

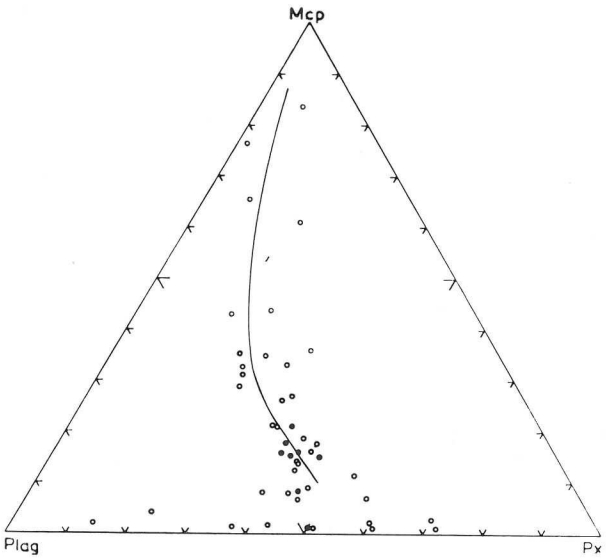


FIG. 1. Triangular diagram of modal plagioclase, pyroxene and micropegmatite plus remaining phases in 46 specimens of Ferrar Dolerite. Solid circles represent undifferentiated rocks. Plagioclase and hypersthene cumulates are at the base and granophyres and pegmatoids near the upper apex.

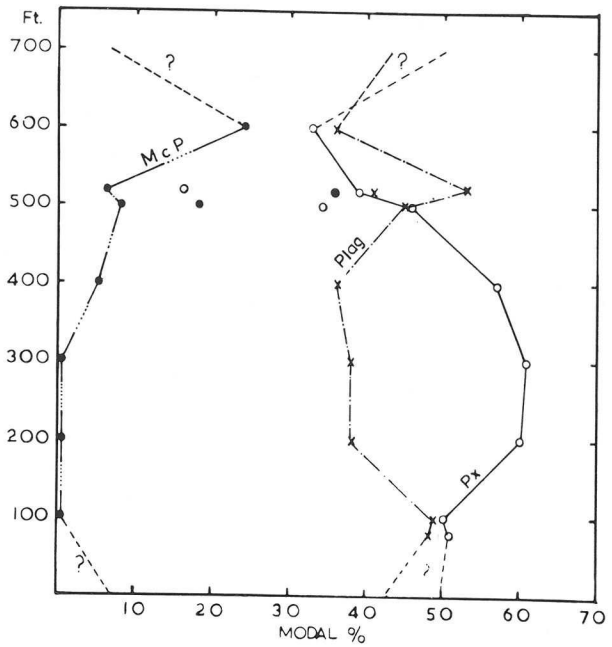


FIG. 2. Distribution of modal % of total pyroxene, plagioclase and micropegmatite with height in Basement Sill at Kukuri Hills with upper and lower margins conjectured from bulk averages. Composition of pegmatoids at 500 feet and 540 feet are shown. Hypersthene is found only at 200 and 300 feet where it constitutes 20% and 26% of the rock.

Typically then a sill of hypersthene-bearing Ferrar Dolerite about 800 feet in thickness displays the following layered structure:

(a) A glassy margin containing a few plagioclase phenocrysts and rarely, hypersthene, passing inwards to augite-pigeonite-plagioclase-mesostasis dolerite.

(b) A lower zone of augite-pigeonite-plagioclase dolerite in which the amount of interstitial micropegmatite is sometimes rather less than near the margins.

(c) A zone of hypersthene dolerite extending from about 150 to about 350 to 500 feet above the base.

(d) Lenses not more than a few inches thick of anorthosite within the hypersthene zone formed of bytownitic plagioclase.

(e) An upper zone of granophyric pigeonite dolerite extending from the top of the hypersthene zone to the upper chilled margin, and containing schlieren of coarse-grained pegmatoid.

(f) Lenses of fine-grained granophyre which occur within the granophyric dolerites are found only rarely in the sills but form bands up to 200 feet in thickness in the dike-like bodies.

A typical range of modal distribution with height in a sill is shown in Fig. 2. compiled from data from the Basement sill near Ferrar Glacier. Hypersthene occurs only at 200 and 300 feet, the pyroxene at 400 feet being augite with some pigeonite.

Dolerite bosses and dike-like bodies more than 1500 feet in thickness often show a regular layering at

about 10 feet intervals. The layers are slightly concave upwards and are accentuated by weathering but petrographic study of the layers in a boss in the Lashly Mountains failed to show any marked differences in mineral composition. Rhythmic layers have been described from elsewhere in the Ferrar Dolerites by Gunn and Warren (1962).

### Cryptic Layering

Optical determinations of mineral composition as well as whole-rock chemical analyses show that the early-formed ferromagnesian minerals now found near the base of the hypersthene zones consist of highly magnesian hypersthene ($Mg_{83-70}$) and augite ($Ca_{45}$ $Mg_{46}$ $Fe_9$) in contrast to the iron-rich ferroaugites ($Ca_{39}$ $Mg_{11}$ $Fe_{50}$) which have crystallized from the last fractions of the melt in the granophyres and pegmatoids. In the same way the early-formed plagioclases are highly calcic ($An_{82-78}$) while the last to crystallize are more sodic ($An_{45-10}$).

This process has been thoroughly described for other differentiated basic bodies, eg. the sills of Tasmania (Edwards 1942; McDougall 1961) and the regularity of the variation in the Ferrar sills supports the contention of original homogeneity.

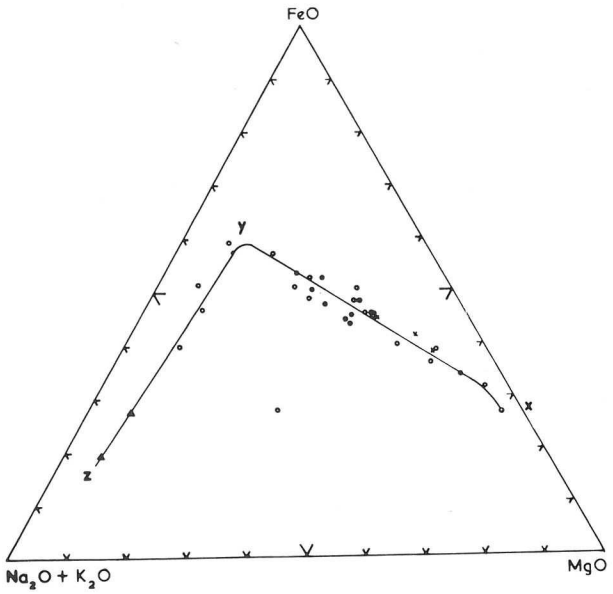


Fig. 3. F M A diagram (ferrous iron, magnesia, and total alkalis) of Ferrar Dolerites. Solid circles represent undifferentiated dolerites, circles differentiated doleites, (analyst B. Gunn), crosses three analyses of Ferrar Dolerites quoted by Benson (1916), triangles two Ferrar Dolerite granophyres kindly supplied by Dr. W. Hamilton, (U.S.G.S. unpublished analyses, Nos. F208 and 154597; analysts: Smith, and Elmore, Barlow, Botts and Chloe). Hypersthene cumulates fall near X, granophyric dolerites near Y and granophyres and pegmatoids near Z. The single isolated rock is an anorthosite.

Variation in normative plagioclase is different in sills of different marginal composition but the composition alters regularly from the margins ($An_{60-70}$) to the hypersthene zones ($An_{75-83}$) and to the granophyres and pegmatoids ($An_{31-56}$). The range of chemical composition is shown in Fig. 3.

### Examples of Layered Bodies of Ferrar Dolerite

Due to the reconnaissance nature of Antarctic fieldwork only limited amounts of material are available from each sill and this was usually obtained in the course of a single traverse across an exposure. There is no case in which good examples of all the features described above have been found in one locality in one sill. Detailed descriptions of one sill and one dike are given which illustrate most but not all of the features which appear to be typical of the Ferrar Dolerites. Similar detailed descriptions of other differentiated sills have been published separately (Gunn, 1962).

*Mt. Egerton sill.* A series of samples of dolerite were collected by Mr. D. Skinner of the New Zealand Antarctic Division, from a sill 800 feet thick exposed on the slopes of Mt. Egerton, 250 miles south of McMurdo Sound. The sill is in part intruded between the Kukri Peneplain surface and Beacon Sandstone and in part into basement limestones.

Field relationships have shown that there were at least three phases of intrusion of the Ferrar Dolerites and that there are several distinct magma types (Table 1). The Egerton sill belongs to the type low in silica and high in magnesia. The hypersthene zone in this sill extends from about 150 to possibly 500 feet above the base and within it are bands of contrasting mineralogy. At 400 feet there are numerous lenses of anorthosite about 18 inches long and $1\frac{1}{2}$ inches thick while at 440 feet there is a continuous band of unusually coarse-grained augite pigeonite-plagioclase rock about 4 feet in thickness. Small pods of pegmatoid up to $3\times6\times10$ inches are found between 600 and 770 feet above the base and tend to occur subhorizontally. These show only slight quartz enrichment and no bands of granophyre were found though a dike-like body at Detour Nunatak with a similar margin composition to the Egerton sill contains an upper band of granophyre more than 200 feet thick.

(a) Petrography

The chilled rock near the lower margin is unremarkable (16793)[1] consisting of sub-ophitic intergrowths of

[1] Numbers are those of the collection of the Geology Department, University of Otago.

TABLE 1. MAGMA TYPES OF FERRAR DOLERITES AND OTHERS

| | A | B | C | D | E | F |
|---|---|---|---|---|---|---|
| $SiO_2$ | 55.68 | 55.14 | 53.57 | 53.05 | 52.65 | 51.59 |
| $Al_2O_3$ | 15.98 | 14.62 | 15.71 | 16.95 | 16.23 | 15.95 |
| $TiO_2$ | 0.80 | 0.71 | 0.67 | 0.65 | 0.58 | 0.89 |
| $Fe_2O_3$ | 1.81 | 1.76 | 1.25 | 0.79 | 0.51 | 1.38 |
| FeO | 8.01 | 7.78 | 7.87 | 6.69 | 8.21 | 7.52 |
| MnO | 0.17 | 0.18 | 0.17 | 0.07 | 0.15 | 0.14 |
| MgO | 4.17 | 5.82 | 6.36 | 6.91 | 6.64 | 7.56 |
| CaO | 8.42 | 10.07 | 10.63 | 11.56 | 11.34 | 9.52 |
| $Na_2O$ | 2.34 | 2.19 | 1.85 | 2.05 | 1.58 | 2.04 |
| $K_2O$ | 1.12 | 0.81 | 0.82 | 0.97 | 0.90 | 0.65 |
| $P_2O_5$ | 0.10 | 0.09 | 0.08 | tr. | 0.01 | 0.19 |
| $H_2O^+$ | 0.93 | 0.48 | 0.74 | 0.49 | 0.48 | 1.77 |
| $H_2O^-$ | 0.62 | 0.23 | 0.36 | 0.43 | 0.85 | 0.57 |
| $CO_2$ | n.d. | 0.06 | n.d. | n.d. | n.d. | 0.44 |
| Total | 100.15 | 99.94 | 100.08 | 100.61 | 100.13 | 100.21 |

A = Average margin of Peneplain Sill (23092, 23093).

B = Average upper and lower margins of Basement Sill, unpublished U.S.G.S. analyses (F2502, F2509), V. C. Smith analyst.

C = Average chilled margins of Detour Nunatak dike, Carapace Nunatak lava, and Mt Egerton Sill (21841, 21846, 16793).

D = Horn Bluff Dolerite (Browne, 1923).

E = Tasmanian Dolerite (average of six undifferentiated samples, Edwards, 1942).

F = Theron Dolerite (average of two chilled margins (350/6, 351/7), J. Stephenson, unpublished analyses.

augite-pigeonite with 0.2 mm plagioclase ($An_{70}$), very fine-grained intergrowths of quartz and orthoclase, apatite needles and iron ores. A hundred feet above the base (16794) there is also a little hypersthene present both as separate coroded crystals and as cores mantled by zones containing copious blebs of augite which is interpreted as having exsolved on inversion from pigeonite which is in turn mantled by uninverted pigeonite. The exsolution lamellae are parallel to (001) of the original pigeonite, the *b* and *c* axes of which have sometimes been retained on inversion. Pigeonite is also present as corroded separate grains and intergrown with augite. At 200 feet (16795) hypersthene is present to the extent of 40% of the rock. Euhedral 4 mm cumulus crystals ($Mg_{83-71}$) are closely packed and fine-grained plagioclase is interstitial. Augite is coarser in grain than the plagioclase (1 mm) but is anhedral and there is a complete lack of pigeonite either marginal to the hypersthene or as separate grains. Fine-grained, almost glassy micropegmatite and iron ores are present only in very minor amounts and the rock has the characteristic porphyritic texture of al hypersthene dolerites. Similar hypersthene dolerite is found at 400 feet (16796) but the texture is glomeroporphyritic with, in an average of three sections, considerably less hypersthene. The separation of hypersthene in such large quantity must have greatly enriched the liquid fraction in lime and alumina.

The thin lenses of anorthosite (16797) consist of about 85% of bytownitic plagioclase ($An_{83}$) together with a little interstitial and ophitic augite some of which is much altered and may be pigeonite (Fig. 4). A few of the larger plagioclase crystals (0.6 mm) show weak oscillatory zoning but the majority of the crystals are unzoned and are less than 0.3 mm long. A strong horizontal banding is caused by parallelism of feldspars and differences in concentration of pyroxene. The coarse-grained 4 foot band at 440 feet is similar to the anorthosites but here coarse (6 mm) poikilitic augites and inverted pigeonites are surrounded by fine-grained plagioclase, and iron ores are present. Unfortunately there is no sample of normal rock from this level but at 600 feet (16799) a little hypersthene is still present as cores mantled by inverted pigeonite. Some of these composite crystals are coarse in grain (3 mm) but there is a complete lack of euhedral outlines, the texture is granular to subophitic and uninverted pigeonite occurs as separate crystals and intergrown with augite. Rods of magnetite-ilmenite and some interstitial micropegmatite are present.

The pegmatoid lenses at 600 feet (16800) are coarse-

FIG. 4. Photomicrograph, of anorthosite, Mt. Egerton Sill (16797). A little augite is ophitically intergrown with the bytownite which shows a roughly parallel orientation. ×30.

grained with pyroxenes up to 2 cm long. Quartz-feldspar intergrowth is present to the extent of 25% but this is much less than in pegmatoids found in other sills where quartz-sanidine intergrowths may make up to 60% of the rock. The texture is granitoid or rarely ophitic with sub-hedral 2 mm plagioclase ($An_{68-56}$), and greenish-brown hornblende but augite, probable pigeonite and fine biotite are secondarily altered to chlorite. Titano-magnetite and ilmenite form coarse 2 mm grains. The pegmatoid from 770 feet is similar with coarse pyroxenes and plagioclase, abundant iron ores and micropegmatite and a little hornblende. The normal rock at 770 feet is a fine grained (0.2–1 mm) augite-inverted pigeonite-plagioclase-micropegmatite rock. Thirty feet above, the chilled marginal rock contains rare phenocrysts of hypersthene.

(b) Modal variation

In this sill the lower pigeonite zone which contains roughly equal amounts of augite and pigeonite extends not more than about 150 feet above the base while the zone of hypersthene accumulation is difficult to define because of the spread of sampling. At 200 feet augite is present in about the same amount as in an undifferentiated rock, (Table 2) plagioclase and micropegmatite are greatly reduced and 50% of hypersthene has been added while pigeonite is entirely absent. At 400 feet total pyroxene is present in normal amount except that hypersthene has taken the place of pigeonite. Probably the residual liquid more ferriferous than about Mg/Mg+Fe=45 (mol %) was expelled by the accumulating pyroxene and plagioclase. Pyroxene is still slightly in excess over its concentration in the margins at 600 feet though this could be a mafic band complementary to the anorthsite lenses below. In the upper 200 feet of the sill there is a general increase in micropegmatite especially in the pegmatoids.

(c) Mineral composition and variation

Progressive variations in normative plagioclase and pyroxene can be seen in Table 3. Optical determinations of plagioclase give consistent results but clinopyroxenes are unusually magnesian and optically variable in this sill, in the main due to exsolution of fine lamellae of hypersthene and pigeonite, the host augites therefore appearing to be more calcic than is usually the case. The lowest values of 2V have accordingly been used in determining composition (Table 4). Determinative data used are those of Hess (1960), for orthopyroxene, Tröger (1956) for plagioclase, Brown (1957) for augites and Muir (1951) for pigeonites and ferro-augites.

*Mt. Harmsworth dike.* A poorly exposed dike-like body of dolerite extends eastward from Mt. Harms-(9080 feet) for about three miles and descends to the Delta Glacier, a tributary of the Skelton Glacier, at about 4800 feet. Several sheets of dolerite are exposed in nearby granites and may branch from the dike, the width of which is unknown but is not less than about 600 feet. Some 200 feet of rock is exposed at the summit of Mt Harmsworth and this is all a fine-grained, light grey granophyre. At about 8000 feet the rock is a pigeonite dolerite while at the visible base the rock is a hypersthenite and is streaked with curved anorthositic bands which are usually less than 1 cm thick.

(a) Petrography

The hypersthenite rock at the base is an extreme example of an accumulative rock in which euhedral weakly pleochroic hypersthenes up to 6 mm long are closely packed and show a strong tendency to a parallel orientation (Fig. 5). A few pseudomorphs after

TABLE 2. MODES OF MT. EGERTON SILL.

| No. | Height above base (ft) | Total Px. | Hypers. | Augite | Pigeon. | Plag. | Micropeg. | Hornbl. Biotite Chlorite | Opaques |
|---|---|---|---|---|---|---|---|---|---|
| 16801 (a) | 770 (peg.) | 21.1 | | 10.9 | 10.2 | 43.7 | 27.8 | 3.6 | 3.8 |
| 16801 | 770 (Norm.) | 41.8 | | 19.3 | 22.5 | 44.1 | 10.8 | 1.9 | 1.4 |
| 16800 | 600 (peg.) | 23.0 | | n.d. | n.d. | 44.1 | 25.6 | 2.6 | 4.7 |
| 16799 | 600 | 52.7 | 8.0 | 21.7 | 23.0 | 36.0 | 10.0 | 0.6 | 0.7 |
| 16798 | 440 | 22.2 | | 12.1 | 10.1 | 73.5 | 2.8 | 0.3 | 1.2 |
| 16797 | 400 | 13.5 | | 10.7 | 2.8 | 84.5 | 1.2 | 0.3 | 0.5 |
| 16796 | 400 | 43.0 | 19.5 | 21.6 | 1.9 | 55.3 | 1.4 | — | 0.3 |
| 16795 | 200 | 70.0 | 50.0 | 20.0 | | 27.3 | 2.3 | — | 0.4 |
| 16794 | 100 | 43.4 | 1.5 | 24.5 | 17.4 | 48.8 | 6.4 | 0.4 | 1.0 |
| 16793 | base | 45.0 | | n.d. | n.d. | 40.0 | 10.8 | 1.5 | 2.7 |

TABLE 3

| | Analyses of Mt Egerton Sill | | | | Analyses of Mt Harmsworth Dike | |
|---|---|---|---|---|---|---|
| No. | 16793 | 16795 | 16797 | 16800 | 16790 | 16792 |
| Feet above base | 0 | 200 | 400 | 600 | 50 | 4,300 |
| S.G. | 2.94 | 3.08 | 2.76 | 2.84 | 3.12 | 2.78 |
| $SiO_2$ | 53.41 | 53.05 | 47.34 | 56.64 | 53.18 | 63.02 |
| $Al_2O_3$ | 16.53 | 11.10 | 30.65 | 15.33 | 9.29 | 13.70 |
| $TiO_2$ | 0.67 | 0.30 | 0.18 | 1.20 | 0.30 | 1.17 |
| $Fe_2O_3$ | 0.88 | 0.62 | 0.61 | 2.60 | 0.42 | 5.37 |
| FeO | 7.73 | 8.54 | 1.44 | 7.64 | 8.17 | 4.83 |
| MnO | 0.18 | 0.19 | 0.02 | 0.18 | 0.18 | 0.19 |
| MgO | 6.61 | 17.26 | 1.66 | 3.19 | 21.27 | 1.02 |
| CaO | 10.90 | 7.63 | 15.85 | 7.86 | 6.18 | 4.80 |
| $Na_2O$ | 1.78 | 0.72 | 1.84 | 2.60 | 0.60 | 2.41 |
| $K_2O$ | 0.81 | 0.32 | 0.29 | 0.91 | 0.30 | 2.07 |
| $P_2O_5$ | 0.09 | n.p. | n.p. | n.d. | n.p. | 0.23 |
| $H_2O^+$ | 0.27 | 0.45 | 0.21 | 1.46 | 0.35 | 0.83 |
| $H_2O^-$ | 0.32 | 0.29 | 0.25 | 0.24 | 0.10 | 0.12 |
| Total | 100.18 | 100.47 | 100.34 | 99.85 | 100.34 | 99.76 |
| *Norm. wt. %* | | | | | | |
| ap | 0.19 | n.p. | n.p. | n.d. | — | 0.50 |
| il | 1.27 | 0.58 | 0.35 | 2.28 | 0.58 | 2.22 |
| mt | 1.27 | 0.90 | 0.88 | 3.77 | 0.60 | 7.78 |
| or | 4.79 | 1.89 | 1.73 | 5.40 | 1.78 | 12.25 |
| ab | 15.05 | 6.08 | 15.58 | 21.98 | 5.09 | 20.40 |
| an | 34.72 | 26.12 | 74.51 | 27.49 | 21.76 | 20.45 |
| di wo | 7.87 | 4.90 | 1.72 | 4.81 | 3.72 | 0.85 |
| di en | 4.29 | 3.34 | 1.10 | 2.12 | 2.66 | 0.39 |
| di fs | 3.31 | 1.17 | 0.50 | 2.68 | 0.73 | 0.45 |
| hy en | 12.17 | 39.64 | 0.81 | 5.82 | 47.31 | 2.15 |
| hy fs | 9.38 | 13.85 | 0.38 | 7.48 | 12.92 | 2.41 |
| ol fo | | | 1.55 | | 2.11 | — |
| ol fa | | | 0.77 | | 0.63 | — |
| Q | 5.26 | 1.25 | | 14.30 | — | 28.97 |
| $H_2O$ | 0.59 | 0.74 | 0.46 | 1.70 | 0.45 | 0.95 |
| Total | 100.16 | 100.46 | 100.34 | 99.83 | 100.34 | 99.77 |
| Norm. Plag. | $An_{70}$ | $An_{81}$ | $An_{83}$ | $An_{56}$ | $An_{81}$ | $An_{50}$ |
| Norm. pyrox. | $Mg_{63}$ | $Mg_{79}$ | $Mg_{74}$ | $Mg_{51}$ | $Mg_{83}$ | $Mg_{54}$ |

olivine are enclosed by the hypersthene, but there are few plagioclase inclusions and crystal margins are entire and uncorroded. Plagioclase tablets are rarely as much as 1 mm in length and fit in the interstices between the hypersthene phenocrysts whereas augite tends to be moulded between orthopyroxene. There is no micropegmatite and traces of iron-ores and biotite are the only other minerals.

The rock at 800 feet appears to be a normal pigeonite dolerite with intergrowths of augite and partly inverted pigeonite with plagioclase and with interstitial micropegmatite.

At the summit the granophyre contains isolated plagioclase ($An_{55-51}$) which are surrounded by quartz sometimes intergrown with extensions of the plagioclase with a composition of about $An_{15-10}$ but more often with potash feldspar (Fig. 6). Interstices between the intergrowths tend to be filled by coarser

TABLE 4. (a) EGERTON SILL

| | | |
|---|---|---|
| 16801 | 770 ft | |
| | *Augite* | $2V_\gamma$ 49–56°, $\beta$ 1.706, $Ca_{42}$ $Mg_{33}$ $Fe_{25}$ |
| | *Plagioclase* | Min. $\alpha'$ 1.562, max. $\gamma'$ 1.572, $An_{69-67}$ |
| 16801 | (pegmatoid) 770 ft | |
| | *Augite* | $2V_\gamma$ 55°, $\beta$ n.d. |
| | *Pigeonite* | n.d. |
| | *Plagioclase* | Min. $\alpha'$ 1.561, max. $\gamma'$ 1.571, $An_{67-64}$ |
| 16800 | (pegmatoid) 600 ft | |
| | *Augite* | $2V_\gamma$ 56±2°, $\beta$ n.d. |
| | *Plagioclase* | Min. $\alpha'$ 1.557, max. $\gamma'$ 1.572, $An_{68-56}$ |
| 16799 | 600 ft | |
| | *Augite* | $2V_\gamma$ 47–53° (variable), $\beta$ 1.688±.004 (variable) |
| | *Hypersthene* | $2V_\gamma$ 62–80°, $Mg_{82-70}$*; $2V_\gamma$ 49–62°, $Mg_{70-56}$* |
| | *Pigeonite* | $2V_\gamma$ 15°, 1.682, $Ca_8$ $Mg_{65}$ $Fe_{27}$ |
| | *Plagioclase* | Min. $\alpha'$ 1.563, max. $\gamma'$ 1.578, $An_{79-68}$ |
| 16798 | (pigeonite band) 440 ft | |
| | *Augite* | $2V_\gamma$ 47–51°, $\beta$ 1.691, $Ca_{43}$ $Mg_{46}$ $Fe_{11}$ |
| | *Pigeonite* | $2V_\gamma$ 17°, $\alpha$ 1.687, $Ca_8$ $Mg_{61}$ $Fe_{31}$ |
| | *Plagioclase* | Min. $\alpha'$ 1.565, max. $\gamma'$ 1.581, $An_{84-73}$ |
| 16797 | (anorthosite lens) 400 ft | |
| | *Augite* | $2V_\gamma$ 55°, $\beta$ 1.698±.003, $Ca_{49}$ $Mg_{36}$ $Fe_{15}$ |
| | *Plagioclase* | $\alpha'$ 1.569, $\gamma'$ 1.580, $An_{83}$ |
| 16796 | 400 ft | |
| | *Augite* | $2V_\gamma$ 51–57° (variable), $\gamma$ 1.680±.003, $Ca_{45}$ $Mg_{50}$ $Fe_5$ |
| | *Hypersthene* | $2V_\gamma$ 62–81°, $Mg_{82-69}$ |
| | *Plagioclase* | Min. $\alpha'$ 1.570, max. $\gamma'$ 1.582, $An_{85}$ |
| 16795 | 200 ft | |
| | *Augite* | $2V_\gamma$ 49–53°, $\beta$ 1.688±.002, $Ca_{45}$ $Mg_{46}$ $Fe_9$ |
| | *Hypersthene* | $2V_\alpha$ 64–82°, $Mg_{83-71}$ |
| | *Plagioclase* | Min. $\alpha'$ 1.568, max. $\gamma'$ 1.581, $An_{81-80}$ |
| 16794 | 100 ft | |
| | *Augite* | $2V_\gamma$ 48–56°, $\beta$ 1.688, $Ca_{44}$ $Mg_{47}$ $Fe_9$ |
| | *Pigeonite* | $2V_\gamma$ 15°, $\alpha$ 1.704, $Ca_7$ $Mg_{48}$ $Fe_{45}$ |
| | *Hypersthene* | $2V_\alpha$ 64–76°, $Mg_{79-71}$; $2V_\alpha$ 55–58*, $Mg_{67-63}$ |
| 16793 | *Plagioclase* | $\alpha'$ 1.564, $\gamma'$ 1.573, $An_{70}$ |

* Inverted pigeonite.

granular quartz and orthoclase but even here the grainsize does not exceed 0.5 mm. Altered and corroded pyroxene, dark green hornblende ($\gamma$=1.698) and primary and secondary biotite are intergrown with granular magnetite-ilmenite. Apatite needles are plentiful and sphene is an accessory.

(b) Modes

The modal analyses (Table 5) show the hypersthene rock at the base to be a similar though more extreme form of cumulate rock to that found in the Egerton Sill. The bulk of the rock contains up to 72% pyroxene but in the thin anorthosite streaks pyroxene is almost absent. As in the Egerton Sill pigeonite is entirely absent but here plagioclase greatly exceeds the amount of augite. The granophyre shows the characteristic features of abundant quartz, orthoclase, hornblende and iron ores and only minor pyroxene.

(c) Mineral composition

The pyroxene from the Harmsworth granophyre is too altered for optical determination but pyroxene from a similar granophyre at Detour Nunatak has

$$2V\gamma\ 47°, \quad \beta\ 1.737, \quad Ca_{34}Mg_{13}Fe_{53}$$

The difference in normative pyroxene between base and summit, ($Mg_{81-54}$) and in normative plagioclase ($An_{81-50}$) is extreme and optical determinations (Table 6) show a greater range.

The amounts of magnesia in the basal rock (Table 3) is comparable with that of picrites and is the most extreme example of hypersthene accumulation yet found in the Ferrar Dolerites.

## CRYSTALLIZATION OF HYPERSTHENE

The asymmetric distribution of pyroxenes as a whole with height in the sills coupled with the markedly higher specific gravities of the hypersthene rocks points strongly to gravitative settling (Fig. 2). However the existence of hypersthene in such large quantity in sills, the marginal phases of which contain little or none, clearly demands explanation. Work done to date has not been detailed enough to answer this problem decisively but the following tentative suggestions are offered:

FIG. 5. Close packed hypersthenes with interstitial bytownite, Mt. Harmsworth Dike, (16790) ×30.

TABLE 5. MODES OF MT HARMSWORTH DIKE.

| No. | Height above S.L. (ft) | Total Px. | Hypers. | Augite | Plag. | Micropeg. | Hornbl. Biotite | Opaques | Apatite |
|---|---|---|---|---|---|---|---|---|---|
| 16792 | 9,050 | 7.6 | | | 27.1 | 52.5 | 8.5 | 3.8 | 0.5 |
| 16791 | 8,000 | 43.1 | | | 49.3 | 5.9 | 0.8 | 0.8 | 0.1 |
| 16790 | 4,800 | 71.7 | 67.3 | 4.4 | 27.6 | 0.3 | 0.1 | 0.3 | |

(1) Either the hypersthene dolerites have crystallized from a magma of the same composition as the margin or from one more magnesian. As single sills have been traced over areas of more than 10,000 sq. mi. volumes of more than 2000 cubic miles of magma have been injected in a single phase of intrusion. Considering the variability shown in sequences of lava flows (Tilley, 1960), it is unlikely the magmas were completely homogenous, indeed lateral variations have been found in single sills, but it is unlikely that several sills being filled from many different conduits could all have central zones more magnesian than the margins. Moreover, no highly magnesian glassy rocks, lavas or dikes have been found, the textures of the hypersthene dolerites is always porphyritic and the hypersthenes are enclosed in a groundmass which often has a composition of a normal dolerite minus the more refractory components.

(2) Assuming the magma to have been initially homogenous it does not seem likely that more than about 7% of hypersthene could crystallize even under conditions of perfect fractionation. Up to 21% of normative hypersthene is present in marginal rocks but in the mode this contains a little augite in solid solution and appears as pigeonite. Normative pyroxene in the Egerton Sill has a composition of $Mg_{63}$ and hypersthene began to crystallize at $Mg_{83}$. Under conditions of perfect fractionation about a third of the normative pigeonite would have crystallized as hypersthene before the inversion composition at $Mg_{70}$ was reached. Work has not yet been done in sufficient detail on any of the Ferrar sills to show whether this

TABLE 6. (b) MT. HARMSWORTH DIKE

Hypersthene zone
16790
*Hypersthene* $2V_\alpha$ 65–81°, $Mg_{82-72}$, $\gamma$ 1.679–1.686, $Mg_{83-74}$
*Augite* $2V_\gamma$ 50±2°, $\beta$ 1.690, $Ca_{45}$ $Mg_{46}$ $Fe_9$
*Plagioclase* Min. $\alpha'$ 1.565, max. $\gamma'$ 1.581, $An_{84-73}$
Granophyre zone
16792
*Plagioclase* Min. $\alpha'$ 1.554, max. $\gamma'$ 1.564, $An_{55-51}$
Plagioclase intergrown with quartz has $\alpha'$ 1.535 $An_{15}$

FIG. 6. Granophyric intergrowths of quartz-orthoclase and quartz-albite grouped about plagioclase. Iron ores and hornblendes also present. Granophyre, summit, Mt. Harmsworth. (16792) ×70.

FIG. 7. Basement Sill, Kukri Hills, intruded into granodiorite, with Peneplain Sill above overlain by Beacon Sandstone. Lower sill is here 800 feet thick, hypersthene zone begins 150 feet above base.

amount is sufficient to account for the concentrations found.

(3) The non-appearance of hypersthene in marginal rocks appears to be in part due to the pyroxenes of a rapidly chilled magma crystallizing with compositions close to that of the norm. Only in the central part of sills where crystallization must have been exceedingly slow are pyroxenes found with compositions markedly more magnesian.

(4) Recent experimental work on the stability fields of ortho- and protoenstatite by Boyd and England (1961) coupled with a consideration of the unit cell dimensions of the three polymorphs of enstatite and of pigeonite (Morimoto *et al.*, 1959) suggests that high pressures favour the crystallization of magnesian orthopyroxene as the stable phase. A column of magma rising from below the Mohorovičič Discontinuity in the manner postulated by Kuno (1959) might well crystallize pigeonite under low pressure near the surface and magnesian hypersthene at depth.

(5) No hypersthene was found in the 1300 foot Peneplain Sill at Solitary Rocks in the Taylor Valley. However the margin of this sill (Table 1) is considerably less magnesian than the hypersthene-bearing sills. Comparison of the ratio

$$\frac{\text{MgO} \times 100}{\text{MgO} + \text{FeO} + \text{MnO}}$$

(mol %) of margins with that of the most magnesian hypersthene to form shows that in four sills hypersthene began to crystallize with 25–30% more MgO than the magma. This separation of solidus and liquidus is rather greater than that deduced by Kuno (1959) and by Brown (1957) from analysed phenocryst and groundmass pyroxenes but using the lower

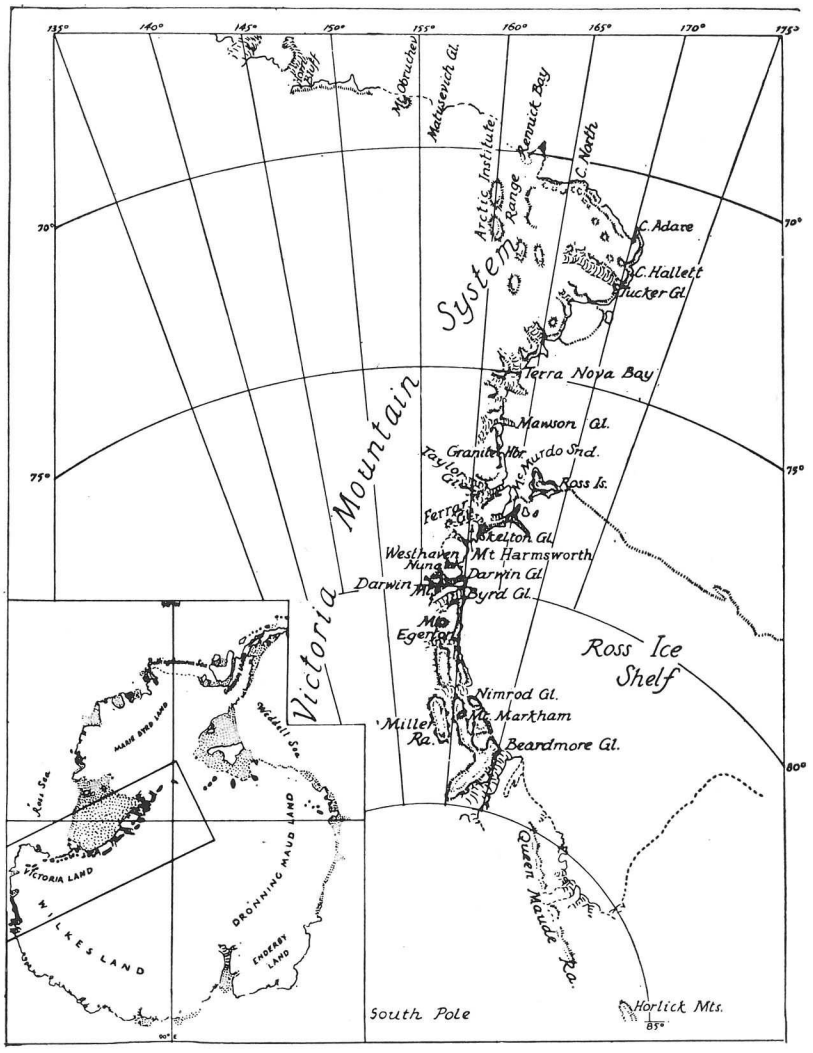


FIG. 8. Distribution of Ferrar Dolerites Group, Antarctica.

figure it is not likely that a magma in which the ferromagnesian ratio is less than about 45 could crystallize hypersthene. In the Peneplain Sill this ratio is 47 compared with 60 for the Egerton Sill, a difference which is probably significant.

Convective circulation appears to have been minimal during crystallization of the sills and the anorthositic lenses of the Egerton Sill are difficult to account for, though convective currents probably account for the rhythmic layers seen in the dike-like bodies. The presence of hydrated minerals in the pegmatoids suggests that these have formed during the last stages of crystallization in localities where the water vapour pressure has exceeded the confining pressure and water has appeared as a separate phase, whereas the granophyres are merely accumulations of residual liquids.

Phase layering is usually inconspicuous in the Ferrar Dolerites even in strongly differentiated sills (Fig. 7).

## Acknowledgments

The writer is indebted to Professor Douglas S. Coombs for suggestions and criticism of the project, and to Mr D. Skinner for loan of material. Field work was partly carried out in the course of the New Zealand Trans-Antarctic Expedition and partly under the N. Z. Antarctic Research Programme. Laboratory work was done with the aid of a New Zealand Research Fund Fellowship.

## References

Benson, W. N. (1916) Report on the petrology of the dolerites collected by the British Antarctic Expedition 1907–1909. *Rep. Brit. Antarct. Exped. 1907–9. Geol* **2** (9), 153–60.

Bowen, N. L. (1935) "Ferrosilite" as a natural mineral. *Am. J. Sci.* **30,** 481–94.

Boyd, F. R. and J. L. England (1961) Melting of silicates at high pressures. *Carn. Inst. Wash. Year Book.* **60,** 113–125.

Brown, G. M. (1957) Pyroxenes from the early and middle stages of fractionation of the Skaergaard intrusion, East Greenland. *Mineral. Mag.* **31,** 511–43.

Browne, W. R. (1923) The dolerites of King George Land and Adelie Land. *Sci. Rep. A'asian Antarct. Exped. 1911–14,* **3,** 245–58.

Edwards, A. B. (1942) Differentiation of the dolerites of Tasmania. *J. Geol.* **50,** 451–80, 579–610.

Ferrar, H. T. (1907) Report on the field geology of the region explored during the 'Discovery' Antarctic Expedition, 1901–4. *Nat. Antarct. Exped. 1901–1904, nat. Hist.* **1,** 1–100.

Gould, L. M. (1931) Some geographical results of the Byrd Antarctic Expedition. *Geogr. Rev.* **31,** 177–200.

Gunn, B. M. (1962) Differentiation in Ferrar Dolerites, Antarctica. *New Zealand Jour. Geol. Geophys.* **5,** 820–863.

——— and Walcott, R. I. (1962) The geology of the Mt Markham region, Ross Dependency, Antarctica. *New Zealand Jour. Geol. Geophys.* **5,** 407–426.

——— and G. Warren (1961) Geology of Victoria Land between the Mawson and Mulock Glaciers. Antartica. *New Zealand Geol. Surv. Bull.* **71.**

Harrington, H. J. (1958) Nomenclature of rock units in the Ross Sea region, Antarctica. *Nature, Lond.* **182,** 290.

Hess, H. H. (1960) Stillwater igneous complex, Montana. *Geol. Soc. Am. Mem.* **80.**

Klimov, L. V. and D. S. Solovyev (1958) Some features of the geological structure of the littoral of Wilkes Land, King George V Land and Oates Land, East Antarctica. *Dokl. Akad. Nauk. S.S.S.R.* **123,** 141–4.

Kulp, J. L. (1961) Geologic time scale. *Science,* **133.** 1105–14.

Kuno, H. (1959) Origin of Cenozoic Petrographic provinces of Japan and surrounding areas. *Bull. Volcanol.* (2) **20,** 37–76.

Laird, M. (1961) Geology of the Nimrod Glacier—Beaumont Bay Area, Antarctica. *Prelim. Rep. to N.Z. Ant. Div. D.S.I.R.*

McDougall, I. (1958) A note on the petrography of the Great Lake dolerite sill. "Dolerite, a Symposium." *University Tasmania Publ., Hobart,* 52–60.

——— (1961) Optical and chemical studies of pyroxenes in a differentiated Tasmanian dolerite. *Am. Mineral.* **46.** 661–87.

Morimoto, N., D. E. Appleman and H. T. Evans, (1959) The structural relations between diopside, clinoenstatite and pigeonite. *Carn. Inst. Wash. Year Book.* **58,** 193–7.

Muir, I. D. (1951) The clinopyroxenes of the Skaergaard Intrusion, eastern Greenland. *Mineral. Mag.* **29,** 690–714.

Roots, E. F. (1953) Preliminary note on the geology of western Dronning Maud Land. *Norsk. Geol. Tidssk.* **32,** 18–33.

Skinner, D. (1961) Geology of the Beaumont Bay—Byrd Glacier Area, Antarctica. *Prelim. Rep. to N.Z. Ant. Div. D.S.I.R.*

Spry, A. (1958) Some observations of the Jurassic dolerite of the Eureka cone sheet near Zeehan, Tasmania. "Dolerite, a Symposium," *University Tasmania Publ., Hobart,* 93–129.

Starik, I. E., M. G. Ravich, A. Krylov and I. Silin (1959) The absolute age of the rocks of the East Antarctic platform. *Dokl. Akad. Nauk. S.S.S.R.* **126,** 144–6.

Tilley, C. E. (1960) Differentiation of Hawaiian basalts: some variants in lava suites of dated Kilauean eruptions. *Jour. Petrol.* **1,** 47–55.

Tröger, W. E. (1956) *Optische Bestimmung der gesteinbildenden Minerale.* E. Schweizerbart'sche Verlagsbuchhandlung, Stuttgart.

Wager, L. R. and W. A. Deer (1939) Geological investigations in east Greenland. Pt. 3. The petrology of the Skaergaard Intrusion, Kangerdlugssuak, East Greenland. *Medd. Grønland* **105.**

Walker, F. (1940) Differentiation of the Palisade diabase. New Jersey. *Geol. Soc. Am. Bulletin* **51,** 1059–1106.

——— and A. Poldervaart (1940) The petrology of the dolerite sill of Downes Mountain, Calvinia. *Geol. Soc. South Africa Trans. Proc.* **43,** 159–73.

——— and A. Poldervaart, (1941) The Hangnest dolerite sill. *Geol. Mag.* **78,** 429–50.

Webb, P. N. and B. C. McKelvey (1959) Geological investigations in South Victoria Land, Antarctica. Pt. I. Geology of Victoria Dry Valley. *New Zealand Jour. Geol. Geophys.* **2,** 120–36.

Weihaupt, J. G. (1961) Reconnaissance of a newly discovered area of mountains in Antarctica. *Jour. Geol.* **68,** 669–73.

MINERALOGICAL SOCIETY OF AMERICA, SPECIAL PAPER 1, 1963
INTERNATIONAL MINERALOGICAL ASSOCIATION, PAPERS, THIRD GENERAL MEETING

## LAYERED BASIC INTRUSIVE ROCKS OF THE WICHITA MOUNTAINS, S.W. OKLAHOMA

H. E. HUNTER
*Department of Geology, Harpur College, State University of New York, Endicott, New York*

ABSTRACT

Basic igneous rocks crop out along the axis of the Wichita Mountains of southeastern Oklahoma. Five stratigraphic units have been distinguished on the basis of mineralogical and textural features. The three lower units which have been mapped at a scale of 1 inch to 1000 feet are discussed in this paper. The lowermost unit includes alternating layers of troctolite and anorthosite with olivine gabbro at some horizons. The second unit consists predominantly of anorthosite in which poikilitic pyroxene crystals ranging from 6 inches to 3 feet in diameter are randomly distributed. Enclosed plagioclase grains are of the same size and composition and show the same degree of preferred planar orientation as the grains outside the intergrowth. Some larger grains have cores of more calcic plagioclase. The third unit comprises anorthosite, gabbro, olivine gabbro, and troctolite. Poikilitic pyroxene grains from one-quarter to two inches in diameter enclose plagioclase grains which are fine-grained and anhedral in contrast to medium-grained, subhedral plagioclase outside the intergrowth. Plagioclase within the pyroxene is randomly oriented whereas in most specimens plagioclase in the enclosing rock shows some degree of preferred planar orientation.

Textures correspond closely to examples cited in the classification proposed by Waner, Brown and Wadsworth in 1960. Texturally the troctolites are adcumulates to mesocumulates and the gabbro containing large poikilitic pyroxene is an extreme example of a heteradcumulate. There is some question whether adcumulus growth could have been restricted to a narrow zone at the interface between crystal mush and magma. The small poikilitic intergrowths appear to have formed by simultaneous crystallization of plagioclase and pyroxene. Later adcumulus and/or intercumulus growth enlarged some of these clusters to approach the size and texture of the intergrowths in the lower units.

## INTERNAL STRUCTURE OF A DIFFERENTIATED TESCHENITE INTRUSION, PROSPECT HILL, NEW SOUTH WALES

H. G. WILSHIRE
*U. S. Geological Survey, Paducah, Kentucky*

ABSTRACT

Internal structures of a 350-ft thick, dish-shaped teschenite intrusion are of four main types: (1) lineation, parallel to contacts, of minerals in the basalt margins, in picrite within 100 ft of the lower contact, and in dolerite and olivine-rich dolerite within 80 to 120 ft of the upper contact; (2) flow layers, which differ in mineral proportions and fabric, in the basalt margins and picrites within 80 ft of the lower contact; (3) rhythmic layering of felsic and mafic rocks inclined to abrupt changes in slope of the basalt-shale contact and to internal contacts between different rock types; and (4) deformation of pegmatite and other schlieren by slip along subsequently healed fractures at a high angle to basalt-shale contacts or by slip along planes parallel to the schlieren.

Progressive decrease in perfection of lineation away from contacts and occurrence of lineations in "complementary" (dolerite) as well as "cumulative" (picrite) rock types indicate an origin by viscous flow. Flow layers are considered to have formed by mechanical concentration of olivine during viscous flow and accompanying fabric variations by volatile redistribution over pressure gradients formed by slip along laminar flow planes. Rhythmically layered units are considered to result from tension fracturing accompanied by concentration of vapor-rich magma and reciprocal diffusion between layers. Deformation of schlieren was caused by initial injection processes because schlieren over and under a deformed one are undisturbed.

Response to viscous flow of material making up 49 to 60 per cent of the intrusion and of rock types representing the most acid differentiates indicates that the rate of intrusion was slow relative to the rate of differentiation.

MINERALOGICAL SOCIETY OF AMERICA, SPECIAL PAPER 1, 1963
INTERNATIONAL MINERALOGICAL ASSOCIATION, PAPERS, THIRD GENERAL MEETING

# SYMPOSIUM ON THE MINERALOGY OF THE SULFIDES

## THE PHYSICAL PROPERTIES OF SEMICONDUCTING SULFIDES, SELENIDES AND TELLURIDES

WAYNE W. SCANLON
*U. S. Naval Ordnance Laboratory, White Oak, Silver Spring, Maryland*

ABSTRACT

Research leading to an understanding of the fundamental properties of materials is becoming more and more an area of common interest which brings together the viewpoints of the traditional scientific disciplines, such as physics or chemistry. In the case of solid state materials, many of the physical properties are intricately interwoven with chemical properties, crystallographic properties and the metallurgy of materials. This paper will discuss some of the interrelations between physical and chemical properties of a group of heavy metal sulfide compounds. Among the materials discussed will be PbS, PbSe, PbTe, CdS, $Bi_2Te_3$ and SnTe. Some of the methods and techniques used by the solid state physicist for studying semiconductors will be described along with details on specific physical properties of the materials.

### INTRODUCTION

Research leading to an understanding of the fundamental properties of materials is an area of interest which is pursued simultaneously by several of the traditional scientific disciplines, such as physics, chemistry, and metallurgy. In the case of solid state materials many of the physical properties are intricately interwoven with chemical properties, crystallographic properties and the metallurgy of the materials. A comprehensive research program in solid state materials must therefore bring in the viewpoints of many different scientific disciplines for effective understanding of the properties of solids.

In the case of semiconductors the greatest interest concerns the behavior of the relatively free electrons and holes within the crystal. These charges may originate from two types of sources. First the electrons in the valence energy levels of the atoms of the crystal are but weakly bound to a given atom. The binding energy, or intrinsic activation energy, for these electrons is of the order of an electron volt or less. Thus the addition of energy in the form of heat or radiation of the proper wavelength can dissociate some of these electrons from lattice atoms so that they may contribute to the conduction process until they recombine once more. At the same time the vacancy in the electronic structure of the atom caused by the removal of the electron is also free to conduct. This charge is effectively positive and is called a hole. A semiconductor can conduct electric current at the same time by both positive and negative carriers. The concentrations of these carriers is a strong function of temperature, increasing rapidly with increasing temperature according to an exponential law.

The second and important source of charge carriers in a semiconductor crystal is the presence of certain crystal imperfections such as vacant lattice sites, foreign atoms of valence different from the normal atoms occupying lattice sites or interstitial positions, or normal atoms in interstitial positions. Each of these imperfections may contribute a conduction electron or hole to the crystal so that the concentration and kind of imperfection in the crystal plays an important role in the electrical properties of a semiconductor. The binding energy for these charges is an order of magnitude smaller than for the intrinsic electrons so that even at room temperature most of these electrons or holes are dissociated from their respective imperfections.

The laws governing the concentration of lattice defects and impurities in a crystal lattice and the ways in which the concentrations change with temperature or other environmental conditions are known to the specialist in fields of physical chemistry or chemistry. Their help is therefore needed in order to interpret and guide some of the experiments on semiconducting materials.

The movement of charges through the crystal lattice and their lifetime in conducting states is influenced among other things by dislocations, grain boundaries or polycrystalline structure. To account for the effect of these defects upon the electrical properties of a semiconductor the solid state physicist must refer to the work of the specialist in crystallography or metallurgy.

Hence we find that the solid state physicist, who has primary responsibility for understanding the various properties of semiconductors, must consult specialists in other areas of science in order to account for some of the phenomena observed in semiconductors.

The studies made on the heavy metal sulfides illus-

trate in an effective way the interdisciplinary nature of solid state research and the importance of bringing together as many different viewpoints as possible to understand the fundamental properties of materials. The materials to be discussed will be principally the lead compounds though other sulfides such as Cd and Bi compounds will be referred to when appropriate.

We shall first consider the composition of the semiconductor crystal and the possible role of lattice vacancies, foreign impurity atoms, and interstitial atoms upon the electrical behavior. Factors governing changes in concentration of these defects in the crystal will be discussed. This will then be followed by a detailed description of various measurements which the physicist makes to understand the behavior of semiconductors. Finally a few of the applications of sulfide semiconductors will be given.

## Defects in Compound Semiconductor Crystals

Crystalline defects such as foreign impurity atoms in normal lattice sites may contribute electrons or holes to the conduction bands in semiconductors. In the case of the sulfides of lead certain elements such as Sn, Ge, Fe, Co, Ni, Pt, Mg, Nb and Bi contribute electrons to the conduction band making the crystal electron conducting or n-type. Similarly other elements such as Au, Ag, Cu, In, Al, Zn and Cd produce holes in the valence band making the crystal p-type. The concentration and kind of foreign impurity atoms in the semiconductor is directly related to the number of mobile electric charge carriers in the crystal and determines its electrical conductivity. In the case of compound semiconductors additional concentrations of electrons or holes may arise from the presence of point defects in the crystals such as ions missing from normal sites or occupying interstitial sites. In crystals of the pure compound these latter point defects are the chief source of electrons or holes in the conduction bands. The concentration of these defects in a crystal is a complicated function of temperature and the composition of liquid or solid phases of the compound in equilibrium with the crystalline phase.

In principle any real crystal of a compound may incorporate in its structure vacant sites from which the atoms or ions are missing or atoms occupying interstitial positions. Statistical theories predict that all ionic or covalent crystals should have finite concentrations of these defects at any temperature above O° K., although these concentrations may be very small in some crystals. When these defects are predominantly of one atom or ion species, which is the

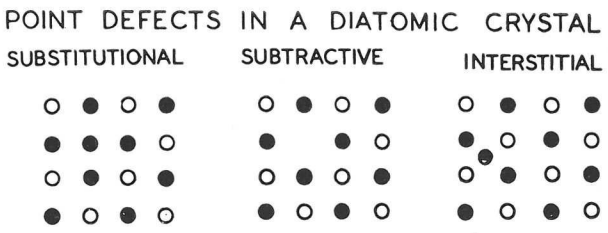


Fig. 1. Types of defects in a diatomic crystal.

usual case, then the composition of the crystal will deviate from the ideal or stoichiometric chemical proportions of the compound. Generally the departures from the stoichiometric proportions are less than 1% since larger departures tend to distort and break up the crystal structure. A deviation of only 0.01% from the stoichiometric proportions in a binary compound semiconductor such as PbTe results in about $10^{18}$ conducting electrons or holes/cm$^3$ in the crystal which is very high for a semiconductor. Thus we see that even very small departures from ideal stoichiometry are very important in determining the electrical properties of a compound semiconductor.

In a binary compound having the formula AB, stoichiometric deviations may be incorporated in the lattice in three ways. For the case where there is an excess of B atoms in the crystal, Anderson (1946) lists the following types of nonstoichiometric solids:

1. Substitutional: Extra B atoms replace A atoms on sites normally occupied by A atoms.
2. Subtractive: B atoms occupy normal B sites, but some A sites are vacant.
3. Interstitial: Extra B atoms occupy interstitial positions.

The three types of defects are illustrated in Fig. 1. In any real crystal all three types of defects could be present simultaneously, but generally one type dominates. It is possible to identify the important defect type on the basis of certain tests. In semiconductors with substitutional defects the crystal will be p-type with an excess of the cation, and n-type with an excess of the anion. On the other hand, with subtractive or interstitial defects the reverse is true; the excess cation crystal is n-type and the excess anion crystal is p-type.

A distinction between interstitial and subtractive defect solids can sometimes be made on the basis of careful $x$-ray and density measurements. Most nonstoichiometric crystals contain defects of the subtractive or interstitial types and only a few incorporate substitutional defects.

Substitutional crystals are likely to be intermetallic compounds in which ion repulsion is weak. Fur-

thermore, a difference in atom valency of unity is desirable. The compounds of the group $Bi_2S_3$, $Bi_2Se_3$ and $Bi_2Te_3$ show substitutional defects. For example, excess Te may occupy Bi sites in the crystal, resulting in n-type conductivity, while excess Bi may reside in Te sites making the crystal p-type.

The family of compounds PbS, PbSe and PbTe may incorporate subtractive defects in either cation or anion lattice positions, being n-type for excess cation and p-type for excess anion concentrations.

## Equilibrium Conditions for Defects in Crystals

Departures from the stoichiometric composition are smallest in crystals having covalent bonding and are generally somewhat larger in crystals having appreciable ionic bonding. In the family of lead sulfides there is a fairly large ionic component to the bond between atoms in the solid state, and these materials can exist with significant departures from stoichiometry.

In a given crystal, addition or removal of excess atoms or ions generally takes place with the gas or liquid phases surrounding the solid. The equilibrium concentration of the excess atoms in the solid depends upon the temperature and composition of the vapor phase or liquid phase contacting the solid. The principle of this phase relationship was established over 30 years ago by Wagner and Schottky (1930) but only recently has been used effectively to control the composition of binary compound semiconductors.

Consider the system composed of a crystal of PbS in equilibrium with its vapor, which might be composed of atoms of Pb and S as well as of molecules of PbS and perhaps other molecular species of Pb and S. By Gibbs' phase rule, this system has only two degrees of freedom. By fixing the temperature and the pressure of one component of the vapor, one fixes all the related properties of the system, such as the crystal composition and its electrical properties.

While in principle the idea of controlling the crystal stoichiometry through control of the pressure of a component of the vapor is simple, in practice the process is complex.

Changes in crystal composition appropriate to the equilibrium values for the solid and vapor states at a given temperature start at the solid-vapor boundary and are propagated to the interior of the crystal by a diffusion process. Diffusion coefficients must be large enough to permit reaching equilibrium in a reasonable length of time. In the sulfides these times are of the order of a day for temperatures of about 400° to 500° C. and decrease to a few minutes for temperatures around 900° to 1000° C. Below about 300° C. diffusion becomes so slow that for all practical purposes the solid composition becomes fixed and independent of the surrounding vapor condition.

The maximum departure from stoichiometry in the solid at various temperatures has been established by Bloem (1956) for PbS, by Brebrick and Gubner (1962) for PbSe, and by Brebrick and Allgaier (1960) for PbTe. Figure 2 represents the limits of stability obtained by Brebrick and Allgaier for the PbTe system. It can be noted that the maximum solubility of excess Pb in the crystal is only about .005 atomic per cent and the maximum solubility of excess Te is only about .012 atomic per cent. Even such small deviations from the ideal composition result in about $10^{18}$ conducting electrons or holes per $cm^3$ in the crystal. Similar limits exist for lead sulfide and lead selenide.

The composition of PbTe at the maximum melting temperature is seen to be in the excess Te range and hence the first material to crystallize from a stoichiometric liquid will have excess Te atoms and will be hole-conducting or p-type. In the case of PbS, Bloem has shown that the maximum melting temper-

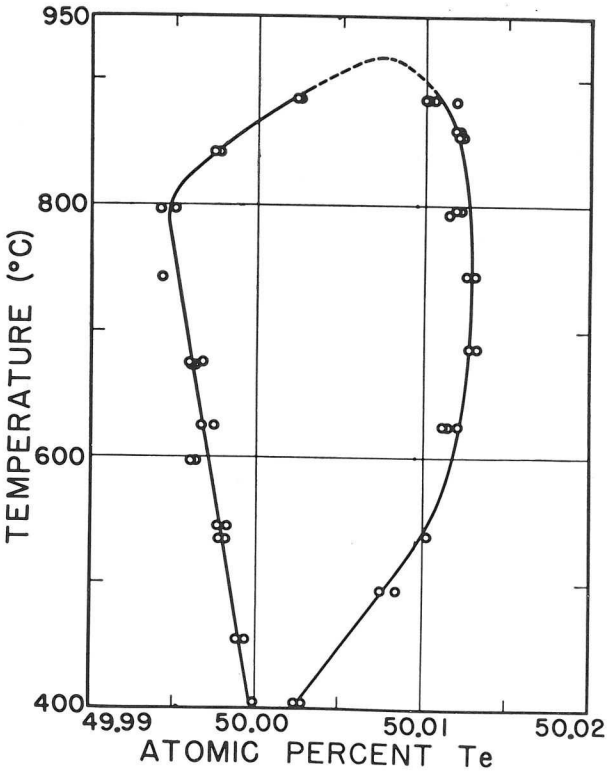


Fig. 2. Composition limits of stability for PbTe (courtesy of Dr. R. F. Brebrick and Dr. R. S. Allgaier).

ature composition results in the excess Pb or n-type conductivity.

The solid may exist with stoichiometric deviations less than the maximum values indicated by the curve in Fig. 2. The crystal composition is established through equilibrium with the gaseous phase at various temperatures. Some of this internal structure in the phase diagram has been obtained by Bloem and Kroger (1956) and by Brebrick and Scanlon (1954) for PbS. Figure 3 summarizes the data. The lines of constant composition as a function of temperature are determined by suitably adjusting the partial pressure of the sulfur component of the vapor.

Studies of the electrical properties of these crystals at high temperatures are complicated by the changing composition of the crystal unless special care is taken to suitably adjust the vapor composition at each temperature in order to maintain a fixed crystal composition. The phase diagrams show the equilibrium conditions required to produce any desired crystal composition which define the electrical properties within the limits of solid stability of the compound.

## Precipitation in Crystals

It can be seen in Fig. 2 that the maximum solubility of excess Pb or Te in a PbTe crystal decreases at temperatures below about 700° C. This is called retrograde solubility. Within the retrograde solubility region a crystal containing the maximum concentration of one of the atom species at a given temperature will be come supersaturated upon being cooled to a lower temperature. The crystal may dispose of the excess atoms by precipitating them as neutral atoms on imperfections such as edge dislocations in the crystal. There is an accompanying reduction in free electron or hole concentration in the crystal. This process is reversible. The time required to come to

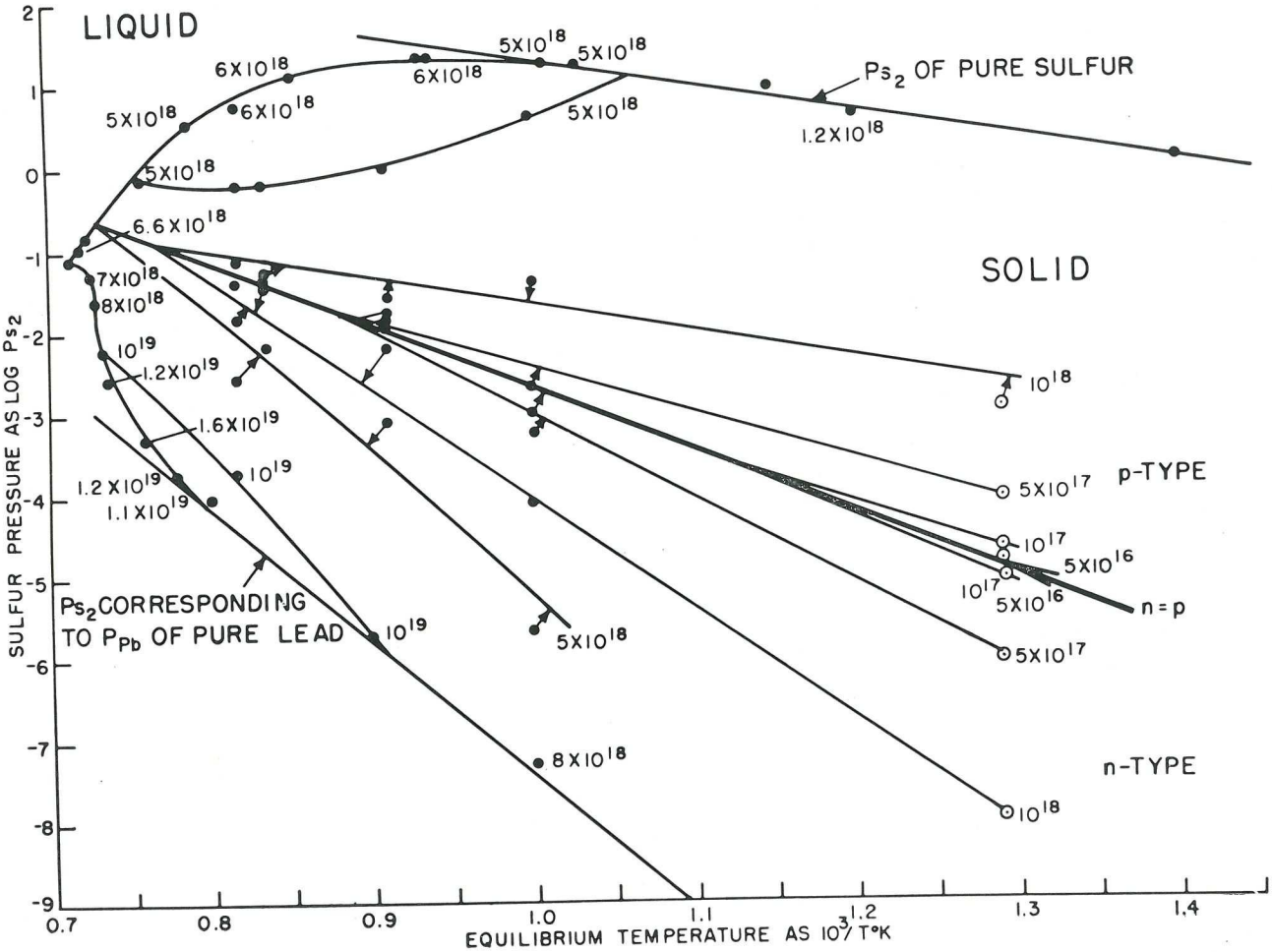


Fig. 3. Solid-vapor phase diagram for PbS.

equilibrium for this internal process is much less than for exchange of material with the external gaseous or liquid phase discussed previously, since the diffusion distance to precipitation sites is small relative to the diffusion distances to the surface of the crystal.

A study of precipitation phenomena in PbTe (Scanlon, 1962) shows it to be a useful technique for altering the carrier concentration in semiconducting crystals. It is particularly useful in preparing crystals having low carrier concentrations.

Figure 4 shows the maximum solubility of Te in PbTe crystals as a function of temperature. These data were obtained from precipitation experiments. The times required to reach approximate equilibrium ranged from a few hours at 400° C. to a month at 180° C. The slope of the curve indicates an activation energy of 0.58 ev for the process.

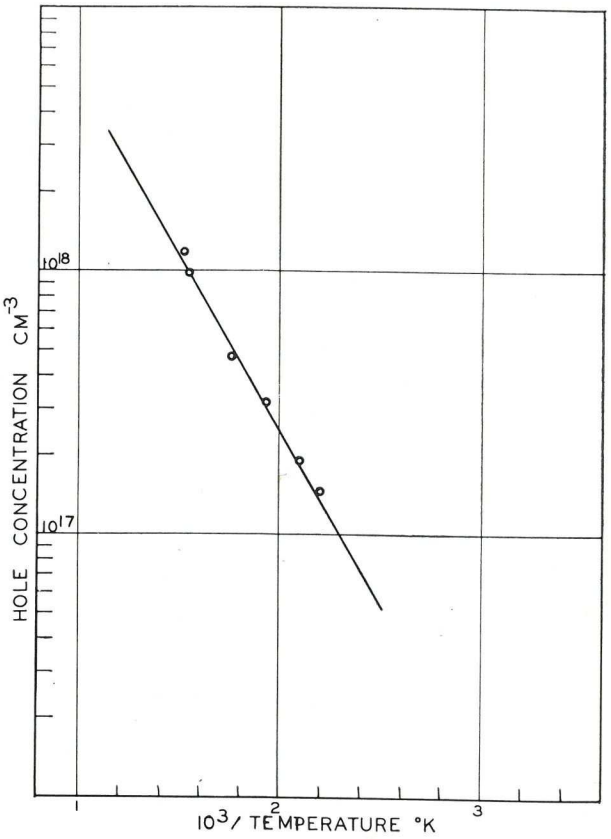


FIG. 4. Solubility of Te in a crystal of PbTe as a function of temperature.

## ELECTRICAL PROPERTIES

The behavior of the free carriers has an important bearing on the electrical properties of semiconductors. This behavior is determined to a large extent by the nature of the energy bands in the crystal and by the various charge scattering processes which are present in the crystal. Information on these properties may be deduced from a variety of interrelated electrical, magnetic, thermal and optical experiments.

The electron energy bands govern the excitation-recombination mechanism for charge carriers in the semiconductor as well as their effective masses. An important and useful characteristic of these bands is the minimum width of the forbidden energy gap between the valence and the conduction bands. Experimental information on the width of the forbidden energy band can be obtained from the temperature dependence of the free carrier concentration as determined from studies of the Hall effect or resistivity. This gives the minimum separation of the band edges for the case when quantum selection rules are relaxed due to the interaction of a lattice phonon in the excitation-recombination process. This energy gap is sometimes called the thermal activation energy. Its interpretation in small-energy-gap (less than about 0.5 volt) semiconductors, such as the lead sulfides, is questionable since the band edges in these semiconductors generally display multiple minima and maxima. Variations in the positions of the band edges due to thermal dilation or contraction of the lattice, thermal changes in the effective masses, and other thermal effects appear to play an appreciable role in these small-energy-gap semiconductors. These factors are not accounted for in the simple theory generally used in interpreting resistivity or Hall effect data in terms of the forbidden energy gap, hence gap values so obtained should not be taken too seriously.

A much more satisfactory experiment for evaluating the minimum forbidden energy gap is to measure the transmission of the semiconductor to visible or infrared radiation. Photons having insufficient energy to excite electrons across the forbidden gap pass through with relatively little absorption. Photons with energies equal to or greater than the gap are strongly absorbed by the electrons in the valence band resulting in their excitation to the conduction band. Thus, there is a sharp drop in the transmission as the radiation energy corresponds to the band gap. Analysis of spectral transmission curves reveals not only the energy gaps for which quantum selection rules are obeyed, direct transitions, but also the energy gap for which lattice phonons assist in the transition, indirect transitions. Figure 5 shows optical transmission data for PbS, PbSe and PbTe crystals, and the analysis in terms of energy gaps is given in Table 1 (Scanlon 1959). It is interesting to point out

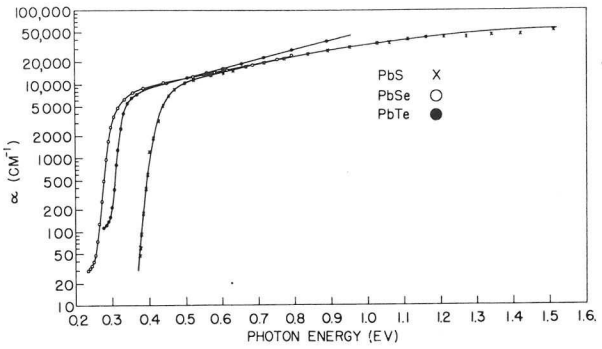


FIG. 5. Optical absorption in PbS, PbSe and PbTe crystals.

that the order of the energy gaps is not the same as the order of molecular weights as might be expected.

The lead sulfides are unusual in regard to the variation of the width of the forbidden energy gap with temperatures. In all three crystals the gap increases approximately $4\times10^{-4}$ev/°K. with increasing temperature. Most semiconductors have negative temperature dependence of the gap.

## TRANSPORT PHENOMENA

The movement of free carriers in a perfect periodic crystal should, in theory, be unimpeded by scattering processes so that free path lengths should be infinite. In real crystals the free path length of an electron or hole is determined by the concentration of imperfections in the lattice which act as scattering centers. Free path lengths are generally very much greater than the atomic spacing, however. The mean time between collisions, $\tau$, is called the relaxation time and is an important quantity in calculations of transport phenomena. Under the influence of various force fields the free electron gas in the crystal acquires a drift velocity in the direction of the applied force given by

$$dv_x = \frac{F_x}{m^*}\,dt \tag{1}$$

where m* is the effective mass of the charge carriers.

TABLE 1. ENERGY GAPS OBTAINED FROM THE OPTICAL ABSORPTION EDGE

| Energy Gap at 300° K (ev) | | |
|---|---|---|
| Material | Direct | Indirect |
| PbS | 0.41 | 0.37 |
| PbSe | 0.29 | 0.26 |
| PbTe | 0.32 | 0.29 |

In the case of an electric field the mean drift velocity becomes

$$\bar{v}_x = \frac{eE\tau}{m^*} \tag{2}$$

We may write this expression in the form

$$\bar{v}_x = \mu E \tag{3}$$

where $\mu$ is the mobility of the charge carrier and is

$$\mu = \frac{e\tau}{m^*} \tag{4}$$

The temperature dependence of the relaxation time for various electron scattering processes can be calculated and the theoretical behavior of the mobility can be determined. Some of these calculations are summarized by Smith (1959).

Experimentally the mobility is readily obtained from measurements of the electrical resistivity and Hall effect. The electrical resistivity $\rho$ for an electron conducting solid is

$$\rho = \frac{1}{ne\mu} \tag{5}$$

while the Hall coefficient is

$$R = \frac{1}{ne}$$

Thus

$$\frac{R}{\rho} = \mu \tag{6}$$

Typical experimental data on Hall effect and resistivity for the sulfides is shown in Fig. 6. At high temperatures the R and $\rho$ behavior is seen to become independent of sample composition and is referred to as the intrinsic conductivity region. At lower temperatures carrier concentrations become constant as indicated by the constant value of the Hall coefficient. This is the extrinsic conductivity region where the carriers arise from low energy level imperfection centers which remain ionized even to the lowest temperatures studied, about 4° K.

By combining R and $\rho$ data one obtains mobility curves such as are shown in Fig. 7 for typical crystals of PbS, PbSe and PbTe. There is a marked similarity in the general behavior for the three materials though the magnitudes differ. These semiconductors are unusual in that their mobility increases rapidly with decreasing temperature, even with carrier concentrations up to about $10^{19}/cm^3$. At the present time known electron and hole scattering models are unable satisfactorily to account for the observed behavior of the mobility. Recent studies by Allgaier (1962) are encouraging in that they qualitatively explain the ob-

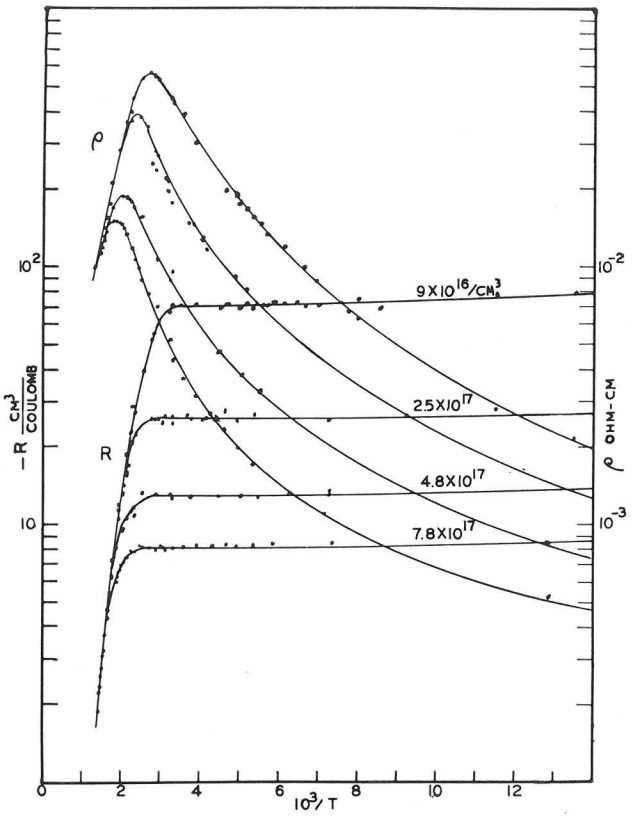


FIG. 6. Typical curves of Hall effect, R and electrical resistivity $\rho$ for PbTe crystals of different compositions.

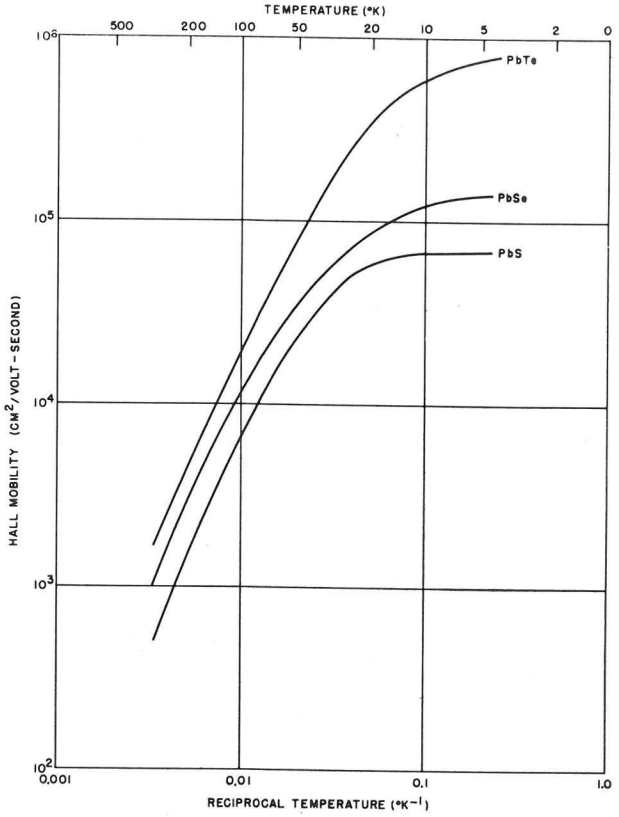


FIG. 7. Typical curves of mobility in n-type PbS, PbSe and PbTe crystals (courtesy of Dr. R. S. Allgaier).

served curves by considering the combined influence of lattice scattering and defect scattering along with the variation of the effective mass and energy gap with temperature.

Thermal gradients in crystals also result in a drift of charge carriers giving rise to thermal-electric effects. One of these is the Seebeck effect, also known as the thermoelectric power. In the lead sulfides the thermoelectric power is relatively large for a material of low electrical resistance and low thermal conductivity. Curves of the thermoelectric power in PbTe as a function of temperature and carrier concentration are shown in Fig. 8. This group of crystals were p-type. An interesting feature is the reversal of the sign of the thermoelectric power at high temperatures. This is due to the increased number of electrons arising from excitations across the forbidden energy gap at high temperatures. When the number of these electrons approaches the number of holes the sign changes because the mobility of the electron is greater than the hole mobility. At absolute zero the thermoelectric power should, in theory, approach zero as $1/T$ and the low-temperature experimental data appear to verify this prediction.

## PHOTOCONDUCTIVITY

The lead sulfides are of particular interest because of their infrared photoconductivity. Their energy gaps

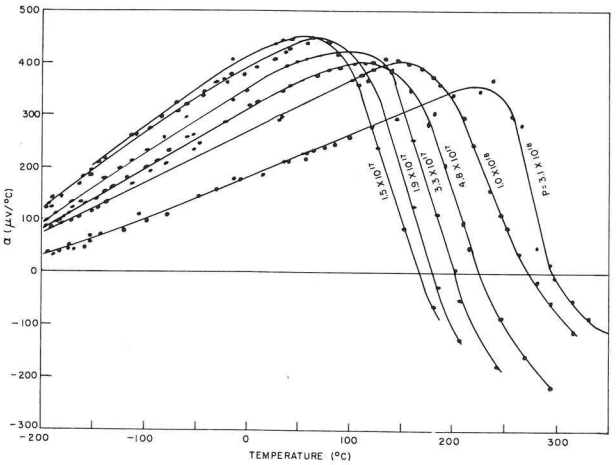


FIG. 8. Thermoelectric power in $p$-type PbTe crystals.

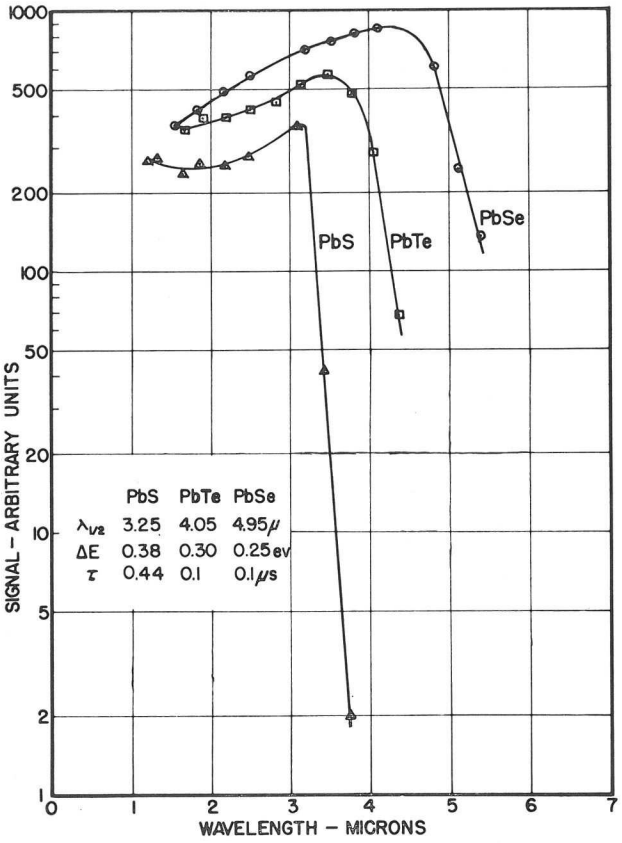


FIG. 9. Infrared photoeffect in PbS, PbSe and PbTe.

fall in the range from about 0.4 ev to 0.2 ev. Photons having wavelengths as long as 3 to 5 microns are energetic enough to excite electrons and holes into conduction bands. This results in a temporary increase in the electrical conductivity of the semiconductor, which returns to the dark value of conductivity upon the removal of the radiation. The relative spectral dependence of the photo effect is shown in Figure 9 for PbS, PbSe and PbTe crystals. The sensitivity for each material was arbitrarily adjusted so that the curves would not cross one another. The sharp fall-off in sensitivity at long wavelengths was used to estimate the energy gaps. The values so obtained are in reasonably good agreement with the more precise values obtained from absorption edge studies. The time $\tau$ for the signal to decay to 1/e of the maximum value is also given on the curve. Oxygen atoms in thin films of these materials act as traps for electrons and have the effect of increasing the decay time by orders of magnitude. The equilibrium concentration of charge carriers under illumination is correspondingly increased and the sensitivity is higher for these oxygen treated films. Thin evaporated or chemically deposited films of the lead sulfides on glass or similar substrate are among the most sensitive infrared detectors known.

## APPLICATIONS

One of the principal uses of the lead sulfide semiconductors is based upon their highly sensitive infrared photoconductivity. Numerous types of infrared cells are being manufactured today for use in military devices, such as target seekers or for mapping out ground areas. These detectors are also widely used by spectroscopists in studying molecular structure or for chemical analysis. The high sensitivity of the photoconductive detectors permits analysis of fine structure in molecular spectra far beyond the capacities of conventional bolometer or thermocouple infrared detectors.

Another application of these materials is somewhat related to photoconductivity in that it is also based upon the energy gap. This application is infrared filters. The sharp absorption edge in these semiconductors falls in a useful region of the infrared spectrum at about 3, 4 and 5 microns. Radiation of wavelengths shorter than the edge value are essentially cut off while longer wavelengths are transmitted. The transmission loss that occurs is principally reflection losses due to the high dielectric constant of the materials.

A more recent application for these materials is in thermoelectric devices for converting heat into electrical energy or for refrigeration. Lead telluride is one of the most useful semiconductors in these applications. Power supplies for isolated equipment such as weather reporting stations in the arctic regions or in satellites have been made using PbTe as the convertor and nuclear waste material such as $Sr^{90}$ or other nuclear fuel elements of the uranium series as the heat source. Such power supplies will last for many years.

Thermoelectric refrigeration devices for small scale cooling applications are now commercially available. Recently household size thermoelectric refrigerators and ice makers have been placed on the market. In these applications n and p-type PbTe are used for the two members of the thermocouple.

## CONCLUSIONS

The lead sulfide semiconductors, owing to their large ionic bonding component, may incorporate significant departures from the stoichiometric proportions in the crystalline state. These imperfections

control the electrical properties in pure crystals. Studies of the maximum deviations in stoichiometry as a function of temperature have been made as well as studies of the internal composition of the solid in equilibrium with the vapor phase. The transport properties of electrons and holes and the detailed structure of the energy band edges in these semiconductors are beginning to be clarified. Applications for the lead sulfides are increasing and include a number of infrared as well as thermoelectric devices.

## References


Allgaier, R. S. and B. B. Houston (1962) Mobility studies in semiconductors with very high carrier densities. International Conference on Semiconductors, Exeter, England (in press.)

Anderson, J. S. (1946) Non-stoichiometric compounds. *Ann. Rept. Prog. Chem. Soc. London*, 104.

Bloem, J. (1956) Controlled conductivity in lead sulfide single crystals. *Philips Res. Rept.* **11,** 273.

——— and F. A. Kroger (1956) The $p$-$T$-$x$ phase diagram of the lead-sulfur system. *Zeit. Phys. Chem.* **7,** 1.

Brebrick, R. F. and R. S. Allgaier (1960) Composition limits of stability of PbTe. *Jour. Chem. Phys.* **32,** 1826.

——— and E. Gubner (1962) PbSe composition stability limits. *Jour. Chem. Phys.* **36,** 170.

——— and W. W. Scanlon (1954) Electrical properties and the solid-vapor equilibrium of lead sulfide. *Phys. Rev.* **96,** 598.

Scanlon, W. W. (1959) Recent advances in the optical and electronic properties of PbS, PbSe, PbTe and their alloys. *Jour. Phys. Chem. Solids*, **8,** 423.

——— (1962) Precipitation of Te and Pb in PbTe crystals. *Phys. Rev.* **126,** 509.

Smith, R. A. (1959) *Semiconductors*. Cambridge.

Wagner, C. and W. Schottky (1960) Theory of regular mixed phases. *Zeit. Physik. Chem.* **11,** 467.

MINERALOGICAL SOCIETY OF AMERICA, SPECIAL PAPER 1, 1963
INTERNATIONAL MINERALOGICAL ASSOCIATION, PAPERS, THIRD GENERAL MEETING

# VARIOUS ASPECTS OF ATOMIC DISPLACEMENTS IN METALLIC SULFIDES

JEAN PROUVOST
*Faculté des Sciences de Lille (Nord), France*

ABSTRACT

Movements of atoms can be observed and even brought about in metallic sulfides. A change in the structure may result from a large number of these movements. These displacements can be studied by various methods. Three examples are given: 1) atomic displacement involving another cell, causing a polymorphic form to appear; 2) atomic displacement bringing about the unmixing of several phases; and 3) artificial introduction of a new metal into a given mineral, where the introduced atoms either enter into solid solution or cause the appearance of new phases. The distances traveled by the atoms can be estimated. Such displacements can explain a number of commonly observed phenomena.

The most common metallic sulfides still pose numerous problems, which become obvious when the minerals are examined under a polarizing metallographic microscope. Many optical anomalies, many features of their mutual arrangements, and the occurrence of unidentified phases make optical interpretations difficult (Prouvost, 1959).

We attribute these surprising features to the facts that, when they were formed, the nutrient material was not so well determined as those which we reproduce in the laboratory, and numerous elements were present in variable quantities. As a result of this variation, each distinct phase contains a certain number of elements, probably in the form of a solid solution, which will be stable under certain conditions. Since conditions vary in the course of geological ages, the balance tends to shift. New phases appear or disappear, certain crystalline states can no longer exist and are replaced by others. All this is accompanied by a regrouping of the atoms and, consequently, by movements of atoms which leave their previous positions to reach new equilibrium positions.

To study these phenomena, it is normal to resort to methods which grasp each of the variables arising from the above observations: the variation of thermodynamic energy is clearly shown by the differential thermal analysis; crystalline modifications are indicated by $x$-ray diffraction; changes of reflecting power (in quantity and quality) and appearance or disappearance of new phases can be seen with the aid of a metallographic polarizing microscope. Finally, there is the analysis, at specific locations, of the elements of the different phases.

Let us consider each of these experimental techniques. DTA, for our purposes, must be particularly sensitive. In fact, it is advantageous to modify the heating rate during the observation of the phenomena, thus permitting the control of their reversibility. The analysis must be sensitive in order to show very slight variations of energy. (Both the dilution techniques and the protection of thermocouples generally used for sulfides are to be avoided, even if it means the destruction of these thermocouples during each experiment.) It should be added that the instability of sulfides heated in an oxidizing medium necessitates the use of an inert gas.

The $x$-ray examination of phases that are stable only in a fixed range of temperatures requires the use of a high-temperature camera, and up to now, with the apparatus at our disposal, we have succeeded only in obtaining Debye-Scherrer powder patterns.

Optical study, in its present form, falls short of giving the results we could expect to obtain with the apparatus that we eventually intend to build, *i.e.*, a heating stage for polished sections. Now we can observe the samples only before thermal treatment and after cooling.

The chemical study of a certain location is effected with the Castaing microsonde, an apparatus based on the emission of $x$-rays, which permits optical observation simultaneously with an analysis of the elements. In some cases it can be supplemented by the scanning apparatus.

Let us recall the results that such a combination of techniques has enabled us to obtain. Let us first examine the case where no arrival or departure of any element is to be expected during thermal treatment. As an example, let us take antimony trisulfide, which we have particularly studied and which can be obtained from pure chemical substances (Prouvost, 1960).

After the transformation at 215° C. of the red precipitate to an orthorhombic crystalline sulfide with $a=11.229$, $b=11.310$, $c=3.839$ Å (Swanson, 1955), we observe, by DTA (Fig. 1), two endothermic peaks at temperatures of 260° and 330° C. By

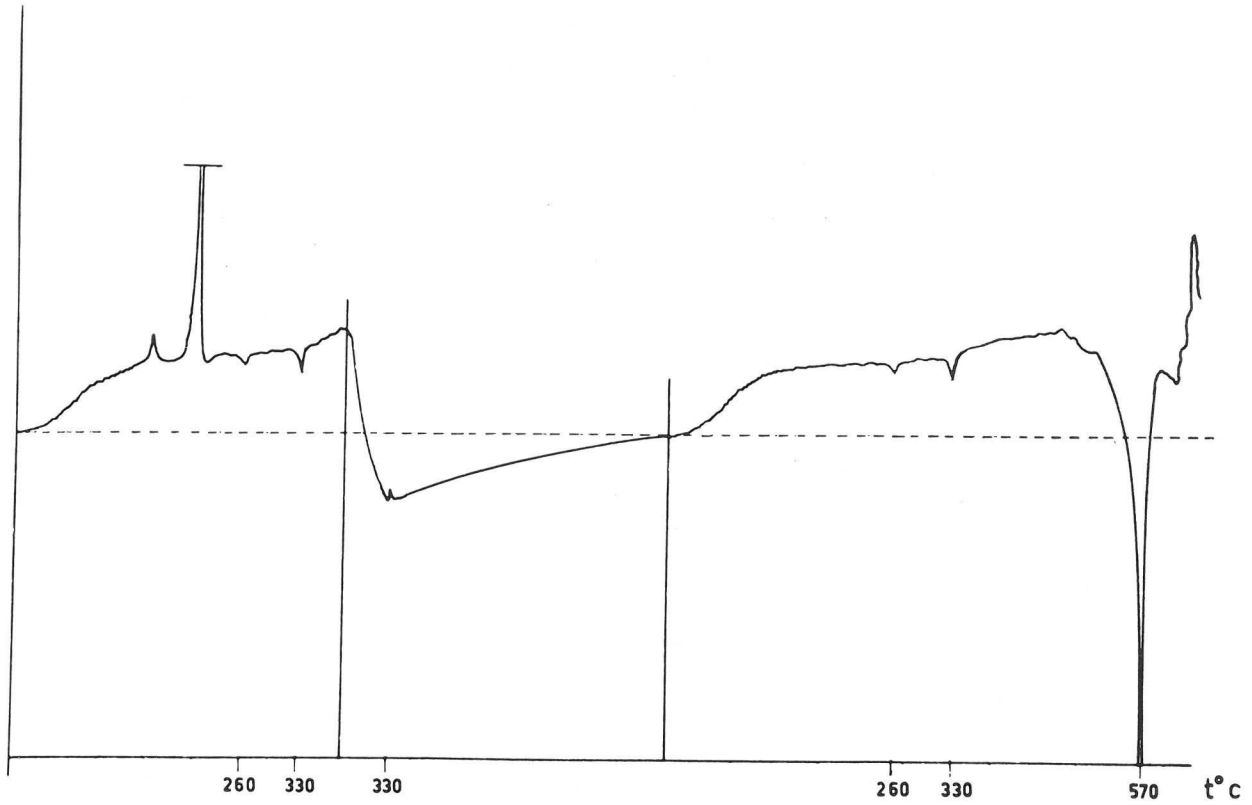


FIG. 1. Differential thermal analysis curves of antimony trisulfide, $Sb_2S_3$.

stopping the heating almost immediately and by letting the sample cool, we can observe an exothermic peak corresponding to 330°; then, as the temperature rises again, the two peaks are reproduced at 260° and 330° C. This example is particularly striking. It is an almost perfect example of reversibility: in the region under consideration, the two curves of thermoanalysis are superimposable. The high-temperature polymorphic phase has probably never before been observed, since it is stable only in a restricted range of temperatures, from 330° C. to the comparatively low melting point, recorded at 570° C. under our conditions. An $x$-ray investigation with the aid of a heating camera seems to indicate that this phase must be cubic, with $a = 5.57$ Å.

The above phenomena, which are commonly observed when different stable phases exist, are certainly very frequent, and each case studied has revealed interesting observations. The passage from one form to another is accompanied by atomic displacements, the magnitude of which is always very slight.

We can now treat the more complex sulfide, bornite ($Cu_5FeS_4$), in the same way. In this case the sulfur is combined with two different metals, and we have a greater number of possibilities: different forms of bornite; formation of other compounds, either of iron or of copper with incidental exclusion of the other metal; and ordered or disordered compounds (Frueh, 1950).

We have analyzed by DTA the purest sample available to us (Fig. 2). The chemical analysis shows close agreement with the chemical formula:

| | *theoretical* | *sample* |
|---|---|---|
| Cu | 63.33 | 62.8 |
| Fe | 11.12 | 11.3 |
| S | 25.55 | 25.5 |

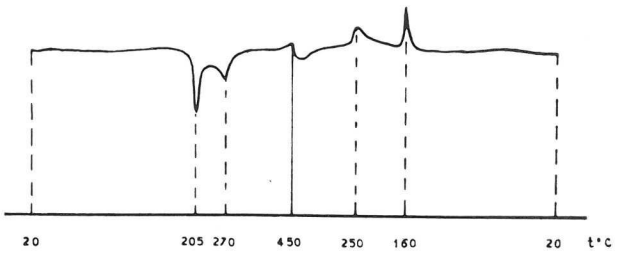


FIG. 2. Differential thermal analysis curves of bornite.

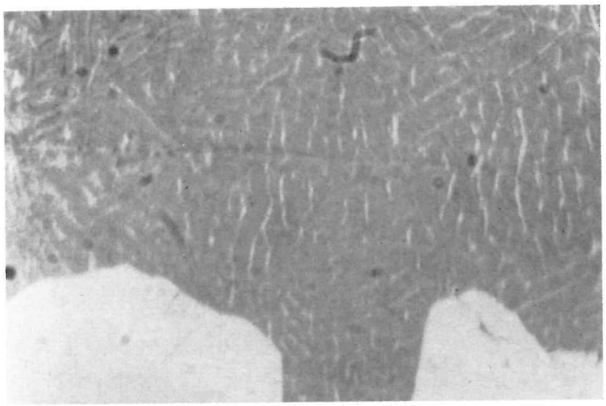

FIG. 3. Micrograph of bornite after thermal treatment. Note two specks of chalcopyrite and segregation of copper sulfide forming Widmannstätten patterns. Ordinary light, ×1000.

The first endothermic peak is noticed at 205° C., and the balance is not yet restored when a new peak is traced at 270° C. The temperature continues to rise without incident to 450° C., when the heating is stopped. Analogous phenomena are observed on cooling, but at lower temperatures.

The run was repeated several times, and the same phenomena were observed each time. There are, therefore, two points of energy change. Since it was impossible to carry out an optical investigation at these temperatures, *x*-ray diffraction was used. Powder photographs were taken at temperatures of 20°, 230°, 270° and again at 20° C. At 230° C. (*i.e.* above the endothermic peak), chalcopyrite lines appeared, and above 270° C. chalcocite lines were also noted. These lines disappeared on cooling to room temperature. Therefore, the formation of chalcopyrite and then of chalcocite must encounter some difficulty, since the diffraction pattern of bornite still persists, with only the main lines of chalcopyrite and chalcocite showing, and since the return to the low-temperature state was considerably delayed.

In order to carry out an optical examination, we used quenching in the hope that it would freeze the structure at a fixed point. The polished sections, which initially consisted only of one phase (bornite), showed, after treatment, minute specks of chalcopyrite scattered in the center of the bornite. Crystallographic planes of chalcopyrite often formed the boundaries of these statistically distributed specks. One could also observe, albeit with great difficulty, the segregation of the copper sulfide. This difficulty arises from the fact that we are dealing with very thin elongated zones, probably oriented along the planes of the original bornite and forming Widmannstätten patterns (Fig. 3).

The examination of such zones with the Castaing microsonde did not give satisfactory results, because we had reached the limit of resolving power. A drop in iron content was nevertheless ascertained when the electron beam embraced such a zone. The scanning process did not yield any better results.

The transformation just described is completely different from the one previously studied. Here we are dealing with unmixing, with the appearance of several solid phases. The atomic displacement, which is relatively large judging by the photographs, takes place only comparatively slowly, which probably explains the difference in the temperatures at which the individual peaks occur on heating and on cooling.

In the course of some other work, we noted particularly interesting phenomena in Cu-Ag-S. Unfortunately, equipment was not available for a study of this compound either by DTA or by *x*-ray diffraction at elevated temperatures. It is known that a mixture of these three elements shows quite different optical properties depending upon the temperature at which they are combined. If we assume that the total composition remains constant, this compound must obviously occur in several forms.

Let us now study the transformation obtained when a new element is introduced from the outside. In this case we increased the energy either by raising the temperature or by applying an electric field. So far, all the experiments which I have attempted, to bring about transformations by the action of an electric field compatible with natural conditions, have ended in failure. The presence of at least one liquid has always proved indispensable. Electrolytic phenomena, therefore, seem in this case to control the movement of the ions (Prouvost, 1960).

By raising the temperature, we were able to make a metal enter the crystal structure of a mineral, and thus bring about the transformation of the latter. It again was the Castaing microsonde that gave the proof of the atomic displacements. Curves of established percentages along lines cutting through the transformed parts give us an idea of the concentration of the various elements at each point (Prouvost, 1962).

As an example, let us consider the deposits of silver and tin on chalcopyrite. On the photograph (Fig. 4) we can see, adjoining the transformed areas, the percentage curves of the constituent elements. These curves show that the enrichment is not

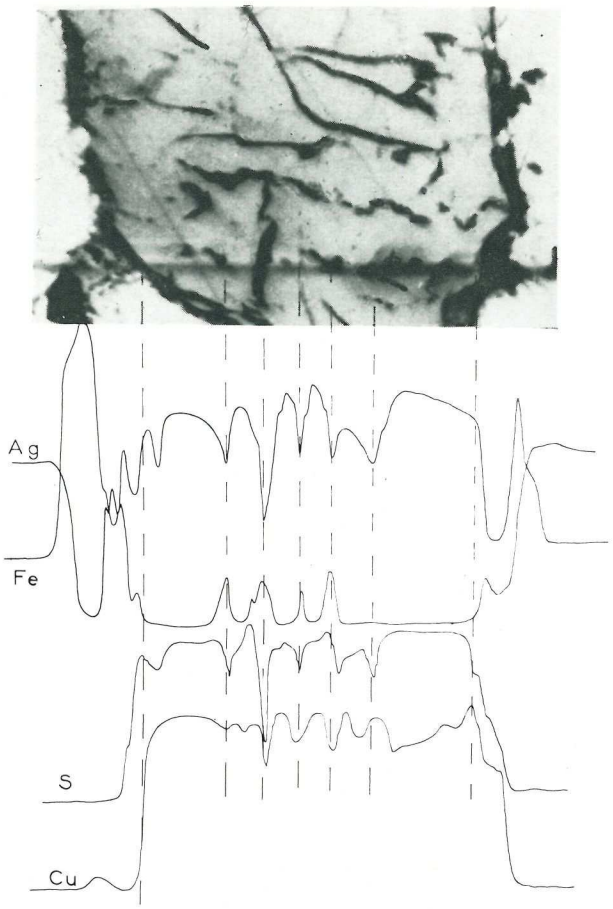


FIG. 4. Examination with Castaing "microsonde" of chalcopyrite treated by silver. Silver is white (some on the left and on the right). Chalcopyrite is gray. The black specks are the transformed areas. The horizontal dark line is the trace of the electron beam. Ordinary light ×350.

gradual; that, on the contrary, there is a sudden variation in concentration at the boundary of the transformation. The percentage of the particular metal is remarkably constant throughout the crossing of the chalcopyrite, and in the case of silver it is about 5 to 8%. The presence of silver in solid solution is probably the reason for the greenish appearance of the treated chalcopyrite, which has been observed in some samples from Peruvian silver deposits. This is a third type of diffusion of the atoms. In this particular case we deal with a supernumerary element. The percentage curves give some information as to its movement.

We have thus shown three aspects of the movements of atoms in metallic sulfides. In the first case, which is the simplest and the most completely studied, the movement of atoms develops quickly, but is slight: because the crystal structures of the two forms are only slightly different from each other, the atom will move to a neighboring position without circulating through the crystal structure. The other cases are different. Let us examine the areas of thermally treated bornite, in which chalcopyrite and copper sulfide have appeared. The segregation points of chalcopyrite are rarely more than 0.1 mm apart. We must not forget that their organization is statistical. We are led to think that, under the conditions of our experiments, the ferrous ions taking part in the regrouping have traveled about 0.1 mm; in the present state of our research we have reason to believe that the material is homogeneous between the particles of chalcopyrite. Finally, in the case of the deposition of a new element, the greater number of parameters makes our study more uncertain. With the same mineral, results are different according to the metal deposited. The thickness transformed under our experimental conditions (8 days at 300° C., or a bit less in the case of tin to avoid fusion) was about 0.01 mm. However, we must distinguish several problems. Up to a certain concentration, movements can take place in a solid solution, without transformation, over distances which can be large. If there is a change of phase, we must take into account the fact that other atoms must occupy the areas in which a new mineral crystallizes. This is possibly the explanation for the slight penetration of the total transformation with appearance of a new phase.

In conclusion, it may be said that the atomic movement of elements or of groups of elements trying to reach a state of equilibrium takes place very slowly as compared to our own time scale. However, the atomic velocities are sufficient to account for the textures commonly encountered in polished sections of ore minerals. In some cases, bornite for instance, we have succeeded in producing typical microstructures in a comparatively short time and under very similar conditions.

## ACKNOWLEDGMENTS

The writer is grateful to the Centre National de la Recherche Scientifique (France) and the Bureau de Recherches Géologiques et Minières (France) for the use of the Castaing apparatus. He wishes to thank Dr. Guillemin for encouraging the study. He has benefited from discussions with Dr. A. J. Frueh, Jr. and Professor H. Curien.

References

Frueh, A. J., Jr. (1950) Disorder in the mineral bornite, $Cu_5FeS_4$. *Am. Mineral.* **35,** 185–192.

——— (1954) The use of zone theory in problems of sulphide mineralogy. *Geochim. Cosmochim. Acta,* **6,** 79–89.

Prouvost, J. (1959) Remarques sur la composition et le pouvoir reflecteur de la bornite ($Cu_5FeS_4$). *Compt. Rend. Congrès des soc. sav.,* **84***ème,* 365.

——— (1960) Quelques variétés polymorphiques du trisulfure d'antimoine. *Bull. soc. franç. Minér. Crist.* **83,** 228.

——— (1960) Transformations expérimentales des sulfures métalliques naturels, étude de leur mécanisme. *Bull. soc. franç. Minér. Crist.* **83,** 265–294.

——— (1962) Variations de la composition de la chalcopyrite soumise à un apport d'étain, d'argent et de fer. *Bull.soc.franç. Minér. Crist.* **85,** 97.

Swanson, H. E., N. T. Gilfrich and G. M. Ugrinic (1955) Standard X-ray diffraction powder patterns. *Nat'l. Bur. Stand. Circ.* **539,** 5.


---

**Discussion**

B. J. Skinner (Washington, D. C.): What is the composition of the yellow mineral, which you called chalcopyrite, that appeared in the heated bornite sample?

Author's reply: (Lille): The yellow mineral that I called chalcopyrite has not been chemically analyzed by classical methods because the specks were too small. I determined the optical properties by means of the dispersion curve of the reflecting power, and the lattice parameters from $x$-ray powder patterns. I also used the Castaing microsonde to obtain the ratios of the elements.

MINERALOGICAL SOCIETY OF AMERICA, SPECIAL PAPER 1, 1963
INTERNATIONAL MINERALOGICAL ASSOCIATION, PAPERS, THIRD GENERAL MEETING

# ÉTUDE STRUCTURALE DE QUELQUES SULFURES DE PLOMB ET D'ARSENIC NATURELS DU GISEMENT DE BINN

M-TH. LE BIHAN
*Laboratoire de Minéralogie-Cristallographie, Faculté des Sciences, Paris, France*

ABSTRACT

Baumhauerite, $Pb_5As_9S_{18}$, is triclinic, with $a=22.78$, $b=8.33$, $c=7.90$ Å, $\alpha=\gamma=90°$, $\beta=97°$ 24; space group is $P\bar{1}$. Material called rathite consists of three species: Rathite I, $Pb_7As_9S_{20}$, monoclinic, $a=8.43$, $b=25.8$, $c=7.91$ Å, $\beta=90°$; space group is $P2_1$. Rathite II, $Pb_9As_{13}S_{28}$, monoclinic, $a=8.43$, $b=70.9$, $c=7.91$ Å, $\beta=90°$; space group $P2_1$. Rathite III, $Pb_6As_{10}S_{20}$, monoclinic, $a=24.52$, $b=7.91$, $c=8.43$ Å, $\beta=90°$; space group $P2_1$. The structures of the four minerals are similar to that of sartorite. They contain two types of chains: one of $As\text{-}S_2$, and the other, a mixed chain (not found in sartorite) of-S-As-S-Pb-.

Nous avons déterminé les structures atomiques de quatre minéraux: baumhauérite, rathite I, rathite II et rathite III.

La différenciation des espèces minérales a été faite par une étude aux rayons X, puis chaque minéral a été identifié à l'aide de mesures goniométriques et de mesures de densités. L'identité des diagrammes de rayons X obtenus à partir de différents échantillons d'une même espèce prouve qu'il s'agit d'espèces bien définies. Nous n'avons pas décelé l'existence d'espèces intermédiaires d'après l'étude des échantillons dont nous disposions.

Pour chaque cristal, les paramètres linéaires et angulaires de la maille élémentaire ont été mesurés respectivement sur des diagrammes de cristal tournant et de Weissenberg, effectués avec la radiation CuK$\alpha$; les résultats sont les suivants:

*La baumhauérite*, $Pb_5As_9S_{18}$, est triclinique; $a=22{,}78$ $b=8{,}33$ $c=7{,}90$ Å; $\alpha=\gamma=90°$, $\beta=97°24'$. Le groupe spatial est $P\bar{1}$: la méthode statistique de Rogers a mis en évidence l'existence du centre de symétrie.

*La rathite I* est monoclinique; la formule est $Pb_7As_9S_{20}$; $a=8{,}43$ $b=25{,}8$ $c=7{,}91$ Å; $\beta=90°$. Le groupe spatial est $P2_1$; ce minéral présente un fort module piézoélectrique.

*La rathite II* est monoclinique; la formule est $Pb_9As_{13}S_{28}$; $a=8{,}43$ $b=70{,}9$ $c=7{,}91$ Å; $\beta=90°$. Le groupe spatial, $P2_1$, a été confirmé par l'étude des diagrammes de Patterson.

*La rathite III*, $Pb_6As_{10}S_{20}$, est monoclinique; $a=24{,}52$ $b=7{,}91$ $c=8{,}43$ Å; $\beta=90°$. Le groupe spatial est $P2_1$; l'absence de miroir a été déduite de l'aspect de la projection de Patterson sur le plan (001).

Des analyses spectrographiques ont été effectuées, et nous ont renseignés sur le degré de pureté de nos échantillons.

La recherche de ces structures présentait des difficultés, dont la principale était due au fait que la composition chimique exacte de chaque minéral était mal connue, et difficile à établir au moyen d'une analyse chimique quantitative, les différentes espèces se trouvant intimement associées.

Nous avons déterminé le nombre et les positions approximatives des atomes de plomb, dans chaque structure, à partir de l'examen des fonctions de Patterson calculées à deux et à trois dimensions; nous avons dû recourir à l'étude des projections généralisées de Patterson pour préciser certains points délicats. Le nombre et les positions approchées des atomes d'arsenic ont été déduits de l'analyse des projections de Fourier, et des projections partielles de densité électronique effectuées entre deux niveaux. Avant de déterminer le nombre et les positions des atomes de soufre, nous avons précisé les coordonnées des atomes lourds au moyen de "séries-dérivées" et de "séries-différences." Les atomes de soufre apparaissent sur les dernières séries-différences, lorsque les contributions calculées de tous les atomes lourds ont été soustraites, après que les coordonnées de ces atomes lourds aient été ajustées une à une.

Ainsi, nous avons montré qu'il était possible de déduire la composition chimique de recherches structurales, dans un cas où les atomes composant le motif sont de poids atomiques suffisamment différents. Les séries-différences révèlent alors facilement une erreur commise sur la nature chimique d'un atome donné.

La structure de la sartorite ($PbAs_2S_4$), déterminée par Nowacki (1961), et les structures des quatre minéraux que nous avons étudiés, ont été comparées (Le Bihan, 1962). Nous trouvons dans chacune d'elles le même arrangement d'atomes de soufre autour des atomes de plomb, d'une part, et des atomes d'arsenic, d'autre part. On rencontre, dans ces structures, deux types de chaînes infinies s'étendant parallèlement à la direction d'allongement de chaque minéral; ce sont, d'une part des chaînes ($As\text{-}S_2$) qui existent dans chaque structure et dont la

périodicité, le long de la chaîne, est 4.2 Å, et d'autre part des chaînes mixtes (-S-As-S-Pb-), qu'on ne trouve pas dans la sartorite et qui admettent une périodicité de 8,4 Å. Le nombre et les positions de ces chaînes mixtes, dans la maille élémentaire, déterminent le type de structure.

La structure de la sartorite est composée de chaînes ($As\text{-}S_2$) groupées trois par trois autour d'une rangée d'atomes de plomb. Les structures de la baumhauérite (Fig. 1) et de la rathite III présentent le même arrangement avec, en outre, des chaînes mixtes qui s'intercalent entre les divers groupements composés de trois chaînes ($As\text{-}S_2$). On trouve, pour la rathite I et pour la rathite II (Fig. 3), des rangées d'atomes de plomb entourées chacune de trois chaînes infinies qui peuvent être soit trois chaînes ($As\text{-}S_2$), soit deux chaînes ($As\text{-}S_2$) et une chaîne mixte ($PbAsS_4$). D'autres chaînes mixtes se placent entre ces groupements, comme dans le cas de la baumhauérite.

Nous avons projeté ces structures parallèlement à la direction des chaînes (Fig. 2). Les rangées constituées d'atomes de plomb superposés et distants de 4,2 Å, se projettent aux sommets d'hexagones de différents types. Nous avons reconnu trois types d'hexagones correspondant à trois types de groupements d'atomes, que nous avons appelés S, $R_I$ et $R_{III}$, et qui diffèrent selon le nombre et la nature des chaînes qu'ils contiennent.

*Le type S* donne en projection un petit contour hexagonal joignant des atomes de plomb, à l'intérieur duquel se trouvent quatre chaînes ($As\text{-}S_2$). La périodicité selon la direction de projection est 4,2 Å. Le contenu chimique de ce groupement S, ramené à une période de 8,4 Å est $Pb_4As_8S_{16}$.

*Le type $R_{III}$* donne en projection un grand hexagone aux sommets duquel se projettent des atomes de plomb dont la périodicité, parallèlement à la direction de projection, est 4,2 Å. A l'intérieur de cet hexagone, se trouvent quatre chaînes ($As\text{-}S_2$) et deux chaînes mixtes (-S-As-S-Pb-). Ce groupement atomique correspond à la formule chimique $Pb_6As_{10}S_{20}$.

*Le type $R_I$* contient trois chaînes ($As\text{-}S_2$) et trois chaînes mixtes. Cette unité structurale a pour formule chimique $Pb_7As_9S_{20}$.

Les trois structures les plus simples (sartorite,

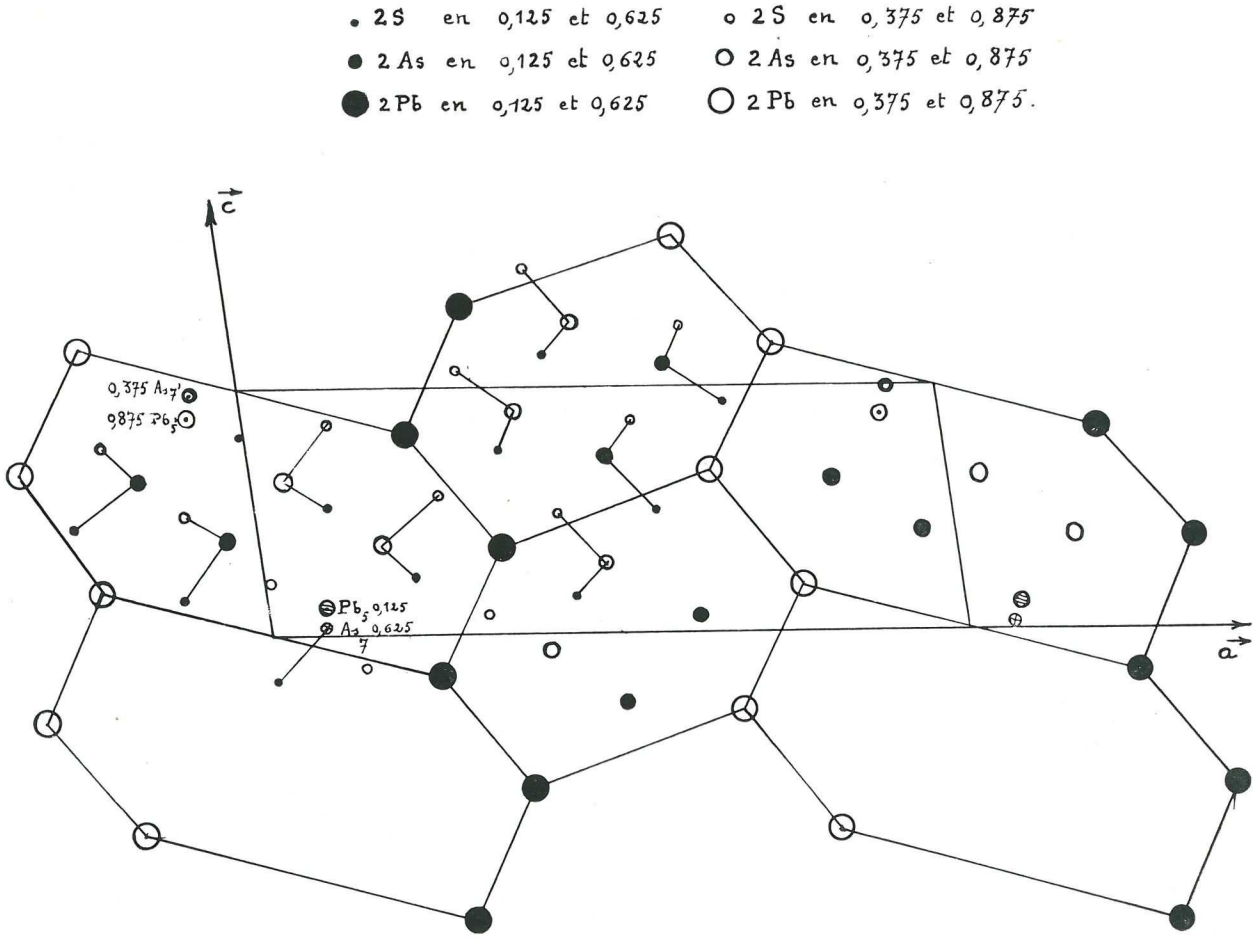


FIG. 1. Baumhauérite.

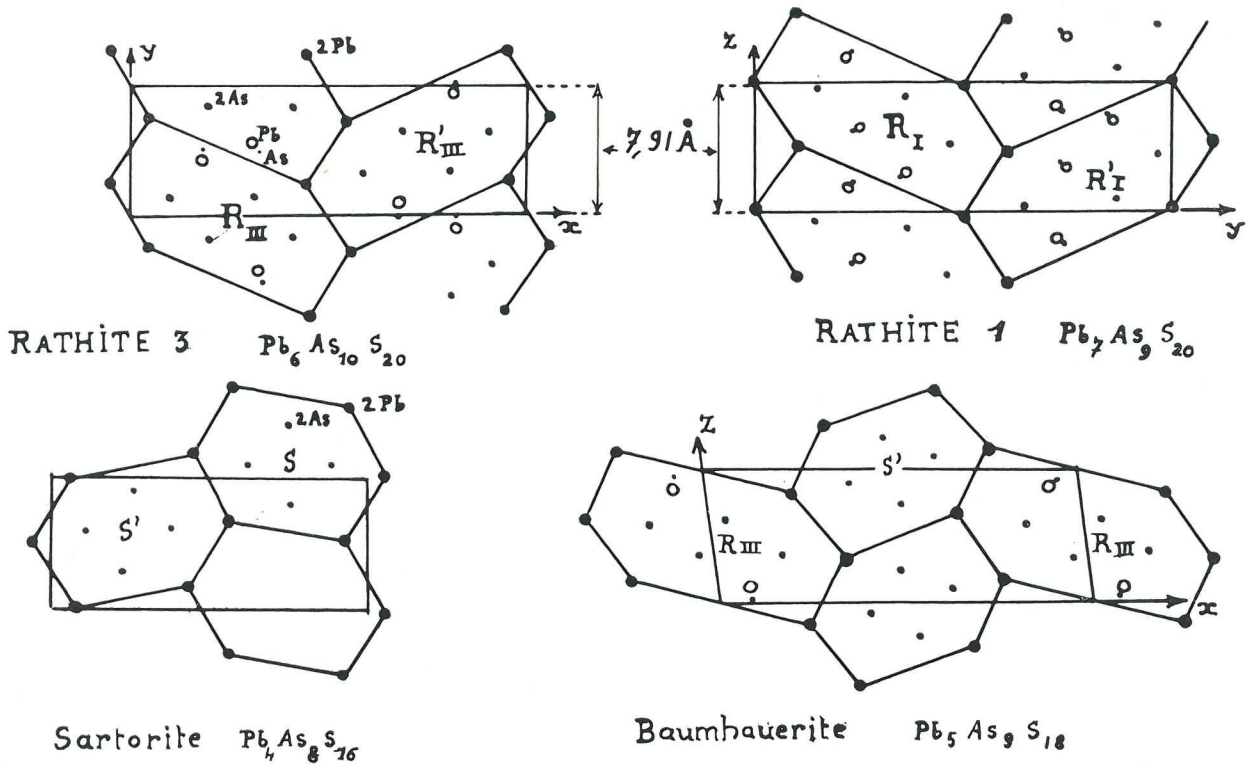


FIG. 2.

rathite I, rathite III), résultent chacune de l'association de deux unités de même type se correspondant par l'opération d'un axe binaire hélicoïdal; ainsi la rathite I (Fig. 2) résulte de l'association de deux "unités" de type $R_I$ que se déduisent l'une de l'autre par l'axe binaire hélicoïdal; nous avons appelé $R_I$ et $R_I'$ ces deux "unités" identiques qui ont, par rapport à la maille élèmentaire, deux orientations différentes.

Dans la structure de la baumhauérite, nous rencontrons l'arrangement ($R_{III}+S'$).

La maille de la rathite II est composée de la juxtaposition des éléments: $R_I+S'+R_{I'}+R_I'+S+R_{I'}$; les hexagones $R_I$ et $R_{I'}$ ont mêmes dimensions, même orientation dans la maille, et même composition chimique; on obtient le contenu de $R_{I'}$ en prenant le symétrique du contenu de $R_I$ par rapport au centre de l'hexagone.

Ainsi, les mêmes figures structurales se conservent d'une espèce à l'autre, mais selon des arrangements différents.

De la connaissance des paramètres et du groupe spatial d'un sulfure d'arsenic et de plomb, on devrait pouvoir déduire la composition chimique et la structure; il suffirait, pour cela, de choisir parmi les divers

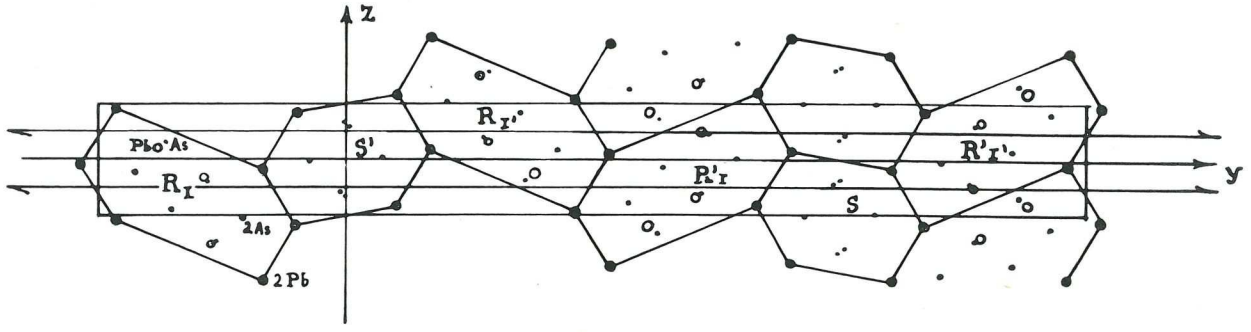


FIG. 3. Rathite II.

arrangements possibles des différentes unités S, $R_I$ et $R_{III}$, le seul arrangement compatible avec les dimensions et les éléments de symétrie de la maille élémentaire. La composition chimique du motif serait donnée par la somme des compositions chimiques des éléments constituants.

On peut admettre que ceci est valable pour les minéraux constitués uniquement de plomb, d'arsenic et de soufre, et dont la composition est telle que: $0{,}50 \leq Pb/As \leq 1$.

## Bibliographie

Le Bihan, M-Th. (1962) Etude structurale de quelques sulfures de plomb et d'arsenic naturels du gisement de Binn. *Bull. soc. franç. Minér. Crist.* **85,** 15–47.

Nowacki, W., Y. Iitaka, H. Bürki and V. Kunz (1961) Structural investigations on sulfosalts from the Lengenbach, Binn Valley (Ct. Wallis). Part 2. *Schweiz. Min. Petrogr. Mitt.* **41,** 103–116.

MINERALOGICAL SOCIETY OF AMERICA, SPECIAL PAPER 1, 1963
INTERNATIONAL MINERALOGICAL ASSOCIATION, PAPERS, THIRD GENERAL MEETING

# ON THE TRANSITION OF BORNITE

NOBUO MORIMOTO
*Mineralogical Institute, University of Tokyo, Tokyo, Japan, and Geophysical Laboratory, Carnegie Institution of Washington, Washington, D. C.*

ABSTRACT

Three polymorphs were confirmed for synthetic and natural bornite: a high-temperature form with a cubic cell of $a=5.50$ Å, a metastable form with a cubic cell of $a=10.94$ Å, and a low-temperature form with a tetragonal cell of $a=10.94$ Å and $c=21.88$ Å. The crystal structures of the high-temperature form and the metastable form were studied by $x$-ray single-crystal methods in order to elucidate the transition mechanisms of bornite.

The transition of bornite from the high-temperature form to the metastable form takes place by an ordering of the metal atoms. A single crystal with its metal atoms in a mobile state changes to many domains with a low symmetry, without changing the face-centered lattice of the sulfur atoms. These domains are in twin relations and collectively give a diffraction aspect of higher symmetry. The transition from the metastable form to the low-temperature form is also discussed.

## INTRODUCTION

The existence of three polymorphs of bornite was confirmed (Morimoto and Kullerud, 1961). These are a high-temperature form, a transitional metastable form, and a low-temperature form. The high-temperature form occurs in face-centered cubic crystals, with $a=5.50$ Å, diffraction aspect $F^{***}$; the transitional metastable form occurs in face-centered cubic pseudocrystals, with $a=10.94$ Å, diffraction aspect $Fd^{**}$; and the low-temperature form occurs in primitive tetragonal pseudocrystals, with $a=10.94$ Å, $c=21.88$ Å, space group $P\bar{4}2_1c$. The term "pseudocrystals" is used to designate very finely twinned edifices that simulate single crystals.

Various cell dimensions and symmetries, found in natural bornite, are explained by twinning of the low-temperature form, the twin operation being a 120° rotation about the row [221] of the tetragonal lattice (the body diagonal of the cubic cell).

The high-temperature form of bornite is unquenchable. When it is cooled below $230°\pm5°$ C. it instantly changes to the metastable form. The metastable form gradually transforms to the low-temperature form at room temperature.

The easy transitions between polymorphs and the simple relations between their unit cells suggest that the three structures are closely related. In this paper the transitions between polymorphs are discussed from the structural viewpoint.

## CRYSTAL STRUCTURE OF THE HIGH-TEMPERATURE FORM

The crystal structure of the high-temperature form was determined by using single-crystal $x$-ray data, which were obtained at $240°\pm5°$ C. (Morimoto, in preparation).

The crystal structure is essentially the anti-fluorite structure, only slightly more complicated. The sulfur atoms occupy the nodes of the cubic face-centered lattice, being cubically close-packed. Each tetrahedron of sulfur atoms, on the average, contains $\frac{3}{4}$ of a metal atom. This fractional atom is itself statistically distributed over twenty-four equivalent sites inside the sulfur tetrahedron. No distinction between Cu and Fe atoms could be made. Thus, in the whole unit cell, six metal atoms are statistically distributed over $24\times8=192$ sites. This can be considered a kind of "mobile" state of metal atoms in the cubic close-packing of sulfur atoms. The properties of bornite at high temperatures, such as high conductivity, wide range of solid solution, etc., are well understood on the basis of this dynamic state of the metal atoms in the high-temperature form.

## CRYSTAL STRUCTURE OF THE METASTABLE FORM

The metastable form is a transitional state between the high-temperature form and the low-temperature form. The crystal structure of the metastable form is, therefore, the key to the understanding of the transition mechanism.

The metastable form shows two characteristics: (a) the existence of a cubic sub-cell with $a=5.47$ Å and (b) a special extinction rule that only reflections with indices $(4m\pm l,\ 4n\pm l,\ l)$ appear.

It was tried in vain to find a *single-crystal* structure that would account for the observed cubic reflections. The nature of the pseudocrystal became apparent, as the twinning hypothesis proposed by Donnay *et al.* in 1958 for digenite was found to apply also in the case of metastable bornite (Morimoto, in preparation).

The cubic edifice of the metastable form is inter-

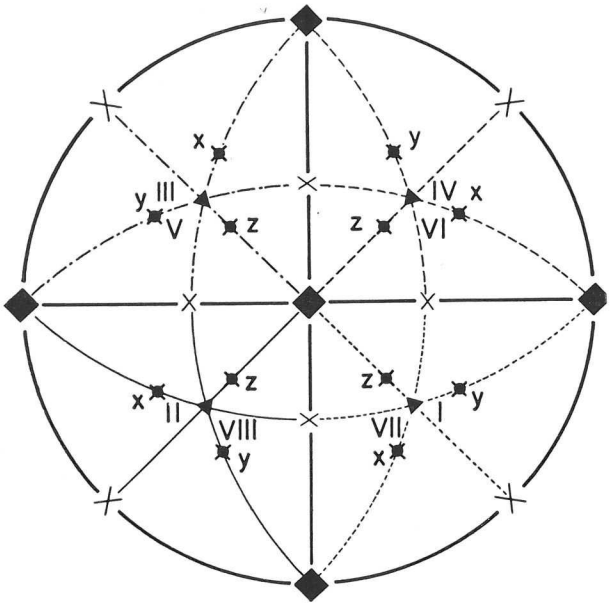


FIG. 1. Stereographic projection on $(001)_c$ of the twin in metastable bornite.

preted as an aggregate of a large number of small domains in eight different orientations. All the domains that have the same orientation constitute *one crystal*, even if they are not singly connected. Each such crystal has rhombohedral symmetry with $a_{rh} = 6.70$ Å and $\alpha = 33°\ 32'$, and the space group $R3m$. These eight crystals are in twin relations, shown in Fig. 1.

Figure 2 shows the structure of the rhombohedral metastable form. This structure can be derived from that of the cubic high-temperature form as follows. All the sulfur atoms remain in place, retaining the cubic close-packing. Of the four sulfur tetrahedra sites, two do not change at all. One becomes vacant, and the metal atom which occupied it in the high-temperature form is redistributed among the other three sites. The corresponding three sulfur tetrahedra now contain one full metal atom each. To compensate for the vacant site, the last metal site is moved slightly. The statistical distribution of $\frac{3}{4}$ of a metal atom among twenty-four possible sites inside each sulfur tetrahedron changes to the statistical distribution of one metal atom among four possible sites.

## Low-temperature Form

Strong and medium reflections have similar intensity distribution in both the metastable and the low-temperature forms, indicating that the two structures have a common basic structure. The reflections of the low-temperature form, however, do not obey the special extinction rule.

There are two different ways to explain the disappearance of the special extinction rule in the low-temperature form: (a) disappearance of the twinning or (b) lowering of the crystal symmetry (or symmetry of the domain orientation) from rhombohedral to monoclinic keeping the twin relation.

It is unlikely that the low-temperature form would have higher symmetry form. The structure of the low-temperature form, therefore, can be derived as twinning of domains with monoclinic symmetry.

## The Transition

Figure 3 shows the structural relations among the three polymorphs, all of which are represented as layer structures parallel to $(111)_{rh}$. The structures of single crystals (= domain orientations) are shown for the metastable and low-temperature forms.

All three structures are built on the basis of the cubic close-packing of the sulfur atoms. The statistically distributed metal atoms are represented as bands in the high-temperature and metastable forms. The MI layers move closer to sulfur layers to compensate for the vacant layers in the metastable and low-temperature forms. The distance between the MI layer and the sulfur layer becomes shorter, which sug-

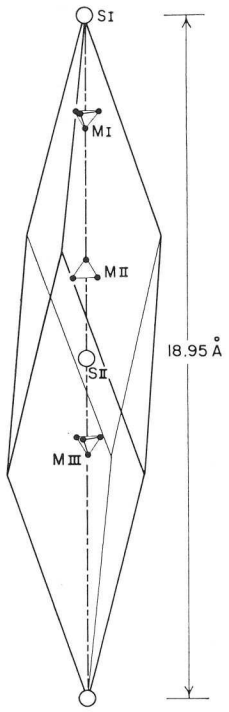


FIG. 2. The crystal structure of metastable bornite.

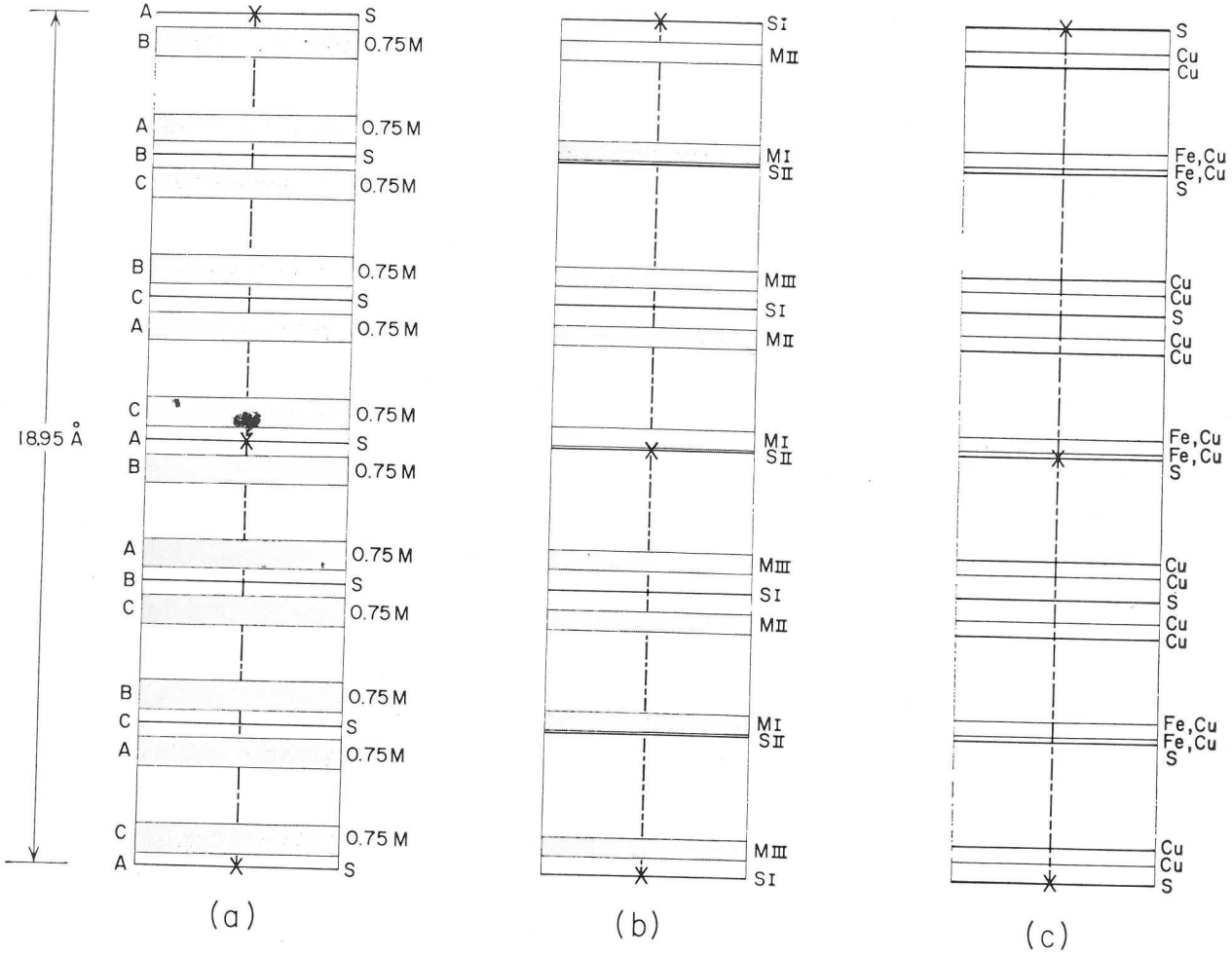


FIG. 3. Layer structures of three polymorphs of bornite: (a) high-temperature, (b) metastable, and (c) low-temperature form.

gests the possibility that the Fe atoms concentrate in the MI layers.

Although the structure of the low-temperature form was not actually determined, it seems likely that the metal atom, statistically distributed at the four corners of a tetrahedron in the metastable form, will occupy one of the four sites in the low-temperature form. Assuming the stoichiometric composition for the low-temperature bornite the Fe atoms must take some special positions, the MI tetrahedra, which give a distance of 2.20 Å from the sulfur atom. The other metal positions are more than 2.27 Å away from sulfur atoms and are supposedly occupied by Cu atoms. This relation in the low-temperature form is shown by lines in Fig. 3.

The arrangements of the metal vacant layers change their orientation according to a simple *twin law* in the metastable and low-temperature forms, as already mentioned. Domain structures always take place on transition from the high-temperature to metastable or low-temperature forms, indicating that the vacant metal layers cannot stably keep their orientation over a long distance. The diffracted *x*-rays from each crystal (= domain orientation) are not coherent with those from other crystals. The domains themselves must be small since the twins cannot be recognized as such by direct methods of observation. The volumes of the different domain orientations must be nearly equal so as to give cubic or tetragonal symmetry for the specimen as a whole.

## TWINNING DOMAIN STRUCTURE

Specimens of the metastable and low-temperature bornites can be described as twins in which the individual crystals are composed of a large number of small domains that need not be singly connected. They are different from usual twins, however, in that most of the atoms build a continuous periodic struc-

ture throughout the whole edifice, so that the twin relations apply only to the vacant metal positions. It follows that the prerequisite for twinning, namely the existence of a multiple cell with higher symmetry or pseudosymmetry, is here exactly satisfied, and twinning should be frequent—as indeed it is; it always accompanies the transition. Such slight structural rearrangements take place that the heat of transition should be very small and the transition unquenchable.

## References

Donnay, G., J. D. H. Donnay and G. Kullerud (1958) Crystal and twin structure of digenite, $Cu_9S_5$. *Am. Mineral.* **43,** 230–242.

Morimoto, N. and G. Kullerud (1961) Polymorphism in bornite. *Am. Mineral.* **46,** 1270–1282.

MINERALOGICAL SOCIETY OF AMERICA, SPECIAL PAPER 1, 1963
INTERNATIONAL MINERALOGICAL ASSOCIATION, PAPERS, THIRD GENERAL MEETING

# ON THE SUPERSTRUCTURE AND TWINNING OF PYRRHOTITE

BERNHARDT J. WUENSCH
*Crystallographic Laboratory, Massachusetts Institute of Technology, Cambridge, Massachusetts*

ABSTRACT

Pyrrhotite of composition $Fe_{.889}S$ from Morro Velho, Brazil, is pseudohexagonal. Precession photographs suggest a superstructure with cell dimensions which appear to be two and four times the $A$ and $C$ dimensions of a NiAs-type substructure. Small displacements of superstructure reflections in the patterns indicate the presence of twinning. A previously proposed twin law does not explain the observed reflections or the symmetry of the twin.

It is shown that the true lattice is at least dimensionally monoclinic and is twinned by a 2-fold rotation about [110]. The $a$ and $b$ translations of the cell are twice the orthohexagonal $B$ and $A$ dimensions of the substructure respectively, and $\beta$ is 91.79°. The $c$ dimension and lattice type are uncertain because of certain non-space-group extinctions which are still unexplained. Patterson projections suggest that the superstructure intensities are primarily due to distortion of a NiAs-type arrangement about iron vacancies.

## INTRODUCTION

The iron sulfide minerals found in nature include troilite, FeS; pyrrhotite, having a variable composition $Fe_{1-x}S$ with $x$ between 0 and approximately .2; smythite, $Fe_3S_4$; and pyrite and marcasite, $FeS_2$. Near composition FeS the system is extremely complex. These compositions have been studied extensively because of their unusual magnetic properties. Despite numerous investigations, the phase relations and magnetic properties are still not understood in detail.

The voluminous literature on pyrrhotite permits but a brief survey of pertinent work. The general nature of the pyrrhotite structure was determined some while ago by Alsen (1925) who assigned to it the arrangement now known as the NiAs-type (B8) structure. Hägg and Sucksdorff (1933) demonstrated that the compositional variations occurred through omission of Fe from sites normally occupied in the NiAs-type structure. Furthermore, they found that troilite and compounds with Fe deficiencies up to $Fe_{.953}S$ displayed a hexagonal superstructure with $a_1=a_2=\sqrt{3}A_1$, $c=2C$†. Following a series of studies of the magnetic properties of artificial Fe-S preparations, Haraldsen (1941) proposed a phase diagram for the system. No phases of symmetry lower than hexagonal were reported and a superstructure was again observed only for "paramagnetic" compositions near troilite. The superstructure was found to invert to a NiAs-type structure at 138° C. Bertaut (1956) subsequently determined the crystal structure of both troilite phases and found that the superstructure was caused by small displacements of Fe atoms normal to $c$ and small displacements of S atoms parallel to $c$. This structure was confirmed by Andresen (1960) who determined improved parameters using neutron diffraction. Also, it is now known that troilite is antiferromagnetic, not paramagnetic as previously proposed. At the 138° C. phase transition the Fe spins shift from an alignment parallel to $c$ to a new antiferromagnetic alignment perpendicular to $c$. A further transition to a paramagnetic structure occurs at a Néel temperature of 325° C. The "ferromagnetic" iron-deficient structures probably possess unbalanced antiferromagnetism, *i.e.*, ferrimagnetism.

The structures with higher iron deficiencies are less well understood. As mentioned above, Haraldsen observed no phases with symmetry lower than hexagonal, and no superstructures other than that of the "paramagnetic" troilite. Byström (1945), however, in investigating powder patterns of natural magnetic pyrrhotite from a number of Swedish localities, surprisingly discovered that the majority of these pyrrhotites were monoclinic with $a\approx B$, $b\approx A$, $c\approx C$; $\beta=90.4°$. No superstructures were observed. In a single-crystal $x$-ray study Buerger (1947) discovered that naturally occurring magnetic pyrrhotites from Morro Velho, Brazil, and Schneeberg, Saxony, exhibited hexagonal superstructures with $a_1=a_2=2A$, $c=4C$. The presence of non-space-group extinctions in the pattern, however, indicated that the specimens were probably twinned, and that the true symmetry of pyrrhotite was perhaps monoclinic or orthorhombic. This superstructure was confirmed by Bertaut (1953) on material of an unspecified nature. Twin-

† Throughout this paper normal lower-case symbols are used to denote the crystallographic axes of the superstructures based on the NiAs-type arrangement, since these are true unit-cell translations. The NiAs-type substructure will be denoted by the hexagonal axes $A_1$, $A_2$, $C$ or, where convenient, by the orthohexagonal axes $A$, $B$, $C$ with $|A|=A_1$, $|B|=\sqrt{3}A_1$. In the past, most authors have used upper-case symbols for the pyrrhotite superstructures.

ning of a monoclinic cell was used to explain the non-space-group extinctions. An additional hexagonal superstructure, $a_1=a_2=3A_1$, $c=2C$, was reported by Graham (1949) for a synthetic pyrrhotite. The composition was unknown but was presumably close to troilite since it was "non-magnetic." Erd *et al.* (1957) discovered naturally occurring $Fe_3S_4$, smythite, which had a rhombohedral superstructure $a_1=a_2=A_1$, $c=6C$.

Further work on the Fe-S phase relations has been done by Eliseev and Denisov (1957), and Grønvold and Haraldsen (1952). The latter authors resolved some of these existing contradictions and, in particular, showed that Byström's monoclinic distortion of the NiAs structure did indeed exist for a very narrow range of compositions around $Fe_7S_8$. This composition was taken as the limit of Fe deficiency, however, and did not extend to $Fe_3S_4$. Also, superstructures (other than that for troilite compositions) were observed only in the range $Fe_{.971}S$-$Fe_{.924}S$ where an unidentifiable superstructure was observed at 185° C.

The superstructures exhibited by the iron-deficient structures are primarily due to ordered arrangement of the iron vacancies. These arrangements have been determined for $Fe_7S_8$ (Bertaut, 1953), $Fe_3S_4$ (Erd *et al.*, 1957) and for several defect superstructures in the iron selenide system where an analogous and equally complex situation exists (Okazaki and Hirakawa, 1956; Okazaki, 1959, 1961). With the exception of $Fe_3S_4$, where unfortunately the crystals were of very poor quality, these structures have been determined only through observation of qualitative relations among the superstructure intensities, and have not been refined. The proposed pyrrhotite superstructure (Bertaut, 1953), with which most of the latter structures have been compared, was determined by finding the ordered array of vacancies which was most favorable energetically. The present study was intended as an attempt to confirm this arrangement by a direct structure determination and refinement. In view of the curious physical properties of the structure, information about atomic displacements around the vacancies and accurate interatomic distances would be of great interest.

## Selection and Composition of Crystals

Natural pyrrhotite from Morro Velho, Brazil, was used in the present study. This material (Harvard Cat. No. 81821) was the same as that previously used by Buerger (1947). Fragments for a single-crystal study were broken from small, well formed hexagonal platelets and ground into spheres using an apparatus similar to that described by Bond (1951). Although care was taken to obtain specimens as free as possible from lineage structure, its effect was still present to some degree even in the best crystals. Polished sections examined in reflected light revealed no evidence for the presence of a second phase even when treated with a variety of etchants.

The pyrrhotite's composition was determined with the aid of an empirical curve relating $d_{10\cdot2}$ to metal content (Arnold and Reichen, 1962). Powder-diffractometer patterns, obtained using CuK$\alpha$ radiation, showed the $10\cdot2$ reflection to be split into two peaks of about equal intensity. This indicated symmetry lower than hexagonal. The superstructure reflections were undetectable. Following Arnold and Reichen's procedure, the powder was then annealed for 26 hours at 575° C. in a sealed, evacuated Vycor tube. This treatment removed the splitting of the $10\cdot2$ reflection. The tungsten powder used in the International Union of Crystallography precision lattice-parameter project (Parrish, 1960) was used as an internal standard. The resulting hexagonal $d_{10\cdot2}$ was was found to be $2.0632\pm.0002$ Å, corresponding to $Fe_{.889}S$ (supposedly accurate to $\pm.23$ atomic per cent). This composition is exactly $Fe_8S_9$, although the deviation from ideal composition $Fe_7S_8$ is slight.

## X-ray Investigation

A single-crystal study of an unannealed spherical crystal was made using the precession method. A zero-level precession photograph taken about one of the supposedly hexagonal $a$ axes is given in Fig. 1. The very strong reflections of the NiAs-type substructure are immediately apparent. A large number of weak superstructure reflections may also be observed which, upon first inspection, appear to require doubling of $A_1$, and quadrupling of $C$. This would require

$$a_1 = a_2 = 2A_1 = 6.88 \text{ Å}$$
$$c = 4C = 22.81.$$

Closer inspection of the reciprocal lattice rows parallel to $C$, however, indicates that those rows which do not contain substructure reflections exhibit only superstructure reflections with $l$ not equal to $4n$. In other words, these reflections occur only in triplets between $l$ values corresponding to substructure reflections. This is the non-space-group extinction rule previously observed by Buerger (1947) and Bertaut (1953), and was found to hold true for such superstructure reflections on *all* levels.

A curious feature of these triplets is illustrated in Fig. 2, in which four sets of these spots from the same

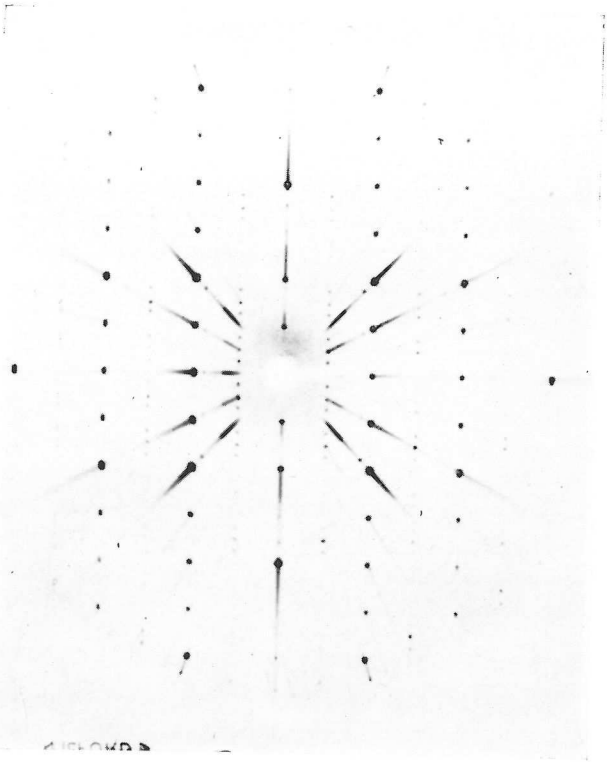

FIG. 1. Precession photograph of pyrrhotite taken about one of the pseudohexagonal $a$ axes. Zero-level MoK$\alpha$, 39 Kv, 15 ma., 39 hour exposure; $c^*$ is vertical, $a^*$ is horizontal. The strong reflections correspond to the NiAs-type substructure.

first-level $a$ axis precession film have been enlarged and assembled together. If pyrrhotite were hexagonal, this level should display symmetry $2mm$ and corresponding spots in the triplet should be equivalent. It may be seen, however, that the intensities do not display this symmetry. In addition, they are not equally spaced, but have small and unequal displacements parallel to $C^*$. The displacements of corresponding spots in the four triplets also bear no symmetric relation to one another. A general reciprocal-lattice level for an axis normal to $C$ is therefore without symmetry of any kind. Furthermore, the irregular displacement of spots parallel to $C^*$ indicates that the superstructure reflections cannot lie on a single reciprocal lattice. This demonstrates conclusively that pyrrhotite is twinned.

## THE TWIN LAW OF PYRRHOTITE

Bertaut (1953) postulated that the pyrrhotite twin was composed of two monoclinic crystals related by a 60° rotation about the pseudohexagonal $c$ axis. A unit cell was proposed with $a=2B$, $B=2a$, $c\approx 4C$, $\beta=90.45°$, and space group $F\ 2/d$. Fig. 3 gives views

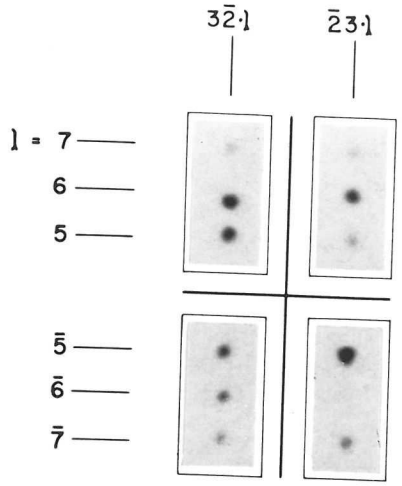


FIG. 2. Enlargement of four sets of superstructure "triplets" taken from a single first-level pseudohexagonal $a$ axis precession photograph. Pseudohexagonal indices have been assigned to the reflections. Hexagonal symmetry would require that the triplets be equivalent. The intensities of corresponding reflections bear no symmetric relation. The spots also have small, unequal displacements parallel to $c^*$.

along the pseudohexagonal axis for two such reciprocal lattices in this orientation. The slight monoclinic distortions have been neglected. The extinction rules for reciprocal-lattice rows parallel to $c^*$ are given by the special symbols indicated. Rows containing substructure reflections are represented by solid symbols; rows containing only superstructure reflections are represented by open symbols. Figure 3 also gives the resulting composite reciprocal lattice. It may be seen that the $l=4n$ extinction rule appears only on two zero levels. Most of the superstructure

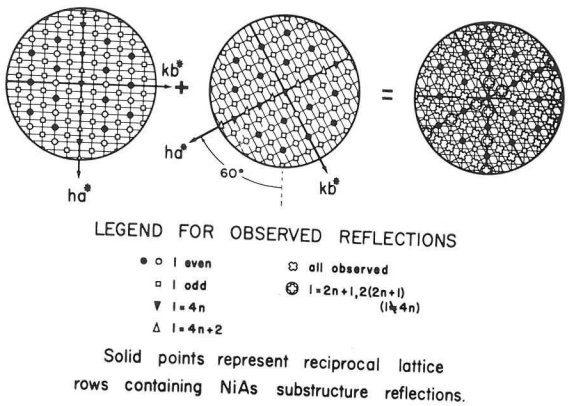


FIG. 3. The twin law previously proposed for pyrrhotite. A face-centered monoclinic cell was postulated. Views along $c^*$ are given for two reciprocal lattices related by the twin operation, and the result of superposing the reciprocal lattices is shown. The various extinction rules are denoted by special symbols.

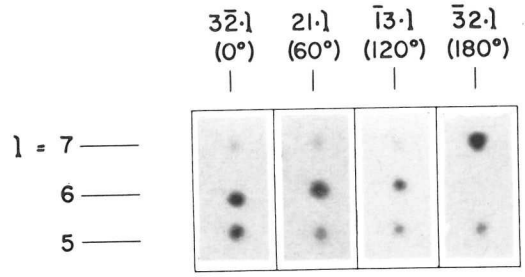


FIG. 4. Comparison of one of the superstructure reflection triplets of Fig. 2 with corresponding sets from precession photographs taken about the neighboring pseudohexagonal $a$ axes. (Pseudohexagonal indices have been assigned to the reflections.)

rows not containing substructure reflections exhibit no extinctions, whereas this "strange" extinction rule is, in fact, observed for most of these rows. Bertaut's cell and twin law therefore do not explain the unobserved reflections.

Only a single set of NiAs-type substructure reflections are observed in the diffraction patterns. Therefore the twin operation must be one which transforms the substructure into itself (or nearly so, if slightly distorted). This situation is common in crystals having substructures, and, indeed, is the physical basis for the twinning. Clearly, no operation isogonal with a hexagonal lattice can give rise to small displacements of the superstructure spots such as those observed if the superstructure lattice is orthogonal. Therefore the true symmetry of pyrrhotite must be monoclinic or triclinic.

Buerger (1960) has shown that the symmetry of a twinned reciprocal lattice is given by the common symmetry of the individuals (when in twinned orientation) augmented by the symmetry of the twin law. If pyrrhotite is monoclinic, a 2-fold axis cannot be oriented parallel to the pseudohexagonal $c$ axis since all candidate operations isogonal with a pseudohexagonal lattice transform this axis into itself. This would require the twin to exhibit at least 2-fold symmetry about this axis. Diffraction symmetry would then introduce a symmetry plane normal to this axis. This is not observed. Therefore if a 2-fold axis is present in pyrrhotite it must be normal to the pseudohexagonal axis.

To determine the symmetry of the twin, zero- and first-level precession patterns were obtained for all of the pseudo-orthohexagonal $a$ and $b$ axes. No rotation about the pseudohexagonal $c$ axis was found which related any two patterns. Figure 4, for example, compares one of the triplets of Fig. 2 with corresponding sets from films taken at 60, 120 and 180 degree intervals. No equivalence is observed. The previously proposed twin law, however, would require two sets to be equivalent.

Only two directions in the twin proved to give identical diffraction patterns upon suitable transformation. Two sets of pseudo-orthohexagonal $b$-axis photographs, for example, were found to be equivalent provided one was rotated 180°. Figure 5 compares pairs of reciprocal lattice rows in this orientation which were taken from first-level films about these two directions. The twinning operation therefore consists of a 60° rotation about the pseudohexagonal $c$ axis followed by a 2-fold rotation about the pseudohexagonal $b$ axis. The combination of these two operations is equivalent to a single 2-fold rotation about the pseudohexagonal $a$ axis midway between the two related $b$ axes.[1] The twin therefore contains crystals corresponding to each operation of the twin axis, unlike the twin resulting from the previously proposed mechanism.

## Orientation of the Twin Axis and Unit Cell

The preceding discussion has described a twinning operation relative to a pseudohexagonal lattice. The nature of the true unit cell and the orientation of the twin axis relative to it have yet to be specified. It may readily be shown that the displacement of spots observed in the precession patterns can arise only if the untwinned lattice is monoclinic.

Let a sublattice of the NiAs-type with true orthohexagonal symmetry be used as a reference system. The diffraction patterns of the twinned crystal indicate apparent doubling of $A$ and $B$. With the twin operation proposed, this may occur only if the actual $a$ and $b$ of the individuals are doubled. Assuming that the superstructure is based on a monoclinic distortion of this substructure, two cases not precluded by the previous discussion are possible. The distortion may be such that the projection of $c$ lies along either the orthohexagonal $A$ or the orthohexagonal $B$ axis of the substructure. The corresponding superstructures for the two possibilities may be expressed by the following general relations:

| *proj. c parallel to A:* | *proj. c parallel to B:* |
|---|---|
| $a = 2A$ | $a = 2B$ |
| $b = 2B$ | $b = -2A$ |
| $c = -\Delta A + nC$ | $c = -\Delta B + nC$ |

*matrix for the transformation:*

$$\begin{matrix} 2 & 0 & 0 \\ 0 & 2 & 0 \\ -\Delta & 0 & n \end{matrix} \qquad \begin{matrix} 0 & 2 & 0 \\ -2 & 0 & 0 \\ 0 & -\Delta & n \end{matrix}$$

[1] See discussion by Professor J. D. H. Donnay following this paper.

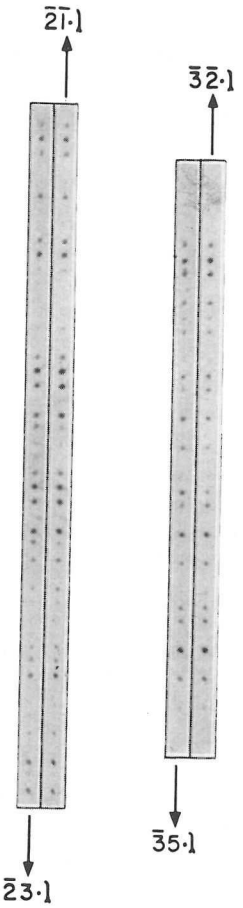


FIG. 5. Comparison of reciprocal-lattice rows related by the twin operation. Rows are compared from precession photographs taken about two first-level pseudo-orthohexagonal $b$ axes which are separated by 60°. One of the films has been rotated 180°. These operations are equivalent to a 2-fold rotation about the pseudohexagonal $a$ axis between the two axes. (Pseudohexagonal indices have been assigned to the reflections.)

where $\Delta$ is a fraction, and $n$ is an integer. Corresponding matrices for the transformation in reciprocal space are given by the transpose of the inverses of the above matrices. Using this relation one obtains:

| *proj. c parallel to A:* | | *proj. c parallel to B:* | |
|---|---|---|---|
| $a^* = \frac{1}{2}A^*$ | $+\frac{1}{2}\frac{\Delta}{n}C^*$ | $a^* =$ | $\frac{1}{2}B^* + \frac{1}{2}\frac{\Delta}{n}C^*$ |
| $b^* = \frac{1}{2}B^*$ | | $b^* = -\frac{1}{2}A^*$ | |
| $c^* =$ | $\frac{1}{n}C^*$ | $C^* =$ | $\frac{1}{n}C^*$ |

From these relations it may be seen that $a^*$ and $b^*$ are halved in the directions of $A^*$ and $B^*$. In both possibilities, however, $a^*$ has an additional component along the pseudohexagonal axis $C^*$. This is the nature of the displacement of spots observed. A triclinic lattice would involve additional components normal to $C^*$. Therefore the pyrrhotite lattice is at least dimensionally monoclinic.

The two monoclinic possibilities may be distinguished from the nature of the splitting of the pseudohexagonal peaks in the powder pattern.[1] It was noted above that the $10\cdot 2$ reflection was spliti nto two components. This behavior will be observed if proj. $c$ is parallel to $B$. If proj. $c$ were parallel to $A$, the peak would be split into three components. Therefore the distortion of the NiAs arrangement is the second of the two cases considered. As mentioned above, $a$ and $b$ appear to be integral multiples of $B$ and $A$ respectively. Since the substructure dimensions are known, it is necessary to assume only that $c$ is also an integral multiple of $C$ in order to permit computation of $\beta$ from the splitting of a substructure reflection. From the magnitude of the $10\cdot 2$ splitting, $\beta$ was found to be 91.79°.

All possible settings of $c$ relative to the twin axis were found to be equivalent upon suitable relabeling of the twins or redefinition of the cell. (Proj. $c$ cannot, however, be normal to the twin axis, for in this case the twin operation is a symmetry element of the lattice.) The twin operation may therefore be described as a 2-fold rotation about [110].

The $l=4n$ extinction rule observed for certain reciprocal lattice rows must be explained by superposition of lattice rows from each of the crystals composing the twin. Since this rule is observed on all levels, it must involve space-group extinctions due to the lattice type. The apparent doubling of $A_1$ can be explained only by assuming that $a=2B$ and $b=2A$. The non-space-group extinctions require superposition of rows with modulo 4 and modulo 2 extinction rules for $l$. It is impossible to find a lattice type which predicts absences with both of these periodicities. The lattice type and the magnitude of the $c$ translation of pyrrhotite are therefore not certain at this time.

This difficulty might arise because of several possible reasons. The superstructure reflections are extremely weak. The superstructure may be such that reflections with a certain periodicity are too weak to be detectable. Another possibility is that further twinning exists, and that the twin actually consists of two or more crystals in twinned orientation which are then further repeated by a rotation about [110]. Also, the composition determined for the specimens was exactly $Fe_8S_9$. While this represents but a slight excess of iron over ideal $Fe_7S_8$, this result may be sig-

[1] Splitting of the peaks in the single-crystal diffraction patterns was suspect because of the presence of lineage structure. In a powder pattern, however, any splitting must be entirely due to the symmetry of the lattice.

nificant. The smallest cell containing a multiple of $Fe_8S_9$ requires $c=9C$. This is incompatible with the apparent quadrupling of $C$. It is therefore possible that the specimens investigated were actually intergrowths of two phases despite the fact that no physical evidence for this could be found.

### The Nature of the Superstructure

If the superstructure were primarily due to ordering of Fe vacancies, a determination of the structure would be comparatively simple. The superstructure reflections would have zero intensity if all Fe sites in the NiAs-type structure were occupied. Therefore, if only superstructure reflections are considered, the diffraction effect of an ordered arrangement of vacancies is completely equivalent to a structure in which Fe atoms alone occupy the vacancy sites. A Patterson function based on superstructure reflections should then exhibit maxima only in locations corresponding to certain of the Fe-Fe peaks of a NiAs arrangement. Consideration of the NiAs structure shows that in projection these peaks may occur only on a sublattice given by $a'=\frac{1}{2}A$, $c'=\frac{1}{2}C$; or $b'=\frac{1}{2}B$, $c'=\frac{1}{2}C$.

A complete set of three-dimensional intensities was collected from a twinned crystal of pyrrhotite. Some reflections were slightly split due to lineage structure or imperfect superposition of reflections arising from different crystals in the twin. Therefore the intensities were recorded with an integrating precession camera. The effect of splitting of spots is minimized in this technique since all portions of the spot eventually contribute to the "plateau" of the integrated spot as the film is moved through a cycle. No symmetry was assumed for the twin. An amount of data equivalent to a complete CuK$\alpha$ sphere was recorded.

Patterson projections along the $a$ and $b$ axes of one of the twins were synthesized using only superstructure reflections. Surprisingly, virtually none of the peaks fell on locations corresponding to Fe-Fe interactions for a NiAs arrangement. The calculated weight of such interactions was only slightly above the background of the maps. The observed maxima were not circular, but rather suggested interactions between portions of atoms. It therefore appears that the superstructure intensities are primarily due to distortions of the NiAs-type structure about the vacancies. Analysis of 3-dimensional Patterson maps is currently in progress.

### Acknowledgments

The authors are indebted to Professor Clifford Frondel for supplying the specimen of pyrrhotite used in the study, and to Dr. Donald Peacor for many helpful discussions. The necessary computations were performed on the I.B.M. 7090 computer at the M.I.T. Computation Center. This work was performed under a grant from the National Science Foundation.

### References

Alsen, Nils (1925) Röntgenographische Untersuchung der Kristallstrukturen von Magnetkies, Breithauptite, Pentlandite, Millerite und verwandten Verbindungen. *Geol. Fören. Stockh. Förh.*, **47**, 19–72.

Andresen, Arne F. (1960) Magnetic phase transitions in stoichiometric FeS studied by means of neutron diffraction. *Acta Chem. Scand.*, **14**, 919–926.

Arnold, R. G. and Laura E. Reichen (1962) Measurement of the metal content of naturally occurring, metal-deficient, hexagonal pyrrhotite by an x-ray spacing method. *Am. Mineral.* **47**, 105–111.

Bertaut, E. F. (1953) Contribution a l'étude des structures lacunaires: La pyrrhotine. *Acta Cryst.* **6**, 557–561.

——— (1956), Structure de FeS stoechiométrique. *Bull. soc. franç. Minér. Crist.* **79**, 276–292.

Bond, W. L. (1951) Making small spheres. *Rev. Sci. Inst.* **22**, 344–345.

Buerger, M. J. (1947) The cell and symmetry of pyrrhotite. *Am. Mineral.* **32**, 411–414.

——— (1960) *Crystal Structure Analysis.* John Wiley and Sons, New York, 53–67.

Byström, Anders (1945) Monoclinic magnetic pyrites. *Ark. Kemi. Mineral. Geol.* **19**, 1–8.

Eliseev, E. N. and A. P. Denisov (1957) X-ray studies of pyrrhotite. *Vestnik Leningrad Univ.* **12**, No. 18, *Ser. Geol. Geog.* **3**, 68–78.

Erd, Richard C., Howard T. Evans and Donald H. Richter (1957) Smythite, a new iron sulfide, and associated pyrrhotite from Indiana. *Am. Mineral.* **42**, 309–333.

Graham, A. R. (1949) Artificial pyrrhotite. *Am. Mineral.* **34**, 462–464.

Grønvold, Fredrik and Haakon Haraldsen (1952) On the phase relations of synthetic and natural pyrrhotites ($Fe_{1-x}S$). *Acta Chem. Scand.* **6**, 1452–1469.

Hägg, Gunnar and Ingrid Sucksdorff (1933) Die Kristallstruktur von Troilite und Magnetkies. *Zeit. physik. Chem.* **B22**, 444–452.

Haraldsen, Haakon (1941) Über die Hochtemperaturumwandlungen der Eisen (II)-Sulfidmischkristalle. *Zeit. anorg. Chem.* **246**, 195–226.

Okazaki, Atsushi (1959) The variation of superstructure in iron selenide $Fe_7Se_8$. *Jour. Phys. Soc. Japan*, **14**, 112–113.

——— (1961) The superstructures of iron selenide $Fe_7Se_8$. *Jour. Phys. Soc. Japan*, **16**, 1162–1170.

——— and Kinshiro Hirakawa (1956) Structural study of iron selenides $FeSe_x$. I. Ordered arrangement of defects of Fe atoms. *Jour. Phys. Soc. Japan*, **11**, 930–936.

Parrish, William (1960) Results of the I. U. Cr. precision lattice-parameter project. *Acta Cryst.* **13**, 838–850.

### Discussion

J. D. H. Donnay (Baltimore): 1. Does the twin contain only two crystals?

2. If the twin operation consists of the product of two rotations $[c \text{ axis}]_{60°} \times [\text{horizontal axis}]_{180°}$, it should be possible to define it as a single rotation about another axis. If crystal I and crystal II in the twin are related by a 180°-rotation, it is easier to understand why the twinning is not repeated by further 60°-rotations. H. Curien (Paris, France) remarks that the new axis is horizontal and lies at 30° to the horizontal axis used in the two-rotation definition.

Author's reply: 1. Only one operation was found which related the diffraction effects observed. Therefore it was assumed that only two crystals were present in the twin.

2. The two-rotation definition was useful since it consists of operations which may actually be performed with precession photographs, taken about different directions of the twin. It is correct that the operations may be described in terms of a single rotation and that this is obviously the best crystallographic description of the twinning operation. Accordingly, this is the final description of the twin law which has been given in the text.

MINERALOGICAL SOCIETY OF AMERICA, SPECIAL PAPER 1, 1963
INTERNATIONAL MINERALOGICAL ASSOCIATION, PAPERS, THIRD GENERAL MEETING

# THE CRYSTAL STRUCTURE OF CHALCOCITE, $Cu_2S$

BERNHARDT J. WUENSCH AND M. J. BUERGER
*Crystallographic Laboratory, Massachusetts Institute of Technology, Cambridge, Massachusetts*

ABSTRACT

The crystal structures of the high- and low-temperature forms of Bristol, Conn., chalcocite have been investigated with single-crystal methods. At 125° C., high-chalcocite has lattice constants $a=3.95$ and $c=6.75$ Å, and space group $P6_3/mmc$. The sulfur atoms are arranged in hexagonal close-packing. The copper atoms are disordered. The most satisfactory approximation to the structure contains Cu atoms statistically distributed in three types of sites. Cu′ is in three-fold coordination and forms of trigonal Cu-S layer. Cu″ occupies the tetrahedral interstices. Cu‴ is in two-fold coordination and links S atoms in neighboring Cu-S sheets.

All electron density in the low-chalcocite substructure is confined to locations corresponding to positions on the 3-fold or 6-fold axes of high-chalcocite. A structure similar to that of stromeyerite, CuAgS, may be derived from that of high-chalcocite by appropriate displacements of the copper atoms. The low-chalcocite structure is very likely a similar derivative structure.

## INTRODUCTION

Until about twenty years ago, it was believed that chalcocite, $Cu_2S$, was dimorphous and existed in orthorhombic and isometric modifications. N. W. Buerger (1941), however, showed that while chalcocite was indeed orthorhombic below about 110° C, stoichiometric $Cu_2S$ actually transformed to a hexagonal phase. Compositions deficient in copper, on the other hand, transformed into this hexagonal phase plus an isometric phase. The isometric structure had composition near $Cu_9S_5$ and was shown to be identical with what had been called isometric chalcocite (N. W. Buerger, 1942). The name digenite was proposed for this cubic modification. Electrical conductivity measurements (Hirahara, 1947) indicated a further phase transition in $Cu_2S$ at 450° C. Ueda (1949) found that this new phase was similar to digenite. In a careful re-examination of the phase relations in the system, Djurle (1958*a*) confirmed this transformation, but, in addition, discovered two new phases at composition $Cu_{1.96}S$. At room temperature crystals of this composition had an unidentifiable structure of low symmetry. At higher temperatures a relatively simple metastable tetragonal structure was formed. It was found that all compositions between $Cu_2S$ and $Cu_{1.8}S$ transformed into a digenite-like phase at a sufficiently high temperature. Dignite may therefore be described as $Cu_{2-x}S$ with $x$ between 0 and at least 0.2.

The nomenclature "low-chalcocite" and "high-chalcocite" will be preserved in this paper for the orthorhombic and hexagonal modifications, respectively, of stoichiometric $Cu_2S$. The two phases are related by a reversible transformation. The high-temperature form cannot be quenched. M. J. Buerger and N. W. Buerger (1944) showed that an interesting substructure-superstructure relation exists between the unit cells of the two structures. The diffraction patterns of low-chalcocite contained weak reflections in addition to those displayed by the hexagonal form. These additional reflections indicated that the axes of the low-chalcocite unit cell were multiples of 3, 4 and 2 of the cell edges of the orthohexagonal cell of high-chalcocite in the $a$, $b$ and $c$ directions respectively. This relation is illustrated in Fig. 1, in which the lattice points of the $A$-centered low-chalcocite cell are given by solid points and the lattice points of the hexagonal high-chalcocite cell by open points. The diffraction symbol for high-chalcocite permitted $P6_3mc$, $P3/m2c$ and $P6_3/mmc$ as possible space groups; low-chalcocite had $Abmm$, $Ab2m$ and $Abm2$ as possible space groups. By assuming that the space

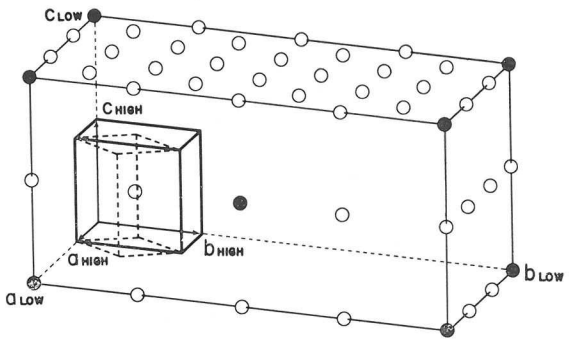


FIG. 1. Relation between the orthohexagonal unit cell of high-chalcocite and the $A$-centered orthorhombic unit cell of low-chalcocite. The lattice points of high-chalcocite are indicated by open points, and those of low-chalcocite by solid points. The hexagonal cell of high-chalcocite is indicated by heavy dotted lines.

group of low-chalcocite was derived from that of high-chalcocite through the suppression of certain symmetry elements, it was possible to assign space group $Ab2m$ ($C_{2V}^{15}$) to low-chalcocite, and space group $P6_3/mmc$ ($D_{6h}^{4}$) to high-chalcocite. The acentric orthorhombic structure contains 96 $Cu_2S$ per unit cell and is quite complex. The hexagonal cell of high-chalcocite, on the other hand, contains only 2 $Cu_2S$ per cell.

An attempt to solve the relatively simple high-chalcocite structure from powder data (Klubock and Buerger, 1945, unpublished) was unsuccessful. Belov and Butuzov (1946), however, considered the several reasonable structures permitted by the high-chalcocite space group. They proposed as a structure that model which gave the best fit with a set of intensities estimated from a high-chalcocite Weissenberg photograph published by Buerger and Buerger (1944). The agreement was rather unsatisfactory. Ueda (1949) attempted a structure determination on the basis of visual estimation of intensities from powder patterns. None of the likely structures permitted by the space group yielded a satisfactory set of structure factors. Calculations were also made for arrangements of sulfur atoms alone. Curiously, it was found that a hexagonal close-packed arrangement gave structure factors in reasonable agreement with those observed. From this Ueda concluded that the copper atoms were in complete disorder.

The present paper describes a single-crystal investigation of the structure of high-chalcocite and discusses the probable relation of this structure to that of low-chalcocite. Refinement of the low-chalcocite structure is in progress and will be described in a subsequent paper.

## Equipoint Restrictions and Nature of the Patterson Function for High-Chalcocite

The unit cell of high-chalcocite contains only 2 $Cu_2S$. This requires that ordered Cu and S atoms occupy special positions. Table 1 lists posible equipoints for the probable high-chalcocite space group $P6_3/mmc$. (It is interesting to note that examination of the other two possible space groups, $P3/m2c$ and $P6_3mc$, shows that the former has special positions identical with those listed, and that the latter has but two possibilities which are included in the list.) The S atoms may be accommodated in only one equipoint of rank 2. The Cu atoms may be accommodated in either two equipoints of rank 2, or a single equipoint of rank 4. A total of 20 arrangements of atoms in these equipoints is possible. Three possibilities, however, result in $c$ being half that actually observed and may be discarded. Of the remaining arrangements, only 9 combinations are distinct.

Table I. Special Positions Lying on the 6-fold and 3-Fold Axes in Space Groups $P\,6_3/mmc$ and $P3/m2c$

| Equi-point | Coordinates in hexagonal cell | | Corresponding coordinates in 2-dimensional representation | |
|---|---|---|---|---|
| 2*a* | 0 0 0 | 0 0 $\frac{1}{2}$ | 0 0 | 0 $\frac{1}{2}$ |
| 2*b* | 0 0 0 | 0 0 $\frac{3}{4}$ | 0 0 | 0 $\frac{3}{4}$ |
| 2*c* | $\frac{1}{3}$ $\frac{2}{3}$ $\frac{1}{4}$ | $\frac{2}{3}$ $\frac{1}{3}$ $\frac{3}{4}$ | $\frac{2}{3}$ $\frac{1}{4}$ | $\frac{1}{3}$ $\frac{3}{4}$ |
| 2*d* | $\frac{1}{3}$ $\frac{2}{3}$ $\frac{3}{4}$ | $\frac{2}{3}$ $\frac{1}{3}$ $\frac{1}{4}$ | $\frac{2}{3}$ $\frac{3}{4}$ | $\frac{1}{3}$ $\frac{1}{4}$ |
| 4*e* | 0 0 $z$<br>0 0 $\frac{1}{2}+z$ | 0 0 $\bar{z}$<br>0 0 $\frac{1}{2}-z$ | 0 $z$<br>0 $\frac{1}{2}+z$ | 0 $\bar{z}$<br>0 $\frac{1}{2}-z$ |
| 4*f* | $\frac{1}{3}$ $\frac{2}{3}$ $z$<br>$\frac{2}{3}$ $\frac{1}{3}$ $\frac{1}{2}+z$ | $\frac{2}{3}$ $\frac{1}{3}$ $\bar{z}$<br>$\frac{1}{3}$ $\frac{2}{3}$ $\frac{1}{2}-z$ | $\frac{2}{3}$ $z$<br>$\frac{1}{3}$ $\frac{1}{2}+z$ | $\frac{1}{3}$ $\bar{z}$<br>$\frac{2}{3}$ $\frac{1}{2}-z$ |

Solution of a three-dimensional Patterson function involving atoms in these equipoints may be considerably simplified by noting that these special positions lie on the 3-fold and 6-fold axes in the hexagonal cell. These axes all lie on a (110) plane through the hexagonal cell. Fig. 1 shows that this plane is equivalent to the section (0$yz$) in the orthohexagonal cell. Analysis of three-dimensional Patterson maps is therefore reduced to a two-dimensional problem, since only this special section need be considered. Equipoint coordinates in this section are also given in Table 1.

## Investigation of the Low-Chalcocite Structure

An attempt was at first made to determine the crystal structure of low-chalcocite directly. A small fragment of Bristol, Connecticut, chalcocite was used in collecting a three-dimensional set of intensities. Using an equi-inclination Geiger-counter diffractometer, all of the accessible independent reflections in a MoK$\alpha$ sphere were investigated. The superstructure reflections were generally quite weak and a large number were not detectable. A total of 584 independent intensities were collected. Of these 76, or roughly 13%, were substructure reflections. Appropriate corrections were made for Lorentz and polarization factors. Absorption effects were not too serious and corrections were not made at this stage of the analysis.

A set of three-dimensional Patterson maps were synthesized. As might be expected, these were completely dominated by the marked substructure and

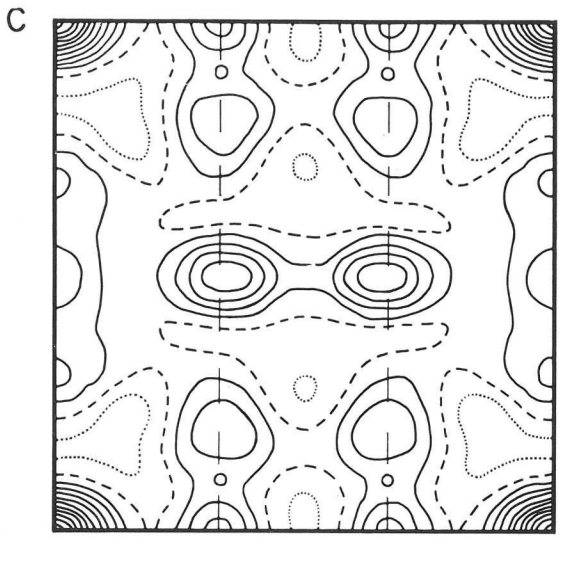


FIG. 2. Low-chalcocite substructure Patterson section $P(0yz)$. The lines $\frac{1}{3}z$ and $\frac{2}{3}z$ correspond to the location of the 3-fold axes in high-chalcocite. Contours at equal but arbitrary intervals. Negative contours dotted, zero contour dashed, positive contours solid lines.

proved to be uninterpretable. It was then hoped that analysis of the substructure alone might indicate the structure of high-chalcocite and yield some clue to the nature of the distortions responsible for the low-chalcocite superstructure.

Accordingly, three-dimensional Patterson maps were synthesized using only squares of structure factors obtained from the substructure reflections. These data had marked pseudo-hexagonal symmetry. The departures from this symmetry were significant enough, however, to warrant treatment of the data as orthorhombic. It was found that all peaks in the maps lay in the section $0yz$ of the orthorhombic cell. The coordinate $y$ had only values of 0, $\frac{1}{3}$ or $\frac{2}{3}$. Therefore all electron density in the substructure is located at positions corresponding to special positions on the 3-fold and 6-fold axes in the hexagonal high-chalcocite cell.

The problem could then be treated as a two-dimensional one, as outlined in the preceding section. The Patterson section $P(0yz)$ is given in Fig. 2. None of the nine possible high-chalcocite structures yield Patterson maps which compare favorably with this section. In fact, it is readily seen that this map contains contradictory features: the peaks having coordinates of roughly (0, .3) and ($\frac{1}{3}$, .2) would require Cu in the 4-fold position having a variable parameter $z$. On the other hand, the strong peak at ($\frac{1}{3}$, 0) requires Cu in a position having the same $z$ parameter as S, that is, in a symmetry-fixed 2-fold position. This map therefore had no clear-cut interpretation and suggested that an appreciable amount of electron density of displaced atoms in the low-chalcocite structure contributes to the substructure. This made a direct determination of the high-chalcocite structure advisable.

## INVESTIGATION OF THE HIGH-CHALCOCITE STRUCTURE

*Selection of material.* Well-crystallized chalcocite from Bristol, Connecticut, was also used for this investigation. An attempt was made to grind spheres from this material using an apparatus similar to that described by Bond (1951). It was found that irregular fragments rapidly assumed the form of oblate ellipsoids but, upon further grinding, became misshapen pellets. The specimen finally selected was untwinned and had the form of an oblate ellipsoid of revolution with dimensions .505×.505×.251 mm. ($\mu r_{max}=6.26$, $\mu r_{min}=3.11$ for MoK$\alpha$ radiation). It was felt that this regular shape, for which exact absorption corrections could be made, was to be preferred to an irregular pellet which would require a smaller but less exact correction. Also, the specimen must be held at an elevated temperature while the intensities are collected. Chalcocite gradually deteriorates when heated in air. The larger regular shape had the advantage of having a higher volume-to-surface ratio, which makes this effect less serious.

*Collection of intensities.* A photographic technique was used to record the intensities. All reflections on a given level were therefore equally affected by any slight deterioration of the crystal. The method also had the advantage of providing evidence that no superstructure reflections were present. This would have permitted detection of a drop in temperature had the heating unit malfunctioned during the course of collecting the intensities.

Intensities were recorded with the aid of an integrating precession camera. The crystal was maintained at 125°±5° C. by a small radiant heater similar to one described by Morimoto and England (1960). The unit cell dimensions determined are in good agreement with those determined by Buerger and Buerger (1944) and Djurle (1958) as shown in Table II.

A disadvantage of recording intensities by the precession method is that the blind region in the center of upper level films obscures certain reflections. This usually requires use of several settings of the spindle

axis if all attainable reflections are to be recorded. Because high-chalcocite has high symmetry and a small unit cell, all independent reflections lay outside of the blind region. It was therefore possible to record all intensities with one setting of the spindle axis. Several exposure times were used to insure that the linearity range of the film was not exceeded.

All films were developed simultaneously. Intensities were determined with a Joyce-Loebl Company double-beam recording microdensitometer. A total of 106 reflections were measured. Of 37 independent reflections, 7 were undetectable and were assigned half the minimum observable value. Lorentz and polarization corrections were computed for each reflection of the pair which compose a spot on the film. Transmission factors for each reflection of the pair were determined using a program for the I.B.M. 7090 computer (Wuensch and Prewitt, 1962). These transmission factors were suitably combined with the individual Lorentz and polarization factors. After applying these corrections, the average deviation between equivalent $F^2$'s was 9.5%.

*Solution of the structure.* A three-dimensional Patterson function was synthesized using the I.B.M. 7090 program ERFR2 (Sly, Shoemaker and Van den Hende, 1962, unpublished). The problem was again reduced to a two-dimensional problem by considering the ortho hexagonal section $P(0yz)$, Fig. 3. It may be noted that this map is similar to the corresponding low-chalcocite substructure Patterson section, Fig. 2, except that the contradictory peak at $\frac{1}{3}$, 0 has diminished. The maxima with variable parameter, $z$, however, are no longer discrete peaks, but are instead smeared out over a considerable region of the cell. Fig. 4, for example, gives the Patterson section $P(xy\frac{1}{6})$. The distribution of the maximum is practically uniform except for very slight peaks in three symmetric locations about the 3-fold axis. The

TABLE II. UNIT-CELL DIMENSIONS OF HIGH-CHALCOCITE

| T | Buerger and Buerger (1944) | Present[1] study | Djurle (1958) | | |
|---|---|---|---|---|---|
| | 112° | 1.25° | 152° | 300° | 460° |
| c (Å) | 6.68 | 6.75 | 6.722 | 6.761 | 6.806 |
| a (Å) | 3.89 | 3.95 | 3.961 | 3.981 | 4.005 |
| c/a | 1.717 | 1.710 | 1.697 | 1.698 | 1.699 |

[1] Precision .3%, accuracy about 1%.

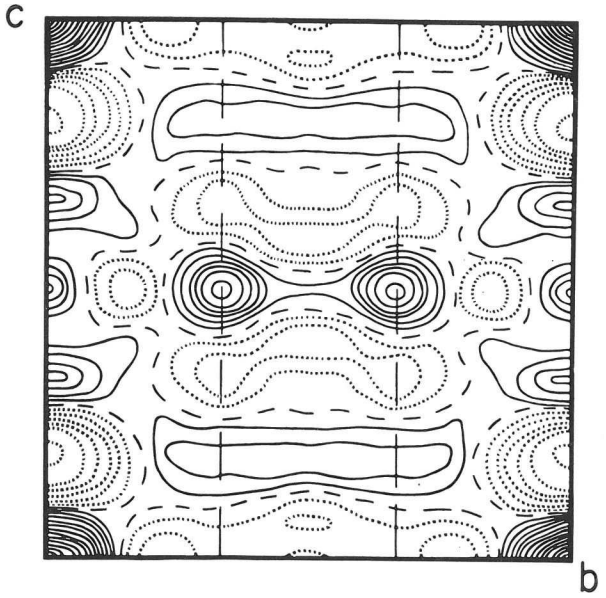


FIG. 3. High-chalcocite Patterson section $P(0yz)$ for the orthohexagonal cell. The lines $\frac{1}{3}z$ and $\frac{2}{3}z$ correspond to the location of the 3-fold axes. Countours at equal but arbitrary intervals. Negative contours dotted, zero contour dashed, positive contours solid lines.

copper atoms are therefore disordered. This suggests that the Cu atoms are disordered. As a result, none of the nine "ideal" structures considered in the previous section predicted Patterson functions in reasonable agreement with Fig. 3.

The structure was solved with the aid of implication diagrams (Buerger, 1959) and successive electron density and difference maps. For structures containing a $6_3$ axis of symmetry, the implication map $I_3(xy0)$ gives a projection of the structure along $c$ with a 3-fold ambiguity (*i.e.*, the projected atoms are

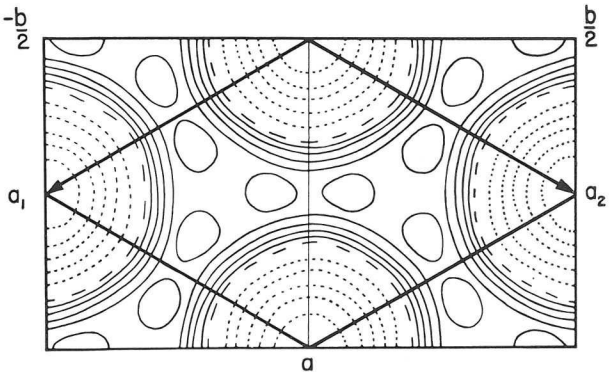


FIG. 4. High-chalcocite Patterson section $P(xy\frac{1}{6})$. Both the hexagonal cell and the orthohexagonal cell are indicated. Negative contours dotted, zero contour dashed, positive contours solid lines at half the interval of Fig. 3.

produced about both the $6_3$ axis and the two 3-fold axes of the cell). The implication map $I_6(xy\frac{1}{2})$ gives the structure without ambiguities, but with satellite peaks located at distances from the origin which are twice those of the atomic coordinates. These maps revealed that the main part of the electron density not confined to the $6_3$ and 3-fold axes had $x$, $y$ coordinates of 0, $\frac{1}{2}$. In space group $P6_3/mmc$ this is special position $6g(0\frac{1}{2}0)$.

Three-dimensional electron density maps were then synthesized using structure-factor signs based on hexagonal close-packed sulfur atoms and various fractions of Cu in equipoint 6*g*. These maps all indicated positions $2b(00\frac{1}{4})$ and $4f(\frac{1}{3}\frac{2}{3}z)$, with $z\approx.6$ as additional sites of high Cu density. Further electron density and difference maps based on Cu atoms in one or two of these three suggested sites always returned the density in the remaining sites. This distribution of Cu was therefore taken as the correct approximation to the mobile Cu atoms. The final electron density maps showed electron density connecting the three Cu sites. The Cu atoms are therefore "smeared" as suggested above.

*Refinement.* Refinement was performed on the I.B.M. 7090 computer with the full-matrix least-squares program SFLSQ3 (Prewitt, 1962, unpublished). Only one scale factor was used. Reflections were initially assigned equal weights, but were weighted by $1/F_o$ in the final cycles.

In addition to the usual parameters, the weights of the three types of Cu atoms were also refined, subject to the restraint that the sum of the Cu atoms per unit cell be equal to 4. Following each series of cycles the distribution of weight was tested with electron density and difference maps. The Cu distribution given in Table III yielded a disagreement factor $R=\Sigma\big|\,|F_o|-|F_s|\,\big|/\Sigma|F_o|$ of 32% when the unobserved reflections were excluded. Observed and calculated structure factors are compared in Table IV. Investigation of the improvement of the agreement between $F_c$ and $F_o$ with variations in Cu distribution is being continued.

TABLE III. COORDINATES AND WEIGHTS OF ATOMS IN FINAL APPROXIMATION TO DISORDERED HIGH-CHALCOCITE STRUCTURE

| Atom | Equipoint | Coordinates | Temperature factor |
|---|---|---|---|
| 1 S | 2*d* | $\frac{2}{3}\ \frac{1}{3}\ \frac{1}{4}$ | .43 |
| .870 Cu′ | 2*b* | 0 0 $\frac{1}{4}$ | .15 |
| .355 C″ | 4*f* | $\frac{1}{3}\ \frac{2}{3}$ .568 | 4.73 |
| .140 Cu‴ | 6*g* | 0 $\frac{1}{2}$ 0 | 3.28 |

TABLE IV. OBSERVED AND CALCULATED STRUCTURE FACTORS

| *hkl* | $F_o$ | $F_c$ | *hkl* | $F_o$ | $F_c$ |
|---|---|---|---|---|---|
| 00·4 | 11.56 | 11.94 | 30·0 | 6.06 | 10.63 |
| 00·6 | 9.86 | −10.02 | 30·1 | 0.83[1] | 0.00 |
| 00·8 | 3.24 | 2.42 | 30·2 | 6.37 | − 6.41 |
| 10·1 | 2.06 | 2.26 | 30·3 | 1.89 | 0.00 |
| 10·2 | 10.81 | − 8.85 | 30·4 | 3.67 | 2.76 |
| 10·3 | 14.95 | − 7.41 | 11·0 | 5.60 | 16.26 |
| 10·4 | 2.68 | 4.80 | 11·2 | 8.48 | − 9.12 |
| 10·5 | 2.05 | 1.24 | 11·4 | 6.83 | 9.02 |
| 10·6 | 0.99[1] | − 1.69 | 11·6 | 6.01 | − 2.92 |
| 10.7 | 3.40 | − 2.31 | 21·0 | 4.01 | 2.96 |
| 20·0 | 2.93 | 4.57 | 21·1 | 3.02 | 2.10 |
| 20·1 | 5.11 | − 2.07 | 21·2 | 1.79 | − 5.06 |
| 20·2 | 5.12 | − 5.01 | 21·3 | 3.33 | − 4.23 |
| 20·3 | 5.11 | 5.42 | 21·4 | 0.84[1] | 0.04 |
| 20·4 | 6.73 | 4.77 | 21·5 | 1.09[1] | − 2.32 |
| 20·5 | 1.87 | − 1.92 | 21·6 | 1.00[1] | 1.21 |
| 20·6 | 7.40 | 1.31 | 31·0 | 1.88 | − 1.31 |
| | | | 31·1 | 2.60 | − 2.33 |
| | | | 31·2 | 1.26[1] | 1.30 |
| | | | 31·3 | 0.73[1] | − 2.17 |

[1] One-half minimum observable value.

## DISCUSSION OF THE STRUCTURE

The disordered high-chalcocite structure contains sulfur atoms in hexagonal close-packing and mobile Cu atoms statistically occupying 3 types of sites. Cu′ lies in the S layers forming a trigonal Cu-S sheet. Cu″ occupies the available tetrahedral sites. Covellite, CuS, also exhibits a curious combination of CuS layers and tetrahedrally coordinated Cu. The remaining Cu‴ atoms are located on three edges of the S tetrahedron and thus statistically link an S atom to three S atoms in the neighboring sheet. Two-fold coordination is found also in $Cu_2O$.

The Cu-S bond lengths are 2.28 and 2.06 Å for Cu′ and Cu‴ respectively. Cu″ is not located in the center of the S tetrahedron, but has three neighbors at 2.59 Å and one at 2.15 Å. With the exception of Cu‴-S, these distances are in reasonable agreement with values of 2.26 and 2.29 Å found in CuAgS (Frueh, 1955). The distance Cu′-Cu″ is 2.59 Å, in good agreement with the distance 2.556 Å found in metallic copper. Cu″ and Cu‴, however, are too close to be occupied simultaneously in an ordered structure.

It is of interest to compare the disordered high-chalcocite structure with that of stromeyerite (Frueh, 1955) which is illustrated in Fig. 5. The structure

consists of alternate layers of hexagonal Cu-S rings and close-packed Ag sheets. The mineral is orthorhombic, but is markedly pseudohexagonal as illustrated by the bond angles indicated in the Cu-S and Ag layers. The Cu-S sheets are stacked in nearly hexagonal close-packing. The Ag layers, however, are displaced along *b* such that each Ag atom is coordinated by two S atoms in neighboring layers. The sheets are knit together by these zig-zag Ag-S chains.

The relative arrangement of the layers in stromeyerite is perhaps best illustrated by the arrangement of atoms lying in the section (0*yz*) of the unit cell. This section is compared with the corresponding section of the idealized high-chalcocite structure in Fig. 6. The unit-cell dimensions of the two structures are quite similar, with the exception of the *c* axis. This difference is in part due to the larger radius of the Ag atom.

It may be seen that the structures differ only in two respects. The Ag atom in stromeyerite links a S atom to only one S atom in the neighboring sheet, while the corresponding S in high-chalcocite is statistically linked to all three neighboring S. Secondly, some of the Cu has escaped into the tetrahedral sites. Consequently, stromeyerite may be considered a derivative structure of the disordered high-chalcocite structure, formed by ordering the linkage between

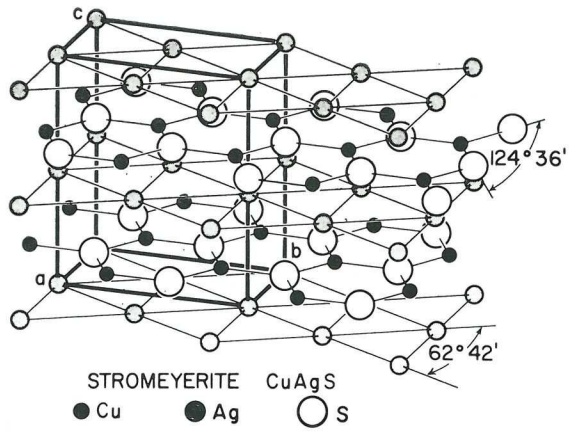


FIG. 5. The crystal structure of stromeyerite, CuAgS.

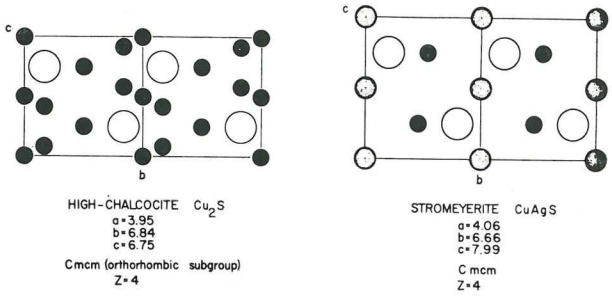


FIG. 6. Comparison of crystallographic data and electron density sections 0*yz* for the disordered high-chalcocite structure and stromeyerite.

Cu-S sheets and by relegating the remaining tetrahedral Cu to the Cu-S sheet.

At 93° C stromeyerite undergoes a phase transformation to a hexagonal modification (Djurle, 1958*b*), in striking similarity to the transformation in low-chalcocite at 110° C. The structures therefore have similar thermal properties and it seems very likely that the structure of high-stromeyerite may involve disorder of the type found for high-chalcocite. Furthermore, this may be the nature of the displacements relating high- and low-chalcocite. As mentioned above, the low-chalcocite substructure Patterson maps indicate a larger fraction of Cu occupying the Cu-S sheets. The relation between stromeyerite and high-chalcocite is compatible with such a displacement. Refinement of a model structure for low-chalcocite based on a suitable stromeyerite-like arrangement of atoms is in progress and will be described in a subsequent paper.

## ACKNOWLEDGEMENTS

The authors are indebted to Dr. J. T. England of the Geophysical Laboratory for the design of the precession camera heating unit, and to Professor Alexander Rich of the Department of Biology, M.I.T., for the use of his laboratory's densitometer. All computations were performed on the I.B.M. 7090 computer at the M.I.T. Computation Center. This work was supported by a grant from the National Science Foundation.

## REFERENCES

BELOV, N. V. AND V. P. BUTUZOV (1946) The structure of high-chalcocite, $Cu_2S$. *C. R. Acad. Sci. U. S. S. R.* **54,** 717–720.

BOND, W. L. (1951) Making small spheres. *Rev. Sci. Inst.* **22,** 344–345.

BUERGER, NEWTON W. (1941) The chalcocite problem. *Econ. Geol.* **36,** 19–44.

——— (1942) *X*-ray evidence of the existence of the mineral digenite, $Cu_9S_5$. *Am. Mineral.* **27,** 712–716.

BUERGER, M. J. (1959) *Vector Space and Its Application Its Crystal-Structure Investigation.* John Wiley & Sons, New York, pp. 145–167.

——— AND NEWTON W. BUERGER (1944) Low-chalcocite and high-chalcocite. *Am. Mineral.* **29,** 55–65.

DJURLE, SEVED (1958a), An x-ray study on the system Cu-S. *Acta Chem. Scand.* **12,** 1415–1426.

——— (1958b) An x-ray study on the system Ag-Cu-S. *Acta*

*Chem. Scand.* **12,** 1427–1436.

FRUEH, ALFRED J. (1955) The crystal structure of stromeyerite, AgCuS: A possible defect structure. *Zeit. Krist.* **106,** 299–307.

HIRAHARA, EIJI (1947) Experimental studies on the electric conduction and heat capacity of cuprous sulfide semiconductors. *Jour. Phys. Soc. Japan,* **2,** 211–213.

MORIMOTO, N. AND J. T. ENGLAND (1960) High-temperature Buerger precession camera. *Carnegie Institution of Washington Year Book,* **59,** 175.

UEDA, RYUZO (1949) X-ray and thermal studies on the phase transitions of cuprous sulfide $Cu_2S$. *Jour. Phys. Soc. Japan,* **3,** 287–292.

WUENSCH, BERNHARDT J. AND C. T. PREWITT (1962) X-ray absorption corrections for a crystal of arbitrary shape (to be published).

---

## DISCUSSION

N. MORIMOTO (Tokyo): 1. How do you deal with the moving Cu atoms in the structure in order to calculate structure factors?

2. What is the most important difference between your structure and Belov's structure?

AUTHOR'S REPLY: 1. Inasmuch as the Cu atoms are somewhat "smeared," there is no really satisfactory way of treating this problem. The best approximation used was to split the Cu atoms into fractional parts. Even this treatment, however, assumes atoms distributed statistically in an equipoint of higher rank and not a continuous "cloud."

2. Belov and Butuzov proposed an ordered, symmetry-fixed structure with 2S in 2*c*, 2Cu in 2*b* and 2Cu in 2*d*. The structure consists of S atoms in hexagonal close-packing. The Cu atoms occupy all the triangular interstices in the S layers.

P. R. BRETT (Washington, D. C.): Have the authors analyzed the chalcocite with which they worked? *X*-ray diffractometer studies at the Geophysical Laboratory on synthetic chalcocite show that both the position and intensity of reflections can change markedly by a variation in the sulfur content of the chalcocite as little as 0.1 wt. per cent. It is impossible to analyze natural chalcocite to this degree of accuracy.

AUTHORS' REPLY: We have not analyzed the specimens used, but analyses reported for Bristol, Conn. chalcocite show nearly ideal stoichiometry. Posnjak, Allen and Merwin,[1] for example, report Cu:S=2.007:1.

An excess of 0.1 wt. per cent S would correspond to a composition of approximately $Cu_{1.99}S$. A variation of 0.4 wt. per cent, however, would result in Djurle's (1958*a*) new phase $Cu_{1.96}S$. The powder pattern of this phase is quite similar to low-chalcocite. This phase, however, inverts to a cubic digenite-like structure at 100° C. Since the hexagonal high-chalcocite structure was actually observed, Djurle's work would require any S excess to be less than 0.4 wt. per cent at most.

[1] *Econ. Geol.* **10,** 508 (1915).

MINERALOGICAL SOCIETY OF AMERICA, SPECIAL PAPER 1, 1963
INTERNATIONAL MINERALOGICAL ASSOCIATION, PAPERS, THIRD GENERAL MEETING

# EQUILIBRIUM IN ORE DEPOSITS[1]

PAUL B. BARTON, JR., PHILIP M. BETHKE AND PRIESTLEY TOULMIN, 3RD
*U. S. Geological Survey, Washington 25, D. C.*

ABSTRACT

This paper discusses the terminology, concepts, and criteria involved in the recognition of equilibrium assemblages in ores, especially with reference to the determination of the physico-chemical environment of ore deposition. Equilibrium is attained much more rapidly in reactions between the depositing solution and the surfaces of crystals than in solid-state reactions; thus the solution acts as an equilibrating agent, while the sluggishness of the solid-state reactions may preserve some record of the ore-forming process. In general, the ease of studying phase relations in the laboratory is inversely related to the likelihood of the same minerals preserving their original compositions on cooling. Studies of ore minerals indicate that a wide range of departures from equilibrium can be recognized, and thus care must be taken to evaluate the effects of possible departures from equilibrium in terms of the precision of results desired.

## INTRODUCTION

The application of laboratory phase-equilibrium studies to mineral deposits to obtain quantitative information on the physico-chemical environment of ore deposition has become increasingly popular in recent years. Most such applications rely either on the coexistence of two or more minerals or on the compositions of individual minerals in a given assemblage. The interpretation is usually based on the assumption of equilibrium among the minerals involved. In this paper we shall consider some of the problems in designating equilibrium assemblages in ores, for it appears that the recognition and selection of samples for meaningful analysis is at least as difficult as the laboratory determination of the equilibria with which the minerals are to be compared.

We shall first introduce some terminology and concepts, then consider reaction rates of interest to ore deposits, and end with a discussion of the application of equilibrium studies to the interpretation of ore-forming processes. This paper is oriented principally toward deciphering the conditions of initial mineral deposition. Most of our discussion is in terms of open space filling but the principles are also applicable to processes leading to replacement.

Most careful investigators have recognized the requirement of equilibrium in the application of experimental data to geologic situations, and thus many of the ideas incorporated into this paper are not original with us. We wish to thank Robin Brett, Eugene Roseboom, and Wayne Hall for reviewing the manuscript and to acknowledge discussions with many of our colleagues including Bruce Doe, Robert Fournier, Irving Friedman, Verne Fryklund, Dick Holland, Gunnar Kullerud, Edwin Roedder, Paul Sims, Brian Skinner and E-an Zen, but we hasten to absolve them of responsibility for what follows.

[1] Publication authorized by the Director, U. S. Geological Survey.

## CONCEPTS AND TERMINOLOGY

In this section we discuss equilibrium from two viewpoints: the thermodynamic and the observational. The thermodynamic approach is concerned with the analysis, on very general grounds, of the concepts of equilibrium and the description of any physical system. The observational approach deals with the reconstruction of past states of a system from observation of its present state.

*Thermodynamic approach.* In the following paragraphs we will discuss briefly various ramifications of the concept of equilibrium. More detailed, rigorous, and elegant treatments of these and related matters may be found in Guggenheim (1950), Prigogine and Defay (1954), Denbigh (1955) and Lewis and Randall (1961). We have not burdened this section with many specific examples because these will be found in succeeding sections.

a) Equilibrium

*Equilibrium* refers to a state from which a *system* has no spontaneous tendency to change. A *system* is that specific quantity of matter, or region of space, we choose to consider.

b) Types of equilibrium

We will discuss many types of equilibrium; these may be grouped in three different ways: (1) according to their relative stabilities, (2) according to the processes which give rise to each variety, (3) according to the degree to which equilibrium is attained.

A primary, and from a geological point of view most

important, distinction to be drawn is between *true equilibrium*, in which there is no driving force tending to change the state of the system, and *false equilibrium*, in which a driving force exists but is unable to overcome some reluctance factor (*e.g.*, friction) to produce a finite velocity of whatever process should occur (Prigogine and Defay, 1954, 40–41).

i) Grouping according to relative stabilities. The only geologically important types of equilibrium within this group are *stable* and *metastable equilibrium*.[1]

A system in a state of stable equilibrium (or, in short, a stable system) is stable relative to all possible alternative states; there is no other state into which the system will transform spontaneously. A system in a state of metastable equilibrium is stable relative to all *adjacent* states and will return spontaneously to the metastable equilibrium state if displaced only a short way. It is, however, unstable relative to some *more distant* state or states; the system, if displaced sufficiently far from the metastable equilibrium state, will transform spontaneously to a more stable state. In the familiar mechanical analogy, a brick resting on one of its smaller faces is metastable relative to the stable state of resting on its largest face.[2]

ii) Grouping according to processes giving rise to equilibrium. The most important processes driving geological systems toward equilibrium are *thermal*, *mechanical*, and *chemical*.[3] The criterion for thermal equilibrium is that the temperature be uniform throughout the system. For mechanical equilibrium, in the simplest case, pressure must be uniform throughout the system. At chemical equilibrium the chemical potential of each component is uniform throughout the system. Since it is relatively easy to choose geologic systems in which temperature and pressure are uniform, our principal concern will be chemical equilibrium and the factors affecting it.

No completely satisfactory theoretical treatment of *textural equilibrium* exists, though it is of considerable geologic interest. This concept is closely allied to the theory of interfacial stresses, and may be regarded as a fine-scale modification of chemical and/or mechanical equilibrium. We regard a system as being in a state of textural equilibrium when the energetic contributions of the surfaces between phases are minimized; these contributions will depend on the size and shape of grains and perhaps on the compositions of the very thin regions adjacent to intergrain contacts. One would suppose that, other things being equal, the energetic contributions of the intergrain contact films should decrease as the area of contact decreases, leading ultimately to complete segregation of each phase into a single mass. It is not now clear whether the common occurrence in geological systems of even- but fine-grained fabrics reflects too small a driving force to produce a finite rate of recrystallization or whether unconsidered factors come into play to minimize the energy of the inter-grain surfaces in polygrain aggregates.

iii) Grouping according to degree of equilibrium. A system may be in complete or partial equilibrium. *Complete equilibrium* is equilibrium with respect to all processes considered in a particular analysis. The situation in which a system is in equilibrium with respect to at least one process and out of equilibrium with respect to any others is known as *partial equilibrium*. For example, a solution may be in equilibrium with barite in regard to the amounts of $Ba^{2+}$ and $SO_4^{2-}$ in the solution, but the sulfate may be out of equilibrium with the other sulfur-bearing ionic species in solution with respect to oxidation-reduction reactions. Partial equilibrium should not be confused with false equilibrium as defined earlier.

*Observational approach.* We shall now consider some of the possible relations between coexisting minerals. To describe the relations between minerals as observed in the field, it is desirable to have some terms unencumbered by connotations of equilibrium. We shall follow the usage of Bartholomé (1958) and refer to those minerals occurring in direct contact with one another without the presence of an intermediate phase as an *assemblage*. If the minerals are believed to have been in equilibrium at some specific time the term *equilibrium assemblage* is applied. The term *association* will be used for minerals occurring together, the spatial and equilibrium relationships being unspecified.

Mineral associations have many possible complex relationships. It is most convenient to consider these in terms of idealized "end member" situations. Figure 1 (cases 1–4) illustrates the more important of these "end member" relations *at the time of deposition*.

[1] Other possible but geologically unimportant stability types of equilibria are *unstable* and *neutral* equilibrium. In the former, the system is not stable relative to at least one adjacent state; in the latter a finite range of contiguous states is all equally stable.

[2] The difference between metastable true equilibrium on the one hand and false equilibrium on the other is in most instances a matter of the scale on which the system is considered.

[3] Except for special considerations, other types of processes such as those arising from magnetic, electrical or gravitational fields, may be, and are, neglected.

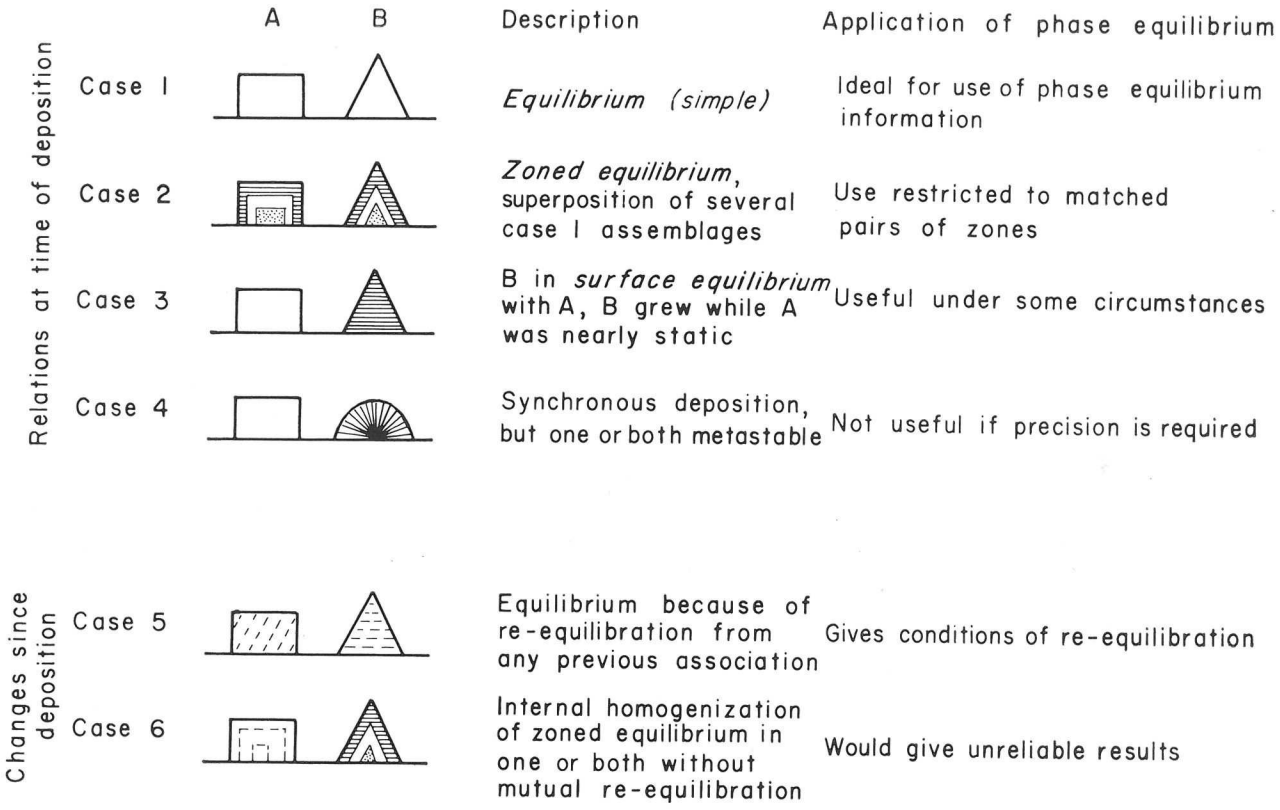


FIG. 1. Some possible relations between coexisting minerals.

It is assumed that the minerals have been preserved in unaltered (or reconstructable) condition.

a) Conditions at initial deposition

i) Case 1. The crystals formed in complete equilibrium with one another and with their environment, which was constant throughout crystal growth. The grains are therefore uniform throughout. Since the minerals have been preserved in unaltered condition, this case is ideal for the application of laboratory equilibrium studies to determine the physico-chemical environment in which the minerals formed. It should be clearly realized, however, that not all associations of homogeneous crystals fall into case 1 (note cases 5 and 6). We shall refer to this case as "*simple equilibrium*" when necessary to avoid ambiguity.

ii) Case 2. The crystals of A and B were deposited simultaneously from solutions whose character changed gradually or spasmodically during crystal growth. A given growth zone in A is matched by a correlative growth zone in B. The array is equivalent to a series of superposed equilibria of the type described in case 1 above. We shall refer to this relation as "*zoned equilibrium.*" It is an especially useful variation of the partial equilibrium described previously; equilibrium is maintained between crystal surface and solution while solid state reactions within the crystal are in a state of false equilibrium.

iii) Case 3. This might be considered as a special variety of case 2 in which mineral A neither grew nor dissolved to an appreciable extent while mineral B was being deposited. As will be discussed more fully later, in many cases equilibration between crystals and solution is rapid. Therefore, the fact that mineal A neither grew nor was dissolved appreciably suggests that its surface was approximately in equilibrium with the fluid and so with mineral B throughout the growth of B. We thus have the unilateral situation wherein mineral B is in equilibrium with the surface of mineral A, but the bulk of mineral A is not necessarily in equilibrium with B. In this case we may refer to mineral B as being in *surficial equilibrium* with mineral A. To judge from the literature, this is an extremely common case and is potentially very useful (for example, see Sims and Barton, 1961).

iv) Case 4. This is synchronous or successive deposition but with one (or both) phases metastable. At present no reliable inference on the environment of ore deposition may be drawn from such relations

except that the rate of precipitation was too rapid for equilibrium to be attained.

b) *Postdepositional changes*

In the previous four cases we have assumed that the minerals were preserved in their original condition, but this assumption is frequently not valid. Two significant examples of postdepositional changes are described as cases 5 and 6 below and illustrated in Fig. 1.

i) Case 5. The minerals have re-equilibrated under conditions different from those obtaining at the time of deposition. This may be the result of failure to quench as the deposit cools or of a later metamorphic event. Although the end product may be difficult to distinguish from case 1, geologic evidence ranging from regional field relations to microscopic mineral textures may help make this distinction (see, for example, Sales and Meyer, 1951; Fryklund and Fletcher, 1956; and Skinner, 1958). Some minerals react much more readily than others; a special situation that is potentially very misleading is illustrated separately by case 6.

ii) Case 6. The minerals were originally associated in zoned equilibrium but during postdepositional history one or both of the crystals has homogenized. Although it is easy to visualize this possibility, its recognition in real ores requires detailed study. Suppose that crystals of galena and sphalerite coexist in zoned equilibrium as described in case 2 above. We know from laboratory studies (see Fig. 2) that diffusion rates of almost any kind are much higher in galena than in sphalerite. All vestiges of zoned equilibrium may be annealed out of the galena even though the coexisting sphalerite retains its original compositional banding.

iii) Exsolution. Although this phenomenon is part of case 5, it is more convenient to discuss it separately. True exsolution textures should present no difficulty for equilibrium studies provided that the state of the original single phase can be reconstructed. A major problem, of course, is distinguishing exsolution from replacement or simultaneous precipitation.

## Reaction Rates and Attainment of Equilibrium

The purpose of this section is to note some of the experimental observations on reaction rates and to discuss in general terms the implications of the differences in rates to the interpretation of processes of ore genesis.

An extensive theoretical discussion of kinetics oriented toward metamorphic petrology has been presented by Fyfe and Verhoogen (1958) as part of GSA Memoir 73. We can add little to their treatment and will not discuss it at length. Their compilation of data summarizes most of the pertinent quantitative information on the kinetics of silicate equilibria and points up the fact that appropriate kinetic studies are scarce and that the problem of reaction rates is among the most challenging for the metamorphic petrologist and for the geologist in general. Garrels (1959) gives some very useful guides to the rates of geochemical reactions at low temperatures and has noted several examples of very important metastable equilibria under near-surface environments.

With very few exceptions, none of which are important to the present discussion, reaction rates increase with temperature. The rates of most reactions in the vicinity of room temperature increase by a factor of from 1.5 to 3 or 4 (and rarely more) for each 10° C. rise in temperature. The change in reaction rate with temperature at high temperatures is similar but less well defined (Figs. 2, 3).

Depending on the specific reaction, pressure may either increase or decrease reaction rates; unless a vapor phase is involved, however, the effect of pressure is small and is negligible compared to temperature for most reactions.

It is not easy to specify, operationally, just when a given reaction has reached equilibrium. The rates of many reactions depend on the concentrations of the reactants, and such reactions must approach equilibrium asymptotically. Thus, for many reactions under constant conditions, equilibrium is, in theory, never reached. This is another way of saying that no strictly reversible process can proceed to a finite extent in finite time. In the laboratory we speak of equilibrium being obtained when no further change is observed with time or when the "same" product is reached by diametrically opposite or very different paths. Thus the operational definition of attainment of equilibrium in the laboratory is controlled by our ability to observe the reaction, and we would recognize as "equilibrium" in most applications of experimental geology those reactions (depending on the particular system) which are between 90 and 99.9 per cent complete. Thus we use the parameter "time for equilibration" rather than the more rigorous term "rate of reaction" as the axis of abscissae in Figs. 2 and 3.

The degree of departure from equilibrium that can be tolerated in the geological application of chemical data depends on whether the purpose is to set broad

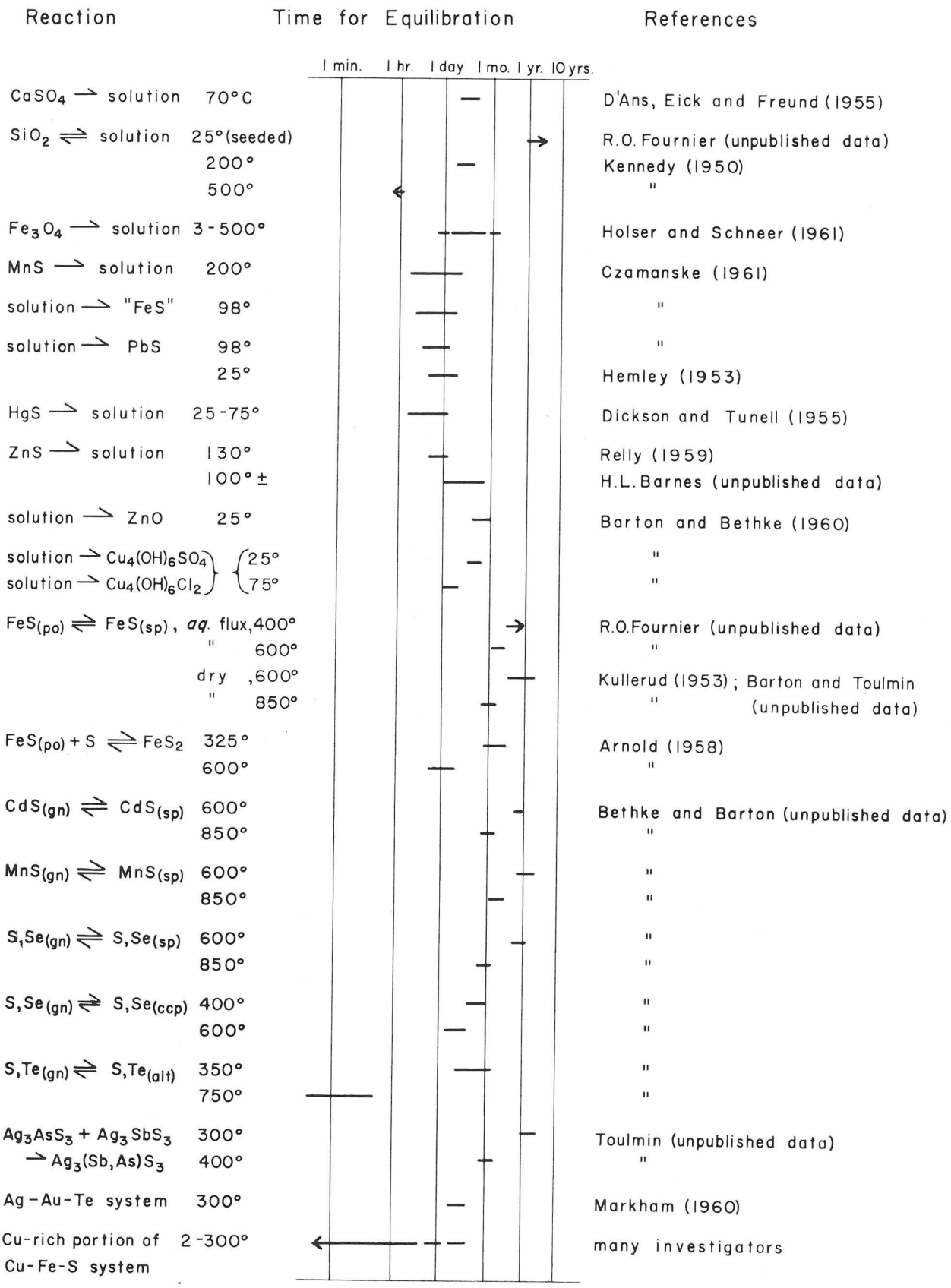


FIG. 2. Time for equilibration for some reactions of interest. The equations representing the reactions are abbreviated. Subscripts refer to phases in which the reacting component is in solid solution; po, pyrrhotite; sp, sphalerite; gn, galena; ccp, chalcopyrite; and alt, altaite. The solutions are of dominantly aqueous composition.

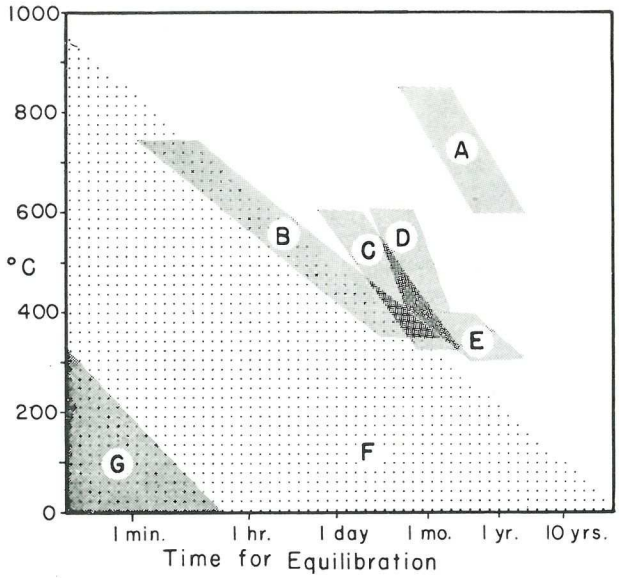


FIG. 3. Plot of time for equilibration against temperature for some of the data given in Fig. 2. A is the general curve for most solid-state reactions involving sphalerite. B is for the distribution of sulfur and tellurium between galena and altaite. C is for the equilibration of pyrite with pyrrhotite. D is for the distribution of selenium between galena and chalcopyrite. E is for equilibration between the ruby silvers. F is the general region within which lie most solution-crystal equilibria. G is the general region for most homogeneous reactions within the aqueous phase.

limits on the environment or to specify as precisely as possible the conditions under which a particular process operated. Thus, Barton (1957) and Krauskopf (1959), in estimating the general range of chemical environments of ore formation, were able to use data orders of magnitude less precise than those required by Sims and Barton (1961) in attempting to define the temperature and chemical potential of sulfur under which some deposits in the Central City District were formed. The most generally applied criteria of equilibrium in natural systems are based only on the presence or absence of particular minerals in particular associations. These criteria, however, do not guarantee the attainment of equilibrium with respect to the compositions of coexisting minerals. These considerations emphasize the importance of specifying the exact meaning of the unmodified term "equilibrium" in any particular context.

Reaction rates in homogeneous systems (those containing only a single phase) are amenable to quantitative study. Most reactions of interest to the geologist, however, are heterogeneous (involving two or more phases) and involve so many variables that quantitative treatment of their kinetics is seldom even attempted. Because the overall rate of a reaction that involves several steps is governed by the rate of the slowest step, kinetic studies of appropriate simple reactions may be applied to complex geologic processes.

*Reactions in homogeneous aqueous solution.* Most reactions between molecules and ions in solution (such as: $H_2O = H^+ + OH^-$, $HCO_3^- = H^+ + CO_3^{2-}$, and $Fe^{2+} = Fe^{3+} + e^-$) are rapid even at room temperature, and equilibrium is quickly attained. A few such reactions, as pointed out by Garrels (1959), may be very sluggish; important examples are the inertness of sulfate ion to changes in redox potential and the slow rate of formation and decomposition of some polymerized aqueous species such as the molybdates.

*Reactions in the solid state.* Solid-state reactions are generally much slower than those in aqueous solution, but there is a tremendous variation in geologically important solid-state reactions, as indicated in Figure 2.

Aside from difficulties of nucleation, solid-state reaction rates are controlled principally by solid-state diffusion, which in turn is related to such things as bond strength and structural defects. High bond strength tends to be associated with hardness, brittleness, high melting point (if congruent or nearly so) and low vapor pressure. In support of this line of reasoning, we may note that sphalerite, arsenopyrite, pyrite, alabandite, Fe-Co-Ni arsenides, hematite, and magnetite are much more sluggish in their solid-state reactions than are galena, chalcopyrite, most sulfosalts, argentite, electrum, chalcocite, and pyrrhotite. The effects of structural defects are hard to evaluate, but it is obvious that gross-defect structures such as those of pyrrhotite, bornite, or tetrahedrite may favor more rapid diffusion than would be possible if the phases were "stoichiometric." Defects of lesser magnitude, such as those of semiconductors or phosphors, are possibly important, but not enough is known about the role of such defects in minerals to generalize at present.

The broad generalizations about relative reaction rates noted above and semiquantified in Figs. 2 and 3 must be tempered by a careful appraisal of the geologic environment and history of the mineral assemblage considered. Even the normally fickle minerals such as galena or tetrahedrite may yield valuable clues regarding equilibrium conditions during deposition for some deposits formed at low temperature. Conversely, even the sulfides considered most likely to have preserved the record of their origin may not

have done so if subjected to extreme conditions.

Bartholomé (1958) has summarized the work of many previous investigators, demonstrating the fact that equilibration between chalcopyrite, bornite, chalcocite, digenite, and copper takes place so rapidly, even at relatively low temperatures, that the compositions and textures of the minerals record only their most recent history. He also emphasizes the frequent observations that reactions involving chalcopyrite are slower than the rest and that those involving the nucleation of pyrite are very much slower than other reactions in the Cu-Fe-S system. The commonly observed tendency for ores representing the copper-rich portion of the Cu-Fe-S system to violate the mineralogical phase rule is usually attributed to the inertness of pyrite.

The rapid reaction rates suggested by the data in Figs. 2 and 3 present an incompletely resolved problem—why isn't re-equilibration in ores almost universal? For example, synthetic pyrrhotite "equilibrates" with pyrite in a few weeks at temperatures as low as 300° C. regardless of whether the starting material is (1) stoichiometric FeS+pyrite or (2) a very iron-deficient pyrrhotite. Yet studies of natural pyrrhotites often reveal pyrrhotite compositions consistent only with temperatures higher than 300° C.; why didn't the pyrrhotite continuously change its composition as the ore cooled from its high temperature of formation? Edwards' (1954) answer to this question is that ores cool extremely rapidly by the mechanism of being injected into "cold" country rock. Barton and Toulmin (1961) have proposed that other probable cooling mechanisms (especially the throttling of high pressure-temperature solutions into cool ground water) may be adequate to explain rapid cooling. They further suggest that effective "quenching" of some ore deposits may be accomplished during the waning phases of mineralization by the entrance of cool ground water into the region previously occupied by high temperature ore solutions. The mechanisms they propose would produce much more rapid cooling than would heat flow through the wall rock. Nevertheless, there remain deposits to which none of these "rapid-cooling" explanations can apply. As an example, the Nairne pyrite deposit described by Skinner (1958) is a regionally metamorphosed sedimentary sequence containing significant amounts of pyrite and pyrrhotite. Skinner determined the composition of the pyrrhotite, which is consistent with an equilibration temperature of about 300° C. (Toulmin and Barton, 1962). It is very difficult to explain how this pyrrhotite was effectively quenched since the entire metamorphic sequence must have taken many thousands of years to cool.

The problem of re-equilibration has also been considered in detail by Kullerud (1959) and Lyon (1959). Laboratory work by Kullerud showed that synthetic FeS-rich sphalerite exsolved more rapidly at 500° C. than did natural sphalerite of similar iron content from Broken Hill. He attributed this behavior to the inhibiting effect of other elements (Cd, Mn, etc.) in the natural material. Similarly, we have observed that a per cent or so of each of a dozen minor elements appeared to inhibit reaction in the Cu-Fe-Zn-Pb-S system at 600° C. While these observations suggest another possible solution to the problem, other as yet undetermined factors must also be important in retarding solid-state reactions in sulfides, for many workers (*e.g.*, Lyon, 1959) have gotten at least partial reaction in short-term heating experiments on natural materials at geologically reasonable temperatures.

Most geothermometers involving phase equilibria must be regarded as providing only minimum temperatures of ore formation, unless it can be shown that subsequent processes have not erased the earlier record. For example, a zoned crystal offers evidence that complete re-equilibration of that crystal has not occurred. The use of exsolution relationships as quantitative geothermometers is extremely hazardous because of the many unevaluated complexities concerning the equilibrium phase relations and the rates of reaction, nucleation and recrystallization. In particular, part or all of the exsolved material may migrate completely out of the host grain, making reconstruction of the original state of the grain difficult, if not impossible. The presence of exsolution lamellae, however, does not guarantee that some additional material has not migrated completely out of the grain. The results of an extended study on the problem of exsolution textures are being prepared for publication by Robin Brett at the Geophysical Laboratory, and we shall not dwell on this problem.

*Solution-crystal equilibrium.* In general, equilibration between crystals and aqueous solution is rapid relative to the time involved for ore-forming processes. With few exceptions crystal-solution reaction rates are intermediate between those of homogeneous reactions in aqueous solutions and solid-state reactions (Figs. 2, 3).

a) Growth of crystals. Crystal growth is conveniently discussed in terms of the degree of supersaturation in the medium from which the crystal grows. We

shall begin by considering crystal growth under near-reversible conditions, and then proceed to consider growth under conditions progressively further removed from equilibrium. Equilibrium may be maintained as long as crystal nucleation and growth keep pace with the changes causing precipitation in the solution. Failure of crystal-solution equilibration to keep up with changes in solution may lead to appreciable amounts of supersaturation and this, in turn, may allow metastable precipitates to form. Some supersaturation is needed for primary nucleation, and solutions of some substances can become highly supersaturated. As an extreme example, solutions supersaturated with respect to quartz by about 2000 per cent can be maintained for years at 25° C. Highly supersaturated solutions are not necessary for crystal growth, however, for crystals can grow from very slightly supersaturated solutions. The importance of spiral dislocations of crystal growth (Frank, 1949), in fact, lies in the mechanism they provide for avoiding the nucleation of successive layers. Thus it is possible that crystals may grow from almost imperceptibly supersaturated solutions (*i.e.*, at "equilibrium") provided that a seed is present. The seed may be a crystal of the same mineral or a crystal of some other phase whose surficial atomic configuration is similar to that of the crystallizing phase. It is probable that, other things being equal, the rate of crystal growth will be roughly proportional to the degree of supersaturation.

Details of the history of crystal growth are more readily obtained for transparent than for opaque minerals, and for this reason much of the evidence we cite comes from observations of sphalerite. Our conclusions are compatible with the much smaller amount of observational data on fluorite, quartz, barite, and carbonates.

Study of polished "thick sections" of sphalerite from a variety of localities reveals sharp and delicate color banding (reflecting principally variation in iron content) that preserves the growth history of the crystals in minute detail (Fig. 4). Analyses of individual color bands of such sphalerite from Creede, Colorado, show that compositional differences as small as a few hundredths of a per cent Fe in iron-poor sphalerite (<1 weight per cent Fe) may be distinguished readily by color differences (Figs. 4A and 4B). The growing crystal's ability to respond quickly (relative to the rate of crystal growth) to apparently subtle changes in the environment is thus a strong argument that crystal-solution equilibrium was nearly attained for these growth bands.

We shall now consider briefly some of the processes taking place at the surface of a growing crystal of variable composition. Various investigators have treated the surface layer(s) of a growing crystal as a "phase" distinct from either the depositing solution or the interior of the crystal. The composition of the surface "phase" will be controlled by the equilibrium between it and the solution. Surface "phases" of different crystal forms may be distinct from one another, so that different ions are selectively taken up by certain forms. On the other hand, the equivalent structural sites in the interior of the crystal should have equal probability of containing a given atom. Thus, in order for the interior of the crystal to reflect the composition of the depositing fluid there must be equilibrium between the interior and surface "phases." This equilibrium is apparently frequently attained, but visible hour-glass features are common enough in minerals to cast suspicion on all crystals whose habit during growth includes more than a single form. In the absence of pertinent experimental data, we suspect that the elements that are more

»»→

FIG. 4. Photographs of polished thick sections (1–2 mm thick) of sphalerite. Transmitted light. Spots are opaque or fluid inclusions in the sphalerite or air bubbles in the epoxy resin used to cement the specimen to a glass slide. The black lines are cleavages.

A. Delicate growth banding in sphalerite; note sharp color differences between bands and uniformity of individual bands. Specimen from Creede, Colorado.

B. Delicate growth banding in sphalerite. Interpreted as near-equilibrium crystal growth (except for the very earliest patchy sphalerite just above the point of the white area at the lower left). The white area at the lower left is the mold left by the complete removal by hydrothermal leaching of an octahedral fluorite crystal. Specimen from Creede, Colorado.

C. Finely banded (not very prominent) early light sphalerite growing around a core of wallrock (black). A later, darker generation of sphalerite contains growth bands showing very patchy distribution of iron within the same growth zone, obviously a disequilibrium feature. The latest sphalerite is a discontinuous light marginal growth band which has been partially leached away. A surface of strong hydrothermal leaching (shown as a dark line of fluid and opaque inclusions generally paralleling, but in detail crosscutting, growth banding in the inner light sphalerite) is preserved in the inner light sphalerite generation 2 or 3 mm below the darker growth band. Specimen from Creede, Colorado. Temperature of formation from fluid inclusions on the order of 200–250° C. (Roedder, 1960).

D. Portion of sphalerite crystal showing very irregular coloration which is at least partly controlled by twinning (the "ENE striking" straight lines). The growth zones are very difficultly visible as color bands crudely concentric about a center somewhere off the photo to the right. Specimen probably from the Joplin area.

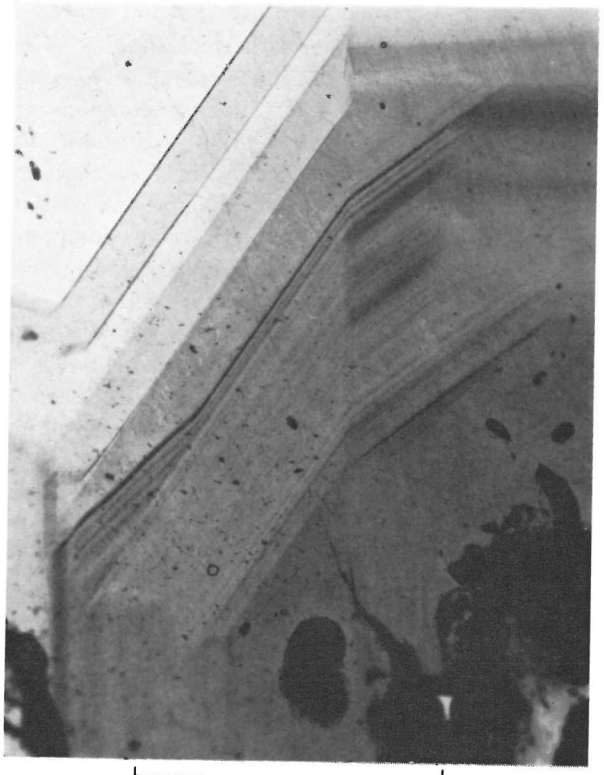

1 cm
A

1 cm
B

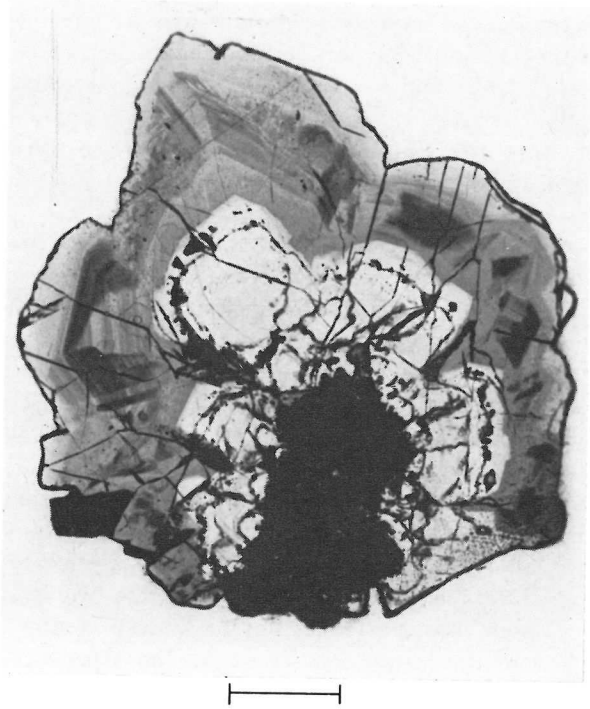

1 cm
C

1 cm
D

likely to show strong fractionation between various crystal forms are those which are minor components because of stereochemical factors rather than solely because of geochemical abundance. Components capable of extensive solid solution are presumably similar to the host in terms of crystal chemistry and thus fractionation between forms may not be as pronounced. Sphalerites from many localities, particularly but not exclusively those from Mississippi Valley type deposits, often show a very patchy incorporation of pigmenting components (probably iron) within individual growth bands (Figs. 4C and especially 4D). The surface of a single face of the growing crystal appears not to have been in equilibrium even with itself and thus the solution from which it crystallized cannot have been in equilibrium with the whole surface. Obviously, we cannot use such a crystal for purposes that depend critically on the composition of the crystal.

At Creede, growth zones of such patchy sphalerite alternate with zones of the delicately banded sphalerite described earlier (see figure 4C). Therefore we infer that the conditions of crystal growth alternated between near equilibrium and considerable supersaturation.

Even higher supersaturation may lead to the development of many new nuclei, with the result that growth of individual crystals is inhibited. Extreme supersaturation may yield colloidal precipitates which, judging from the literature, are not uncommon, especially in low-temperature deposits.

One feature of solution-crystal equilibrium presents difficulty in practical applications. As mentioned above, "equilibrium" crystal growth tends to produce large crystals with few intercrystal contacts. Thus the crystals most likely to have grown in equilibrium with the same solution are apt to show few textural criteria of it. A possible way to "prove" simultaneous deposition and equilibrium, based on the distribution of trace elements between coexisting phases, has been suggested by Bethke and Barton (1959), but as should be clear from the preceding pages, many problems remain.

b) Hydrothermal leaching. The partial or complete re-solution of hydrothermal minerals by later hydrothermal solutions has occurred in many ore deposits. It is perhaps most frequently recognized in connection with replacement, wherein the replaced mineral (or some of its constituents) is redissolved either before or during deposition of the later mineral. Leaching without immediate replacement is also common, though to judge from the literature its recognition is not so widespread. Several examples (from the literature) of hydrothermal leaching of ore minerals are cited later in this paper; our observations (Bethke *et al.* 1960) at Creede, Colorado, seem to be typical. Examination of doubly polished slabs of individual sphalerite crystals reveals repeated "solution unconformities," which round and corrode previous crystal forms; later deposition usually reconstructs the earlier forms. As pointed out previously (Barton, 1959) hydrothermal leaching of well crystallized materials demonstrates that hydrothermal environments contain solutions capable of dissolving sulfide minerals; thus it is not necessary to resort to colloids or other mechanisms involving metastability in order to explain ore transport. In the Creede deposit the leaching surfaces are associated with delicately banded sphalerite and never with the patchy sphalerite (see Fig. 4C), even though both types of sphalerite are present (in different growth zones) in the same crystal. The leaching thus supports the contention that the finely banded material was deposited under quasi-equilibrium conditions, the concentration of sphalerite in solution varying just above and below the solubility of sphalerite.

If the surfaces of crystals are in "equilibrium" with the solution surrounding them, the composition of the solution will be buffered at the saturation level for the various minerals in contact with it. Thus the concept of surficial equilibrium mentioned earlier is applicable, and we may be able to make use of equilibrium relations that are not obviously applicable from the simple examination of ore textures (Sims and Barton, 1961).

*Summary of reaction rates.* The discussion in the preceding sections implies that, in considering the initial equilibrium and the requirements for its preservation, the geologically important types of reactions are crystal-solution and solid-state reactions. For a given system there appear to be broad, frequently poorly defined limits to the conditions under which its phase relations will be capable of furnishing quantitative information on the environment of deposition. On one hand there is an upper "temperature-time" limit above which the original mineral assemblage reacts internally or with its environment to provide a new assemblage that does not preserve a complete record of the initial deposition; on the other hand there is a lower "temperature-rate of deposition" limit below which there is such a departure from equilibrium during deposition that calculations in-

volving the equilibrium assumption are not meaningful. Useful equilibrium studies must therefore deal with assemblages falling between these limits. It is possible that under some circumstances (high solid-state reaction rates combined with sluggish solution-crystal equilibration) the upper and lower limits may effectively overlap, as in the case of colloidal Cu-Fe sulfide deposits. Such an assemblage may provide a better indication of present than of past temperatures. Minerals having high bond strengths (sphalerite, pyrite, iron oxides, arsenopyrite, etc.) are much more likely to preserve the record of their history than others in which the rates of solid-state diffusion are large (chalcocite, digenite, bornite, chalcopyrite, galena, etc.). In general, the ease of studying phase relations in the laboratory (by DTA, *x*-ray heating camera, short-term phase-equilibrium investigations) is inversely related to the reliability of applying them to mineral assemblages in the field.

## Application to the Study of Ore Deposits

*Deposition of a simple zoned ore body.* It is of interest to consider the emplacement of a hypothetical ore body in light of the foregoing discussion of equilibrium behavior.

To show more clearly the general solubility relations in an ore-forming process, let us consider a hypothetical and greatly simplified vein system. Figure 5 is an attempt to construct a model showing some of the salient features as they pertain to this discussion. The diagram is for a steady-state model which, unrealistically, does not change with time. The diagram shows solubility or concentration plotted against the ensemble of temperature, pressure, and composition variables that affect the solubility of minerals. This horizontal coordinate is plotted simply as distance from the source, but it must be remembered that many factors may affect the shape of the curves. For each crystalline phase, two curves are drawn: a solid line representing the concentration of the substance in the solution; and a line of "o's" representing its solubility in the solution. Dashed segments of the concentration curves represent metastable conditions. The actual construction of the curves in Fig. 5 is arbitrary, and the curves are meant only as illustrations of general principles.

As the solution leaves its source, in this case supposed to be of granitic composition, it is probably in surficial equilibrium with the minerals of the granite. As it passes outward the solution goes through various changes in physicochemical environment, the net result generally being to decrease the solubilities of the various compounds present in solution. The solution was originally saturated with quartz, and thus as it moves outward quartz is deposited. Near the source, only quartz is at the saturation level, and a barren quartz vein results; further along, however, the solubility of pyrite drops until it reaches the concentration of $FeS_2$ in the solution and pyrite begins to deposit with the quartz. In a like manner, sphalerite and galena may be deposited successively to form pyrite-quartz, pyrite-quartz-sphalerite, and finally pyrite-quartz-sphalerite-galena veins. The solution may never become saturated in some phases, *e.g.*, halite, and thus halite does not occur as a mineral in this model even though the concentration of NaCl in the ore fluid may be very high.

In some environments, particularly at low temperatures, the physicochemical environment may change more rapidly than the solution can adjust its composition; the resulting supersaturation may permit the formation of metastable phases. This possibility is illustrated for silica and pyrite. It is a common observation that quartz veins may pass laterally (or vertically) into chalcedony veins even though the associated sulfides may not take on a colloidal aspect. In the case of pyrite, some sluggishness in nucleation (corresponding to a supersaturation of only a few per cent) has been sketched for the point of initial precipitation. Thus pyrite enters the mineral assemblage of the vein much less abruptly than do sphalerite and galena, as shown in the bottom part of Fig. 5. In actual ores, the variations of the loci of deposition with time, and possible momentary supersaturation prior to nucleation and crystal growth, would tend to smooth out the abrupt appearance of minerals in the zoning pattern.

The model given in Fig. 5 makes it easy to visualize at least two ways in which an ore body may become zoned. The incoming solutions may reach saturation in different minerals at different places (as indicated by the intersections of the curves for solubility (circles) and concentration (solid lines) for each of the various minerals), or the slopes of the saturation curves may vary for a given mineral as well as from one mineral to another.

Although the relative amounts of phases deposited are indicated in the lower part of Fig. 5, the absolute amounts are indeterminate and will vary across the diagram. The shapes of the solubility curves are arbitrarily chosen to obtain a zoned ore body; but, in defense of the model, it must be realized that ores are most likely to be deposited in regions where the

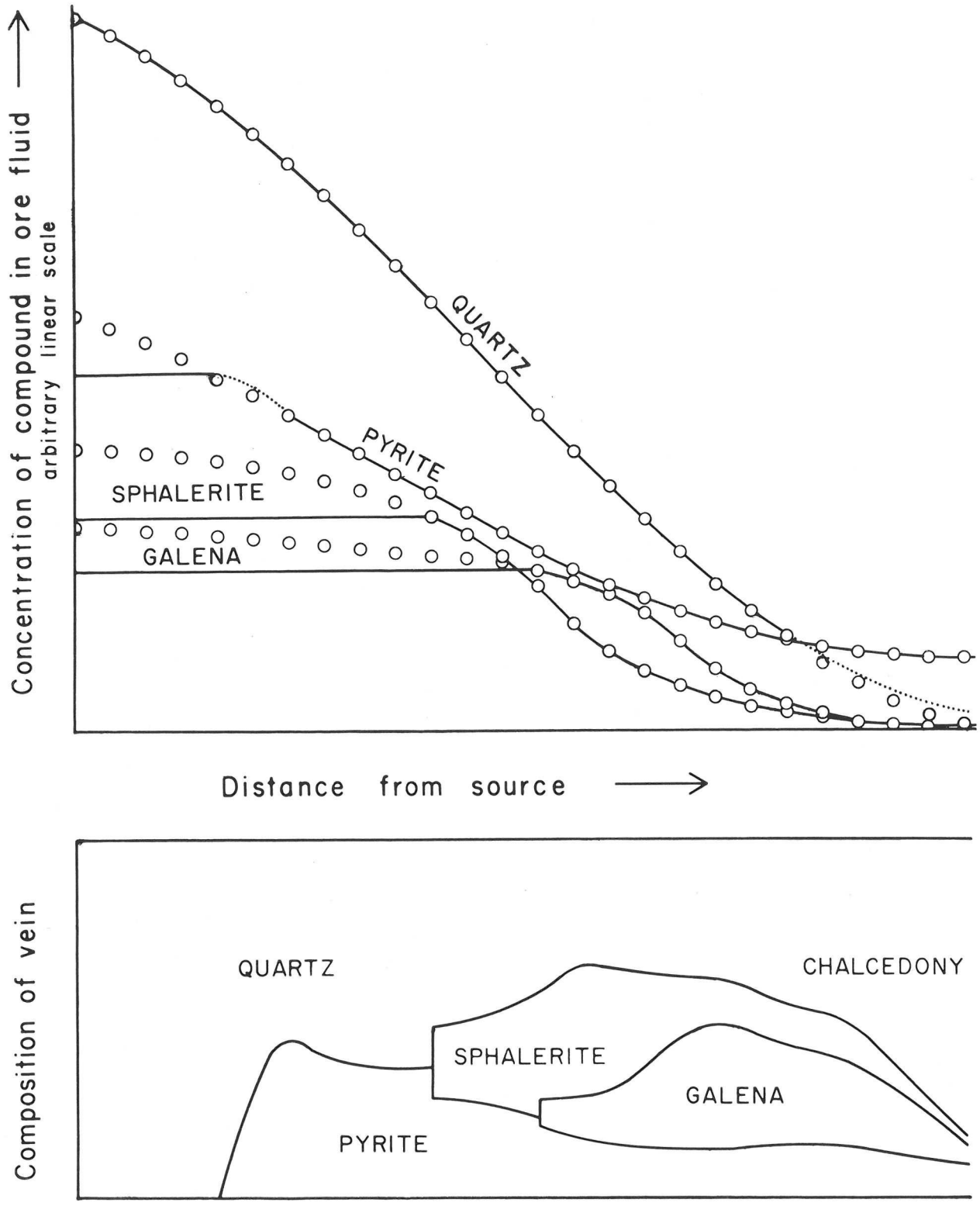


FIG. 5. Schematic diagram for the deposition of an ore body.

Upper part: Solubility vs distance diagram
Solubility indicated by circles; concentration by solid lines; supersaturation by dotted lines.
Lower part: Character of ore body deposited in the model, showing relative proportions of minerals deposited

solubility changes most rapidly. The shapes of the solubility curves will be controlled by such complex processes as throttling, mixing with ground water, and other factors affecting the chemistry of the ore fluid; these are beyond the scope of the present discussion.

*Mineralogical bottoming of ore.* Let us now consider how hydrothermal leaching might operate in the model ore-forming system just described; we may as well confess at the outset our intention to develop a criterion for the impending bottoming of an ore body.

The position of a zoned Zn-Pb ore body is evident from Fig. 5. The incoming solution at the bottom of the incipient ore body (on the left side of the diagram) is just reaching saturation with sphalerite, and sphalerite is depositing from there to the end of the model. If for some reason the region of undersaturation with respect to sphalerite should shift into the region where sphalerite had previously been deposited, the sphalerite there would be leached. Such encroachment of the region of undersaturation on the region of saturation would be expected to occur most commonly near the lower limit of the range of sphalerite deposition. Thus observation of increasing amounts of leaching in the lower part of an ore body would be a criterion for the impending bottoming of the ore body.

Let us compare the leaching in the model described above with several recent descriptions of hydrothermal corrosion of ores. Lacy and Hosmer (1956) describe the hydrothermal leaching of barite, tetrahedrite, galena, sphalerite, pyrite, chalcopyrite and carbonates in several Peruvian mines; the almost complete leaching was generally *below* known ore on the same structure. Turneaure (1960) notes the hydrothermal corrosion of pyrrhotite, leaving pyrite boxworks, in the central zones of some Bolivian tin-silver deposits. Sims and Barton (1961) found hydrothermal leaching of sphalerite near the zinc-poor core of the symmetrically zoned Central City district in Colorado. We have recognized several periods of leaching of sphalerite and galena at Creede, Colorado. The intensity of leaching increases with depth and is at a maximum at the bottom of the present workings. We therefore conclude that detailed study of hydrothermal leaching may in some cases provide the mining geologist with another tool to bring to bear on the problem of the continuation of ore with depth.

It is not necessary that the solubility of minerals in a hydrothermal solution decrease outward from the source; it may remain nearly constant, or increase, or fluctuate. For example, because of the rapid changes in the density of water as temperature changes at constant pressure in the P-T region just above the critical point, the solubility of quartz (and by analogy, most other minerals) increases as the temperature drops in the interval from 600 to 400° C. Further, because of complex chemical reactions within the ore fluid and between the ore fluid and its environment, solubilities could behave in almost infinitely varied ways. Some minerals, *e.g.*, calcite and anhydrite, have a negative thermal coefficient of solubility in simple aqueous solutions and might well be leached by solutions that had been saturated with them at higher temperatures.

*Determination of the physicochemical environment of ore formation.* Knowledge of the physicochemical conditions under which an ore deposit formed is obviously a prerequisite to reliable inference of the ore-forming process. For this reason, much of the laboratory effort in sulfide studies has been devoted to measuring those properties of minerals that may indicate the temperature, pressure, and chemical environment at the time the minerals formed. To apply these studies to mineral deposits, however, we must have some criteria by which to evaluate the degree of attainment of equilibrium. In developing these criteria, we must carefully distinguish the indications of equilibrium at the time of initial deposition from those of postdepositional equilibration (or re-equilibration). Concordant "readings" by several independent methods constitute the best available evidence for equilibrium in an assemblage, though by itself the concordance gives no indication whether the conditions of equilibrium refer to the time of initial deposition. Textural or structural evidence may permit the possibility of postdepositional re-equilibration to be evaluated—euhedral, zoned crystals in a vuggy, banded vein, for example, are unlikely to have re-equilibrated.

In contrast to the foregoing "positive" lines of evidence, most criteria for equilibrium are negative: they amount to the absence of evidence for disequilibrium. Thus if an assemblage does not violate the phase rule, or if a mineral does not show compositional variation in a single association, we infer that the minerals under study are (or were) in equilibrium. Again we must rely on textural and structural evidence to decide *when* the equilibrium occurred.

Complete attainment of equilibrium is rarely, if ever, demonstrable, so we should also consider the extent to which departures from equilibrium may be evaluated, and tolerated, in the interpretation of ore

deposits. Obviously, a growth-zoned sphalerite (Fig. 4) is not in equilibrium even with itself, and yet each zone may represent a fleeting set of equilibrium conditions during the formation of the deposit. Growth-zoning on a very fine scale, which we have observed in sphalerites from many deposits of the open-space filling type, suggests that the crystal responded to minor fluctuations in physicochemical conditions during ore formation, and also indicates that complete re-equilibration of the crystal has not occurred after deposition. Provided (1) that the range of composition in the zoned crystal is not too great, and (2) that we have reason to believe that the solution was in contact with the minerals required for a useful assemblage, we may be able to set broad limits on the temperature, pressure, and chemical activities at deposition from the bulk composition of the zoned crystal. Of course, much more detailed information, including the important feature of the sequence of changing conditions, could be obtained if it were feasible to analyze the crystal zone by zone, as by use of an electron micro-probe.

We should re-emphasize at this point the important distinction between equilibrium in the sense of compatibility of phases (basis of the concept of mineral facies) and equilibrium in the sense of compatibility of mineral composition (basis of quantitative geothermometry, etc.).

If the available evidence against disequilibrium is only that the number of minerals in an association or assemblage does not exceed that allowed by the phase rule, we can, in general, infer only broad limits to the conditions of deposition. Here again, textural and structural observations are often significant. If in a specimen composed largely of pyrrhotite, magnetite, and hematite, for example, we observed that pyrite was restricted to thin bands separating grains of pyrrhotite from grains of hematite, we might infer that the association had formed under conditions where the assemblage pyrrhotite-magnetite-hematite was stable and had later partially reacted internally under conditions permitting the alternative assemblages, pyrite-magnetite-hematite and pyrrhotite-pyrite-magnetite. In the light of Barnes and Kullerud's (1961) demonstration that the reaction of pyrite and magnetite to form hematite and pyrrhotite takes place above about 675° C., we could interpret our observations to mean that the deposit had formed above 675° C. and that partial re-equilibration had occurred as the deposit cooled below 675° C. Obviously, the principles we have illustrated with reference to temperature changes may equally well be applied to changes of pressure or of chemical parameters.

In conclusion, there may be a close enough approach to equilibrium between crystals and the depositing solution for various equilibrium systems to be applied to interpretation of the physico-chemical processes and environment of ore deposition. However, successive stages of mineralization and possible subsequent processes of metamorphism of the ore may tend to mask or destroy the record of initial mineral deposition. Even the most careful laboratory equilibrium studies and the most precise analytical data thus are of little use without detailed knowledge of the paragenetic relations among the minerals.

## References


Arnold, R. G. (1958) The FeS-S system. *Carnegie Inst. Washington Yearbook* **57,** 218–222.

Barnes, H. L. and G. Kullerud (1961) Equilibria in sulfur-containing aqueous solutions, in the system Fe-S-O and their correlation during ore deposition. *Econ. Geol.* **56,** 648–688.

Bartholomé, P. (1958) On the paragenesis of copper ores. *Studia Universitatis Lovanium,* Leopoldville.

Barton, P. B., Jr. (1957) Some limitations on the possible composition of the ore-forming fluid. *Econ. Geol.* **52,** 333–353.

——— (1959) The chemical environment of ore deposition and the problem of low-temperature ore transport, in *Researches in Geochemistry,* John Wiley & Sons, New York.

——— and P. M. Bethke (1960) Thermodynamic properties of some synthetic zinc and copper minerals. *Am. Jour. Sci. Bradley Vol.* **258A,** 21–34.

——— and P. Toulmin, 3rd. (1961) Some mechanisms for cooling hydrothermal fluids. *U. S. Geol. Survey Prof. Paper* **424-D,** D348–D352.

Bethke, P. M. and P. B. Barton, Jr. (1959) Trace element distribution as an indicator of pressure and temperature of ore deposition (abs.). *Geol. Soc. Am. Bull.* **70,** 1569–1570.

——— P. B. Barton, Jr. and W. C. Bodine, Jr. (1960) Time-space relationships of the ores at Creede, Colorado (abs.). *Geol. Soc. Am. Bull.* **71,** 1825–1826.

Czamanske, G. K. (1961) A study of the solubilities of iron, lead, and manganese sulfides at elevated temperatures. Ph.D. thesis, Stanford University.

D'ans, J., H. Eick, and H. E. Freund (1955) Untersuchungen über die Calciumsulfate. *Kali und Steinsalz,* **9,** 17–38.

Denbigh, K. (1955) *The Principles of Chemical Equilibrium.* Cambridge Press.

Dickson, F. W. and G. Tunnell (1955) Geochemical and petrographic aspects of mercury ore deposits. *Final Rept., ONR Project* **NR 801-174.**

Edwards, A. B. (1954) *Textures of the Ore Minerals.* Austral. Inst. Min. Metal.

Frank, F. C. (1949) The influence of dislocation on crystal growth. *Disc. Faraday Soc.* **5,** 48–54.

FRYKLUND, V. C. AND J. D. FLETCHER (1956) Geochemistry of sphalerite from the Star Mine, Coeur d'Alene district, Idaho. *Econ. Geol.* **51,** 223–247.

FYFE, W. S. AND J. VERHOOGEN, in FYFE, W. S., F. J. TURNER, AND J. VERHOOGEN (1958) Metamorphic reactions and metamorphic facies. *Geol. Soc. Am. Mem.* **73,** 53–103.

GARRELS, R. M. (1959) Rates of geochemical reactions at low temperatures and pressures, in *Researches in Geochemistry,* John Wiley & Sons, New York, pp. 25–37.

GUGGENHEIM, E. A. (1950) *Thermodynamics.* North-Holland Co., Amsterdam.

HEMLEY, J. J. (1953) A study of lead sulfide solubility and its relation to ore deposition. *Econ. Geol.* **48,** 113–138.

HOLSER, W. T. AND C. J. SCHNEER (1961) Hydrothermal magnetite. *Geol. Soc. Am. Bull.* **72,** 369–386.

KENNEDY, G. C. (1950) A portion of the system silica-water. *Econ. Geol.* **45,** 629–653.

KRAUSKOPF, K. B. (1959) The use of equilibrium calculations in finding the composition of a magmatic gas phase, in *Researches in Geochemistry,* John Wiley & Son, New York.

KULLERUD, G. (1959) Sulfide systems as geological thermometers, in *Researches in Geochemistry,* John Wiley & Sons, New York.

LACY, W. C. AND H. L. HOSMER (1956) Hydrothermal leaching in central Peru. *Econ. Geol.* **51,** 69–79.

LEWIS, G. N. AND M. RANDALL (1961) *Thermodynamics,* rev. by K. S. Pitzer and L. Brewer, 2nd ed., McGraw-Hill Book Co., New York.

LYON, R. J. P. (1959) Time aspects of geothermometry. *Mining Engr.* **11,** 1145–1151.

MARKHAM, N. L. (1960) Synthetic and natural phases in the system Au-Ag-Te, Part I. *Econ. Geol.* **55,** 1148–1178.

PRIGOGINE, I. AND R. DEFAY (1954) *Chemical Thermodynamics.* Longmans, Green and Co., New York. Transl. by D. H. Everett.

RELLY, B. H. (1959) A method for determining solubility at high temperatures and pressures. *Econ. Geol.* **54,** 1496–1505.

ROEDDER, E. (1960) Primary fluid inclusions in sphalerite crystals from the OH vein, Creede, Colorado (abs.). *Geol. Soc. Am. Bull.* **71,** 1958.

SALES, R. H. AND C. MEYER (1951) Effect of post-ore dike intrusions on Butte ore minerals. *Econ. Geol.* **46,** 813–820.

SIMS, P. K. AND P. B. BARTON, JR. (1961) Some aspects of the geochemistry of sphalerite, Central City district, Colorado. *Econ. Geol.* **56,** 1211–1237.

SKINNER, B. J. (1958) The geology and metamorphism of the Nairne pyritic formation, a sedimentary sulfide deposit in South Australia. *Econ. Geol.* **53,** 546–562.

TOULMIN, P., 3rd AND P. B. BARTON, JR. (1962) Thermodynamic study of pyrrhotite and pyrite (abs.). *Am. Mineral.* **47,** 205–206.

TURNEAURE, F. S. (1960) A comparative study of major ore deposits of central Bolivia. *Econ. Geol.* **55,** 217–254, 574–606.

---

### DISCUSSION

G. DEICHA (Paris): Le fait de retrouver dans les minerais sulfures des effets d'un déséquilibre cristallogénétique manifeste (*Bull. Trim. Inform. B.R.G.M.*, Paris, **47,** 1, 1960), vient renforcer les conclusions analogues qui fournit souvent l'étude des gangues: des observations au microscope électronique, poursuivies en collaboration avec M. Cl. SELLA (C.N.R.S., Bellevue), montrent en particulier que l'abondance des lacunes de cristallisation et des pores intergranulaires (*C. R. Acad. Sci.*, Paris, **253,** 1774, 1961), est très variable dans le quartz tant stérile que métallifère (Mine de Saint-Véran, dans les Alpes françaises, par example).

P. M. BETHKE (Washington): Our observations of fluid inclusions in sphalerite are consistent with your broader generalizations.

G. W. LEO (Washington): Insofar as it is necessary for you to determine precise compositions of distinct zones in zoned crystals, what is the technique you use for such determinations, especially in the case of small crystals and/or their compositional zones?

P. M. BETHKE (Washington): Thus far all of our analyses have been on relatively coarse grained material from which several milligrams could be separated from each zone by hand picking. Presumably the electron micro-probe would be very satisfactory for those elements within its range.

MINERALOGICAL SOCIETY OF AMERICA, SPECIAL PAPER 1, 1963
INTERNATIONAL MINERALOGICAL ASSOCIATION, PAPERS, THIRD GENERAL MEETING

# A STUDY OF DISTORTED PYRITE CRYSTALS FROM SPAIN

M. FONT-ALTABA
*Laboratorio de Mineralogia, Universidad de Barcelona, Barcelona, Spain*

ABSTRACT

In Fuente Valoria, Province of Soria, Spain, medium-sized crystals of pyrite with a pronounced distorted cubic habit occur in calcareous rocks that are mined for ornamental use. The variations of the angles between the cubic faces have been measured. A qualitative spectrographic analysis, as well as an *x*-ray study by single-crystal and powder methods, have been carried out. A study of the faces of these crystals has been made by means of a reflecting microscope. From the data obtained it is deduced that the deformation of these crystals was due to irregularities in their growth.

## INTRODUCTION

On the border between the provinces of Soria and Logroño there are, in a zone of about 30 km by 10 km, four localities in which perfectly crystallized pyrites occur in the calcareous rocks of the Wealden beds. The pyrite crystals exhibit cubic habit in Fuente Valoria, Villerijo and Valdenegrillos (Soria), and have less well-developed pyritohedral and cubic habit in Muro de Aguas (Logroño). Only in Fuente Valoria are the deformed crystals found.

The Wealden, in this region discordant with the Lias, has a thickness of 800 m and is formed by alternating layers of limestones and clay-marl. The pyrites appear only in some layers of the limestones, and never in the clay-marl. Cuttings were observed in which the limestone layers abounded in pyrite cubes whose edges ranged from 1 cm to 25 cm in length.

In Valdenegrillos, the blackish limonitized pyrite cubes, called "negrillos" in this region, are surrounded by twinned (swallow-tail) gypsum crystals that reach a size of 20 cm. These gypsum crystals are produced by the reaction of sulfuric acid, released in the process of the limonitization of the pyrite, with the calcium carbonate of the limestones.

In a preliminary, unpublished study of the deformed pyrite cubes of Fuente Valoria (José F. de Villalta), it was indicated that the distortion of these crystals seemed to result from homogeneous deformations attributable to external pressures. This particularity aroused our interest.

## MAGNITUDE AND REGULARITY OF THE DEFORMATION

A group of 250 was chosen from among the thousand or so distorted crystals that were placed at our disposal by the mining company. From this group a second selection was made, eliminating those crystals whose face irregularities did not permit measurements to be made with sufficient accuracy.

The dihedral angles of the 200 selected crystals were measured with a contact goniometer. Although the goniometer could be read to 0.1°, the accuracy of the measurements was estimated to be $\pm 0.5°$. Forty-three of the crystals were found to be completely regular and were eliminated from further consideration. Only the remaining 157 were used for calculations.

A distribution curve (Fig. 1) was plotted by grouping the values at intervals of 1 degree, so that those measurements falling between 89.6° and 90.5° were plotted at the value 90°. The average value of all values less than 90° (between 81° and 89°) is 87°, and the average of all values over 90° (between 91° and 107°) is 93°. The overall average value is 91°. These results immediately caused us to doubt that a question of homogeneous deformation was involved.

## *X*-RAY AND SPECTROGRAPHIC STUDY

*X*-ray Laue diagrams were obtained from different parts of various crystals. None of them showed the spot deformation typical of a crystal lattice distorted by pressure. In addition to the characteristic diffraction lines of pyrite, the *x*-ray powder diagrams of these pyrites revealed some very weak lines attributable to calcite. This calcite is found as an inclusion in the distorted pyrite crystals.

For the spectrographic analysis, specimens were chosen that were representative of all types of crystals occurring in the pyrite deposits of Fuente Valoria. Only those portions of the pyrite were analyzed that were found, by microscopic observation, to be free of any inclusions. A carbon arc using direct current, graphite electrodes, and a Hilger spectrograph were employed. The film used was Mafe positive, sensitive only to the ultra-violet region of the spectrum.

Al, Si, Mg and Ag were present as minor elements

in all of the crystals. Ti was present in a quantity that permits us to say that the pyrites from Fuente Valoria are "titaniferous pyrites." The samples from the other deposits of this region do not contain as large a quantity of Ti.

### Microscopic Study of the Crystal Faces

The deformation of the pyrites of Fuente Valoria may be due to phenomena occurring during the growth of these crystals. Should this be so, the microscopic observation of the irregularities existing on the faces, as well as of the lines and surfaces of growth, which give us information about the conditions of crystallization, will clear up the problem.

A series of crystals with faces of varying nature were chosen for this study. They were all treated with $H_2O_2$ and washed with water acidulated with HCl and alcohol to bring out the features of the faces and remove the impurities contained thereon.

The microscopic examinations were carried out with a Zeiss photomicroscope fitted out with reflected-light and dark-field equipment. The photomicrographs (24×35 mm) were taken on a 13° DIN Adler film, and the exposure times were estimated automatically. The photomicrographs were enlarged to the size 90×120 mm on glossy paper of high contrast.

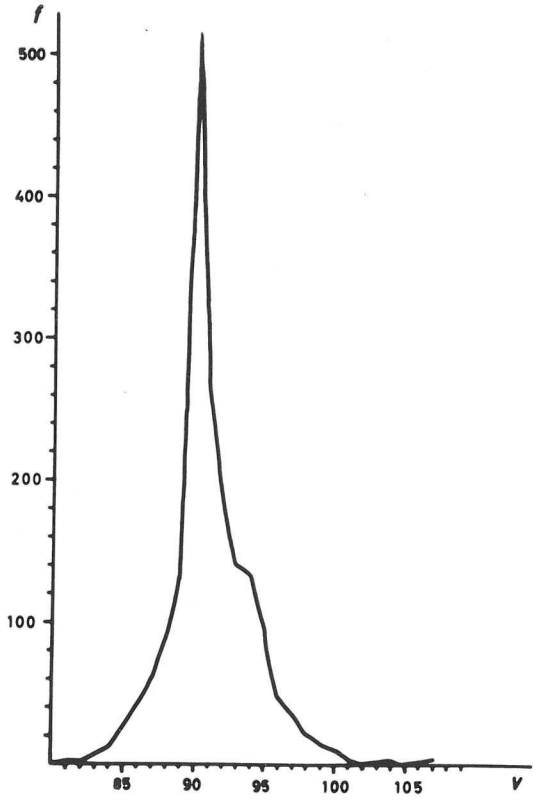


Fig. 1. The distribution curve of the deformation (frequency of occurrence, *f*, *vs.* angle between cube faces, *v*.)

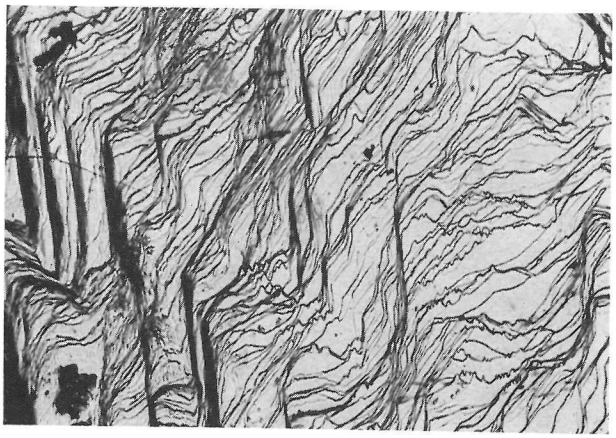

Fig. 2. General view of the crystal face of a pyrite from Fuente Valoria. The growth steps are of irregular outline; however, they follow two general directions corresponding to the cubic faces (100) and pyritohedral faces (320). ×75.

On studying the surfaces of these crystals we can distinguish: a) growth features, and b) dislocations.

*Growth features.* A general view of the cubic faces is shown in Figs. 2 and 3. In these low-magnification photomicrographs it is observed that the crystalline surfaces are formed by blocks limited by real cracks. In each of these blocks the growth steps are of a different form, a fact which accentuates the differences of the various blocks. The faces of these crystals are of

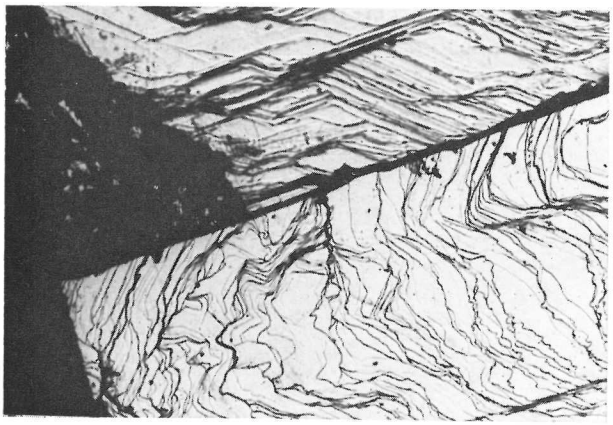

Fig. 3. General view of crystal face exhibiting two blocks outlined by surfaces closely parallel to the cubic faces (100). The growth steps in the two blocks are of different types. On the upper block the steps are straight and regular and are parallel to the (100) and (320) faces. On the lower block the steps are of warped and irregular outline but tend to develop into (100) and (320) faces. The blocks are separated by a split in the crystal faces. ×75.

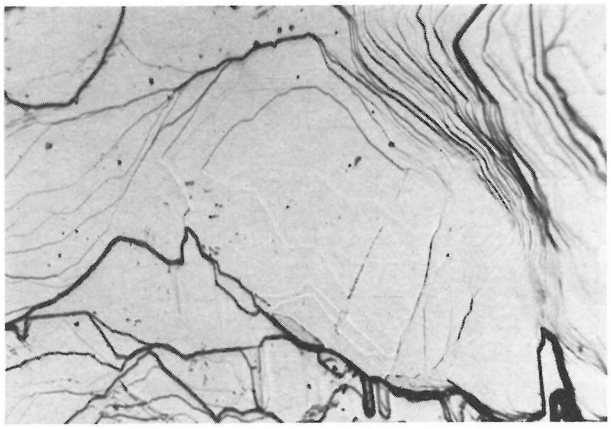

FIG. 4. Details of growth steps showing triangular disposition of the primary steps and dislocation lines. ×480.

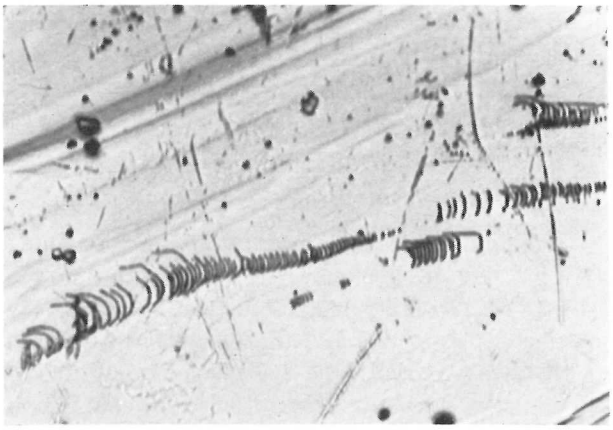

FIG. 6. Lineal series of dislocations lying nearly parallel to the (320) faces. ×750.

mosaic type due to the "lineage structure" type growth as described by Buerger.

These differences in the blocks of the crystalline faces are increased in the case of the pyrites of Fuente Valoria through the existence of abundant inclusions of $CaCO_3$ in the interior of the crystal. The inclusions of $CaCO_3$ are located in the small cracks and force the crystal to grow with exaggerated distortion. The final result is complete deformation of the crystal.

In some blocks the growth steps are of irregular form, although they tend to develop in the direction of the (100) and (320) faces. In others, the steps are straight and develop parallel to the above-mentioned faces. Figures 4 and 5 show the growth steps with a higher magnification. In Fig. 4 it is possible to observe the triangular disposition of the primary steps and also some dislocation bands, which are independent of the growth of the crystal and cut the growth steps (Fig. 5).

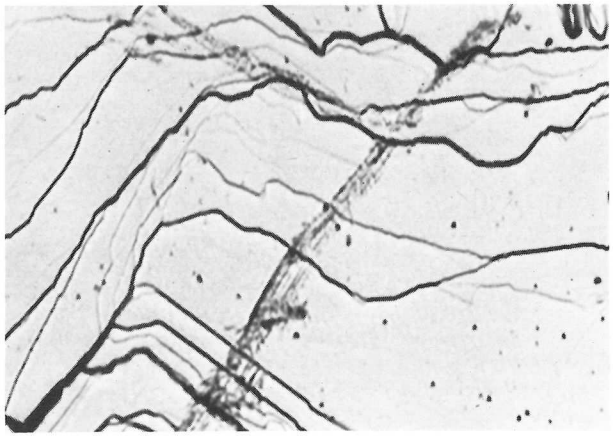

FIG. 5. Dislocation bands cutting growth steps. ×750.

*Dislocations*. Two kinds of dislocation were observed: one kind independent of the lines of growth, and the other closely related to them. The former are disposed in a linear series lying almost parallel to the (320) faces. Figure 6 shows these dislocations highly magnified, and in Fig. 5 bands of the same kind of dislocation can be observed cutting the growth steps without mutual interference. Figures 7 and 8 illustrate the type of dislocation closely related to the growth lines. The dislocations are on one side of the step and can be perpendicular to and develop along it as in Fig. 7, or they can be parallel to the step and develop perpendicular to it as in Fig. 8. Figure 9 shows a series of dislocations starting from the edge of a crystalline block. A growth step arises from them, and another one is being formed.

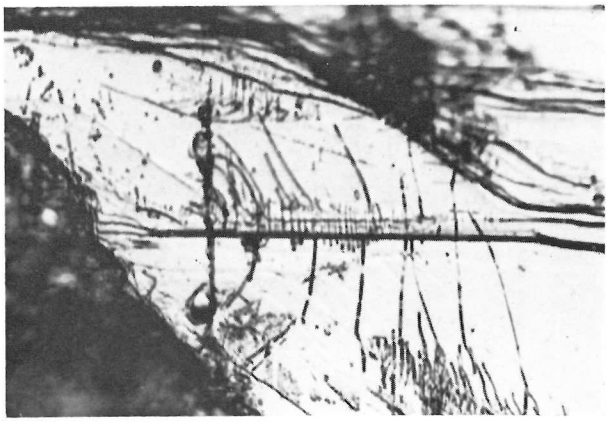

FIG. 7. Dislocations lying parallel to a growth step. Note that the dislocations are on only one side of the step—the side which is growing. ×750, with green interferential filter.

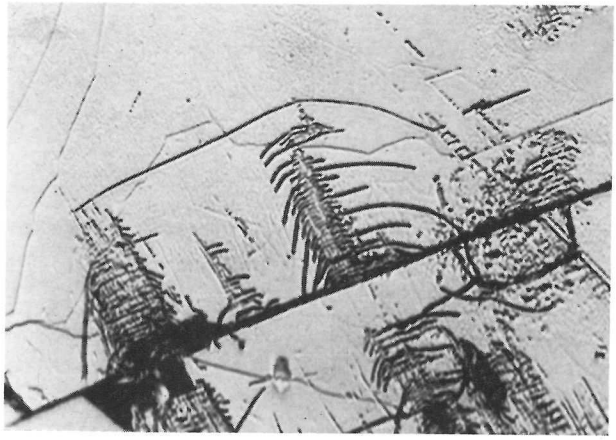

FIG. 8. Series of dislocations lying perpendicular to a growth step and parallel to the direction of the step. ×1200, with green interferential filter.

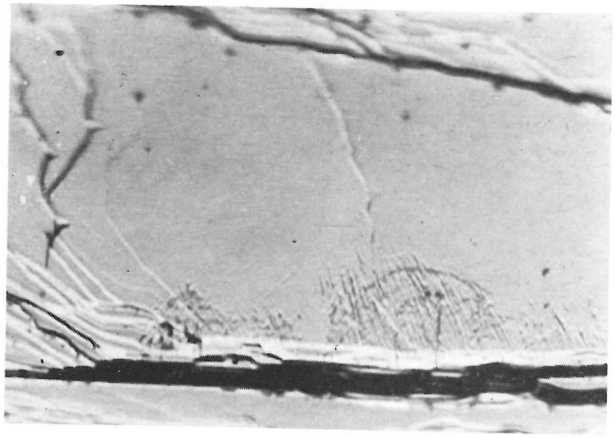

FIG. 9. Dislocations starting from the edge of a crystalline block. Note the growth step which arises from them, and another that is in process of formation. ×1200, with green interferential filter.

## CONCLUSIONS

The morphological, *x*-ray and microscopic study of the pyrites of Fuente Valoria does not support the idea that the crystals are distorted as a result of homogeneous deformation attributable to external pressures. From the observation of nearly three thousand specimens carried out at the deposit, and from the study of a series of crystals chosen in such a way that the greatest number of different types would be found amongst them, we have deduced that the deformation of these crystals was due to irregularities in their growth, chiefly produced by the abundant inclusions of $CaCO_3$.

On studying the local geological conditions of the deposits where the distorted pyrite cubes occur we did not observe in the limestone layers any signs of pressure great enough to produce the deformation found in the crystals. The microscopic examination of the crystal faces indicated that these crystals grew from a liquid phase. This agrees entirely with their sedimentary origin. As the Wealden is of continental facies (in Spain it presents the typical facies of Numancia), it can be supposed that these pyrites formed under reducing conditions during lacustrian deposition. This explains why the pyrites appear only in certain layers while in others there is no trace of them.

The conditions producing the simultaneous formation of pyrite and calcite that existed when the limestone layers of the Fuente Valoria deposits were formed determined the deformed cubic habit of the pyrites and explain the existence of abundant calcareous inclusions in these crystals.

## ACKNOWLEDGMENTS

We wish to express our thanks to Dr. José F. de Villalta for making specimens available to us, and to Prof. J. Codina for permission to use the spectrographic equipment and for many helpful suggestions during the spectrographic study.

## REFERENCES

AMORÓS, J. L., M. A. BRANDOLY AND PEREZ PEÑASCO M. (1955) *Publ. Dept. Crist. Min.* **2**, 89.

A.S.T.M. *X*-ray powder data file, 6-0710 and 5-0586.

DANA'S SYSTEM OF MINERALOGY (1946). Elements, sulfides, sulfosalts and oxides. I, 282.

FRONDEL, C. (1936) *Am. Mus. Nat. Hist.* Nov. **829**.

INST. GEOL. MIN. ESPAÑA, *Hojas y memorias explicativas del Mapa Geológico.*

LÓPEZ DE AZCONA, J. M. (1961) *Notas Com. Inst. Geol. Min. Expaña*, **63**, 119.

SHANNON, F. (1922) *U. S. Natl. Mus. Proc.* **62**, 9.

VILLALTA, J. F. DE (1961) Private communication.

MINERALOGICAL SOCIETY OF AMERICA, SPECIAL PAPER 1, 1963
INTERNATIONAL MINERALOGICAL ASSOCIATION, PAPERS, THIRD GENERAL MEETING

# A STATISTICAL STUDY OF BRAVOITE ZONING

FAROUK EL BAZ AND G. C. AMSTUTZ
*The University of Missouri, School of Mines and Metallurgy, Rolla, Missouri*

ABSTRACT

Bravoite-pyrite grains occur in sulfide ores of the Fredericktown area, Missouri, in the transition facies between the Lamotte sandstone and the Bonneterre dolomite. These ores also include galena, marcasite, siegenite, chalcopyrite and small amounts of sphalerite. Geopetal features[1] displayed by sulfide agglomerations suggest their formation during diagenesis.

A systematic recording of specific characteristics of 4575 grains leads to a classification into eight zoning types. The internal regularities of the grains as well as their relationship to the surroundings are discussed.

Finally, the question of the possible causes for zoning is raised. Although no definite answer to the problem is reached, it is suggested that at the constant temperatures and pressures of formation other factors than these control such crystallization phenomena as zoning. Among the important factors are the surface properties of the crystallizing minerals.

## INTRODUCTION

The incidence of bravoite in North America was first established in 1943 in an iron concentrate from the Fredericktown area in the southeastern part of the so-called "Lead Belt" of Missouri (Rasor, 1943). The Fe-Pb-Cu-Ni-Co-Zn-sulfide ores occur here in the shaly and glauconitic zone between the Lamotte sandstone and the Bonneterre dolomite. These upper Cambrian sediments were laid down on an irregular erosion surface of Precambrian granites, and these formations pinch out and lap up against Precambrian hills known as "granite knobs." The Fredericktown mining district is located between two of these knobs and alongside the larger of the two.

The paleogeographic positions of the sulfide-rich sedimentary layers are flat coastal areas of brackish water; glauconite and traces of hydrocarbons are abundant. Several geopetal structures are displayed by the sulfide agglomerations in the shaly sediments (Amstutz, *et al.*, 1961). These features and certain geochemical considerations suggest a diagenetic age for the sulfides (Amstutz, 1959; Amstutz and El Baz, 1962).

The sulfides associated in variable proportions in these sediments are galena, marcasite and pyrite, siegenite and chalcopyrite, and small amounts of sphalerite and wurtzite. They occur in layers, layered disseminations, concretionary agglomerations and sulfide nodules.

## SCOPE AND PURPOSE

Bravoite from the Fredericktown area, and that from most localities described in the literature, occurs as intergrowths with alternating zones of pyrite. The bravoite problem consists of the open question whether or not there are gaps in the solid-solution series between the bravoite ($NiFeS_4$) and pyrite ($FeS_2$) end members and, if so, under what conditions they occur.

There are two approaches to the solution of this problem—observations, measurements and analyses of natural material, on the one hand, and laboratory syntheses and phase-equilibrium studies on the other. The solution to the problem will probably develop from integration of both methods of investigation.

The present study is based on an analysis of certain observations on natural bravoite, on the assumption that there must be physico-chemical reasons for the features that can be observed in nature. Ultimately, a classification and evaluation of a great number of observations should allow us to draw limiting conclusions about the phase-relationships between two or more components and about other factors controlling the deposition of natural minerals. It will be interesting to compare the present study with the results of experimental work on bravoite done by Kullerud (pers. comm., 1962; Clark and Kullerud, 1960; Ramdohr and Kullerud, 1961) and by Springer (pers. comm. D. Schachner, 1962).

## LITERATURE REVIEW

*Discovery and definitions.* In their early investigations, several authors reported Ni and Co-rich varieties of pyrite (*e.g.* Hunt, 1866; Dana, 1871; Egleston, 1889; Penfield, 1893; Walker, 1894; Doelter and Leitmeier, 1926). Hillebrand (1907) appears to have been the first to describe and analyze bravoite. He found it in sulfide nodules from the vanadium mines of Mina Ragra, Peru, and proposed the name after J. J. Bravo, the Peruvian writer on the vanadium deposits of the same locality.

[1] Geopetal:—Indicating top to bottom relations in rocks at the time of formation.

Strunz (1957) gives the formula (Ni, Co, Fe)$S_2$ for bravoite, and defines it as occupying a solid-solution field between pyrite ($FeS_2$), vaesite ($NiS_2$) and cattierite ($CoS_2$). Ramdohr (1960) uses the same nomenclature, but puts more emphasis on the FeS-$NiS_2$ side. He states (p. 749) that Hillebrand may have had material which actually consisted of "an unusual" (Ni-Fe-rich) violarite.

*Bravoite zoning.* Short and Shannon (1930; Short, 1940) recognized and analyzed two different internal zones in bravoite, one yellow and the other violet. According to their data, the violet zones contain more Ni and Co than the yellow ones. Schneiderhöhn and Ramdohr (1931) and Eskola (1946) refer to the remarkable zonal structure displayed by bravoite.

Kalb (1951, 1952) concluded from habit changes of zoned bravoite-pyrite grains from Mechernich that these minerals do not form a complete solid-solution series. The same conclusion was reached by Hegemann (1942).

An environmental mechanism causing zoning is suggested by Edwards (1960). Maucher and Rehwald (1961) picture zoned and unzoned bravoite grains. They describe different geometric forms in which these grains can occur.

*Reported zoned bravoite.* In addition to Rasor (1943), Kidwell (1946) lists bravoite among the minerals of the Fredericktown area. El Baz (1961) and Amstutz *et al.* (1961) describing zoned bravoite as one of the sulfides in the Cambrian sediments of the Fredericktown mine, attribute to these sulfides a diagenetic origin, based largely on geopetal features (Amstutz, 1959).

Extensive literature on experimental studies of the bravoite-pyrite group minerals, as well as other occurrences of bravoite, is available and will be reviewed at some later time.

## Techniques

The methods used so far are microscopic only. *X*-ray microprobe analyses to obtain quantitative compositional information have been initiated.

### A. Reflectivity measurements

Bravoite grains from the Fredericktown ores range from 5 to 200 microns in diameter. Most of them are, however, below 50 microns. Many of the grains show internal zoning, the individual zones averaging about 3 microns in width, so that none of the available photometers could be used. The reflectivity of the zoned portions had to be recorded by visual comparison with associated sulfides and gangue minerals. All variables of microscopic observation were standardized as much as possible, thus narrowing down the error of reflectivity estimates into a $\pm 2\%$ to $\pm 3\%$ range, justifying the choice of 10% reflectivity intervals in Figs. 11 and 12. The reflectivity in oil appears to vary from about 20 to about 40. Vachromeiev (1950, 1954) is the only one to give reflectivity values in air. His value of 41% is, of course, only an average.

### B. Recording of properties

Reflectivity profiles of all grains were drawn and other properties were recorded, and statistical tables were made by compiling these data. Profile portions within reflectivity intervals of 2.5% were measured. However, this range was too close to the accuracy limit, and also showed a subjective tendency of the observer to draw the profile line on the 25, 30, 35, etc. lines. The summation of these results appears below.

## Observations and Results

*Observations*—Bravoite occurrences in the Fredericktown sediments can be classified as follows:

1. Dark, isolated bravoite grains without any zoning or pyrite intergrowth; these are rare, and occasionally form colloform aggregates; they always occur in association with common rock-forming minerals.
2. Minute cores enclosed in bacteria-like disseminated pyrite spheres identical with the so-called bacterial pyrite grains of Mt. Isa (Allen *et al.*, 1912; Love, 1958; Omera, 1961; and others).
3. Bravoite zones in layered intergrowths with pyrite or with transitional compounds and, in rare cases, locked to other sulfides such as siegenite and galena. The present study deals mainly with this property of zonal intergrowth.

The Fredericktown bravoites may be separated into eight zoning types. A total of 4575 zoned grains was recorded, including a few grains of the unzoned end member (type I, below). Figure 1 illustrates the eight essential zoning types arranged according to consecutive geometric differences. On the right side of the triangle are the types with abrupt zone boundaries, whereas on the left side most of the types display gradational zoning. The characteristics of the various types are as follows.

*Zoning type I:* Grains that belong to this type show no internal zones. They display a slightly brownish tint and, as shown in Fig. 2, are always enclosed in siegenite and/or galena.

*Zoning type II:* Bravoite grains included under this type also show a slightly brownish tint. They are either free or locked to other sulfides, and in most cases bravoite occupies the center of the grain, as shown in Fig. 3. Pyrite grains with a core of bravoite are usually slightly darker than those free of bravoite. Reflectivity differences in such cases may range from 2 to 4%. In Fig. 4 a bravoite grain with a core of pyrite is shown. It must be mentioned that the bravoite layer closer to the pyrite region is the darkest of all zones. This is not an optical illusion, as the difference in tone remains even when the pyrite zone is covered up.

*Zoning type III:* Grains of this type are irregular modifica-

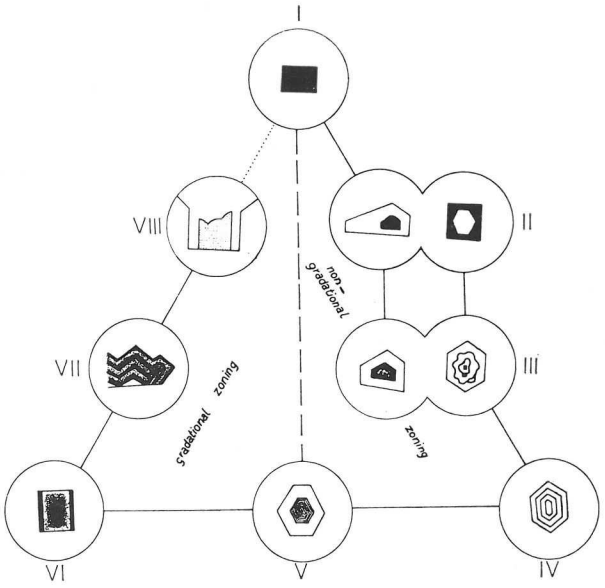


FIG. 1. A classification of the zoning types of bravoite-pyrite grains from the Federicktown sulfide ores, subdivided into non-gradational or abrupt zoning and gradational or solid solution zoning.

tions of similar grains of zoning type II. Most of them in this case are not intergrown with any other sulfides, but they always surround larger dolomite and/or quartz grains. They occur with the above-mentioned bacteria-like disseminations. Figure 5 shows an irregular geometric pattern displayed by bravoite. Central holes in the pyrite grains sometimes take the place of bravoite regions.

*Zoning type IV:* In this type, pyrite grains commonly occur with linear zonal structures. In many cases the lines separating these zones are represented by a hole 2 to 5 microns thick. In other rarer cases, this feature is displayed by bravoite instead of by pyrite. Figure 6 shows a zoned bravoite grain where the intermediate zones consist of galena.

FIG. 2. Bravoite grains (dark gray) enclosed in siegenite (upper right, medium light gray), and in galena (gray). Type I zoning. Oil immersion, 550×.

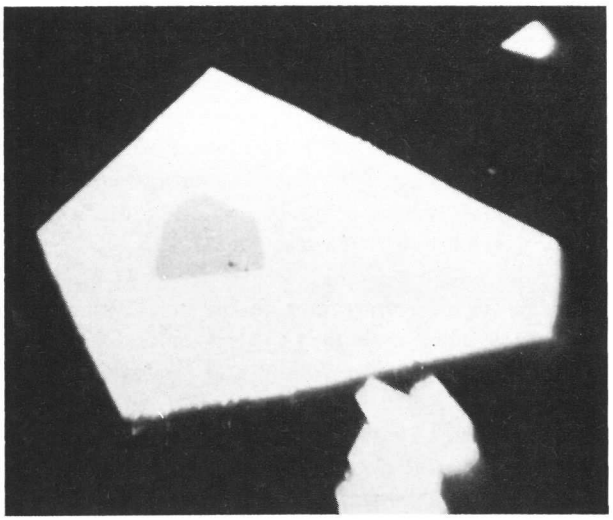

FIG. 3. Bravoite occupying the center of a pyrite grain, a very common occurrence. Zoning type II. Oil immersion, 550×.

*Zoning type V:* Grains of this type are composed of bravoite in the center and a distinct pyrite rim. The bravoite region is always zoned. Individual zones in this case show clear changes of reflectivity, which are either abrupt or gradational. The zoning in such regions can be simple or intricate. Holes occur in or at the end of the darkest bravoite zones. In some cases they are occupied by galena (or possibly by cattierite, $CoS_2$). Intergrown grains are common to this type.

*Zoning type VI:* This type includes grains with linear broad zones of bravoite and pyrite. In many cases the bravoite regions show gradational zoning. Figure 7 is an illustration of the broad zones of bravoite, which show an internal set of

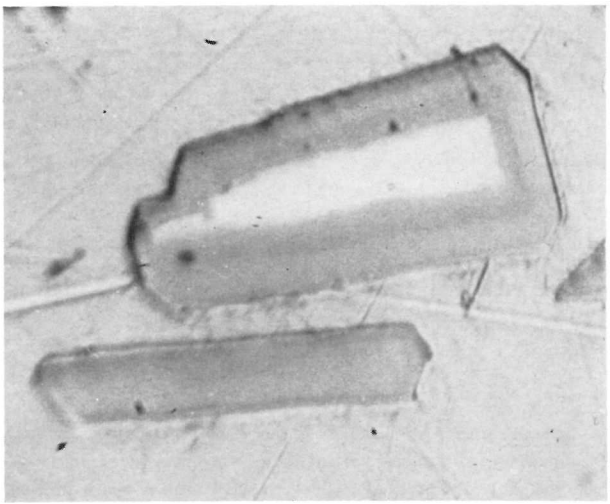

FIG. 4. Bravoite layers (dark gray) surrounding a pyrite cone (white) in a matrix of galena. The smaller area of bravoite can be regarded as a shallower cut in a similar grain. Zoning type II. Oil immersion, 550×.

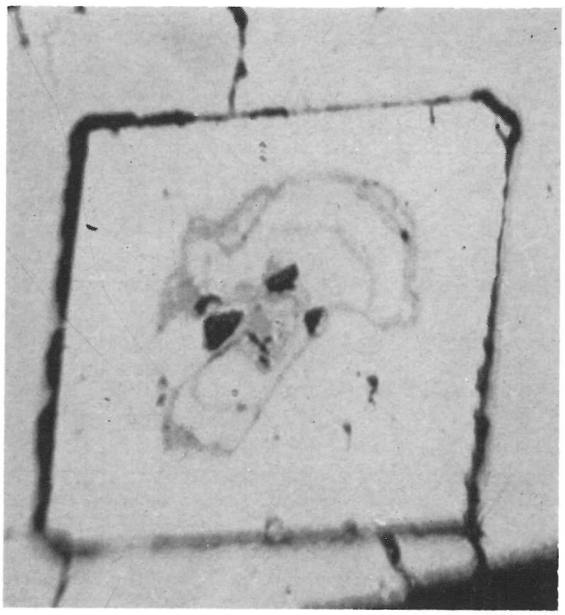

FIG. 5. A grain belonging to zoning type III. Irregular bravoite layers occur in the central part of the pyrite grain. The habit change is conspicuous. Oil immersion, 550×.

zones. Many of the grains classified under this type display a complex crystal form.

*Zoning type VII:* This type includes all grains which are formed of bravoite or "nickeliferous pyrite" layers showing definite gradational zoning. Bravoite generations displaying reflectivities from 20 to about 30% usually show a definite gradation from darker to brighter zones. The darkest bravoite generations are found at the rim of the grains, and surrounding holes in them. Parallel holes are also common and occur nearest to or within the darkest portions of the bravoite zones. Some of the holes are filled with galena or perhaps with cattierite. This mineral appears to be later than the dark type of bravoite. In many cases it fills these "crystallographic" holes. Galena is, on the whole, later in the diagenetic paragenesis of these holes. It fills, for example, cracks in bravoite as well as in most other minerals.

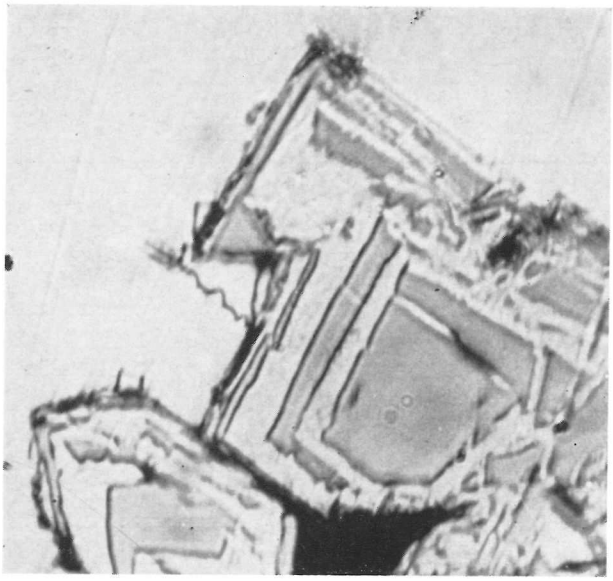

FIG. 6. Bravoite layers enclosed in lighter galena. Zoning type IV. Oil immersion, 550×.

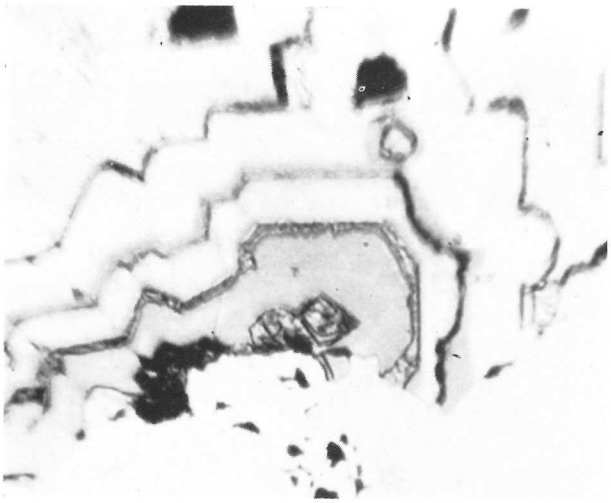

FIG. 7. Broad zones of bravoite (dark gray) locked to pyrite layers (white). Zoning type VI. Oil immersion, 550×.

*Zoning type VIII:* Type VIII includes linear as well as massive disseminations of very tiny specks of bravoite and/or "nickeliferous pyrite" peppered over certain portions of pyrite crystals. The borders of the areas containing these disseminations can be either parallel or non-parallel to the boundaries of the enclosing pyrite crystal, as shown in Fig. 8. Bravoite patterns falling under this classification have been observed in sulfide nodules and in concentration products. They do not occur anywhere else in the ores. In the sulfide nodules, they follow the contact boundaries of locked pyrite and marcasite, which occupy the central portions of these nodules.

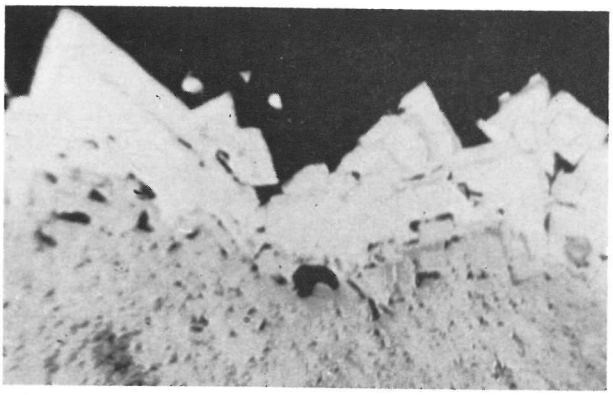

FIG. 8. Bravoite disseminations peppered through a distinct portion of a pyrite mass. Zoning type VIII. Oil immersion, 550×.

TABLE 1. CLASSIFICATION OF 4575 BRAVOITE GRAINS COUNTED IN FREDERICKTOWN ORE, MISSOURI

| Zoning type | Size (microns) | Crystal habit | Dark zones | Bright zones | Holes | Direct locking | Enclosing rock | Quantity |
|---|---|---|---|---|---|---|---|---|
| I | 60% 5–20<br>40% 20–50 | simple<br>(Δh=0) | dark-brownish<br>(δR=0) | absent | none | # sg or py<br>(some # gn) | dolomite or<br>mixed facies | 59 gr.<br>1.3% |
| II | 45% 5–20<br>34% 20–50<br>21% 50–80 | simple<br>(Δh=n<br>or=0) | dark-brownish<br>(δR=0) | whitish-<br>yellow | 10% with<br>90% without | free<br>(or # gn, sg,<br>mr, ct) | dolomite or<br>mixed facies | 1275 gr.<br>28.0% |
| III | 38% 5–20<br>56% 20–50<br>4% 50–100<br>2% 100–150 | simple<br>(Δh=n<br>or=0) | violet-cream<br>(δR=0 or=n) | whitish-<br>yellow | 30% with<br>70% without | free<br>(or # mr, cp, ct) | sandy dolo-<br>mitic or<br>mixed facies | 2272 gr.<br>50.0% |
| IV | 10% 5–20<br>75% 20–50<br>15% 50–100 | simple<br>(Δh=0) | absent | whitish-<br>yellow | 100% with | free<br>(or # gn, mr) | mixed facies<br>or dolomite | 380 gr.<br>10.1% |
| V | 15% 5–20<br>26% 20–50<br>38% 50–100<br>15% 100–150<br>6% 150–200 | simple<br>(Δh=0) | lavender<br>(δR=0 or=n) | whitish-<br>yellow | 50% with<br>50% without | free<br>(or # gn, ct) | dolomite | 490 gr.<br>8.4% |
| VI | 33% 5–20<br>15% 20–100<br>52% 100–200 | simple<br>(Δh=0) | dark-brownish<br>(δR=n) | absent or<br>whitish-<br>yellow | 85% with<br>15% without | # gn<br>(or mr, sg)<br>some free | mixed facies | 33 gr.<br>0.7% |
| VII | From 175 to 200 | complex<br>(Δh=0) | dark-brownish<br>(δR=n) | absent | 100% with | # gn<br>(or mr, sg, ct) | mixed facies | 45 gr.<br>1.0% |
| VIII | 200 or more | variable<br>(Δh=0) | spotted<br>lavender | whitish-<br>yellow | disseminated | # mr only | sulphide<br>nodules | 21 gr.<br>0.5% |

Δh=habit changes; δR=gradational change in reflectivity; # means "locked to"; sg=siegenite, py=pyrite, mr=marcasite, gn=galena, ct=cattierite, cp=chalcopyrite; gr=grains observed.

*Results*

Table I represents the results of the statistical recording of the characteristics of the 4575 bravoite grains. The columns of the table list the parameters of importance to this study, and are here briefly discussed.

*Grain size:* Grains showing simple zoning (types I to IV) are usually small. Most of them fall below the 50 micron limit. However, grains of types V to VIII are large, averaging about 100 or more microns in diameter.

*Crystal habit:* There is a change of habit (Δh) in types II and III only. Fig. 9 shows various forms that display such a change. Most of the drawings represent bravoite-pyrite grains from the Fredericktown ores. The two typical types in the lower right are drawn after Kalb (1951). Kalb interprets the habit changes as proof of a solid-solution gap. Habit changes are common, even from one generation of pyrite to another, and therefore can hardly be taken as proof of a gap in the bravoite-pyrite solid-solution series.

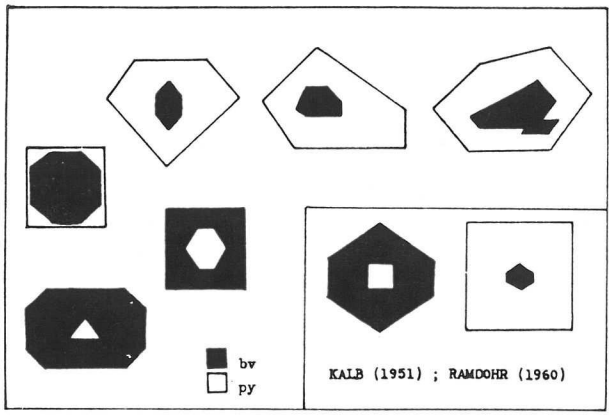


FIG. 9. Various habit changes of bravoite-pyrite grains from Fredericktown and as reported from Maubach-Mechernich.

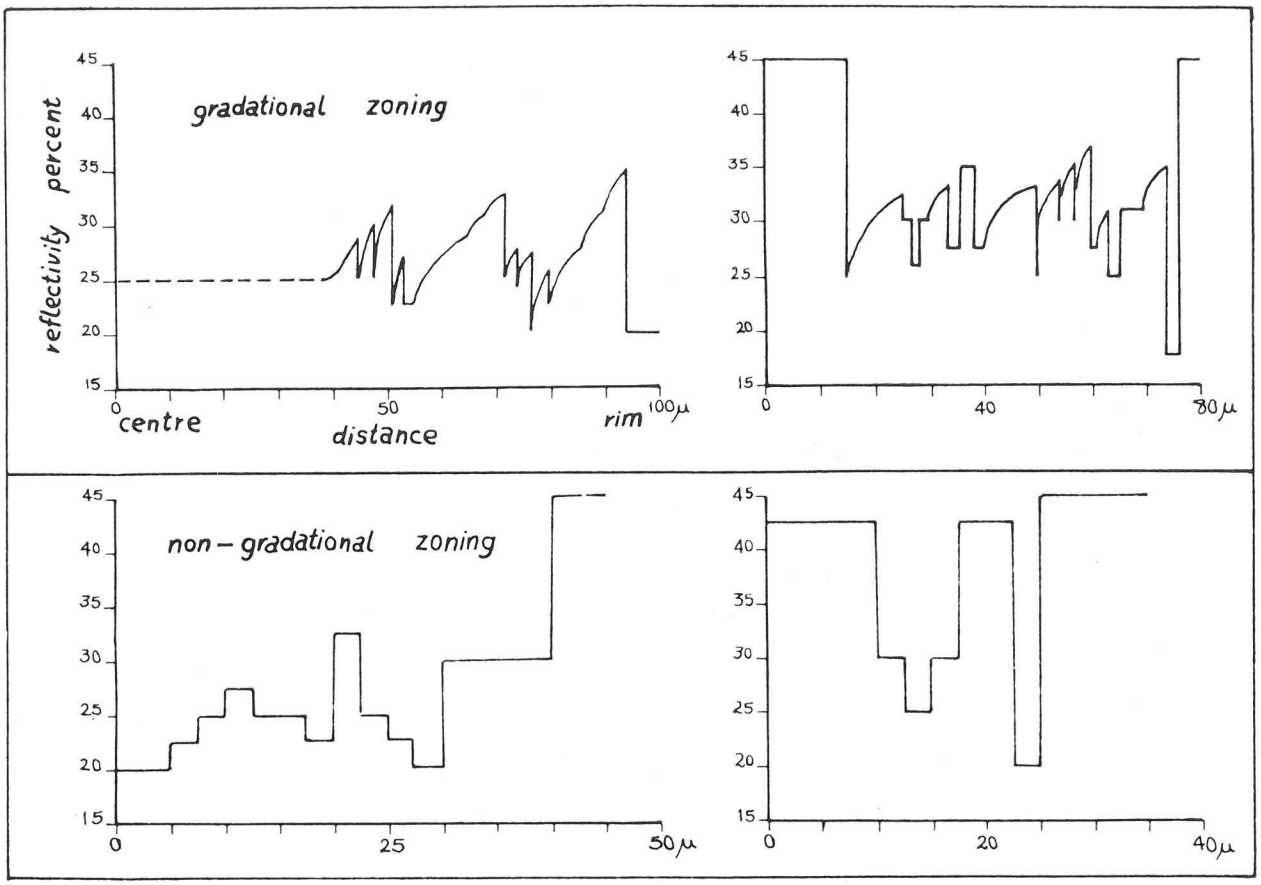


FIG. 10. Reflectivity profiles of four grains showing abrupt and gradational zoning.

*Dark zones:* The dark zones in the grains show variable characteristics. The darkest bravoite areas are found in the first two types and as rims of type VII grains. Violet-cream and lavender zones are common in larger grains. Usually they show gradational zoning. Gradational changes of reflectivity ($\delta R$) can be found mainly in types VI and VII. Two illustrations in Fig. 10 show gradational zoning. The gradational color slopes trend towards the Fe-rich member. Reversed slopes have never been observed with certainty.

*Bright zones:* When intergrown with bravoite, pyrite layers appear to be darker than those free of bravoite, as mentioned above. This might be due to a certain content of Ni and/or Co.

The relationships between dark and bright zones of the bravoite-pyrite grains can be seen on the reflectivity profiles (see four examples in Fig. 10.) The components of all measurements made on the reflectivity profiles are shown in Fig. 11. Separate histograms are drawn here for each zoning type. Proceeding from type I to type IV, there is a tendency of area decrease on the side of bravoite and an increase on the side of pyrite. In types V to VIII a maximum shows up in the area of intermediate reflectivity, *i.e.*, in the range from 20 to 35%.

Figure 12 is a histogram made by compiling data from the eight drawings of Fig. 11. Note that there are three maxima. Also, within the accuracy of the methods used so far, there does not seem to be any compositional gap between the bravoite and the pyrite.

*Holes within the grains:* The distribution of holes in the grains belonging to the eight zoning types is shown in the 6th column of Table I. These holes are regarded as natural rather than as produced by polishing, for the following reasons:

1. They always run parallel to crystallographic growth planes.
2. They occupy definite positions in certain zones.
3. They generally display smooth linear boundaries.
4. Frequently, their place is taken by galena and possibly by cattierite.
5. Since we are dealing with zonal structures, we may expect periods of interruptions during the growth of the grains.

*Direct locking:* Bravoite grains of types II, III and IV are mostly not intergrown with other sulfides. Grains of other types are commonly locked to siegenite, galena and marcasite.

*Enclosing rock:* Relations to the enclosing rock are listed in the 8th column of Table I. Types from I to IV occur in dolomites as well as in rocks of mixed facies, *i.e.* in finely interbedded shaly, sandy, glauconitic and dolomitic layers,

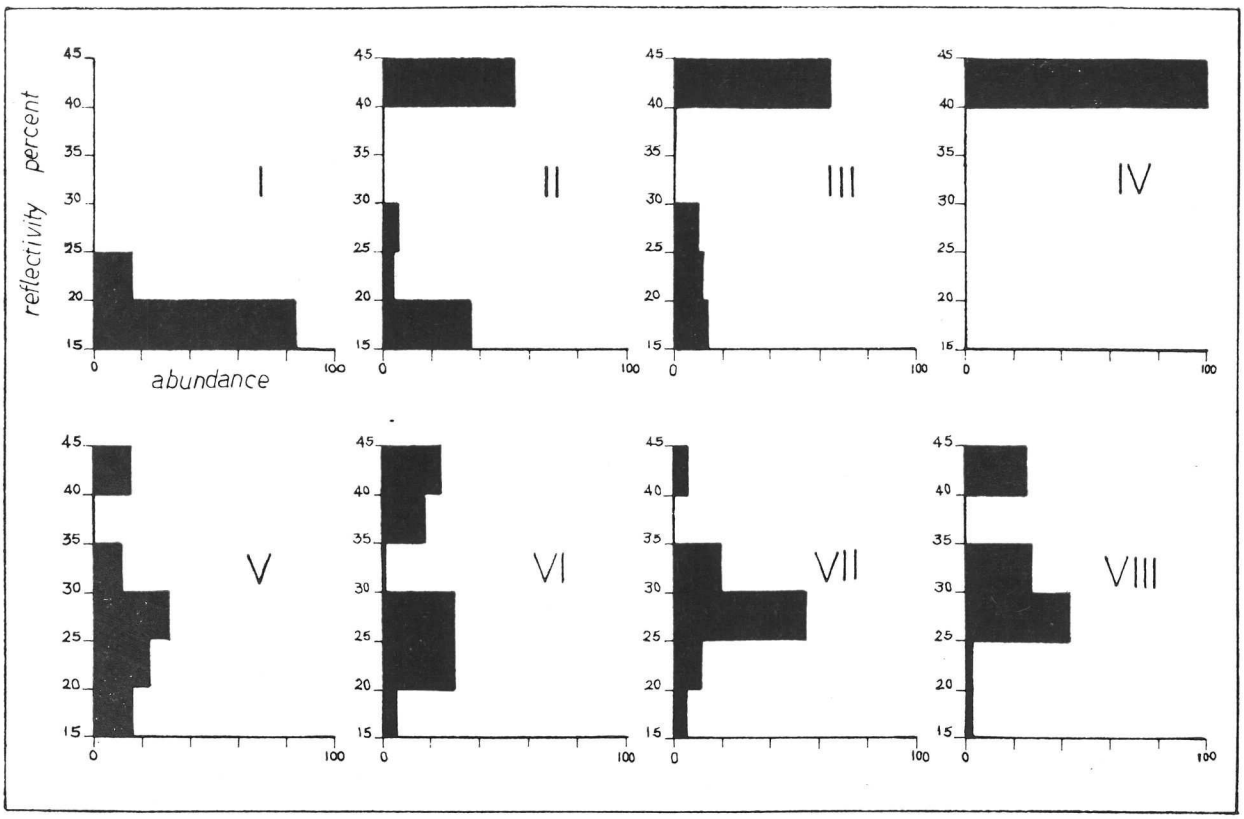


FIG. 11. Histograms of reflectivity areas as measured for each zoning type (*cf.* Fig. 1).

or variable mixtures of these rocks. Type V occurs in dolomites only. Types VI and VII occur in rocks of mixed facies, and type VIII occurs in sulfide nodules which are common in black shales, and in cavities in the Bonneterre dolomite.

*Quantitative counting:* With regard to their abundance, grains of types II and III comprise 78% of the total, and types IV and V constitute about 18%. The rest make up the remaining 4%, half of which represents grains of types VI and VII displaying clear gradational zoning, while the other half consists of grains that belong to types I and VIII.

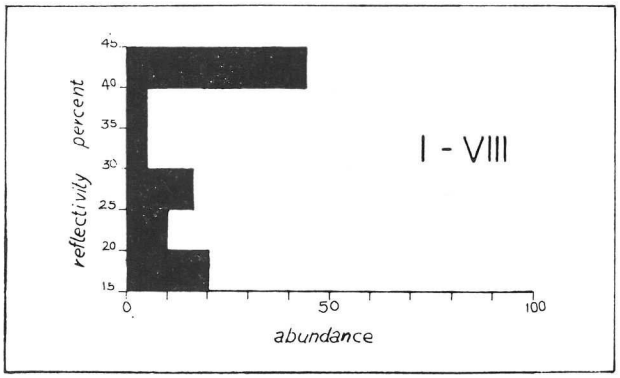


FIG. 12. Histogram representing the summation of cumulative graphs of Fig. 11.

## POSSIBLE CAUSES FOR ZONING

The different observations and measurements discussed above illustrate various types of zoning in bravoite. Zoning is produced by compositional differences between successive crystal layers. It appears that conventional theories on zoning factors (Niggli, 1941, p. 608; Eitel, 1954, pp. 83 and 711; Buckley, 1951, p. 403) do not apply in this case. The coexistence of abrupt and gradational zoning, with many subvarieties in the same rock, suggests that factors other than straight pressure-temperature equilibria may play a substantial role. Possible factors that might be responsible for producing zones are these:

a) Possible internal factors
   - Lattice energy.
   - Electric properties of the crystallizing surfaces.
   - Types of lattice defects.
   - Size and polarization effects.
   - Rate of unmixing.
   - Number and rate of nucleation.

b) Possible external factors
   - Excess or deficiency of cations.
   - Partial pressures of anions.
   - pH and Eh values of the environment.
   - Network modifiers (in a surrounding colloidal "matrix.")

Cation fixation and periodic release by organic complexes. Temperature and pressure of the depositing solutions.

It seems likely that a combination of one or more factors, of both internal and external parameters, constitutes the working hypothesis. Among other observations, the presence of both abrupt *and* gradational zoning within the same small laminae of sediment can hardly be attributed to the same process. Preliminary considerations appear to suggest that in addition to concentration changes, surface properties during crystallization may act as a "screen" responsible for the formation of abrupt zones in one case and gradational in another. These relationships are being investigated.

## References


Allen, E. T., I. L. Crenshaw, L. Johnson, and E. S. Larsens (1912) Die mineralischen Eisensulfide. *Zeit. anorg. Chem.* **76,** 201–273.

Amstutz, G. C. (1959) Syngenetic zoning in ore deposits. *Proc. Geol. Assn. Canada,* **11,** 95–113.

——— and F. El Baz (1962) The diagenetic behavior of the sulfides in Fredericktown, Missouri (in press).

——— R. P. Uhley, and F. El baz (1961) Sedimentary features in the layered sulphide deposits of Fredericktown, Missouri (abs.). *Geol. Soc. Am. Spec. Paper,* **68,** 128.

Buckley, H. E. (1951) *Crystal Growth.* John Wiley & Sons, New York.

Clark, L. A. and G. Kullerud (1960) The Fe-Ni-S system: Bravoite synthesis. *Ann. Rept. Geophys. Lab.,* 1959–1960, 126–127.

Dana, E. S. (1871) System of Mineralogy. 5th ed. John Wiley & Sons, New York, p. 63.

Doelter, C. and H. Leitmeier (1926) Handbuch der Mineralchemie. Steinkopf, Dresden, **4,** I, p. 643.

Edwards, A. B. (1960) *Textures of the Ore Minerals and Their Significance.* Austral. Inst. Min. Metal. Melbourne, pp. 16–17.

Egleston, T. (1889) Catalogue of minerals and synonyms. *U. S. Nat. Mus. Bull.* **33,** 138.

Eitel, W. (1954) *The Physical Chemistry of the Silicates.* Univ. of Chicago Press.

El baz, F. (1961) Sedimentary features and geochemistry of the sulphide facies in the transition between the Lamotte sandstone and the Bonneterre formation in the Ferdericktown area, Madison County, Missouri. Thesis, University of Missouri, Rolla.

Eskola, P. (1946) *Kristalle und Gesteine.* Springer, Wien, p. 313.

Hegemann, F. (1942) Die geochemische Bedeutung von Kobalt und Nickel im Pyrit. *Zeit. angew. Mineral.* **4,** 121.

Hillebrand, W. F. (1907) The vanadium sulphide patronite and its mineral associates from Mina Ragra, Peru. *Am. Jour. Sci. Ser. 4,* **24,** 151.

Hunt, H. S. (1866) Geological exploration of Canada from 1863 to 1866. Ottawa, p. 225.

Kalb, G. (1951) Crystal morphology as criterion for isomorphy. *Naturwissenschaften,* **38,** 560–561.

——— (1952) The crystal habit of bravoite and pyrite as a criterion of isomorphism. *Neues Jb. Mineral. Monatsh. 1952,* 90–93.

Kidwell, A. L. (1946) Minerals of Fredericktown, Missouri, mining district. *Rocks and Minerals,* **21,** 750–753.

Love, L. G. (1958) Micro-organisms and the presence of syngenetic pyrite. *Jour. Geol. Soc. London,* **113,** 429–440.

Maucher, A. and G. Rehwald (ed.) (1961) Card index of ore photomicrographs. Umschau Verlag, Frankfurt, p. 0040.

Niggli, P. (1941) *Lehrbuch der Mineralogie und Kristallchemie.* Bornträger, Berlin.

Omera, A. E. (1961) Contribution to the study of the Mount Isa copper ore bodies. *Proc. Austral. Inst. Min. Metal.* **197,** 163–192.

Penfield, S. L. (1893) On pentlandite from Sudbury with remarks upon three supposed new species from the same region. *Am. Jour. Sci.* **45,** 493.

Ramdohr, P. (1960) *Die Erzmineralien und ihre Verwachsungen.* Akademie-Verlag, Berlin, pp. 747–754.

——— and G. Kullerud (1961) Meteorites. *Ann. Rept. Geophys. Lab., 1960–1961,* 182–183.

Rasor, C. A. (1943) Bravoite from a new locality. *Econ. Geol.* **38,** 399–407.

Schneiderhöhn, H. and P. Ramdohr (1931) *Lehrbuch der Erzmikroskopie.* Gebrüder Bornträger, Berlin, pp. 173–178.

Short, M. N. (1940) Microscopic determination of the ore minerals. *U. S. Geol. Survey Bull.* **914,** 164, 270.

——— and E. V. Shannon (1930) Violarite and other rare nickel sulphides. *Am. Mineral.* **15,** 1–22.

Strunz, H. (1957) *Mineralogische Tabellen.* Becker und Erler, Leipzig, p. 80.

Vachromeiev, S. A. (1950) *Erzmikroskopie.* Moscow. (German translation: Oelsner, 1954) p. 129.

Walker, T. L. (1894) Notes on nickeliferous pyrite from Murray Mine, Sudbury, Ont. *Am. Jour. Sci.* **47,** 312–314.

MINERALOGICAL SOCIETY OF AMERICA, SPECIAL PAPER 1, 1963
INTERNATIONAL MINERALOGICAL ASSOCIATION, PAPERS, THIRD GENERAL MEETING

## SULFUR ISOTOPE MINERALOGY OF SULFIDES

MEAD LEROY JENSEN
*Department of Geology, Yale University, New Haven, Connecticut*

ABSTRACT

Sulfur from the troilite phase in meteorites exhibits a remarkably uniform $S^{32}/S^{34}$ composition of 22.21 $\pm 0.02$, which value is taken as a reference standard for $\delta S^{34}$ measurements. Primordial sulfur is identical to or at least very near this composition; nevertheless, sulfide minerals, even juxtaposed sulfides of the same species, are known to vary by more than 5% from this value, although no evidence has yet been found to indicate that specific sulfide species are characterized by specific isotopic compositions, even though sulfates are generally enriched in $S^{34}$. Information, therefore, on the processes by which this isotopic fractionation occurs is of assistance in determining the genesis of the sulfur in sulfide minerals.

For example, a large $\delta S^{34}$ variation for sulfides in one deposit is indicative of a biogenic rather than a magmatic hydrothermal origin for the sulfur in the sulfides. Biogenic sulfur is derived from hydrogen sulfide gas evolved from anaerobic bacteria of the *Desulfovibrio* genus. Sulfides in concretions, "red beds" copper deposits, and sandstone-type uranium deposits exhibit broad $\delta S^{34}$ variations, suggesting that they contain sulfur derived almost entirely from this biogenic process. The sulfur in magmatic hydrothermal sulfides, on the other hand, is quite uniform in its $\delta S^{34}$ composition. It is suggested that the reason for such is that as magmatic hydrothermal solutions become more and more concentrated in a cupola zone during progressive crystallization of their host or parent magma, the solutions become well mixed, resulting in a homogenization of what isotopic variations there may have been.

Further $\delta S^{34}$ studies corroborate the inference that one mechanism of sulfide replacement and exsolution is by diffusion of the smaller cations through the framework of the larger sulfur anions because the replacing sulfide exhibits the same original isotopic composition of the replaced sulfide. Even supergene sulfides form by this same mechanism of replacement, as indicated by $\delta S^{34}$ analyses plus the additional realization that sulfates are reduced to sulfides only at temperatures of several hundred degrees C. in the presence of an effective reducing agent such as carbon. Enrichment of $S^{34}$ (a common feature of sulfates) in sulfides, which has been noted for a few sulfide deposits, in correlation with geologic data, is rather suggestive of this source of sulfur.

Mass spectrometric measurements of the stable sulfur isotopic composition of sulfide minerals is an additional important mineralogical step in determining the composition and variation in composition of sulfide minerals.

## THERMODYNAMIC STUDY OF PYRRHOTITE AND PYRITE

PRIESTLEY TOULMIN, 3RD AND PAUL B. BARTON, JR.
*U. S. Geological Survey, Washington, D. C.*

ABSTRACT

Through the use of the electrum tarnish method (Barton and Toulmin, 1959; Toulmin and Barton, 1960) the following equation has been found to interrelate the composition of pyrrhotite, fugacity of sulfur, and temperature:

$$\log_{10} f_{S_2} = (70.03 - 85.83N)\left(\frac{1000}{T} - 1\right) + 39.301\sqrt{1 - 0.99808N} - 11.9113. \quad (1)$$

In this equation $f_{S_2}$ is the fugacity of sulfur relative to the ideal diatomic gas at 1 atm, N is the mole fraction of FeS in pyrrhotite (in the system FeS-$S_2$), and T the absolute temperature. The experimental uncertainty in the equation is 0.002 in N. Substituting equation 1 into the Gibbs-Duhem equation and inte-

grating leads to the following expression for the activity of FeS ($a_{FeS}$) relative to the pure substance at the temperature of consideration:

$$\log_{10} a_{FeS} = 85.83\left(\frac{1000}{T} - 1\right)(1 - N + \ln N) + 39.301\sqrt{1 - 0.99808N} - 39.226\tanh^{-1}\sqrt{1 - 0.99808N} - 0.0024. \quad (2)$$

The electrum tarnish method has permitted us to determine the $f_{S_2}$ *vs* T curve for the univariant assemblage pyrrhotite-pyrite-vapor from 743° to 325° C. (a considerably greater range than previously studied). The curve passes through the points indicated in the table below. Our determinations of the composition of pyrrhotite are in excellent agreement with the results of Arnold (1958). The activity of FeS in pyrite-saturated pyrrhotite is very different from unity (Table 1), a fact that greatly influences the interpretation of some other phase equilibrium studies involving pyrrhotite and their application to sulfide mineral assemblages, but has little effect on the more general calculations of composition of hydrothermal or magmatic fluids.

TABLE 1. POINTS ALONG THE SMOOTHED PYRITE-PYRRHOTITE CURVE

| t° C. | $N_{FeS}$ | log $f_{S_2}$ | $a_{FeS}$ |
|---|---|---|---|
| 743 | 0.8993 | + 0.76 | 0.375 |
| 599 | 0.9202 | − 2.00 | 0.455 |
| 514 | 0.9298 | − 4.00 | 0.496 |
| 410 | 0.9395 | − 7.00 | 0.536 |
| 354 | 0.9440 | − 9.00 | 0.554 |
| 325 | 0.9462 | −10.17 | 0.564 |

Combining these data with the well-known standard free-energy of the reaction Fe ($\alpha$)+$\frac{1}{2}S_2$(g, 1 atm) = FeS (pyrrhotite), we calculate the standard free energy of formation of pyrite from the elements (Fe, $S_2$) at 1 atm:

$$\Delta G^\circ = -71{,}260 + 47.09\ T \text{ cal (T in degrees K)} \quad (3)$$

The temperature coefficient of equation (3) is in excellent agreement with calorimetric data.

MINERALOGICAL SOCIETY OF AMERICA, SPECIAL PAPER 1, 1963
INTERNATIONAL MINERALOGICAL ASSOCIATION, PAPERS, THIRD GENERAL MEETING

# MISCELLANEOUS PAPERS

## THE ROLE OF ORIENTED TRANSFORMATIONS IN MINERALOGY

L. S. DENT GLASSER, F. P. GLASSER AND H. F. W. TAYLOR
*Department of Chemistry, University of Aberdeen, Aberdeen, Scotland*

ABSTRACT

Topotactic reactions are discussed with special reference to those of proved or possible mineralogical significance. It is suggested that some mineralogical phenomena might be reinterpreted in terms of such mechanisms, which are probably more common than has generally been supposed.

There has recently been an increasing interest in oriented transformations; that is, reactions in which a single crystal of the starting material is transformed directly into something approaching a single crystal of the product (or products). Such reactions have been termed topotactic (Lotgering, 1959; Mackay, 1960). For their occurrence, there must in general be some measure of three-dimensional correspondence between the two structures, implying that at least some chemical elements are common to both. This is in contrast to epitaxy, which demands only two dimensional correspondence; indeed one substance may grow epitaxially on another without being chemically related to it (*e.g.* the growth of hydrocarbons on mica).

Studies of such topotactic reactions can give information about their mechanisms. For example, study of the transformation of rhodonite, (Mn, Ca) $SiO_3$, to a wollastonite solid solution showed conclusively that the reaction proceeded by the migration of silicon and of some of the associated oxygen atoms; the remainder of the structure was relatively unchanged (Dent Glasser and Glasser, 1961). Furthermore, study of a topotactic reaction may give clues to a previously unknown structure; for example, knowledge of the orientation of the dehydration products of foshagite helped in the determination of its structure (Gard and Taylor, 1958). Because the details of such studies are complex, they will not be discussed here. We shall limit ourselves to a general survey of topotactic reactions, emphasizing their possible mineralogical importance.

Table I lists some types of reaction, all of geologic interest, which can occur topotactically; the examples given are all drawn from substances which occur as minerals. All the examples quoted involve major structural changes; processes which involve only minor changes, such as the $\alpha-\beta$ quartz inversion, have been omitted.

Topotactic reactions vary widely in the extent to which the composition of the crystal changes. At one extreme are polymorphic transitions which involve no change in composition. At the other are reactions such as the dehydration of brucite to periclase, in which, according to the chemical equation

$$Mg(OH)_2 \rightarrow MgO + H_2O$$

half the oxygen atoms are lost from the crystal. It was originally assumed that the elements of water were lost uniformly from all parts of the crystal by condensation of adjacent hydroxyl groups. A "homogeneous" mechanism of this type would result in such a disturbance of the crystal framework that it is difficult to see how it could account for a topotactic reaction. An alternative "inhomogeneous" mechanism, of the kind postulated by Taylor and co-workers (Freeman and Taylor, 1960; Ball and Taylor, 1961), and by Brindley (1961), resolves this difficulty. The oxygen for the expelled water comes entirely from certain parts of the structure which are destroyed, leaving pores. $H^+$ ions diffuse into these regions (which probably begin to form around defects in the crystal) while $Mg^{2+}$ ions diffuse into the parts of the crystal where MgO is formed topotactically. These regions thus lose no oxygen, but gain $Mg^{2+}$ to replace the lost $H^+$ ions. It has been suggested that the dehydroxylation of clay minerals should also be approached in this way (Taylor, 1962).

In most topotactic reactions, the arrangement of the bulkiest atoms or ions in the structure appears to control the orientation relationship. In oxides and silicates it is therefore the oxygen packing which is important, together with any large cations which may be present (*e.g.* $Ca^{2+}$, $Na^+$). Smaller cations, *including silicon*, diffuse through the oxide framework, which remains relatively unchanged. Gay and LeMaitre (1961) present a detailed picture of this process in the formation of iddingsite from olivine. They visualize a continuous series of highly disordered states, from which regions of comparative

TABLE I. SOME TOPOTACTIC REACTIONS

| Type of reaction | Examples | References |
|---|---|---|
| Redox reactions | magnetite → hematite | Gruner, 1926 |
| | cryptomelane → bixbyite → hausmannite | Faulring *et al.*, 1960 |
| Hydrations | olivine → iddingsites | Gay and LeMaitre, 1961 |
| Thermal dehydrations | brucite → periclase | Ball and Taylor, 1961 |
| | amphiboles → pyroxenes | Thilo and Rogge, 1939; Freeman and Taylor, 1960 |
| | xonotlite → wollastonite | Dent and Taylor, 1956 |
| | gypsum → anhydrite | Flörke, 1952 |
| | kaolinite → metalaolin → spinel → mullite | Brindley and Nakahira, 1959 |
| | talc → enstatite | Thilo and Rogge, 1939 |
| | sepentine → forsterite | Brindley and Zussman, 1957 |
| Other thermal decompositions | dolomite → calcite | Haul and Wilsdorf, 1952 |
| | smithsonite → zincite | Rose, 1939 |
| Hydrothermal reactions | tobermorite → xonotlite | Taylor, 1959 |
| | chrysotile → forsterite | Ball and Taylor, 1962 |
| Exsolution | *e.g.* lamellae in pyroxenes | —[1] |
| | feldspars | —[1] |
| | olivines | Hurlbut, 1961 |
| Anion exchange | calcite → fluorite | Glasser, 1962 |
| | wurtzite → zincite | Prewitt-Hopkins and Frondel, 1956 |
| Polymorphic transitions | rhodonite → wollastonite | Dent Glasser and Glasser, 1961 |
| | wurtzite → sphalerite | Kröger, 1940. |
| | rhombic enstatite ⇄ proto enstatite ↖? ↙ clino enstatite | Brown *et al.*, 1961 |
| Alteration | ilmenite → rutile | Bailey *et al.*, 1956; Yanulov and Chulkova, 1961. |

[1] Extensive literature; see, for example, papers by M. G. Bown, P. Gay, N. Morimoto, J. V. Smith, W. S. Mackenzie, F. Laves, O. F. Tuttle and N. L. Bowen.

order become differentiated. Composition and degree of structural order may vary continuously through the "crystal". Iddingsite may be in any of these states of disorder, and is therefore always rather poorly crystallized, but it seems likely that transformations resulting in well crystallized end products may proceed via similar disordered states.

Anions are in general bulkier than cations, but in anion exchange reactions it appears to be the cations which exert structural control. The transformation calcite→fluorite is especially interesting; fluorite pseudomorphous after calcite occurs in nature. Calcite crystals can be partially replaced with fluorite in the laboratory (Ames, 1961); examination of such crystals shows that the fluorite is oriented (Glasser, 1962; Glover and Sippel, 1962).

The hydrothermal reactions of single crystals have so far been little studied. The mechanism of the reaction sometimes, though not always, changes with increase in water vapor pressure. Thus, dehydration of chrysotile at 520° and 500 kg/cm² gives forsterite in an orientation different from that found on heating in air at this temperature; at still higher pressures (1200 kg/cm²) the forsterite is randomly oriented (Ball and Taylor, 1962). Further studies of the effects of water pressure on topotactic reactions are badly needed.

Topotactic control over the crystal size and perfection may help explain minor discordance between different sets of P-T data obtained for hydrothermal reactions such as $Mg(OH)_2 \rightleftarrows MgO + H_2O$. Thus if the reactions A→B and B→A proceed by different mechanisms, yielding products with characteristic textures, defect contents, etc., determination of the actual "equilibrium" may be a formidable task.

It should be pointed out that Table I is by no

means an exhaustive list. Nevertheless, it includes most mineralogically important types of reaction, and the minerals listed include representatives of most important groups. We do not wish to imply that all the examples of transformations which are listed actually do occur in nature, but it does seem likely that topotactic reactions may be very much more common than has sometimes been supposed. It might be profitable to examine from this standpoint the textures of minerals and mineral assemblages, particularly those believed to record a genetic history of solid-solid transition (*i.e.* replacement, etc.). Lauder (1961) has attempted this, using mainly optical techniques.

It is hoped that this brief review of topotactic processes may be helpful to those interested in these problems.

ACKNOWLEDGMENT

This paper forms part of a study on the structural chemistry of silicates and related substances sponsored by the Office of Aerospace Research of the United States Air Force, through its European Office.

REFERENCES

AMES, L. L. (1961) The metasomatic replacement of limestones by alkaline, fluoride-bearing solutions. *Econ. Geol.* **56,** 730–739.

BAILEY, S. W., E. N. CAMERON, H. R. SPEDDEN, AND R. J. WEEGE (1956) The alteration of ilmenite in beach sands. *Econ. Geol.* **51,** 263–279.

BALL, M. C. AND H. F. W. TAYLOR, (1961) The dehydration of brucite. *Mineral Mag.* **32,** 754–766.

——— AND H. F. W. TAYLOR (1962) The dehydration of chrysotile in air and under hydrothermal conditions. *Mineral. Mag.* (in press).

BRINDLEY, G. W. (1961) The crystal structure and thermal behaviour of some ceramic materials. *Dainippon Yôgyô Kyôkai Zasshi,* **69,** 23–28 (in Japanese).

——— AND M. NAKAHIRA (1959) The kaolinite-mullite reaction series, Parts I, II, III. *Jour. Am. Ceram. Soc.* **42,** 311–324.

——— AND J. ZUSSMAN (1957) A structural study of the thermal transformation of serpentine minerals to forsterite. *Am. Mineral.* **42,** 461–474.

BROWN, W. L., N. MORIMOTO AND J. V. SMITH (1961) A structural explanation of the polymorphism and transitions of $MgSiO_3$. *Jour. Geol.* **69,** 609–616.

DENT, L. S. AND H. F. W. TAYLOR (1956) The dehydration of xonotlite. *Acta Cryst.* **9,** 1002–1004.

DENT GLASSER, L. S. AND F. P. GLASSER (1961) Silicate transformations. rhodonite—wollastonite. *Acta Cryst.* **14,** 818–822.

FAULRING, G. M., W. K. ZWICKER AND D. W. FORGENG (1960) Thermal transformations and properties of cryptomelane. *Am. Mineral.* **45,** 946–959.

FLÖRKE, O. W. (1952) Kristallographische und röntgenometrische Untersuchungen im System $CaSO_4-CaSO_4\cdot 2H_2O$. *Neues Jahrb. Mineral., Abh.* **84,** 189–240.

FREEMAN, A. G. AND H. F. W. TAYLOR (1960) Die Entwässerung von Tremolit. *Silikattech.* **11,** 390–392; and unpublished work.

GARD, J. A. AND H. F. W. TAYLOR (1958) Foshagite; composition, unit cell and dehydration. *Am. Mineral.* **43,** 1–15.

GAY, P. AND R. W. LEMAITRE (1961) Some observations on "iddingsite". *Am. Mineral.* **46,** 92–111.

GLASSER, F. P. (1962) Unpublished work.

GLOVER, F. D. AND SIPPLE, R. F. (1962) Experimental pseudomorphs: replacement of calcite by fluorite *Am. Mineral.* **47,** 1156–1165.

GRUNER, J. W. (1926) Magnetite—martite—hematite. *Econ. Geol.* **21,** 375–393.

HAUL, R. A. W. AND H. WILSDORF (1952) Röntgenographische Untersuchung der thermischen Zersetzung von Dolomitkristallen. *Acta Cryst.* **5,** 250–255.

HURLBUT, C. S. (1961) Tephroite from Franklin, New Jersey. *Am. Mineral.* **46,** 549–559.

KRÖGER, F. A. (1940) Note on the wurtzite—sphalerite transition of zinc sulphide. *Zeit. Krist.* **102,** 136–7.

LAUDER, W. R. (1961) Reaction of crystal structures and reaction fabric. *Am. Mineral.* **46,** 1317–1328.

LOTGERING, F. K. (1959) Topotactical reactions with ferrimagnetic oxides having hexagonal crystal structures, I. *Jour. Inorg. Nucl. Chem.* **9,** 113–123.

MACKAY, A. L. (1960) Some aspects of the topochemistry of the iron oxides and hydroxides. *4th Int. Symp. React. Solids, Amsterdam,* 571–583.

PREWITT-HOPKINS, J. AND C. FRONDEL (1956) Thermal decomposition of zinc sulfide polymorphs. *Am. Mineral.* **35,** 116.

ROSE, A. (1939) Sur la dissociation thermique du carbonate de zinc. *Compt. rend.* **208,** 1914–1916.

TAYLOR, H. F. W. (1959) The transformation of tobermorite into xonotlite. *Mineral. Mag.* **32,** 110–116.

——— (1962) Homogeneous and inhomogeneous mechanisms in the dehydroxylation of minerals. *Clay Min. Bull.* (in press).

THILO, E. AND G. ROGGE (1939) Chemische Untersuchungen von Silikaten, VIII: Über die thermische Umwandlung des Anthophyllits $Mg_7Si_8O_{22}(OH)_2$. Über die Polymorphie des Magnesium—metasilikates und über den Mechanismus der Umwandlung von Anthophyllit und Talk beim Erhitzen. *Berichte,* **72B,** 341–362.

YANULOV, K. P. AND I. V. CHULKOVA (1961) Oriented pseudomorphs of rutile after ilmenite. *Dokl. Akad. Nauk. S.S.S.R.* **140,** 215–217.

## DISCUSSION

D. R. WONES (Washington, D. C.): The growth of feldspar and magnetite lamellae during oxidation of biotite phenocrysts in volcanic rocks might provide examples of topotactic inversions.

Walter (U.S.A.) brought up the problem of metastable transitions due to "inherited" structural features. It would appear that in the reaction

$$\tfrac{3}{5}O_2 + \underset{KFe_3FeSi_3O_{10}(OH)_2}{\text{Ferri-annite}} \rightleftarrows \underset{KFeSi_3O_8}{\text{Fe-sanidine}} + \tfrac{3}{5}\underset{\text{hematite}}{Fe_2O_3} + \tfrac{3}{5}\underset{\text{magnetite}}{Fe_3O_4} + H_2O$$

the Fe-sanidine "inherits" a disordered structure from the ferri-annite. In time the Fe-sanidine will convert to the more stable Fe-microcline. The structure of ferri-annite is being worked out by Morimoto and Donnay.

AUTHORS' REPLY: The evidence certainly suggests that the reaction proceeds topotactically, but this cannot be established without crystallographic evidence. Examination of the naturally occurring lamellae to establish whether or not their orientations are consistent with a topotactic reaction would provide indirect evidence. Direct evidence could be obtained by study of the oxidation of a single crystal of ferri-annite in the laboratory, using single crystal X-ray methods to determine whether the product of the reaction is oriented. For the interpretation of such a study, a knowledge of the crystal structure of ferri-annite would be essential.

It must be emphasized that the occurrence of a metastable phase is not in itself proof of topotaxy. It is tempting to hypothesize that the appearance of a metastable phase inheriting certain structural features of the parent does indicate a topotactic mechanism. We are hoping that mineralogists will study reactions of this sort to establish the degree of structural correspondence necessary for solid-solid transformations to proceed topotactically

MINERALOGICAL SOCIETY OF AMERICA, SPECIAL PAPER 1, 1963
INTERNATIONAL MINERALOGICAL ASSOCIATION, PAPERS, THIRD GENERAL MEETING

# EFFECTS OF THE CHANGES IN SLOPE OCCURRING ON LIQUIDUS AND SOLIDUS PATHS IN THE SYSTEM DIOPSIDE-ANORTHITE-ALBITE[1]

PETER J. WYLLIE
*Department of Mineralogy, The Pennsylvania State University, University Park, Pennsylvania*

ABSTRACT

Liquidus and solidus paths in the system diopside-anorthite-albite exhibit changes in slope. When plagioclase crystallizes alone from a ternary liquid both paths are steeper than in the system anorthite-albite, but when plagioclase is joined by diopside both paths become much less step than in the binary system. This fact, together with other evidence, suggests that the liquidus profile of an igneous rock series may be characterized by three shelves (where small temperature changes cause much fusion or crystallization, and large compositional changes) separated by steep slopes (where large temperature changes cause little crystallization or fusion, and small compositional changes). The shelves extend across picritic compositions (upper), basic and intermediate compositions (middle), and acid compositions (lower). The changes in slope may help to account for the relative proportions of various igneous rocks in different petrographical associations. The origin of primary basaltic and intermediate magmas, and the rarity of intermediate rocks in basic-acid igneous associations are discussed. Marginal zoning, oscillatory zoning, and the development of two generations of crystals (with continuous cooling) are discussed in terms of changes in slope of solidus paths.

## INTRODUCTION

During the fractional crystallization of basaltic magma, the composition and behavior of early precipitates of olivine, plagioclase feldspar, and pyroxene are important in determining the composition and amount of later differentiates. Concepts of basaltic differentiation have therefore been influenced by the phase diagrams for the systems forsterite-fayalite (Bowen and Schairer, 1935) and anorthite-albite (Bowen, 1913). Each system forms a complete series of solid solutions, with melting intervals at temperatures intermediate between the melting points of the end members, and the liquidus and solidus curves form simple loops with no abrupt changes in slope. This simple pattern, of course, does not persist in more complex systems. Addition of $Ca_2SiO_4$ to the system forsterite-fayalite produces an extensive shelf on both liquidus and solidus surfaces of the orthosilicate plane (Ricker, 1952[2]). Possible effects of this shelf, if it persists in the natural peridotite-basalt system, were discussed in an earlier paper (Wyllie, 1960; Buddington pointed out, in conversation, that the term "plateau" used in this paper to describe the gently sloping areas on the liquidus and solidus surface is inappropriate, and the term "shelf" is now adopted). Examination of Bowen's (1915) results in the system diopside-anorthite-albite reveals that addition of diopside to the system anorthite-albite produces a pattern of slopes for liquidus and solidus paths which is rather similar to that produced by addition of $Ca_2SiO_4$ to the system forsterite-fayalite.

[1] Contribution No. 61-27 from the College of Mineral Industries.

[2] The solidus surface must be intersected by a solvus between the forsterite-fayalite and the monticellite-kirschteinite series, and this certainly contributes to the shelf feature on the solidus, which is indicated by Ricker's preliminary data.

## LIQUIDUS AND SOLIDUS PATHS

Equilibrium and fractionation liquidus paths have frequently been discussed in geological literature, but solidus paths have received less attention. Liquidus and solidus paths illustrate the compositional changes of coexisting liquids and crystals with increase or decrease in temperature. If a path is steep, large temperature changes produce small compositional changes, whereas if a path crosses a gently sloping shelf, small changes in temperature produce large compositional changes.

In each of the binary systems forsterite-fayalite and anorthite-albite there is one liquidus path and one solidus path, and their slopes change continuously from one component to the other. In a multicomponent system there are many liquidus paths which vary with the composition of the initial liquid (crystallization processes) or crystalline mixture (fusion processes), and with the degree of fractionation. For each liquidus path there are several solidus paths giving the compositions of minerals in equilibrium with the liquids at various temperatures. With decreasing temperature the minerals may be precipitated or resorbed. An example of the latter situation is offered by the reaction relationship exhibited by olivine in many silicate systems and in some basic magmas. A discontinuity occurs in the slope of liquidus and solidus paths whenever a phase

appears in or disappears from the system. In many systems, rather abrupt changes in slope occur with no change in the number of phases.

A certain amount of supersaturation is required to initiate crystallization of most liquids, and the amount required depends upon the properties of the liquid and crystals. A moderate degree of supersaturation in silicate magmas probably leads to the precipitation of a few crystals which attain large sizes. If crystallization is initiated at a higher degree of supersaturation the number of crystals precipitated increases markedly but they remain small (Turner and Verhoogen, 1960, p. 47). When a liquidus path is steep the liquid temperature must fall quite far below the liquidus to produce much supersaturation, but when the slope is gentle a high degree of supersaturation can be produced if the liquid temperature falls only slightly below the liquidus.

The nature of the continuous zoning developed in minerals depends upon many factors, including the slope of the solidus path for the mineral. If the solidus path is steep the compositions of successive zones change only slightly even in large temperature intervals, but if the slope is gentle a wide range of zoning can be developed in a small temperature interval.

## The System Diopside-Anorthite-Albite

The main features of this system are summarized in Figs. 1 and 2, and a comprehensive account of equilibrium and fractional crystallization for various liquids has been presented by Bowen (1915). It is now known that the phase relationships are more complex than indicated, because appreciable substitution of alumina occurs in the pyroxene (Hytönen and Schairer, 1961). Schairer and Yoder (1960) have shown that there is no eutectic on the join diopside-albite, but that the point labeled C in Fig. 2 is a piercing point at a considerable higher temperature, 1133° C. However, revised data for the whole system are not available, and it will be assumed in the following discussion that the system remains ternary. Since most of the compositions considered lie in the plagioclase field, departures from ternary behavior probably have little effect on the general pattern of crystallization.

Each liquid on the field boundary coexists with diopside and a plagioclase feldspar of fixed composition, and the three phases coexisting at each temperature are represented by the corners of a three-

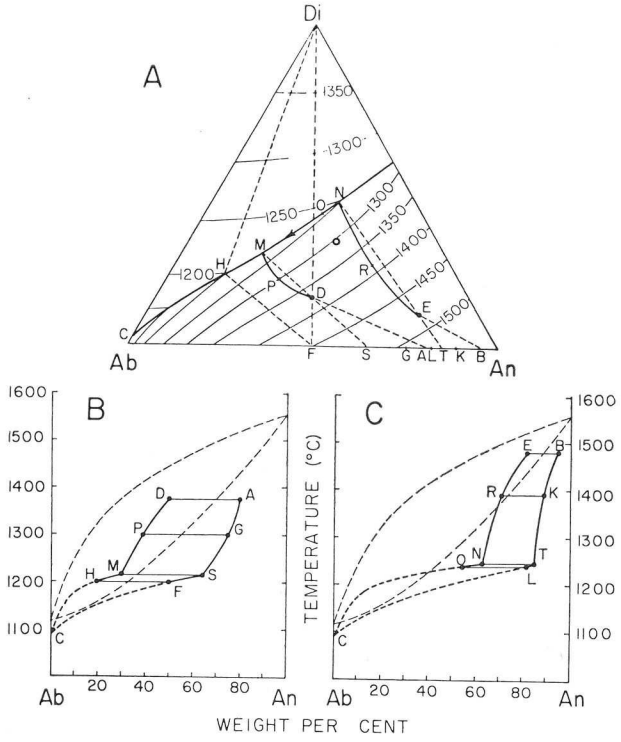


Fig. 2. Equilibrium crystallization in the system diopside-anorthite-albite.

A. Crystallization of liquids D and E, after Bowen (1915). For explanation see text and Bowen's paper. The open circle is the projected composition of Nockold's (1954) average "central" basalt (see text and Fig. 3).

B and C. Perspective TX projections of the liquidus and solidus paths for the liquid D (DPMH and AGSF) and for the liquid E (ERNO and BKTL) in Fig. 2A. With fractional crystallization, these paths would continue down the heavy dashed curves to C. The liquidus and solidus for the system anorthite-albite are shown as light dashed curves.

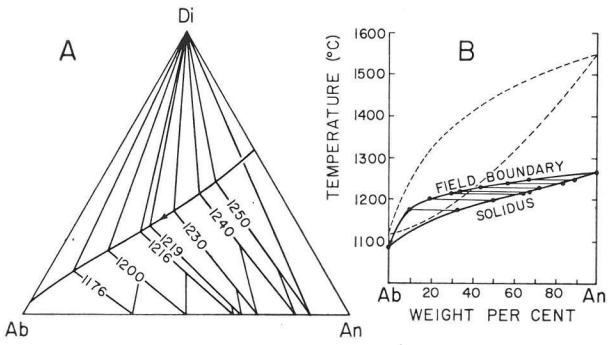


Fig. 1. The system diopside-anorthite-albite, after Bowen (1915).

A. Three-phase triangles measured by Bowen.

B. Perspective TX projection of the solidus and the liquidus field boundary. Three-phase triangles project as horizontal lines connecting pairs of points on the field boundary and solidus. The liquidus and solidus for the system anorthite-albite are shown as dashed curves (Bowen, 1913).

phase triangle. Those experimentally measured by Bowen are illustrated in Fig. 1A. During crystallization, the liquid and the plagioclase feldspar are enriched in albite relative to anorthite. The extent of this enrichment is indicated by the ratio of albite/anorthite (Ab/An), and it is illustrated in Fig. 1B, a projection of the field boundary and of the solidus from within the TX prism on to the An-Ab-T face of the prism. The three-phase triangles project as lines connecting pairs of points on the field boundary and the solidus. The proportion of diopside in the liquid is not represented because the projection is made horizontally through the diopside-T edge. Liquidus and solidus boundaries for the system anorthite-albite (Bowen, 1913) are plotted for comparison. Ternary crystallization temperatures are lower and, except near albite, the projected ternary field boundary and the solidus both slope much more gently than in the binary system. The difference in composition between coexisting liquid and plagioclase in terms of the ratio Ab/An is smaller in the ternary system than in the binary system. This is also true for plagioclase precipitated from multicomponent magmatic liquids (Wager, 1960a, Fig. 12).

Addition of other components to the system, in moderate amounts, would cause the field boundary to generate a surface with the form of a shelf. The boundary is only a line passing across this shelf, but, for convenience, whenever this feature appears on a liquidus or solidus path it will be referred to as a shelf.

Bowen described the equilibrium crystallization of the mixtures D and E in Fig. 2. The liquid D follows the path DPMH while the plagioclase changes composition from A to F, and the liquid E follows the path ERNO while the plagioclase changes from B to L. The enrichment of liquid and plagioclase in the ratio Ab/An is illustrated by the liquidus and solidus paths in Figs. 2B and C. These diagrams were obtained in the same way as Fig. 1B, by projecting the tie-lines for coexisting liquid and plagioclase. Liquidus and solidus paths in the binary plagioclase system are plotted for comparison. When plagioclase crystallizes alone from a ternary liquid the projected liquidus and solidus paths are steeper than in the binary system, but as soon as plagioclase is joined by diopside they become less steep than in the binary system. It should be noted that the slope of a projected liquidus path is not the same as its actual slope on the liquidus surface. However, although the slopes of the paths DPM and ERN are not quite as steep as indicated in the projection, they are steeper than the slopes in the binary system during the corresponding composition intervals (compare Figs. 2A, 2B, 2C).

The slopes of the liquidus paths in these projections may be considered as measures of differentiation of the liquid. The steep slopes DM and EN indicate that little differentiation occurs while plagioclase alone crystallizes from a multicomponent liquid, whereas the gentle slopes MH and NO indicate that when plagioclase is joined by other crystalline phases much differentiation occurs in a small temperature interval.

The influence of the slopes of liquidus paths on the rate of crystallization of liquids is demonstrated by Bowen's data for the liquids D and E (Fig. 2A). Liquid D begins to crystallize at 1,375° C., and approximately 50% crystallizes while its composition changes from D to M in a temperature interval of 159° C. The remaining 50% crystallizes while it changes composition from M to H in a temperature interval of only 16° C. Similarly, approximately 75% of liquid E crystallizes along the path EN in a temperature interval of 235° C. and the remaining 25% crystallized along the path NO in a temperature interval of only 8° C.

Bowen also discussed fractional crystallization in this system. Continuous zoning of the plagioclase lowers the temperature of final consolidation, and causes enrichment of the liquid, and of the outer plagioclase zones, in the ratio Ab/An. The liquids D and E then follow paths similar to those illustrated in Figs. 2B and C, with two modifications. The liquidus paths DPM and ERN, and the solidus paths AGS and BKT become somewhat less steep, joining the projected field boundary and solidus at temperatures lower than those indicated by MS and NT. However, Bowen's diagrams confirm that the paths for these compositions remain steeper than the corresponding paths in the binary system. The final liquid persists to much lower temperatures than indicated by HF and OL, and with strong fractionation the late liquids, and the outer plagioclase zones, could continue to the point C, the albite-diopside eutectic (assuming, for convenience, that the albite-diopside join remains binary).

Fusion processes can be traced by following the liquidus and solidus paths in the direction of increasing temperature. Partial fusion of the crystalline mixtures D and E, composed of diopside and homogeneous plagioclase feldspar, produces first a trace of liquid with compositions H and O, respectively. Because these liquids lie on the shelf, small increases of

temperature are followed by considerable melting as the liquid changes composition up the gentle slope of the shelf. Once the liquid leaves the shelf (at M and N respectively), much larger temperature increases are required to cause much further melting or change in liquid composition. For example, if equilibrium is maintained, an increase in temperature of 16° C. is sufficient to melt 50% of the mixture D while the liquid changes from H to M, but a further increase of 159° C. is required to melt the remaining 50%. Even if equilibrium is not maintained, *i.e.* if the crystalline plagioclase fails to react continuously with the liquid developed, the general pattern is unchanged. If the mixture D is composed of diopside and zoned plagioclase crystals, the first liquid developed is richer in the ratio Ab/An than H, and it forms at a lower temperature.

### Haplobasaltic, Haplodioritic and Haplogranitic magmas

The compositions of many igneous rocks can be represented approximately in the system diopside-anorthite-albite-orthoclase-silica. Bowen (1915) pointed out the close chemical and mineralogical correspondence of some natural basalts and diorites with mixtures lying close to the field boundary in the system diopside-anorthite-albite. The assemblages labradorite+diopside and andesine+diopside, with bulk compositions lying close to the field boundary, he called haplobasaltic and haplodioritic, respectively. Liquids with these compositions were similarly called haplobasaltic and haplodioritic magmas. Haplogranitic compositions lie close to the system albite-orthoclase-silica, but if these compositions are projected from within the five-component system onto the system diopside-anorthite-albite, with orthoclase+albite+silica plotted jointly as albite, they are represented by points not far removed from the field boundary in the system diopside-anorthite-albite. Therefore, although the assemblage albite+diopside (with bulk composition close to the field boundary) is not closely related in composition to granites, it is considered useful in this review to refer to this assemblage as haplogranitic. The assemblage oligoclase+diopside can be referred to as haplogranodioritic. These terms are used in Fig. 3.

It is often stated that typical basalts are composed essentially of labradorite and pyroxene, and that these minerals begin to crystallize almost simultaneously (Bowen, 1928, pp. 64–69; Hess, 1960, p. 178). This has been demonstrated experimentally for some basalts by Yoder and Tilley (1957). Such basalts are described as "normal" in this paper to distinguish them from what are here referred to as "olivine-," "pyroxene-," and "feldspar-basalts." "Olivine-basalts" precipitate olivine first, followed later by plagioclase and pyroxene. "Pyroxene-" and "feldspar-basalts" first precipitate either pyroxene or plagioclase, respectively. Normal basalts correspond to haplobasaltic compositions lying on the field boundary in the system diopside-anorthite-albite. Pyroxene-basalts correspond to haplobasaltic compositions lying in the diopside field, and feldspar-basalts correspond to haplobasaltic compositions lying in the plagioclase field. Nockold's (1954) average "central" basalt is plotted in Fig. 2A in terms of its normative pyroxene and plagioclase; it corresponds to a feldspar-basalt. Liquidus and solidus paths for a haplomagma with the composition of this point in the system diopside-anorthite-albite (feldspathic haplobasaltic magma) can be estimated from Bowen's (1915) data, and the result is shown in the projection of Fig. 3.

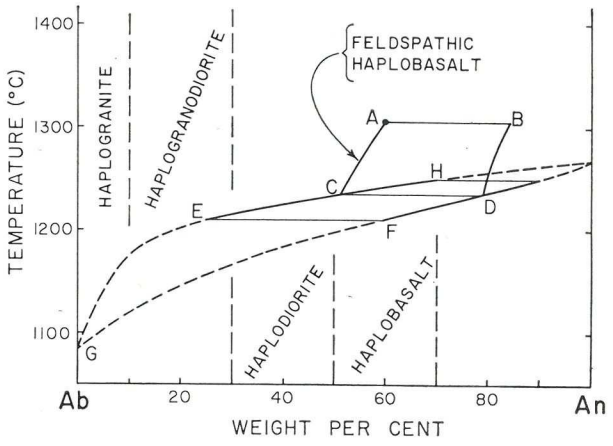


FIG. 3. Perspective TX projection of the liquidus and solidus paths (ACE and BDF) for equilibrium crystallization of the feldspathic haplobasaltic magma, A, representing the "central" basalt projected onto Fig. 2A. With fractional crystallization the paths would continue down the heavy dashed lines to G (the lettering in this figure does *not* correspond to that in Fig. 2). The liquid compositions on the path ACEG are related to their nearest igneous equivalents by their designation as haplomagmas. Normal haplobasaltic magmas lie on or close to the field boundary between C and H.

The liquid (A) begins to crystallize at 1,305° C. and, with equilibrium cooling, approximately 20% crystallizes in an interval of 70° C. (AC), while the plagioclase changes composition from about An84 to An79 (BD). Plagioclase is then joined by diopside. The remaining 80% of the liquid crystallizes in a temperature interval of only 25° C. (CE) while the

plagioclase changes compositon to $An_{59}$ (from D to F). The final liquid (E) at 1,210° C., with a ratio Ab/An of 0.75, is haplogranodioritic in composition. With strong fractional crystallization, zoning of plagioclase would cause the liquid to change composition to G, reaching haplogranitic compositions.

In order to examine the final stages of crystallization of haplogranitic magmas it is necessary to consider the effect of the additional components orthoclase and silica. Bowen (1928, pp. 104–110) briefly discussed the systems diopside-anorthite-albite-orthoclase and anorthite-albite-orthoclase-silica in connection with the crystallization of basaltic magma. Many parts of the complete five-component system have since been determined experimentally (*cf.* Schairer, 1957). The effects of adding moderate amounts of the components orthoclase and silica to mixtures corresponding to haplobasaltic magmas in Fig. 3 would be insignificant until the later stages of fractional crystallization. (During the middle and late stages of crystallization of natural magmas, the components of diopside in the synthetic system appear in hydrous phases such as amphibole and mica.) If Ab in Fig. 3 were replaced by albite+orthoclase+silica, the general pattern of fractional crystallization would be similar to that illustrated, except that the final temperature of consolidation at G would be lower, the final liquids and feldspar crystals would contain an appreciable proportion of $K_2O$, and quartz would be precipitated in the closing stages of crystallization. All liquidus temperatures would be somewhat lower, increasingly so for the more acid compositions. Final crystallization of haplogranitic magmas would occur near the feldspar-quartz field boundary of the Residua System, and this stage may be represented by another shelf on the liquidus surface.

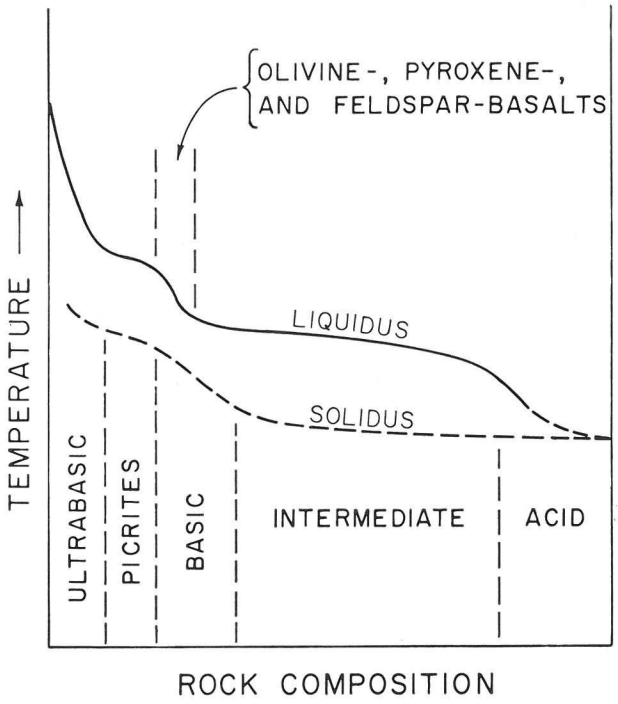


FIG. 4. Possible liquidus and solidus profiles for an igneous rock series. The liquidus profile represents one liquidus path through multicomponent space. The solidus profile does *not* represent a solidus path for any particular mineral. This tentative diagram illustrates schematically the temperatures of beginning of melting and of complete melting for a series of igneous rocks.

## Liquidus Slopes for Igneous Rock Series

Combination of extrapolations from Fig. 3 with the inferences discussed above and in the earlier paper (Wyllie, 1960) provides the liquidus profile illustrated in Fig. 4. This is a tentative working model representing one possible liquidus path through the multicomponent system including all igneous rocks. The stage of differentiation can be represented by a parameter such as the differentiation index (Thornton and Tuttle, 1960). The liquidus temperatures, the gradients of the slopes, and the positions of changes in gradient probably vary from one igneous series to another. The effects of pressure, with or without volatile components, are considerable. A temperature scale on Fig. 4 would thus be meaningless unless for a specific suite of rocks under specific conditions. Thermal data of this kind are not yet available.

The liquidus profile illustrates the rate of change of liquid composition for a constant rate of temperature change during the fractional crystallization of a magma, or the fusion of a crystalline igneous rock. It should be stressed that this representation need not imply that the rocks plotted have ever existed as completely liquid magmas. Shelves extend across picritic compositions (ranging from olivine-rich basalts to peridotite), across the composition range of basic and intermediate rocks, and across acid compositions. These will be referred to as the upper, middle, and lower shelves, respectively. They are connected by steeper liquidus slopes.

Evidence for the existence of the middle shelf and the steeper slope above it is reviewed in the preceding pages. Nockolds (1936) hinted at the possible existence of a shelf feature for this compositional range when discussing the rarity of intermediate magmas in basic-acid igneous associations. He suggested that

perhaps the pyroxene and plagioclase crystallized from a basic magma through a comparatively small temperature range, so that unless the residual magma was removed during a comparatively short space of time, intermediate rocks would not form.

Below the middle shelf, the liquidus slope for acid melts appears to increase in steepness (Fig. 3). The increase may be only apparent in the system diopside-anorthite-albite, because the temperature of the point G in Fig. 3 is now known to be 1133° C. (Schairer and Yoder, 1960). However, similar changes in slope occur in several systems for compositions corresponding to approximately the same stage of differentiation. In the systems leucite-forsterite-silica, leucite-diopside-silica, leucite-anorthite silica, and nepheline-anorthite-silica (illustrated in Figs. 30, 31, 32 and 35 of Schairer's useful review paper, 1957) the field boundaries separating the primary fields of forsterite, enstatite, diopside and anorthite, respectively, from the primary fields of one of the minerals of the Residua System, follow rather gently sloping paths at higher temperatures. At lower temperatures, as the field boundaries approach the Residua System, the slopes of the field boundaries increase appreciably. This increase in slope occurs with no change in the number of coexisting phases. That the steep slope at the low-temperature end of the middle shelf (Fig. 4) does exist is therefore suggested by the pattern of crystallization exhibited by several synthetic systems.

The existence of a steep liquidus slope for residual acid melts has been inferred from petrological studies. Bailey *et al.* (1924) suggested that after the crystallization of the gabbroic minerals in the Glen More ring dike, there was "a marked pause in the process of crystallization" before the granitic residuum crystallized. Holmes and Harwood (1928) suggested that after crystallization of the main part of tholeiitic sills, the residual acid liquid passed down a steeply-dipping groove in multi-dimensional space until it finally crystallized as micropegmatite.

The crystallization of the final liquid as granophyre or micropegmatite may be compared with the crystallization of liquids on the feldspar-quartz field boundary of the Residua System. From the data obtained by Tuttle and Bowen (1958, Fig. 23) it can be seen that, in a given temperature interval, much more crystallization occurs when feldspar and quartz crystallize together than when feldspar crystallizes alone. The final stages or crystallization of magmas, marked by the appearance of quartz, may thus be represented by the lower shelf indicated in Fig. 4.

A steep liquidus for the composition range including feldspar-, pyroxene-, and olivine-basalts connects the middle and upper shelves. The steep slope for feldspar-basalts is illustrated by AC in Fig. 3. A similar pattern is found for compositions corresponding to "olivine-basalts" in the system MgO-FeO-$SiO_2$ (Bowen and Schairer, 1935). Few basalts contain more than a small excess of either plagioclase or pyroxene, and the compositional range of such basalts may be limited to the lower part of the steep slope just above the middle shelf. There is no similar limit on the amount of olivine contained by crystalline basalts and other basic rocks (although there may be a limit on the amount of olivine contained in solution in basic magmas, as suggested by Bowen in 1928), and the liquidus path thus continues up the steep slope for rocks approaching picritic compositions. There are indications from the system CaO-FeO-MgO-$SiO_2$ that as the content of dissolved forsteritic olivine increases in liquids of certain compositions, at least, a steep liquidus gives way to a shelf feature. Possibly, therefore, the steep liquidus corresponding to olivine-basalts may give way to an upper shelf for picritic compositions (Wyllie, 1960). For ultrabasic rocks above the upper shelf, liquidus temperatures are high and the slope is steep.

The dashed line in Fig. 4 is a possible solidus profile reflecting the liquidus pattern of shelves and steep slopes. It is *not* a solidus path for any particular mineral.

Several liquidus profiles of this type for different igneous rock series could be represented on a surface illustrating not only the stage of differentiation but also the compositional variations between rocks at the same stage of differentiation (*e.g.* between alkaline, calc-alkaline, and tholeiitic series). The problem lies in finding suitable parameters to separate the different series (Wager, 1960b).

## Petrological Applications

The thermal regime of a magmatic system is complex. The rate of temperature change depends upon many factors, in particular upon the heat balance between the magma, the phases crystallizing from the magma or being dissolved by it, and the regional surroundings. Most of these factors cannot be evaluated because insufficient thermodynamic data are available. For simplicity, therefore, the preliminary petrological applications which follow refer only to a constant rate of temperature change. It is unlikely that these conditions ever obtain in natural systems, but the conclusions reached by making this assumption

will serve as working hypotheses. *It should be borne in mind that although only small changes of temperature are required to cause considerable melting or crystallization of compositions on shelf features, the amount of heat involved is much larger than for corresponding temperature intervals on steep liquidus slopes. The latent heat of fusion is an important item in the thermal budget.*

Applications of two types may be considered: (a) changes in the slope of liquidus paths in igneous systems may help to account for the relative proportions of various igneous rocks in different petrographical associations, and (b) the nature of continuous zoning in minerals will be dependent on changes in slope of their solidus paths.

*Primary basalts.* Basalts may be formed by partial fusion of feldspathic peridotite (Bowen, 1928). The intermediate magma first developed on the middle shelf (Fig. 4) increases rapidly in amount while it changes composition up the gentle slope of the shelf. Basaltic magma is formed at the high-temperature end of the shelf and on the lower part of the steep slope above it. A similar pattern would persist if the crystals involved were the high pressure phases (Yoder and Tilley, 1961). Garnet, clinopyroxene, and olivine would melt together while the liquid changed composition across the shelf, and when only liquid plus olivine remained, the middle shelf would give way to a steep slope, as illustrated in Fig. 4. Both the rate of fusion and the rate of change of composition (for a constant rate of temperature increase) decrease markedly when the steeper slope above the shelf is reached. This change in slope might well be a vital factor in limiting the products of fusion to the chemical composition of primitive basaltic magmas.

*Ultrabasic magmas.* If ultrabasic magmas are ever formed their composition may similarly be limited by the steep liquidus rising above the upper shelf (Fig. 4). The behavior of picritic magmas, which would lie on the upper shelf if they exist, was discussed in the previous paper (Wyllie, 1960).

*Primary intermediate magmas.* Partial fusion of sialic rocks in the earth's crust initially yields an acid melt. Its composition and the amount developed depend upon the bulk composition and mineralogy of the sialic rocks. When the temperature exceeds the threshold of the middle shelf (Fig. 4), rapid melting follows with the formation of large amounts of intermediate magma. If the original acid melt has not previously been separated from the rock this is incorporated in the magma. It changes composition rapidly up the gentle slope of the shelf, but its composition is limited by a steep liquidus path rising from the shelf, the exact position of which depends on the composition of the rock being fused. By the time this stage is reached, most sialic rocks would contain only a small residue of crystalline material. Other crustal rocks, more basic in composition, or containing an excess of aluminous minerals compared to compositions on the middle shelf, may retain a higher proportion of crystalline material when the liquidus path leaves the shelf. It is unlikely that the product of partial fusion of crustal rocks would reach the upper end of the middle shelf to yield a basic magma. The general pattern envisaged is illustrated in Fig. 2B, where D represents the projection of a hypothetical sialic rock from the multicomponent natural system onto the plane diopside-anorthite-albite. A process of this kind may account for the dominant role of intermediate rocks in the calc-alkaline series.

*Basic-acid associations.* The final liquid developed by equilibrium or moderate fractional crystallization of basalt is of intermediate composition. Strong fractional crystallization yields successively intermediate and acid liquids, and a small temperature interval suffices to change the liquid composition from basic to acid across the middle shelf. With the relatively rapid cooling which might be expected in intrusions of small or moderate size, the intermediate liquid stage is therefore unlikely to be represented by rocks of intermediate composition (*cf.* Nockolds, 1936). It is, however, represented by zones in plagioclase feldspar and in ferromagnesian minerals.

*Hybridization.* Acid magma developed by fractional crystallization of basic magma persists, with little crystallization and little change in composition, while the temperature falls from the middle to the lower shelf (Fig. 4). Hybridization could occur between the acid magma and the crystalline basic rocks during the interval of slow crystallization. Indeed, this drop from the middle shelf, if it exists, could be the cause of the hybridization which occurs in many basic-acid associations (*e.g.* Bailey *et al.*, 1924).

*Oscillatory zoning.* It has proved difficult to explain

[1] In other circumstances, if conditions are such that the heat of crystallization is lost only by conduction then the rate of crystallization on the shelf feature may be retarded, leading to the development of a wide range of intermediate differentiates.

the oscillatory zoning exhibited by plagioclase feldspars in terms of the steep solidus path for the system anorthite-albite (*e.g.* Hills, 1936). However, the various explanations which have been proposed appear much more feasible if the plagioclase solidus path is gentle in the appropriate composition range. Figures 1B and 3 suggest that this could be the situation for many magmas ranging in composition from basic to intermediate.

*Marginal zoning.* A feldspathic basaltic magma may precipitate plagioclase before other crystalline phases. The solidus path for the plagioclase is then characterized by a steep slope followed by a shelf, as illustrated in Fig. 3. This leads to the precipitation of plagioclase crystals of fairly uniform calcic composition (solidus path BD), or crystals of fairly uniform calcic composition with narrow, marginal zones (BD followed by DF). Both types are present in rocks of the porphyritic central magma type in Mull (Bailey *et al.*, 1924, p. 241 and p. 369), and in the Stillwater complex (Hess, 1960, p. 41). Olivine crystals precipitated from basic magmas may follow similar solidus paths.

*Crystals in two generations.* Many petrologists have stressed the fact that a mineral may give the appearance of crystallization in two generations, although crystallization was perfectly continuous (*e.g.* Hawkes, 1930). The liquidus and solidus paths illustrated in Fig. 3 illustrate one of the ways in which this appearance could result during continuous crystallization of a feldspathic basalt. Crystallization of the magma on the slope AC produces a few large crystals of plagioclase with fairly uniform composition. When the plagioclase is joined by diopside (which can be regarded as representing the other minerals precipitated from the magma) crystallization on the shelf CE causes precipitation of many smaller plagioclase crystals, in addition to the marginal zones formed around the existing large crystals. Calcic plagioclase phenocrysts in basic rocks therefore need not represent intratelluric crystallization. A similar conclusion may be valid for olivine phenocrysts in some basic rocks.

## Concluding Remarks

Phase relationships in several synthetic systems indicate a pattern for liquidus and solidus paths which is characterized by changes in the slopes of these paths. Possibly, therefore, a similar pattern applies also in natural systems. A rather abrupt change in slope occurs on a liquidus path whenever a new crystalline phase appears in the system. This occurs at the high-temperature end of the middle shelf where olivine (or more rarely, plagioclase or pyroxene) is joined by other phases, and at the high-temperature end of the lower shelf where quartz begins to crystallize. The changes in slope illustrated at the low-temperature ends of the middle and upper shelves in Fig. 4 may not persist in the natural systems (although changes of this kind, involving no change in the number of phases, do exist in several synthetic systems) because they could be smoothed out either by fractional processes or simply by the presence of additional components. The writer intends to study the melting relationships of series of rocks in the appropriate compositional ranges in order to test the hypothesis embodied in Fig. 4 (*cf.* Wyllie, 1960). If these studies confirm the suggested liquidus profile, this introduces a "tempo" into igneous processes which may help to explain some petrogenetic problems.

## Acknowledgements

The writer wishes to thank H. I. Drever, P. G. Harris, R. Johnston, W. Q. Kennedy, W. S. Mackenzie, P. L. Roeder and O. F. Tuttle, for kindly reviewing drafts of the manuscript. Their suggestions have led to many improvements in the paper. Parts of this study are being supported by the National Science Foundation.

## References

Bailey, E. B. and W. B. Wright (1924) Tertiary and post-tertiary geology of Mull. *Geol. Surv. Scotland, Memo.*

Bowen, N. L. (1913) The melting phenomena of the plagioclase feldspars. *Am. Jour. Sci.* Ser. 4, **35,** 577–599.

——— (1915) The crystallization of haplobasaltic, haplodioritic, and related magmas. *Am. Jour. Sci.*, Ser. 4, **40,** 161–185.

——— (1928) *The Evolution of Igneous Rocks.* Princeton University Press.

——— and J. F. Schairer (1935) The system MgO-FeO-$SiO_2$. *Am. Jour. Sci.* Ser. 5, **29,** 151–217.

Hawkes, L. (1930) On rock glass, and the solid and liquid states. *Geol. Mag.* **67,** 17–24.

Hess, H. H. (1960) Stillwater igneous complex, Montana. *Geol. Soc. Am. Mem.* **80.**

Hills, E. S. (1936) Reverse and oscillatory zoning in plagioclase feldspars. *Geol. Mag.* **73,** 49–56.

Holmes, A. and H. F. Harwood (1928) The age and composition of the Whin Sill and the related dikes of the north of England. *Mineral. Mag.* **21,** 493–542.

Hytönen, K. and J. F. Schairer (1961) Carnegie Inst. *Washington Year Book,* **60,** 134–139.

Nockolds, S. R. (1936) The idea of contrasted differentiation: a reply. *Geol. Mag.* **73,** 529–535.

——— (1954) Average chemical composition of some igneous

rocks. *Bull. Geol. Soc. Am.* **65,** 1007–1032.

RICKER, R. W. (1952) Phase equilibria in the quaternary system CaO-MgO-FeO-$SiO_2$. Ph.D. dissertation. College of Mineral Industries, Pennsylvania State University.

SCHAIRER, J. F. (1957) Melting relations of the common rock-forming oxides. *Jour. Am. Ceram. Soc.* **40,** 215–235.

——— AND H. S. YODER (1960) The nature of residual liquids from crystallization, with data on the system nepheline-diopside-silica. *Am. Jour. Sci. Bradley Vol.* **258**-A, 273–283.

THORNTON, C. P. AND O. F. TUTTLE (1960) Chemistry of igneous rocks. I. Differentiation index. *Am. Jour. Sci.* **258,** 664–684.

TURNER, F. J. AND J. VERHOOGEN (1960) *Igneous and Metamorphic Petrology.* 2nd ed., McGraw-Hill Book Co., New York.

TUTTLE, O. F. and N. L. BOWEN (1958) Origin of granite in the light of experimental studies in the system $NaAlSi_3O_8$-$KAlSi_3O_8$-$SiO_2$-$H_2O$. *Geol. Soc. Am. Mem.* **74.**

WAGER, L. R. (1960a) The major element variation of the layered series of the Skaergaard intrusion and a re-estimation of the average composition of the hidden layered series and of the successive residual magmas. *Jour. Petrol.* **1,** 364–398.

——— (1960b) The relationship between fractionation stage of basalt magma and the temperature of beginning of its crystallization. *Geochim. Cosmochim. Acta,* **20,** 158–160.

WYLLIE, P. J. (1960) The system CaO-MgO-FeO-$SiO_2$, and its bearing on the origin of ultrabasic and basic rocks. *Mineral. Mag.* **32,** 459–470.

YODER, H. S. AND C. E. TILLEY (1957) Carnegie Institution of Washington Year Book, **56,** 158.

———, ———, 1961. Carnegie Institution of Washington Year Book, **60,** 111.

## DISCUSSION

E. H. ROSEBOOM, JR. (Washington, D. C.): There are theoretical difficulties to predicting zoning by means of phase diagrams. There are only two types of crystallization which we can discuss on a theoretical basis, perfect equilibrium crystallization and perfect fractional crystallization. Dr. Wyllie has used the former in his diagrams to illustrate zoning. However, by definition the crystals react perfectly to maintain equilibrium and thus no zoning can occur. In perfect fractional crystallization, the bulk composition by definition equals the liquid composition and the lever law cannot be used to predict how the proportions of the crystals and liquid will change with temperature.

P. J. WYLLIE: I agree completely with Dr. Roseboom's statements, and I hope that the complete text will answer the query. The diagrams do illustrate only perfect equilibrium conditions, and they are used in most of the text to describe equilibrium conditions. It is then pointed out that with perfect fractional crystallization (for the original compositions used in this paper) liquidus and solidus paths follow patterns similar to those illustrated for perfect equilibrium crystallization; the changes in slope are less abrupt. Conditions in natural environments probably lie somewhere between perfect equilibrium and perfect fractional crystallization, and liquidus and solidus paths in natural systems may therefore be characterized by slopes similar to those illustrated. The equilibrium diagrams can not give the range of zoning developed with fractional crystallization, but in view of the foregoing remarks, they do give an indication of the differences between the ranges of zoning which could be developed when (a) paths are steep, and (b) paths cross gentle slopes. In the brief sections dealing with tentative applications to zoning in minerals, the equilibrium diagrams have been used in this qualitative fashion.

H. D. MEGAW (Cambridge, England): Does Dr. Wyllie think that there can be any explanation of the shape of these curves in terms of what we know of felspar structure? Anorthite has perfect Si/Al alternation; this seems to be a very stable pattern. As we move away from the pure anorthite composition, the perfect order *can* still be maintained within domains—and recent structural work suggests that it *is* maintained—the substitutions being segregated in domain boundaries, perhaps one or two cells thick. When compositions are too far from anorthite, this can not be maintained without great complication. Good order is not found again till low albite, if then. Is this apparent preference for the Si/Al pattern of anorthite not likely to have a bearing on the course of crystallization?

P. J. WYLLIE: I am tempted to answer "yes" to such an elegant proposal. However, a similar change occurs in most systems when a crystalline phase exhibiting solid solution is joined by another crystalline phase. An example is provided by the system MgO-FeO-$SiO_2$, when olivine is joined by pyroxene, and here there is no ordering of Si and Al to consider. Among the controlling factors are the composition and amount of material being subtracted from the liquid phase. When a new phase begins to crystallize, both these factors change discontinuously, and together they cause discontinuities in liquidus and solidus paths.

MINERALOGICAL SOCIETY OF AMERICA, SPECIAL PAPER 1, 1963
INTERNATIONAL MINERALOGICAL ASSOCIATION, PAPERS, THIRD GENERAL MEETING

# CELL PARAMETERS OF ORTHOPYROXENES

R. A. HOWIE
*Dept. of Geology, The University, Manchester, England*[1]

ABSTRACT

The cell parameters have been determined for forty-seven analyzed orthopyroxenes from metamorphic rocks, the majority of them from the charnockite series or from related rock types in the granulite facies. In general the cell dimensions are each smaller than those determined by Hess and by Kuno for igneous orthopyroxenes of equivalent compositions. The *a* and *b* dimensions may be considerably less: these are both apparently affected particularly by the amount of Al in the octahedral position and also by the $Fe^{3+}$, Ti, Ca and Mn content of the mineral. The *c* dimension is relatively less affected by these ionic substitutions and may be used to give an approximate value for the $Fe^{2+}$:Mg ratio; the *b* dimension may then be used to give some indication of the alumina content of the orthopyroxene. It is suggested that the departure from linearity of the cell dimensions of various orthopyroxenes reported by Ramberg and De Vore, and taken as evidence of the non-ideal nature of the orthopyroxene mixed crystal series, may be interpreted also in terms of variation in the alumina content (and paragenesis) of the orthopyroxenes studied. Thirteen new orthopyroxene analyses are presented.

## INTRODUCTION

The structure and cell parameters of the orthorhombic pyroxene enstatite were investigated by Warren and Modell (1930), and the relationship between the cell parameters and composition of the orthopyroxene series was examined by Ramberg and De Vore (1951). The latter authors concluded both from cell parameters and refractive indices that the orthopyroxenes do not form an ideal mixed-crystal series. Hess (1952) and Kuno (1954), however, have demonstrated straight line relationships between cell parameters and mol. per cent. enstatite in orthopyroxenes from volcanic and plutonic igneous rocks, provided that the proportion of Ca and Al is constant. Clavan *et al.* (1954) investigated orthopyroxenes ranging from 27.8 to 44.3 mol. per cent. $FeSiO_3$ but, within the limits of error of measurement, found no differences in the spacing between the mineral with the lowest iron content and that with the highest. The present work was undertaken to investigate the variation in cell parameters of orthopyroxenes which had crystallized under granulite facies conditions, and it was soon apparent that the cell dimensions, *a*, *b* and *c*, of these orthopyroxenes were appreciably smaller than for those of equivalent composition but of igneous origin. This investigation has therefore been extended to cover the whole of the common range of $Fe^{2+}$:Mg ratios in the orthopyroxene series and also to include varieties relatively rich in alumina.

## CHEMISTRY

New chemical analyses for thirteen orthopyroxenes are given in Tables 1 and 2 and previously published analyses for 34 orthopyroxenes investigated in the present study are collected together in Table 3. The analyses were mostly made using the "classical" or mianly gravimetric methods of Washington (1930). The development of the flame photometer, however, has allowed more accurate and reliable determinations of the alkalis in minerals such as these, with a relatively low alkali content, compared with results previously obtainable from the Lawrence Smith method in which the 'blank' values were often considerably in excess of the values being determined. It has thus been possible to re-determine the alkali content of several of the previously analysed orthopyroxenes (Howie, 1955), and the revised values are quoted here. In selecting specimens for this investigation it was desired to select orthopyroxenes of widely varying Fe:Mg ratios and also to study minerals particularly rich in Mn or Al. A fairly wide range of compositions was in fact obtained (Fig. 1) and gaps in the sequence have been obviated by the inclusion of data for seven orthopyroxenes analysed by other investigators. The metal ions, on the basis of six oxygens, have been calculated and are also given in Tables 1 to 3, together with such optical data as are available.

## CELL DIMENSION DETERMINATIONS

The measurements of cell dimensions were made over a period of some years, employing in the early stages of the investigation powder cameras of radius 19 cm and later Philips *x*-ray diffractometers. For the majority of specimens two determinations have been made, and in particular all the early results using a film technique have been re-checked using the

[1] Present address: Dept. of Geology, King's College, London.

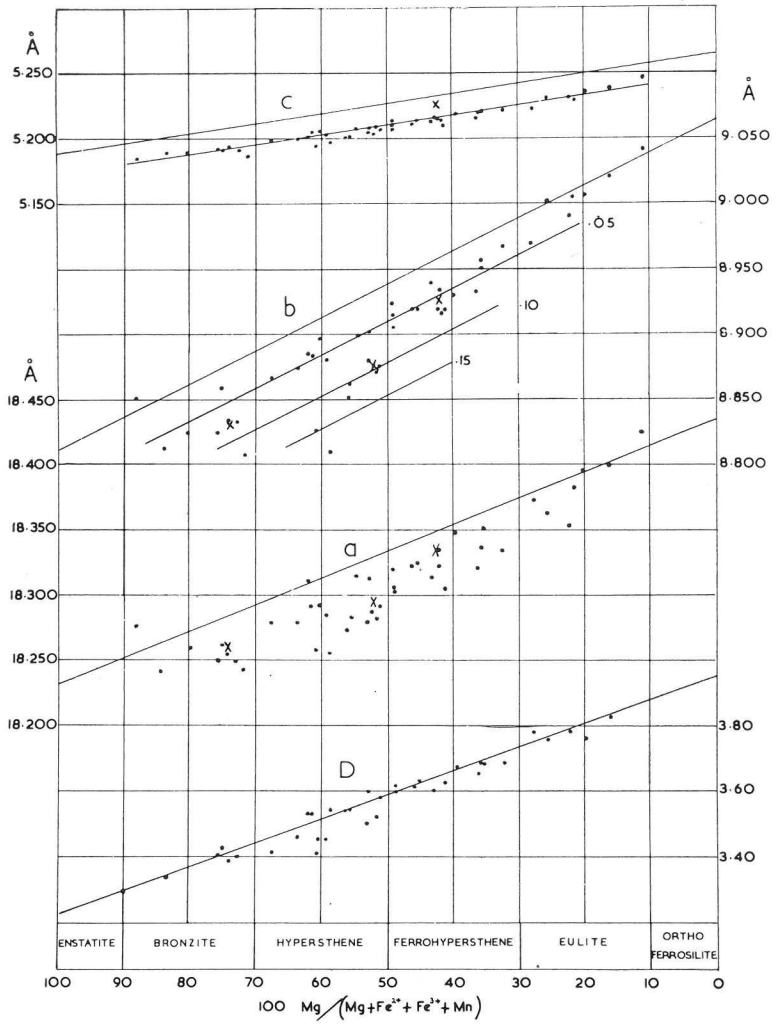


FIG. 1. Variation in cell parameters and specific gravity of orthopyroxenes. For *a*, *b* and *c* the top curve is that of Hess (1952), and for *b* and *c* the lower curves are those plotted to fit the determinations in this paper, as shown by dots; crosses represent values obtained by Hess for three of the author's specimens.

chart recorder. Filtered Fe$K\alpha$ or Co$K\alpha$ radiation was used in conjunction with a silicon standard: the error for *b* is estimated to be $\pm 0.006$ Å.

Following Ramberg and De Vore (1951), the *a* and *b* dimensions were measured initially on 12, 0, 0 and 060 and refined by reference to 14, 5, 0, 650, 250 and also 840. The *c* dimension was measured from the 004 reflection.

## *X*-RAY RESULTS

The *a* and *b* dimensions for twleve orthorhombic pyroxenes from the Madras charnockite series were initially determined. The *c* dimensions were not at first measured as little change was expected in the direction of the $SiO_3$ chains, and because 004, the only reflection of the type 00*l*, was weak. Shortly after the *x*-ray work on these twelve minerals had been completed (Howie, 1953), a study on the ion substitutions and changes in unit cell dimensions in orthopyroxenes of the Bushveld type was published (Hess, 1952). It was immediately obvious that there was an apparent discrepancy between the curves drawn for the orthopyroxenes examined by Hess, of which only one was metamorphic, and the results obtained for the charnockitic orthopyroxenes. Professor Hess kindly examined seven of the author's specimens and found general agreement: the average variation in $2\theta$ for $14,5,0_{\alpha_1}$ was $-0.06°$. He also investigated an orthopyroxene (12700 of Table 3) from his own specimen of a Madras charnockite and found that the results gave smaller cell dimensions than indicated by his curves for Bushveld type orthopyroxenes.

It was therefore evident that the Madras charnockitic orthopyroxenes have smaller *a* and *b* cell dimensions than those of Bushveld type igneous orthopyroxenes of equivalent Fe/Mg ratio, and that this contraction might be due to the substitution of smaller ions in place of $Fe^{2+}$ or $Mg^{2+}$. Further investigations were thus made on orthopyroxenes covering a wide range of chemical compositions and from many other areas, though the study was restricted primarily to metamorphic orthopyroxenes. Hess (1952) demonstrated that the *c* dimension also increased with $Fe^{2+}$ and this dimension was determined on the Madras minerals already examined. The results of the cell parameter determinations on forty-seven analysed orthopyroxenes are given in Tables 1 to 3, and the values are plotted in Fig. 1 against molecular percentage En, or more exactly as 100 $Mg^{2+}/(Mg^{2+}+Fe^{2+}+Fe^{3+}+Mn^{2+})$, following Hess (*loc. cit.*).

TABLE 1. NEW ANALYSES, CELL PARAMETERS, ETC. OF ORTHOPYROXENES FROM AMERICA

| | A | 177/54 | KS137/59 | B310 | 400 | 186b/54 | 355 |
|---|---|---|---|---|---|---|---|
| $SiO_2$ | 51.45 | 47.11 | 48.71 | 48.75 | 49.54 | 48.21 | 48.70 |
| $TiO_2$ | 0.08 | 0.19 | 0.06 | 0.10 | 0.30 | 0.17 | 0.10 |
| $Al_2O_3$ | 2.52 | 9.48 | 4.52 | 3.90 | 1.89 | 1.37 | 1.04 |
| $Fe_2O_3$ | 0.63 | 2.65 | 1.63 | 0.75 | 0.57 | 1.46 | 0.16 |
| FeO | 22.60 | 21.15 | 26.80 | 29.05 | 33.23 | 36.90 | 42.35 |
| MnO | 0.51 | 0.30 | 0.27 | 0.35 | 0.73 | 0.68 | 0.06 |
| MgO | 21.20 | 19.05 | 17.04 | 16.25 | 12.65 | 10.45 | 6.88 |
| CaO | 0.65 | 0.10 | 0.69 | 0.58 | 0.93 | 0.43 | 0.85 |
| $Na_2O$ | 0.02 | tr. | 0.04 | 0.07 | 0.07 | 0.00 | 0.01 |
| $K_2O$ | 0.01 | 0.00 | 0.08 | 0.04 | 0.03 | 0.00 | 0.00 |
| $H_2O^+$ | 0.05 | 0.05 | — | — | 0.05 | — | 0.02 |
| $H_2O^-$ | 0.09 | 0.17 | 0.05 | 0.02 | 0.22 | 0.09 | 0.08 |
| Total | 99.81 | 100.25 | 99.89 | 99.86 | 100.21 | 99.76 | 100.25 |
| D | 3.53 | 3.545 | 3.52(+) | — | 3.67 | 3.68 | 3.78 |
| *a*Å | 18.290 | 18.255 | 18.282 | 18.305 | 18.348 | 18.334 | 18.354 |
| *b*Å | 8.882 | 8.810 | 8.871 | 9.805 | 8.930 | 8.967 | 8.990 |
| *c*Å | 5.206 | 5.195 | 5.208 | 5.211 | 5.218 | 5.222 | 5.232 |
| *Atomic percentages of end-members* | | | | | | | |
| Fe | 38.0 | 41.2 | 47.7 | 50.3 | 59.2 | 67.0 | 76.1 |
| Mg | 60.7 | 58.6 | 50.8 | 48.5 | 38.8 | 32.1 | 22.0 |
| Ca | 1.3 | 0.2 | 1.5 | 1.2 | 2.0 | 0.9 | 1.9 |
| En | 61.5 | 58.7 | 51.5 | 49.0 | 39.6 | 32.4 | 22.4 |
| *Numbers of metal ions on the basis of 6(O)* | | | | | | | |
| Si | 1.927 | 1.759 | 1.871 | 1.888 | 1.961 | 1.952 | 1.999 |
| Al | 0.073 | .241 | .129 | .112 | .039 | .048 | .001 |
| Al | 0.047 | .178 | .076 | .066 | .049 | .017 | .051 |
| $Fe^{3+}$ | 0.018 | .075 | .046 | .022 | .017 | .045 | .005 |
| Mg | 1.183 | 1.060 | .975 | .938 | .746 | .631 | .421 |
| Ti | 0.002 | .005 | .002 | .003 | .009 | .005 | .003 |
| $Fe^{2+}$ | 0.708 | .660 | .861 | .941 | 1.100 | 1.249 | 1.454 |
| Mn | 0.016 | .009 | .009 | .011 | .024 | .023 | .002 |
| Na | 0.001 | — | .003 | .005 | .005 | — | .001 |
| Ca | 0.026 | .004 | .028 | .024 | .039 | .018 | .038 |
| K | — | — | .004 | .002 | .001 | — | — |
| $\Sigma Y$ | 2.00 | 1.99 | 2.00 | 2.01 | 1.99 | 1.99 | 1.98 |

Analyst: R. A. Howie.

A. Hypersthene, enclave of basic rock in granite gneiss, 300 yards W.S.W. of 177/54, S.W. of Dadanawa, South Savannas, British Guiana.

177/54. Hypersthene, enclave of basic rock in granite gneiss, 6 miles S.W. of Dadanawa, South Savannas, British Guiana ($\gamma$ 1.724).

KS137/59. Hypersthene, pyroxene granulite with charnockitic affinities, northern Quebec, Canada (55°09′ N., 68°47′ W.).

B310. Hypersthene, intermediate member of the charnockite series, Bahia, Brazil (Beagle Collection).

400. Ferrohypersthene, charnockite, Panguirtung, east coast of Baffin Island.

186b/54. Ferrohypersthene, enderbite, 3 miles W. of Dadanawa, South Savannas, British Guiana.

355. Eulite, garnet-orthopyroxene-quartz rock, 6 miles E.S.E. of Pond Inlet, northeast Baffin Island ($\gamma$ 1.769).

TABLE 2. NEW ANALYSES, CELL PARAMETERS, ETC. OF ORTHOPYROXENES FROM ELSEWHERE

| | 20486 | SP.18 | 116 | 7725 | 1002 | XI-132 |
|---|---|---|---|---|---|---|
| $SiO_2$ | 53.25 | 50.39 | 48.98 | 48.29 | 47.55 | 47.67 |
| $TiO_2$ | 0.19 | 0.20 | 0.17 | 0.40 | 0.07 | 0.07 |
| $Al_2O_3$ | 4.05 | 2.83 | 5.76 | 2.83 | 1.90 | 0.43 |
| $Fe_2O_3$ | 1.58 | 1.25 | 1.04 | 1.23 | 0.41 | 0.95 |
| FeO | 11.05 | 23.84 | 24.85 | 33.67 | 39.37 | 43.05 |
| MnO | 0.09 | 0.46 | 0.17 | 0.67 | 0.89 | 0.20 |
| MgO | 28.78 | 20.52 | 18.50 | 10.77 | 8.68 | 6.24 |
| CaO | 0.88 | 0.58 | 0.20 | 2.29 | 1.23 | 1.45 |
| $Na_2O$ | 0.03 | 0.04 | 0.02 | 0.03 | — | 0.06 |
| $K_2O$ | 0.01 | 0.01 | 0.02 | 0.04 | — | 0.03 |
| $H_2O^+$ | 0.02 | 0.05 | — | 0.03 | 0.05 | — |
| $H_2O^-$ | 0.04 | tr. | 0.13 | 0.04 | 0.09 | 0.03 |
| Total | 100.13 | 100.17 | 99.84 | 100.29 | 100.24 | 100.18 |
| D | 3.36 | 3.53 | 3.54 | 3.68 | 3.78 | 3.76 |
| *a*Å | 18.255 | 18.288 | 18.272 | 18.352 | 18.374 | 18.396 |
| *b*Å | 8.824 | 8.868 | 8.850 | 8.950 | 8.969 | 9.102 |
| *c*Å | 5.192 | 5.200 | 5.201 | 5.221 | 5.233 | 5.236 |
| *Atomic percentages of end-members* | | | | | | |
| Fe | 19.3 | 40.5 | 43.8 | 61.3 | 70.1 | 77.3 |
| Mg | 79.0 | 58.3 | 55.8 | 33.6 | 27.2 | 19.5 |
| Ca | 1.7 | 1.2 | 0.4 | 5.1 | 2.7 | 3.2 |
| En | 80.3 | 59.0 | 56.1 | 35.5 | 27.8 | 20.0 |
| *Numbers of metal ions on the basis of 6(O)* | | | | | | |
| Si | 1.888 | 1.901 | 1.856 | 1.921 | 1.941 | 1.981 |
| Al | .112 | .099 | .144 | .079 | .059 | .019 |
| Al | .061 | .027 | .114 | .052 | .034 | .002 |
| $Fe^{3+}$ | .042 | .036 | .030 | .040 | .012 | .030 |
| Mg | 1.521 | 1.153 | 1.045 | .642 | .531 | .386 |
| Ti | .005 | .006 | .005 | .012 | .002 | .002 |
| $Fe^{2+}$ | .328 | .752 | .787 | 1.115 | 1.338 | 1.496 |
| Mn | .003 | .015 | .006 | .023 | .031 | .007 |
| Na | .002 | .003 | .001 | .002 | — | .005 |
| Ca | .033 | .023 | .008 | .098 | .054 | .064 |
| K | .001 | .001 | .001 | .003 | — | .001 |
| $\Sigma Y$ | 2.00[1] | 2.02 | 2.00 | 1.99 | 2.00 | 1.99 |

Analyst: R. A. Howie.

20486. Bronzite, pyroxenite ("ultrabasic charnockite"), Dangin, Western Australia (rock analysis and description given by Prider, 1945). (Anal. includes $Cr_2O_3$ 0.08, $P_2O_5$ 0.08).

SP.18. Hypersthene, norite, Namaqualand, South Africa.

116. Hypersthene, garnetiferous enderbite, Magazine Hill, Madras, India.

7725. Ferrohypersthene, two-pyroxene granulite, Eie, Hitterö, Norway.

1002. Eulite, eulysitic rock, Madial, southern Sudan ($\alpha$ 1.736, $\beta$ 1.747, $\gamma$ 1.752; $2V_\alpha$ 63°).

XI-132. Eulite, "ferrohypersthenite" with orthopyroxene, grunerite and hastingsite, Okopi valley, Okandja, central Gabon, Africa (rock analysis and description given by Choubert, 1954).

[1] Includes Cr 0.002.

(*Text continued on page 219, Col. 2*)

TABLE 3. ORTHOPYROXENE ANALYSES, CELL PARAMETERS, ETC.

| | 1 | R.62 | H.66 | R.104 | 3709 | 4645 | 35 | 1631 | H.67 |
|---|---|---|---|---|---|---|---|---|---|
| $SiO_2$ | 55.456 | 53.63 | 52.94 | 54.57 | 52.10 | 51.69 | 50.14 | 51.76 | 51.22 |
| $TiO_2$ | — | 0.19 | 0.09 | 0.08 | 0.10 | 0.15 | 1.05 | 0.17 | 0.13 |
| $Al_2O_3$ | 2.026 | 4.53 | 4.45 | 1.53 | 4.35 | 4.55 | 6.02 | 2.82 | 2.59 |
| $Fe_2O_3$ | — | 1.54 | 1.27 | 1.52 | 1.38 | 0.55 | 1.83 | 1.46 | 1.87 |
| FeO | 8.424 | 9.07 | 13.85 | 14.54 | 15.28 | 16.51 | 15.38 | 18.30 | 20.76 |
| MnO | — | 0.25 | 0.26 | 0.26 | 0.28 | 0.27 | 0.36 | 0.35 | 0.62 |
| MgO | 34.483 | 30.31 | 26.72 | 27.24 | 26.65 | 25.74 | 24.58 | 23.21 | 22.30 |
| CaO | — | 0.53 | 0.35 | 0.35 | 0.06 | 0.50 | 0.30 | 1.75 | 0.57 |
| $Na_2O$ | — | 0.02 | tr. | 0.02 | 0.01 | 0.03 | 0.06 | 0.03 | 0.03 |
| $K_2O$ | — | 0.00 | 0.00 | 0.00 | tr. | 0.02 | 0.05 | 0.00 | 0.00 |
| $H_2O^+$ | — | 0.03 | n.d. | 0.02 | 0.04 | 0.04 | 0.18 | n.d. | 0.05 |
| $H_2O^-$ | — | 0.04 | 0.03 | 0.03 | 0.05 | 0.05 | 0.06 | 0.03 | 0.06 |
| Total | 100.389 | 100.14 | 99.96 | 100.16 | 100.30 | 100.10 | 100.32 | 99.88 | 100.20 |
| Fe | 12.0 | 16.2 | 24.1 | 24.5 | 26.1 | 27.0 | 28.2 | 31.4 | 36.0 |
| Mg | 88.0 | 82.7 | 75.2 | 74.8 | 73.8 | 72.0 | 71.2 | 65.1 | 62.9 |
| Ca | — | 1.1 | 0.7 | 0.7 | 0.1 | 1.0 | 0.6 | 3.5 | 1.1 |
| En | 88.0 | 83.6 | 75.8 | 75.0 | 73.9 | 72.6 | 71.6 | 67.5 | 63.6 |
| *Cell parameters and optical properties* | | | | | | | | | |
| $a$Å | 18.276 | 18.243 | 18.250 | 18.261 | 18.254 | 18.248 | 18.242 | 18.278 | 18.278 |
| $b$Å | 8.850 | 8.812 | 8.824 | 8.858 | 8.833 | 8.833 | 8.807 | 8.865 | 8.874 |
| $c$Å | 5.184 | 5.190 | 5.191 | 5.191 | 5.194 | 5.191 | 5.186 | 6.199 | 5.200 |
| D | — | 3.339 | 3.40 | 3.429 | 3.39 | 3.40 | — | 3.415 | 3.46 |
| $\gamma$ | 1.671 | — | — | — | 1.690 | 1.690 | 1.704 | — | 1.703 |
| $2V_\alpha$ | 94° | — | — | — | 73° | 76° | 76° | 62½° | 62° |
| *Numbers of metal ions on the basis of 6(O)* | | | | | | | | | |
| Si | 1.924 | 1.884 | 1.899 | 1.962 | 1.878 | 1.883 | 1.822 | 1.911 | 1.910 |
| Al | .076 | .116 | .101 | .038 | .122 | .117 | .178 | .089 | .090 |
| Al | .007 | .072 | .087 | .027 | .063 | .076 | .080 | .034 | .022 |
| $Fe^{3+}$ | — | .041 | .034 | .041 | .037 | .015 | .050 | .041 | .049 |
| Mg | 1.783 | 1.585 | 1.428 | 1.457 | 1.432 | 1.384 | 1.331 | 1.277 | 1.247 |
| Ti | — | .006 | .002 | .002 | .003 | .004 | .029 | .005 | .003 |
| $Fe^{2+}$ | .244 | .266 | .415 | .436 | .461 | .499 | .467 | .565 | .644 |
| Mn | — | .007 | .008 | .008 | .008 | .009 | .011 | .011 | .019 |
| Na | — | .001 | — | .001 | .001 | .002 | .004 | .002 | .001 |
| Ca | — | .020 | .014 | .014 | .002 | .019 | .012 | .069 | .022 |
| K | — | — | — | — | — | .001 | .002 | — | — |

1. Bronzite, sagvandite, Sagvandet, 15 km southwest of Lyngen, Troms, Norway (Barth, 1926). Anal. H. Rosenbusch.

R.62. Bronzite, ultrabasic gneiss, Loch Ossigary, Rodil, South Harris (Howie, 1963).

H.66. Bronzite, pyroxenite, ⅓ mile northwest of Scourie House, Scourie, Sutherland (O'Hara, 1961). Anal. R. A. Howie (note: $SiO_2$ value is 52.94, not 52.44 as quoted in O'Hara, 1961).

R.104. Bronzite, pegmatitic vein in pyroxene granulite, Caisteal Ard, Ardvourlie, North Harris (Howie, 1963).

3709. Bronzite, ultrabasic rock of the charnockite series, Pammal Hill, Pallavasa, Madras (Howie, 1955; alkalis redetermined).

4645. Bronzite, pyroxenite (charnockite series), Pammal, Madras (Howie, 1955).

35. Bronzite, metamorphosed peridotite, Dawros, Connemara, Eire (Rothstein, 1958). Anal. E. A. Vincent (includes $Cr_2O_3$ 0.26, NiO 0.05; Cr 0.008, Ni 0.001).

1631. Hypersthene, bytownite-orthopyroxene-hornblende-biotite rock, southwest of Lough Fadda, Co. Galway (Leake, 1958). Anal. R. A. Howie.

H.67. Hypersthene, intermediate charnockitic rock, northwest of Pairc a'Chladaich, Scourie, Sutherland (Howie, 1963).

TABLE 3. ORTHOPYROXENE ANALYSES, CELL PARAMETERS, ETC.—*Cont.*

| | R.13b | B.20 | 2270 | 4641B | R.96 | 80258 | 2941 | 80270 |
|---|---|---|---|---|---|---|---|---|
| $SiO_2$ | 51.78 | 48.48 | 51.17 | 50.47 | 49.68 | 49.52 | 49.55 | 50.21 |
| $TiO_2$ | 0.08 | 0.52 | 0.15 | 0.65 | 0.11 | 0.15 | 0.30 | 0.12 |
| $Al_2O_3$ | 1.96 | 7.21 | 1.97 | 3.55 | 4.41 | 2.86 | 2.42 | 2.52 |
| $Fe_2O_3$ | 1.55 | 1.97 | 0.59 | 0.90 | 1.68 | 0.62 | 1.92 | 1.93 |
| FeO | 21.56 | 20.62 | 23.01 | 23.59 | 24.21 | 26.31 | 26.51 | 26.10 |
| MnO | 0.64 | 0.49 | 0.87 | 0.54 | 0.48 | 0.23 | 0.32 | 0.70 |
| MgO | 21.70 | 19.97 | 20.75 | 20.18 | 18.32 | 18.10 | 17.67 | 17.80 |
| CaO | 0.67 | 0.46 | 0.90 | 0.10 | 0.76 | 0.96 | 0.70 | 0.66 |
| $Na_2O$ | 0.01 | 0.02 | 0.01 | 0.04 | 0.02 | tr. | 0.02 | 0.02 |
| $K_2O$ | tr. | 0.00 | tr. | 0.02 | 0.01 | 0.00 | 0.02 | tr. |
| $H_2O^+$ | n.d. | n.d. | n.d. | 0.09 | 0.07 | 0.70 | 0.06 | 0.04 |
| $H_2O^-$ | 0.12 | 0.07 | 0.14 | 0.10 | 0.05 | 0.27 | 0.05 | 0.02 |
| Total | 100.07 | 99.81 | 99.56 | 100.23 | 99.80 | 99.72 | 99.54 | 100.12 |
| Fe | 37.2 | 38.8 | 39.1 | 40.8 | 43.9 | 44.7 | 46.8 | 46.6 |
| Mg | 61.4 | 60.2 | 59.1 | 59.0 | 54.5 | 53.3 | 51.8 | 52.0 |
| Ca | 1.4 | 1.0 | 1.8 | 0.2 | 1.6 | 2.0 | 1.4 | 1.4 |
| En | 62.0 | 60.8 | 60.2 | 59.1 | 55.5 | 54.4 | 52.6 | 52.6 |
| *Cell parameters and optical properties* | | | | | | | | |
| $a$Å | 18.311 | 18.257 | 19.292 | 18.283 | 18.282 | 18.315 | 18.278 | 18.312 |
| $b$Å | 8.884 | 8.825 | 8.896 | 8.879 | 8.862 | 8.898 | 8.878 | 8.902 |
| $c$Å | 5.202 | 5.193 | 5.206 | 5.203 | 5.202 | 5.208 | 5.205 | 5.209 |
| D | 3.530 | 3.41 | 3.54 | 3.45 | 3.55 | — | 3.50 | 3.60 |
| $\gamma$ | — | 1.719 | 1.708 | 1.708 | — | 1.726 | 1.722 | 1.725 |
| $2V_\alpha$ | — | — | 58° | 58° | — | — | 54° | — |
| *Numbers of metal ions on the basis of 6(O)* | | | | | | | | |
| Si | 1.936 | 1.811 | 1.936 | 1.897 | 1.886 | 1.914 | 1.911 | 1.920 |
| Al | .064 | .189 | .064 | .103 | .114 | .086 | .089 | .080 |
| Al | .022 | .128 | .024 | .057 | .084 | .044 | .021 | .034 |
| $Fe^{3+}$ | .045 | .056 | .017 | .025 | .048 | .018 | .056 | .056 |
| Mg | 1.207 | 1.112 | 1.170 | 1.130 | 1.037 | 1.043 | 1.016 | 1.015 |
| Ti | .002 | .015 | .004 | .018 | .003 | .004 | .009 | .004 |
| $Fe^{2+}$ | .673 | .644 | .728 | .741 | .769 | .850 | .855 | .835 |
| Mn | .020 | .015 | .028 | .017 | .016 | .008 | .010 | .023 |
| Na | — | .001 | .001 | .003 | .001 | — | .001 | .001 |
| Ca | .027 | .018 | .036 | .004 | .031 | .039 | .029 | .027 |
| K | — | — | — | .001 | — | — | .001 | — |

R.13b. Hypersthene, hornblende-pyroxene-plagioclase gneiss, north of Rodil, South Harris (Howie, 1963).

B.20. Hypersthene, hypersthene-spinel-plagioclase hornfels, Belhelvie, Aberdeenshire (Howie, 1963).

2270. Hypersthene, intermediate rock of the charnockite series, Salem, Madras (Howie, 1955; alkalis redetermined).

4641B. Hypersthene, intermediate rock of the charnockite series, Shevaroy Hills, Madras (Howie, 1955; alkalis redetermined).

R.96. Hypersthene, plagioclase—two pyroxene granulite, north of Leverburgh, South Harris (Howie, 1963).

80258. Hypersthene, charnockitic gneiss, Bemato, Betroka, Madagascar (Howie, 1958).

2941. Hypersthene, basic member of charnockite series, Nagaramalai, Salem, Madras (Howie, 1955; alkalis redetermined).

80270. Hypersthene, charnockitic gneiss, Fort Dauphin, Madagascar (Howie, 1958).

J.32. Hypersthene, charnockitic granulite, Kailasgarh, Vellore, India (Naidu, 1954). Anal. H. Schwander (Includes $P_2O_5$ 0.05).

Ch.113. Hypersthene, garnetiferous enderbite, Pallavaram, Madras (Howie and Subramaniam, 1957).

TABLE 3. ORTHOPYROXENE ANALYSES, CELL PARAMETERS, ETC.—*Cont.*

| | J.32 | Ch.113 | 137 | 7286 | 3 | 68671 | S.347 | 12700 | 4642A |
|---|---|---|---|---|---|---|---|---|---|
| $SiO_2$ | 48.65 | 50.05 | 49.44 | 49.98 | 47.10 | 49.73 | 49.48 | 49.49 | 49.50 |
| $TiO_2$ | 1.60 | 0.30 | 0.15 | 0.18 | 0.20 | 0.11 | 0.13 | 0.14 | 0.11 |
| $Al_2O_3$ | 1.66 | 4.08 | 2.21 | 2.26 | 3.25 | 1.96 | 1.77 | 1.78 | 2.01 |
| $Fe_2O_3$ | 5.55 | 0.68 | 1.93 | 1.05 | 1.74 | 1.72 | 1.84 | 0.54 | 1.31 |
| FeO | 24.40 | 27.50 | 28.06 | 27.97 | 29.03 | 29.64 | 31.56 | 32.48 | 32.60 |
| MnO | 0.30 | 0.27 | 1.03 | 0.60 | 0.64 | 0.53 | 0.49 | 0.66 | 0.59 |
| MgO | 17.65 | 16.51 | 16.61 | 15.82 | 14.76 | 14.66 | 14.25 | 13.73 | 13.74 |
| CaO | 0.12 | 0.46 | 0.23 | 1.81 | 3.43 | 1.24 | 0.80 | 1.16 | 0.16 |
| $Na_2O$ | 0.27 | 0.09 | 0.10 | 0.11 | tr. | 0.10 | 0.01 | 0.00 | 0.03 |
| $K_2O$ | tr. | 0.03 | tr. | 0.07 | 0.00 | 0.01 | tr. | 0.00 | 0.02 |
| $H_2O^+$ | 0.03 | 0.02 | 0.04 | n.d. | n.d. | 0.04 | 0.02 | 0.04 | 0.01 |
| $H_2O^-$ | 0.01 | 0.11 | 0.29 | 0.21 | — | 0.11 | 0.04 | 0.09 | 0.02 |
| Total | 100.29 | 100.10 | 100.09 | 100.06 | 100.15 | 99.85 | 100.39 | 100.11 | 100.10 |
| Fe | 48.5 | 48.5 | 50.5 | 49.1 | 50.4 | 53.3 | 55.8 | 56.3 | 58.2 |
| Mg | 51.3 | 50.5 | 49.0 | 47.1 | 42.5 | 44.1 | 42.5 | 41.3 | 41.5 |
| Ca | 0.2 | 1.0 | 0.5 | 3.8 | 7.1 | 2.6 | 1.7 | 2.4 | 0.3 |
| En | 51.4 | 51.0 | 49.2 | 49.0 | 45.7 | 45.3 | 43.2 | 42.4 | 41.6 |
| *Cell parameters and optical properties* | | | | | | | | | |
| $a$Å | 18.286 | 18.291 | 18.320 | 18.302 | 18.323 | 18.325 | 18.314 | 18.334 | 18.322 |
| $b$Å | 8.875 | 8.876 | 8.923 | 8.915 | 8.919 | 8.918 | 8.939 | 8.919 | 8.933 |
| $c$Å | 5.204 | 5.207 | 5.213 | 5.207 | 5.212 | 5.216 | 5.214 | 5.216 | 5.215 |
| D | 3.33 | 3.58 | 3.60 | 3.61 | 3.60± | 3.63 | 3.60 | 3.65 | — |
| $\gamma$ | 1.724 | 1.728 | 1.724 | 1.725 | 1.735 | 1.732 | 1.733 | 1.737 | 1.735 |
| $2V_\alpha$ | 54° | — | 52° | — | 57° | 52° | 54° | 54.5° | 56° |
| *Numbers of metal ions on the basis of 6(O)* | | | | | | | | | |
| Si | 1.868 | 1.918 | 1.917 | 1.937 | 1.851 | 1.945 | 1.940 | 1.949 | 1.946 |
| Al | .075 | .082 | .083 | .063 | .149 | .055 | .060 | .051 | .054 |
| Al | — | .102 | .019 | .041 | .001 | .034 | .020 | .034 | .039 |
| $Fe^{3+}$ | .106 | .019 | .056 | .031 | .051 | .052 | .054 | .014 | .039 |
| Mg | 1.010 | .943 | .965 | .915 | .864 | .854 | .837 | .810 | .805 |
| Ti | .046 | .009 | .005 | .005 | .006 | .002 | .004 | .005 | .003 |
| $Fe^{2+}$ | .784 | .879 | .907 | .903 | .954 | .968 | 1.030 | 1.065 | 1.072 |
| Mn | .010 | .009 | .034 | .019 | .021 | .018 | .016 | .021 | .020 |
| Na | .020 | .009 | .009 | .008 | — | .009 | .001 | — | .002 |
| Ca | .005 | .018 | .009 | .075 | .144 | .051 | .034 | .047 | .007 |
| K | — | .001 | — | .003 | — | — | — | — | .001 |

137. Ferrohypersthene, intermediate member of the charnockite series, Ambagamudam Pothai, Tinnevelly, Madras (Howie, 1955).

7286. Ferrohypersthene, basic member of the charnockite series, Lafit Mountains, Sudan (Howie, 1958).

3. Ferrohypersthene, basic charnockitic granulite, near Lafler Canyon, Santa Lucia range, California (Compton, 1960).

68671. Ferrohypersthene, intermediate member of the charnockite series, Hatton, Ceylon (Howie and Subramaniam, 1957).

S.347. Ferrohypersthene, intermediate member of the charnockite series, Mt. Wati, West Nile district, Uganda (Howie and Subramaniam, 1957).

12700. Ferrohypersthene, charnockite, Pallavaram, Madras (Howie, 1955). Anal. Rock Anal. Lab., Univ. of Minnesota.

4642A. Ferrohypersthene, basic member of the charnockite series, Pallavaram, Madras (Howie, 1955, alkalis redetermined).

Ch.199. Ferrohypersthene, basic member of the charnockite series, Pallavaram, Madras (Howie and Subramaniam, 1957).

4639. Ferrohypersthene, charnockite, Pallavaram, Madras (Howie, 1955).

6436. Ferrohypersthene, charnockite, Trisul Hill, Meanambakam, Madras (new analysis).

115. Ferrohypersthene, intermediate member of the charnock-

TABLE 3. ORTHOPYROXENE ANALYSES, CELL PARAMETERS, ETC.—*Cont.*

| | Ch.199 | 4639 | 6436 | 115 | V.2 | H.4 | UG.29a | A.50 |
|---|---|---|---|---|---|---|---|---|
| $SiO_2$ | 49.28 | 47.98 | 47.11 | 47.23 | 47.33 | 47.8 | 46.65 | 47.1 |
| $TiO_2$ | 0.17 | 0.94 | 0.29 | 1.02 | 0.29 | — | 0.10 | — |
| $Al_2O_3$ | 2.09 | 3.39 | 2.79 | 2.47 | 1.37 | 0.2 | 2.10 | 0.2 |
| $Fe_2O_3$ | 0.98 | 1.54 | 1.98 | 1.60 | 1.09 | 2.3 | 0.57 | 4.1 |
| FeO | 32.01 | 32.16 | 33.72 | 34.03 | 39.41 | 40.4 | 44.02 | 40.1 |
| MnO | 0.47 | 0.26 | 0.28 | 0.89 | 0.94 | 0.52 | 0.55 | 3.1 |
| MgO | 13.32 | 13.16 | 13.34 | 11.14 | 8.02 | 6.67 | 4.90 | 3.4 |
| CaO | 1.38 | 0.03 | 0.47 | 1.57 | 1.25 | 1.74 | 0.81 | 1.6 |
| $Na_2O$ | 0.06 | 0.06 | tr. | 0.05 | 0.05 | 0.09 | 0.01 | 0.10 |
| $K_2O$ | 0.01 | 0.00 | 0.00 | 0.12 | 0.01 | 0.02 | 0.01 | 0.03 |
| $H_2O^+$ | n.d. | 0.31 | 0.09 | n.d. | 0.07 | — | 0.08 | — |
| $H_2O^-$ | 0.04 | 0.42 | 0.14 | 0.06 | 0.23 | — | 0.03 | — |
| Total | 99.81 | 100.25 | 100.21 | 100.18 | 100.06 | 99.7 | 99.83 | 99.7 |
| Fe | 56.6 | 57.7 | 59.5 | 62.5 | 72.0 | 75.2 | 82.2 | 85.4 |
| Mg | 40.5 | 42.2 | 39.5 | 34.1 | 25.2 | 20.9 | 15.9 | 10.9 |
| Ca | 2.9 | 0.1 | 1.0 | 3.4 | 2.8 | 3.9 | 1.9 | 3.7 |
| En | 41.6 | 41.1 | 40.0 | 35.3 | 25.7 | 21.8 | 16.2 | 11.4 |
| *Cell parameters and optical properties* | | | | | | | | |
| *a*Å | 18.334 | 18.307 | 18.320 | 18.337 | 18.364 | 18.384 | 18.401 | 18.426 |
| *b*Å | 8.916 | 8.917 | 8.932 | 8.957 | 9.003 | 9.006 | 9.021 | 9.040 |
| *c*Å | 5.214 | 5.210 | 5.215 | 5.221 | 5.232 | 5.228 | 5.238 | 5,246 |
| D | 3.62 | — | 3.65 | 3.68 | 3.75 | — | 3.83 | — |
| $\gamma$ | 1.734 | 1.738 | 1.737 | 1.743 | 1.758 | — | 1.763 | — |
| $2V_\alpha$ | — | 57° | 56° | 58° | 66° | — | 78° | — |
| *Numbers of metal ions on the basis of 6(O)* | | | | | | | | |
| Si | 1.943 | 1.895 | 1.876 | 1.892 | 1.949 | 1.982 | 1.954 | 1.987 |
| Al | .057 | .105 | .124 | .108 | .051 | .010 | .046 | .010 |
| Al | .045 | .051 | .007 | .009 | .015 | — | .058 | — |
| $Fe^{3+}$ | .028 | .045 | .059 | .048 | .034 | .072 | .018 | .130 |
| Mg | .785 | .779 | .792 | .664 | .492 | .412 | .306 | .214 |
| Ti | .005 | .028 | .009 | .031 | .010 | — | .003 | — |
| $Fe^{2+}$ | 1.054 | 1.059 | 1.123 | 1.138 | 1.354 | 1.401 | 1.542 | 1.415 |
| Mn | .017 | .010 | .009 | .031 | .033 | .018 | .020 | .111 |
| Na | .005 | .005 | — | .005 | .004 | .007 | .001 | .008 |
| Ca | .057 | .001 | .020 | .067 | .055 | .077 | .037 | .072 |
| K | — | — | — | .006 | — | .001 | .001 | .002 |

ite series, Nambran Paramba, Tinnevelly, Madras (Howie, 1955).

V.2. Eulite, basic garnetiferous granulite, Fästningsberget, Varberg, Sweden (Howie and Subramaniam, 1957).

H.4. Eulite, two pyroxene-calcite-quartz rock, Mount Reed area iron formation, northern Quebec (Kranck, 1961). Anal. S. H. Kranck.

UG.29a. Eulite, charnockitic adamellite, Oribi Gorge, Marble Delta, Natal (Howie, 1958).

A.50. Eulite, quartz-magnetite-two pyroxene rock, Mount Reed area iron formation, northern Quebec (Kranck, 1961). Anal. S. H. Kranck.

Analyses except 1, 35, J.32, 3, 12700, H.4 and A.50 by R. A. Howie.

(*Text continued from page 215*)

Although ideally simply (Mg, Fe)$SiO_3$, all orthopyroxenes contain appreciable amounts of other ions substituting for the metal ions in the structure: this is particularly true for the orthopyroxenes which have crystallized under the P,T conditions of the granulite facies. The principal ions thus entering their structure are $Al^{3+}$, $Ti^{4+}$, $Fe^{3+}$, $Cr^{3+}$, $Mn^{2+}$, $Ca^{2+}$ and $Na^+$: the interionic distances for the appropriate octahedral and tetrahedral positions are given in Table 4. It will be seen from Tables 1 to 3 that Na is

TABLE 4. APPROXIMATE INTERIONIC DISTANCES

| Six-fold coordination (after Green, 1959) | |
|---|---|
| $Mg^{2+} \cdots O^{2-} = 2.06$ Å | $Al^{3+} \cdots O^{2-} = 1.91$ Å |
| $Fe^{2+} \cdots O^{2-} = 2.14$ Å | $Cr^{3+} \cdots O^{2-} = 2.03$ Å |
| $Ca^{2+} \cdots O^{2-} = 2.39$ Å | $Fe^{3+} \cdots O^{2-} = 2.04$ Å |
| $Mn^{2+} \cdots O^{2-} = 2.20$ Å | $Ti^{4+} \cdots O^{2-} = 2.08$ Å |
| $Na^{+} \cdots O^{2-} = 2.37$ Å | |
| **Four-fold coordination (Smith, 1954)** | |
| $Si^{4+} \cdots O^{2-} = 1.60$ Å | $Al^{3+} \cdots O^{2-} = 1.78$ Å |

virtually absent, $Cr^{3+}$ is also very low (Table 1, 20486; see also Howie, 1955, where for 13 orthopyroxenes Cr varies from 300 to $<2$ ppm). $Ti^{4+}$ is low and relatively constant in amount at around 0.002 to 0.006 per six oxygens: where it has a higher value this may be due to its occurrence as exsolved crystallites of rutile or ilmenite, giving rise to the schiller effect visible in some specimens. $Mn^{2+}$ is also relatively constant at 0.015 to 0.030, and becomes important only at the iorn-rich end of the series. The chief substituent ions are thus $Al^{3+}$, $Fe^{3+}$ and $Ca^{2+}$. $Al^{3+}$ may exist in four-fold coordination partly replacing $Si^{4+}$ or in six-fold coordination replacing $Mg^{2+}$ or $Fe^{2+}$. In the former case the relatively larger interionic distance of 1.78 Å as compared with 1.60 Å for $Si^{4+}$ and $O^{2-}$ would be expected to bring about an increase in the cell parameters, while the substitution of $Al^{3+}$ in the octahedral position giving an $Al^{3+} \cdots O^{2-}$ distance of 1.91 Å compared with that of $Mg^{2+}$ and $Fe^{2+}$ or 2.06 and 2.14 Å respectively will clearly lead to a decrease in cell parameters. In re-calculating the chemical analyses on the basis of six oxygens, sufficient $Al^{3+}$ (where available) has been placed with $Si^{4+}$ to make the *Z* group exactly 2.00, the remainder of the $Al^{3+}$ being placed in the *Y* group. The resulting distribution of $Al^{3+}$ between the tetrahedral and octahedral positions does not lead to significantly different results from those obtained by using the recalculation method of Hess (1949). The replacement of $Fe^{2+}$ by $Fe^{3+}$ would lead to a decrease in interionic distances though the $Fe^{3+} \cdots O^{2-}$ distance is only slightly less than that of $Mg^{2+} \cdots O^{2-}$. The $Ca^{2+}$ ion, however, is considerably larger than any others in the orthopyroxene structure and its entry may be expected to cause an increase in the cell parameters: the entry of $Mn^{2+}$ would give a similar effect.

It was initially supposed that the partial replacement of ions in the octahedral position by others of different size would cause variations in all three parameters, *a*, *b* and *c*. Hess (1952), however, recorded the empirical results for Bushveld type igneous pyroxenes and showed that the introduction of the larger $Ca^{2+}$ ion increased only the *a* dimension, whereas the substitution of the smaller $Al^{3+}$ decreased only the *b* dimension. The expected increase in cell parameters due to the substitution of $Al^{3+}$ for $Si^{4+}$ in the tetrahedral position was not observed by Hess, nor is it apparent from the present data.

The cell parameters are plotted in Fig. 1, where the line for *a* and the uppermost lines for *b* and *c* are those of Hess (1952). The points represent new cell parameter determinations, with the addition of repeated determinations by Professor Hess for three of the present specimens (3709, 2941 and 12700). The lower line for *c* is considered to be the best fit for the new data and indicates that the *c* dimension is less strongly affected by ion substituions than are *a* and *b*. It should thus be possible to obtain an estimate of the Fe/Mg ratio of an orthopyroxene to approximately $\pm 7$ mol. % from a simple determination of *c*, by measuring the position of the 004 reflection ($d \simeq 1.30$ Å).

The entry of $Ca^{2+}$ can be seen to have a slight effect in increasing the *b* dimension, *e.g.* for specimen V.2 (En 25.7%) with 0.055 Ca (1.25% CaO) and $[Al]^6$ only 0.015 the *b* dimension lies above Hess's curve. The main control of the *b* dimension, however, appears to be the amount of substitution of Al in the octahedral position. In Fig. 1 curves have been drawn for 0.05, 0.10 and 0.15 $[Al]^6$ indicating that it is possible to estimate the amount of $Al^{3+}$ entering the octahedral position in an orthopyroxene if the Fe/Mg ratio is already known from measurement of the *c* dimension or by other means. For orthopyroxene 177/54 (En 58.7, $Al_2O_3$ 9.48%) the $[Al]^6$ value is 0.178, giving the biggest deviation from the normal curve. It is interesting to note that the rock containing the mineral outcrops only three hundred yards from a similar rock type containing orthopyroxene A with En 61.5, $Al_2O_3$ 2.52%, and normal cell parameters. Thus these two orthopyroxenes closely associated both in outcrop and apparently in PT conditions of crystallization nevertheless contain entirely different amounts of alumina. It is proposed to investigate the chemistry of these particular rocks in the hope of providing a further clue to this problem.

The effect on the cell parameters of the entry of $Mn^{2+}$ can be seen by reference to specimens H.4 (En 21.8) and A.50 (En 11.4). Both specimens contain only 0.2% $Al_2O_3$ and both have similar amounts of CaO and FeO, but orthopyroxene A.50 contains 3.1%

MnO compared with 0.52% in H.4. It can be seen from Table 3 and Fig. 1 that the result for specimen A.50 is to increase all three cell parameters more than the equivalent Mol. % of $Fe^{2+}$, etc.; this is in accord with the relatively larger ionic radius of $Mn^{2+}$.

For the *a* dimension it is clear that the entry of $Al^{3+}$ into the octahedral position causes a decrease, but the relationship is not quite as clear as for *b*.

Ramberg and De Vore (1951) concluded that, considering only the aluminium-poor orthopyroxenes, the *a* and *b* dimensions of the unit cell plotted against the Fe/Mg ratio gave curved lines which are not what one should expect unless the orthopyroxenes are not ideal mixtures between Fe and Mg silicates. The present author's contention, however, is that from the work of Hess (1952) and Kuno (1954), and from the data given here, the cell parameters show straight line variations in terms of $Mg^{2+}$ and $Fe^{2+}$, providing that the proportion of $Mn^{2+}$, $Ca^{2+}$ and $Al^{3+}$ is constant. Ramberg and De Vore (1951) plotted curves for five analysed "alumina-poor" orthopyroxenes but of these the one causing an appreciable departure from linearity for the *a* and *b* curves contained 0.035 Al in the octahedral position. The present investigation has shown that the orthopyroxenes from charnockitic and associated granulite facies metamorphic rocks do have cell parameters consistently smaller than those from Bushveld type plutonic or volcanic rocks earlier studied. This seems to be related mainly to the increasing ability of orthopyroxenes in the granulite facies to accept greater amounts of alien ions. It is felt, however, that in cell parameter studies of this type it is essential to specify the paragenesis of the minerals, as the inclusion in one investigation of specimens from unspecified sources but including both igneous and metamorphic minerals which have crystallized under very different conditions may possibly obscure slight but important differences in their chemistry and in their physical properties.

## Specific Gravity

The specific gravity was determined for 35 of the analysed orthopyroxenes and the results are included in Tables 1 to 3 and in Fig. 1. This property was measured using a 10 ml pycnometer, the final reading being taken after several preliminary checks over 3 to 4 days to eliminate trapped air bubbles. That the specific gravity also varies linearly with variation in the Fe/Mg ratio is illustrated in Fig. 1, where the line drawn is taken directly from Deer *et al.* (1963) and is seen to fit reasonably well the data here presented.

## Acknowledgments

In attempting to correlate cell parameters with chemical composition in the orthopyroxene series, it has been important to obtain mineral samples covering a wide range of compositions. The author is particularly grateful to Dr. B. A. O. Randall (1), Dr. A. T. V. Rothstein (35), Dr. P. R. J. Naidu (J. 32), Dr. R. R. Compton (3), Prof. H. H. Hess (12700), and Prof. H. W. Fairbairn and Dr. S. H. Kranck (H.4 and A.50) for providing samples of analysed orthopyroxenes, and to Mr. C. N. Barron (A, 177/54, 186b/54), Dr. K. E. Eade (KS. 137/54), Prof. W. A. Deer (400, 355), Prof. R. T. Prider (20486), Dr. M. Mathias (SP. 18) and Dr. B. Choubert (XI-132) for supplying suitable rock specimens from which it has been possible to separate the orthopyroxenes for analysis and further study. It is also a particular pleasure to acknowledge permission from Prof. H. H. Hess to plot values for cell parameters determined by him for three of the orthopyroxenes used in the present work, and to thank Dr. J. Zussman for helpful advice on the *x*-ray side of this work.

## References

Barth, T. F. W. (1926) Sagvandite, a magnesite-bearing igneous rock. *Norsk Geol. Tidssk.* **9,** 271–303.

Clavan, W., W. M. McNabb and E. H. Watson (1954) Some hypersthenes from southeastern Pennsylvania and Delaware. *Am. Mineral.* **39,** 566–580.

Choubert, B. (1954) Recherches géologiques au Gabon Central. *Bull. Dir. Mines. Géol. de l'A.E.F.*, No. **6**.

Compton, R. R. (1960) Charnockitic rocks of Santa Lucia range, California. *Am. Jour. Sci.* **258,** 609–636.

Deer, W. A., R. A. Howie and J. Zussman (1963) *Rock-forming Minerals. Vol. 2: Chain Silicates.* Longmans, London (John Wiley & Sons, Inc., New York).

Green, J. (1959) Geochemical table of the elements for 1959. *Geol. Soc. Am. Bull.* **70,** 1127–1184.

Hess, H. H. (1949) Chemical composition and optical properties of common clinopyroxenes, Part I. *Am. Mineral.* **34,** 621–666.

——— (1952) Orthopyroxenes of the Bushveld type, ion substitutions and changes in unit cell dimensions. *Am. Jour. Sci., Bowen vol.* 173–187.

Howie, R. A. (1953) The geochemistry of the charnockite rock group. Ph.D. Thesis, Univ. of Cambridge.

——— (1955) The geochemistry of the charnockite serires of Madras, India. *Trans. Roy. Soc. Edinburgh,* **62,** 725–768.

——— (1958) African charnockites and related rocks. *Serv. Géol. Congo Belge Bull.* **8,** Fasc. 2.

——— (1963) Some orthopyroxenes from Scottish metamorphic rocks. *Mineral. Mag.* **33** (in press).

——— and A. P. Subramaniam (1957) The paragenesis of garnet

in charnockite, enderbite, and related granulites. *Mineral. Mag.* **31,** 565–586.

KRANCK, S. H. (1961) A study of phase equilibria in a metamorphic iron formation. *Jour. Petrol.* **2,** 137–184.

KUNO, H. (1954) Study of orthopyroxenes from volcanic rocks. *Am. Mineral.*, **39,** 30–46.

LEAKE, B. E. (1958) The Cashel—Lough Wheelaun intrusion, Co. Galway. *Proc. Roy. Irish Acad.* **59,** (B) 155–203.

NAIDU, P. R. J. (1954) Minerals of charnockites from India. *Schweiz. Min. Petr. Mitt.* **34,** 203–279.

O'HARA, M. J. (1961) Zoned ultrabasic and basic gneiss masses in the early Lewisian metamorphic complex at Scourie, Sutherland. *Jour. Petrol.* **2,** 248–276.

PRIDER, R. T. (1945) Charnockite and related cordierite-bearing rocks from Dangin, Western Australia. *Geol. Mag.* **82,** 145–150.

RAMBERG, H. AND G. DE VORE (1951) The distribution of $Fe^{++}$ and $Mg^{++}$ in coexisting olivines and pyroxenes. *Jour. Geol.* **59,** 193–210.

ROTHSTEIN, A. T. V. (1958) Pyroxenes from the Dawros peridotite and some comments on their nature. *Geol. Mag.* **95,** 456–462.

SMITH, J. V. (1954) A review of the Al-O and Si-O distances. *Acta Cryst.* **7,** 479–481.

WARREN, B. E. AND D. I. MODELL (1930) Structure of enstatite $MgSiO_3$. *Zeit. Krist.* **75,** 1–14.

WASHINGTON, H. S. (1930) *The Chemical Analysis of Rocks.* John Wiley & Sons, Inc., New York.

## ADDENDUM

### PLEOCHROISM

Earlier work has shown that the strength of the pleochroism of orthopyroxenes is not related to the iron content (Howie, 1955), nor does it appear to be simply related to the amount of Ti or Mn, or to any one trace element. The orthopyroxenes of granulite facies rocks, however, are typically markedly pleochroic. The strongest pleochroism is shown by specimens 177/54, 2048b, 116, 3709 and 4645, all of which have more than 4% $Al_2O_3$, and it is here suggested that the strength of the pleochorism can be correlated with the alumina content and with the contraction of the cell parameters, *i.e.* it may be largely a physical effect.

MINERALOGICAL SOCIETY OF AMERICA, SPECIAL PAPER 1, 1963
INTERNATIONAL MINERALOGICAL ASSOCIATION, PAPERS, THIRD GENERAL MEETING

# SUR LES CONSTITUANTS PHOSPHATÉS DES MINERAIS DE FER OOLITHIQUES DE FRANCE

S. CAILLÈRE AND F. KRAUT
*Laboratoire de Minéralogie du Muséum, Paris and Laboratoire de Pétrographie de l'Ecole Nationale Supérieure des Mines, Paris*

ABSTRACT

Les minerais de fer oolithiques sont constitués en grande partie par des minéraux cristallisés, reconnaissables au microscope en lumière transmise ou en lumière réfléchie. Leur identification est aisée lorsqu'ils sont assez largement développés. Ce n'est pas le cas des minéraux phosphatés qui sont relativement rares et se présentent en général en petits cristaux.

Il a été néanmoins possible de déterminer dans de nombreaux minerais le minéral responsable de la teneur en phosphore, il s'agit toujours de phosphates de calcium.

En France, les minerais de fer oolithiques constituent trois dépôts importants, ceux de Lorraine, de Normandie et de l'Anjou.

Le premier est d'âge secondaire (aalénien); les autres, d'âge primaire, appartiennent au silurien à l'exception du gisement de Diélette qui est dévonien.

En Lorraine et en Normandie, les constituants essentiels du minerai sont des hydroxydes et des oxydes de fer, des carbonates et des silicates. En Anjou les couches minéralisées sont siliceuses et peu carbonatées. Tous ces minerais renferment des quantités variables de phosphore qui dépassent rarement 1%.

Malgré son importance quantitative faible, le phosphore dans les minerais de fer pose un problème en raison de son influence sur les procédés sidérurgiques.

## LES CONSTITUANTS PHOSPHATÉS DES MINERAIS DE LORRAINE

Le minerai contient 0,40 à 1% de phosphore, et l'expérience montre que le rapport P/Fe, assez constant, est égal à environ 2%.

D'après L. Cayeux (1902, 1922), les constituants phosphatés peuvent être visibles dans les débris osseux et dans des concrétions microscopiques ou invisibles, et dans ce cas le phosphore est combiné au fer.

En 1939, J. Bichelonne et P. Angot (1939) confirment les observations de L. Cayeux, sans préciser davantage sous quelle forme minéralogique se présente le phosphore visible.

Nous avons repris l'étude des concrétions et des organismes phosphatés et recherché, en outre, des minéraux bien cristallisés renfermant cet élément.

*Concrétions.* Les concrétions phosphatées se présentent, en lames minces, comme des masses jaunes ou incolores ayant un aspect colloforme et une texture concentrique. Elles sont partiellement ou entièrement anisotropes et polarisent dans le gris du premier ordre. Leurs indices de réfraction sont supérieurs à 1,60. Des essais microchimiques ont montré qu'elles sont formées par le phosphore et le calcium.

*Phosphates cristallisés.* Dans la couche grise de Moulaine, on trouve des échantillons riches en phosphore. On a dosé dans un spécimen 5% de $P^2O^5$ et 12,7% de CaO. L'examen microscopique de ce minerai s'est révélé particulièrement intéressant. On y voit, dans les espaces interoolithiques, des plages de "chlorites" qui renferment des cristaux hexagonaux bien développés.

En lumière naturelle le minéral est incolore, son indice moyen est d'environ 1,62. Entre nicols croisés, on constate que sa biréfringence dépasse légèrement celle de l'apatite. Les sections hexagonales se divisent en 6 secteurs dont chacun est biaxe négatif, avec, un angle 2V de l'ordre de 30°.

Les propriétés optiques de ce phosphate et ses caractères morphologiques correspondent à ceux de la francolite, carbonatofluoapatite de formule $Ca^5(F(PO^4,CO^3OH)^3)$ (3) (4) .

Au puits de Martinvaux le minerai vert renferme 1,3% de $P^2O^5$. En lames minces on observe dans les espaces interoolithiques des agrégats sphérolitiques dont les fibres polarisent dans le gris du premier ordre. Elles ont un allongement négatif et une extinction droite. Par endroits on remarque des sections transversales montrant des contours hexagonaux. Il s'agit d'un phosphate de calcium cristallisé probable-

ment de la staffélite, faciès fibreux de francolite, ou de la dahllite (apatite hydroxylée) $Ca^5(OH(PO^4)^3)$.

Des agrégats semblables ont été observés dans plusieurs minerais de la région.

*Organismes phosphatés.* Le minerai lorrain renferme d'innombrables fragments de fossiles. En lumière naturelle ils sont pour la plupart, jaunes et entre nicols croisés ils polarisent dans des teintes grises et s'éteignent parallèlement à l'allongement.

Nous allons insister sur un cas exceptionnel qui a permis d'étudier en détail non seulement les propriétés optiques, mais aussi la composition chimique d'un de ces os fossiles.

Un fragment d'os de plésiosaure, d'environ 20 cm de longueur a été trouvé dans la mine de Moulaine. Il se présente comme une masse poreuse entourée d'une croûte jaune rougeâtre.

L'examen microscopique montre que la carapace externe est constituée par des fibres faiblement biréfringentes à extinction droite et à allongement négatif. En se rapprochant de la zone centrale on voit des perforations de plus en plus nombreuses. Autour de ces cavités les fibres sont enroulées en anneaux concentriques, tandis que dans leurs interstices elles forment des agrégats rectilignes d'un jaune plus intense et plus biréfringents. Le signe d'allongement de ces fibres est positif. Les cavités sont remplies par des oxydes et des sulfures de fer.

A. Lacroix a signalé, dans les quercyites de Mouillac, deux variétés de dahllite ayant la même composition chimique et des propriétés optiques différentes.

Nous avons comparé les échantillons de A. Lacroix avec l'organisme de Moulaine et nous avons trouvé, entre eux, une grande analogie morphologique et optique. L'analyse chimique de la carapace donne les résultats suivants:

| | |
|---|---|
| $P^2O^5$ | 31,90 |
| CaO | 49,50 |
| $Al^2O^3$ | 0,30 |
| $Fe^2O^3$ | 2,80 |
| $TiO^2$ | 0,10 |
| MgO | 0,20 |
| $H^2O-$ | 1,70 |
| $+$ | 1,70 |
| $CO^2$ | 9 |
| $SO^3$ | 1,75 |
| F | 0,30 |
| | 99,25 |

Les proprotions moléculaires des principaux constituants $P^2O^5$, CaO et $CO^2$ sont les suivantes:

| | | |
|---|---|---|
| 3 | 11,6 | 2,6 |

En déduisant la quantité de CaO nécessaire pour saturer le $CO^2$, il reste:

| $P^2O^5$ | CaO |
|---|---|
| 3 | 8,94 |

ce qui donne pour $CaO/P^2O^5$ un rapport voisin de 3.

On peut conclure, d'après les résultats de l'analyse chimique, que l'on a affaire à une carbonatoapatite qui contient une certaine quantité d'eau dans son réseau.

Le diagramme de rayons X, fait avec ce fragment d'os, est indentique à celui de la dahllite de Mouillac (Geiger, 1950).

Nous pensons que certains débris d'organismes ayant le faciès fibreux de l'os de Moulaine sont également formés de dahllite. Dans une lame mince du minerai de la couche grise d'Ottange, nous avons observé des dents de poissons. L'une d'elles a été étudiée à l'aide de la sonde de Castaing, qui a bien confirmé que l'on est en présence d'un phosphate de calcium.

En dehors du phosphate visible le minerai lorrain renferme, comme le pensaient les anciens auteurs, du phosphate dispersé submicroscopique. En effet les teneurs en $P^2O^5$ que font apparaitre les analyses ne sont pas toujours justifiées par la quantité visible de phosphate.

Par exemple dans le couche grise d'Ottange, les oolithes silicatées et ferrugineuses sont presque opaques en lame mince, cependant un certain nombre d'entre elles comportent des anneaux concentriques relativement transparents. Dans ces "zones claires" la sonde de Castaing met en évidence le phosphore et le calcium. Il semble, par conséquent, que le phosphate invisible au microscope est lié au calcium plutôt qu'au fer.

En résumé, dans le minerai lorrain le phosphore se trouve toujours à l'état de phosphate de calcium, le plus souvent dans les organismes, assez rarement sous forme bien cristallisée, et en partie à l'état d'inclusions submicroscopiques.

## Les Constituants Phosphatés Des Minerais de Normandie

Le problème des phosphates est beaucoup moins ardu dans les minerais de Normandie que dans ceux de Lorraine (Courty, 1961).

Effectivement on observe souvent des cristaux bien développés dont les propriétés optiques sont celles de l'apatite. Par exemple dans certains minerais de May-sur-Orne, les espaces interoolithiques sont occupés par l'apatite.

Nous avons analysé dix échantillons provenant de ce gisement. En saturant le phosphore avec du calcium dans le rapport moléculaire $\frac{1}{3}$ on obtient pour l'apatite les valeurs suivantes:

APATITE DANS MINERAL DE MAY SUR ORNE

| | $P^2O^5$ | Apatite |
|---|---|---|
| I | 0,16 | 0,30 |
| II | 0,27 | 0,67 |
| III | 0,34 | 0,67 |
| IV | 0,34 | 0,67 |
| V | 0,34 | 0,67 |
| VI | 1 | 2,35 |
| VII | 1,05 | 2,35 |
| VIII | 2,60 | 6 |
| IX | 4 | 9,45 |
| X | 6,35 | 13,50 |

Les cinq premiers échantillons représentent le minerai moyen, qui renferme moins de 1% de phosphate. Les autres ont été choisis en raison de leur forte teneur en apatite observée au microscope.

L'un d'entre eux, le N°X, a été étudié à la sonde de Castaing. On a pu vérifier ainsi que les cristaux repérés en lame mince sont bien du phosphate de calcium.

Ajoutons que l'exploration à la sonde a montré que le phosphore est localisé uniquement dans le ciment et fait défaut dans les oolithes.[1]

Le minerai de Soumont renferme aussi, localement, de l'apatite en quantité non négligeable. La sonde de Castaing montre à nouveau que le phosphore est concentré dans le ciment associé au calcium. On ne trouve ni l'un ni l'autre de ces éléments dans les oolithes. Par contre à St-Rémy et à la Ferrière-aux-Etangs l'apatite constitue le noyau de quelques oolithes.

A Diélette nous avons observé des agrégats d'apatite dans plusieurs couches minéralisées, en particulier dans la couche N° 2. En général, le phosphate forme des amas allongés ou des lentilles parallèles à la stratification du minerai.

[1] M. Courty (1961) a signalé la présence de phosphate de calcium dans les oolithes de certains minerais de May-sur-Orne.

## LES CONSTITUANTS PHOSPHATÉS DES MINERAIS DE L'ANJOU

C'est principalement dans des échantillons provenant de Chazé Henry et d'Ombrée que nous avons observé de beaux exemples de phosphate cristallisé. L'apatite accompagne parfois la magnétite. Dans le minerai d'Ombrée on trouve des veinules microscopiques remplies par la calcite et l'apatite. Ce dernier minéral a été identifié par ses propriétés optiques et par son diagramme de rayons X. Des plages de phosphate prélevées dans la lame mince ont donné un diagramme de Debye et Scherrer caractéristique de la fluoapatite. Le même échantillon a été étudié à la sonde de Castaing, qui a mis en évidence le phosphore et le calcium dans tous les agrégats reconnus comme apatite par leurs propriétés optiques. On a également constaté qu'aucune plage ferrugineuse ne renferme de phosphore. L'analyse chimique a montré que ce minerai renferme 5,5% de $P^2O^5$ et 6,5% de CaO, ce qui correspond exactement au rapport moléculaire 1:3 de l'apatite.

Le minerai de Segré, qui a la même composition minéralogique que ceux de Chazé Henry et d'Ombrée, renferme par endroits des quantités notables d'apatite. Les cristaux hexagonaux de ce minéral y sont souvent très bien développés.

Dans deux échantillons analysés on a trouvé les valeurs suivantes: dans la couche A 3,65% d'apatite; dans la couche B 3,3%.

En conclusion, cette étude montre que dans les minerais étudiés le phosphore se trouve toujours à l'état de phosphate de calcium de type apatite, et nous avons vu qu'il peut revêtir des formes très variées.

Dans les minerais primaires le phosphore est souvent contenu dans des cristaux visibles que l'on a pu identifier à une fluoapatite. Dans les minerais secondaires ce sont des variétés carbonatées d'apatite qui ont été reconnues: la francolite et la dahllite, cette dernière le plus souvent dans des débris d'organismes.

Enfin il est probable qu'une partie du phosphate de calcium se trouve dans ces minerais à l'état d'inclusions submicroscopiques.

## BIBLIOGRAPHIE


BICHELONNE, J. ET P. ANGOT (1939) *Le Bassin Ferrifère de Lorraine.* Berger-Levrault, Nancy-Strasbourg.

CAILLÈRE, S. ET F. KRAUT (1954) Les Gisements de fer du Bassin Lorrain. Edition du Muséum, Paris.

CAYEUX, L. (1902, 1922) *Les Minerais de Fer Oolithiques de France. Fasc. I et II.* Imprimerie Nationale, Paris.

COURTY, G. (1961) *C. R. Acad. Sci.* **252,** 1486–1488.

GEIGER, TH. (1950) *Bull. Schweiz. Mineral Petrog. Mitt.* **30,** 161–181.

MCCONNELL, DUNCAN (1952) *Bull. Soc. Franc. Mineral. Cryst.* **75,** 428–445.

### Discussion

W. Wimmenauer (Freiburg, Germany): Est-ce-que les apatites bien cristallisées sont une repartition plus générale ou sont-ils liées aux zones de diagénèse plus avancée?

Authors reply: Les apatites bien cristallisées sont assez fréquentes.

Les minerais où on les rencontre renferment aussi du phosphore à l'état dispersé, si bien qu'il n'existe pas de relation apparente entre la diagénsèe et l'état plus ou moins cristallin des substances phosphatées.

MINERALOGICAL SOCIETY OF AMERICA, SPECIAL PAPER 1, 1963
INTERNATIONAL MINERALOGICAL ASSOCIATION, PAPERS, THIRD GENERAL MEETING

# TRENDS AND AFFINITIES OF BASALTIC MAGMAS AND PYROXENES AS ILLUSTRATED ON THE DIOPSIDE—OLIVINE—SILICA DIAGRAM

D. S. COOMBS
*Geology Department, University of Otago, Dunedin, New Zealand*

ABSTRACT

The major normative components of basalts can be accommodated in the tetrahedra plagioclase—diopside—olivine—silica or plagioclase—diopside—olivine—nepheline. Average compositions of magma batches from basaltic provinces project from the plagioclase point as a broad band extending across the base of the tetrahedra. At one extreme are types in which an "indicator ratio"

$$\frac{Hy + 2Qz}{Hy + 2(Qz + Di)} = 0.65 - 0.85,$$

and from which early precipitation of hypersthene is common. Differentiation leads to granophyric products. Where the indicator ratio is less than 0.60—0.65 hypersthene, if present, tends to follow augite. Hypersthene is seldom found where the ratio is less than 0.50. For typical tholeiites, the indicator ratio is $0.65 \pm 0.20$. In the range 0.40 to 0.00 is a rather heterogeneous group including the high-alumina basalts of Medicine Lake Highlands as well as mildly alkaline suites such as Ascension Island, Easter Island and Réunion. The latter examples tend to show a pantelleritic differentiation trend. Averages for the more typical alkaline suites have normative nepheline instead of hypersthene and have trachytic and phonolitic associates. Analyses of pyroxenes from alkaline basalts contain normative Ne; those from tholeiites commonly contain normative Di, Ol, Hy. Separation of such pyroxenes from their parent magma in general accentuates the undersaturated or oversaturated nature of the magma with respect to the plagioclase—diopside—olivine plane. Consideration of crystallization trends allows the approximate location of a five-phase "point" (olivine, augite, hypersthene, plagioclase, liquid) and interpretation of reaction relationships. Clustering of analyses of typical tholeiites around this point suggests that they have originated as liquids coexisting with the four solid phases mentioned.

## INTRODUCTION

Yoder and Tilley (1957) have recently emphasized the importance in basaltic petrogenesis of the relations described by Bowen (1914) in the system $CaMgSi_2O_6$-$Mg_2SiO_4$-$SiO_2$. For ordinary pressures, the olivine-pyroxene reaction relationship should be shown by those liquids which start their crystallization in that part of the forsterite field below and to the right of a line joining $Mg_2SiO_4$ to the point where the pyroxene-forsterite field boundary crosses the $MgSiO_3$-$CaMgSi_2O_6$ join (Fig. 1). Such liquids may be compared with simplified tholeiitic magmas. In contrast alkali basalt magmas do not show this reaction relationship and if they may be represented on this diagram at all, they may be compared with liquids that commence their crystallization in the wedge-shaped area to the left of the join referred to, that is near the forsterite-diposide side of the triangular diagram.

In spite of the fundamental significance to petrogenesis of relationships in this system, systematic attempts to plot appropriate rock compositions on a corresponding diagram do not appear to have been published.[1] Some of the relationships which are revealed by the use of such diagrams are explored in the present paper.

The diagrams here used may be regarded as projections from the plagioclase apex onto the bases of a plagioclase-ferroan diopside-olivine-silica tetrahedron, and of a corresponding plagioclase-nepheline-olivine-ferroan diopside tetrahedron for more strongly undersaturated compositions. Compositions are plotted in terms of molecular proportions of the normative components. In the case of common basaltic rocks virtually all constituents, except iron ores, are accommodated by the tetrahedra concerned. The projections are designed primarily to portray variation in silica saturation. Variations in iron/magnesium and alkali/lime ratios, effectively illustrated in certain other diagrams, are not revealed. An advantage sought by Murata (1960) in a proposed method for plotting basaltic rock analyses is achieved, namely that compositions of the major minerals are

[1] Since this was written Tilley (1961) has plotted Hawaiian basalts on diagrams of this sort, though he favours plots in weight per cent rather than molecular per cent as here employed.

clearly represented. Furthermore rock compositions are portrayed in a manner which with certain qualifications, directly reflects the crystallization history of the rock as has long been achieved in phase diagrams of synthetic systems and in plots of rocks whose compositions approach those of petrology's residua system $NaAlSiO_4$-$KAlSiO_4$-$SiO_2$.

ACKNOWLEDGMENTS

For some years the writer has used in his lecture courses diagrams of the type presented here. During late 1959 and 1960 he had the opportunity of discussing problems of basalt petrogenesis with many geologists including Drs. G. A. Chinner, I. D. Muir, K. J. Murata, S. R. Nockolds, D. H. Richter, Professors C. E. Tilley and O. F. Tuttle and Dr. H. S. Yoder. While he accepts full responsibility for the general approach and the opinions here expressed, the writer is conscious that the treatment has been greatly enriched through these discussions. Several of those mentioned critically read a manuscript of the present paper during late 1960, a number of additional data and minor changes having been incorporated since. The writer is particularly grateful to Professor E. F. Osborn for critical comments on the manuscript, to Professor Tilley and Dr. Muir for much interesting information and to Professor Tilley for the hospitality of the Department of Mineralogy and Petrology, Cambridge, where most of the manuscript was prepared, to the United States Educational Foundation for a Fulbright travel award and to the Pennsylvania State University

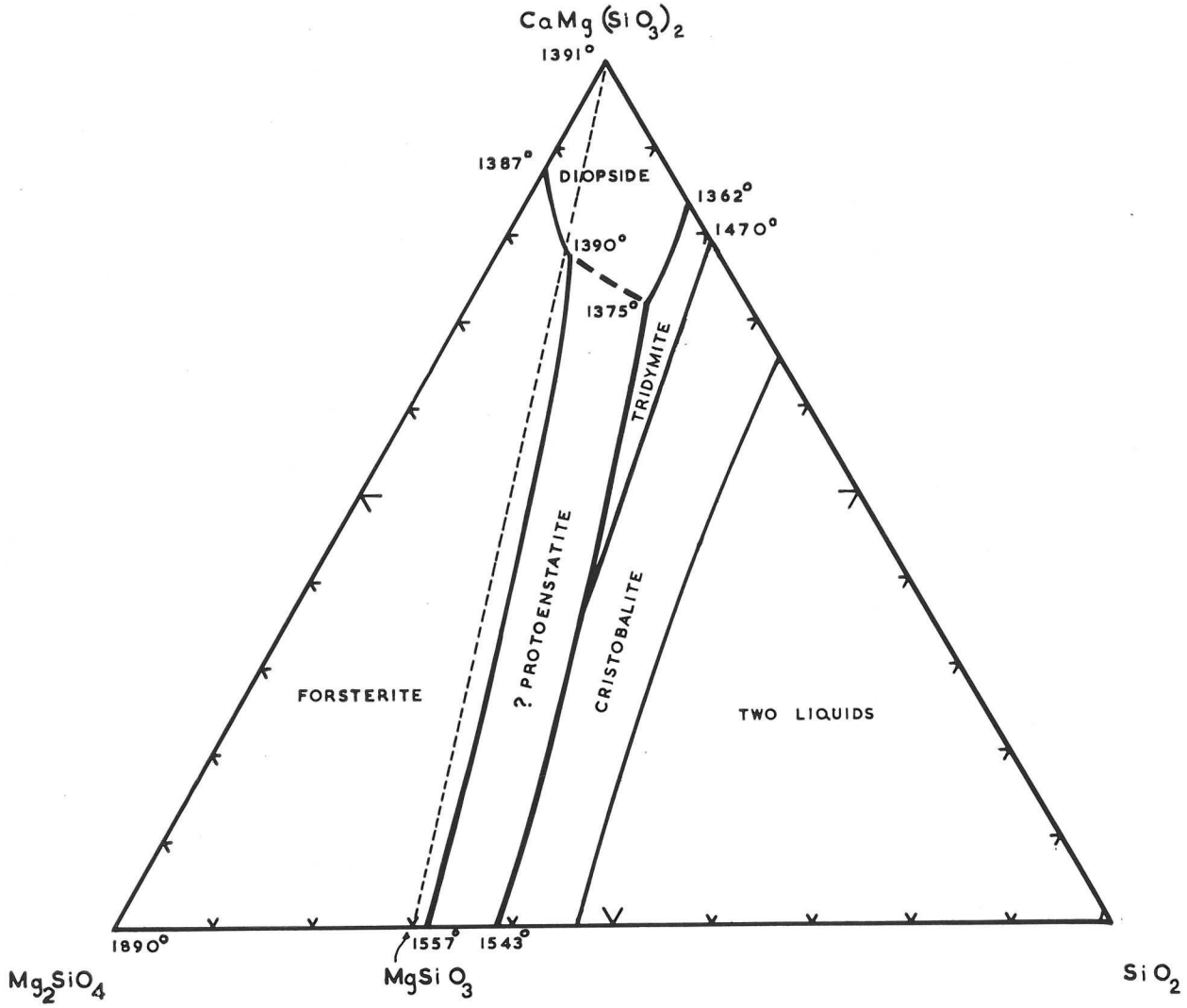


FIG. 1. The system $CaMgSi_2O_6$-$Mg_2SiO_4$-$SiO_2$, after Bowen (1914) and Osborn and Muan (1960).
Note added in proof: For revised diagram, see Schairer and Yoder (1962) *Carn. Inst. Wash. Year Book*, **61**, 76.

whose guest the writer was during the Spring Semester of 1960.

### Effects of Added Components on Relations in the System $CaMgSi_2O_6$-$Mg_2SiO_4$-$SiO_2$

Probable relationships in the four-component system diopside-forsterite-anorthite-silica (Fig. 2), based on interpolation from the four bounding ternary systems, have been illustrated by Osborn and Tait (1952). Boyd and Schairer (1957) have subsequently demonstrated an immiscibility gap in the diopside-clinoenstatite series. This requires subdivision of the pyroxene field in the ternary system (Fig. 1) as indicated tentatively by Osborn and Muan (1960, Plate 2). The pyroxene volume in the quaternary system must also be subdivided into separate volumes for at least two pyroxenes. The anorthite volume forms a roof to those of forsterite, pyroxenes and the silica minerals. Disregarding the subdivision of the pyroxene volume, the projection of this "roof" from

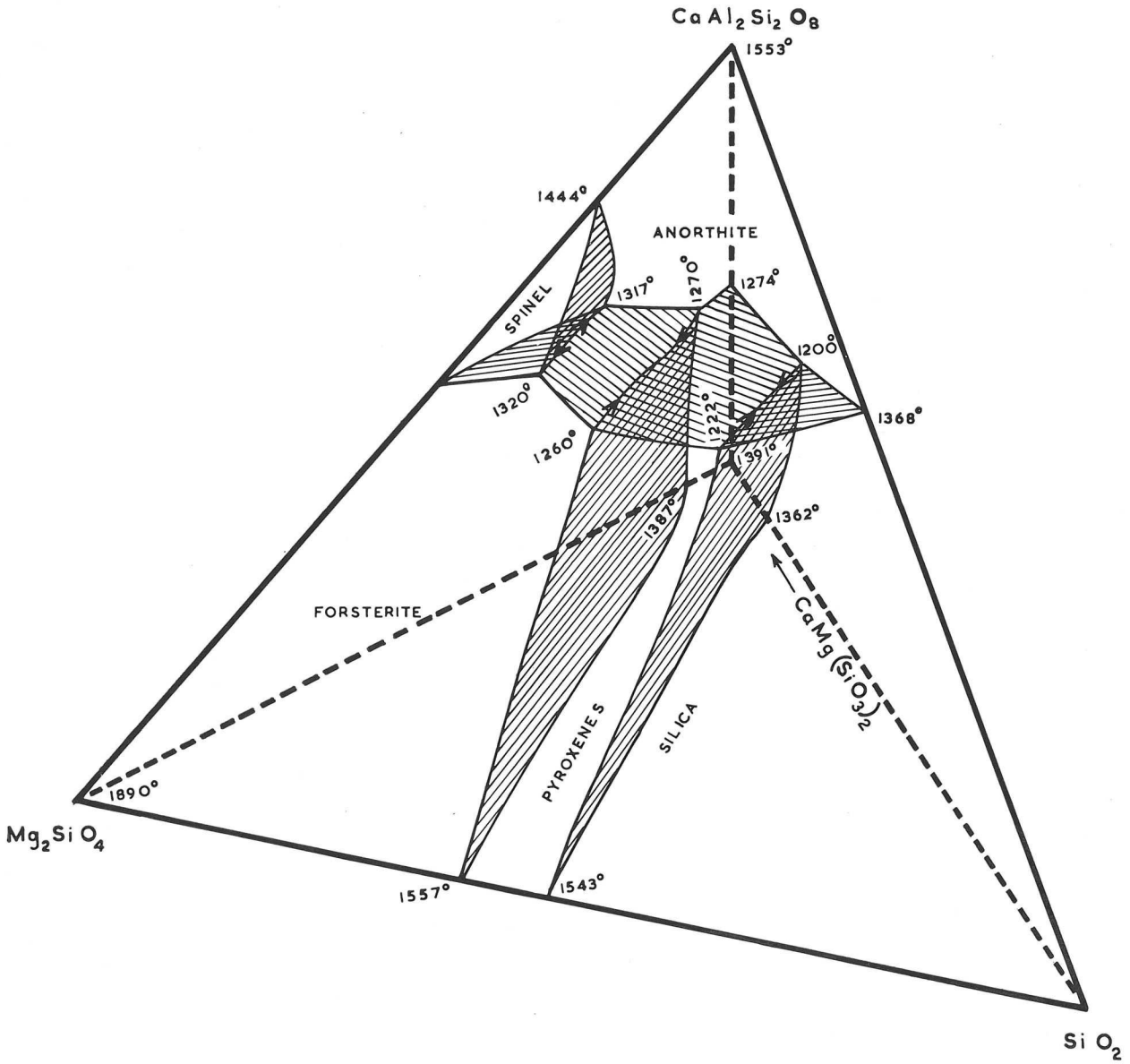


Fig. 2. Schematic representation of relations in the four component system $CaAl_2Si_2O_8$-$CaMgSi_2O_6$-$Mg_2SiO_4$-$SiO_2$ neglecting subdivision of the pyroxene volume (adapted from Osborn & Tait, 1952). The "floor" of the anorthite volume is shown shaded. It is crossed by three four-phase invariant lines: anorthite-spinel-forsterite-liquid, anorthite-forsterite-pyroxene-liquid, anorthite-pyroxene-silica-liquid, where it intersects other boundary surfaces, which are also shown shaded.

the anorthite point onto the base of the tetrahedron is shown schematically in Fig. 3, recast into molecular proportions for reasons discussed later. Following Osborn and Tait, temperature minima are indicated on the forsterite-pyroxene-anorthite-liquid and silica-pyroxene-anorthite-liquid univariant lines. It is probable that a two-pyroxene boundary surface will in fact intersect these univariant lines in five-phase invariant points that may also be the minima on the two boundary curves. Compositions and temperatures of the ternary and binary univariant points are indicated and the shape of the anorthite crystallization surface is shown schematically by contour lines indicating weight percentage anorthite, these being interpolated between the bounding ternary systems and the plane anorthite-enstatite-diopside studied by Hytönen and Schairer (1960).

From the position of the trace of the anorthite-metasilicate plane, it appears that the reaction relationships of Fig. 1 are unlikely to be upset by the presence of anorthite. In fact Andersen (1915) showed that in the plane anorthite-forsterite-silica the effect of anorthite is to extend the field in which the forsterite-enstatite reaction relationship prevails

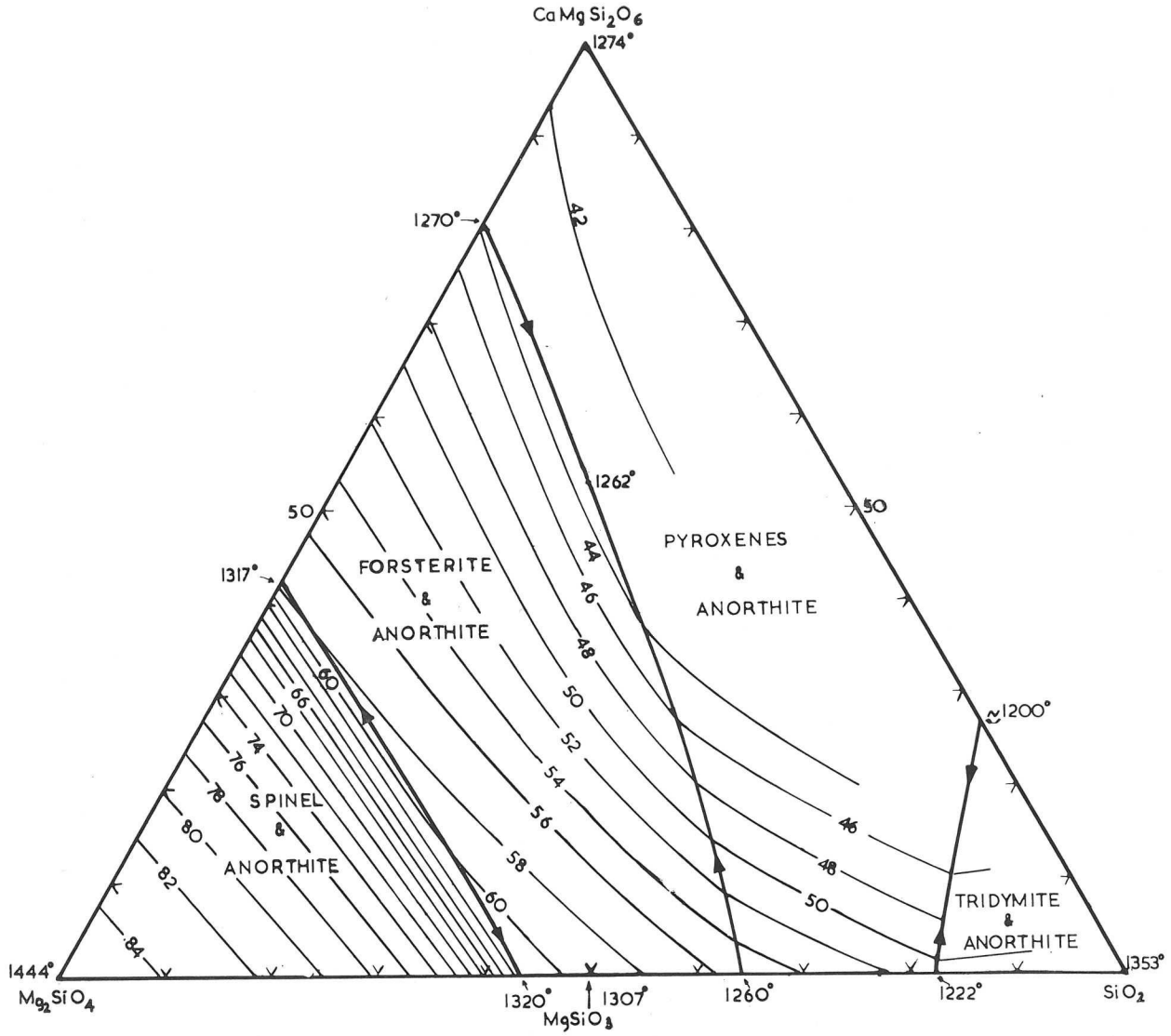


FIG. 3. Probable form of surface of the anorthite volume projected onto the base of the tetrahedron anorthite-diopside-forsterite-silica, disregarding subdivision of the pyroxene field; compositions in molecular per cent. Contours (marked in weight per cent) represent anorthite content of liquids existing on the three-phase surfaces as interpolated from boundary faces and the section enstatite-anorthite-diopside. Data from Andersen (1915), Osborn and Tait (1952), Hytönen and Schairer (1960).

However, if the interpretation of Osborn and Tait (1952) is correct, fractionation of liquids near the forsterite-diopside-anorthite plane should lead towards a minimum on the four-phase univariant line within the tetrahedron instead of to a eutectic or piercing point on the forsterite-diopside join as indicated by Bowen (1914) for the ternary system without anorthite. This fact could be crucial to the interpretation of the crystallization history of alkali olivine basalt magmas.

Presently published data do not allow the effect of albite to be evaluated in detail. Nevertheless behaviour in the planes enstatite-albite-diopside (Schairer and Morimoto, 1959) and albite-forsterite-silica (Schairer and Yoder, 1960) indicate that as albite replaces anorthite the plagioclase volume must shrink away from the diopside-forsterite-silica face, and that an olivine-"enstatite" reaction still prevails and may be further extended. The detailed effects of progressive substitution of iron for magnesium in the system are similarly uncertain, but as is well known from the work of Bowen and Schairer (1935) the olivine-pyroxene reaction relationship is destroyed by increasing iron content in the system $MgO$-$FeO$-$SiO_2$ so that ultimately fayalitic olivine can coexist stably with a silica mineral and a liquid whose composition is now on the olivine side of the metasilicate join. One may infer that in an infinite series of tetrahedra such as that in Fig. 2 in which iron progressively replaces magnesium and in which albite replaces anorthite, the position of the various three-phase surfaces and four-phase curves will progressively migrate. Increasing Fe/Mg ratios apparently reduce the range of compositions showing the olivine-"hypersthene" reaction relationship whereas increasing ratios of albite/anorthite may have the converse effect.

From the fact that typical basaltic liquids do coexist with the phases olivine, pyroxene and plagioclase feldspar and furthermore from the consistent pattern revealed when basaltic rocks and their pyroxenes are plotted in the tetrahedron, it may be inferred that crystallization relations for the common basaltic liquids have a general similarity in form to those of Fig. 2. It will be shown later that for common basalts the projected position of the four-phase curve olivine-pyroxene-plagioclase-liquid is remarkably close to its inferred position for the iron-free, albite-free system. Furthermore as normative feldspar constitutes about 50% by weight of total normative olivine or quartz plus pyroxenes plus feldspar in common basaltic rocks, it may also be inferred that the floor of a feldspar volume in a system plagioclase-ferroan diopside-olivine-silica must be in about the same position for basaltic compositions as it is in the system $CaAl_2Si_2O_8$-$CaMgSi_2O_6$-$Mg_2SiO_4$-$SiO_2$. Melts containing substantially more feldspar than this appear to commence crystallization in a plagioclase volume, as in the case of a hawaiite from Papalele Gulch, Mauna Kea, containing 61.2% normative feldspar (Yoder and Tilley, 1957). Melts containing lower plagioclase contents commonly commence crystallization in an olivine volume, apart from the more markedly oversaturated tholeiitic basalts in which the early crystallization products are pyroxenes and plagioclase to the exclusion of olivine.

## Procedure

The metasilicate join, arbitrary indicator of silica saturation in igneous rocks, varies in its position on a weight per cent diopside-olivine-silica diagram as the Fe/Mg ratio is varied, and furthermore owing to the differing Fe/Mg ratios in crystals and liquid, liquids in the olivine field of a weight per cent diagram would follow a slightly curving instead of a straight course away from the olivine point, even though olivine may be the only phase separating. For clarity of interpretation rather than ease of plotting, diagrams based on molecular proportions are here adopted.

Compositions to the right of the metasilicate join in Fig. 3, conventionally considered as oversaturated, contain silica in the norm; those to the left are undersaturated and contain olivine. When silica is inadequate to satisfy diopside, olivine and feldspar, then nepheline and leucite appear in turn instead of hypersthene. It is therefore convenient to plot a second triangle $Ca(Mg,Fe)Si_2O_6$-$(NaAlSiO_4+KAlSi_2O_6)$-$(Mg,Fe)_2SiO_4$ alongside the first and having one edge in common. This may be considered as the base of a tetrahedron with feldspar at the apex and sharing a "critical plane of silica undersaturation" (Yoder and Tilley, 1960) with the plagioclase-ferroan diopside-olivine-silica tetrahedron. Compositions of rocks and minerals are thus plotted in this paper in terms of molecular proportions of $(NaAlSiO_4+KAlSi_2O_6)$: $Ca(Mg,Fe)Si_2O_6$: $(Mg,Fe)SiO_3$: $(Mg,Fe)_2SiO_4$: $SiO_2$ as computed during the calculation of the C.I.P.W. Norm, and recalculated to 100%. Well known tables for the calculation of the norm give molecular proportions (weight per cent divided by molecular weight) to three places of decimals. For some constituents this involves significantly less precision than is justified by the chemical analysis and furthermore the use of these three-figure tables invalidates the fourth

significant figure often cited in published norms. Revised molecular weights and a fourth figure have therefore been used during the calculation of norms for the present paper, and rounding to one place of decimals has been carried out at the end of the computation.

### Effects of Analytical Error and Secondary Alteration

It is easy to demonstrate the amount and direction of scatter that is produced by given analytical errors in plots based on relative proportions of normative pyroxenes, olivine, silica or nepheline. Overestimation of alumina increases normative anorthite, olivine and nepheline or hypersthene at the expense of diopisde, whereas overestimation of lime or underestimation of $P_2O_5$ will result in overestimation of normative diopside. On account of the large amount of silica required to combine with alkalis in normative feldspar, errors in alkalis are of considerable importance, whereas normal errors in silica cause relatively minor disturbance. The effects of secondary oxidation and of analytical error in $Fe_2O_3/FeO$ ratio are especially significant. It is well known that oxidation of ferrous iron tends to increase hypersthene in the norm at the expense of olivine (*e.g.* see Muir and Tilley, 1957, p. 251). As an example we may consider the effect of reducing the 3.14% $Fe_2O_3$ recorded for a certain basalt to 1.5% $Fe_2O_3$ with corresponding increase of FeO. In terms of relative molecular proportions of Qz, Di, Hy and Ol, Di remains constant at 35.4%, Hy drops from 62.6% to 56.4% and 8.2% Ol appears instead of 2.1% Qz. This type of difficulty is particularly perplexing in the case of alkaline basalts in which $Fe_2O_3$ and $H_2O$ are commonly high, perhaps in part the result of an inherent property of alkali basalt magmas.

Two other types of secondary alteration are likely to be especially important. Serpentinization of olivine results in an increase of normative hypersthene with respect to olivine while alteration of glass to chlorite, palagonite or chlorophaeite appears to result commonly in a loss of lime, no doubt promoting the formation of calcite and zeolites in amygdaloidal horizons, and causing a serious decrease in normative diopside with respect to normative hypersthene and olivine in the massive rock. In the writer's view the many analyses of basaltic rocks in which such processes have been operative, cannot safely be regarded as precise representations of the composition of the original magma.

From this discussion and that of Fairbairn *et al.* (1951) it is obvious that analytical error and secondary alteration will produce an appreciable scatter on the Di-Ol-Qz and Di-Ol-Ne diagrams and for rocks such as some mugearites where total normative Di+Ol+Ne or Qz is 25% or less of the total rock, the plots will be of qualitative value only. The scatter of points which can be obtained by plotting the more aberrant individual analyses of the diabase W1 (Fairbairn *et al.*, 1951) emphasizes that too much significance must not be attached to individual analyses, but nevertheless it also appears that many generalized trends can be clearly portrayed. In fact batches of analyses of related unaltered rocks often show remarkably consistent patterns as in the case of the various phases of the 1921 and 1955 Kilauea eruptions (Fig. 8). In such cases the internal consistency can be appreciably enhanced by reducing $Fe_2O_3$ to some arbitrary value throughout the series, suggesting that even in very fresh rocks at least part of the $Fe_2O_3$ variation is due to secondary oxidation or to error in the determination of FeO.

### A Series of Basaltic Magmas

It is obvious from the analyses that in typical tholeiitic basalts such as those from Tholey itself the ratio of normative hypersthene to diopside is in general rather high, whereas in those basalts having high alkali/silica ratios such as the alkali series of Hawaii (Tilley, 1950), hypersthene tends to be subordinate or absent. Such relationships are clearly relevant to the reaction relationship and the subsequent crystallization trend likely to be followed by a magma. Are these relationships capable of more systematic treatment?

In Table 1 the average compositions, norms and other data are given for basalts from a number of provinces, an attempt being made, in so far as the data allow, to ensure that the average represents a suite of rocks that is reasonably homogeneous in type, place and time. Except where special points are illustrated, the objective has been to obtain analyses representative of relatively voluminous batches of magma. The effects of averaging are both to smooth out analytical error and also to conceal real variation within the single volcano or province. Aspects of such intraprovincial variation are discussed later. The data are plotted on a Ne-Di-Ol-Qz diagram in Fig. 4.

Many of the averages have been taken from the literature; a few have been computed by the writer. In the latter case individual analyses showing more than 5% $Fe_2O_3$ or 5% $H_2O$ have been discarded owing to the probability of secondary alteration and where published averages show more than 5% $Fe_2O_3$, these averages have also been rejected. Where the average

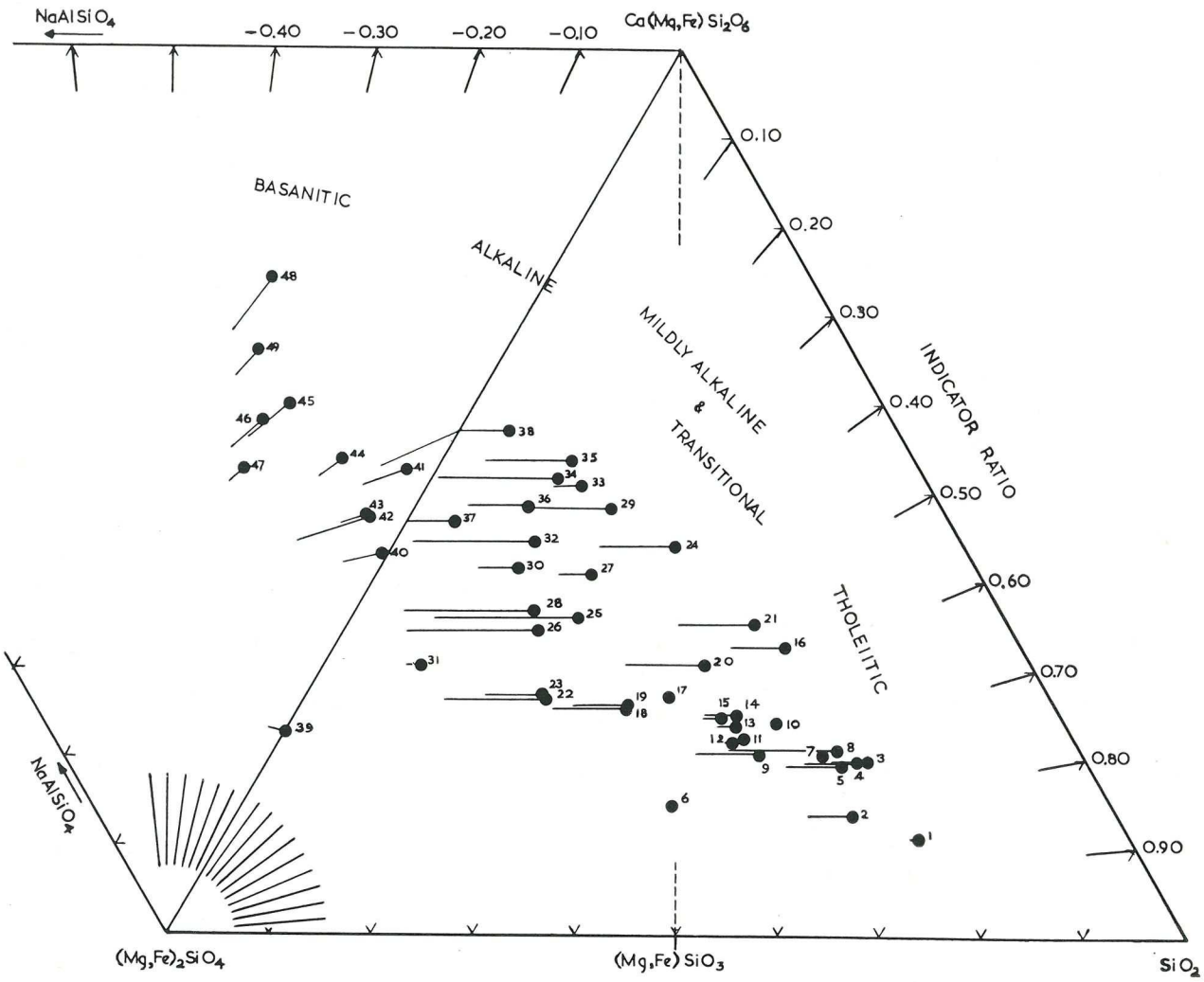


FIG. 4. Average compositions of basalts of various petrographic provinces plotted on a Ne-Di-Ol-Qz diagram (molecular proportions). See Table 1.

shows more than 1.5% $Fe_2O_3$, a line is drawn from the plotted point to where the analysis would plot if $Fe_2O_3$ were reduced to 1.5% and FeO increased correspondingly. This line gives an indication of the probable range of uncertainty in the plot in so far as oxidation effects are concerned.

Olivine is the first silicate phase to crystallize from perhaps the majority of basaltic magmas. In terms of the tetrahedral model of Fig. 2, crystallization commonly commences in the olivine volume and residual liquids must then move away from the point representing the olivine composition until they reach either the olivine-pyroxene or olivine-plagioclase boundary surface. They will then move along this towards an olivine-pyroxene-plagioclase-liquid four-phase curve, which as discussed above is not univariant but migrates with changing Fe/Mg and albite/anorthite ratios as well as with other variables in the natural system. The probability that basalts with high normative feldspar content may commence crystallization in the feldspar volume has already been referred to, but whether feldspar commences to crystallize early or late, so long as it carries neither an excess nor deficiency of silica, its separation does not affect the position of residual liquids on the projections here employed. It may be noted that many plagioclase analyses do in fact show a slight excess of silica. If this is real and not analytical, separation of plagioclase would thus tend to leave a residual liquid slightly impoverished in silica and to displace it slightly away from the silica corner of the projection. This possible effect will be neglected in the ensuing discussion.

No matter, then, at what stage plagioclase com-

KEY TO TABLE 1 AND FIG. 4

1. Peneplain Sill chilled margins, Ferrar dolerite, Victoria Land (Gunn, 1962).
2. Izu basalts, Japan, with $SiO_2 < 52\%$ (Kuno, 1950).
3. Columbia River basalt; Yakima basalt (Waters, 1961).
4. Izu basalts, Japan; aphyric types and groundmasses (Kuno, 1950).
5. Paleozoic tholeiites and quartz dolerites of north England and Scotland (Walker and Poldervaart, 1949).
6. Stillwater complex, border facies (Hess, 1960).
7. Ferrar dolerite chilled margins, moderate silica type, Victoria Land (Gunn, 1962).
8. Tholey tholeiites, Saar; two least oxidized analyses (Jung, 1958).
9. Koolau basalts, Oahu (Wentworth and Winchell, 1947).
10. Tasmanian dolerites; chilled phases (Edwards, 1942).
11. Karroo dolerites (Walker and Poldervaart, 1949).
12. Palisade diabase, chilled contacts (Walker, 1940).
13. Japanese "parental tholeiite" (Kuno, 1960).
14. Mauna Loa basalts, Hawaii (Macdonald, 1949a).
15. Columbia River basalts; late Yakima and early Ellensburg flows (Waters, 1961).
16. Deccan basalts (Sukheswala and Poldervaart, 1958).
17. Kilauea basalts, Hawaii (Macdonald, 1949a).
18. Greenstone flow, Lake Superior, weighted average (Cornwall, 1951).
19. Japanese "parental high-alumina basalt" (Kuno, 1960).
20. Columbia River (early) basalts; Picture Gorge basalt (Waters, 1961).
21. Non-porphyritic central magma type, Britain (Walker and Poldervaart, 1949).
22. Plateau basalts of Scotland (Green and Poldervaart, 1955).
23. Central Cascade Range, olivine basalts (Waters, 1961).
24. Western Australian Tertiary tholeiites (Edwards, 1938).
25. Ascension Island (Daly, 1925; Coombs and Harris, unpublished data).
26. Banks Peninsula, N.Z. (Benson, 1941).
27. Skjaldbreith shield volcano, Iceland (Tryggvason, 1943).
28. Tutuila, American Samoa (Daly, 1924).
29. Easter Island (least oxidized and hydrated; Bandy, 1937).
30. Galapagos Islands (Richardson, 1933).
31. Medicine Lake, California; high alumina basalt (Green and Poldervaart, 1955; Anderson, 1941).
32. Mauritius; Older Volcanic Series aphyric and microphyric basalts (Walker and Nicolaysen, 1954).
33. Réunion; basalt and dolerite, Volcan Actif (Walker and Nicolaysen, 1954).
34. Gambier Island (Mangareva), (Green and Poldervaart, 1955).
35. Réunion; basalts "des cônes interne et externe" (Lacroix, 1936, p. 192).
36. Réunion; Piton des Neiges (Lacroix, 1936, p. 211).
37. Mauna Kea, Hawaii; Hamakua volcanic series (Macdonald, 1949a).
38. Juan Fernandez; Mas-a-tierra (Green and Poldervaart, 1955).
39. Réunion; oceanites from Piton des Neiges (Lacroix, 1936, p. 214).
40. Alkali olivine basalts of Japan (Kuno, 1960).
41. Hualalai basaltic rocks, Hawaii (Macdonald, 1949a).
42. St. Helena (Daly, 1927).
43. Society Islands; Bora-Bora and neighbourhood (Lacroix, 1927).
44. Mauritius; late younger series basalts and dolerites (Walker and Nicolaysen, 1954).
45. Rungwe, East Africa; basaltic lavas excluding melanephelinites (Harkin, 1960).
46. East Otago, N.Z.; peripheral subprovince weighted average (Benson, 1942).
47. Auckland city basanitic basalts (Searle, 1960).
48. Tahiti basanitoid (Williams, 1933).
49. Honolulu series basanites (Winchell, 1947).

---

mences to crystallize, most basaltic liquids should appear to move radially away from the olivine composition on the Di-Ol-Qz or Ne-Di-Ol projection until they reach the projection of an olivine-pyroxene field boundary. The point at which this occurs is indicated by a radial line drawn from the olivine point through the projected liquid composition. For compositions on the high-silica side of the critical plane of silica undersaturation this radial may be defined by its intercept Qz/(Qz+Di) on the Qz-Di side of the Di-Ol-Qz diagram (Fig. 4). For any point lying within the triangle Di-Ol-Qz this intercept is given by the ratio

$$\frac{\text{Hy} + 2\text{Qz}}{\text{Hy} + 2(\text{Qz} + \text{Di})}$$

in molecular proportions. This ratio is here referred to as the *indicator ratio* (I.R.) since it indicates the projected course of any liquid from which olivine or olivine and plagioclase are the only phases crystallizing (*cf.* Fig. 8). Where Qz is absent from the norm, as in the presence of normative Ol, the ratio simplifies to

$$\frac{\text{Hy}}{\text{Hy} + 2\text{Di}}.$$

The indicator ratio is related to the silica-saturation expected for liquids as they reach the olivine-pyroxene field boundary. For compositions so deficient in silica as to contain normative nepheline, the indicator ratio may be considered to be negative and may be defined as

$$\frac{\text{NaAlSiO}_4}{\text{NaAlSiO}_4 + \text{Ca(Mg, Fe)Si}_2\text{O}_6}$$

in molecular proportions. Provision could also be made for normative leucite, if present.

It is instructive to consider various basaltic provinces in order of decreasing indicator ratio (Fig. 4),

TABLE 1. AVERAGED COMPOSITIONS FOR SOME BASALTIC SUITES

| | 1 | 2 | 3 | 4 | 5 | 6 | 7 | 8 | 9 | 10 | 11 | 12 | 13 | 14 | 15 | 16 | 17 | 18 | 19 | 20 | 21 | 22 | 23 | 24 |
|---|---|---|---|---|---|---|---|---|---|---|---|---|---|---|---|---|---|---|---|---|---|---|---|---|
| No. of analyses | 2 | 9 | 8 | 11 | 32 | 1 | 3 | 2 | 10 | 6 | 43 | 4 | 3 | 14 | 4 | 10 | 24 | 17 | 11 | 16 | 11 | 9 | 13 | 3 |
| $SiO_2$ | 55.68 | 50.60 | 53.8 | 52.3 | 51.6 | 50.68 | 53.57 | 52.35 | 50.45 | 52.65 | 52.5 | 52.2 | 49.78 | 50.42 | 50.0 | 50.56 | 49.80 | 47.84 | 50.19 | 49.3 | 51.6 | 46.9 | 49.79 | 50.39 |
| $TiO_2$ | 0.80 | 0.86 | 2.0 | 1.1 | 2.7 | 0.45 | 0.67 | 1.09 | 2.33 | 0.58 | 1.0 | 1.3 | 0.68 | 2.97 | 3.2 | 2.78 | 2.68 | 1.53 | 0.75 | 1.6 | 1.6 | 2.4 | 1.71 | 0.96 |
| $Al_2O_3$ | 15.98 | 19.52 | 13.9 | 14.5 | 15.0 | 17.64 | 15.71 | 17.63 | 14.94 | 16.23 | 15.4 | 15.4 | 15.69 | 11.62 | 13.5 | 12.79 | 12.42 | 16.98 | 17.58 | 15.6 | 14.3 | 15.4 | 16.74 | 14.80 |
| $Fe_2O_3$ | 1.81 | 2.82 | 2.6 | 3.8 | 3.4 | 0.26 | 1.25 | 4.21 | 3.38 | 0.51 | 1.2 | 1.6 | 2.73 | 2.71 | 1.9 | 3.23 | 1.53 | 3.18 | 2.84 | 3.5 | 3.5 | 3.9 | 2.65 | 3.38 |
| FeO | 8.01 | 7.21 | 9.3 | 10.2 | 9.6 | 9.88 | 7.87 | 4.23 | 7.55 | 8.21 | 9.3 | 8.7 | 9.20 | 9.07 | 12.5 | 11.28 | 9.91 | 7.92 | 7.19 | 7.8 | 9.2 | 9.8 | 7.82 | 8.31 |
| MnO | 0.17 | 0.17 | 0.2 | 0.3 | 0.2 | 0.15 | 0.17 | 0.15 | 0.08 | 0.15 | 0.2 | 0.1 | 0.35 | 0.10 | 0.25 | 0.22 | 0.13 | 0.17 | 0.25 | 0.2 | 0.3 | 0.3 | 0.17 | 0.20 |
| MgO | 4.17 | 4.49 | 4.1 | 5.1 | 4.9 | 7.71 | 6.36 | 5.42 | 7.67 | 6.64 | 7.1 | 7.3 | 7.79 | 10.11 | 4.4 | 5.40 | 10.31 | 6.73 | 7.39 | 6.5 | 5.3 | 8.4 | 7.16 | 6.03 |
| CaO | 8.42 | 11.04 | 7.9 | 10.0 | 8.9 | 10.47 | 10.63 | 9.13 | 9.17 | 11.34 | 10.3 | 10.0 | 11.93 | 9.74 | 8.3 | 10.29 | 10.32 | 10.01 | 10.50 | 10.3 | 10.1 | 9.6 | 9.07 | 10.93 |
| $Na_2O$ | 2.34 | 1.94 | 3.0 | 2.1 | 2.4 | 1.87 | 1.85 | 3.02 | 2.84 | 1.58 | 2.1 | 2.4 | 1.21 | 2.09 | 2.9 | 2.55 | 1.96 | 2.63 | 2.75 | 2.7 | 2.8 | 2.5 | 3.32 | 2.93 |
| $K_2O$ | 1.12 | 0.31 | 1.5 | 0.4 | 1.1 | 0.24 | 0.82 | 1.27 | 0.35 | 0.90 | 0.8 | 0.8 | 0.29 | 0.39 | 1.4 | 0.59 | 0.45 | 0.48 | 0.40 | 0.5 | 1.1 | 0.6 | 0.82 | 0.57 |
| $P_2O_5$ | 0.10 | 0.10 | 0.4 | 0.2 | 0.2 | 0.09 | 0.08 | 0.21 | 0.27 | 0.01 | 0.1 | 0.2 | 0.07 | 0.27 | 0.7 | 0.31 | 0.29 | 0.18 | 0.14 | 0.3 | 0.3 | 0.2 | 0.31 | 0.04 |
| $H_2O$ | 1.55 | 0.85 | 1.2 | — | — | 0.48 | 1.10 | 1.56 | 0.96 | 1.33 | — | — | — | — | 0.9 | — | — | 2.23 | — | 1.8 | — | — | 0.41 | 1.70 |
| Others | — | — | — | — | — | 0.04 | — | 0.04 | 0.12 | — | — | — | 0.29 | — | 0.09 | — | — | 0.12 | — | 0.04 | — | — | 0.02 | 0.02 |
| Total | 100.15 | 99.91 | 99.9 | 100.0 | 100.0 | 99.96 | 100.08 | 100.31 | 100.11 | 100.13 | 100.0 | 100.0 | 100.01 | 99.49 | 100.04 | 100.00 | 99.80 | 100.00 | 99.98 | 100.14 | 100.1 | 100.0 | 99.99 | 100.26 |
| Norms (weight per cent) | | | | | | | | | | | | | | | | | | | | | | | | |
| qz | 10.7 | 5.9 | 6.9 | 7.8 | 6.0 | — | 6.2 | 4.4 | 2.8 | 4.2 | 2.6 | 2.0 | 2.9 | 2.7 | 1.3 | 3.8 | — | — | — | 0.8 | 2.3 | — | — | — |
| or | 6.6 | 1.8 | 8.9 | 2.2 | 6.7 | 1.4 | 4.8 | 7.5 | 2.1 | 5.3 | 4.5 | 4.5 | 1.7 | 2.3 | 8.4 | 3.5 | 2.7 | 2.8 | 2.3 | 2.8 | 6.7 | 3.3 | 4.8 | 3.4 |
| ab | 19.8 | 16.4 | 25.2 | 17.8 | 20.4 | 15.8 | 15.6 | 25.5 | 23.5 | 13.4 | 17.8 | 20.5 | 10.2 | 17.7 | 24.7 | 21.6 | 16.6 | 22.2 | 23.3 | 23.1 | 23.6 | 21.0 | 28.1 | 24.8 |
| ne | — | — | — | — | — | — | — | — | — | — | — | — | — | — | — | — | — | — | — | — | — | — | — | — |
| an | 29.8 | 43.7 | 20.0 | 28.9 | 26.7 | 39.0 | 32.2 | 30.8 | 27.3 | 34.6 | 30.3 | 28.9 | 36.5 | 21.2 | 19.5 | 21.7 | 23.8 | 33.1 | 34.5 | 29.8 | 23.1 | 29.2 | 28.4 | 25.5 |
| di wo | 4.8 | 4.4 | 7.0 | 8.2 | 6.7 | 5.4 | 8.4 | 5.5 | 7.0 | 9.0 | 8.5 | 7.9 | 9.6 | 10.7 | 7.3 | 11.4 | 10.8 | 6.5 | 7.0 | 8.6 | 10.6 | 7.2 | 6.2 | 11.9 |
| di en | 2.2 | 2.3 | 3.2 | 3.8 | 3.5 | 2.7 | 4.5 | 4.1 | 4.6 | 4.7 | 4.5 | 4.4 | 5.3 | 7.1 | 2.9 | 5.5 | 6.8 | 3.9 | 4.3 | 5.2 | 5.4 | 4.4 | 3.8 | 6.5 |
| di fs | 2.6 | 2.0 | 3.7 | 4.4 | 3.1 | 2.5 | 3.6 | 0.9 | 1.8 | 4.0 | 3.7 | 3.2 | 3.9 | 2.7 | 4.5 | 5.7 | 3.3 | 2.2 | 2.3 | 2.9 | 4.9 | 2.4 | 2.0 | 4.9 |
| hy en | 8.2 | 8.9 | 7.0 | 8.9 | 8.7 | 16.1 | 11.3 | 9.4 | 14.4 | 11.8 | 13.1 | 13.8 | 14.1 | 18.0 | 8.0 | 7.9 | 18.1 | 9.7 | 10.8 | 10.9 | 7.7 | 7.9 | 6.5 | 8.2 |
| hy fs | 9.7 | 7.8 | 8.3 | 9.9 | 7.7 | 14.6 | 9.0 | 1.9 | 5.5 | 10.0 | 11.0 | 9.5 | 10.3 | 7.0 | 12.1 | 8.2 | 9.0 | 5.6 | 5.9 | 6.3 | 7.0 | 4.2 | 3.5 | 6.1 |
| ol fo | — | — | — | — | — | 0.3 | — | — | — | — | — | — | — | — | — | — | 0.5 | 2.2 | 2.4 | — | — | 6.1 | 5.3 | 0.2 |
| ol fa | — | — | — | — | — | 0.3 | — | — | — | — | — | — | — | — | — | — | 0.3 | 1.4 | 1.4 | — | — | 3.7 | 3.2 | 0.2 |
| il | 1.5 | 1.6 | 3.8 | 2.1 | 5.2 | 0.9 | 1.3 | 2.1 | 4.4 | 1.1 | 2.0 | 2.4 | 1.3 | 5.6 | 6.0 | 5.3 | 5.1 | 2.9 | 1.4 | 3.0 | 3.0 | 4.6 | 3.3 | 1.8 |
| mt | 2.6 | 4.1 | 3.7 | 5.6 | 4.9 | 0.4 | 1.8 | 6.1 | 5.0 | 0.7 | 1.9 | 2.3 | 4.0 | 3.9 | 2.8 | 4.7 | 2.2 | 4.6 | 4.1 | 5.1 | 5.1 | 5.6 | 3.8 | 4.9 |
| ap | 0.2 | 0.2 | 0.9 | 0.3 | 0.4 | 0.2 | 0.2 | 0.5 | 0.6 | 0.0 | 0.2 | 0.6 | 0.2 | 0.6 | 1.5 | 0.7 | 0.6 | 0.4 | 0.3 | 0.6 | 0.6 | 0.4 | 0.7 | 0.1 |
| Others | 1.5 | 0.9 | 1.2 | — | — | 0.5 | 1.1 | 1.6 | 1.1 | 1.3 | — | — | — | — | 1.0 | — | — | 2.4 | — | 1.8 | — | — | 0.4 | 1.7 |
| Total | 100.2 | 100.0 | 99.8 | 99.9 | 100.0 | 100.1 | 100.0 | 100.3 | 100.1 | 100.1 | 100.1 | 100.0 | 100.0 | 99.5 | 100.0 | 100.0 | 99.8 | 99.9 | 100.0 | 100.0 | 100.0 | 100.0 | 100.0 | 100.2 |
| Molecular porportions $NaAlSiO_4$:Ca(Mg, Fe)$Si_2O_6$:(Mg, Fe)$SiO_3$:(Mg, Fe)$_2SiO_4$:$SiO_2$ (recalculated to 100%) | | | | | | | | | | | | | | | | | | | | | | | | |
| $NaAlSiO_4$ | — | — | — | — | — | — | — | — | — | — | — | — | — | — | — | — | — | — | — | — | — | — | — | — |
| Ca(Mg, Fe)$Si_2O_6$ | 11.0 | 13.4 | 19.5 | 19.5 | 19.1 | 14.5 | 20.2 | 20.8 | 20.5 | 22.9 | 22.1 | 21.8 | 23.7 | 24.9 | 24.4 | 32.4 | 26.7 | 25.5 | 25.6 | 30.3 | 35.0 | 26.6 | 26.9 | 43.9 |
| (Mg, Fe)$SiO_3$ | 41.5 | 52.2 | 43.3 | 44.8 | 47.9 | 84.5 | 50.8 | 47.1 | 63.6 | 56.7 | 64.6 | 67.2 | 62.6 | 63.1 | 67.0 | 46.5 | 71.8 | 64.1 | 64.3 | 64.4 | 50.0 | 47.2 | 46.3 | 55.1 |
| (mg, Fe)$_2SiO_4$ | — | — | — | — | — | 1.0 | — | — | — | — | — | — | — | — | — | — | 1.5 | 10.4 | 10.1 | — | — | 26.2 | 26.8 | 1.0 |
| $SiO_2$ | 47.5 | 34.4 | 37.2 | 35.7 | 33.0 | — | 29.0 | 32.1 | 15.9 | 20.5 | 13.3 | 10.9 | 13.7 | 12.0 | 8.6 | 21.1 | — | — | — | 5.3 | 15.0 | — | — | — |
| Molecular proportions of $Fe^{3+}$ reduced to $Fe^{2+}$ to leave 1.50% $Fe_2O_3$ | | | | | | | | | | | | | | | | | | | | | | | | |
| $NaAlSiO_4$ | — | — | — | — | — | — | — | — | — | — | — | — | — | — | — | — | — | — | — | — | — | — | — | — |
| Ca(Mg, Fe)$Si_2O_6$ | 11.0 | 13.4 | 19.5 | 19.5 | 19.1 | — | — | 20.8 | 20.5 | — | — | 21.8 | 23.7 | 24.9 | 24.4 | 32.4 | — | 25.5 | 25.6 | 30.3 | 35.0 | 26.6 | 26.9 | 43.9 |
| (Mg, Fe)$SiO_3$ | 43.0 | 61.0 | 50.2 | 55.5 | 59.8 | — | — | 69.4 | 75.7 | — | — | 68.2 | 69.2 | 69.8 | 70.5 | 57.2 | — | 49.6 | 53.7 | 59.1 | 65.0 | 27.9 | 35.4 | 39.9 |
| (Mg, Fe)$_2SiO_4$ | — | — | — | — | — | — | — | — | — | — | — | — | — | — | — | — | — | 24.9 | 20.7 | 10.7 | — | 45.5 | 37.7 | 16.2 |
| $SiO_2$ | 46.0 | 25.6 | 30.3 | 25.0 | 21.1 | — | — | 9.8 | 3.8 | — | — | 10.0 | 7.1 | 5.3 | 5.1 | 10.4 | — | — | — | — | 0.0 | — | — | — |
| Indicator Ratio | | | | | | | | | | | | | | | | | | | | | | | | |
| Unadjusted | 0.86 | 0.82 | 0.75 | 0.75 | 0.75 | 0.74 | 0.73 | 0.73 | 0.70 | 0.68 | 0.67 | 0.67 | 0.66 | 0.64 | 0.63 | 0.58 | 0.57 | 0.56 | 0.56 | 0.55 | 0.53 | 0.47 | 0.46 | 0.39 |
| For $Fe_2O_3$=1.5% | 0.86 | 0.81 | 0.74 | 0.73 | 0.73 | — | — | 0.68 | 0.67 | — | — | 0.67 | 0.64 | 0.62 | 0.62 | 0.55 | — | 0.49 | 0.52 | 0.49 | 0.48 | 0.34 | 0.40 | 0.31 |

TABLE 1. AVERAGED COMPOSITIONS FOR SOME BASALTIC SUITES—*Continued*

| | 25 | 26 | 27 | 28 | 29 | 30 | 31 | 32 | 33 | 34 | 35 | 36 | 37 | 38 | 39 | 40 | 41 | 42 | 43 | 44 | 45 | 46 | 47 | 48 | 49 |
|---|---|---|---|---|---|---|---|---|---|---|---|---|---|---|---|---|---|---|---|---|---|---|---|---|---|
| No. of analyses | 6 | 14 | 7 | 5 | 5 | 6 | 7 | 5 | 23 | 5 | 7 | 5 | 5 | 3 | 3 | 7 | 6 | 4 | 4 | 6 | 11 | 19 | 13 | 13 | 3 |
| $SiO_2$ | 49.65 | 49.14 | 47.56 | 48.44 | 48.12 | 47.61 | 48.4 | 47.0 | 48.4 | 46.96 | 47.24 | 47.12 | 47.17 | 46.62 | 44.04 | 48.11 | 47.18 | 47.62 | 47.05 | 45.8 | 44.7 | 46.16 | 44.80 | 44.26 | 43.98 |
| $TiO_2$ | 2.86 | 3.17 | 2.00 | 4.29 | 3.66 | 2.35 | 0.9 | 3.5 | 2.9 | 2.46 | 3.17 | 3.16 | 2.43 | 3.47 | 1.92 | 1.72 | 2.79 | 3.57 | 2.42 | 2.5 | 2.0 | 2.45 | 1.96 | 3.46 | 2.73 |
| $Al_2O_3$ | 16.41 | 15.71 | 14.65 | 13.27 | 15.02 | 16.68 | 19.2 | 14.5 | 13.9 | 14.76 | 14.23 | 14.94 | 14.14 | 15.41 | 7.64 | 15.55 | 14.64 | 16.27 | 13.17 | 14.9 | 15.7 | 15.32 | 13.86 | 14.30 | 13.49 |
| $Fe_2O_3$ | 3.71 | 3.64 | 2.35 | 4.06 | 2.93 | 2.31 | 1.8 | 4.0 | 2.3 | 3.68 | 3.30 | 2.73 | 3.05 | 4.57 | 3.05 | 2.99 | 3.17 | 3.87 | 2.67 | 3.0 | 4.1 | 3.50 | 2.91 | 4.61 | 3.53 |
| FeO | 7.38 | 8.17 | 9.92 | 8.27 | 9.79 | 8.80 | 7.3 | 9.0 | 9.2 | 7.68 | 8.76 | 9.34 | 8.81 | 7.66 | 9.45 | 7.19 | 9.00 | 8.17 | 8.76 | 9.9 | 8.5 | 9.67 | 9.63 | 7.79 | 8.79 |
| MnO | 0.23 | 0.15 | 0.24 | 0.15 | 0.14 | 0.22 | 0.1 | 0.2 | 0.1 | 0.16 | 0.13 | 0.11 | 0.12 | 0.19 | 0.11 | 0.16 | 0.09 | 0.11 | 0.15 | 0.2 | 0.1 | 0.21 | 0.17 | 0.21 | 0.10 |
| MgO | 5.08 | 6.03 | 8.53 | 8.21 | 4.42 | 6.89 | 8.0 | 7.5 | 7.8 | 8.12 | 7.16 | 6.63 | 9.23 | 6.73 | 22.78 | 9.31 | 8.19 | 6.33 | 10.65 | 8.8 | 8.4 | 7.25 | 11.07 | 8.34 | 10.19 |
| CaO | 8.43 | 8.38 | 12.59 | 7.72 | 9.45 | 11.26 | 11.2 | 10.1 | 11.9 | 11.94 | 11.15 | 10.42 | 10.96 | 10.49 | 7.22 | 10.43 | 10.70 | 8.65 | 9.99 | 11.1 | 11.6 | 9.58 | 10.16 | 11.26 | 11.11 |
| $Na_2O$ | 3.81 | 3.69 | 1.78 | 3.47 | 3.48 | 2.66 | 2.7 | 2.7 | 2.3 | 2.31 | 2.51 | 2.65 | 2.54 | 2.98 | 1.64 | 2.85 | 3.04 | 3.82 | 2.63 | 2.9 | 2.9 | 3.74 | 3.19 | 3.48 | 3.49 |
| $K_2O$ | 1.48 | 1.39 | 0.32 | 1.55 | 0.97 | 0.51 | 0.3 | 1.1 | 0.9 | 0.65 | 0.93 | 1.07 | 0.78 | 0.96 | 0.53 | 1.13 | 0.80 | 1.14 | 1.37 | 0.6 | 1.2 | 1.34 | 1.09 | 1.59 | 0.99 |
| $P_2O_5$ | 0.68 | 0.73 | 0.20 | 0.57 | 0.30 | 0.26 | 0.1 | 0.4 | 0.3 | 0.22 | 0.15 | 0.19 | 0.38 | 0.30 | 0.07 | 0.56 | 0.49 | 0.45 | 0.33 | 0.3 | 0.8 | 0.65 | 0.55 | 0.70 | 0.54 |
| $H_2O$ | 0.69 | — | — | — | 1.57 | 0.43 | — | — | — | 1.05 | 1.44 | 2.03 | 0.64 | 0.61 | 1.88 | — | 0.42 | — | 0.69 | — | — | — | 0.73 | — | 0.84 |
| Others | — | — | — | — | 0.16 | — | — | — | — | — | — | — | 0.05 | — | — | — | — | — | 0.04 | — | — | 0.20 | — | — | 0.29 |
| Total | 100.41 | 100.20 | 100.14 | 100.00 | 100.01 | 99.98 | 100.0 | 100.0 | 100.0 | 99.99 | 100.17 | 100.39 | 100.30 | 99.99 | 100.33 | 100.00 | 100.51 | 100.00 | 99.92 | 100.0 | 100.0 | 100.07 | 100.12 | 100.00 | 100.07 |
| **Norms (weight per cent)** | | | | | | | | | | | | | | | | | | | | | | | | | |
| qz | — | — | — | — | — | — | — | — | — | — | — | — | — | — | — | — | — | — | — | — | — | — | — | — | — |
| or | 8.7 | 8.2 | 1.9 | 9.2 | 5.7 | 3.0 | 1.8 | 6.5 | 5.3 | 3.8 | 5.5 | 6.4 | 4.6 | 5.7 | 3.1 | 6.7 | 4.7 | 6.7 | 8.1 | 3.6 | 7.1 | 7.9 | 6.5 | 9.4 | 5.8 |
| ab | 32.2 | 31.2 | 15.0 | 29.4 | 29.4 | 22.5 | 22.9 | 22.9 | 19.5 | 19.6 | 21.2 | 22.4 | 21.5 | 25.2 | 13.9 | 23.8 | 24.2 | 30.8 | 19.6 | 18.6 | 13.6 | 20.4 | 13.0 | 11.7 | 11.0 |
| ne | — | — | — | — | — | — | — | — | — | — | — | — | — | — | — | 0.2 | 0.8 | 0.8 | 1.4 | 3.2 | 5.9 | 6.1 | 7.6 | 9.6 | 10.1 |
| an | 23.4 | 22.2 | 31.0 | 16.0 | 22.5 | 32.1 | 39.4 | 24.2 | 24.9 | 28.0 | 24.8 | 25.7 | 24.9 | 25.8 | 11.9 | 26.3 | 23.9 | 23.9 | 20.1 | 25.8 | 26.3 | 21.1 | 20.3 | 18.7 | 18.2 |
| di wo | 6.0 | 6.3 | 12.6 | 7.9 | 9.1 | 9.2 | 6.5 | 9.8 | 13.5 | 12.4 | 12.4 | 10.4 | 11.5 | 10.1 | 9.8 | 9.2 | 11.0 | 6.8 | 11.4 | 11.5 | 11.1 | 9.6 | 11.2 | 13.7 | 14.1 |
| di en | 3.8 | 4.0 | 7.4 | 5.7 | 4.7 | 5.4 | 4.0 | 6.5 | 8.3 | 8.4 | 7.9 | 6.2 | 7.5 | 7.2 | 7.3 | 6.3 | 7.0 | 4.5 | 7.7 | 7.0 | 7.2 | 5.6 | 7.2 | 9.9 | 9.6 |
| di fs | 1.9 | 1.9 | 4.7 | 1.4 | 4.2 | 3.4 | 2.1 | 2.7 | 4.4 | 3.1 | 3.7 | 3.7 | 3.2 | 2.1 | 1.5 | 2.2 | 3.3 | 1.8 | 2.9 | 3.8 | 3.1 | 3.5 | 3.3 | 2.5 | 3.4 |
| hy en | 4.7 | 4.5 | 7.6 | 5.6 | 3.8 | 3.6 | 2.6 | 4.1 | 5.1 | 4.1 | 3.8 | 2.9 | 1.6 | 1.2 | 0.2 | — | — | — | — | — | — | — | — | — | — |
| hy fs | 2.3 | 2.0 | 4.8 | 1.4 | 3.4 | 2.2 | 1.4 | 1.7 | 2.7 | 1.5 | 1.8 | 1.7 | 0.7 | 0.4 | 0.0 | — | — | — | — | — | — | — | — | — | — |
| ol fo | 2.9 | 4.6 | 4.4 | 6.4 | 1.8 | 5.7 | 9.3 | 5.7 | 4.3 | 5.4 | 4.3 | 5.2 | 9.8 | 5.9 | 34.5 | 11.9 | 9.4 | 7.9 | 13.2 | 10.5 | 9.6 | 8.7 | 14.3 | 7.6 | 11.0 |
| ol fa | 1.6 | 2.4 | 3.1 | 1.7 | 1.7 | 4.0 | 5.5 | 2.7 | 2.5 | 2.1 | 2.2 | 3.4 | 4.6 | 1.9 | 8.0 | 4.6 | 4.8 | 3.4 | 5.5 | 6.3 | 4.6 | 6.0 | 7.0 | 2.1 | 4.3 |
| il | 5.4 | 6.0 | 3.8 | 8.1 | 6.9 | 4.5 | 1.7 | 6.6 | 5.5 | 4.7 | 6.0 | 6.0 | 4.6 | 6.6 | 3.6 | 3.3 | 5.3 | 6.7 | 4.6 | 4.7 | 3.8 | 4.6 | 3.7 | 6.6 | 5.2 |
| mt | 5.4 | 5.3 | 3.4 | 5.9 | 4.3 | 3.4 | 2.6 | 5.8 | 3.3 | 5.3 | 4.8 | 4.0 | 4.4 | 6.6 | 4.4 | 4.3 | 4.6 | 5.6 | 3.9 | 4.4 | 6.0 | 5.1 | 4.2 | 6.7 | 5.1 |
| ap | 1.5 | 1.6 | 0.4 | 1.2 | 0.9 | 0.6 | 0.2 | 0.9 | 0.7 | 0.5 | 0.3 | 0.4 | 0.8 | 0.7 | 0.2 | 1.2 | 1.1 | 1.0 | 0.7 | 0.7 | 1.8 | 1.4 | 1.2 | 1.6 | 1.2 |
| Others | 0.7 | — | — | — | 1.7 | 0.4 | — | — | — | 1.1 | 1.4 | 2.0 | 0.7 | 0.6 | 1.9 | — | 0.4 | — | 0.7 | — | — | 0.1 | 0.7 | — | 1.1 |
| Total | 100.5 | 100.2 | 100.1 | 99.9 | 100.1 | 100.0 | 100.0 | 100.1 | 100.0 | 100.0 | 100.1 | 100.4 | 100.4 | 100.0 | 100.3 | 100.0 | 100.5 | 99.9 | 99.8 | 100.1 | 100.1 | 100.1 | 100.2 | 100.1 | 100.1 |
| **Molecular Proportions** | | | | | | | | | | | | | | | | | | | | | | | | | |
| $NaAlSiO_4$ | — | — | — | — | — | — | — | — | — | — | — | — | — | — | — | 0.6 | 3.0 | 4.0 | 4.4 | 10.0 | 18.3 | 19.9 | 18.7 | 27.1 | 24.3 |
| $Ca(Mg, Fe)Si_2O_6$ | 35.8 | 34.2 | 40.6 | 36.3 | 48.1 | 41.3 | 30.2 | 44.2 | 50.6 | 51.5 | 53.4 | 48.2 | 46.7 | 56.9 | 22.8 | 42.4 | 49.7 | 43.1 | 42.9 | 43.6 | 41.7 | 38.0 | 33.8 | 47.1 | 41.6 |
| $(Mg, Fe)SiO_3$ | 44.3 | 36.1 | 42.2 | 35.0 | 38.9 | 27.4 | 19.5 | 27.9 | 30.9 | 25.2 | 25.7 | 22.7 | 9.7 | 9.8 | 0.4 | — | — | — | — | — | — | — | — | — | — |
| $(Mg, Fe)_2SiO_4$ | 19.9 | 27.7 | 17.2 | 28.8 | 13.0 | 31.3 | 50.3 | 27.9 | 18.5 | 23.3 | 20.9 | 29.1 | 43.6 | 33.3 | 76.8 | 57.0 | 47.3 | 52.9 | 52.7 | 46.4 | 40.0 | 42.1 | 47.5 | 25.8 | 34.1 |
| $SiO_2$ | — | — | — | — | — | — | — | — | — | — | — | — | — | — | — | — | — | — | — | — | — | — | — | — | — |
| **Molecular Proportions if $Fe^3$ reduced to $Fe^2$ to leave 1.50% $Fe_2O_3$** | | | | | | | | | | | | | | | | | | | | | | | | | |
| $NaAlSiO_4$ | — | — | — | — | — | — | — | — | — | — | — | — | 1.0 | 5.9 | 1.8 | 4.0 | 6.4 | 9.8 | 6.4 | 11.2 | 20.4 | 21.4 | 19.5 | 28.0 | 25.1 |
| $Ca(Mg, Fe)Si_2O_6$ | 35.8 | 34.2 | 40.6 | 36.3 | 48.1 | 41.3 | 30.2 | 44.2 | 50.6 | 51.5 | 53.4 | 48.2 | 45.4 | 47.0 | 21.6 | 38.1 | 44.2 | 34.6 | 40.0 | 40.2 | 35.9 | 33.5 | 31.7 | 40.1 | 37.9 |
| $(Mg, Fe)SiO_3$ | 16.3 | 12.8 | 36.2 | 9.4 | 22.3 | 19.4 | 16.4 | 3.5 | 24.4 | 0.8 | 8.7 | 10.2 | — | — | — | — | — | — | — | — | — | — | — | — | — |
| $(Mg, Fe)_2SiO_4$ | 47.9 | 53.0 | 23.1 | 54.3 | 29.6 | 39.2 | 53.3 | 52.3 | 25.0 | 47.8 | 37.9 | 41.6 | 53.6 | 47.1 | 76.6 | 57.9 | 49.3 | 55.6 | 53.7 | 48.6 | 43.7 | 45.1 | 48.8 | 31.9 | 37.0 |
| $SiO_2$ | — | — | — | — | — | — | — | — | — | — | — | — | — | — | — | — | — | — | — | — | — | — | — | — | — |
| **Indicator Ratio** | | | | | | | | | | | | | | | | | | | | | | | | | |
| Unadjusted | 0.38 | 0.36 | 0.34 | 0.33 | 0.29 | 0.25 | 0.24 | 0.24 | 0.23 | 0.20 | 0.19 | 0.19 | 0.09 | 0.08 | 0.01 | −0.01 | −0.06 | −0.09 | −0.09 | −0.19 | −0.31 | −0.34 | −0.36 | −0.37 | −0.37 |
| For $Fe_2O_3$=1.5% | 0.19 | 0.16 | 0.31 | 0.12 | 0.19 | 0.19 | 0.21 | 0.04 | 0.19 | 0.01 | 0.08 | 0.10 | −0.02 | −0.11 | −0.08 | −0.10 | −0.13 | −0.22 | −0.14 | −0.22 | −0.36 | −0.39 | −0.38 | −0.41 | −0.40 |

*Indicator ratio 0.85 to 0.65.* Magma batches for which this ratio exceeds 0.65 include the Izu basalts of Japan (2, 4), Ferrar dolerites of Antarctica (1, 7), the Yakima basalts of the Columbia River group (3), British Paleozoic tholeiites and quartz-tholeiites (5), Stillwater border facies (6), the type tholeiites from Tholey, Saar (8), Koolau Series of Oahu (9), the Tasmania (10), Karroo (11) and Palisade (12) dolerites and Kuno's average Japanese tholeiite (13). In these provinces, except in the somewhat altered rocks of Tholey where hypersthene is rare (Jung, 1958), and the Columbia River basalts, hypersthene characteristically appears early. It is soon joined by clinopyroxene, although this situation may occasionally be reversed, and olivine shows the reaction relationship to hypersthene or pigeonite. Differentiation in place leads to granophyric residua as demonstrated in many quartz dolerite sills and in the Palolo quartz dolerite of the Koolau Series, Oahu (Kuno *et al.*, 1957).

*Indicator ratio 0.65 to 0.50.* In the range of indicator ratio from 0.65 to 0.50 are the average basalt from Mauna Loa (14), the late Yakima flows of Columbia River (15), Deccan (16), Kilauea (17), the Keweenawan Greenstone flow of Lake Michigan (18), Kuno's average Japanese high-alumina basalt (19), Picture Gorge basalts (early Columbia River, 20) and the non-porphyritic central magma type of Scotland (21). In the case of Kilauea, olivine occurs as phenocrysts and occasionally in the groundmass, usually without any conspicuous reaction relationship (Macdonald, 1949a). Throughout the group hypersthene appears to be distinctly less common than in the group with I.R. 0.85 to 0.65 above. For example the pyroxenes reported by West (1958) and Naidu (1960) for the Deccan basalts of central India (I.R.=0.58) are augite, subcalcic augite and rarer pigeonite. Hypersthene occurs in rare examples of the Kilauea basalts (average I.R. 0.59) whereas Macdonald (1949a) shows that in the Mauna Loa basalts (I.R. 0.64) microphenocrysts of hypersthene are present in a substantial minority of specimens and in the analysed Koolau basalts (I.R. 0.70) microphenocrysts of hypersthene are normal (Wentworth and Winchell, 1947).

*Indicator ratio 0.50 to 0.39.* The average Scottish plateau basalt (22, probably rather altered), olivine basalts from the Central Cascade Range (23) and the Tertiary tholeiites of south-western Australia (24) belong here. The suite appears to be transitional towards alkali olivine basalts. Edwards (1938) reports that augite and pigeonite are the pyroxenes of the Western Australian rocks, but in the suite as a whole hypersthene appears to be characteristically absent and pigeonite rare.

*Indicator ratio 0.38 to 0.00.* In the range 0.38 to 0.00 are Ascension Island (25), Banks Peninsula, New Zealand (26), Skjaldbreith shield volcano, Iceland (27), Tutuila (28), Easter Island (29), Galapagos (30), Medicine Lake Highlands of California (31), older series of Mauritius (32), Gambier Island (34), the Hamakua series of Mauna Kea (37), Juan Fernandez (38) and Réunion (33, 35, 36, 39). The alkali-silica ratio for Ascension basalts (mostly in fact hawaiites with normative ab>an) is essentially that characteristic of alkali olivine basalt suites (Tilley, 1950) and one new analysis shows a very small amount of normative nepheline. However, as in the case of the other provinces mentioned, most Ascension Island analyses show significant amounts of normative hypersthene and one analysed specimen to be described elsewhere contains modal hypersthene and a siliceous pegmatoid. Otherwise hypersthene appears to be virtually unknown in these suites and pigeonite is rare or absent. It is usual for olivine to occur as groundmass microlites as well as phenocrysts (*e.g.* Lacroix, 1936) without obvious reaction relationship to pyroxene and for augite or titanaugite to appear sometimes as phenocrysts as well as in the groundmass. A group of Réunion oceanites (38) illustrates the effects on the diagram of olivine accumulation.

The Skjaldbreith lavas (Tryggvason, 1943) are of tholeiitic aspect in their low alkali/silica ratio and the high-alumina basalts of the Medicine Lake Highlands (Anderson, 1941) while variable in alkali and normative hypersthene contents, tend also to have rather low alkali/silica ratios. Apart from these two magma-batches, the others cited may be described as mildly alkaline in the sense that even though the analyses show minor normative hypersthene, they have relatively high ratios of alkalis to silica. This results in the common presence of groundmass alkali feldspar. Such suites are in fact commonly referred to in petrological literature as olivine basalts of alkaline type. It is notable that those from Réunion, Easter Island, Galapagos, Banks Peninsula, Tutuila and Ascension all have pantellerites or pantelleritic trachytes as associates while the older volcanic series of Mauritius includes trachytes that may be either slightly oversaturated or moderately undersaturated

(Lacroix, 1936; Bandy, 1937; Richardson, 1933; Speight, 1938; Daly, 1924; 1925; Walker and Nicolaysen, 1954).

*Nepheline present in norm.* The average Japanese alkali basalt (40), Hualalai, Hawaii (41), St. Helena (42), Bora-Bora and neighbouring islands of the N.W. Society Islands (43), and younger basalts of Mauritius (44) are representatives of typical undersaturated alkali basalt suites. On St. Helena the differentiation trend is clearly phonolitic (Daly, 1927). Finally, averages are plotted for five more strongly alkaline, basanitic provinces having indicator ratios −0.30 to −0.40, namely Rungwe Volcano, East Africa (45), the peripheral subprovince of the Dunedin district (46), Auckland city (47), Tahiti (48) and basanites of the Honolulu series, Oahu (49). For all these more alkaline basalts the pyroxene is typically titanaugite, olivine occurs both as phenocrysts and in the groundmass and a reaction relationship between olivine and a lime-poor pyroxene is unknown, although reaction between olivine and titanaugite has been reported.

*Discussion.* The above survey suggests that, at least in a general way, there is a close correlation between the normative composition of magma batches, the pyroxene crystallization history and ultimate differentiation trends. Typical tholeiites showing a strong reaction relationship and yielding granophyric differentiates, more mildly tholeiitic types such as those of Kilauea, mildly alkaline and transitional types which follow a pantelleritic or trachytic trend, and finally the more strongly alkaline types differentiating to phonolite, appear to plot in an essentially continuous band across the diagram. There is a heavy clustering of points representing the most voluminous and typical tholeiites. Nevertheless, in terms of the variables here considered and in confirmation of the views of Green and Poldervaart (1955) and others, there appears to be a continuous series of basaltic magmas ranging from calcalkaline and tholeiitic at one extreme through transitional types to the typical alkali basalts and thence to the basanites.

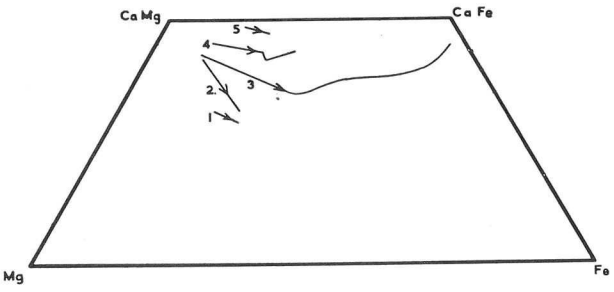


FIG. 5. Some clinopyroxene trends in terms of relative proportions of Ca, Mg, Fe.

1. Prehistoric flow, Kilauea (Yoder and Tilley, 1957).
2. Kilauea flow of 1921 (Yoder and Tilley, 1957).
3. Skaergaard (Brown, 1957; Muir, 1951).
4. Garbh Eilean (Murray, 1954).
5. Black Jack teschenite (Wilkinson, 1957).

## Interrelation Between Pyroxene and Host Rock

The familiar Di-En-Fs-He or Ca-Mg-Fe diagram (Fig. 5) clearly portrays the progressive relative variation of Ca, Mg and Fe in pyroxenes during fractionation of basic magmas. It is generally believed that pyroxene crystallization history is of fundamental importance to the mutual relationship of tholeiitic and alkali basalt magmas, in effect to questions of saturation or undersaturation in silica. It would be helpful to have a projection of pyroxene compositions which had a direct bearing on this problem, and a norm, calculated from pyroxene analyses, appears to be a convenient starting point for this purpose. Many examples are set out in Tables 2–7.

The alumina of pyroxene analyses appears in the norm as feldspars or feldspathoids[1] and inspection will show that for the clinopyroxenes treated, normative feldspar ranges from 3.5 to 27.2% by weight. Furthermore almost all analyses examined contain significant amounts of normative olivine, and in the case of pyroxenes from alkaline rocks, normative nepheline and sometimes leucite and calcium orthosilicate as well. In the Pl-Di-Ol-Qz tetrahedron, clinopyroxene compositions thus plot somewhat above the base and occupy an irregular volume stretching from the Pl-Di-Hy plane to the Pl-Di-Ol face and thence into the neighbouring Pl-Ne-Di-Ol tetrahedron.

In the case of one analysis examined, Table 5, No. II, from the strongly alkaline Black Jack Sill, N.S.W. (Wilkinson, 1957), a total of 12.7% normative $Ca_2SiO_4$+Il+Mt cannot be represented within the tetrahedra employed. Usually however, not more than a few per cent of the pyroxene components are unaccounted for. It is of interest to note that clinopyroxene analyses commonly contain only 70–90% of normative pyroxene components, in one case examined (Table 4, No. 26) only 58%. In such rocks,

[1] Also as corundum in the case of the high-alumina enstatites of peridotitic inclusions in basaltic rocks.

substantially more pyroxene should appear in the mode than in the norm.

*Skaergaard and Stillwater* (*Fig. 6, Tables 2, 3*). The chemical analysis of augitic pyroxene from the Skaergaard border group gabbro-picrite (Brown, 1957) contains a negligible trace of normative nepheline. In Brown's series (1957, 1960) from augite to ferroaugite, not only do the augitic pyroxenes become more iron-rich and lime-poor (*cf.* Fig. 5), their analyses are also seen to move progressively in terms of normative components (Fig. 6) from the Di-Ol join to the metasilicate join, becoming effectively saturated in silica in the middle gabbros (nos. 5, 6). Brown (1957) and Muir (1951) have demonstrated that for still more iron-rich compositions, not normally attained in basaltic crystallization, the later clinopyroxenes become progressively more lime-rich again, a fact reflected by migration of the later members of the series back towards the $Ca(MgFe)Si_2O_6$ apex of Fig. 6. Skaergaard olivines (Wager and Deer, 1939, pp. 72–73), bronzite and pigeonites (Brown, 1957) are plotted on the same diagram. One of the olivine analyses contains normative $Ca_2SiO_4$ which is not represented on the diagram.

For comparative purposes, five clinopyroxenes and five orthopyroxenes from the Stillwater Complex (Hess, 1960) are also plotted. In Fe/(Fe+Mg) ratio these correspond to the two most iron-poor of the Skaergaard augites.

TABLE 2. SKAERGAARD PYROXENES

Norms (weight per cent)

| Ref. No. | 1 | 2 | 3 | 4 | 5 | 6 | 7 | 8 | 9 | 10 | 11 | 1′ | 4′ | 6′ | 7′ |
|---|---|---|---|---|---|---|---|---|---|---|---|---|---|---|---|
| qz | — | — | — | — | — | 0.2 | — | — | — | — | — | — | — | — | — |
| or | 0.3 | 0.3 | 0.2 | 0.4 | 0.1 | 0.1 | 0.2 | 0.2 | 0.1 | 0.1 | 0.2 | 0.2 | — | 0.2 | 0.6 |
| ab | 5.4 | 3.1 | 3.3 | 3.0 | 2.2 | 2.2 | 2.0 | 2.1 | 2.1 | 2.0 | 1.9 | 1.7 | — | 0.8 | 1.6 |
| ne | 0.1 | — | — | — | — | — | — | — | — | — | — | — | — | — | — |
| an | 5.7 | 6.3 | 4.7 | 4.9 | 5.0 | 4.2 | 4.8 | 4.6 | 2.4 | 2.6 | 1.8 | 5.3 | 6.2 | 4.4 | 2.5 |
| di {di | 68.2 | 53.6 | 48.7 | 47.4 | 41.2 | 39.0 | 36.1 | 35.1 | 34.2 | 31.8 | 13.9 | 3.0 | 8.0 | 6.9 | 7.1 |
| di {he | 7.6 | 17.3 | 20.2 | 21.1 | 24.6 | 26.4 | 26.8 | 28.6 | 32.4 | 39.8 | 66.1 | 0.7 | 5.3 | 6.7 | 7.7 |
| hy {en | — | 8.6 | 10.4 | 9.8 | 13.9 | 13.9 | 13.6 | 12.9 | 11.6 | 7.6 | 1.9 | 64.7 | 40.1 | 37.1 | 33.4 |
| hy {fs | — | 3.2 | 5.0 | 5.0 | 9.5 | 10.8 | 11.6 | 12.0 | 12.5 | 11.0 | 10.3 | 16.5 | 30.2 | 41.1 | 42.2 |
| ol {fo | 7.0 | 2.8 | 1.9 | 2.6 | 0.3 | — | 0.7 | 0.4 | 0.3 | 0.7 | 0.2 | 3.8 | 4.3 | 0.4 | 1.4 |
| ol {fa | 1.0 | 1.1 | 1.0 | 1.5 | 0.2 | — | 0.7 | 0.4 | 0.3 | 1.2 | 1.0 | 1.1 | 3.6 | 0.4 | 1.8 |
| il | 1.8 | 1.4 | 1.8 | 2.5 | 1.5 | 1.6 | 1.2 | 1.4 | 2.5 | 1.5 | 1.3 | 0.9 | 1.0 | 0.9 | 0.8 |
| mt | 2.2 | 2.5 | 2.7 | 1.9 | 1.8 | 1.8 | 2.3 | 2.5 | 2.2 | 2.2 | 2.1 | 1.9 | 1.6 | 1.0 | 0.9 |
| cm | 0.6 | 0.2 | 0.1 | — | — | — | — | — | — | — | — | 0.4 | — | — | — |
| Total | 99.9 | 100.4 | 100.0 | 100.1 | 100.3 | 100.2 | 100.0 | 100.2 | 100.6 | 100.5 | 100.7 | 100.2 | 100.3 | 99.9 | 100.0 |
| Molecular proportions $NaAlSiO_4$:$Ca(Mg, Fe)Si_2O_6$:$(Mg, Fe)SiO_3$:$(Mg, Fe)_2SiO_4$:$SiO_2$ | | | | | | | | | | | | | | | |
| $NaAlSiO_4$ | 0.1 | — | — | — | — | — | — | — | — | — | — | — | — | — | — |
| $Ca(Mg, Fe)Si_2O_6$ | 86.3 | 70.2 | 65.7 | 65.3 | 57.7 | 56.1 | 54.2 | 55.3 | 57.4 | 64.3 | 76.2 | 2.0 | 7.9 | 7.9 | 8.7 |
| $(Mg, Fe)SiO_3$ | — | 24.3 | 30.3 | 29.2 | 41.8 | 43.2 | 44.2 | 43.8 | 41.9 | 33.4 | 22.4 | 94.1 | 85.5 | 91.5 | 88.7 |
| $(Mg, Fe)_2SiO_4$ | 13.6 | 5.5 | 5.0 | 5.5 | 0.5 | — | 1.6 | 0.9 | 0.7 | 2.3 | 1.4 | 3.9 | 6.6 | 0.6 | 2.6 |
| $SiO_2$ | — | — | — | — | — | 0.7 | — | — | — | — | — | — | — | — | — |
| Atomic ratio Fe/Fe+Mg | | | | | | | | | | | | | | | |
| Fe/Fe+Mg | 0.17 | 0.28 | 0.33 | 0.33 | 0.38 | 0.41 | 0.43 | 0.46 | 0.49 | 0.55 | 0.81 | 0.19 | 0.38 | 0.47 | 0.50 |

KEY TO TABLE 2 Norms of Skaergaard Pyroxenes

1. Augite from gabbro picrite, 4526 (Brown, 1957)
2. Augite from lower olivine gabbro, 30 m., 4392 (Brown, 1957)
3. Augite from lower olivine gabbro, EG4389 (Brown, 1960, p. 18)
4. Augite from lower olivine gabbro, 600 m., 4385A (Brown, 1957)
5. Augite from middle gabbro, 1060 m., 4369 (Brown, 1957)
6. Augite from middle gabbro, 1310 m., 4341 (Brown, 1957)
7. Augite from ferrogabbro, 1600 m., 4430 (Brown, 1957)
8. Augite from ferrogabbro, 1740 m., 4306 (Brown, 1957)
9. Augite from ferrogabbro, 1830 m., 4309 (Brown, 1957)
10. Ferroaugite from ferrogabbro, 2000 m., 4314 (Brown, 1957)
11. Ferroaugite from ferrogabbro, EG 4318 (Brown, 1960, p. 18)
1′. Bronzite from gabbropicrite, 4526 (Brown, 1957)
4′. Pigeonite from lower olivine gabbro 4385A (Brown, 1957)
6′. Pigeonite from middle gabbro 4341 (Brown, 1957)
7′. Pigeonite from ferrogabbro 4430 (Brown, 1957)

*Contrasting pyroxenes from alkaline and tholeiitic provinces.* Norms of phenocrystic and groundmass pyroxenes from hawaiites, mugearites and Japanese alkali dolerites are set out in Table 4. Those of pyroxenes from the Black Jack teschenite sill (Wilkinson, 1957, 1958) and the Garbh Eilean picritic and crinanite sill (Murray, 1954), are set out in Table 5. Norms of pyroxenes from tholeiitic rocks are recorded in Tables 2, 3 and 6. The pyroxenes listed in Tables 4, 5 and 6 are plotted in Fig. 7 and fields for pyroxenes of all tables are summarized on the same diagram. Clearly, clinopyroxenes from alkaline basaltic rocks (field A) differ from those of tholeiites (field B) not only in a tendency towards a higher Ca/(Mg+Fe) ratio (*cf.* Fig. 5) and higher titanium content, but also in a greater degree of silica undersaturation in terms of normative components. Thus normative nepheline is absent from only 3 of 23 pyroxene analyses examined from alkaline basaltic rocks, and the exceptions (42–44, Table 5) are all from the upper portions of the mildly alkaline Garbh Eilean Sill. In contrast tholeiitic pyroxenes from Japan (Kuno, 1955) and Hawaii range from diopside-rich compositions near the Di-Ol join to subcalcic

TABLE 3. PYROXENES FROM THE STILLWATER COMPLEX, MONTANA

Norms (weight per cent)

| Ref. no. | 11A | 12 | 13 | 14 | 15 | 16 | 17 | 18 | 19 | 20 | 21 |
|---|---|---|---|---|---|---|---|---|---|---|---|
| Authors' No. | MVL 101/2 | I52 | EB175 | EB43 | EB41 | 7666 | 7704 | EB13 | EB38 | EB130 | EB41[1] |
| qz | — | — | — | — | 0.4 | — | — | 0.2 | 0.6 | 0.5 | 1.8 |
| or | — | — | 0.1 | 0.1 | — | — | — | — | — | — | — |
| ab | 2.4 | 2.7 | 2.4 | 2.3 | 1.9 | — | — | — | — | — | 0.4 |
| ne | — | — | — | — | — | — | — | — | — | — | — |
| an | 6.9 | 6.7 | 6.1 | 7.1 | 5.3 | 4.4 | 4.2 | 4.7 | 4.1 | 4.5 | 4.3 |
| di (di) | 58.6 | 63.6 | 63.2 | 56.2 | 51.9 | 2.1 | 1.7 | 2.3 | 3.5 | 2.6 | 11.0 |
| di (he) | 5.8 | 6.3 | 12.8 | 14.3 | 19.5 | 0.3 | 0.3 | 0.5 | 0.9 | 1.0 | 6.3 |
| hy (en) | 14.1 | 13.2 | 9.4 | 10.9 | 12.0 | 79.0 | 77.3 | 73.2 | 68.6 | 62.0 | 44.2 |
| hy (fs) | 1.6 | 1.5 | 2.2 | 3.2 | 5.2 | 12.1 | 14.9 | 17.3 | 20.7 | 26.8 | 29.1 |
| ol (fo) | 5.0 | 1.9 | 0.7 | 2.0 | — | — | 0.1 | — | — | — | — |
| ol (fa) | 0.6 | 0.2 | 0.2 | 0.7 | — | — | 0.0 | — | — | — | — |
| il | 0.5 | 0.5 | 0.8 | 0.9 | 1.0 | 0.2 | 0.2 | 0.3 | 0.4 | 0.5 | 0.7 |
| mt | 2.0 | 1.7 | 2.0 | 2.0 | 2.3 | 1.4 | 0.7 | 0.8 | 1.2 | 1.6 | 1.6 |
| cm | 1.6 | 1.7 | — | — | — | 0.7 | 0.8 | 0.7 | 0.1 | 0.1 | — |
| Total | 99.1 | 100.0 | 99.9 | 99.7 | 99.5 | 100.2 | 100.2 | 100.0 | 100.1 | 99.6 | 99.4 |
| Molecular proportions $NaAlSiO_4$:$Ca(Mg, Fe)Si_2O_6$:$(Mg, Fe)SiO_3$:$(Mg, Fe)_2SiO_4$:$SiO_2$ recalculated to 100% | | | | | | | | | | | |
| $NaAlSiO_4$ | — | — | — | — | — | — | — | — | — | — | — |
| $Ca(Mg, Fe)Si_2O_6$ | 60.6 | 66.9 | 74.6 | 67.8 | 65.6 | 1.2 | 1.0 | 1.4 | 2.3 | 1.9 | 9.9 |
| $(Mg, Fe)SiO_3$ | 31.4 | 30.2 | 24.1 | 28.5 | 33.0 | 98.8 | 98.9 | 98.2 | 96.5 | 97.1 | 86.2 |
| $(Mg, Fe)_2SiO_4$ | 8.0 | 2.9 | 1.3 | 3.7 | — | — | 0.1 | — | — | — | — |
| $SiO_2$ | — | — | — | — | 1.4 | — | — | 0.4 | 1.2 | 1.0 | 3.9 |
| Atomic ratio Fe/Fe+Mg | | | | | | | | | | | |
| Fe/Fe+Mg | 0.14 | 0.13 | 0.20 | 0.23 | 0.30 | 0.12 | 0.14 | 0.16 | 0.20 | 0.27 | 0.35 |

[1] Augite impurity.

KEY TO TABLE 3

Norms of Stillwater pyroxenes
Specimen numbers as in Hess (1960, pp. 25, 28, 36)

11A–15. Clinopyroxenes.
16–20. Orthopyroxenes of Bushveld Type.
21. Orthopyroxene of Stillwater Type (inverted pigeonite).

augites or pigeonitic augites which lie near the metasilicate join. Two analyses of iron-poor phenocrystic augites from Taga Volcano, Japan (Kuno, 1955) show trace amounts of normative nepheline and can in this respect be compared with the earliest Skaergaard augite, but the other analyses examined show normative hypersthene and olivine or occasionally minor quartz.

Lines are drawn connecting a number of the pyroxenes to points representing their host rocks. It is to be emphasized that the host rock compositions shown will not in general represent the composition of the melt phase at the time the pyroxene was crystallizing. Nevertheless the orientations of these tie-lines suggest that the degree of effective undersaturation of the pyroxene bears a crude relationship to the degree

TABLE 4. PYROXENES FROM ALKALINE BASALTIC ROCKS

Norms (weight per cent)

| Ref. No. | 22 | 23 | 24 | 25 | 26 | 27 | 28 | 29 | 30 | 31 |
|---|---|---|---|---|---|---|---|---|---|---|
| qz | — | — | — | — | — | — | — | — | — | — |
| or | 0.6 | 0.4 | 1.7 | 0.3 | 4.0 | 0.3 | 3.5 | 0.5 | 1.3 | — |
| lc | — | — | — | — | — | — | — | — | — | 1.3 |
| ab | 3.0 | 3.4 | 6.7 | 0.3 | 11.0 | 3.6 | 11.8 | 6.8 | 0.2 | — |
| ne | 1.0 | 5.2 | 2.5 | 4.8 | 4.8 | 2.4 | 2.8 | 4.6 | 2.2 | 2.0 |
| an | 9.7 | 2.7 | 11.8 | 5.4 | 12.2 | 2.6 | 7.4 | 2.2 | 6.1 | 14.3 |
| di di | 61.1 | 68.6 | 54.9 | 64.8 | 46.7 | 59.7 | 43.0 | 29.3 | 67.4 | 51.9 |
| di he | 12.8 | 14.4 | 13.0 | 16.7 | 11.4 | 24.2 | 24.6 | 45.2 | 13.4 | 16.0 |
| hy en | — | — | — | — | — | — | — | — | — | — |
| hy fs | — | — | — | — | — | — | — | — | — | — |
| ol fo | 4.9 | 0.4 | 2.8 | 2.1 | 1.4 | 1.6 | 2.7 | — | 1.2 | 4.2 |
| ol fa | 1.3 | 0.2 | 0.8 | 0.7 | 0.4 | 0.8 | 1.9 | — | 0.3 | 1.6 |
| cs | — | — | — | — | — | — | — | 2.8 | — | 0.6 |
| il | 2.7 | 2.1 | 4.4 | 3.0 | 5.3 | 2.0 | 1.5 | 4.5 | 5.4 | 5.6 |
| mt | 2.8 | 3.2 | 1.8 | 3.4 | 2.7 | 3.3 | 0.9 | 4.6 | 3.1 | 2.1 |
| cm | — | — | — | — | — | — | — | — | — | — |
| Total | 99.9 | 100.6 | 100.4 | 101.5 | 99.9 | 100.5 | 100.1 | 100.5 | 100.6 | 99.6 |
| **Molecular proportions** | | | | | | | | | | |
| $NaAlSiO_4$ $+KAlSi_2O_6$ | 1.7 | 8.9 | 5.1 | 8.0 | 10.9 | 4.2 | 5.6 | 9.3 | 3.9 | 5.5 |
| $Ca(Mg, Fe)Si_2O_6$ | 78.8 | 90.3 | 88.1 | 87.7 | 85.1 | 92.1 | 86.1 | 90.7 | 93.5 | 84.0 |
| $(Mg, Fe)SiO_3$ | — | — | — | — | — | — | — | — | — | — |
| $(Mg, Fe)_2SiO_4$ | 19.5 | 0.8 | 6.8 | 4.3 | 4.0 | 3.7 | 8.3 | — | 2.6 | 10.5 |
| $SiO_2$ | — | — | — | — | — | — | — | — | — | — |
| **Atomic ratio Fe/Fe+Mg** | | | | | | | | | | |
| Fe/Fe+Mg | 0.25 | 0.26 | 0.27 | 0.29 | 0.33 | 0.34 | 0.36 | 0.66 | 0.29 | 0.32 |

KEY TO TABLE 4

Pyroxenes from alkaline basaltic rocks

22. From hawaiite 60464, Papalele Gulch, Mauna Kea (Muir and Tilley, 1961, Table 9, No. 6).
23. From "soda mugearite" 72881, Ulva Ferry, Mull (Muir and Tilley, 1961, Table 9, No. 8).
24. From hawaiite 68219, Kahului, Maui (Muir and Tilley, 1961, Table 9, No. 3).
25. From mugearite basalt 7568, River Rha, above Uig, Skye (Muir and Tilley, 1961, Table 9, No. 2).
26. From hawaiite 57361, Noonaohae Cone, Mauna Kea (Muir and Tilley, 1961, Table 9, No. 4).
27. From "mugearite" (hawaiite) 76503, Jeffreys Hill, E. Otago, N. Z. (Muir and Tilley, 1961, Table 9, No. 12).
28. From mugearite, 9384, Druim na Criche, near Mugeary, Syke (Muir and Tilley, 1961, Table 9, No. 1).
29. From "mugearite" (hawaiite) 76505, Scroggs Hill, E. Otago, N. Z. (Muir and Tilley, 1961, Table 9, No. 13.)
30. Titanaugite from dolerite 1507, Tahara Bridge, Sakhalin (Yagi, 1953).
31. Titanaugite from dolerite 607, Morotu Cape, Sakhalin (Yagi, 1953).

of undersaturation of the host rock. From the figure it would seem that the effect of separation of clinopyroxene from those basaltic magmas that initially carry substantial amounts of normative Ne, will be to displace the liquid towards more strongly undersaturated compositions whereas magmas plotting clearly to the right of the Di-Ol join, will be displaced towards more siliceous compositions. Present data do not allow a decisive appraisal of the effect on silica saturation of the separation of pyroxenes, olivine or plagioclase from basaltic liquids lying close to the Di-Ol join, and hence to the plagioclase-diopside-olivine plane. Nevertheless a number of rock-pyroxene tie-lines plotted in this region are roughly parallel to the join and suggest that separation of pyroxene, like separation of olivine and plagioclase, may have little effect on the degree of silica saturation of such liquids. This accords with the observation already made that basaltic magma batches that appear to have differentiated towards trachyte, do in fact plot close to the Di-Ol join.

*Chromian diopsides from peridotitic inclusions in basaltic rocks.* Norms (Table 7) have been calculated for the ten modern analyses of chromian diopsides listed by Ross *et al.* (1954), eight of them from the peridotitic inclusions commonly found in alkaline basaltic rocks, and two from dunites. In spite of the presence of appreciable $Cr_2O_3$ and $TiO_2$ which in the norm calculation are combined with FeO releasing $SiO_2$ for other purposes, all but two of the analyses of diopsides from inclusions carry normative nepheline. The analyses of these plot in a field C (Fig. 7), overlapping that of pyroxenes from alkaline basaltic rocks, but with its centre of gravity nearer the Di-Ol join and displaced somewhat towards the olivine point.

*Hawaiian tholeiitic basalts and their pyroxenes.* Variants of the Kilauea flows of 1921 (*e.g.* Tilley, 1960a), 1959 (Tilley, 1960b), 1955 (Macdonald, 1955), 1840 (Macdonald, 1949b), the Uwekahuna laccolith of Kilauea (Murata and Richter, 1961), the Mauna Loa and Kilauea flows of 1868 (Tilley and Scoon, 1961) and Palolo quarry, Oahu (Kuno *et al.*, 1957) are plotted on Fig. 8 together with the 1887 hypersthene basalt of Mauna Loa (illey, 1961) and average Koolau basalt. In each case the points for each suite fall in a well defined band, in general order of increasing ratio of Fe/Mg from left to right, the sharpness of the

TABLE 5. PYROXENES FROM THE BLACK JACK (32–35) AND GARBH EILEAN (36–44) SILLS

(Data from Wilkinson, 1957 and Murray, 1954)

Norms (weight per cent)

| Ref. No. | 32 | 33 | 34 | 35 | 36 | 37 | 38 | 39 | 40 | 41 | 42 | 43 | 44 |
|---|---|---|---|---|---|---|---|---|---|---|---|---|---|
| Author's No. | I | II | III | IV | I | 17 | 20 | P1 | 31L | P2 | 25 | 29 | 31H |
| or | — | — | — | 0.2 | — | — | tr. | tr. | tr. | tr. | tr. | 0.3 | tr. |
| lc | 0.2 | 0.5 | 0.6 | 0.2 | tr. | tr. | — | — | — | — | — | — | — |
| ab | — | — | — | — | — | — | 1.8 | 0.7 | 2.2 | 1.9 | 3.7 | 1.0 | 2.6 |
| ne | 3.0 | 3.7 | 3.2 | 3.1 | 1.8 | 2.1 | 1.0 | 2.8 | 0.2 | 2.4 | — | — | — |
| an | 15.0 | 11.7 | 6.3 | 8.0 | 7.3 | 6.2 | 8.3 | 7.6 | 9.3 | 7.0 | 5.7 | 8.4 | 5.8 |
| di {di | 56.9 | 57.2 | 57.7 | 55.6 | 68.4 | 70.0 | 67.2 | 64.6 | 63.6 | 68.1 | 56.7 | 50.2 | 44.6 |
| di {he | 9.9 | 11.0 | 21.3 | 25.0 | 8.8 | 8.6 | 11.8 | 14.2 | 14.1 | 11.8 | 23.4 | 22.7 | 34.4 |
| hy {en | — | — | — | — | — | — | — | — | — | — | 1.2 | 5.8 | 2.4 |
| hy {fs | — | — | — | — | — | — | — | — | — | — | 0.6 | 3.0 | 2.1 |
| ol {fo | 3.0 | 2.7 | 1.4 | 0.9 | 4.0 | 4.5 | 3.2 | 3.3 | 3.4 | 1.2 | 2.5 | 1.8 | 1.7 |
| ol {fa | 0.7 | 0.6 | 0.7 | 0.5 | 0.7 | 0.7 | 0.7 | 0.9 | 1.0 | 0.3 | 1.3 | 1.0 | 1.7 |
| cs | 3.6 | 3.9 | 1.6 | — | 3.3 | 1.6 | — | — | — | — | — | — | — |
| il | 5.8 | 6.1 | 4.6 | 4.1 | 3.5 | 2.7 | 2.6 | 4.3 | 2.4 | 4.1 | 2.5 | 2.6 | 2.6 |
| mt | 2.2 | 2.7 | 2.6 | 2.1 | 2.7 | 3.9 | 3.7 | 1.7 | 3.3 | 3.4 | 2.5 | 3.4 | 2.2 |
| Total | 100.3 | 100.1 | 100.0 | 99.7 | 100.5 | 100.3 | 100.3 | 100.1 | 99.5 | 100.2 | 100.1 | 100.2 | 100.1 |
| Molecular proportions $NaAlSiO_4$+$KAlSi_2O_6$:$Ca(Mg, Fe)Si_2O_6$:$(Mg, Fe)SiO_3$:$(Mg, Fe)_2SiO_4$ | | | | | | | | | | | | | |
| $NaAlSiO_4$+$KAlSi_2O_6$ | 6.2 | 7.9 | 6.4 | 5.8 | 3.3 | 3.6 | 1.7 | 4.9 | 0.4 | 4.3 | — | — | — |
| $Ca(Mg, Fe)Si_2O_6$ | 86.8 | 85.9 | 90.1 | 91.8 | 88.8 | 87.8 | 91.5 | 88.2 | 92.0 | 93.1 | 84.6 | 76.8 | 85.0 |
| $(Mg, Fe)SiO_3$ | — | — | — | — | — | — | — | — | — | — | 3.8 | 19.0 | 9.9 |
| $(Mg, Fe)_2SiO_4$ | 7.0 | 6.2 | 3.5 | 2.4 | 8.0 | 8.7 | 6.8 | 6.9 | 7.6 | 2.6 | 11.6 | 4.2 | 5.1 |
| Atomic ratio Fe/Mg+Fe | | | | | | | | | | | | | |
| Fe/Fe+Mg | 0.27 | 0.29 | 0.35 | 0.37 | 0.21 | 0.22 | 0.25 | 0.25 | 0.27 | 0.27 | 0.34 | 0.36 | 0.46 |

bands having been somewhat improved by reducing $Fe_2O_3$ to an arbitrary value based on the least oxidized specimens and increasing FeO accordingly. The value of 1.5% has been used except for Kilauea 1955 for which 1.87% $Fe_2O_3$ has been used. In the case of the rather highly oxidized Palolo quarry variants two points are shown for each analysis, that on the right representing the unadjusted analysis, the other after reduction of $Fe_2O_3$ to 1.5%.

Also shown are points for the five pyroxene analyses so far available: two fractions of augitic pyroxene separated from the 1840 picrite basalt, clinopyroxene and hypersthene from the Uwekahuna laccolith, and pigeonitic groundmass augite from the

TABLE 6. PYROXENES FROM SOME THOLEIITIC AND RELATED ROCKS OF JAPAN AND HAWAII

Norms (weight per cent)

| Ref. No. | 45 | 46 | 47 | 48 | 49 | 50 | 51 | 52 | 53 | 54 | 55 | 56 | 57 |
|---|---|---|---|---|---|---|---|---|---|---|---|---|---|
| qz | — | — | — | — | — | — | — | — | — | — | 1.5 | 1.1 | — |
| or | 0.0 | — | 1.0 | 0.7 | 0.7 | 0.4 | 0.9 | 0.8 | 0.1 | 0.3 | 1.2 | 1.5 | 0.2 |
| ab | 0.0 | — | 2.7 | 0.7 | 2.9 | 2.7 | 3.2 | 2.8 | 2.7 | 3.8 | 5.9 | 8.1 | 1.4 |
| ne | — | 0.9 | — | 0.7 | — | — | — | — | — | — | — | — | — |
| an | 14.9 | 12.5 | 3.8 | 6.0 | 4.5 | — | — | 0.8 | 7.1 | 8.3 | 7.2 | 9.4 | 5.0 |
| ac | — | — | — | — | — | 0.8 | 2.0 | — | — | — | — | — | — |
| di di | 67.1 | 60.3 | 61.9 | 73.4 | 25.1 | 23.5 | 24.0 | 25.8 | 61.0 | 58.7 | 42.7 | 25.3 | 5.3 |
| di he | 8.4 | 13.5 | 13.9 | 10.7 | 12.4 | 15.3 | 16.3 | 28.8 | 9.8 | 10.0 | 11.7 | 10.5 | 1.5 |
| hy en | — | — | 5.0 | — | 19.2 | 26.9 | 22.6 | 14.9 | 8.5 | 8.5 | 18.1 | 27.2 | 60.0 |
| hy fs | — | — | 1.3 | — | 10.8 | 20.2 | 17.5 | 19.1 | 1.6 | 1.6 | 5.8 | 12.9 | 18.8 |
| ol fo | 4.4 | 6.3 | 5.1 | 3.1 | 12.8 | 2.2 | 4.6 | 2.5 | 4.6 | 4.3 | — | — | 2.8 |
| ol fa | 0.7 | 1.8 | 1.5 | 0.6 | 8.0 | 1.8 | 4.0 | 3.5 | 0.9 | 0.9 | — | — | 1.0 |
| cs | 0.1 | 2.3 | — | — | — | — | — | — | — | — | — | — | — |
| il | 0.8 | 0.8 | 1.4 | 0.5 | 0.6 | 1.4 | 1.1 | 0.3 | 1.4 | 1.7 | 2.7 | 1.8 | 2.1 |
| mt | 3.5 | 1.1 | 1.5 | 4.0 | 2.9 | 5.0 | 3.8 | 0.5 | 1.8 | 1.3 | 2.4 | 1.6 | 1.6 |
| cm | — | — | — | — | — | — | — | — | 0.7 | 0.8 | 0.8 | — | 0.2 |
| Total | 99.9 | 99.5 | 99.1 | 100.4 | 99.9 | 100.2 | 100.0 | 99.8 | 100.2 | 100.2 | 100.0 | 99.4 | 99.9 |
| Molecular proportions $NaAlSiO_4$: $Ca(Mg, Fe)Si_2O_6$: $(Mg, Fe)SiO_3$: $(Mg, Fe)_2SiO_4$: $SiO_2$ | | | | | | | | | | | | | |
| $NaAlSiO_4$ | — | 1.6 | — | 1.3 | — | — | — | — | — | — | — | — | — |
| $Ca(Mg, Fe)Si_2O_6$ | 90.8 | 84.7 | 76.8 | 92.7 | 29.1 | 27.4 | 30.1 | 41.7 | 70.6 | 70.3 | 49.5 | 29.1 | 3.8 |
| $(Mg, Fe)SiO_3$ | — | — | 13.4 | — | 48.0 | 68.7 | 61.0 | 52.1 | 21.3 | 21.8 | 45.4 | 67.5 | 93.1 |
| $(Mg, Fe)_2SiO_4$ | 9.2 | 13.6 | 9.8 | 6.0 | 22.9 | 3.9 | 8.9 | 6.2 | 8.1 | 7.9 | — | — | 3.1 |
| $SiO_2$ | — | — | — | — | — | — | — | — | — | — | 5.1 | 3.3 | — |
| Atomic ratio Fe/Fe+Mg | | | | | | | | | | | | | |
| Fe/Fe+Mg | 0.19 | 0.20 | 0.21 | 0.21 | 0.34 | 0.42 | 0.42 | 0.50 | 0.18 | 0.18 | 0.27 | 0.30 | 0.22 |

KEY TO TABLE 6

Pyroxenes from some tholeiitic and related rocks of Japan and Hawaii

A. *Salite and augite phenocrysts, Hakone and Taga Volcanoes, Japan*

45. Salite phenocrysts, basalt tuff, Taga Volcano (Kuno, 1955, No. 2, p. 73).
46. Salite phenocrysts, olivine eucrite in tuff, Taga Volcano (Kuno, 1955, No. 1, p. 73).
47. Augite phenocrysts, hypersthene-olivine-augite andesite, Hakone (Kuno, 1955, No. 5, p. 74).
48. Augite phenocrysts, olivine-augite basalt, Taga Volcano (Kuno, 1955, No. 4, p. 73).

B. *Groundmass subcalcic augites from Japanese tholeiites*

49. From aphyric basalt, Okata, Ō-Sima (Kuno, 1960, No. 3, p. 128).
50. From pyroxene basalt flow of 1778, Ō-Sima (Kuno, 1955, No. 9, p. 75).
51. From hypersthene-augite basalt, extruded 1950, Ō-Sima Island (Kuno, 1955, No. 8, p. 75).
52. From olivine basalt, Hatu-Sima, east of Taga (Kuno, 1955, No. 7, p. 74).

C. *Clinopyroxenes from Hawaii*

53. From Uwekahuna gabbroic laccolith, Kilauea (Muir and Tilley, 1957, Table 4).
54. Phenocrysts from picrite basalt flow of 1840, Nanawale Bay (Muir and Tilley, 1957, Table 4).
55. Groundmass clinopyroxene, picrite basalt flow of 1840, as for No. 54.
56. Pigeonitic augite of groundmass, hypersthene-olivine basalt of 1887, Mauna Loa (Tilley, 1961).

D. *Hypersthene from Hawaii*

57. From Uwekahuna laccolith, as for No. 53.

hypersthene basalt of 1887. In addition the Ca-Mg-Fe ratios of successive clinopyroxene fractions from the 1921 Kilauea flows are known (Muir *et al.* 1957) and their general position within the field of tholeiitic pyroxenes can be confidently predicted.

At least two trends are clearly shown by the rock suites. The first of these is approximately away from the olivine point and graphically demonstrates the effect of olivine separation and accumulation. Thus Uwekahuna no. 1 represents the lower chilled margin of the intrusion and 6 the upper margin, whereas 2, 3 and 4 represent olivine-enriched phases. In the case of the 1840 variants, if indeed they have a common parent, some separation of pyroxene as well as olivine is indicated as already concluded by Muir *et al.* (1957), the necessary crystal extract having a pro-

TABLE 7. CHROMIAN DIOPSIDES FROM PERIDOTITIC INCLUSIONS IN BASALTIC ROCKS (58–65) AND FROM TWO DUNITES (66–67)

Norms (weight per cent)

| Ref. No. | 58 | 59 | 60 | 61 | 62 | 63 | 64 | 65 | 66 | 67 |
|---|---|---|---|---|---|---|---|---|---|---|
| Authors' No. | 8 | 7 | 1 | 3 | 2 | 4 | 9 | 11 | 12 | 13 |
| qz | — | — | — | — | — | — | — | — | — | — |
| or | 0.4 | 0.2 | 0.5 | 0.4 | 0.6 | 0.5 | 0.1 | 0.2 | 0.2 | 0.6 |
| ab | 8.6 | 2.7 | 7.7 | 6.9 | 5.7 | 8.6 | 2.8 | 4.9 | 3.3 | 3.2 |
| ne | 5.2 | 1.9 | 0.7 | 2.7 | 3.2 | 0.9 | — | — | — | — |
| an | 1.3 | 9.5 | 9.0 | 11.4 | 9.9 | 12.0 | 3.2 | 9.7 | — | — |
| ac | — | — | — | — | — | — | — | — | 0.5 | — |
| di (di) | 72.3 | 72.0 | 69.7 | 61.7 | 66.0 | 57.9 | 73.9 | 65.5 | 82.4 | 82.5 |
| di (he) | 1.6 | 4.7 | 2.0 | 2.2 | 3.9 | 3.9 | 5.0 | 4.6 | 4.6 | 6.2 |
| hy (en) | — | — | — | — | — | — | 5.5 | 1.7 | 0.3 | — |
| hy (fs) | — | — | — | — | — | — | 0.4 | 0.1 | 0.0 | — |
| ol (fo) | 5.3 | 5.1 | 5.3 | 8.9 | 6.8 | 12.1 | 3.5 | 6.4 | 5.9 | 4.3 |
| ol (fa) | 0.1 | 0.4 | 0.2 | 0.4 | 0.5 | 1.0 | 0.3 | 0.6 | 0.5 | 0.4 |
| cs | — | — | — | — | — | — | — | — | — | 1.2 |
| il | 1.5 | 0.6 | 0.7 | 1.5 | 0.5 | 0.5 | 1.2 | 1.4 | 0.3 | 0.2 |
| mt | 1.2 | 1.0 | 2.5 | 2.2 | 2.1 | 1.2 | 2.3 | 3.7 | 0.2 | — |
| cm | 2.1 | 1.5 | 1.4 | 1.4 | 1.2 | 1.8 | 1.6 | 1.8 | 1.3 | 1.0 |
| Total | 99.6 | 99.6 | 99.7 | 99.7 | 100.4 | 100.4 | 99.8 | 100.6 | 100.2[1] | 99.9[2] |
| Molecular proportions $NaAlSiO_4$+$KAlSi_2O_6$:$Ca(Mg, Fe)Si_2O_6$:$(Mg, Fe)SiO_3$:$(Mg, Fe)_2SiO_4$:$SiO_2$ | | | | | | | | | | |
| $NaAlSiO_4$ | 8.8 | 3.2 | 1.2 | 5.0 | 5.6 | 1.6 | — | — | — | — |
| $Ca(Mg, Fe)Si_2O_6$ | 82.0 | 87.3 | 88.5 | 77.7 | 81.4 | 74.5 | 81.1 | 82.9 | 89.4 | 92.5 |
| $(Mg, Fe)SiO_3$ | — | — | — | — | — | — | 13.1 | 4.7 | 0.7 | — |
| $(Mg, Fe)_2SiO_4$ | 9.3 | 9.5 | 10.3 | 17.3 | 13.0 | 23.9 | 5.8 | 12.4 | 9.9 | 7.5 |
| $SiO_2$ | — | — | — | — | — | — | — | — | — | — |
| Atomic ratio Fe/Fe+Mg | | | | | | | | | | |
| Fe/Fe+Mg | 0.09 | 0.11 | 0.11 | 0.12 | 0.12 | 0.13 | 0.14 | 0.14 | 0.06 | 0.07 |

[1] Includes ns 0.7.
[2] Includes ns 0.3.

KEY TO TABLE 7

(Data from Ross *et al.*, 1954, p. 709)

A. *Chromian diopsides from peridotitic inclusions in basaltic rocks*

58. Salt Lake Crater, Honolulu Series, Oahu, Hawaii.
59. Ichinomegata, Japan.
60. Chihuahua, Mexico.
61. Peridot Cove, Arizona.
62. Ludlow, California.
63. Dreiser Weiher, Eifel, Germany.
64. Grove Farm Quarry, Kauai, Hawaii.
65. Flow of 1801, Hualalai, Hawaii.

B. *Diopsides from "dunites"*

66. Twin Sisters, Whatcom County, Washington.
67. Webster, North Carolina.

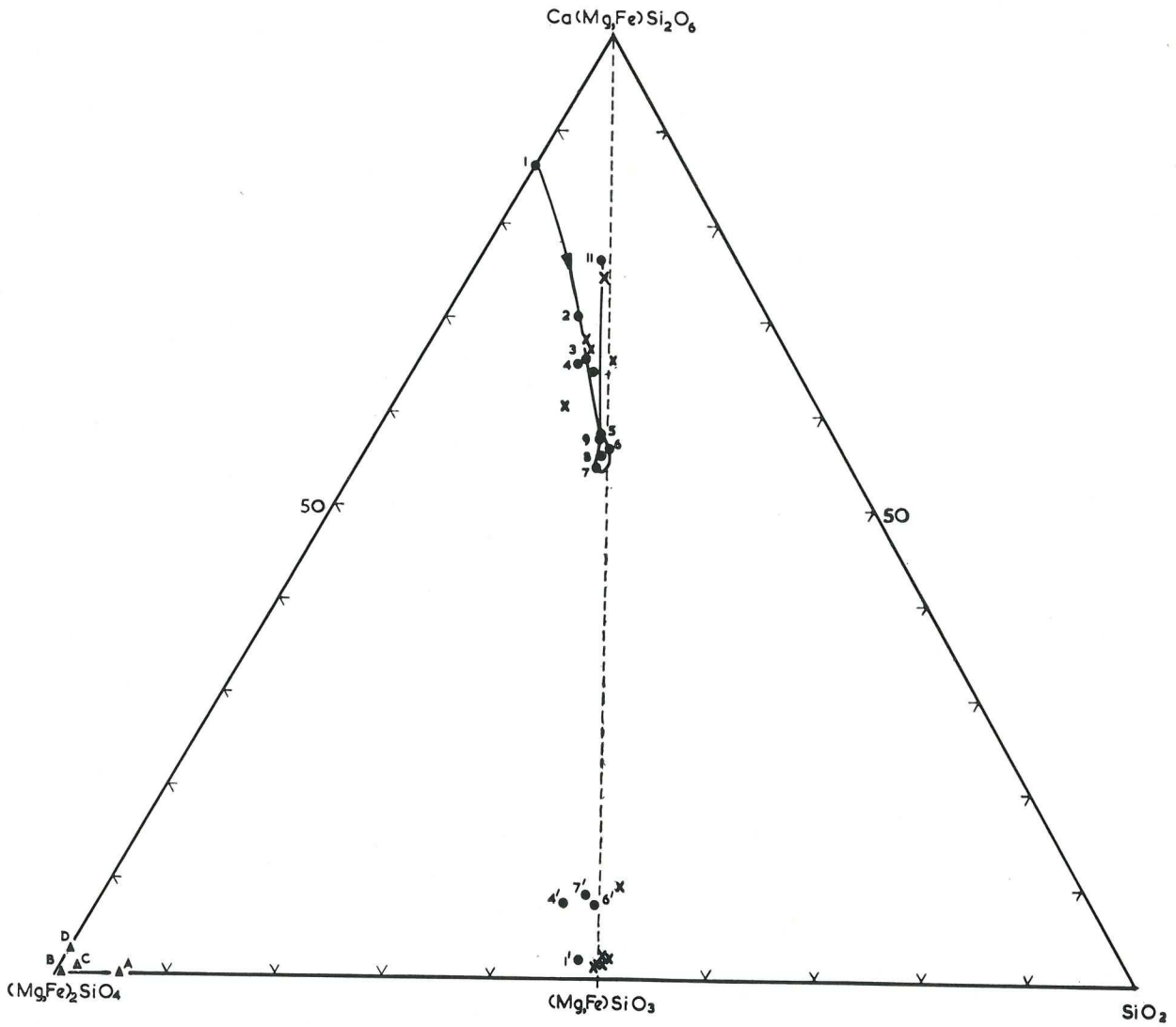


FIG. 6. Normative compositions of pyroxenes and olivines from the Skaergaard and Stillwater complexes in molecular proportions ferroan diopside:olivine:silica.

● Skaergaard pyroxenes 1 to 11; 1′–7′ (see Table 2).

× Stillwater pyroxenes (see Table 3).

▲ Skaergaard olivines A–D (olivines I to IV of Wager and Deer, 1939, pp. 72, 73).

jected composition such as E given by the intersection of the lava trend line with a join from the olivine point to the appropriate clinopyroxene composition. The same may apply to the 1921 variants. The trachyte and Pele's hair which constitute the least basic variants, numbers 5 and 6, of the 1921 suite, may well have reached the limits of the olivine field, and the same applies to the 1955 Kilauea lavas. These follow a trend athwart the trend of olivine separation, a trend clearly controlled by the separation of clinopyroxene. The more basic members of the 1955 series may well approximate to the position of an olivine-augitic pyroxene-plagioclase-liquid four-phase curve. Hypersthene appears in the less basic members, that is those having indicator ratio greater than about 0.60.

Late segregation veins (no. 7) from the Uwekahuna laccolith continue the 1955 trend and in a general way the Palolo quarry quartz dolerite and granophyres extend it still further. These rocks appear to represent liquids which have left the olivine surface entirely (a few deeply corroded relics remain) and are moving along a two pyroxene-feldspar-liquid four-phase curve, one of the pyroxenes ultimately no

doubt disappearing. In the Uwekahuna rocks and in the 1840 picrite basalt (indicator ratio approximately 0.55) the early pyroxene appears to be augitic pyroxene. On the other hand in the Koolau basalts (I.R.=0.70) and apparently in the 1868 and 1887 Mauna Loa flows (I.R. 0.62–0.65) hypersthene appears early, to be joined by pigeonitic augite. Separation of olivine in these cases presumably displaces the liquid to an olivine-*hypersthene*-plagioclase-liquid four-phase curve which must then be followed to the five-phase "point." A trend in this direction is suggested by the Izu basalt whole-rock and groundmass fractions (Fig. 4, Nos. 2 and 4). It is to be emphasized again that in the natural rock systems the four-phase curves and five-phase "point" are not fixed in position but will migrate with changing ratios of Fe/Mg, albite/anorthite and other variables; the present approach merely fixes their approximate position for typical magma compositions.

## A Model for Tholeiitic Crystallization

The inferred relationships are summarized in Fig. 9 which is to be compared with Fig. 3. Figure 9 is a reconstruction of the inferred form of the plagioclase surface projected onto the base of the tetrahedron plagioclase-ferroan diopside-olivine-silica for natural basaltic compositions. A five-phase reaction point R is indicated in the general region $Di_{26}Hy_{54}Qz_{20}$ in normative molecular proportions. The width of the immiscibility gap shown between the two pyroxene composition fields is undoubtedly variable, being a

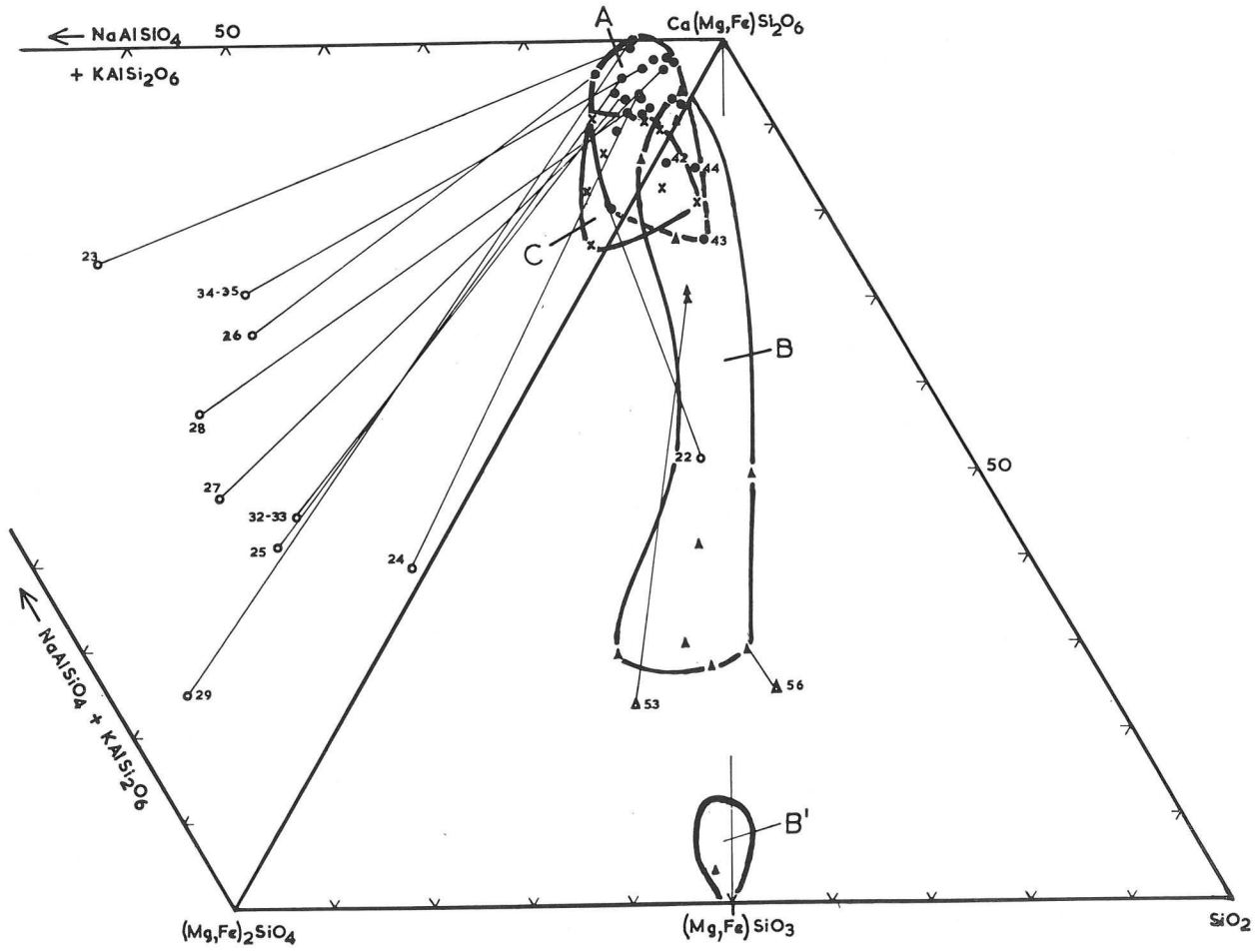


Fig. 7. Pyroxenes from alkaline basaltic rocks (field A), tholeiites (field B) and peridotitic inclusions (field C) and bulk composition of some host rocks. Compositions in molecular percentages of normative components. For explanation of numbers, see Tables 4–7.

●——○ Pyroxenes of alkaline basaltic rocks (solid symbols) and host rock (open symbols).

▲——△ Pyroxenes of tholeiitic rocks (solid symbols) and their host rock (open symbols).

× Pyroxenes from peridotitic inclusions in basaltic rocks.

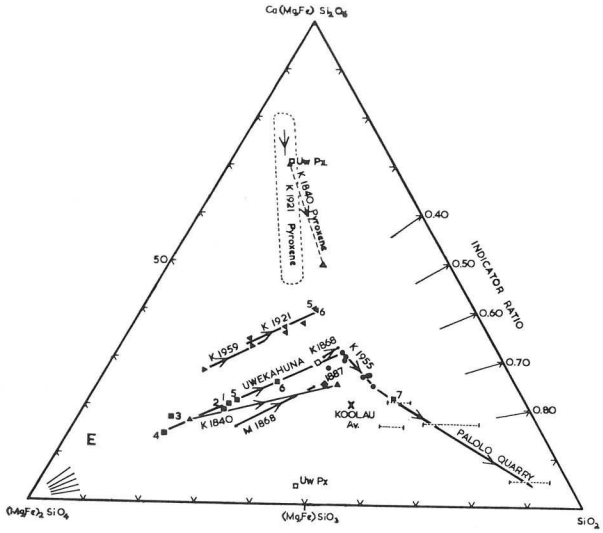


FIG. 8. Some Hawaiian differentiation trends. Solid symbols: rock analyses; open symbols: pyroxenes.

K1921: Kilauea 1921 lava variants; similarly for K1840, etc.

M1868: Mauna Loa 1868 lava variants.

Arrows indicate direction of increasing ratio Fe:Mg. For discussion, see text.

function of magmatic temperatures and pressures as well as Fe/Mg ratios. It is normally wider in intrusive rocks than it is in extrusives.

It is commonly considered that crystallization of hypersthene will give way to pigeonite when the pyroxene inversion temperature falls below the magma temperature. It should also be borne in mind (Gunn, 1962) that as the molar volume of pigeonite appears to be higher than that of a corresponding hypersthene-augite assemblage, intratelluric high-pressure crystallization will tend to extend the field of hypersthene with respect to that of pigeonite. Although the procedure of the present paper allows the approximate position of the five-phase point to be determined for a series of magmas, it does not portray the contrasting conditions for early separation of pigeonite as against hypersthene.

As demonstrated by Yoder and Tilley (1957), typical Hawaiian lavas commence to precipitate olivine, plagioclase and pyroxene within a relatively narrow temperature range. A liquid such as X is comparable to the 1921 and 1959 Kilauea magmas. Early separation of olivine should lead to a projected line of descent to point L on the olivine-augite-liquid surface on or near the plagioclase-olivine-augite-liquid curve. At this stage augite such as L′ should begin to crystallize, the liquid then following the course LMR, and the coexisting pyroxene the course L′M′R′. Hence if equilibrium were preserved, the residual liquid from liquid X would reach some point between M and R where the last trace of liquid would be in equilibrium with a homogeneous subcalcic augite of composition lying on the straight line X-L. If the relations are correctly drawn, olivine will continue to crystallize in minor amount together with pyroxene for liquids on the field boundary near L, but for liquids somewhere between M and R, the projected tie-lines will have crossed the trace of the field boundary in which case olivine would now be undergoing resorption. As the trend of the projected curve LR (*cf.* trend of 1955 lavas, Fig. 8) is in the main away from the precipitated clinopyroxene neither voluminous precipitation of olivine, nor its strong resorption are to be expected in this range. This inference accords with petrographic observation and contrasts with the crystallization of plentiful groundmass olivine together with augite in more alkaline basalts such as one represented by point W. Unless fractionation is extreme hypersthene is not to be expected from a liquid X, and it is to be remembered that if fractionation were extreme, the Fe/Mg and albite/anorthite ratios may be so modified as to upset the basic form of the diagram shown.

From a liquid Y, representative of the Uwekahuna chilled magma and the Ascension Island hypersthene-bearing basalt referred to above, separation of

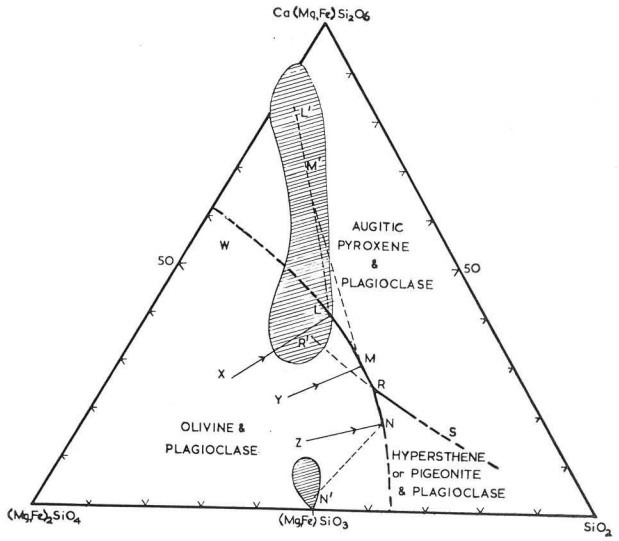


FIG. 9. Possible form of equilibrium relations for basaltic liquids within the olivine-pyroxene-silica-plagioclase tetrahedron, the floor of the plagioclase volume being projected from the plagioclase point onto the base of the tetrahedron. Composition fields of tholeiitic pyroxenes are shaded. Compositions are in molecular proportions.

olivine would yield accumulates comparable to the 1840 picrite basalt and the olivine-rich phases of the Uwekahuna mass, together with a liquid fraction reaching the augite-olivine boundary at M. Augite or subcalcic augite trending from M′ to R′ should then crystallize while the liquid moves from M to R. In the later stages of this process olivine is partly resorbed. At R, pigeonitic augite R′ should be joined by hypersthene or a related pigeonite and olivine would undergo continued resorptive reaction. The position of the five-phase point R is not fixed, but will migrate as this reaction proceeds as well as with other compositional changes and any pressure change. Fractionation of such a liquid by effective removal of olivine should lead to crystallization along a plagioclase-two pyroxene-liquid curve (RS), and the eventual appearance of free silica.

Separation of olivine from a liquid Z would displace it to the hypersthene or pigeonite field boundary at N where hypersthene (or pigeonite) should start to appear. The liquid should then move upwards along a curve such as NR as olivine is resorbed, hypersthene and olivine being joined at R by groundmass pigeonitic augite.

It will be noticed that for magmas with indicator ratios progressively smaller than the theoretical maximum of 1.00, the proportion of olivine resorbed to pyroxene crystallized becomes progressively smaller, in other words the Bowen reaction relationship becomes weaker. For indicator ratios somewhere near the middle of the range the reaction relationship disappears altogether and for lower values groundmass olivine can crystallize side by side with augitic pyroxene. For indicator ratios less than about 0.60 also, the appearance of hypersthene or pigeonite becomes progressively more unlikely and can only be achieved after increasingly strong fractionation.

## Origin of Tholeiitic Magmas

It is noticeable that the compositions of the voluminous batches of typically tholeiitic magma plotted on Fig. 4, fall close to the inferred five-phase point olivine-augitic pyroxene-hypersthene-plagioclase-liquid of Fig. 9. In so far as the equilibria are not displaced by high pressure, partial fusion of a crystalline aggregate containing the solid phases mentioned would give rise to such liquids. This suggests a possible origin for tholeiitic magmas. Partial fusion of crystalline aggregates lacking hypersthene would be freed of this control.

As shown by Macdonald (1949b), Tilley (1960a) and others, the variation between the different variants of particular Kilauean eruptions may well be explained on the basis of crystal fractionation in upper crustal levels, the effects being clearly illustrated in Fig. 8. Differences in indicator ratio between such different batches of magma are much more difficult to account for on this basis. Increasing oxidation will slightly increase the indicator ratio and separation of pyroxene from liquids on the olivine-pyroxene-plagioclase-liquid curve will displace them towards tholeiitic composition if they fall initially within the diopside-olivine-plagioclase-silica tetrahedron, and probably towards more alkaline compositions if they contain substantial normative nepheline. The simplest interpretation of magma batches occupying intermediate positions in the basalt series of Fig. 4 (*e.g.* Réunion, Easter Island) is that these, like the more tholeiitic and alkaline extremes, may be true parental rather than derivative magmas. Yoder and Tilley (1961) and Kuno (1960) have indicated a possible mechanism that might bring this about.

## Summary of Conclusions

(a) Averaged basalt analyses from various petrographic provinces plot across the normative Di-Ne-Ol-Qz diagram in a broad band. They range from typically tholeiitic suites with high indicator ratio $(Hy+2Qz)/Hy+2(Qz+Di)$, through transitional and mildly alkaline types with indicator ratio 0.40 to 0.00, to alkaline types with nepheline in the norm and in effect a negative indicator ratio. The first group gives rise to granophyric differentiates, at least some of the transitional group follow a pantelleritic trend the later stages of which cannot be properly represented in the tetrahedron here employed, whereas a phonolitic line of descent is followed by more strongly alkaline basalts. A trachytic trend appears to be characteristic of magmas with an indicator ratio near zero, that is, with neither significant normative nepheline nor hypersthene.

(b) Early crystallization of olivine and feldspar from most basaltic magmas may be considered to displace the liquid composition to an olivine-pyroxene-plagioclase boundary curve within the tetrahedron diopside-olivine-silica (or -nepheline).

(c) Clinopyroxenes are commonly strongly undersaturated in terms of normative components, the degree of undersaturation varying with that of the host rock. Clinopyroxene from alkaline basaltic rocks

usually contains normative nepheline and olivine, that from tholeiites, normative olivine and hypersthene.

(d) Except for liquid compositions falling close to the Pl-Di-Ol plane, separation of clinopyroxene will usually tend to offset the liquid away from that plane, either towards greater undersaturation if sufficient normative nepheline is originally present, or towards more silica-rich compositions if normative hypersthene or quartz is present.

(e) Detailed consideration of Hawaiian lavas and their pyroxenes suggests a five-phase, two-pyroxene reaction "point" on the olivine-pyroxene-plagioclase-liquid "curve" in the general region Di 26, Hy 54, Qz 20 in normative molecular proportions. In more approximate fashion this conclusion is compatible with the common behaviour of basaltic rocks in a substantial number of petrographic provinces.

(f) If the indicator ratio in a magma exceeds about 0.60 to 0.70 hypersthene or an equivalent pigeonite is likely to be the first pyroxene to commence to crystallize. If the ratio is between 0.50 and 0.65, a pyroxene trend from diopsidic pyroxene to subcalcic or pigeonitic augite may culminate in the subsequent appearance of a separate lime-poor phase. If the ratio is less than 0.50, hypersthene is unlikely to appear during the period of normal magmatic crystallization. The olivine-pyroxene reaction relationship progressively fades away for decreasing values of the indicator ratio and in many mildly alkaline rocks (low indicator ratio) olivine and augite crystallize simultaneously in comparable amounts.

## References


Andersen, O. (1915) The system anorthite-forsterite-silica. *Am. Jour. Sci.* 4th ser., **39,** 407–454.

Anderson, C. A. (1941) Volcanoes of the Medicine Lake Highland, California. *Bull. Dept. Geol. Sci., Univ. Calif. Publ.* **25,** 347–422.

Bandy, M. C. (1937) Geology and petrology of Easter Island. *Geol. Soc. Am. Bull.* **48,** 1589–1610.

Benson, W. N. (1941) Cainozoic petrographic provinces in New Zealand and their residual magmas. *Am. Jour. Sci.* **239,** 537–552.

——— (1942) The basic igneous rocks of Eastern Otago and their tectonic environment. Part II. *Trans. Roy. Soc. New Zealand,* **72,** 85–110.

Bowen, N. L. (1914) The ternary system diopside-forsterite-silica. *Am. Jour. Sci.* 4th ser., **38,** 207–264.

——— and J. F. Schairer (1935) The system MgO-FeO-$SiO_2$. *Am. Jour. Sci.* ser 5, **29,** 151–217.

Boyd, F. R. and J. F. Schairer (1957) The join $MgSiO_3$-$CaMgSi_2O_6$. *Carnegie Inst. Washington Year Book,* **56,** 223–225.

Brown, G. M. (1957) Pyroxenes from the early and middle stages of fractionation of the Skaergaard intrusion, East Greenland. *Mineral. Mag.* **31,** 511–543.

——— (1960) The effect of ion substitution on the unit cell dimensions of the common clinopyroxenes. *Am. Mineral.* **45,** 15–38.

Cornwall, H. R. (1951) Differentiation in magmas of the Keweenawan series. *Jour. Geol.* **59,** 151–172.

Daly, R. A. (1924) The geology of American Samoa. *Carnegie Inst. Papers Dept. Marine Biol.* **19,** 93–143.

——— (1925) The geology of Ascension Island. *Proc. Am. Acad. Arts Sci.* **60,** (1).

——— (1927) The geology of Saint Helena Island. *Proc. Am. Acad. Arts Sci.* **62,** 31–92.

Edwards, A. B. (1938) Tertiary tholeiite magma in western Australia. *Jour. Roy. Soc. West. Austr.* **24,** 1–12.

——— (1942) Differentiation of the dolerites of Tasmania. *Jour. Geol.* **50,** 451–480, 579–610.

Fairbairn, H. W. and others (1951) A cooperative investigation of precision and accuracy in chemical, spectrochemical and modal analysis of silicate rocks. *U. S. Geol. Surv. Bull.* **980.**

Green, J. and A. Poldervaart (1955) Some basaltic provinces. *Geochim. Cosmochim. Acta,* **7,** 177–188.

Gunn, B. M. (1962) Differentiation in Ferrar Dolerites, Antarctica. Ph.D. thesis, University of Otago.

Harkin, D. A. (1960) The Rungwe volcanics at the northern end of Lake Nyasa. *Geol. Surv. Tanganyika Mem.* **2.**

Hess, H. H. (1960) Stillwater igneous complex, Montana. *Geol. Soc. Am. Mem.* **80.**

Hytönen, K. and F. J. Schairer (1960) The system enstatite-anorthite-diopside. *Carn. Inst. Washington Year Book* 1959–60, 71–72.

Jung, D. (1958) Untersuchungen am Tholeyit von Tholey (Saar). *Beitr. Mineral. Pet.* **6,** 147–181.

Kuno, H. (1950) Petrology of Hakone volcano and the adjacent areas, Japan. *Geol. Soc. Am. Bull.* **61,** 957–1020.

——— (1955) Ion substitution in the diopside-ferropigeonite series of clinopyroxenes. *Am. Mineral.* **40,** 70–93.

——— (1960) High-alumina basalt. *Jour. Petrol.* **1,** 121–145.

——— K. Yamasaki, C. Iida and K. Nagashima (1957) Differentiation of Hawaiian magmas. *Jap. Jour. Geol. Geog.* **28,** 179–218.

LaCroix, A. (1927) La constitution lithologique des îles volcaniques de la Polynésie australe. *Acad. Sci. Paris, Mem.* **59,** 1–82.

——— (1936) *Le volcan actif de l'île de la Réunion et ses produits.* Paris, Gauthier-Villars.

Macdonald, G. A. (1949a) Petrography of the Island of Hawaii. *U. S. Geol. Surv. Prof. Paper,* **214D,** 1–96.

——— (1949b) Hawaiian petrographic province. *Geol. Soc. Am. Bull.* **60,** 1541–1596.

——— (1955) *Catalogue of the active volcanoes of the world. Part III. Hawaiian Islands.* Naples Intl. Volcan. Assoc., 35–36.

——— and J. P. Eaton (1955) Hawaiian volcanoes during 1953. *U. S. Geol. Surv. Bull.* **1021-D,** 160.

Muir, I. D. (1951) The clinopyroxenes of the Skaergaard intrusion, eastern Greenland. *Mineral. Mag.* **29,** 690–714.

——— AND C. E. TILLEY (1957) Contributions to the petrology of Hawaiian basalts. I. The picrite basalts of Kilauea. *Am. Jour. Sci.* **255,** 241–253.

——— C. E. TILLEY AND J. H. SCOON (1961) Mugearites and their place in alkali igneous rock series. *Jour. Geol.* **69,** 186–203.

MURATA, K. J. (1960) A new method of plotting chemical analyses of basaltic rocks. *Am. Jour. Sci.* **258-A,** 247–252.

——— AND D. H. RICHTER (1961) Magmatic differentiation in the Uwekahuna Laccolith, Kileauea Caldera, Hawaii. *Jour. Petrol.* **2,** 427–437.

MURRAY, R. J. (1954) The clinopyroxenes of the Garbh Eilean Sill, Shiant Isles. *Geol. Mag.* **91,** 17–31.

NAIDU, P. R. J. (1960) Optic axial angles of pyroxenes of Deccan Traps. *Indian Mineral.* **1,** 68–75.

OSBORN, E. F., AND A. MUAN (1960) *Phase equilibrium diagrams of oxide systems.* Am. Ceram. Soc.

——— AND D. B. TAIT (1952) The system diopside-forsterite-anorthite. *Am. Jour. Sci. Bowen vol.* 413–433.

RICHARDSON, C. (1933) Petrology of Galapagos Islands. *Bernice P. Bishop Museum Bull.* **110,** 45–64.

ROSS, C. S., M. D. FOSTER AND A. T. MYERS (1954) Origin of dunites and of olivine-rich inclusions in basaltic rocks. *Am. Mineral.* **39,** 693–737.

SCHAIRER, J. F. AND N. MORIMOTO (1959) The system forsterite-diopside-silica-albite. *Carn. Inst. Washington Year Book,* **58,** 113–118.

——— AND H. S. YODER (1960) The system olbite-forsterite-silica. *Carn. Inst. Washington Year Book,* **59,** 69–70.

SEARLE, E. J. (1960) Petrochemistry of the Auckland basalts. *New Zealand Jour. Geol. Geophys.* **3,** 23–40.

SPEIGHT, R. (1938). The dykes of the Summit Road, Lyttleton. *Trans. Roy. Soc. New Zealand* **68,** 82–99.

SUKHESWALA, R. N. AND A. POLDERVAART (1958) Deccan basalts of the Bombay area, India. *Geol. Soc. Am. Bull.* **69,** 1475–1494.

TILLEY, C. E. (1950) Some aspects of magmatic evolution. *Quart. Jour. Geol. Soc. London,* **106,** 37–61.

——— (1960a) Differentiation of Hawaiian basalts: some variants in lava suites of dated Kilauean eruptions. *Jour. Petrol.* **1,** 47–55.

——— (1960b) Kilauea magma, 1959–60. *Geol. Mag.* **97,** 494–497.

——— (1961) The occurrence of hypersthene in Hawaiian basalts. *Geol. Mag.* **98,** 257–260.

——— AND J. H. SCOON (1961) Differentiation of Hawaiian basalts: trends of Mauna Loa and Kilauea historic magma. *Am. Jour. Sci.* **259,** 60–68.

TRYGGVASON, T. (1943) Das Skjaldbreid-Gebiet auf Island. *Bull. Geol. Inst. Upsala,* **30,** 273–320.

WAGER, L. R. (1960) The major element variation of the layered series of the Skaergaard intrusion and a re-estimation of the average compositions of the hidden layered series and of the successive residual magmas. *Jour. Petrol.* **1,** 364–398.

——— AND W. A. DEER (1939) The petrology of the Skaergaard Intrusion, Kangerdlugssuak, East Greenland. *Medd. om. Grønland,* **105.**

WALKER, F. (1940) Differentiation of the Palisade diabase, New Jersey. *Geol. Soc. Am. Bull.,* **51,** 1059–1106.

——— AND NICOLAYSEN, L. O. (1954) The petrology of Mauritius. *Col. Geol. Min. Res.* **4,** 3–43.

——— AND POLDERVAART, A. (1949) Karroo dolerites of the Union of South Africa. *Geol. Soc. Am. Bull.* **60,** 591–706.

WATERS, A. C. (1961) Stratigraphic and lithologic variations in the Columbia River basalt. *Am. Jour. Sci.* **259,** 583–611.

WENTWORTH, C. K. AND H. WINCHELL (1947) Koolau basalt series, Oahu, Hawaii. *Geol. Soc. Am. Bull.* **58,** 49–78.

WEST, W. D. (1958) The petrography and petrogenesis of forty-eight flows of Deccan trap penetrated by borings in western India. *Trans. Nat. Inst. Sci. India.* **IV** (1), 1–56.

WILKINSON, J. F. G. (1957) The clinopyroxenes of a differentiated teschenite sill near Gunnedah, New South Wales. *Geol. Mag.* **94,** 123–134.

——— (1958) The petrology of a differentiated teschenite sill near Gunnedah, New South Wales. *Am. Jour. Sci.* **256,** 1–39.

WILLIAMS, H. (1933) Geology of Tahiti, Moorea, and Maiao. *Bernice P. Bishop Museum Bull.* **105.**

WINCHELL, H. (1947) Honolulu series, Oahu, Hawaii. *Geol. Sco. Am. Bull.* **58,** 1–48.

YAGI, K. (1953) Petrochemical studies of the alkali rocks of the Morotu district, Sakhalin. *Geol. Soc. Am. Bull.* **64,** 769–810.

YODER, H. S. AND C. E. TILLEY (1957) Basalt magmas. *Carn. Inst. Washington Year Book,* **56,** 156–161.

——— AND C. E. TILLEY (1960) Simple basalt systems. *Carn. Inst. Washington Year Book,* **59,** 67–69.

MINERALOGICAL SOCIETY OF AMERICA, SPECIAL PAPER 1, 1963
INTERNATIONAL MINERALOGICAL ASSOCIATION, PAPERS, THIRD GENERAL MEETING

# CRYSTALLIZATION OF LEUCITE-NEPHELINE-SANIDINE IN BASIC DIFFERENTIATES FROM A PERIDOTITE-DUNITE MASS IN SALEM, MADRAS STATE, INDIA

P. R. J. NAIDU
*Department of Geology and Geophysics, University of Madras, Madras, India*

ABSTRACT

The potassic rocks of Salem occur as dikes and sheets within or marginal to a dunite-peridotite mass that has intruded into Archean Peninsular gneisses, charnockite series, pyroxenites and dolerites. The rocks are porphyritic with euhedral crystals of olivine and augite set in a ground mass consisting of (1) leucite-pseudoleucite-sanidine, (2) nepheline, sanidine and nepheline-sanidine intergrowths, (3) sanidine laths or massive sanidine and (4) sanidine or orthoclase cryptoperthites. The texture resembles that of lamprophyres. Both the rocks and the residua have been chemically analysed, and interpreted on the $SiO_2$-$NaAlSiO_4$-$KalSiO_4$ diagram of Schairer and Bowen (1935). It is held that the magma crystallized under high water vapor pressure and that the field of leucite was restricted. Consequently, the pseudoleucite reaction was restricted to a narrow range in time, and the crystallization of nepheline and sanidine, and nepheline-sanidine intergrowths was the end product of the differentiation of these potassic rocks.

## INTRODUCTION

Basic plutonic potassic rocks have been reported by W. H. Weed and L. V. Pirsson (1901) from the Shonkin Sag laccolith. The shonkinite reported from there consists of augite, olivine, biotite, apatite, and magnetite in a matrix of potash feldspar, zeolites and carbonates, with pseudoleucite appearing conspicuously in a chilled marginal phase. A somewhat similar series of rocks was noticed by the author and S. Ramanathan in Salem, Madras State, India, in 1953, and the rocks were described, under the author's guidance, by S. Ramanathan (1954). In these rocks, zeolites and carbonates are absent. Leucite and sporadic pseudoleucite occur in some dike phases. Nevertheless, on account of their close resemblance, mineralogically and chemically, to the shonkinites and missourites, they have been described as the "shonkinite series" of Salem.

A map of the area, prepared for the present paper by N. L. Rao, is presented in Fig. 1. The country consists of Archean Peninsular gneisses, charnockite series, pyroxenites and dolerites, which have been intruded by a dunite-peridotite mass. The potassic rocks occur in this mass as marginal sheets or dikes. The dunite-peridotite mass is now largely converted to magnesite, serpentine, mica, asbestos and other hydrous minerals. The magnesite is the largest deposit of its kind in India.

## DESCRIPTION

The potassic rocks are black to dark gray and look like lamprophyres. Under the microscope they show a panidiomorphic texture with euhedral to subhedral crystals of olivine and augite, set in a groundmass, which may consist of, (1) leucite, pseudoleucite and sanidine, (2) nepheline, sanidine and intergrowths of nepheline-sanidine, (3) sanidine laths or massive sanidine and (4) sanidine, or orthoclase cryptoperthites (Figs. 2–8). Of these four types of matrices, the first two occur in small dykes and the last two in the main mass. Their distribution is indicated in Fig. 1. The percentages of the area occupied by the four varieties of rocks is:- 1.3(1):0.2(2):3.0(3):95.5(4). In the bulk of the mass, therefore, the matrix consists of sanidine or orthoclase cryptoperthites.

The olivine is both fayalitic and forsteritic and shows optic axial angles ranging from $2V(+)=72°$–$85°$ to $2V(-)=78°$–$82°$. In some crystals inclusions are arranged zonally. The augite is diopsidic and gives Optic axial angles ranging from $2V(+)=55°$–$60°$, to $2V(+)=65°$–$78°$, and $Z\wedge C=42°$–$57°$. The crystals are zoned, some having as many as thirty-five zones that show a small variation in extinction angles. Twinning parallel to {100}, lamellar twins, herring-bone twins and staurolite-like twins are common. Rimmed crystals give varying optic axial angles, the core has $2V(+)=59°$, and the rim $2V(+)=61°$. They have sometimes inclusions parallel to all the pinacoids or irrational faces. They are poikilitic with olivine. At contacts with sanidine, both olivine and augite are altered to phlogopite, which may cut across and along the cleavages. Both olivine and augite may occur sparingly as tiny grains in the various matrices. When there is micaisation in the rocks, the iron oxides are also rimmed by phlogopite.

The potash feldspars give optic axial angles ranging from 0° to $44°(-)$ or $50°(-)$ to $66°(-)$. As it

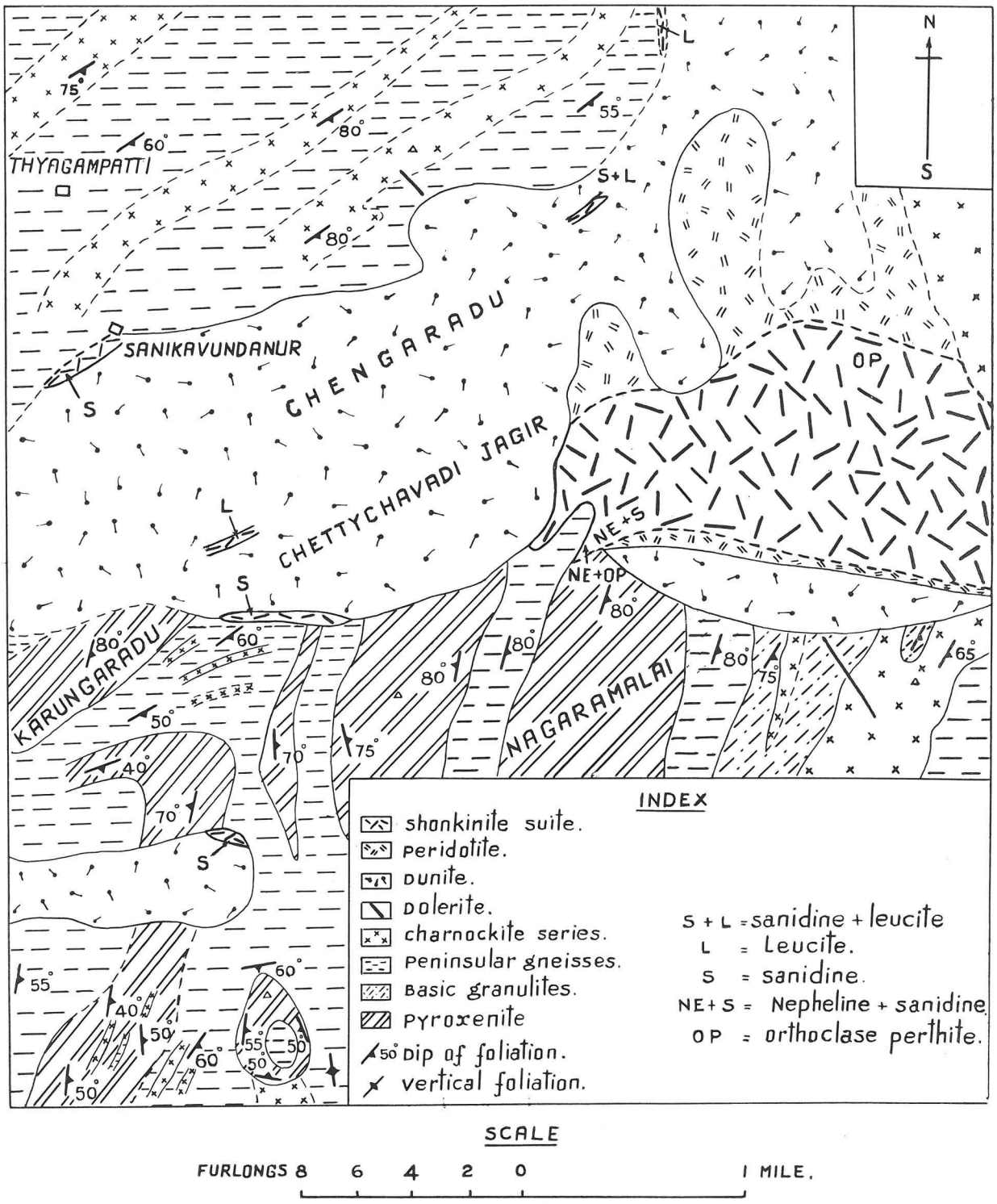


FIG. 1. Geological map of Nagaramalai, Salem, Madras State, India.

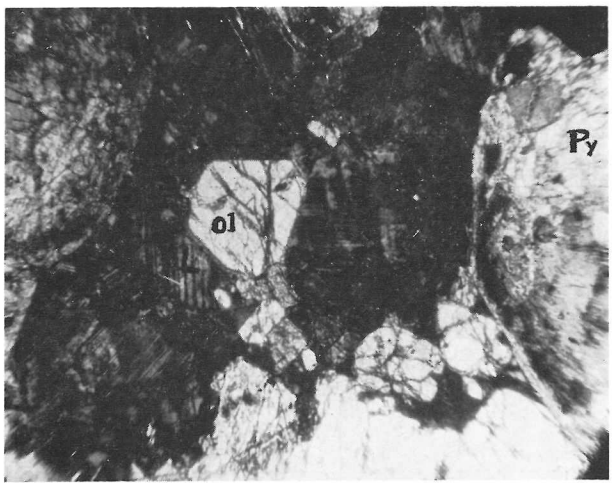


FIG. 2. Interstitial leucite with lamellae, L = Leucite, Ol = Olivine, Py = Pyroxene. Nicols crossed, ×26

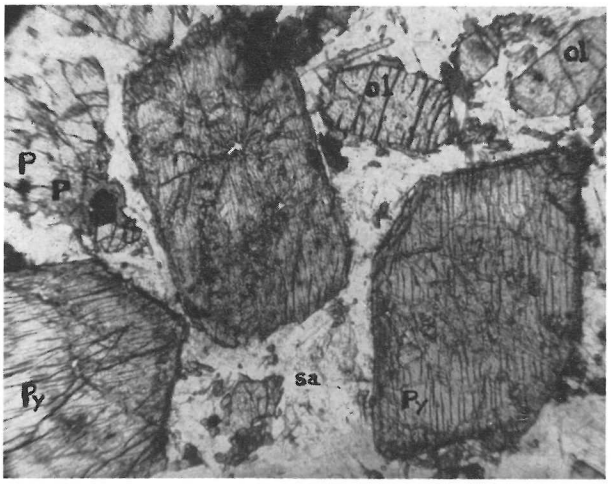


FIG. 4. Interstitial massive sanidine, Sa = Sanidine, Py = Pyroxene with reaction rims, Ol = Olvine, P = Phlogopite. Nicols not crossed, ×26.

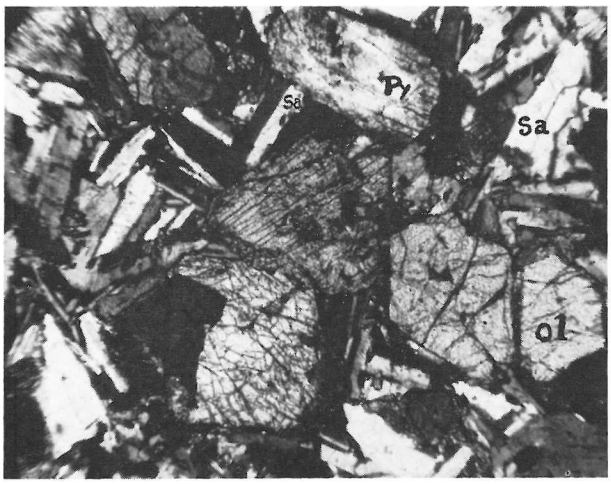


FIG. 3. Interstitial sanidine laths, Sa = Sanidine, Ol = Olivine, Py = Pyroxene. Nicols crossed, ×26

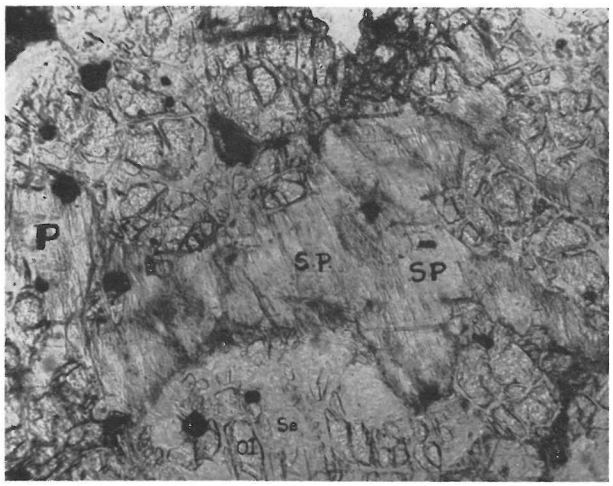


FIG. 5. Interstitial sanidine perthites S.P. = Sanidine perthites, Ol = Unaltered olivine, Se = Serpentine; P = Phlogopite. Nicols not crossed, ×70.

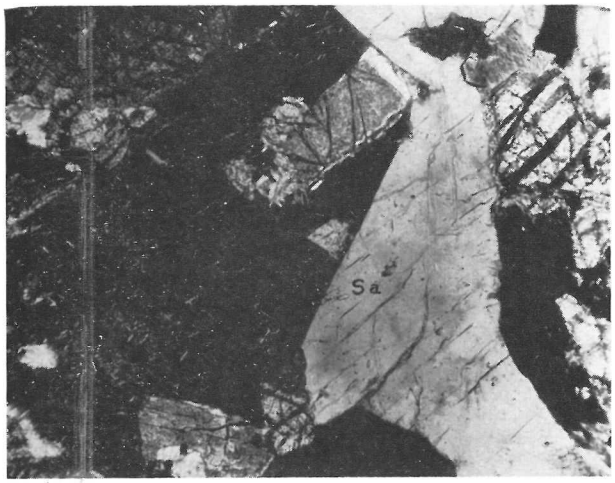


FIG. 6. Symplectitic intergrowths of nepheline and sanidine, (100) of sanidine parallel to prism of nepheline Y=E, Sa=Sanidine. Dark portion with crystallites=Nepheline. Nicols crossed, ×70.

FIG. 8. Interstitial massive sanidine with brown pleochroic patches and faint lamellae. Nicols crossed, ×70

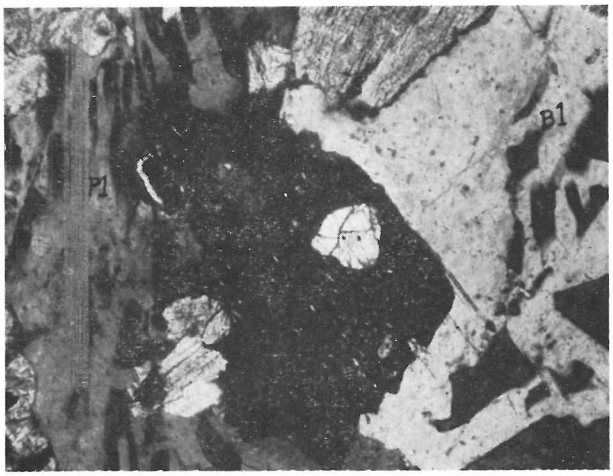


FIG. 7. Intergrowths of nepheline and sanidine, plumose or dactylic and bleb type, Bl=Bleb type; Pl=Plumose type. Dark portion with crystallites=discrete grain of nepheline. Nicols crossed, ×70.

TABLE I. MODES OF THE POTASSIC ROCKS OF SALEM

| | 1 | 2 | 3 | 4 | 5 | 6 | 7 | 8 | 9 | 10 | 11 | 12 |
|---|---|---|---|---|---|---|---|---|---|---|---|---|
| Sanidine including sanidine cryptoperthite | 44.2 | 44.0 | 29.8 | — | 49.2 | 44.3 | 17.9 | 16.4 | 11.2 | 2.2 | 2.5 | 0.7 |
| Orthoclase including orthoclase cryptoperthite | — | — | — | 34.6 | — | — | — | — | — | — | — | — |
| Pseudoleucite | — | — | — | — | — | — | — | — | — | 2.4 | 2.4 | — |
| Nepheline | — | — | 6.1 | — | — | — | — | — | — | — | — | — |
| Nepheline-sanidine intergrowth | — | — | 11.8 | — | — | — | — | — | — | — | — | — |
| Leucite | — | — | — | — | — | — | — | — | — | 13.5 | 17.2 | — |
| Olivine | 12.7 | 13.5 | 16.8 | 20.7 | 15.6 | 10.9 | 26.1 | 74.7 | 75.4 | 43.0 | 37.1 | 24.5 |
| Augite | 36.8 | 37.2 | 22.0 | 34.7 | 29.7 | 42.4 | 53.6 | 4.5 | 3.4 | 36.9 | 37.1 | 71.8 |
| Mica | 5.2 | 4.1 | 12.4 | 6.8 | 4.2 | 1.1 | 1.4 | 4.2 | 6.9 | 1.8 | 3.5 | 0.9 |
| Accessories (Apatite, iron ore) | 1.1 | 1.2 | 1.1 | 3.2 | 1.3 | 1.3 | 1.0 | 0.2 | 3.1 | 0.2 | 0.2 | 2.1 |

TABLE II. ANALYSES OF THE BASIC POTASSIC ROCKS OF SALEM

| | Analyses | | | | | Niggli Basis | | | |
|---|---|---|---|---|---|---|---|---|---|
| | A | B | C | D | | | | | |
| $SiO_2$ | 50.55 | 48.87 | 50.10 | 48.31 | Kp | 14.58 | 16.10 | 13.77 | 35.35 |
| $TiO_2$ | 1.52 | 1.29 | 0.41 | 0.11 | Ne | 7.95 | 13.94 | 14.26 | 11.23 |
| $Al_2O_3$ | 6.97 | 9.44 | 13.81 | 18.73 | Ns | 1.27 | — | — | — |
| $Fe_2O_3$ | 0.29 | 2.33 | 0.35 | 1.79 | Cal | — | 0.33 | 7.94 | 6.94 |
| FeO | 7.93 | 7.57 | 4.91 | 6.16 | Cs | 18.06 | 14.05 | 12.58 | 8.37 |
| MnO | 0.43 | 0.42 | 0.15 | Tr | Sp | — | — | — | — |
| MgO | 13.11 | 12.15 | 11.66 | 4.56 | Fs | 0.33 | 2.43 | 0.43 | 1.82 |
| CaO | 12.22 | 9.57 | 11.45 | 8.14 | Fo | 26.95 | 25.00 | 23.43 | 9.42 |
| $Na_2O$ | 1.97 | 2.61 | 2.74 | 2.11 | Fa | 9.55 | 9.13 | 5.67 | 6.88 |
| $K_2O$ | 4.13 | 4.56 | 3.99 | 10.12 | Ru | 1.05 | 0.88 | 0.27 | 0.05 |
| $P_2O_5$ | Tr | Tr | — | — | Cm | — | — | — | — |
| $H_2O$ | 0.33 | 0.44 | 0.22 | 0.03 | Q | 20.26 | 18.14 | 21.65 | 19.94 |
| $H_2O^-$ | 0.06 | 0.16 | 0.10 | 0.10 | L | 22.53 | 30.57 | 35.97 | 53.52 |
| Total | 99.51 | 99.41 | 99.89 | 100.16 | M | 57.21 | 51.49 | 42.38 | 27.54 |

A. B, C Analyst: S. Ramanathan, Oil and Natural Gas Commission, Government of India.
D Analyst: S. Saravanan, Analytical Chemist, Department of Geology and Geophysics, University of Madras.
A Rock with a matrix of sanidine.
B Rock with a matrix of nepheline, sanidine and nepheline-sanidine intergrowths.
C Rock with a matrix of sanidine and orthoclase perthites.
D Rock with a matrix of leucite and pseudolecuite.

*Q, Kp, Ne recalculated to 100*

| | A | B | C | D |
|---|---|---|---|---|
| Q | 45 | 39 | 43 | 30 |
| Kp | 35 | 33 | 28 | 53 |
| Ne | 20 | 28 | 29 | 17 |

is not possible to determine on the Fedorow stage optic axial angles below 20°, only angles above this value are recorded. The rest are inferred to be uniaxial when they answer the uniaxial test. The optic axial plane, whenever it is possible of determination, is perpendicular to (010). These feldspars are sanidine and orthoclase (Tuttle, 1952) and are classified as follows: Grains showing $2V(-)=0°–40°$ and lath-shaped as sanidine laths; when not lath-like as massive sanidine; when perthitic as sanidine cryptoperthites, grains showing $2V(-)=50°–66°$ as orthoclase; and when perthitic, as orthoclase cryptoperthites. Intergrowths of nepheline and sanidine, occurring in leucite-bearing rocks, are described as pseudoleucites. When there is no leucite present, but the nepheline-sanidine intergrowths occur along with discrete grains of nepheline and sanidine, they are not regarded as pseudoleucites.

Leucite, being interstitial, rarely has its common crystal shape, but, it shows the characteristic lamellar twinning. Some of the lamellae give optic axial

TABLE III. ANALYSES OF THE MATRICES OF POTASSIC ROCKS OF SALEM.

| | Leucite, pseudo-leucite & sanidine (1) | Sanidine laths (2) | Massive sanidine (3) | Sanidine perthites (4) | Nepheline and sanidine (5) |
|---|---|---|---|---|---|
| $SiO_2$ | 55.08 | 64.68 | 64.92 | 66.30 | 59.01 |
| $Al_2O_3$ | 24.01 | 18.10 | 18.05 | 18.41 | 22.69 |
| $K_2O$ | 20.71 | 16.30 | 16.21 | 14.38 | 12.72 |
| $Na_2O$ | 0.99 | 0.25 | 0.33 | 1.67 | 5.37 |
| Total | 100.79 | 99.33 | 99.51 | 100.76 | 99.79 |

Analyses calculated to molecules $SiO_2$ (O), $NaAlSiO_4$ (Ne) and $KAlSiO_4$ (Kp).

| | 1 | 2 | 3 | 4 | 5 |
|---|---|---|---|---|---|
| Q | 26.60 | 43.39 | 43.80 | 44.41 | 32.48 |
| Kp | 68.90 | 55.47 | 54.76 | 47.96 | 42.85 |
| Ne | 4.50 | 1.14 | 1.53 | 7.63 | 24.67 |

Analyst: S. Saravanan, Analytical Chemist, Department of Geology and Geophysics, University of Madras.

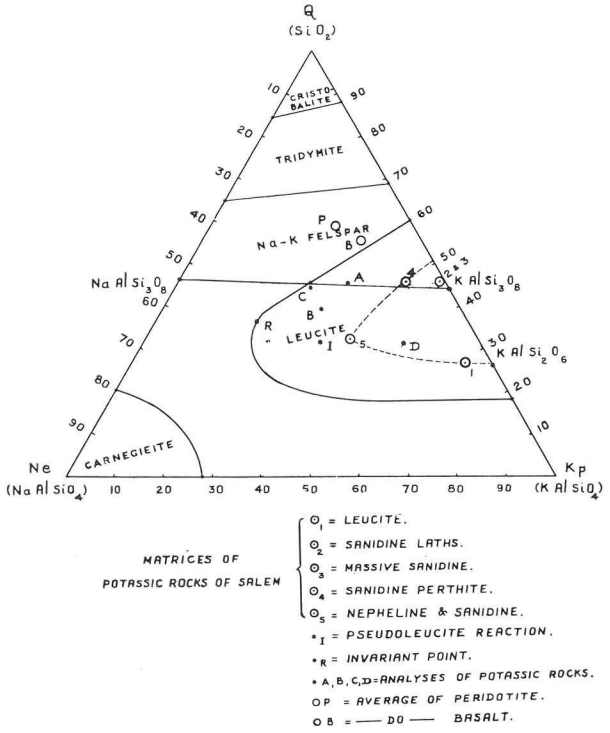


FIG. 9. Phase diagram of the system $SiO_2$(Q), $NaAlSiO_4$(Ne) – $KAlSiO_4$(Kp).

angles of 0° to 44°(−). They have reacted with the liquid to form sanidine. In other instances they have formed pseudoleucite.

## MODES

The modes of the basic potassic rocks are shown in Table I.

The modes show the relative variation of the mafic and felsic minerals indicating the role of crystallization-differentiation in the formation of these rocks. The presence of olivine and augite, in all the rocks, relates them to the peridotites and the dunites. The larger proportion of felsic constituents is generally parallel with the increase of augite. The early abundant crystallization of olivine and later of diopside-augite had rendered the residuum siliceous and alkalic (Bowen 1956).

## CHEMICAL DATA

Four of these rock types have been analyzed. The analyses are given in Table II along with their Niggli basis molecules.

The matrices of these rocks, after separating the mafics from them, were also analysed and the results are given in Table III.

The Q, Kp, Ne values of the analyzed rocks and the matrices are plotted in Fig. 9 which is the $SiO_2$–$KAlSiO_4$-$NaAlSiO_4$ phase diagram of Schairer and Bowen (1935).

## DISCUSSION

Treating the points, as lying in the system investigated, at one bar, all the rock analyses are seen to lie within the leucite field. They may all, therefore be regarded as crystallizing leucite, which reacted with the liquid and formed orthoclase and pseudoleucite in succession. The course of the magma was from D towards A, B and C, by the crystallization of residuum No. 1. At about C, residua Nos. 2, 3 and 4 crystallized. When the magma reached the invariant point R, residuum No. 5 crystallized. But, it may reasonably be assumed that, since the potassic rocks of Salem crystallized under plutonic conditions and high water vapor pressure, the field of leucite was restricted. (Bowen and Tuttle, 1950). The assumed restriction is indicated in dotted lines. Rock No. D is the only fraction that lies in the leucite field. It is regarded that D, by crystallizing fraction 1, moved on to A, where, by crystallization of fractions 2 and 3, the magma moved on to C, when fraction 4 crystallized. By this time, the magma was desilicated and moved on to B, where, it crystallized fraction 5, with the independent crystallization of nepheline and intergrowths of sanidine and nepheline. This fraction is therefore not regarded as pseudoleucite.

TABLE IV. MODES OF DISCRETE GRAINS OF NEPHELINE AND SANIDINE AND NEPHELINE-SANIDINE INTERGROWTHS

| | Discrete grains | | Nepheline-sanidine intergrowth | Percentage of nepheline to sanidine in the intergrowth | | App. proportion of discrete grains of nepheline and sanidine | App. proportion of nepheline to sanidine in the intergrowth | App. proportion of nepheline to sanidine in the whole rock |
|---|---|---|---|---|---|---|---|---|
| | Nepheline % | Sanidine % | | | | | | |
| Slide 1 | 12.90 | 62.03 | 25.07 | 42.06 | 57.94 | 1:5 | 2:3 | 1:3 |
| Slide 2 | 8.59 | 67.13 | 24.10 | 32.96 | 67.04 | 1:8 | 1:2 | 1:5 |
| Slide 3 | 13.61 | 37.04 | 49.35 | 37.89 | 62.11 | 1:3 | 2:3 | 1:2 |

The proportion of discrete grains of nepheline and sanidine to nepheline-sanidine intergrowths and the proportion of nepheline to sanidine in the intergrowths themselves, was estimated in three slides by point-counter, and the results are tabulated in Table IV.

If all the intergrowths of nepheline and sanidine were pseudoleucites, the proportion of nepheline to sanidine in residuum 5, Fig. 9, would be 1:3. This proportion is not born out by all the estimated modal proportion in the slides.

## References


Bowen, N. L. (1956) *The Evolution of the Igneous Rocks*, Dover Publications Inc., New York, 332.

——— and R. B. Ellestad (1937) Leucite and pseudoleucite *Am. Mineral.* **22,** 409–415.

——— and O. F. Tuttle (1950) The system $NaAlSi_3O_8$-$KAlSi_3O_8$-$H_2O$. *Jour. Geol.* **58,** 489–517.

Ramanathan, S. (1954) Shonkinites from the ultrabasic areas of Salem, *Jour. Madras Univ.* **XXIV** (3), 315–333.

Schairer, J. F. and N. L. Bowen (1935) Preliminary report on equilibrium relations between felspathoids, alkali feldspar and silica. *Am. Geophys. Union Trans.* **1,** 325–328.

Tuttle, O. F. (1952) Optical studies on alkali feldspars. *Am. Jour. Sci. Bowen vol.* 553–567.

Weed, W. H. and L. V. Pirsson (1901) Geology of the Shonkin Sag and Palisade Butte, *Am. Jour. Sci.* **12,** 1–17.

MINERALOGICAL SOCIETY OF AMERICA, SPECIAL PAPER 1, 1963
INTERNATIONAL MINERALOGICAL ASSOCIATION, PAPERS, THIRD GENERAL MEETING

# STUDIES OF CRYSTAL SURFACES

ICHIRO SUNAGAWA
*Geological Survey of Japan, Kawasaki-shi, Japan*

ABSTRACT

Four instances of imperfection or disorder in crystals are presented and interpreted in this paper. They are all obtained through the studies of crystal surfaces of silicon carbide and hematite. This paper consists of two parts; part 1 deals with observations on silicon carbide crystals and part 2 deals with the first direct observation of twinning due to stacking faults in hematite.

Part 1: It is clarified that the so-called single crystals are often not single but consist of several different polytypic domains having different $c_0$ values or even belonging to different crystal systems. They also sometimes consist of complicated twinned domains. Existence of stacking faults in silicon carbide crystals is also proved from the orientation of epitaxially grown impurity crystals on the surface of growth layers.

Part 2: The first direct evidence of twinning due to stacking fault is observed on the surface of the basal plane of natural hematite crystals. Three examples are shown. They consist of two sets of oppositely orientated triangular growth layers. In every case, it is noticed that one set of triangular laye has the height of a fractional multiple of that of the other set. The final level difference between the two sets of growth layers is measured to be less than 7Å and is considered to be one layer height in the unit cell. Structural consideration of hematite suggests that stacking faults with an odd number of layers missing from the normal stacking sequence can produce twinning structure parallel to the basal plane. The observed surface patterns can be explained in terms of twinning due to stacking fault.

## INTRODUCTION

Since growth and dissolution of crystals take place through the surface of crystal faces, the crystal surfaces are the places where all phenomena concerning crystal growth and dissolution are most vividly reflected. Therefore, by studying surface structures of crystal faces, we are able to know the mechanism, process or history of crystal growth and dissolution. It is also possible to know the behavior of internal imperfections or disorders of crystals such as dislocations, stacking faults, etc., since their existence will affect greatly the surface patterns formed by growth or dissolution. Surface structures of crystal faces will also exhibit the differences in growth conditions, as well as the history that the crystals have experienced after their formation, since the difference in growth conditions will result in different growth patterns. Therefore, it can be said that the studies of surface structures of crystal faces are very important not only in studying genetical or dynamical nature of crystals, imperfections in crystals, but also to solve various geological or mineralogical problems.

Fortunately, remarkable developments in methods of observation and measurement have recently been achieved, and we are now able to study every minor detail of surface structures. Using a sensitive reflection phase contrast microscope, it is possible to observe growth layers as thin as a few Å. In fact, the writer has succeeded in observing spirals having a step height of only 2.3 Å, 4.6 Å or 7 Å on the basal plane of hematite crystals (Sunagawa, 1961). These values are in fact smaller than the height of one unit cell of hematite. The height or depth of such extraordinary thin growth layers or dissolution features can be precisely measured by the methods of multiple-beam interferometry and of fringes of equal chromatic order (Tolansky, 1948). With these methods, we can measure step height down to 10 Å, and if the indirect method is applied, it is possible to measure a height of less than this value. Therefore by using these sensitive methods of observation and measurement adequately, we can make a thorough survey of every minor detail of crystal surfaces, and so can discuss the mechanism of growth or dissolution and other problems relating to growth or dissolution in terms of a unit cell or on an atomic scale. We are also able to observe directly dislocations or stacking faults in crystals.

The writer has been engaged in studies of crystal surfaces of natural hematite from many localities, silicon carbide made at several different factories, natural and synthetic diamonds, pyrite and quartz. Many interesting results have been obtained through these studies, and some of them were reported previously (Sunagawa, 1958, 1960a, b, c, d, Seager & Sunagawa, 1962; Tolansky and Sunagawa 1959, 1960).

In this paper, four examples showing imperfection or disorder in crystals will be presented and interpreted. They contradict our general beliefs on the

nature of crystals. The first three pieces of evidence to be presented in part 1 are observed on silicon carbide crystals, and the evidence presented in part 2 is observed on hematite. The interpretations to be discussed are all based on the following principles.

1. When growth spirals or growth layers—specifically those not having very big step height, namely less than several unit cell height—take on polygonal forms, the symmetry of the polygons is strictly in accordance with the symmetry of the face on which they appear. If a crystal face has a three-fold axis, polygonal spirals or growth layers will take on triangular forms, and if a face has a six-fold axis they will take on hexagonal form. This has invariably been observed on a large number of crystals which the writer has studied so far. Therefore, it is possible to conjecture the crystal system from the symmetry elements of growth spirals.

2. Growth spirals, growth layers or etch pits which have polygonal forms and have small step heights or depths are orientated in one direction on the whole surface of a crystal face, if the crystal is single, and oppositely orientated on the opposite sides of a twin boundary, if the crystal is a contact twinned (Sunagawa 1960b). If a surface pattern which is contradictory to this is observed, it shows that there must be some kind of disorder.

3. According to Frank's (Frank, 1951) and Mitchell's (Mitchell, 1956, 1957) theory, different polytypes of silicon carbide or cadmium iodide are formed from screw dislocations having different Bergers' vector. If this theory is correct, spirals having different step heights will belong to different polytypes, provided that they originate from single screw dislocation point and that the height of one spiral layer is a fractional multiple of that of the other.

## Part 1. OBSERVATIONS ON SILICON CARBIDE CRYSTALS

### Coexistence of Different Polytypes in Single Crystals

If a crystal possesses single external form and yields a single $x$-ray diffraction pattern, we consider it a single crystal. In practical procedure, we make $x$-ray analyses of a crystal having single external form, presuming that the crystal is single.

However, if detailed studies are made of the surface structures of such single crystals of silicon carbide, we are surprised to find that they often consist of several different polytypic domains. On the surface

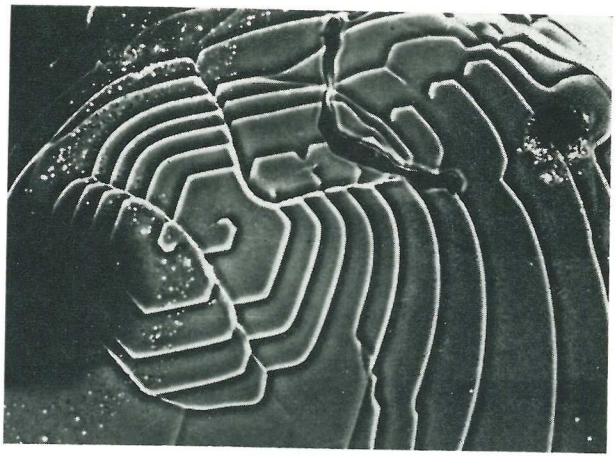

Fig. 1. Hexagonal spiral, positive phase contrast, ×250.

of basal planes, we often find that there are several spirals having different forms and step heights. In Figs. 1 and 2, two different spirals observed on one basal plane of a silicon carbide crystal are shown. The spiral in Fig. 1 has hexagonal form, which suggests that it belongs to a hexagonal polytype, whereas the spiral in Fig. 2 has regular triangular form, which shows that it belongs to a rhombohedral polytype. In Fig. 2, one can see on the lower left part of the photograph layers having regular hexagonal form, which clearly proves the coexistence of hexagonal and triangular spirals on the same surface. Step heights of the two spirals are quite different as can be seen from the width and brightness of white diffraction bands appearing along spiral steps in the phase contrast photomicrographs. Therefore, it can be said that this crystal, though having singular external form of hexagonal platy habit, is in fact not single but consists of two different polytypes.

Fig. 2. Triangular spiral, positive phase contrast, ×1000.

FIG. 3. Hexagonal spiral belonging to 6H polytype, positive phase contrast, ×1000.

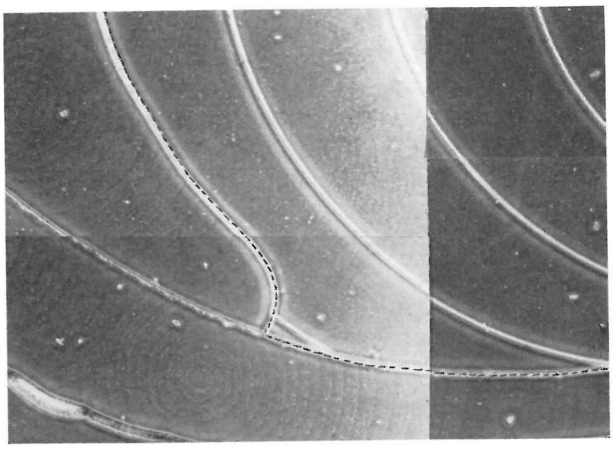

FIG. 5a. Built up positive phase contrast photomicrograph showing domain boundary, ×200.

Fig. 3 and 4 show two hexagonal spirals on the same surface of another silicon carbide crystal which has a regular hexagonal, thin, platy habit. Both spirals have hexagonal forms, but the former's hexagon is regular, while the latter spiral shows typical interlacing pattern. (The meaning of dots observed on both spirals will be reported elsewhere.) The step heights of the two spirals are measured with the method of multiple-beam interferometry. It is found that the former spiral has step height of 15 Å, while the latter has 10 Å. This shows that the former spiral belongs to 6H polytype, while the latter to 4H polytype. Here again, it is definitely proved that on one crystal face of a single crystal there are two different polytypes.

Figure 5 shows another example. In this photograph, we notice a typical circular spiral having very small step height in the lower and left part of the picture and very thick circular growth layers on the upper and right part. At the centre of the latter growth layers, there are typical circular spirals originating from three screw dislocation points, as shown in Fig. 5. The latter circular growth layers originate from these screw dislocations. The step height of the latter spiral layer is estimated to be very large, probably more than 1000 Å, whereas that of the former spiral will not exceed 50 Å. These two possibly belong to different polytypes, although it has not been proved up to the present time as their step heights are not precisely measured. However, the reason that the writer presents this photograph is to show the boundary between the two supposed-to-be polytypes. There is clear discontinuity between the two domains as shown by a dotted line. This sort of

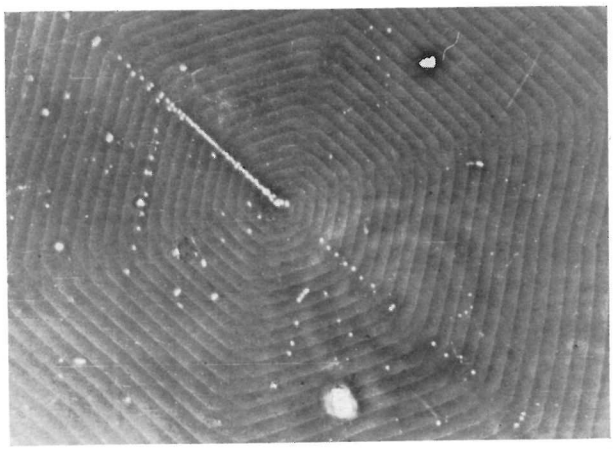

FIG. 4. Hexagonal spiral belonging to 4H polytype, positive phase contrast, ×1000.

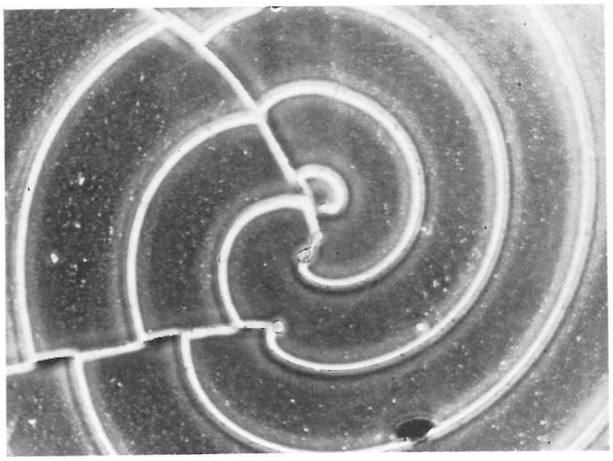

FIG. 5b. Positive phase contrast, ×350.

discontinuity is seen at the boundary between different polytypic domains in every case. Inside of one polytypic domain, no discontinuity of growth layers is seen.

The above described phenomena are not at all exceptional but are commonly observed on many silicon carbide crystals, as well as on some hematite crystals. These observations clearly show that the so-called single crystals are often not single but consist of different polytypes, which have different $c$ and even belong to different crystal systems, and give an alarm to $x$-ray studies of polytypism. In an $x$-ray analysis of this sort of single crystal, we may get an $x$-ray pattern which is an integral of several different polytyes. Such a pattern is difficult to distinguish from the $x$-ray patterns of a real single crystal having a $x$-ray repeat distance which is equal to the integral of several different repeat distances. Therefore, $x$-ray analyses of such crystals may sometimes lead to a wrong conclusion and produce a new polytype which does not really exist. It is strongly suggested to make a thorough study of crystal surfaces before carrying out $x$-ray studies of polytypism.

### Twinning Observed on the So-called Single Crystals of Silicon Carbide

As stated in principle 2, polygonal spirals or growth layers are orientated in one direction on the whole surface of one crystal face of a single crystal. However on some crystals of silicon carbide, evidences which show contradiction to this principle have been found, though the crystals have perfectly single external forms.

Figure 6 shows an example of such a case schematically. Two triangular spirals having rounded corners appear close together on the basal plane of one single crystal. There is a clear discontinuity between the two spirals. It is clearly noticed that the two triangles are oppositely oriented, which shows that the two are in a twin relation.

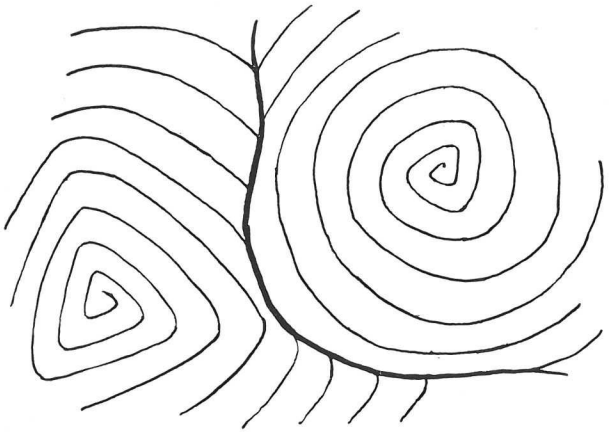

Fig. 6. Schematic figure showing two spirals in twin relation on one crystal face.

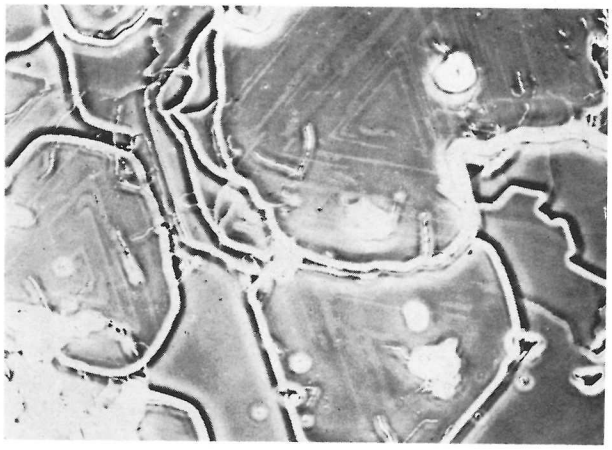

Fig. 7. Complicated twin domains observed on the basal plane of one silicon carbide single crystal. Positive phase contrast, ×250.

Figure 7 shows another example of much complicated twinning. This crystal came from the Norton Co. and has hexagonal habit with perfectly single appearance. The crystal received etching while it was still in furnace, as can be seen from the characteristics of surface structures. There are areas surrounded by broad white lines, which are considered to be domain boundaries. One triangular spiral occurs on one domain. It is noticed that some triangles of these spirals have opposite orientations in respect to the neighboring triangular spirals, but some are in the same orientation. This shows that some domains are in the twin position in respect to the other domains. In other words, this crystal, though having perfectly single appearance, consists of many domains which are in the twin relation with each other.

These observations again show that the crystal which we treat as a single crystal is in fact not single but consists of many twinned domains. It should be noted here that $x$-ray analyses of such crystals will not show the existence of twinning, especially in the case of the first example, since such spirals often occupy only a very thin part of the topmost surface of a crystal, as typical spirals are usually formed at the latest stage of growth. (Sunagawa 1960d, 1962). This again shows the necessity for studies of crystal surfaces before carrying out $x$-ray studies.

### A Proof of Existence of Stacking Fault in Silicon Carbide Crystals

Figure 8 is a positive phase contrast photomicrograph of the surface of a single crystal of silicon carbide from the Norton Co. The crystal has thin hexagonal platy habit. Broad white lines running horizontally across the photograph are edges of very thick growth layers having step height of more than a few thousand Å. On the surface of these thick growth layers are many small star-like patterns. They sometimes aggregate together forming triangular pattern with a white circle at the centre. Since these patterns appear bright on the positive phase contrast photograph, they are all elevated. Since this type of growth feature has never been observed on any silicon carbide crystals and is quite different from ordinary growth features of silicon carbide, both the star-like and triangular elevations are considered to be impurity crystals which are epitaxially grown on the surface of the crystal. As it can be clearly seen on the photograph, these star-like patterns have the same orientation, without a single exception, on the whole surface of one growth layer but have entirely opposite orientation on the surfaces of the two neighboring layers. The stars on A layer are orientated oppositely in respect to those on B and C layers but are orientated in the same direction as those on D layer. If the surface of these thick growth layers have the same atomic arrangement, the epitaxially grown impurity crystals should also be arranged in one direction on the surfaces of every growth layer. However, if there is a stacking fault between the two successive layers, the surface of the two layers will have different (oppositely orientated) atomic arrangement, as silicon carbide has a polar structure. This will naturally result in the opposite orientation of epitaxially grown impurity crystals on the surface of the two layers. This is in fact the case. Therefore, it is quite safe to conclude that there are stacking faults in this crystal.

Fig. 8. Photomicrograph showing the existence of stacking fault in silicon carbide crystal. Positive phase contrast, ×1000.

## Part 2. TWINNING OF HEMATITE DUE TO STACKING FAULT

### Introduction

It has been theoretically conjectured that stacking fault can produce twinning. For instance an attempt has been made to interpret the origin of polysynthetic twinning, such as that of plagioclase feldspar in terms of stacking faults arising during growth. However, these are merely theoretical assumptions, and no clear experimental evidence of twinning due to stacking faults has yet been reported (Cahn, 1954).

Surfaces of the basal plane of hematite crystals usually exhibit thick growth layers of irregular or triangular shape. On the surface of these thick layers there are many thinner growth layers or growth spirals. These thinner growth layers at times have circular form, but in most cases they have a triangular form. These triangles are all orientated in the same direction over the whole surface, if a crystal is single. If the crystal is contact twinned, they have opposite orientations on opposite sides of the twin boundary, irrespective of the orientation of the twin boundaries. This was clearly demonstrated in the writer's previous study (Sunagawa 1960b).

It has been noticed from observations on large numbers of crystals from different localities that almost all crystals have the pattern of either a single or contact twinned crystal. In almost all cases, the triangular growth or etch patterns do not overlap each other, nor do two sets of oppositely orientated triangles coexist on the surface of a single crystal. However, on a very few crystals, it has been observed that on the surface of a single crystal there are two sets of triangular growth layers oppositely orientated. Such a pattern can only be explained in terms of twinning parallel to the basal plane. Considerations of the hematite structure in terms of a layer structure indicate that this twinning formed through a stacking fault during growth. The observations reported here are, as far as the writer knows, the first clear evidences of twinning due to stacking faults. Evidence from three examples showing twinning due to stacking fault will be described.

## Observations

The first evidence is furnished from several crystals from Gihofuji, Japan. The surfaces of the basal planes of these crystals consist of thick triangular growth layers. On the surface of these thick growth layers, there are thinner triangular growth layers which originate from rows of screw dislocations and have very small step heights. They form complicated and combined spiral patterns. The orientation of these thin triangular growth layers is strictly crystallographic and has one direction over all the surface. However, it is noticed that many small tongues project along the fronts of these thin triangular layers (a typical example of which is shown by arrows in Fig. 9). These tongues have several different forms, but they are principally the same and a deviation from a simple triangle. The most noteworthy point is that these tongues have a completely opposite orientation to that of the main thin triangular growth layers. In fact, if they are in the same orientation, no projections will be formed along the fronts of main growth layers.

Under low magnification, the tongues appear to start from a part of a front of main growth triangles and do not cross or cover the other fronts. But, if they are observed under high magnification, it is found that they can cover several growth fronts, as schematically shown in Fig. 10. As it can be seen in this figure, the step height of the tongue is neither the same as that of a single layer of the main thin triangular growth layers nor rational multiples of them. Careful investigation of the boundaries between the tongue and the main growth fronts show

FIG. 9. Positive phase contrast photomicrograph showing triangular tongues projecting along the fronts of triangular thin growth layers. Arrows show the tongues, ×250.

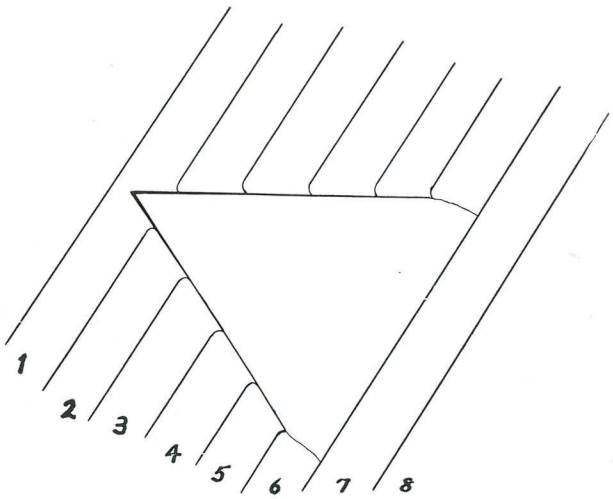


FIG. 10. Schematic figure showing the relation between triangular tongue and triangular thin growth layers.

that the surface of the tongue is higher than the surfaces of 1st, 2nd—6th main growth layers, but lower than the 7th, 8th, etc., layers in Fig. 10. Moreover, the surfaces of the tongue and the 6th layer are not on the same level but there is a very faint level difference between these two. Such relationships can be observed on every tongue.

Since the tongues are very small, it is virtually impossible to measure their step heights. It is also difficult to measure the step heights of the main thin growth layers, since they are irregularly spaced and very shallow. However, from the nature of white diffraction fringes appearing at the edges of these layers, the step heights can be roughly estimated. The heights of the tongues are estimated to be few tens of angstroms and that of the thinnest main growth layer is of the order of one unit cell height or even less than that. Therefore, the final displacement in height of the tongues and the main growth layers is considered to be less than a unit cell.

These observations clearly show that the tongues are not stacked on the substrate in the correct sequence. In other words, there must be stacking fault between the substrate and the tongues. Furthermore as the orientations of the tongues show, it is quite clear that the tongues are in the twin position to the main triangular layers (substrate), the twinning plane of which is c(0001). Therefore, it is safe to conclude that this twinning is formed by a stacking fault.

The second example appeared on a crystal from Saganoshima, Japan. More than half of the surface

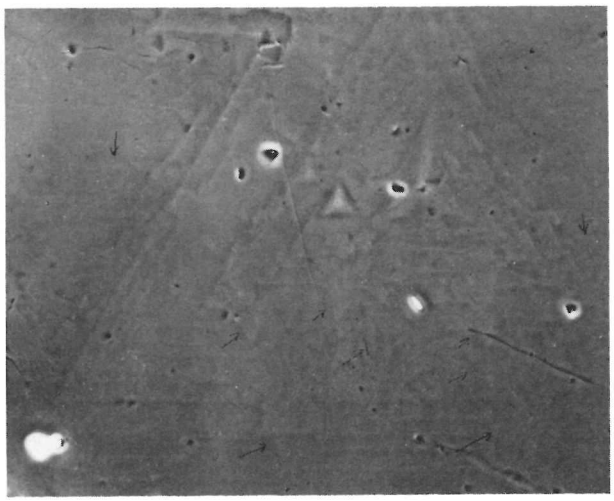

FIG. 11. Positive phase contrast photomicrograph showing the second evidence of twinning due to stacking fault. Arrows show projections, ×250.

of this crystal is flat and on it are more than ten triangular cones. The sides of these triangular cones are not straight but have many small triangular projections; Fig. 11 serves as an example. On the other parts of the surface, very thin straight growth fronts appear. Although the central parts of these growth fronts are not visible, the orientation of these fronts is certainly opposite to that of the triangular cones and nearly parallel to that of the triangular projections appearing along the sides of the cones. At several places on the surface, there are two sets of these oppositely orientated triangular layers. Noteworthy is the fact that the two sets of fronts do not cross each other, which clearly demonstrates that they are growth or etch fronts and not the lines formed by movement of dislocations (Seager and Sunagawa, 1962). For the following two reasons, these fronts are considered to be growth fronts and not etch fronts.

a) Triangular cones are commonly observed on other crystals in which they have been proved to be growth spirals.
b) Another set of triangular layers has very smooth fronts, which again can not be expected in the case of etching.

In the case of a contact twin, the triangular features have opposite orientations on opposite sides of a twin boundary, which appears like a discontinuity line of growth patterns. But on the surface of this crystal, no discontinuity line appears, and the two sets of triangular layers just overlap each other. This crystal therefore is not a contact twin but exhibits repeated twinning parallel to the basal plane. The thickness of the laminae of this polysynthetic twin is of the order of the height of one growth layer, which is estimated to be one unit cell or less.

Close investigation of the region where the two sets of layers coexist shows similar features as observed in the first example. It is reasonably safe to conclude that this polysynthetic twinning is also formed by successive stacking faults during growth.

The third example appears on one crystal from Saganoshima, Japan. Here, there is no projecting pattern on the surface which in fact reveals two different kinds of structure. There are triangular growth spirals with a step height of 7 Å and also triangular growth islands and tongue-like terraces with an average step height of about 40 Å. The tongue-like terraces are proved to be derived from the triangular growth islands. The mutual relationship between these two patterns shows that the spiral was formed after the formation of triangular islands (Sunagawa, 1960a).

These two growth patterns have opposite orientations, as schematically shown in Fig. 12. Close examination of the boundary between spiral fronts and the tongue-like terraces show that the heights of the tongue-like terraces and triangular islands are fractional multiple of the height of a single spiral layer; that is, 7 Å×n+0 to 7 Å. This level difference must be either 2.3 Å (one layer height in the unit cell) or 4.6 Å (two layers). The most probable level difference is 2.3 Å.

From these observations, therefore, it is quite clear that the spiral pattern is not stacked on the substrate in a correct sequence. In other words, there is a stacking fault between the spiral layers and the sub-

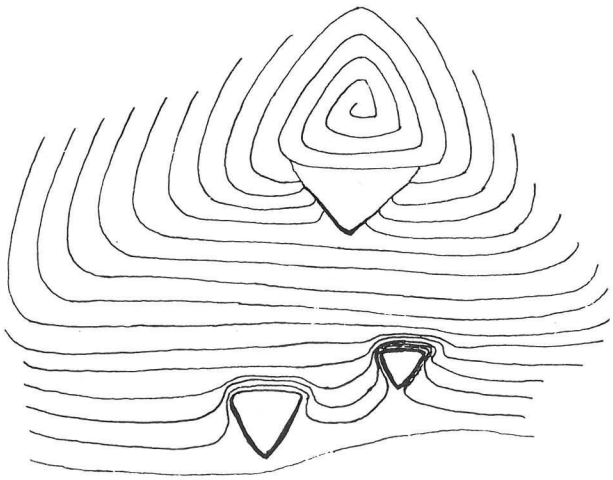

FIG. 12. Schematic figure showing the relation between the spiral and tongue-like terraces, triangular growth island.

strate which consists of triangular islands. Since these two triangular patterns have opposite orientations, it can be said that these two are in the relation of twinning, parallel to the basal plane, Thus, it is concluded that this twinning is formed by stacking faults.

## Structural Considerations

We have observed in this study three different appearances of twinning, the twinning plane of which is (0001) and these are considered to be formed through stacking faults. Perhaps the first and the most primitive example may not be called twinning in the common sense of terminology, but it certainly has the nature of twinning. The second example is certainly polysynthetic twinning, but the laminae are thinner than formerly reported. The third example is again not twinning in the common sense, but its characteristic is without doubt that of twinned crystals. In any case, the appearance is not that of a twinned crystal in the ordinary sense, but the character is exactly that of a twinned crystal, at least in the fundamental meaning of the word twinning.

Two main characteristics commonly observed in the three examples are as follows:

1) there are two sets of triangular features oppositely orientated on the one surface, 2) the step height of the one triangular feature is a fractional multiple of the other.

The first characteristic clearly shows that these two sets of triangular features are stacked upon each other in twin orientation. The second characteristic shows that there is a stacking fault between the two sets of features. Since the final level difference between these two features is less than 7Å as in the case of the second example and from the nature of the stacking in hematite structure, it is considered that the most probable arrangement of stacking faults in these cases is that one layer is missing in the structure.

Now, if we consider the structure of hematite to be in terms of a layer structure, we notice that the unit cell consists of six layers in the sequence of (ABABAB). Triangles consisting of three oxygen atoms in A layer have opposite orientations to those in B layer. If the next growth unit settles on the substrate having one or an odd number of layers missing, the resultant sequence will be (ABABAB) (BABABA) which is exactly the sequence of twinning. If two or an even number of layers are missing, the resultant sequence will be of a single crystal. Therefore, as a result of an odd number of layers missing, twinning can be formed parallel to the basal plane. This mechanism seems to explain satisfactorily the facts reported here. So far as the writer knows, the observations presented here are the first showing the existence of twinning due to stacking fault during growth.

## Conclusion

The evidence from the four examples presented in this paper definitely shows how real crystals are imperfect, far more imperfect than we had generally believed. Such imperfection in crystals is difficult to reveal by ordinary crystallographic methods. Detailed studies of crystal surfaces, using modern techniques can reveal such imperfections. The writer would like to stress the importance of studies of crystal surfaces, not only in studying imperfections of crystals, but also in studying many other crystallographic, mineralogical and geological problems.

## Acknowledgments

Main part of this work was done at Physics Department, Royal Holloway College, London University, and the remaining part at Geological Survey of Japan.

The writer expresses his gratitude to Prof. S. Tolansky of R.H.C. for his encouragement and kind permission of using the facilities of his department. He also wishes to thank the people and organizations who kindly supplied many specimens of hematite and silicon carbide, especially Dr. D. R. Hamilton of Westinghouse Research Laboratory. His thanks are also due to Mr. K. Komatsu, who helped in the observation of stacking fault in silicon carbide.

## References

Cahn, R. W. (1954) Twinned crystals. Advances in Physics, **3,** 363.

Frank, F.C. (1951) The growth of carborundum; dislocations and polytypism. *Phil. Mag.* **42,** 1014.

Mitchell R. S. (1956) Polytypism of cadmium iodide and its relationship to screw dislocations, 1. Cadmium iodide polytypes. *Zeit. Krist.* **108,** 296, 2. Explanation of the formation of polytypes of cadmium iodide. *Zeit. Krist.* **108,** 341.

——— (1957) A correlation between theoretical screw dislocations and the known polytypes of silicon carbide. *Zeit. Cryst.* **109,** 1.

Seager, A. F. and I. Sunagawa (1962) Movement of screw dislocations in hematite. *Mineral. Mag.* **33,** 1–8.

Sunagawa, I. (1958) Crystal growth of hematite from Ayumikotan, Japan. *Jour. Mineral. Soc. Japan,* **3,** 543

——— (1960a) Growth history of hematite. *Am. Mineral.* **45,** 566.
——— (1960b) Surface stucture of the twin boundary of hematite crystals. *Inst. "Lucas Mallada", Cursillos y Conferencias,* **7,** 47.
——— (1960c) Growth and etch features of hematite crystals from the Azores Islands, Portugal. *Serv. Geol. Port., Mem.* **6,** 1–44.
——— (1960d) Mechanism of crystal growth, etching and twin formation of hematite, *Mineral. Jour. Japan,* **3,** 59.
——— (1961) Step height of spirals on natural hematite crystals. *Am. Mineral.* **46,** 1216.
——— (1962a) Mechanism of growth of hematite. *Am. Mineral.* **47,** 1139.
——— (1962b), Mechanism of natural etching of hematite crystals. *Am. Mineral.* **47,** 1332.
TOLANSKY, S. (1948) *Multiple-beam interferometry,* Oxford at the Clarendon Press.
——— AND I. SUNAGAWA (1959) Spiral and other growth forms of synthetic diamonds. *Nature,* **184,** 1526.
——— AND I. SUNAGAWA (1960) Interferometric studies of synthetic diamonds. *Nature,* **185,** 203.

MINERALOGICAL SOCIETY OF AMERICA, SPECIAL PAPER 1, 1963
INTERNATIONAL MINERALOGICAL ASSOCIATION, PAPERS, THIRD GENERAL MEETING

# CLINOAMPHIBOLE REGRESSION STUDIES.
# I. REGRESSIONS OF OPTICAL PROPERTIES AND DENSITY ON COMPOSITION

HORACE WINCHELL
*Department of Geology, Yale University, New Haven, Connecticut*

ABSTRACT

Linear regression coefficients for five physical properties (refractive indices $n_x$, $n_y$, $n_z$; extinction angle $Z/c$; and density G) on 24 variables of chemical composition $(K,Na,Ca)_w(K,Na,Ca,Mn,Fe^{2+},Mg)_2(Ca,Mn,Fe^{2+},Mg,Ti,\ Fe^{3+},Al)_5(Ti,Fe^{3+},Al,Si)_8O_{22}(O,OH,F,H_2O)_2$ have been calculated by least-squares methods from data on about 400 analyses selected from the literature. These regressions yield high values for their coefficients of determination $R^2$ and variance ratio F, showing that they do empirically account for most of the variance.

Direct application of the present equations leads to preliminary predictions of the properties of a few interesting compositions in the clinoamphibole system, as follows: For tremolite $CaMg_5Si_8O_{22}(OH)_2$, $n_x=1.6005\pm.0012$, $n_y=1.6146\pm.0015$, $n_z=1.6266\pm.0017$, $Z/c=16.3°\pm1.7°$, $G=2.974\pm.014$. For tschermakite $Ca_2Mg_3Al_2Si_6Al_2O_{22}(OH)_2$ the same properties are 1.6259, 1.6362, 1.6460, 0.7°, and 3.068. For pargasite $NaCa_2Mg_4AlSi_6Al_2O_{22}(OH)_2$, they are 1.6253, 1.6319, 1.6408, 14.0°, 3.086. For hastingsite $NaCa_2Fe^{2+}{}_4Fe^{3+}Si_6Al_2O_{22}(OH)_2$, they are 1.7033, 1.7181, 1.7113, 30.1°, and 3.496. For glaucophane $Na_2Mg_3Al_2Si_8O_{22}(OH)_2$ they are 1.6083, 1.6064 [sic]. 1.6086, 35.1°, 3.042. The value of "$n_z$" is here the lowest index predicted for sections $\|010$, and "$n_y$" is the predicted value for light vibrating parallel to the symmetry axis $b$. For cummingtonite $FeMg_4Fe^{2+}Si_8O_{22}(OH)_2$ they are 1.6349, 1.6500, 1.6689, 13.5° and 3.239.

Special tests are being made to determine whether non-linear regressions may be required for some of the chemical variables, especially for the regression of extinction angle on composition. Full tables of regression coefficients, predicted values for end-members, and residual errors of prediction for nearly 800 analyzed specimens have been prepared.

Indirect uses for such regressions include the discussion of order-disorder problems, temperature of formation, etc.

## INTRODUCTION

Methods for computing regression coefficients have been well known among statisticians for many years; within the last few years the development of high-speed automatic computing machinery has made it possible for the first time to carry out such computations on a fairly large scale. Hey (1956) used the method to study the properties of a limited number of anthophyllites. Hori (1954), Henriques (1958a, b, c), Winchell and Tilling (1960), and Winchell (1961) applied it to clinopyroxenes. Henriques (1958d) used both first- and second-degree terms, for which there is theoretical, and in some cases practical justification. Similar studies have also been reported on garnet and other mineral groups.

Regression studies are in a sense no more than the analytical (algebraic) extension of the graphical methods that are familiar to all mineralogists. Regressions, however, remove the most serious limitation of charts, namely the necessity of picturing them on two-dimensional paper. After a third dimension is shown on the paper by means of isopleths (contour lines), it is difficult to consider any further dimensions in a meaningful way. A surprisingly rare device is to use many charts, as in the solution of a five-variable problem involving unknown quantities of thickness, birefringence, composition, and two variables of orientation in random sections of plagioclase twins (Nieuwenkamp, 1948; Laffitte, 1950).

For every advance in techniques there is a price to be paid; in the present case this is the price of substituting equations for the more familiar charts. We note the form, structure, and derivation of such equations in the next section, then consider their application to clinoamphiboles, and finally report the regression coefficients and some preliminary conclusions. Detailed discussion of applications will be reserved for a later report.

## LEAST SQUARES METHOD, REGRESSION EQUATIONS

*The least-squares method* (Acton, 1959; Davies, 1958; Fisher, 1958; Williams, 1959) seeks to reduce to a minimum the overall discrepancy between a set of data that presumably contains errors of measurement, and an equation that describes a relationship between two or more of the variables. This "discrepancy" is defined as the sum of the squares of the residuals, or differences between equation and observation. These residuals are commonly assumed to be distributed about zero (their mean) according to the familiar *normal curve of error*, This assumption turns out to be fairly accurate in most cases involving physical measurements; its accuracy affects the

validity of certain statistical estimates, but it seems relatively unimportant with respect to the regression coefficients themselves.

*Regression theory* (Acton, 1959; Davies, 1958; Fisher, 1958; Williams, 1959). In the absence of any information about the independent, or controlling variable x, its mean value $\bar{x}$ is taken as the most probable value, and the corresponding value of the dependent variable y is its mean value, $\bar{y}$. Any deviation of x from its own mean $\bar{x}$ may be due partly to a "random error of measurement," and partly to a real or valid deviation from $\bar{x}$. For a given value x′, the part due to error of measurement should have no effect upon the estimated value y′, but the part due to real deviation of x′ from $\bar{x}$ should cause a proportional difference between y′ and $\bar{y}$. Where there are several independent variables $x_1$, $x_2$, $x_3$, $\cdots$, $x_i$, $\cdots$, each one of these is assumed to contribute a portion, or component, of the deviation of y′ from $\bar{y}$, that is proportional to its own deviation from its own mean. Thus we have

$$y - \bar{y} = b_1(x_1 - \bar{x}_1) + b_2(x_2 - \bar{x}_2) + \cdots + b_i(x_i - \bar{x}_i) + \cdots$$

where the quantities $b_1$, $b_2$, $\cdots$, $b_i$, are the *regression coefficients* of y on the corresponding $x_i$. An alternative form of the same equation can be obtained by removing the parentheses and collecting the constant terms ($b_0 = \bar{y} + b_1\bar{x}_1 + b_2\bar{x}_2 + \cdots$), and rewriting as follows:

$$y = b_0 + b_1x_1 + b_2x_2 + \cdots + b_ix_i + \cdots + b_Ix_I \quad (1')$$

If we introduce a constant quantity $x_0 = 1$ the notation can be made more compact as follows:

$$y = \sum_{i=0}^{I} b_ix_i \quad (1)$$

The regression formula (1) may be made to represent not just one y, but a series of different dependent variables $y_1$, $y_2$, $\cdots$ ($y_p$ with $p = 1, 2, \cdots$) such as refractive indices $n_x$, $n_z$, extinction angle Z/c, density G, lattice constants a, b, c, etc., by introducing another subscript p so as to represent all the different regression equations at once as follows:

$$y_p = \sum_{i=0}^{I} b_{ip}x_i \quad (2)$$

*The standard error*, s, of an estimated quantity, z, is a commonly used measure of the uncertainty, or precision, with which z can be estimated. It is closely analogous to the standard deviation of a population about its mean, and is formally represented by a very similar equation. In the better methods for obtaining the regression coefficients $b_{ip}$, their respective standard errors $s_{ip}$ are made readily available. The standard error of regression may also be obtained; it is symbolized by $s_p$, and calculated from equation (3):

$$s_p^2 = \sum_{n=1}^{N} (y_{pn} - y'_{pn})^2/(N - I - 1) \quad (3)$$

where n designates the nth observation out of a total of N, and y and y′ are the observed and regression-predicted values, respectively, of the dependent variable, and I, as in equations (1) and (2), is the number of computed regression coefficients.

*Student's ratio*, t, is defined as the ratio of any number to its own standard error. For example,

$$t_{ip} = b_{ip}/s_{ip} \quad (4)$$

This ratio provides a means for estimating the probability that the number (here, $b_{ip}$) differs significantly from zero. Most textbooks of statistics give at least abbreviated tables of the distribution of t, which show values of t for given values of Φ (number of degrees of freedom) and P (probability, or confidence level, that a chance distribution would give equally high t). In the present study, many analyses have been used, giving Φ larger than 60: the t-distribution tables show that for such cases, the chance that a random "accident" would give equally great or greater value of t is about 0.3 (30%) if $t = 1$, 0.05 if $t = 2$, 0.01 if $t = 2.66$, and 0.005 if $t = 3$.

Hey (1956) adopted the value $t_{ip} = 1$ as the cutoff point for deciding that a regression coefficient $b_{ip}$ differs significantly from zero. This is a compromise between the usual statistical choice $t = 2$ or 2.5 on the one hand, and the proposition that in the regression of physical properties on chemical composition every chemical component is expected to have an effect on the physical property.

*Computation* of the regression coefficients follows methods that are widely known and well described, and need not be reviewed here. A matrix of the sums of squares and products of all the variables is formed. This matrix is solved by inversion to obtain the matrix of variances and covariances of the x's and y's, augmented with one or more column-vectors containing the regression coefficients. The covariance matrix can be used to find standard errors of the regression coefficients, the standard error of the regression as a whole, and the standard error of a calculated value y′ of the dependent variable y for any particular set of values of the independent variables $x_i$.

*Availability of full data.* A few copies of the matrices used in this study have been prepared, and may be

had while the supply lasts. A full listing of data, matrices, and residuals will be made available in a separate publication.

## The Composition and Properties of Clinoamphibole

*General statement.* Clinoamphiboles have a well-known crystal structure with 48 atoms of oxygen plus fluorine, hydroxyl, etc., per unit cell. Half of this cell is a convenient unit for chemical calculations. Accordingly the chemical analyses $u_i$ (Table 1) were recast as atoms per 24 (O, OH, $H_2O$, F, Cl) using an IBM 650 computer. The details of the program input and output, and the program itself, can be made available as long as the supply of copies lasts.

With 24 (O, etc.) per formula, there is space for 16 cations, but these are located in at least four crystallographically distinct types of formula-positions, one of which may be partly or wholly vacant. The formula of clinoamphibole is accordingly as follows:

$$A_w\ B_2\ C_5\ D_8\ O_{22}\ E_2, \qquad (5)$$

where E represents OH, F, Cl, and either O or $H_2O$ depending upon the amount of H to be accommodated; A, B, C, and D represent cations in crystallographically distinct positions; and $0 \leqq w \leqq 1$.

*Recasting procedure.* A preliminary note (Winchell, 1962) described our program written for the IBM 650 computer for recasting amphibole analyses in terms of formula (5) above. Table 1 shows the method of calculation for an ordinary analysis. The chemical analysis in weights per cent ($u_i$) is first recast as number of atoms $v_i$ of each component per 24,000 (O, F, Cl). The resulting quantities $v_i$ are next distributed into the several positions of the chemical formula (5), the number $w_1$ of smallest atoms (Si) in position D first, then successively larger atoms (Al, $Fe^{3+}$, Ti for $w_2$, $w_3$, $w_4$), stopping when the 8000 spaces of position D are filled. A remainder of Si over this limit is made impossible by an automatic branch to two alternative programs which reduce Si to 8000 by (1) assuming free silica [quartz?] present as impurity in the analyzed sample and by (2) assuming that $H_2O$ was missed in the analysis, and correcting the values of $v_i$ accordingly. Any remainder of Al, $Fe^{3+}$, or Ti is assigned immediately to position C.

Position C is filled in a similar manner using

Table 1. Recasting Analysis 187

| Hornblende from Stark, N. H. (Sandell and Goldich, 1943) recast as atoms ($v_i$) per 24,000 (O, F, Cl) | | | | | Distribution of atoms $v_i$ to positions in formula $(A_wB_2C_5D_8O_{22}E_2)_{1000}$ in 25 variables $w_i$ and selection $x_i$ for regression | | | | |
|---|---|---|---|---|---|---|---|---|---|
| Oxide $M_pO_q$ | Wt. % by anal. $u_i$ | Mol. wt. $m_i$ | Oxygen equiv. $\frac{10{,}000\ q \cdot u}{s \cdot m}$ | Atoms $v_i = \frac{24{,}000\ p \cdot u}{s \cdot m}$ | Position D[c] | Position C[c] | Position B[c] | Position A[c] | Position E[d] |
| | | | | | Symb. Amt. | Symb. Amt. | Symb. Amt. | Symb. Amt. | Symb. Amt. |
| 1 $SiO_2$ | 45.63 | 60.09 | 15,187 | Si 7341 | $w_1$ 7341 | | | | |
| 2 $Al_2O_3$ | 2.52 | 101.96 | 741 | Al 478 | $w_2 = x_1$ 478 | $w_5 = X_3$ 0 | | | |
| 3 $Fe_2O_3$ | 7.47 | 159.70 | 1,403 | $Fe^{3+}$ 905 | $w_3 = X_2$[e] 181 | $w_6 = x_4$ 724 | | | |
| 4 $TiO_2$ | 2.88 | 79.90 | 721 | Ti 348 | $w_4$ 0 | $w_7 = x_5$ 348 | | | |
| 5 MgO | 0.76 | 40.32 | 188 | Mg 182 | | $w_8$ 182 | $w_{12} = x_9$ 0 | | |
| 6 FeO | 27.17 | 71.85 | 3,781 | $Fe^{2+}$ 3655 | | $w_9 = x_6$ 3655 | $w_{13} = x_{10}$ 0 | | |
| 7 MnO | 1.02 | 70.94 | 144 | Mn 139 | | $w_{10} = x_8$ 91 | $w_{14} = X_{11}$ 48 | | |
| 8 CaO | 5.56 | 56.08 | 991 | Ca 958 | | $w_{11} = x_7$ 0 | $w_{15}$ 958 | $w_{18} = x_{14}$ 0 | |
| 9 $Na_2O$ | 4.19 | 61.994 | 676 | Na 1307 | | | $w_{16} = x_{13}$ 994 | $w_{19} = x_{15}$ 313 | |
| 10 $K_2O$ | 1.09 | 94.20 | 116 | K 223 | | | $w_{17} = x_{12}$ 0 | $w_{20} = x_{16}$ 223 | |
| 11 $H_2O^+$ | 1.24 | 18.016 | 688 | H 1331 | | | | | |
| 12 F[a] | 0.73 | 18.999 | 192 | F 371 | | | | | F $= w_{21} = X_{17}$ 371 |
| 13 Cl[a] | 0.00 | 35.457 | 0 | Cl 0 | | | | | Cl $= w_{22} = x_{18}$ 0 |
| Rem. | 0.00[b] | | | | | | | | $H_2O = w_{23}$ 0 |
| | | | | | | | | | OH $= w_{24}$ 1331 |
| | | | | | | | | | O $= w_{25}$ 298 |
| 14 Sum | 100.26 | | S = 24,828 | $v_{14} = \Sigma_1^{10} v_i$ = 15,536 | 8000 | 5000 | [f] $w_{26} = 5536$ | 536 | (E) = 2000 |

[a] For F and Cl, "p" = 1, "q" = 0.5.
[b] $H_2O^-$ = 0.00.
[c] Not more than one line may contain non-zero w-values in two adjacent columns for positions A, B, C, and D; also $w_3 \cdot w_5 = w_4 \cdot w_6 = w_9 \cdot w_{12} = w_{10} \cdot w_{13} = \cdots = 0$.
[d] At least one of the pair $w_{23}$, $w_{25}$ must be zero, hence $w_{23} \cdot w_{25} = 0$.
[e] $x_2 = w_3 + w_4$.
[f] $w_{26} = 3000 + \Sigma(B) + \Sigma(A)$.

available Al ($w_5$), $Fe^{3+}$ ($w_6$), Ti ($w_7$), then Mg ($w_8$), $Fe^{2+}$ ($w_9$), Mn ($w_{10}$), Ca ($w_{11}$), in order, as necessary to make the total 5000 atoms in D. Residues from Mg, $Fe^{2+}$, Mn, Ca, and in addition Na and K, are assigned to position B as $w_{12}$ to $w_{17}$, respectively, following the same procedure again until 2000 atoms have been assigned there. Excess Ca, Na, and K are finally assigned to position A as $w_{18}$ to $w_{20}$, and a check sum equal to 3000+atoms in A+atoms in B is reported out for comparison with the total metals reported previously as $v_{14}$, which should be exactly 10,000 larger.

All F and Cl is first assigned to position E, which is then completed with either OH+O, or OH+$H_2O$, to use up the H and bring total E to 2000. Warning cards are punched if there is a deficiency of atoms for assignment to position D or C, or if there is too much H to be accommodated in position E.

Table 1 shows the 25 quantities $w_i$ available for study as a result of this recasting and assignment procedure.

*Independent chemical variables* $x_i$. The sum of all the atoms in position B must be exactly 2; in position C it is 5; in position D it is 8; in position E it is 2. Moreover, the condition of valency balance must be satisfied, making a linear interdependence among the variables $v_i$ and hence among the $w_i$. Thus by the distribution procedure, some of the 25 chemical variables $w_i$ are really dependent upon others. However, no linear dependence between variables can be tolerated in the matrix-algebraic procedure for solution of the simultaneous equations developed for the regression coefficients. It is therefore necessary to eliminate arbitrarily at least one of the chemical variables in each formula-position, and one more because of the valency balance.

There are several ways to remove these chemical dependences. A convenient and practical choice is to consider Si(D), Mg(C), Ca(B), and O, OH, $H_2O$ in (E) as dependent upon all the other chemical variables. The remaining 19 include Ti in D, which is so rarely non-zero that it has been added to $Fe^{3+}$ in D- and Cl in E, which is so rarely known that it has been ignored (equivalent to assuming it has no effect upon the physical properties). The final 17 independent variables are designated by $x_i$ (i=1 to 17) in table 1. These are linearly independent; in particular, if all 17 are set arbitrarily equal to zero, the composition represented is that of the amphibole component $Ca_2Mg_5Si_8O_{22}(OH)_2$, called tremolite. By this choice of independent variables we assure that the constant term $b_{0p}$ in each of the regression equations will represent the properties of an interesting and significant component of clinoamphibole.

*Inhomogeneous chemical data.* Some analyses are better than others. Particularly, only about 43% of the otherwise satisfactory analyses include determinations of the fluorine content. These 173 analyses seemed too valuable not to use for computing regressions on fluorine, but the whole set of 408, including these and the otherwise good ones, seem to offer equally good opportunity for important information. Accordingly, the regression computations were made on both groups, resulting in equations for physical properties $y_p$, numbered with p=1 to 4 for all 408 analyses, ignoring fluorine determinations, and with p=6 to 9 for 173 with fluorine data. The equation for $y_p$ with p=5 is based upon a third group containing 249 analyses for which density data are available.

*Physical variables*, $y_p$. The indicatrix axis Z is always perpendicular to the crystallographic axis b in clinoamphiboles. There is thus no ambiguity in reference to Z, to the associated refractive index $n_z$, or to the extinction angle Z/c. (These symbols are compatible with and printable by, standard computing machinery, and are therefore adopted here.)

A second indicatrix axis is always perpendicular to Z and to the crystallographic axis b. In nearly all clinoamphiboles it is X, the vibration direction of the lowest principal refractive index; and for regression purposes it is so designated even though in rare cases (as crossite) it might more conventionally be called Y. The third indicatrix axis is always parallel to the crystallographic axis b, and for the regressions here described this is uniformly designated Y. A similar convention was used successfully in a previous regression study (Winchell, 1961).

*Homogeneity of physical variables.* A regression computation can be carried out separately for each dependent variable, y, but if several such variables depend upon the same set of independent variables ($x_i$), then it is much more economical to treat all of the y's and x's together. The formation of the augmented moments matrix, consisting of the squares and the products of all the variables, summed over all the observations (analyses in the present case) is time-consuming, and therefore costly, and should be done in such a manner that no data from a single analysis need be handled more than once individually. Selection of analyses actually used in the computa-

tion of regression coefficients was first made on the basis of chemical considerations as outlined below, and secondly on the basis of homogeneity of physical data and chemical data.

*Homogenization of data.* It is convenient to subdivide the data into five groups, numbered zero to four. Group 0 contains just under half of the analyses, and embraces all that have been rejected for any reason, as outlined below. Group 1 contains 46 acceptable analyses that include determinations of fluorine but not of density. Group 2 includes 113 with neither density nor fluorine data. Group 3 has 127 with both density and fluorine determinations. Group 4 comprises 122 analyses that have density but not fluorine determinations. Groups 1 to 4 include a total of 408 specimens, out of approximately 700 that were available.

The original list of available analyses is essentially unselective. It includes all that were used by A. N. Winchell (1945; 1938; 1932; etc.) in preparing several studies of amphiboles, plus many that have been gathered from the literature subsequently. No truly thorough search of the literature was attempted, although all available lists and bibliographical sources, especially *Mineralogical Abstracts*, volumes 1 to 14, were checked carefully. Dr. Bernard Leake of the University of Bristol, England, has kindly called my attention to a number of errors in these and has contributed a number of references for my use, but not in time for most of them to be included in the regressions. His contribution swelled my list of analyses to more than 850 before the cutoff time for using them in the residuals studies summarized here. (Dr. Leake's magnificently documented list of analyses of the calciferous clinoamphiboles has just become available to me in manuscript form, and swells my total list of clinoamphibole analyses with physical data, to well over 1000. The details of the total list will be published separately.) Several hundred more clinoamphibole analyses, for which no physical data have been published, are omitted from both Dr. Leake's and my lists, and a few score very old ones have been deleted.

Analyses of group 0 that were rejected for chemical and other reasons may be classified as follows into categories that are not mutually exclusive:

0.0 Rejections for essentially chemical reasons.

| Class | Number | |
|---|---|---|
| 0.01 | 59 | cases with $v_{14}$ (Sum of v's from 1 to 10) $<14.900$. |
| 0.02 | 110 | cases with $v_{14}>16.099$ |
| 0.03 | 24 | cases with $v_1>8.000$ (shifted automatically into alternate programs 1 and 2 to make $v_1=8.000$; these were not used in regressions, but were considered among the data for calculations of residuals |
| 0.04 | 10 | cases with $<7.900$ atoms for position D ($w_i$ with $i=1$–4) |
| 0.05 | 19 | cases with $<4.900$ atoms for position C ($w_i$ with $i=5$–11) |
| 0.06 | 13 | cases with too much H ($v_{11}$) to be accommodated in position E, even as $H_2O$ replacing the normal OH. |

Remaining:

586 cases considered chemically acceptable.

In an antilogous manner the chemically acceptable cases were classified on the basis of availability (+) and absence (−) of certain physical measurements, as follows:

0.1 Classification of 586 chemically acceptable cases.

| Class | Number | $n_x$ | $n_y$ | $n_z$ | Z/c | G |
|---|---|---|---|---|---|---|
| 0.11 | 24 | − | − | − | − | − |
| 0.12 | 83 | (other combination) | | | | |
| 0.13 | 7 | + | − | + | − | + |
| 0.14 | 9 | + | − | + | + | − |
| 0.15 | 16 | + | − | + | + | + |
| 0.16 | 28 | + | + | + | − | − |
| 0.17 | 11 | + | + | + | − | + |
| 0.18 | 159 | + | + | + | + | − |
| 0.19 | 249 | + | + | + | + | + |

To accomplish the final homogenization of data in four groups, the 159 analyses in 0.18 were subdivided into two groups, Group 1 with, and Group 2 without fluorine determinations, and the 249 cases in 0.19 were similarly divided into two groups, Group 3 with, and Group 4 without fluorine determinations.

The four homogeneous groups of useful data thus defined were used to generate four augmented moments-matrices of order 24, each of which (except Group 3) contains some rows and columns based on partial data with missing items treated as zeroes.

*Regressions for optics, ignoring fluorine.* The sum of the four matrices, 1, 2, 3 and 4, is a matrix containing rows and columns that are dependent upon the amounts of fluorine and chlorine, which were assumed zero if not determined, and upon the values of G, also assumed zero if not determined. These three columns and rows were therefore dropped from the matrix, reducing it to order 21 with four instead of five dependent variables; the resulting basic moments-matrix, inverted and combined properly with the

four columns containing data on the dependent variables, yields the regression coefficients $b_{ip}$ and their standard errors $s_{ip}$ for four equations (p=1, 2, 3, 4) of the form (2):

$$\left.\begin{aligned}
&\text{for p = 1:}\quad n_x = y_1 = \sum_{i=0}^{16} b_{i1}x_i;\ \text{also}\ s_{i1}, t_{i1}, s_1\\
&\text{for p = 2:}\quad n_y = y_2 = \sum_{i=0}^{16} b_{i2}x_i;\ \text{also}\ s_{i2}, t_{i2}, s_2\\
&\text{for p = 3:}\quad n_z = y_3 = \sum_{i=0}^{16} b_{i3}x_i;\ \text{also}\ s_{i3}, t_{i3}, s_3\\
&\text{for p = 4:}\quad Z/c = y_4 = \sum_{i=0}^{16} b_{i4}x_i;\ \text{also}\ s_{i4}, t_{i4}, s_4
\end{aligned}\right\} \qquad (6)$$

where the regression coefficients are $b_{ip}$, their standard errors are $s_{ip}$, their t-ratios are $t_{ip}$, and the root-mean-square residual for the pth equation is $s_p$. These results are summarized in Table 2.

*Regression for G, ignoring fluorine.* The sum of matrices 3 and 4 contains nearly all the data that give information on the density G. Treating this sum-matrix in the same manner as the previous sum-matrix, but eliminating columns and rows corresponding to F, Cl, $n_x$, $n_y$, $n_z$, and Z/c, we obtain the following:

$$\text{for p = 5:}\quad G = y_5 = \sum_{i=0}^{16} b_{i5}x_i;\ \text{also}\ s_{i5}, t_{i5}, s_5 \qquad (7)$$

where the quantities are all as defined above; their values appear in Table 2.

*Regressions allowing for fluorine.* The sum of matrices 1 and 3 is a matrix that contains all the information about optical properties and fluorine as well as the other chemical variables. Eliminating rows and columns corresponding to Cl and to G, and solving as before, the four equations obtained are as follows:

$$\left.\begin{aligned}
&\text{for p = 6:}\quad n_x = y_6 = \sum_{i=0}^{17} b_{i6}x_i;\ \text{also}\ s_{i6}, t_{i6}, s_6\\
&\text{for p = 7:}\quad n_y = y_7 = \sum_{i=0}^{17} b_{i7}x_i;\ \text{also}\ s_{i7}, t_{i7}, s_7\\
&\text{for p = 8:}\quad n_z = y_8 = \sum_{i=0}^{17} b_{i8}x_i;\ \text{also}\ s_{i8}, t_{i8}, s_8\\
&\text{for p = 9:}\quad Z/c = y_9 = \sum_{i=0}^{17} b_{i9}x_i;\ \text{also}\ s_{i9}, t_{i9}, s_9
\end{aligned}\right\} \qquad (8)$$

The values of $b_{ip}$, $t_{ip}$, and $s_p$ for these equations are in table 2.

*Residuals.* Residuals have been computed for about 750 cases of clinoamphiboles that have been analyzed and at least partially studied optically. These have been grouped and summarized by the classification groups 0–4 defined above, and the summaries are presented in Table 3, in which the boxes surrounded by single lines contain valid data, those surrounded by double lines summarize the data on which regression coefficients are directly based, and data not boxed represent invalid application of equations 6–9 to analyses that do not all contain fluorine determinations. The unboxed data should be ignored in most evaluations; they clearly show that it is not wise to use equations 6–9 for estimating physical properties of specimens on which no fluorine determination is available. The other groups tend to show that the analyses in group 0 (including the individual subgroups as well as the entire collection in group 0) contain more specimens that have large residual earrors of estimation of optical properties and density than the analyses in groups 1–4, taken individually or collectively.

*Interesting compositions.* The key to Table 4 presents a number of interesting hypothetical compositions, together with names that might be applied to them as "end-members" of the clinoamphibole system. The main section of this table presents the estimated optical properties and densities y′ together with respective standard errors $s(y'_p)$ estimated according to equation (9),

$$s(y'_p) = s_p\left\{\sum_i x_i^2 c_{iip} + 2\sum_i\sum_j x_i x_j c_{ijp}\right\}^{1/2} \qquad (9)$$

where symbols are as defined above, $c_{ijp}$ is the component from column i, row j, (i>j) of the covariance matrix for equation p, and $c_{iip}$ is the ith diagonal element of the same matrix. The standard errors are shown in Table 4 in the columns *preceding* the numbers to which they refer. The amount of fluorine is known in these cases, but regressions for $y_p$ with p=1−4 give smaller estimated standard errors in some cases because certain regression coefficients are better known for p=1−4 than for regressions of $y_p$ with p=6−9. The latter, however, are essential for cases where effects of fluorine are specifically studied.

## Discussion

A full discussion of these results, and some further results and comparisons, will be presented elsewhere. As with clinopyroxenes (Winchell, 1961), so also with clinoamphiboles, the prospect arises of making significant comparisons that may lead to immediate tests for degree of order in the distribution of certain atoms. Should such tests succeed, there is a good

TABLE 2. REGRESSION COEFFICIENTS B(I,P) WITH CORRES. S(I,P) AND T(I,P)

| P=1 Y(1) = N(X)<br>R-SQ = .906 F = 236.9<br>V = 16 W = 391<br>S = .007958 MATRIX 5 | | | P=2 Y(2) = N(Y)<br>R-SQ = .877 F = 174.9<br>V = 16 W = 391<br>S = .009889 MATRIX 5 | | | P=3 Y(3) = N(Z)<br>R-SQ = .845 F = 133.0<br>V = 16 W = 391<br>S = .010979 MATRIX 5 | | | |
|---|---|---|---|---|---|---|---|---|---|
| B | S | T | B | S | T | B | S | T | |
| 1.60049 | .00120 | 99.99 | 1.61460 | .00149 | 99.99 | 1.62660 | .00166 | 99.99 | CONST |
| .00807 | .00113 | 7.09 | .00698 | .00141 | 4.93 | .00385 | .00157 | 2.45 | AL(D) |
| .00821 | .00494 | 1.65 | .00895 | .00615 | 1.45 | -.00017 | .00682 | .02 | FE3(D) |
| .00463 | .00156 | 2.96 | .00331 | .00194 | 1.70 | .00583 | .00215 | 2.70 | AL(C) |
| .02583 | .00132 | 19.49 | .03267 | .00164 | 19.84 | .03308 | .00182 | 18.10 | FE3(C) |
| .03849 | .00321 | 11.98 | .04961 | .00399 | 12.42 | .05933 | .00443 | 13.38 | TI(C) |
| .01424 | .00048 | 29.24 | .01420 | .00060 | 23.47 | .01331 | .00067 | 19.82 | FE2(C) |
| .00535 | .00383 | 1.39 | .00733 | .00476 | 1.53 | .01345 | .00528 | 2.54 | MN(C) |
| .01815 | .00454 | 3.99 | .01909 | .00564 | 3.38 | .02178 | .00626 | 3.47 | CA(C) |
| -.00014 | .00120 | .12 | .00049 | .00149 | .32 | .00105 | .00166 | .63 | MG(B) |
| .01010 | .00124 | 8.09 | .01055 | .00155 | 6.80 | .01451 | .00172 | 8.42 | FE2(B) |
| .01061 | .00266 | 3.98 | .01214 | .00330 | 3.66 | .00913 | .00367 | 2.48 | MN(B) |
| .01557 | .01393 | 1.11 | .01021 | .01732 | .58 | .01356 | .01922 | .70 | NA(B) |
| -.00073 | .00154 | .47 | -.00735 | .00192 | 3.82 | -.01477 | .00213 | 6.92 | K(B) |
| .00024 | .00311 | .08 | -.00656 | .00387 | 1.69 | -.01224 | .00430 | 2.84 | CA(A) |
| .00396 | .00185 | 2.14 | .00002 | .00230 | .01 | .00056 | .00255 | .22 | NA(A) |
| .00619 | .00408 | 1.51 | .00582 | .00507 | 1.14 | .00880 | .00563 | 1.56 | K(A) |

| P=4 Y(4) = Z/C<br>R-SQ= .387 F= 15.4<br>V = 16 W = 391<br>S = 11.171 MTX 5 | | | P=5 Y(5) = G<br>R-SQ = .751 F = 43.7<br>V = 16 W = 232<br>S = .06918 MATRIX 6 | | | P=6 Y(6) = N(X)<br>R-SQ = .955 F = 193.6<br>V = 17 W = 155<br>S = .006378 MATRIX 7 | | | |
|---|---|---|---|---|---|---|---|---|---|
| B | S | T | B | S | T | B | S | T | |
| 16.28 | 1.69 | 9.61 | 2.9736 | .0135 | 99.99 | 1.60226 | .00151 | 99.99 | CONST |
| 2.53 | 1.59 | 1.58 | .0437 | .0126 | 3.46 | .00981 | .00175 | 4.60 | AL(D) |
| -5.17 | 6.94 | .74 | .0139 | .0520 | .46 | .01594 | .00605 | 2.63 | FE3(D) |
| -5.24 | 2.19 | 2.38 | .0033 | .0183 | .17 | .00661 | .00258 | 25.55 | AL(C) |
| -1.78 | 1.85 | .95 | .0727 | .0150 | 4.83 | .02863 | .00175 | 16.28 | FE3(C) |
| -14.95 | 4.51 | 3.31 | .0354 | .0343 | 1.03 | .04077 | .00420 | 9.70 | TI(C) |
| 3.16 | .68 | 4.62 | .0854 | .0055 | 15.46 | .01447 | .00074 | 19.55 | FE2(C) |
| -11.52 | 5.37 | 2.14 | -.0198 | .0375 | .52 | .02136 | .01172 | 1.82 | MN(C) |
| -.83 | 6.37 | .13 | .0297 | .0422 | .70 | .02280 | .00709 | 3.21 | CA(C) |
| .37 | 1.69 | .22 | .1308 | .0382 | 3.41 | -.00066 | .00103 | .63 | CA(C) |
| -2.99 | 1.75 | 1.70 | .0899 | .0146 | 6.13 | .01009 | .00197 | 5.10 | FE2(B) |
| -7.83 | 3.73 | 2.09 | .0833 | .0289 | 2.87 | -.00225 | .00558 | .40 | MN(B) |
| -18.50 | 19.56 | .94 | -1.0546 | .2236 | 4.71 | -.00744 | .03221 | .23 | NA(B) |
| 14.66 | 2.17 | 6.75 | .0306 | .0168 | 1.82 | -.00171 | .00227 | .75 | K(B) |
| 12.57 | 4.36 | 2.87 | -.0000 | .0327 | .00 | .00041 | .00381 | .10 | CA(A) |
| 8.07 | 2.59 | 3.10 | .0205 | .0212 | .96 | .00005 | .0276 | .02 | NA(A) |
| 14.60 | 5.72 | 2.54 | .0159 | .0465 | .34 | -.00291 | .0513 | .56 | K(A) |
| | | | | | | -.00567 | .00158 | 3.58 | F(E) |

| P=7 Y(7) = N(Y)<br>R-SQ = .937 F = 135.6<br>V = 17 W = 155<br>S = .008582 MATRIX 7 | | | P=8 Y(8) = N(Z)<br>R-SQ = .909 F = 90.5<br>V = 17 W = 155<br>S = .010301 MATRIX 7 | | | P=9 Y(9) = Z/C<br>R-SQ = .428 F = 6.8<br>V = 17 W = 155<br>S = 9.342 MATRIX 7 | | | |
|---|---|---|---|---|---|---|---|---|---|
| B | S | T | B | S | T | B | S | T | |
| 1.61587 | .00203 | 99.99 | 1.62693 | .00244 | 99.99 | 15.21 | 2.21 | 6.87 | CONST |
| .00407 | .00235 | 1.73 | .00185 | .00282 | .65 | -.85 | 2.56 | .33 | AL(D) |
| .01156 | .00815 | 1.41 | .00936 | .00978 | .95 | -15.28 | 8.87 | 1.72 | FE3(D) |
| .00440 | .00347 | 1.26 | .00492 | .00417 | 1.17 | -.40 | 3.78 | .10 | AL(C) |
| .04388 | .00236 | 18.55 | .04500 | .00283 | 15.85 | -6.12 | 2.57 | 2.37 | FE3(C) |
| .05899 | .00565 | 10.43 | .06949 | .00678 | 10.23 | -13.51 | 6.15 | 2.19 | TI(C) |
| .01464 | .00099 | 14.70 | .01312 | .00119 | 10.98 | 1.34 | 1.08 | 1.23 | FE2(C) |
| .03955 | .01576 | 2.50 | .04361 | .01892 | 2.30 | 23.90 | 17.16 | 1.39 | MN(C) |
| .03075 | .00954 | 3.22 | .02900 | .01145 | 2.53 | -3.71 | 10.38 | .35 | CA(C) |
| -.00034 | .00138 | .25 | .00006 | .00166 | .03 | -.00 | 1.51 | .00 | MG(B) |
| .01123 | .00265 | 4.22 | .01665 | .00319 | 5.21 | -.41 | 2.89 | .14 | FE2(B) |
| -.00337 | .00750 | .44 | -.00291 | .00901 | .32 | -17.18 | 8.17 | 2.10 | MN(B) |
| -.02386 | .04334 | .55 | -.04194 | .00367 | .80 | 12.09 | 47.18 | .25 | NA(B) |
| -.01682 | .00306 | 5.48 | -.02267 | .00367 | 6.16 | 18.67 | 3.33 | 5.59 | K(B) |
| -.00824 | .00513 | 1.60 | -.01067 | .00616 | 1.73 | 10.10 | 5.58 | 1.80 | CA(A) |
| .00304 | .00372 | .81 | .00572 | .00446 | 1.28 | 6.55 | 4.05 | 1.61 | NA(A) |
| -.00214 | .00691 | .31 | -.00285 | .00829 | .34 | 8.40 | 7.52 | 1.11 | K(A) |
| -.00609 | .00212 | 2.86 | -.00594 | .00255 | 2.32 | .15 | 2.31 | .06 | F(E) |

prospect of being able to estimate the metamorphic grade of a rock by a consideration of the properties of its amphibole alone. Ghose (1962) predicts that ordering of Mg and Fe″ should be common in hornblendes, but aside from a few ultra-precise determinations of crystal structure his evidence is inductive from principles of chemical crystallography. No method can replace the refined analysis of crystal structure for ultimate decision on this point, but contributory evidence may be obtainable from other physical measurements. Such measurements must be corrected, however, for all the chemical components. Any residual difference can be examined for correlation with the temperature history of the specimen, as reflected in the order of its cations and/or its geologic setting. Clearly one way of making allowance for chemical components is through empirical regressions based on very many data, as herein presented.

An estimate of the composition of a clinoamphibole cannot be based upon a few measured physical properties alone when there are so many chemical variables. However, as with clinopyroxenes (Winchell, 1961), the geologist ordinarily has at least an approximate idea of the composition, and can calculate the properties of an arbitrary "first approximation." He can then compare these with the observed properties of a specimen in hand, and observe what adjustments in the trial composition will produce better agreement.

## Conclusion. Further Work in Progress

With several non-significant coefficients $b_{ip}$ in each of the regressions here presented, it seems advisable to reconsider the variables $x_i$ to be used, and possibly to assign arbitrary zero values to some b's. This and similar experiments are contemplated. A further investigation of the data that present large residual differences between observed and estimated

Table 3

| | gp 1 (46 anals.) | | | gp 2 (113 anals.) | | | gp 3 (126 anals.) | | | gp 4 (123 anals.) | | |
|---|---|---|---|---|---|---|---|---|---|---|---|---|
| EQ | Ē | s | N | Ē | s | N | Ē | s | N | Ē | s | N |
| 1 | −.00167 | .00700 | 46 | .00053 | .00858 | 113 | −.00104 | .00746 | 126 | .00120 | .00759 | 123 |
| 2 | −.00260 | .01098 | 46 | .00043 | .00988 | 113 | −.00090 | .00955 | 126 | .00150 | .00903 | 123 |
| 3 | −.00429 | .01284 | 46 | .00040 | .01046 | 113 | −.00085 | .01093 | 126 | .00210 | .00984 | 123 |
| 4 | 2.08 | 8.69 | 46 | −.47 | 10.84 | 113 | 1.25 | 10.09 | 126 | −1.62 | 2.49 | 123 |
| 5 | — | — | | — | — | | −.0056 | .0436 | 126 | .0057 | .0841 | 123 |
| 6 | −.00037 | .00603 | 46 | .00461 | .01070 | 113 | .00011 | .00605 | 126 | .00482 | .01092 | 123 |
| 7 | −.00118 | .00820 | 46 | .00363 | .01317 | 113 | .00035 | .00806 | 126 | .00574 | .01448 | 123 |
| 8 | −.00276 | .00986 | 46 | .00341 | .01422 | 113 | .00086 | .00957 | 126 | .00672 | .01536 | 123 |
| 9 | 0.71 | 6.89 | 46 | −.71 | 12.27 | 113 | −0.23 | 9.48 | 126 | −1.29 | 15.89 | 123 |
| | gp 5=Σgps 1–4 | | | gp 6=gp(3+4) | | | gp 7=gp(1+3) | | | gp 0 (280 anals.) | | |
| 1 | −.00000 | .00778 | 408 | +.00007 | .00752 | 249 | −.00121 | .00734 | 172 | −.00063 | .01148 | 158 |
| 2 | −.00000 | .00967 | 408 | .00029 | .00930 | 249 | −.00135 | .00995 | 172 | −.000013 | .01514 | 121 |
| 3 | −.00000 | .01072 | 408 | .00061 | .01041 | 249 | −.00177 | .01147 | 172 | .00072 | .01294 | 156 |
| 4 | .00000 | 10.93 | 408 | −.17 | 11.34 | 249 | 1.47 | 9.74 | 172 | 2.18 | 17.80 | 148 |
| 5 | −.00000 | .0668 | 249 | −.00000 | .0668 | 249 | −.0056 | .0436 | 126 | −.0053 | .0647 | 164 |
| 6 | .00272 | .00911 | 408 | .00244 | .00880 | 249 | −.00001 | .00605 | 172 | .00241 | .01153 | 158 |
| 7 | .00271 | .01178 | 408 | .00301 | .01168 | 249 | −.00006 | .00810 | 172 | .00548 | .01855 | 121 |
| 8 | .00292 | .01290 | 408 | .00375 | .01276 | 249 | −.00010 | .00965 | 172 | .00552 | .01779 | 156 |
| 9 | −.57 | 12.29 | 408 | −.75 | 13.05 | 249 | 0.02 | 8.86 | 172 | 1.81 | 20.07 | 148 |

*Legend.* Mean deviations Ē, root-mean-square deviations s, and number of observations N for equations 1 to 9, inclusive, applied to certain groups of clinoamphibole analyses defined in the text. Note. The boxed sections represent data to which the equations are properly applied; other sections involve data that have not been computed according to the assumptions implied. The double-lined boxes contain data for the observation-sets from which the regression coefficients were actually computed.

properties is also required. No doubt this procedure will identify a few errors, and it will probably also point out a number of suspect analyses or incorrect optical data.

### Acknowledgments

I acknowledge with gratitude the support of the Higgins Trust Fund of Yale University, without which the extensive programming and calculations would have been quite impossible. Theresa Y. Park of the Yale Computer Center did most of the programming, and indeed all of the recasting of the analyses, as well as much of the actual operation of the IBM 650. The Computer Center cooperated generously with me in developing a new program for calculating residuals, which I used on an IBM 1620 machine that supersedes the 650.

Philip Goodell and a number of other students spent long hours with a desk computer doing the standard errors for Table 4.

Key to Table 4 *(On next page)*

| NUMBER | NAME | NUMBER OF ATOMS W(I) (SEE TABLE 1) | | | | | | | | | | | | | | | | | |
|---|---|---|---|---|---|---|---|---|---|---|---|---|---|---|---|---|---|---|---|
| | INDEX I OF W(I) | 2 | | 3 | | 6 | | 8 | | 10 | | 13 | | 15 | | 19 | | 25 | |
| | | 1 | | 5 | | 7 | | 9 | | 12 | | 14 | | 16 | | 24 | | 21 | |
| 9901 | TREMOLITE | 0 | 8 | 0 | 0 | 0 | 0 | 5 | 0 | 0 | 0 | 0 | 0 | 2 | 0 | 0 | 2 | 0 | 0 |
| 9902 | FLUORINE-TREMOLITE | 0 | 8 | 0 | 0 | 0 | 0 | 5 | 0 | 0 | 0 | 0 | 0 | 2 | 0 | 0 | 0 | 0 | 2 |
| 9903 | FERROTREMOLITE | 0 | 8 | 0 | 0 | 0 | 0 | 0 | 5 | 0 | 0 | 0 | 0 | 2 | 0 | 0 | 2 | 0 | 0 |
| 9904 | FLUORINE FERROTREMOLITE | 0 | 8 | 0 | 0 | 0 | 0 | 0 | 5 | 0 | 0 | 0 | 0 | 2 | 0 | 0 | 0 | 0 | 2 |
| 9905 | OXYFERROTREMOLITE | 0 | 8 | 0 | 0 | 2 | 0 | 0 | 3 | 0 | 0 | 0 | 0 | 2 | 0 | 0 | 0 | 2 | 0 |
| 9906 | TSCHERMAKITE | 2 | 6 | 0 | 2 | 0 | 0 | 3 | 0 | 0 | 0 | 0 | 0 | 2 | 0 | 0 | 2 | 0 | 0 |
| 9907 | FERROTSCHERMAKITE | 2 | 6 | 0 | 2 | 0 | 0 | 0 | 3 | 0 | 0 | 0 | 0 | 2 | 0 | 0 | 2 | 0 | 0 |
| 9908 | OXYFERROTSCHERMAKITE | 2 | 6 | 0 | 2 | 2 | 0 | 0 | 1 | 0 | 0 | 0 | 0 | 2 | 0 | 0 | 0 | 2 | 0 |
| 9909 | FERROFERRITSCHERMAKITE | 2 | 6 | 0 | 0 | 2 | 0 | 0 | 3 | 0 | 0 | 0 | 0 | 2 | 0 | 0 | 2 | 0 | 0 |
| 9910 | FLUORINE-TSCHERMAKITE | 2 | 6 | 0 | 2 | 0 | 0 | 3 | 0 | 0 | 0 | 0 | 0 | 2 | 0 | 0 | 0 | 0 | 2 |
| 9911 | PARGASITE | 2 | 6 | 0 | 1 | 0 | 0 | 4 | 0 | 0 | 0 | 0 | 0 | 2 | 0 | 1 | 2 | 0 | 0 |
| 9912 | FERROPARGASITE | 2 | 6 | 0 | 1 | 0 | 0 | 0 | 4 | 0 | 0 | 0 | 0 | 2 | 0 | 1 | 2 | 0 | 0 |
| 9913 | FERRIPARGASITE | 2 | 6 | 0 | 0 | 1 | 0 | 4 | 0 | 0 | 0 | 0 | 0 | 2 | 0 | 1 | 2 | 0 | 0 |
| 9914 | HASTINGSITE | 2 | 6 | 0 | 0 | 1 | 0 | 0 | 4 | 0 | 0 | 0 | 0 | 2 | 0 | 1 | 2 | 0 | 0 |
| 9915 | OXYHASTINGSITE | 2 | 6 | 0 | 0 | 3 | 0 | 0 | 2 | 0 | 0 | 0 | 0 | 2 | 0 | 1 | 0 | 2 | 0 |
| 9916 | EDENITE | 1 | 7 | 0 | 0 | 0 | 0 | 5 | 0 | 0 | 0 | 0 | 0 | 2 | 0 | 1 | 2 | 0 | 0 |
| 9917 | FERROEDENITE | 1 | 7 | 0 | 0 | 0 | 0 | 0 | 5 | 0 | 0 | 0 | 0 | 2 | 0 | 1 | 2 | 0 | 0 |
| 9918 | FLUORINE-EDENITE | 1 | 7 | 0 | 0 | 0 | 0 | 5 | 0 | 0 | 0 | 0 | 0 | 2 | 0 | 1 | 0 | 0 | 2 |
| 9919 | FLUORINE-FERROEDENITE | 1 | 7 | 0 | 0 | 0 | 0 | 0 | 5 | 0 | 0 | 0 | 0 | 2 | 0 | 1 | 0 | 0 | 2 |
| 9920 | OXYFERROEDENITE | 1 | 7 | 0 | 0 | 2 | 0 | 0 | 3 | 0 | 0 | 0 | 0 | 2 | 0 | 1 | 0 | 2 | 0 |
| 9921 | RICHTERITE | 0 | 8 | 0 | 0 | 0 | 0 | 5 | 0 | 0 | 0 | 0 | 0 | 1 | 1 | 1 | 2 | 0 | 0 |
| 9922 | FERRORICHTERITE | 0 | 8 | 0 | 0 | 0 | 0 | 0 | 5 | 0 | 0 | 0 | 0 | 1 | 1 | 1 | 2 | 0 | 0 |
| 9923 | FLUORINE-RICHTERITE | 0 | 8 | 0 | 0 | 0 | 0 | 5 | 0 | 0 | 0 | 0 | 0 | 1 | 1 | 1 | 0 | 0 | 2 |
| 9924 | FLUORINE-FERRORICHTERITE | 0 | 8 | 0 | 0 | 0 | 0 | 0 | 5 | 0 | 0 | 0 | 0 | 1 | 1 | 1 | 0 | 0 | 2 |
| 9925 | OXYFERROFERRIRICHTERITE | 0 | 8 | 0 | 0 | 2 | 0 | 0 | 3 | 0 | 0 | 0 | 0 | 1 | 1 | 1 | 0 | 2 | 0 |
| 9926 | GLAUCOPHANE | 0 | 8 | 0 | 2 | 0 | 0 | 3 | 0 | 0 | 0 | 0 | 0 | 0 | 2 | 0 | 2 | 0 | 0 |
| 9927 | FERROGLAUCOPHANE | 0 | 8 | 0 | 2 | 0 | 0 | 0 | 3 | 0 | 0 | 0 | 0 | 0 | 2 | 0 | 2 | 0 | 0 |
| 9928 | MAGNESIORIEBECKITE | 0 | 8 | 0 | 0 | 2 | 0 | 3 | 0 | 0 | 0 | 0 | 0 | 0 | 2 | 0 | 2 | 0 | 0 |
| 9929 | RIEBECKITE | 0 | 8 | 0 | 0 | 2 | 0 | 0 | 3 | 0 | 0 | 0 | 0 | 0 | 2 | 0 | 2 | 0 | 0 |
| 9930 | OXYRIEBECKITE | 0 | 8 | 0 | 0 | 4 | 0 | 0 | 1 | 0 | 0 | 0 | 0 | 0 | 2 | 0 | 0 | 2 | 0 |
| 9931 | MAGNESIO-ALUMINOARFVEDSONITE | 0 | 8 | 0 | 1 | 0 | 0 | 4 | 0 | 0 | 0 | 0 | 0 | 0 | 2 | 1 | 2 | 0 | 0 |
| 9932 | ALUMINO-ARFVEDSONITE | 0 | 8 | 0 | 1 | 0 | 0 | 0 | 4 | 0 | 0 | 0 | 0 | 0 | 2 | 1 | 2 | 0 | 0 |
| 9933 | MAGNESIO-ARFVEDSONITE | 0 | 8 | 0 | 0 | 1 | 0 | 4 | 0 | 0 | 0 | 0 | 0 | 0 | 2 | 1 | 2 | 0 | 0 |
| 9934 | ARFVEDSONITE | 0 | 8 | 0 | 0 | 1 | 0 | 0 | 4 | 0 | 0 | 0 | 0 | 0 | 2 | 1 | 2 | 0 | 0 |
| 9935 | OXYARFVEDSONITE | 0 | 8 | 0 | 0 | 3 | 0 | 0 | 2 | 0 | 0 | 0 | 0 | 0 | 2 | 1 | 0 | 2 | 0 |
| 9936 | FLUORINE-PARGASITEIL | 2 | 6 | 0 | 1 | 0 | 0 | 4 | 0 | 0 | 0 | 0 | 0 | 2 | 0 | 1 | 0 | 0 | 2 |
| 9937 | FLUORINE-HASTINGSITE | 2 | 6 | 0 | 0 | 1 | 0 | 0 | 4 | 0 | 0 | 0 | 0 | 2 | 0 | 1 | 0 | 0 | 2 |
| 9938 | FLUORINE-GLAUCOPHANE | 0 | 8 | 0 | 2 | 0 | 0 | 3 | 0 | 0 | 0 | 0 | 0 | 0 | 2 | 0 | 0 | 0 | 2 |
| 9939 | FLUORINE-RIEBECKITE | 0 | 8 | 0 | 0 | 2 | 0 | 0 | 3 | 0 | 0 | 0 | 0 | 0 | 2 | 0 | 0 | 0 | 2 |
| 9940 | FLUORINE-ARFVEDSONITE | 0 | 8 | 0 | 0 | 1 | 0 | 0 | 4 | 0 | 0 | 0 | 0 | 0 | 2 | 1 | 0 | 0 | 2 |
| 9941 | CROSSITE | 0 | 8 | 0 | 1 | 1 | 0 | 1 | 2 | 0 | 0 | 0 | 0 | 0 | 2 | 0 | 2 | 0 | 0 |
| 9942 | CHIKLITE | 0 | 8 | 0 | 0 | 2 | 0 | 1 | 0 | 2 | 0 | 0 | 0 | 0 | 2 | 0 | 2 | 0 | 0 |
| 9943 | BARKEVIKITE | 2 | 6 | 0 | 0 | 1 | 1 | 1 | 2 | 0 | 0 | 0 | 0 | 2 | 0 | 1 | 2 | 0 | 0 |
| 9944 | KUPFFERITE | 0 | 8 | 0 | 0 | 0 | 0 | 5 | 0 | 0 | 2 | 0 | 0 | 0 | 0 | 0 | 2 | 0 | 0 |
| 9945 | 5 KUPFFERITE + 2 GRUNERITE | 0 | 8 | 0 | 0 | 0 | 0 | 5 | 0 | 0 | 0 | 2 | 0 | 0 | 0 | 0 | 2 | 0 | 0 |
| 9946 | 3 KUPFFERITE + 4 GRUNERITE | 0 | 8 | 0 | 0 | 0 | 0 | 3 | 2 | 0 | 0 | 2 | 0 | 0 | 0 | 0 | 2 | 0 | 0 |
| 9947 | GRUNERITE | 0 | 8 | 0 | 0 | 0 | 0 | 0 | 5 | 0 | 0 | 2 | 0 | 0 | 0 | 0 | 2 | 0 | 0 |
| 9948 | MANGANESE GRUNERITE | 0 | 8 | 0 | 0 | 0 | 0 | 0 | 5 | 0 | 0 | 0 | 2 | 0 | 0 | 0 | 2 | 0 | 0 |
| 9949 | MANGANESE-CUMMINGTONITE | 0 | 8 | 0 | 0 | 0 | 0 | 3 | 0 | 2 | 0 | 0 | 2 | 0 | 0 | 0 | 2 | 0 | 0 |
| 9950 | F-NA-CUMMINGTONIT (F-NA-RICHTERITE) | 0 | 8 | 0 | 0 | 0 | 0 | 5 | 0 | 0 | 0 | 0 | 0 | 0 | 1 | 1 | 0 | 0 | 2 |

TABLE 4. CALCULATED VALUES FOR INTERESTING COMPOSITIONS

Standard Errors S′(P) and Physical Properties Y′(P), Calculated from Regressions

| | Y(1)=N(X) | | Y(2)=N(Y) | | Y(3)=N(Z) | | Y(4)=Z/C | | Y(5)=G | | Y(6)=N(X) | | Y(7)=N(Y) | | Y(8)=N(Z) | | Y(9)=Z/C | |
|---|---|---|---|---|---|---|---|---|---|---|---|---|---|---|---|---|---|---|
| N | S(X) | N(X) | S(Y) | N(Y) | S(Z) | N(Z) | S(/) | Z/C | S(G) | G | S(X) | N(X) | S(Y) | N(Y) | S(Z) | N(Z) | S(/) | Z/C |
| 9901 | .0012 | 1.6004 | .0015 | 1.6146 | .0017 | 1.6266 | 1.7 | 16.2 | .014 | 2.973 | .0015 | 1.6022 | .0020 | 1.6158 | .0024 | 1.6269 | 2.2 | 15.2 |
| 9902 | . | 1.6004 | . | 1.6146 | . | 1.6266 | . | 16.2 | . | 2.973 | .0030 | 1.5909 | .0040 | 1.6036 | .0049 | 1.6150 | 4.4 | 15.5 |
| 9903 | .0025 | 1.6717 | .0031 | 1.6856 | .0035 | 1.6931 | 3.5 | 32.1 | .027 | 3.400 | .0038 | 1.6746 | .0051 | 1.6891 | .0061 | 1.6925 | 5.5 | 21.9 |
| 9904 | . | 1.6717 | . | 1.6856 | . | 1.6931 | . | 32.1 | . | 3.400 | .0049 | 1.6632 | .0066 | 1.6769 | .0080 | 1.6806 | 7.3 | 22.2 |
| 9905 | .0030 | 1.6948 | .0037 | 1.7225 | .0051 | 1.7327 | 4.2 | 22.2 | .034 | 3.375 | .0041 | 1.7029 | .0056 | 1.7475 | .0067 | 1.7563 | 6.1 | 6.9 |
| 9906 | .0023 | 1.6259 | .0029 | 1.6352 | .0032 | 1.6460 | 3.2 | .7 | .055 | 3.067 | .0036 | 1.6351 | .0049 | 1.6328 | .0059 | 1.6405 | 5.3 | 14.3 |
| 9907 | .0024 | 1.6686 | .0030 | 1.6778 | .0033 | 1.6859 | 3.4 | 10.2 | .056 | 3.324 | .0035 | 1.6785 | .0047 | 1.6767 | .0057 | 1.6798 | 5.1 | 18.3 |
| 9908 | .0035 | 1.6918 | .0043 | 1.7147 | .0048 | 1.7254 | 4.9 | .3 | .063 | 3.298 | .0051 | 1.7068 | .0069 | 1.7352 | .0083 | 1.7436 | 7.5 | 3.4 |
| 9909 | .0024 | 1.7110 | .0030 | 1.7365 | .0033 | 1.7404 | 3.4 | 17.1 | .031 | 3.462 | .0036 | 1.7225 | .0048 | 1.7557 | .0058 | 1.7600 | 5.2 | 5.2 |
| 9910 | . | 1.6259 | . | 1.6352 | . | 1.6460 | . | .7 | . | 3.067 | .0052 | 1.6237 | .0070 | 1.6206 | .0084 | 1.6286 | 7.7 | 14.6 |
| 9911 | .0020 | 1.6252 | .0025 | 1.6319 | .0028 | 1.6407 | 2.8 | 14.0 | .040 | 3.084 | .0023 | 1.6285 | .0031 | 1.6314 | .0037 | 1.6413 | 3.4 | 20.4 |
| 9912 | .0027 | 1.6822 | .0034 | 1.6887 | .0038 | 1.6939 | 3.8 | 26.6 | .044 | 3.426 | .0037 | 1.6864 | .0050 | 1.6900 | .0060 | 1.6938 | 5.4 | 25.8 |
| 9913 | .0023 | 1.6464 | .0029 | 1.6612 | .0032 | 1.6679 | 3.2 | 17.5 | .026 | 3.154 | .0032 | 1.6505 | .0041 | 1.6709 | .0051 | 1.6813 | 4.5 | 13.9 |
| 9914 | .0027 | 1.7034 | .0034 | 1.7180 | .0038 | 1.7212 | 3.8 | 30.1 | .029 | 3.496 | .0042 | 1.7084 | .0057 | 1.7295 | .0068 | 1.7338 | 6.2 | 19.3 |
| 9915 | .0034 | 1.7265 | .0042 | 1.7550 | .0047 | 1.7607 | 4.8 | 20.2 | .061 | 3.470 | .0050 | 1.7367 | .0067 | 1.7880 | .0081 | 1.7976 | 7.4 | 4.3 |
| 9916 | .0017 | 1.6125 | .0021 | 1.6216 | .0023 | 1.6310 | 2.4 | 21.8 | .021 | 3.037 | .0028 | 1.6121 | .0037 | 1.6230 | .0045 | 1.6345 | 4.1 | 20.9 |
| 9917 | .0020 | 1.6837 | .0025 | 1.6926 | .0028 | 1.6976 | 2.8 | 37.6 | .034 | 3.465 | .0048 | 1.6844 | .0065 | 1.6962 | .0078 | 1.7001 | 7.0 | 27.6 |
| 9918 | . | 1.6125 | . | 1.6216 | . | 1.6310 | . | 21.8 | . | 3.037 | .0029 | 1.6007 | .0040 | 1.6108 | .0048 | 1.6226 | 4.3 | 21.2 |
| 9919 | . | 1.6837 | . | 1.6926 | . | 1.6976 | . | 37.6 | . | 3.465 | .0052 | 1.6731 | .0071 | 1.6840 | .0085 | 1.6882 | 7.7 | 27.9 |
| 9920 | .0029 | 1.7069 | .0036 | 1.7295 | .0040 | 1.7371 | 4.1 | 27.7 | .033 | 3.440 | .0045 | 1.7128 | .0061 | 1.7546 | .0073 | 1.7638 | 6.6 | 12.6 |
| 9921 | .0021 | 1.6037 | .0026 | 1.6072 | .0029 | 1.6123 | 2.9 | 39.0 | .029 | 3.024 | .0031 | 1.6006 | .0041 | 1.6021 | .0050 | 1.6099 | 4.5 | 40.4 |
| 9922 | .0032 | 1.6749 | .0040 | 1.6782 | .0044 | 1.6789 | 4.5 | 54.8 | .036 | 3.452 | .0019 | 1.6729 | .0066 | 1.6753 | .0079 | 1.6756 | 7.2 | 47.1 |
| 9923 | . | 1.6037 | . | 1.6072 | . | 1.6123 | . | 39.0 | . | 3.024 | .0031 | 1.5892 | .0042 | 1.5899 | .0050 | 1.5980 | 4.5 | 40.7 |
| 9924 | . | 1.6749 | . | 1.6782 | . | 1.6789 | . | 54.8 | . | 3.452 | .0053 | 1.6616 | .0071 | 1.6631 | .0086 | 1.6637 | 7.7 | 47.4 |
| 9925 | .0028 | 1.6981 | .0035 | 1.7152 | .0039 | 1.7185 | 3.9 | 44.9 | .030 | 3.426 | .0043 | 1.7012 | .0058 | 1.7338 | .0069 | 1.7393 | 5.3 | 32.2 |
| 9926 | .0030 | 1.6082 | .0037 | 1.6065 | .0042 | 1.6087 | 4.3 | 35.1 | .037 | 3.041 | .0054 | 1.6120 | .0073 | 1.5910 | .0087 | 1.5914 | 7.9 | 53.3 |
| 9927 | .0032 | 1.6510 | .0039 | 1.6491 | .0043 | 1.6486 | 4.4 | 44.6 | .038 | 3.297 | .0051 | 1.6554 | .0069 | 1.6349 | .0083 | 1.6308 | 7.5 | 57.3 |
| 9928 | .0025 | 1.6507 | .0031 | 1.6652 | .0034 | 1.6632 | 3.4 | 42.0 | .029 | 3.180 | .0038 | 1.6501 | .0050 | 1.6700 | .0061 | 1.6715 | 5.5 | 40.3 |
| 9929 | .0025 | 1.6934 | .0030 | 1.7078 | .0034 | 1.7031 | 3.4 | 51.5 | .028 | 3.436 | .0036 | 1.6995 | .0048 | 1.7139 | .0058 | 1.7109 | 5.2 | 44.3 |
| 9930 | .0040 | 1.7165 | .0050 | 1.7448 | .0055 | 1.7427 | 5.6 | 41.6 | .047 | 3.411 | .0054 | 1.7278 | .0073 | 1.7724 | .0088 | 1.7747 | 8.0 | 29.3 |
| 9931 | .0033 | 1.6076 | .0041 | 1.6032 | .0045 | 1.6034 | 4.6 | 48.4 | .032 | 3.058 | .0055 | 1.6054 | .0074 | 1.5896 | .0089 | 1.5922 | 8.1 | 59.5 |
| 9932 | .0037 | 1.6645 | .0045 | 1.6600 | .0050 | 1.6567 | 5.1 | 61.1 | .037 | 3.400 | .0041 | 1.6633 | .0055 | 1.6482 | .0066 | 1.6447 | 6.0 | 64.8 |
| 9933 | .0031 | 1.6288 | .0048 | 1.6325 | .0042 | 1.6307 | 4.3 | 51.9 | .028 | 3.128 | .0038 | 1.6275 | .0051 | 1.6291 | .0062 | 1.6323 | 5.6 | 52.9 |
| 9934 | .0035 | 1.6857 | .0043 | 1.6894 | .0048 | 1.6839 | 4.9 | 64.5 | .033 | 3.470 | .0046 | 1.6854 | .0061 | 1.6877 | .0074 | 1.6848 | 6.7 | 58.3 |
| 9935 | .0036 | 1.7089 | .0045 | 1.7263 | .0050 | 1.7235 | 5.1 | 54.6 | .036 | 3.444 | .0048 | 1.7137 | .0064 | 1.7462 | .0077 | 1.7485 | 7.0 | 43.4 |
| 9936 | . | 1.6252 | . | 1.6319 | . | 1.6407 | . | 14.0 | . | 3.084 | .0032 | 1.6172 | .0042 | 1.6192 | .0051 | 1.6294 | 4.6 | 20.7 |
| 9937 | . | 1.7034 | . | 1.7180 | . | 1.7212 | . | 30.1 | . | 3.496 | .0048 | 1.6971 | .0065 | 1.7173 | .0078 | 1.7219 | 7.1 | 19.6 |
| 9938 | . | 1.6082 | . | 1.6065 | . | 1.6087 | . | 35.1 | . | 3.041 | .0065 | 1.6007 | .0087 | 1.5788 | .0105 | 1.5795 | 9.5 | 53.6 |
| 9939 | . | 1.6934 | . | 1.7078 | . | 1.7031 | . | 51.5 | . | 3.436 | .0048 | 1.6881 | .0065 | 1.7017 | .0077 | 1.6990 | 7.0 | 44.6 |
| 9940 | . | 1.6857 | . | 1.6894 | . | 1.6839 | . | 64.5 | . | 3.470 | .0050 | 1.6740 | .0067 | 1.6755 | .0065 | 1.6729 | 7.3 | 58.6 |
| 9941 | .0022 | 1.6579 | .0027 | 1.6642 | .0030 | 1.6626 | 3.0 | 44.9 | .026 | 3.281 | .0040 | 1.6630 | .0054 | 1.6598 | .0080 | 1.6577 | 5.9 | 49.5 |
| 9942 | .0088 | 1.6869 | .0109 | 1.7034 | .0121 | 1.7068 | 12.4 | 40.3 | .081 | 3.239 | .0138 | 1.7016 | .0186 | 1.7315 | .0223 | 1.7296 | 20.2 | 32.8 |
| 9943 | .0037 | 1.7134 | .0045 | 1.7393 | .0050 | 1.7539 | 5.1 | 8.8 | .034 | 3.360 | .0035 | 1.7202 | .0048 | 1.7592 | .0057 | 1.7771 | 5.2 | 3.1 |
| 9944 | .0026 | 1.6001 | .0033 | 1.6155 | .0036 | 1.6287 | 3.6 | 17.0 | .075 | 3.235 | .0025 | 1.6009 | .0034 | 1.6151 | .0041 | 1.6270 | 3.7 | 15.2 |
| 9945 | .0076 | 1.6207 | .0094 | 1.6357 | .0105 | 1.6556 | 10.7 | 10.3 | .028 | 3.153 | .0038 | 1.6224 | .0052 | 1.6383 | .0062 | 1.6602 | 5.6 | 14.3 |
| 9946 | .0066 | 1.6491 | .0082 | 1.6641 | .0091 | 1.6822 | 9.3 | 16.6 | .025 | 3.324 | .0032 | 1.6513 | .0043 | 1.6676 | .0052 | 1.6864 | 4.7 | 17.0 |
| 9947 | .0077 | 1.6919 | .0095 | 1.7067 | .0106 | 1.7222 | 10.8 | 26.1 | .029 | 3.580 | .0034 | 1.6948 | .0046 | 1.7115 | .0055 | 1.7258 | 5.0 | 21.0 |
| 9948 | .0053 | 1.6929 | .0066 | 1.7099 | .0073 | 1.7114 | 7.5 | 16.4 | .057 | 3.567 | .0107 | 1.6701 | .0144 | 1.6823 | .0173 | 1.6867 | 15.8 | 12.4 |
| 9949 | .0092 | 1.6580 | .0115 | 1.6770 | .0127 | 1.6884 | 13.0 | −1.0 | .085 | 3.199 | .0162 | 1.6433 | .0217 | 1.6706 | .0261 | 1.6791 | 23.7 | 26.5 |
| 9950 | . | 1.6035 | . | 1.6077 | . | 1.6134 | . | 39.4 | . | 3.155 | .0031 | 1.5885 | .0042 | 1.5895 | .0050 | 1.5981 | 4.5 | 40.7 |

References

Acton, F. S. (1959) *Analysis of Straight-line Data.* John Wiley & Sons, New York, p. 1–267.

Davies, O. W. (1958) *Statistical Methods in Research and Production,* 3d ed, Oliver and Boyd, London, p. 1–396.

Fisher, R. A (1958) *Statistical Methods for Research Workers,* 13th ed. Hafner Publ. Co. New York, p. 1–356.

——— and F. Yates (1957) *Statistical Tables for Biological, etc. Research.* Hafner Pub. Co., New York, p. 1–138.

Ghose, S. (1962) The nature of $Mg^{2+}$—$Fe^{2+}$ distribution in some ferromagnesian silicate minerals. Am. Mineral. **47,** 388–394.

Henriques, A. (1958a) An attempt to determine the effect of cations on the extinction angle *c/8* with the aid of linear regression equations: *Arkiv Mineral. Geol.* **2,** 337–340.

——— (1958b) The influence of cations on the optical properties of clinopyroxenes, Pt. I. *Arkiv Mineral. Geol.* **2,** 341–348.

——— (1958c) The influence of cations on the optical properties of clinopyroxenes. Pt. II. *Arkiv Mineral. Geol.* **2,** 381–390.

Hey, M. H. (1956) On the correlation of physical properties with chemical composition in multivariate systems. *Mineral. Mag.* **31,** 69–95.

Hori, F. (1954) Effects of constituent cations on the optical properties of clinopyroxene. *Tokyo Univ. Coll. Gen. Educ. Sci. Papers.* **4,** 71–83.

Laffitte, P. (1950) Série d'abaques permettant la détermination rapide des feldspaths maclés albite. *Bull. Soc. Franc. Minéral.* **73,** 425–438.

Leake, B. (unpublished) List of analyses of the calciferous amphiboles.

Mertie, J. B. (1942) Nomogram for optic angle formulae. *Am. Mineral.* **27,** 538–551.

Nieuwenkamp, W. (1948) *Stereograms for the Determination of Plagioclase Feldspars in Random Sections.* Spectrum Publishers, Utrecht, p. 1–29, pls. 1–13.

Rabbitt, J. C. (1948) A new study of the anthophyllite series. *Am. Mineral.* **33,** 263–323.

Williams, E. J. (1959) *Regression Analysis.* John Wiley & Sons, New York, p. 1–214.

Winchell, A. N. (1924) Studies in the amphibole group. *Am. Jour. Sci.* **7,** 287–310.

——— (1925) The $FeSiO_3$—$CaSiO_3$—$NaFeSi_2O_6$ system of monoclinic amphiboles. *Am. Mineral.* **10,** 335–341.

——— (1931) Further studies in the amphibole group. *Am. Mineral.* **16,** 250–266.

——— (1932) Ferrotremolite, oxyhornblende, and tourmaline. *Am. Mineral.* **17,** 472–477.

——— (1938) The anthophyllite and cummingtonite-grunerite series. *Am. Mineral.* **23,** 329–333.

——— (1945) Variations in composition and properties of the calcifeous amphiboles. *Am. Mineral.* **30,** 27–50.

Winchell, H. (1961) Regressions of physical properties on the compositions of clinopyroxenes. II. Optical properties and specific gravity. *Am. Jour. Sci.* **259,** 295–319.

——— (unpublished) List of chemical analyses and physical properties of clinoamphiboles (in preparation).

——— (1962) A computer program for handling chemical analyses of amphiboles and other minerals. *Am. Mineral.* **47,** 411–413.

——— and R. I. Tilling (1960) Regressions of physical properties on the chemical compositions of clinopyroxenes. I. Lattice constants. *Am. Jour. Sci.* **258,** 529–547.


## Discussion

B. Leake, (Bristol, England) Your regression equations should be capable of being modified to find out in any one amphibole in which position in the structure certain elements are really present. This would give some decisive new information to assist in the assignment of elements to particular lattice sites in the structure. Have you obtained any results along these lines yet?

Author's reply: These equations are indeed applicable to studies of the sort you mention. We may, for example, study the distribution of a pair of elements, both of which can reasonably enter the formula in either of two positions, by assuming two or more plausible distributions, computing the physical properties, and comparing the results with observed properties. Moreover, the estimated standard error for each computation will afford the means of deciding whether or not the differences so calculated are significant, and if so at what probability-level.

Allan Wilson (Brisbane, Australia) How can you be sure of the reliability of the fluorine determinations of the analyses which you have used, especially in view of the importance of fluorine in the amphibole structure?

Author's reply: Individual fluorine determinations are hard to carry out, especially by the methods used in many of the analyses here considered. That they are, on the average fairly valid when considered *en masse,* is indicated by the small, but consistent improvement in the standard deviations of observed and calculated $y_p$-values set forth in Table 3, group 7, equations 6–9 compared with equations 1–4, and also compared with group 5, equations 1–4. I have not investigated the statistical significance of these differences.

MINERALOGICAL SOCIETY OF AMERICA, SPECIAL PAPER 1, 1963
INTERNATIONAL MINERALOGICAL ASSOCIATION, PAPERS, THIRD GENERAL MEETING

# CONTRIBUTION TO THE STUDY OF THE FLUORITE DEPOSIT "MINA BERTA" IN SAN CUGAT DEL VALLES (BARCELONA, SPAIN)

J. MONTORIOL POUS, A. SAN MIGUEL AND M. FONT-ALTABA
*Laboratorios de Mineralogia y Petrografia, Universidad de Barcelona, Barcelona, Spain*

ABSTRACT

As a contribution to the mineralogical study of the fluorite deposit "Mina Berta," spectrographical analyses of some samples of fluorite of this deposit are given. No correlation exists between the different colors of fluorite and the presence of certain cations. Mg, Si, Al and Cu appear clearly in all the specimens; Fe appears also in all of them but with notable differences in the quantity.

The fluorite deposit called "Mina Berta" lies about 25 km north northwest of Barcelona (Fig. 1). Formerly, galena and sphalerite as well as fluorite were mined there, but at present only fluorite is mined and, from time to time, small quantities of galena. However, the deposit has a very rich paragenesis, and 25 different mineral species have been identified up to now. The fluorite appears as discontinuous lenses with a predominately vertical attitude included in an aplitic granite.

The samples used in this work were personally collected at the deposit or selected from the mineralogical collections of the Town Museum of Geology of Barcelona and Sabadell or from the private collection of Mr. Folch Girona.

Of the white, green and violet color varieties of the fluorite, only the white and green are abundant and well defined in this deposit. The violet fluorite is very rare and the few specimens having this color offer only a slight pinkish shade. Some fluorite is in nearly perfect octahedrons with a green exterior and a white, slightly violet interior. In crystals like this, the surface separating the two colors is approximately the cleavage plane (111).

Microscopical observation shows that in some fluorite specimens there are inclusions of a biaxial, low birefringent mineral, that seems to be a feldspar. In other specimens, although not very abundant in the deposit, small inclusions of galena give the fluorite a gray color. For the spectrographical study specimens were chosen that, by microscopical observation, are free of inclusions.

A Hilger spectrograph using a direct current carbon arc was employed. The film used was Mafe positive, sensitive only to the ultraviolet region of the spectrum.

Of the many samples studied, the results of 25 which show the greatest variations, are selected for presentation. Figure 2 shows the results of the spectrographical analysis. Mg, Si, Al and Cu appear

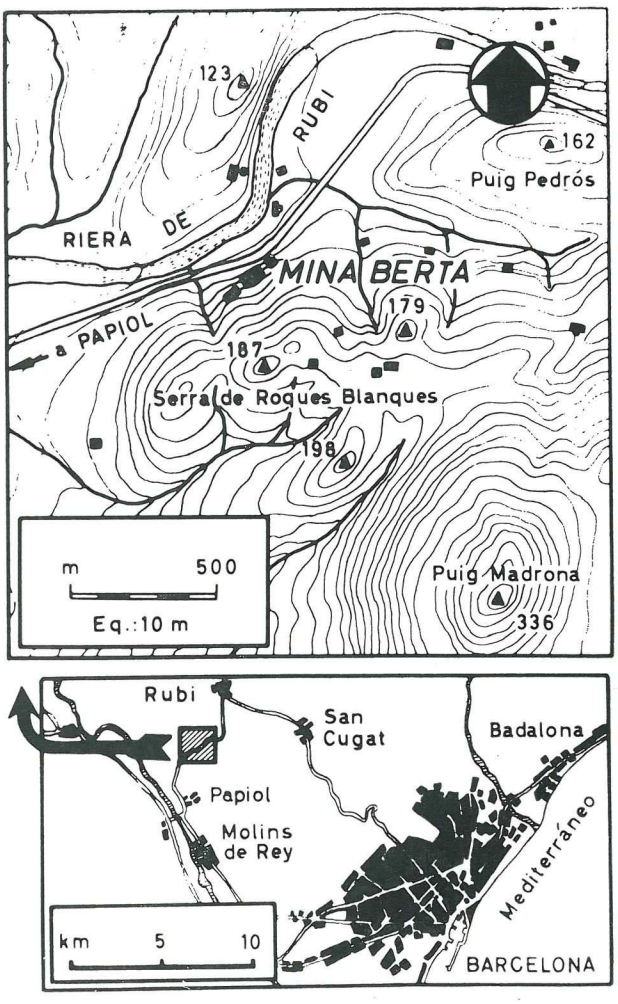


FIG. 1. Map showing the location of "Mina Berta."

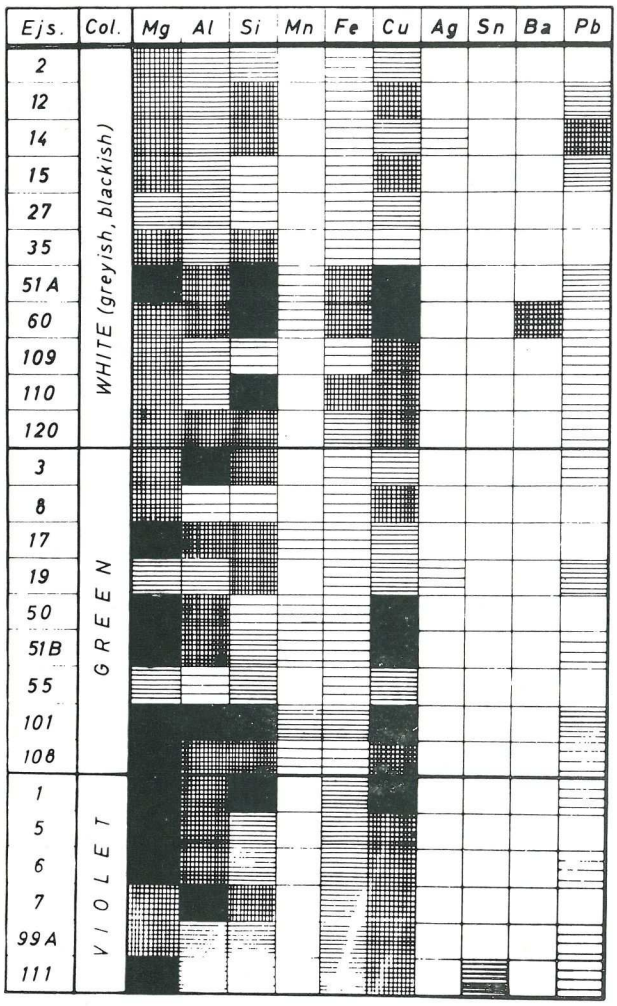


FIG. 2. Minor elements existing in the fluorite. The intensity of the shading is proportional to the intensity of the spectrographic lines of the element.

clearly in all the specimens; Fe appears also in all of them but with notable differences in the quantity.

The spectrographic analysis of the fluorite from Mina Berta was carried out chiefly to see the correlations between the fluorite, associated minerals and the wall rock, with the hope that the results would shed light on the genesis of the deposit. But on doing so, we can see also whether there exists any correlation between the different colors of fluorite and the presence of certain cations.

At the beginning it appeared that there was not such a correlation, since Fe and Cu, elements that could have a certain influence over the coloring, appear indistinctly in the white, violet and green varieties. Further, it has been observed that the intensities of the spectral lines of Cu and Fe are variable in different samples of the same coloring and on the other hand, the same intensities appear in samples of different color.

The work in quantitative aspects is going on now in order to get a complete confirmation of the above as well as to compare the quantity of the trace elements contained in the fluorite and in the rock wall. It can be seen that Ba, Pb, Sn are random and in very small quantities.

As a curiosity it was observed that the white and violet fluorite of this deposit never contain any quantity of Mn, whereas the green samples always contain this element. However, at the present time it is not possible to establish any definite correlation between the green color and Mn.

Of particular interest is the fact that Mg, Al, Fe and Si have been detected systematically in all samples. In no bibliography is any information given about the existence of these elements as impurities in fluorite but at Mina Berta they have even been found in perfect octahedrons of fluorite. Mg is also found in samples of calcite from this deposit, that means that Ca is here always accompanied by Mg.

In all the samples studied Cu is present as a minor element in constant quantity. A great variety of copper minerals is present at "Mina Berta," both primary (chalcopyrite) and secondary (chalcocite, bornite, covellite, azurite, malachite). Although these minerals are included in the mass of fluorite, they are found chiefly near the contacts with the granite walls.

A concentration of azurite and malachite was observed wherever the granite is fractured and slightly altered, even if there are no other copper minerals nearby. This seems to indicate that the water circulating about the deposit has a high copper content. However, this alone does not explain the existence of copper as a minor element in a perfect crystallized fluorite.

In all samples of calcite spectrographically analysed the presence of Cu has been detected. It is believed at the present state of investigation that the presence of Cu in fluorite and calcite shows that the formation of minerals in the deposit was carried out in a single stage, in which the fluorite and the other primary minerals were precipitated simultaneously, and that the original material that formed this deposit was contaminated by Cu.

## References


CALDERÓN, S (1910) Los minerales de España. *Junta Ampliación Estudios*, **1**, 404.

DOELTER, C. AND H. LEITMEIER (1931) *Handbuch der Mineralchemie, Band* **4**, *Teil* **3**, 228. Verlag Theodor Steinkopff, Dresden-Leipzig.

GIMENO, F (1901) Mina de Puig-Pedrós (Papiol). *Bol. Soc. Esp. Hist. Nat.* **1**, 270.

HINTZE, C. (1915) *Handbuch der Mineralogie, Band* **1**, 2381. Verlag Veit und Comp., Leipzig.

INSTITUTO GEOLÓGICO Y MINERO DE ESPAÑA (1930) Memoria explicativa de la hoja nº 420, 77. Mapa geológico a 1:50000.

LÓPEZ DE AZCONA, J. M. (1944) Preparación de electrodos con substancias no conductoras para su análisis espectroquímico. *An. Fís. Quí.* **41**, 791.

——— (1961) Un siglo de aplicación de la espectroquímica a la geoquímica española. *Notas Com. Inst. Geol. Min. Esp.* **63**, 119.

MAESTRE, A. (1878) Descripción geognóstica y minera del distrito de Cataluña y Aragón. *An. de Minas*, **3.**

MAURETA Y THOS, J. AND S. CODINA (1881) Descripción física y geológica de la provincia de Barcelona. *Mem. Comisión mapa geológico.*

RIVAS MATEOS, M. (1903) La fluorita de Papiol. *Bol. Soc. Exp. Hist. Nat.* **3**, 184.

SOLÉ SABARIS, L. (1932) Nota petrográfica sobre una zona metamórfica del Tibidabo. *Bol. Soc. Esp. Hist. Nat.* **32**, 461.

TOMÁS, Ll. (1920) Els minerals de Catalunya. *Trab. Inst. Cat. Hist. Nat.*, 129.

MINERALOGICAL SOCIETY OF AMERICA, SPECIAL PAPER 1, 1963
INTERNATIONAL MINERALOGICAL ASSOCIATION, PAPERS, THIRD GENERAL MEETING

# STRUCTURAL CLASSIFICATION OF ZEOLITES

J. V. SMITH
*Department of the Geophysical Sciences, University of Chicago, Chicago, Illinois*

ABSTRACT

In the past ten years the structures of bikitaite, chabazite, dachiardite, erionite, faujasite, gismondine, gmelinite, harmotome, levyne, mordenite, phillipsite and Linde A have been determined. In addition, proposals have been made for NaP1 and heulandite. Although many structures remain undetermined, it is possible to extend the structural classification started by W. L. Bragg in "Atomic Structure of Minerals" on the basis of the determinations of analcime and the natrolite group.

The zeolites chabazite, gmelinite, erionite and levyne are based on different ways of linking together parallel six-membered rings. Harmotome, phillipsite, NaP1 and gismondine are based on parallel four-membered rings, and are related structurally to feldspar and paracelsian. The structures of faujasite and Linde A are both based on tetrahedra lying at the corners of truncated octahedra linked by other polyhedra, and are thus related to sodalite. The columns of linked five-membered rings in mordenite and dachiardite may also form the basis of other zeolites with a 7.5 Å repeat distance (laumontite and brewsterite) but probably not of ferrierite and heulandite.

## INTRODUCTION

The most recent summary of the crystal structures of zeolites is that given by W. L. Bragg in "Atomic Structure of Minerals" published in 1937 by Cornell University Press. In the last decade, renewed interest in zeolites has led to the determination of the crystal structures of more than a dozen zeolites, and the time is ripe for a new summary.

Classification of structures serves two purposes: first, to make the data more readily available to a wider group of scientists, and secondly, to make it easier to see relationships between structures, thus encouraging the development of ideas on the nature of the crystal structures and on possible solutions of as yet unknown structures. Particular emphasis will be paid to this latter aspect for there are approximately fifteen zeolites whose structures have not been determined. Because zeolites bear important structural relations to other framework silicates such as feldspars, the present classification will be set in as wide a frame as possible.

Defining a zeolite is rather difficult because of the existence of gradational properties, and a broad definition will be used to avoid the danger of excluding a possible candidate from the group. The two characteristic physical properties of a zeolite are those of ion-exchange and reversible dehydration. Detailed study of zeolites has shown that the two phenomena are complex, and that many zeolites show incomplete ion-exchange, and that reversibility occurs only in the initial stage of dehydration. Possibly a more satisfactory definition of a zeolite will come from the nature of the crystal structure. Such a definition might be as follows: a zeolite is an alumino-silicate with a framework structure enclosing cavities occupied by large ions and water molecules, both of which have considerable freedom of movement, permitting ion-exchange and reversible dehydration. Because it is possible that materials with the typical physical properties of zeolites may not have framework structures, the above definition of a zeolite must be applied with caution.

In order to identify the types of linkage in the zeolite structures, and to depict the structures on a two-dimensional paper surface, it has been necessary to resort to various simplifying devices in which tetrahedra and other structural units are denoted by symbols specifying their orientation. Such devices often lead to idealization of the structures, but the details can be found from the original references.

For brevity, no attempt has been made to trace in detail the historical development of the determination of zeolite structures. However the references have been arranged in groups to correspond to the structural classification, and the historical sequence can be determined by inspection of the titles. The author wishes to pay tribute and make grateful acknowledgment to the following scientists who have contributed to this classification of zeolites: Dr. W. H. Taylor for his pioneering studies on analcime and the edingtonite group, Dr. D. W. Breck for ideas on the zeolites such as Linde A which are based on tetrahedra lying at the corners of convex polyhedra, Prof. R. M. Barrer and his group for their pioneering studies on molecular-sieve properties and associated structural effects, Drs. K. Fischer and W. M. Meier for their major contributions to the mordenite, gmelinite and gismondine groups, and also for the

generous way in which they have communicated their data to the author.

## Structural Classification

*Analcime group* The analcime group of zeolites and related silicates consists of three types of analcime, wairakite, pollucite, leucite and viséite. Leucite is anhydrous, and viséite contains phosphorus, so neither fit a strict definition of a zeolite.

*Analcime* $Na(AlSi_2O_6)\cdot H_2O$
Type (a): Isometric, $a$ 13.72 Å, $Ia3d$, optically isotropic.
Type (b): geometrically isometric, $a$ 13.72 Å, not $Ia3d$, anisotropic.
Type (c): geometrically rhombohedral or orthorhombic, if rhombohedral, $a$ 13.71 Å, $\alpha$ 90° 31′, not $Ia3d$, optically anisotropic.

*Wairakite* $Ca(AlSi_2O_6)\cdot 2H_2O$
pseudo-isometric, possibly monoclinic, $a$ 13.69 $b$ 13.68 $c$ 13.56 Å, $\beta$ 90.5°.

*Pollucite* $Ca(AlSi_2O_6)\cdot xH_2O$
tetragonal, pseudo-isometric, $a$ 13.77 Å.

*Leucite* $K(AlSi_2O_6)$
Tetragonal, pseudo-isometric, $a$ 12.98 $c$ 13.68 Å, $I4_1/a$.

*Viseite* $NaCa_5(Al_{10}Si_3P_5O_{30}(OH)_{18})\cdot 8H_2O$
isometric, $a$ 13.65 Å.

All members of the groups have the same type of framework structure that was determined for analcime by Taylor (1930). Depiction of the structure is difficult because of the way in which the different rings of oxygen tetrahedra are twisted and interconnected. Figure 1 is an idealized view down a cube edge (say the $z$-axis). The tetrahedra have been placed into three groups, U (for upwards) with an apex pointing along $+z$ and the base parallel to (001), D (for downwards) with the apex pointing along $-z$, and T (for tilted) in which one edge is parallel and one is perpendicular to $z$. Four-membered rings of type UDUD are connected by T tetrahedra to form rings of type UDTUDTUDTUDT. Each T tetrahedron is joined to a U and a D tetrahedron in a twelve-membered ring and to a U tetrahedron from a lower level and a D tetrahedron from a higher level. There are four levels of four- and twelve-membered rings in each unit cell, linked together by the T tetrahedra. The resultant framework structure has regular six-membered rings parallel to (111), and distorted eight-membered rings parallel to (110). The complex interaction of the 4-, 6-, 8- and 12-membered rings, and the severe distortion of the latter two rings from a regular shape is probably the reason why this structure is so hard to visualize.

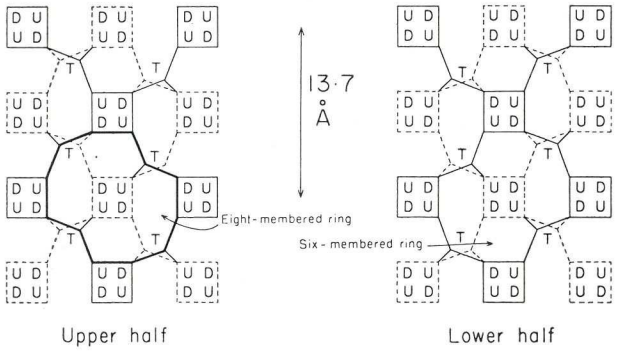


Fig. 1. Schematic crystal structure of analcime. A detailed explanation is given in the text of the method of linkage. The orientations of the terahedra are shown by the symbols U, D and T, and the positions of the tetrahedra are at the intersections of the lines. In each half of the unit cell there are two levels of tetrahedra shown by full (upper) and broken (lower) lines. One of the twelve-membered rings is emphasized by use of a heavy line. The 13.7 Å repeat of the isometric unit cell is shown. The vertical $4_1$ symmetry axes pass between the T tetrahedra which lie at the corners of a square in projection. One each of the six-membered rings and eight-membered rings are pointed out: the six-membered ring is regular in shape, but the eight-membered ring is strongly distorted.

Some of the outstanding structural problems in this group concern the polymorphism of analcime (Coombs, 1955: is it caused by order-disorder of the aluminum and silicon atoms?), the location of cations and water molecules (Náray-Szabó, 1938b; Taylor, 1938; Beattie, 1954), the structural changes occurring between analcime with the usual composition of $NaAlSi_2O_6\cdot H_2O$ and the uncommon silica-rich material (Saha, 1959, 1961) and the detailed structures of wairakite (Steiner, 1955; Coombs, 1955) and viséite (McConnell, 1952).

*Sodalite group*

*Sodalite* Many chemical variants, one example is $Na_4(Al_3Si_3O_{12})Cl$
isometric, $a$ 9.0 Å, $P\bar{4}3n$.

*Linde A* $Na_{12}(Al_{12}Si_{12}O_{48})\cdot 27H_2O$
isometric, $a$ 12.32 Å, Pm3m (pseudo-cell): true cell has $a$ 24.64 Å.

*Faujasite* synthetic forms known as Linde X and Y
$(Na_2, Ca)_{30}(Al, Si_{192}O_{384})\cdot 260H_2O$
isometric, $a$ 24.7 Å, $Fd3m$.

Although sodalite is not a zeolite, it is convenient to use it as a designation for this group of zeolites and related alumino-silicates. (Actually it is possible that a zeolite with the sodalite framework might occur either naturally or synthetically with a composition like $Na_3Al_3Si_3O_{12}\cdot H_2O$). All three known structural types in this group (Reed and Breck, 1956; Barrer, Bultitude and Sutherland, 1957; Bergerhoff, Koyama and Nowacki, 1956; Bergerhoff *et al.* 1956)

are built from linked tetrahedra arranged at the corners of truncated octahedra. (The truncated octahedron is often called a cubo-octahedron: the nomenclature of Encyclopedia Britannica, 1958 edition, vol. 20, p. 945, is used here.) The truncated octahedron contains eight hexagonal faces (octahedral) and six square (cube) faces. In sodalite (Fig. 2) the truncated octahedra share both square and hexagonal faces. The model in Fig. 2 shows eight truncated octahedra arranged at the corners of the isometric unit cell. It will be seen that the truncated octahedra leave just sufficient space for another truncated octahedron at the body center of the cell. In Linde A the truncated octahedra also occupy the corners of the unit cell, but are now joined by cubes to produce a larger cell edge and a larger cavity at the center of the cell. The cavity has the shape of a truncated cubo-octahedron, consisting of six cube faces, eight octahedral faces and twelve dodecahedral faces, all with equal edges.

In faujasite the truncated octahedra are linked by hexagonal prisms at the octahedral faces in such a way as to place the centers of the truncated octahedra at the positions of the carbon atoms in diamond. Because the edges of the hexagons in truncated octahedra are alternatively of two types, those shared between two hexagons, and those shared between a hexagon and a square, adjacent truncated octahedra may be linked in two ways by hexagonal prisms. In faujasite, adjacent truncated octahedra are linked in such a way that the hexagons bordering on the hexagonal prism alternate to give an axis of inverse three-fold symmetry. In the other method of linkage the hexagons face each other across the hexagonal prism to give an axis of three-fold rotational symmetry. A framework can be built from truncated octahedra linked in this pattern, but it is necessary to distort the octahedra. It will be seen from Fig. 2 that large cages are formed, each one comprised of twenty truncated octahedra. There are twelve windows into the cage, each being a prism of ten-fold symmetry. At a casual glance, there are ten three-fold and six ten-fold axes of rotational symmetry, but this is an optical illusion. Ten-fold symmetry requires an angle of 108° between the faces of the prism. If the truncated octahedra are undistorted they are linked through an angle of 109°28′. In the model it is easy to distort the octahedra by 1°28′ thus permitting completion of the cage and yielding apparent high symmetry. It is possible that this unit (or a similar one obtained by removing the hexagonal prisms) may occur in amorphous and gel material where the lack of true symmetry would not matter.

In Fig. 2 is shown a model for a possible structure based on truncated octahedra linked partly in the faujasite manner and partly in the other manner. Dr. D. W. Breck of the Linde Company suggested to the author that there might be a wurtzite equivalent to the zinc blende (or diamond) arrangement found in faujasite, and he showed that if alternate layers of truncated octahedra lying parallel to the (111) planes of faujasite were rotated by 60° and fastened together again, a new framework was obtained which was the wurtzite analog. In this wurtzite form, the bonding between the layers is like that in the hypothetical amorphous variety, but the bonding in the layers is like that in faujasite. The symmetry of the wurtzite form is hexagonal and the cell dimensions are $a$ 19.3 $c$ 28.5 Å.

At the moment the author is studying the ways in which regular polyhedra can be linked together so that he can predict all possible structures of this type. He hopes that it will be possible to find the structures of paulingite and ashcroftine among these possible arrangements, and, indeed, has found a structure with the cell dimensions and symmetry of paulingite, but with too many tetrahedra for the chemical analysis.

### *The chabazite group*

*Chabazite* near $Ca_2(Al_4Si_8O_{24})\cdot 13H_2O$
rhombohedral or pseudo-rhombohedral, possibly monoclinic or triclinic, $a$ 9.44 Å, $\alpha$ 94° 28′, $R\bar{3}m$.

*Gmelinite* near $Na_2(Al_2Si_4O_{12})\cdot 6H_2O$
hexagonal, $a$ 13.72 $c$ 10.02 Å, $P6_3/mmc$.

*Erionite* $(Ca, etc.)_{4.5}(Al_9Si_{27}O_{72})\cdot 27H_2O$
hexagonal, $a$ 13.62 $c$ 15.12 Å, $P6_3/mmc$.

*Levyne* near $Ca(Al_2Si_4O_{12})\cdot 6H_2O$
rhombohedral, $a$ 10.75 Å, $\alpha$ 76° 25′, $R\bar{3}m$.

The structures of the four members of this group were determined in the last four years (Dent and Smith, 1958; Nowacki *et al.*, 1958; Barrer and Kerr, 1959; Staples and Gard, 1959; Fischer, 1960 and personal communication), and are based on parallel six-membered rings of tetrahedra. The group is named from the most commonly-occurring member.

The relations between the structures are shown in Fig. 3 (see Barrer and Kerr, 1959, for additional diagrams). The horizontal six-membered rings of Si, Al tetrahedra are linked either to other rings vertically superimposed giving hexagonal prisms or through tilted four-membered rings to the other horizontal hexagonal rings displaced both vertically and sideways. In projection the centers of the six-membered

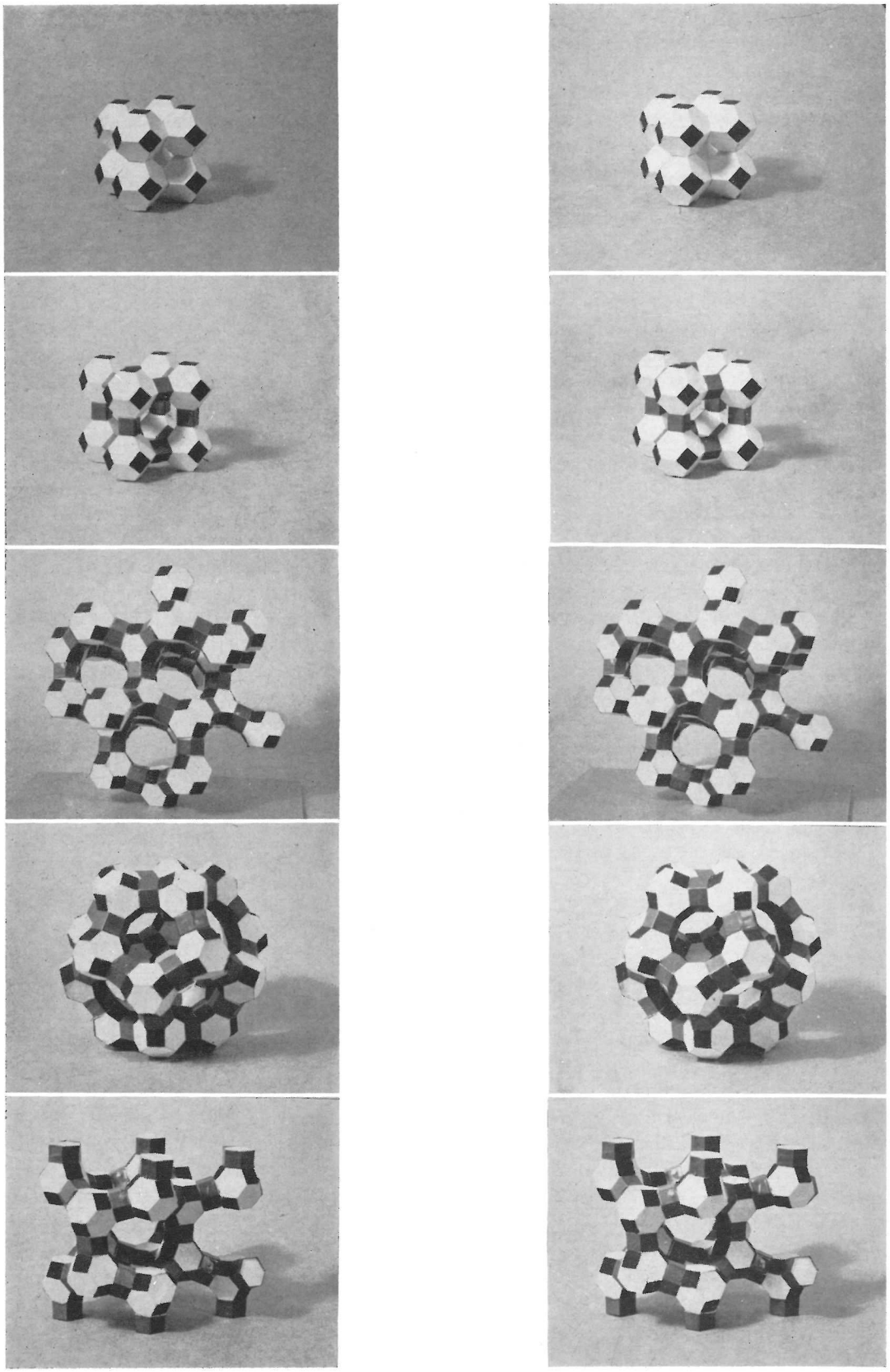

rings lie in the same pattern as close-packed spheres, thus permitting a simple terminology. As is well-known, cubic and hexagonal close-packing can be represented as ABC and AB, where A, B and C represent the three possible horizontal projections of the layers. A similar terminology can be used for the zeolites in the chabazite group if the centers of the hexagonal rings of tetrahedra are specified by the alphabetical symbol. When adjacent layers have the same symbol hexagonal prisms are formed: when they have different symbols, the hexagonal rings are linked by tilted four-membered rings. The possible structures that can be built from parallel six-membered rings are infinite in number, and the simplest are enumerated in the following table. In compiling the list, it should be noted that combinations with three or more identical symbols in sequence are omitted, even though they are possible theoretically.

| | |
|---|---|
| AB | |
| ABC* | |
| AAB | |
| AABC | |
| AABB | gmelinite |
| ABAC | |
| ABABC | |
| AABBC | |
| AABAC | |
| AABBCC* | chabazite |
| AABAAC | erionite |
| AABCCB | |
| AABACC | |
| AABCBB | |
| AABABC | |
| . | |
| . | |
| . | |
| AABCCABBC* | levyne |

All the structures have hexagonal symmetry and a 120° prism for a unit cell except for the three starred ones which have a rhombohedral unit cell. These three structures have a unit cell only one-third as large as that for related structures with the same number of alphabetical symbols. Thus chabazite and levyne have simpler structures than would appear from their position in the list. The combination ABC is the incorrect structure that was proposed for chabazite (Wyart, 1931) thirty years ago.

There is optical and $x$-ray evidence that suggests reduction of symmetry of chabazite from the ideal configuration (possibly to the monoclinic or triclinic systems), and ordering of the silicon and aluminum atoms has been suggested as the cause. The complete structures of hydrated, dehydrated and $Cl_2$-bearing varieties of chabazite have been determined, but only the shape of the framework is known for the other zeolites of this group. Intergrowths of gmelinite and chabazite have been found, indicating stacking errors in the sequence of hexagonal prisms.

*Natrolite group*

| | |
|---|---|
| *Natrolite* | $Na_2(Al_2Si_3O_{10})\cdot 2H_2O$ orthorhombic, $a$ 18.30 $b$ 18.63 $c$ 6.60 Å, *Fdd*2. |
| *Scolecite* | $Ca(Al_2Si_3O_{10})\cdot 3H_2O$ probably monoclinic, $a$ 18.52 $b$ 18.99 $c$ 6.56 Å, *Cc*. |
| *Mesolite* | $Na_2Ca_2(Al_2Si_3O_{10})_3\cdot 8H_2O$ monoclinic (?), $a$ 56.8 $b$ 6.55 $c$ 18.48 Å, $\beta$ 90° 00′. |
| *Edingtonite* | $Ba(Al_2Si_3O_{10})\cdot 3H_2O$ probably orthorhombic pseudo-tetragonal, $a$ 9.58 $b$ 9.70 $c$ 6.54 Å, $P\bar{4}2_1m$ (pseudo ?). |
| *Thomsonite* | near $NaCa_2(Al_5Si_5O_{20})\cdot 6H_2O$ orthorhombic, $a$ 13.0 $b$ 13.0 $c$ 13.3, *Pn*2*n*. |
| *Gonnardite* | $(Ca, Na)_{6-8}(Si, Al_{20}O_{40})\cdot 12H_2O(Al\backsim 9)$ orthorhombic, $a$ and $b$ like thomsonite, $c$ 6.6 Å. |
| *Metanatrolite* | natrolite dehydrated at 300° C. monoclinic (?) $a$ 16.3 $b$ 17.1 $c$ 6.6 Å, $\gamma$ 90°, *F*112. |

Because the structural properties of this group are so well described in Bragg's "Atomic Structure of Minerals," readers are referred there first. The following additional comments may prove useful. All structures are based on cross-linking of columns of tetrahedra and the three possible ways of doing this are all found in nature: edingtonite; natrolite, scolecite and mesolite; thomsonite and gonnardite. Thus this group of zeolites is complete, apart from the possible discovery of further compositional variants. (To prove that there are only three ways of cross-linking the columns, examine Fig. 139 in Bragg's book and subtract 3 from each number in the edingtonite diagram, 2 from the thomsonite and 1 from the natrolite. The numbers around the diamond-shaped



FIG. 2. Stereoscopic pairs of models of structures built from truncated octahedra: from top to bottom, sodalite, Linde A, faujasite, amorphous variety, wurtzite analog of faujasite. To aid in visualization, the square faces of the truncated octahedra are painted black and the square faces of the linking cubes and hexagonal prisms are covered in a neutral tone. The intersection of four edges marks the center of a tetrahedron where a silicon or aluminum atom resides, while oxygen atoms occur near, but not on, the centers of the edges. The sodalite and Linde A models are resting on a (100) face. The faujasite model is arranged with a [111] axis vertical to permit easy comparison with the model of the wurtzite-analog which has an [0001] axis vertical.

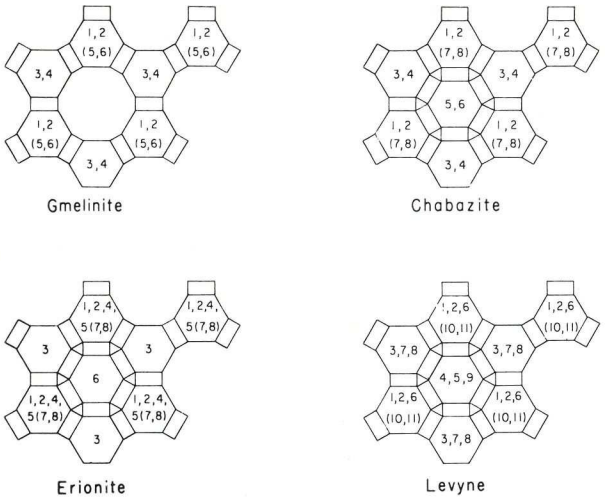


FIG. 3. Schematic representations of the gmelinite, chabazite, erionite and levyne structures. The heights of the six-membered rings of tetrahedra are shown by the numbers, and the positions of the tetrahedra by the intersections of the lines. The structural pattern may be visualized by following the sequence of the numbers. Where adjacent six-membered rings are vertically superimposed, hexagonal prisms are formed: where they are displaced sideways, they are linked by tilted four-membered rings. The number in brackets denotes the next unit cell. Large cavities, linked by apertures, are formed in the framework: see Barrer and Kerr (1959) for perspective drawings.

units become 0202 for edingtonite, 0242 for thomsonite and 0246 for natrolite. Because the numbers must change by 2, and 8 is the unit cell repeat of 0, these are the only three combinations.)

Meier (1960) has shown that the silicon and aluminum atoms in natrolite are ordered, and is known to have a paper in preparation on the ordering in mesolite and scolecite. It seems likely that gonnardite with a 6.6 Å *c*-axis and thomsonite with a 13.2 Å repeat are related by order-disorder of the tetrahedrally-coordinated atoms.

### *Phillipsite group*

*Phillipsite* $(K, Na)_5(Al_5Si_{11}O_{32}) \cdot 10H_2O$
orthorhombic, *a* 9.96 *b* 14.25 *c* 14.25 Å, *B2mb* or monoclinic, *a* 10.02, *b* 14.28 *c* 8.64 Å, $\beta$ 125° 40′, $P2_1$ or $P2_1/m$.

*Harmotome* $Ba_2(Al_4Si_{12}O_{32}) \cdot 12H_2O$
monoclinic (pseudo-orthorhombic), *a* 9.87 *b* 14.14 *c* 8.72 Å, $\beta$ 124° 50′, $P2_1$.

*Gismondine* $Ca(Al_2Si_2O_8) \cdot 4H_2O$
monoclinic, *a* 9.84 *b* 10.02 *c* 10.62 Å, $\gamma$ 92.4°, $P112_1/a$.

*Garronite* $(NaCa_{2.5})(Al_6Si_{10}O_{32}) \cdot 13\frac{1}{2}H_2O$
Tetragonal (?), *a* 10.01 *c* 9.87 Å.

*NaP1* (named by Barrer *et al.*; identical with Linde B and Saha's B)
$Na_2(Al_2Si_3O_{10}) \cdot 5H_2O$
isometric, *a* 10.0 Å
(numerous cationic variants also occur).

The structures of this group are based on parallel four- and eight-membered rings of tetrahedra. The first structure of this group of zeolites to be determined in detail was that of harmotome (Sadanaga, *et al.*, 1961), who found that it consisted of cross-linked chains of tetrahedra of the same kind as those already found in the alumino-silicates feldspar and paracelsian (Fig. 4). It had long been suspected that harmotome and phillipsite were iso-structural, and this was confirmed by the publication of the structure of phillipsite by Steinfink (1961). (This structure is more regular, and based on an orthorhombic unit cell: it is possible that it may need minor modification to fit the monoclinic (pseudo-orthorhombic) geometry generally found for phillipsite.) Upon learning that the harmotome structure was built from the double-crankshaft chains of the feldspar structure, Smith and Rinaldi (1962) developed all the simple structures that could be built from cross-linked feldspar chains. Of the seventeen that resulted, one of

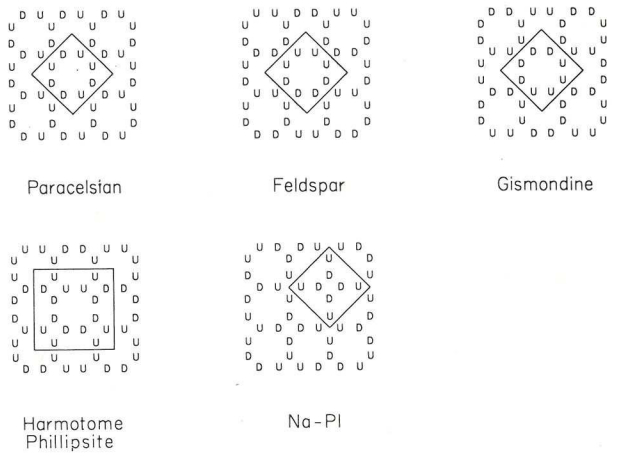


FIG. 4. Schematic representation of members of the harmotome group and the related silicates, feldspar and paracelsian. In each structure four-membered rings of tetrahedra are formed, of type UUDD in paracelsian, feldspar, gismondine and harmotome (or phillipsite), and type UUUU or DDDD in Na-P1. By sharing an oxygen atom between U and a superimposed D tetrahedron infinite chains perpendicular to the plane of the paper are formed in the first four structures, and cubes in the fifth structure. Sharing of oxygen atoms in the plane of the paper leads to eight-membered rings of type UUDUDDUD in paracelsian, and so on in the other structures. The smallest unit cell that is obtained for a regular structure is shown by the squares. Actually the structures of the anhydrous forms, paracelsian and feldspar, collapse in a non-symmetrical way so that a larger unit cell is formed. The structures of gismondine, harmotome (phillipsite) and Na-P1 expand to permit entry of water molecules, but the axes of the unit cell maintain the position shown in these idealized diagrams. Detailed explanation of these structures is given by Rinaldi and Smith (1962).

the fourteen that remained after assignation of three structures to feldspar, paracelsian and harmotome was suggested as a possible structure for gismondine. Fischer (private communication) independently showed that this hypothesis was correct, and has refined the atomic coordinates to a high degree of precision. The four structures are shown in Fig. 4, where U and D have the same significance as earlier.

Barrer, *et al.* (1959) reported on the synthesis and ion-exchange properties of various phases that gave *x*-ray powder patterns related to those of harmotome. One of these, denoted Na-P1, has also been prepared by the Linde Company (denoted Zeolite B), and by Saha (also called B). Barrer *et al.* indexed the powder pattern with an isometric unit cell and proposed a crystal structure based on parallel four- and eight-membered rings, but with UUUU rings instead of the UUDD rings in feldspar. The linkage of these rings leads to the formation of cages with tetrahedra lying at the corners of cubes. At the same time, Dr. G. P. L. Walker of Imperial College, London, was discovering a new zeolite, named garronite, in his study of the vug minerals of the Tertiary basalts of Ireland. Barrer *et al.* synthesized a sodium zeolite Na-P2 which was tetragonal, but otherwise similar to Na-P1. The Ca-exchanged product of Na-P2 gave an *x*-ray powder pattern identical with that of garronite. In addition, Barrer *et al.* made a third sodium zeolite, Na-P3, which is similar to the sodium-exchanged form of harmotome. Smith and Rinaldi extended their study of framework structures built from rings of type UUDD and UUUU to include UDUD and UUUD rings. Three of the resulting structures (labelled 2, $\beta$ and $\gamma$ in their paper) would give cell dimensions and powder patterns similar to those for Na-P1 and garronite. Thus there is still some uncertainty about the structures of these zeolites, but there seems no reasonable doubt that they belong to this structural group because of the general similarities of the *x*-ray powder patterns.

### *Mordenite group*

*Mordenite (ptilolite)* $Na(AlSi_5O_{12})\cdot 3H_2O$
orthorhombic, *a* 18.13 *b* 20.49 *c* 7.52 Å, *Cmc*$2_1$,

*Dachiardite* $(Na_2, Ca)_2(Al_4Si_{20}O_{48})\cdot 12H_2O$
monoclinic *a* 18.35 *b* 7.54 *c* 10.25 Å, $\beta$ 107° 49′, *C*2/*m*.

The structure of mordenite (Fig. 5), as determined by Meier (1961), consists of columns of five-membered rings of type UDDTT (or DUUTT) which are cross-linked by four-membered rings in one direction and by sharing of oxygen atoms in the other direction. Meier showed that there was another way of joining the columns together by four-membered rings, and this has turned out to be the structure of dachiardite (Gottardi and Meier, 1962).

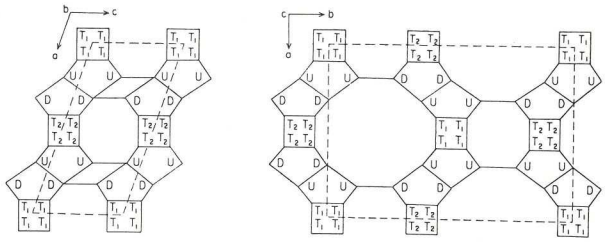


FIG. 5. Schematic representation of the structures of dachiardite and mordenite (ptilolite). The tilted $T_1$ and $T_2$ tetrahedra have a relative displacement of half the repeat distance of the 7.5 Å axis (*b* in dachiardite, *c* in mordenite).

Both structures have a 7.5 Å repeat distance along the columns, which is the length obtained for the total vertical height of three linked tetrahedra, one each with the U, D and T orientations. Other zeolites—heulandite, ferrierite, laumontite (leonhardite) and brewsterite—have this repeat distance and it is tempting to suggest that they may be based on different ways of cross-linking columns of the mordenite type: indeed Rinaldi (personal communication) has discovered several ways of cross-linking these columns with six- and eight-membered rings. One of these fits the cell dimensions, symmetry and cell contents of heulandite, but did not explain the Patterson projection. It seems that at least heulandite is based on a framework that does not contain a mordenite type column: study of the Patterson projection suggests that the structure of this important zeolite will be solved by Rinaldi soon (see later for further discussion of heulandite, ferrierite, laumontite and brewsterite).

### *Bikitaite*

*Bikitaite* $LiAlSi_2O_6\cdot H_2O$
monoclinic, *a* 8.61 *b* 4.96 *c* 7.61 Å, $\beta$ 114° 26′, $P2_1$.

Although an abstract announcing the solution of the structure of bikitaite has been published (Appleman, 1960), a detailed account of the structure has not yet appeared in press. Dr. Appleman has kindly allowed me to see his drawings of the crystal structure: neither he nor I have been able to find any obvious relation to the structures of other zeolites. However, detailed examination of a three-dimensional model may permit later recognition of a relationship.

*Zeolites with unknown structures*

*Paulingite* near $(K, Ca, Na)_{120}(Al, Si)_{580}O_{1160}\cdot 690H_2O$
isometric, $a$ 35.1 Å, probably $Im3m$.

*Ashcroftine* near $(K, Na, Ca)_{120}(Al_{160}Si_{200})O_{720}\cdot 320H_2O$
tetragonal, $a$ 34.0 $c$ 17.5 Å.

*Thaumasite* near $Ca_3H_2(CO_3)(SO_4)(SiO_4)\cdot 13H_2O$
hexagonal, $a$ 11.0 $c$ 10.4 Å, $P6_3$.

*Ferrierite* near $(Na, K)_4Mg_2(Al_6Si_{30})O_{72}(OH)_2\cdot 18H_2O$
orthorhombic, $a$ 19.12 $b$ 14.4 $c$ 7.48 Å, $Immm$, $I222$, $I2_12_12_1$ or $Imm2$.

*Heulandite and Clino-ptilolite* (a compositional variant)
near $(Ca, K, Na)(Al_2Si_7)O_{18}\cdot 6H_2O$
monoclinic, $a$ 15.85 $b$ 17.9 $c$ 7.45 Å, $\beta$ 91° 24′, $I2/m$.

*Laumontite* near $(Ca, Na, K)(Al_2Si_4)O_{12}\cdot 4H_2O$
monoclinic, $a$ 14.90 $b$ 13.17 $c$ 7.55 Å, $\beta$ 111° 30′, $C2$ or $Cm$.
leonhardite, the partially dehydrated form of laumontite, has: $a$ 14.75 $b$ 13.10 $c$ 7.55 Å, $\beta$ 112° 0′.

*Brewsterite* $(Sr, Ba, Ca)(Al_2Si_6)O_{16}\cdot 5H_2O$
monoclinic, $a$ 6.77 $b$ 17.41 $c$ 7.66 Å, $\beta$ 93° 04′.

*Stilbite* near $Na_2Ca_4(Al_{10}Si_{26})O_{12}\cdot 28H_2O$
monoclinic, $a$ 13.6 $b$ 18.2 $c$ 11.3 Å, $\beta$ 129° 10′, $C2/m$.

*Epistilbite* near $Ca(Al_2Si_6)O_{10}\cdot 5H_2O$
monoclinic $a$ 8.9 $b$ 17.7 $c$ 10.2 Å, $\beta$ 124° 20′.

*Yugawaralite* $Ca_4(Al_7Si_{20})O_{54}\cdot 14H_2O$
monoclinic, $a$ 13.26 $b$ 13.65 $c$ 9.73 Å, $\beta$ 111° 30′.

*Rhodesite* $(Ca, Na, K)_8Si_{16}O_{40}\cdot 11H_2O$
orthorhombic, $a$ 23.8 $b$ 6.54 $c$ 7.05 Å.

*Mountainite* $(Ca, Na, K)_8Si_{16}O_{40}\cdot 12H_2O$
monoclinic, $a$ 13.51 $b$ 13.10 $c$ 13.51 Å, $\beta$ 104°.

Although the structures of none of these minerals are known, there are some interesting relations between the cell dimensions of some of them. The $a$ dimension of ashcroftine is similar to that of paulingite, and the $c$ dimension is halved, suggesting that that there may be a structural relationship. A structure has been suggested for heulandite by Ventriglia (1955), but comparison of its vectors with the Patterson projection prepared by Rinaldi (private communication) shows no correspondence. The pseudo-orthorhombic cell of heulandite is similar in dimensions to the truly orthorhombic cell of ferrierite and there is a fair correspondence between the intensities. Consequently it seems likely that these two zeolites have the same structural framework. Dr. K. Fischer is trying to determine the structure of laumontite at the present time, and Dr. F. Rinaldi has taken preliminary measurements of brewsterite. Strunz and Tennyson (1956) have shown that there are interesting geometrical relations between heulandite, stilbite and epistilbite, the most obvious one being the presence of an axis with an 18 Å repeat distance. Three minerals (thaumasite, rhodesite and mountainite) which are not strictly zeolites are included: it was thought best to include them because their water is partly of zeolite type. Hydro-nepheline was not included because there is considerable doubt concerning its identity. At least one other probable zeolite is known to the author (it has cell dimensions similar to those of thomsonite, and it occurs in veins in Oregon granite), and several others are suspected by other zeolite investigators. It seems likely that the list of zeolites will become considerably larger than that given here.

## Conclusion

The first classifications of zeolites were based on external morphology and proved of considerable value in directing the attention of structural crystallographers to zeolites with related structures. Thus the members of the natrolite group have similar morphology, and phillipsite and harmotome were suspected correctly by the morphologists to be isostructural. However, it is unlikely that erionite with its fibrous habit would be linked with the equant zeolite, chabazite. Study of the structural units of zeolites has revealed many other possible arrangements and it seems possible that some of these will be found to fit as yet unknown zeolites.

## References

*Analcime group*

Barrer, R. M., J. W. Baynham and N. McCallum (1953) Hydrothermal chemistry of silicates. Part V. Compounds structurally related to analcite. *Jour. Chem. Soc. London*, 4035–4041.

Beattie, I. R. (1954) The structure of analcite and ion-exchanged forms of analcite. *Acta Cryst.* **7**, 357–359.

Coombs, D. S. (1955) X-ray observations on wairakite and non-cubic analcime. *Mineral. Mag.* **30**, 699–707.

McConnell, Duncan (1952) Viséite, a zeolite with the analcime structure and containing linked $SiO_4$, $PO_4$ and $H_xO_4$ groups. *Am. Mineral.* **37**, 609–617.

Naray-Szabó, St. (1938a) Die Struktur des Pollucits $CsAlSi_2O_6\cdot xH_2O$. *Zeits. Krist.* **99**, 277–282.

——— (1938b) Note on the structure of analcite. *Zeit. Krist.* **99**, 291.

——— (1942) Die Struktur des Leucits $KAlSi_2O_6$. *Zeit. Krist.* **104**, 39–44.

Saha, P. (1959) Geochemical and $x$-ray investigations of natural and synthetic analcites. *Am. Mineral.* **44**, 300–313.

——— (1961) The system $NaAlSiO_4$ (nepheline) $-$ $NaAlSi_3O_8$ (albite) $-$ $H_2O$. *Am. Mineral.* **46**, 859–884.

Steiner, A. (1955) Wairakite, the calcium analogue of analcime, a new zeolite mineral. *Mineral Mag.* **30**, 691–698.

TAYLOR, W. H. (1930) The structure of analcite $NaAlSi_2O_6 \cdot H_2O$. *Zeit. Krist.* **74,** 1–19.

——— (1938) Note on the structures of analcite and pollucite. *Zeit. Krist.* **99,** 283–290.

WYART, J. (1938) Étude sur la leuvcite. *Bull. Soc. Franc. Mineral. Crist.* **61,** 228–239.

——— (1940) Etude cristallographique d'une leucite artificielle: structure atomique et symétrie du minéral. *Bull. Soc. Franc. Mineral. Crist.* **63,** 5–17.

*Sodalite group*

BARRER, R. M., F. W. BULTITUDE AND J. W. SUTHERLAND (1957) Structure of faujasite and properties of its inclusion complexes with hydrocarbons. *Trans. Faraday Soc.* **53,** 111–123.

——— AND W. M. MEIER (1958) Structural and ion-sieve properties of a synthetic crystalline exchanger. *Trans. Faraday Soc.* **54,** 1074–1085.

BERGERHOFF, G., W. H. BAUR AND W. NOWACKI (1958) Über die Kristallstruktur des Faujasites. *Neues Jahrb. Mineral. Mh.* **9,** 193–200.

——— H. KOYAMA AND W. NOWACKI (1956) Zur Kristallstruktur der Mineralien der Chabasit- und der Faujasitgruppe. *Experientia,* **12,** 418.

BRECK, D. W., W. G. EVERSOLE, R. M. MILTON, T. B. REED AND T. L. THOMAS (1956) Crystalline zeolites I The properties of a new synthetic zeolite, Type A. *Jour. Am. Chem. Soc.* **78,** 5963–5971.

BROUSSARD, L. AND D. P. SHOEMAKER (1960) The structures of synthetic molecular sieves. *Jour. Am. Chem. Soc.* **82,** 1041–1051.

HOWELL, P. A. (1960a) Low angle X-ray scattering from synthetic zeolites A, X and Y. *Jour. Phys. Chem.* **64,** 364–367.

——— (1960b) A refinement of the cation positions in synthetic zeolite type A. *Acta Cryst.* **13,** 737–741.

KERR, G. T. AND G. T. KOKOTAILO (1961) Sodium zeolite ZK-4, a new synthetic crystalline aluminosilicate. *Jour. Am. Chem. Soc.* **83,** 4675.

REED, T. B. AND BRECK, D. W. (1956) Crystalline zeolites II. Crystal structure of synthetic zeolite, Type A. *Jour. Am. Chem. Soc.* **78,** 5972–5977.

PAULING, L. (1930) The structure of sodalite and helvite. *Zeit. Krist,* **74,** 213–225.

STRUNZ, H. (1955) Zur Kristallchemie des Wasser-reichsten Zeolithes Faujasite. *Naturwiss.* **42,** 485.

*Chabazite group*

BARRER, R. M. AND I. S. KERR (1959) Intra crystalline channels in levynite and some related zeolites. *Trans. Faraday Soc.,* **55,** 1915–1923.

BERGERHOFF, G., H. KOYAMA AND W. NOWACKI (1955) Zur Kristallstruktur der Mineralien der Chabasit- und der Faujasitgruppe. *Experientia,* **12,** 418–419.

DENT, L. S. AND J. V. SMITH (1958) Crystal structure of chabazite, a molecular sieve. *Nature,* **181,** 1794–1796.

FISCHER, K. (1960) Strukturuntersuchung von Gmelinit. *Fortsch. Mineral.* **38,** 201.

FANG, J. H. AND J. V. SMITH (1962) Crystal structures with a chabazite framework: IV Ca-$Cl_2$-chabazite at room temperature (in prep.).

NOWACKI, W., M. AELLEN AND H. KOYAMA (1958) Einige Röntgendaten über Chabasit, Gmelinit and Lévyn. *Schweiz. Mineral. Petr. Mitt.* **38,** 53–60.

——— H. KOYAMA AND M. H. MLADECK (1958) The crystal structure of the zeolite, Chabazite. *Experientia,* **14,** 396.

RINALDI, F., C. K. KNOWLES AND J. V. SMITH (1962) Crystal structures with a chabazite framework: III Hydrated Ca-chabazite at both room and low temperature (in prep.)

SMITH, J. V. (1962) Crystal structures with a chabazite framework: I Dehydrated Ca-chabazite, *Acta Cryst.* **15,** 835–845.

——— F. RINALDI AND L. S. DENT GLASSER (1963), Crystal structures with a chabazite framework: II Hydrated Ca-chabazite at room temperature. *Acta Cryst.* **16,** 45–53.

STAPLES, L. W. AND J. A. GARD (1959) The fibrous zeolite erionite; its occurrence, unit cell, and structure. *Mineral. Mag.,* **32,** 261–281.

STRUNZ, H. (1956) The zeolites gmelinite, chabazite, levyne (phacolite, herschelite, seebachite, offretite). *Neues. Jahrb. Mineral. Mh.* **11,** 250–259.

WYART, J. (1931) Étude sur la chabasie. *Compt. Rend. Acad. Sci. Paris,* **192,** 1244–1246.

——— (1933) Recherches sur les zéolites. *Bull. Soc. Franc. Mineral.* **56,** 81–187.

*Natrolite group*

FANG, J. H. (1960) Ph.D. dissertation, Pennsylvania State University, Part 2. Dehydrated Natrolite.

HEY, M. H. AND F. A. BANNISTER (1932a) Studies on the zeolites. Part II. Thomsonite (including faroelite) and gonnardite. *Mineral. Mag.* **23,** 51–125.

——— AND F. A. BANNISTER (1932b) Studies on the zeolites, Part III. Natrolite and metanatrolite. *Mineral. Mag.* **23,** 243–289.

——— AND F. A. BANNISTER (1933) Studies on the zeolites. Part V. *Mesolite. Mineral. Mag.* **23,** 412–447.

——— AND F. A. BANNISTER (1934) Studies of the zeolites. Part VI. Edingtonite. *Mineral Mag.* **23,** 483–494.

——— AND F. A. BANNISTER (1936) Studies on the zeolites. Part IX. Scolecite and metascolecite. *Mineral Mag.* **24,** 227–253.

MEIER, W. M. (1960) The crystal structure of natrolite. *Zeit. Krist.* **113,** 430–444.

MEIXNER, H., M. H. HEY AND A. A. MOSS (1956) Some new occurrences of gonnardite. *Mineral Mag.* **31,** 265–271.

PAULING, L. (1930) The structure of some sodium and calcium aluminosilicates. *Proc. Nat. Acad. Sci.* **16,** 453–459.

TAYLOR, W. H. (1935) An X-ray examination of substituted edingtonites. *Mineral Mag.* **24,** 208–226.

——— AND R. JACKSON (1933) The structure of edingtonite. *Zeit. Krist.* **86,** 53–64.

——— C. A. MEEK AND W. W. JACKSON (1933) The structures of the fibrous zeolites. *Zeit. Krist.* **84,** 373–398.

WYART, J. (1931) Sur les reseaux cristallin de la thomsonite et de la mésotype. *Compt. Rend. Acad. Aci. Paris,* **193,** 666–668.

——— (1933), Recherches sur les zéolites. *Bull. Soc. Franc. Mineral.* **56,** 81–187.

*Harmotome group*

BARRER, R. M., F. W. BULTITUDE AND I. S. KERR (1959) Some properties of, and a structure scheme for, the harmotome zeolites. *Jour. Chem. Soc. London,* **294,** 1521–1528.

FISCHER, K. (1962) The crystal structure determination of the zeolite gismondite, $CaAl_2Si_2O_8 \cdot 4H_2O$. Submitted to *Am. Mineral.*

——— AND H. KUZEL (1958) Elementarzelle und Raumgruppe von Gismondin. *Naturwiss.,* **45,** 488.

KRAUS, O. (1939) Röntgenographische Untersuchungen an Gismondin. *Zent. Mineral. Abt, A.* 105–109.

MILTON, R. N. (1959) Crystalline zeolite B. U. S. Patent 3,008,803.

SADANAGA, R., F. MARUMO AND Y. TAKÉUCHI (1961) The crystal structure of harmotome, $Ba_2Al_4Si_{12}O_{32}\cdot 12H_2O$. *Acta Cryst.* **14,** 1153–1162.

SEKANINA, J. AND J. WYART (1937) Sur l'harmotome. *Bull. Soc. Franc. Mineral.* **60,** 139–145.

SMITH, J. V. AND F. RINALDI (1962) Framework structures formed from parallel four- and eight-membered rings. *Mineral Mag.* **33,** 202–212.

STEINFINK, H. (1962) The crystal structure of zeolite, phillipsite. *Acta. Cryst.* **15,** 644–651.

WALKER, G. P. L. (1962a) Garronite, a new zeolite, from Ireland and Iceland. *Mineral. Mag.* **33,** 173–186.

——— (1962b) Low-potash gismondine from Ireland and Iceland. *Mineral. Mag.* **33,** 187–201.

WYART, J. AND P. CHATELAIN (1938) Étude cristallographique de la christianite. *Bull. Soc. Franc. Mineral* **61,** 121–126.

*Mordenite group*

BONATTI, S. (1942) Ricerche sulla dachiardite. *Atti (Mem.) Soc. Toscana Sci. Nat.* **50,** 14–25.

GOTTARDI, G. AND W. M. MEIER (1962) The crystal structure of dachiardite. *Am. Mineral.* **47,** 190–191 (abstract).

MEIER, W. M. (1961) The crystal structure of mordenite (ptilolite). *Zeit. Krist.* **115,** 439–450.

WAYMOUTH, C., P. C. THORNELEY AND W. H. TAYLOR (1938) An X-ray examination of mordenite (ptilolite), *Mineral Mag.* **25,** 212–216.

*Bikitaite and miscellaneous zeolites*

APPLEMAN, D. E. (1960) The crystal structure of bikitaite, $LiAlSi_2O_6\cdot H_2O$. abs. *Acta Cryst.* **13,** 1002.

COOMBS, D. S. (1952) Cell size, optical properties and chemical composition of laumontite and leonhardite. *Am. Mineral.* **37,** 812–830.

GARD, J. A. AND H. F. W. TAYLOR (1957) An investigation of two new minerals: rhodesite and mountainite. *Mineral. Mag.* **31,** 611–623.

HEY, M. H. AND F. A. BANNISTER (1932) Studies on the zeolites. IV. Ashcroftine (kalithomsonite of S. G. Gordon). *Mineral. Mag.* **23,** 305.

KAMB, W. B. AND W. C. OKE (1960) Paulingite, a new zeolite, in association with erionite and filiform pyrite. *Am. Mineral.*, **45,** 79–91.

KNILL, D. C. (1960) Thaumasite from Co. Down, Northern Ireland. *Mineral Mag.* **32,** 416–418. See this paper for complete bibliography.

SAKURAI, K. AND A. HAYASHI (1952) Yugawaralite, a new zeolite. *Sci. Rept. Yokohama Univ. Sec.* **11** (1), 69–77.

SEKANINA, J. AND J. WYART (1936) Sur la stilbite. *Bull. Soc. Franc. Mineral.* **59,** 377–383.

STAPLES, L. W. (1955) *X*-ray investigation of ferrierite, a zeolite. *Am. Mineral.* **40,** 1095–1099.

STRUNZ, H. AND C. TENNYSON (1956) "Polymorphie" in der Gruppe der Blätterzeolithe (Heulandit-Stilbit-Epistilbit; Brewsterit). *Neues Jahrb., Mineral., Mh* 1–9.

VENTRIGLIA, V. (1955) La structura della heulandite. *Period. Mineral.* **24,** 48–83.

WYART, J. (1930) Étude de la heulandite an moyen des rayons X. *Compt. Rend. Acad. Sci. Paris.* **190,** 1564–1566.

## NOTE ADDED AFTER SUBMISSION OF THE PAPER

In preparing this paper, the work of Barrer and White (*Jour. Chem. Soc. London*, 1952, 1561–1571) was accidentally overlooked. They prepared a hydroxy-sodalite whose water was zeolitic in nature, a sodium alumino-silicate labelled L which was monoclinic $a$ 8.10 $b$ 6.10 $c$ 4.88 Å, $\beta$ 105° 20′ and another one labelled M which was orthorhombic $a$ 11.75 $b$5.81 $c$ 8.52 Å.

MINERALOGICAL SOCIETY OF AMERICA, SPECIAL PAPER 1, 1963
INTERNATIONAL MINERALOGICAL ASSOCIATION, PAPERS, THIRD GENERAL MEETING

# THE CRYSTAL STRUCTURE OF DACHIARDITE

G. GOTTARDI AND W. M. MEIER
*Instituto di Mineralogia dell'Università, Pisa, Italy, and Technikum, Winterthur and Institut für Kristallographie und Petrographie der ETH, Zurich, Switzerland*

ABSTRACT

Structural work on mordenite suggested a possible structure for dachiardite, a rare zeolite. This trial structure has been confirmed by 2-dimensional Fourier syntheses.

The crystals are monoclinic with space group *B2/m* or *Bm*. The framework structure of dachiardite is closely related to the mordenite structure. There are comparatively wide channels along both the *b* and *c* axes.

Dachiardite is a rare zeolite which occurs in association with mordenite on Elba, Italy. Its composition, (K, Na, $Ca_{\frac{1}{2}})_5Al_5Si_{19}O_{48}\cdot 12H_2O$, is very nearly that of mordenite. The crystal data of the two zeolites are as follows:

| *Dachardite* (D) | *Mordenite* (M) |
|---|---|
| monoclinic[1] | orthorhombic |
| $a=18.73$ Å | $a=18.13$ Å |
| $b=10.30$ Å | $b=20.49$ Å |
| $c=7.54$ Å $\gamma=107°54'$ | $c=7.52$ Å |
| Space group: *B2/m* or *Bm* | *Cmcm* or *Cmc2* |

The relationship between the unit cells of D and M, as illustrated in Fig. 1, was first noted by Gottardi (1960)

The structure of M is based on characteristic chains shown in Fig. 2 (Meier, 1961). These chains can be linked in two different ways to give the aluminosilicate frameworks of M and D. Figure 3 shows the resultant frameworks in projection along [001]. The trial structure of D (involving framework atoms only) gave an initial R-factor of 0.37 for the *hk0* reflections. Two-dimensional Fourier and difference maps confirmed the general features of the framework

[1] The first monoclinic setting is used in this paper for convenience.

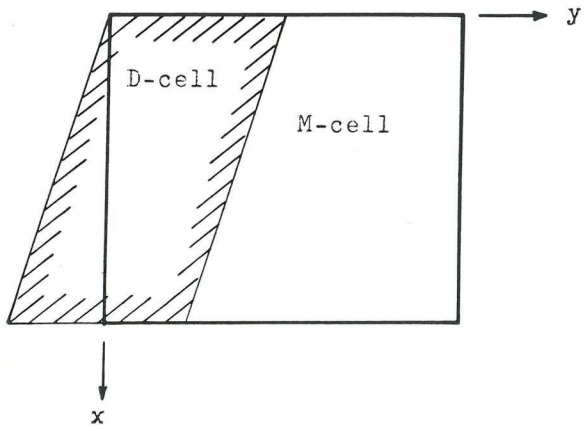


FIG. 1. Unit cells of D and M.

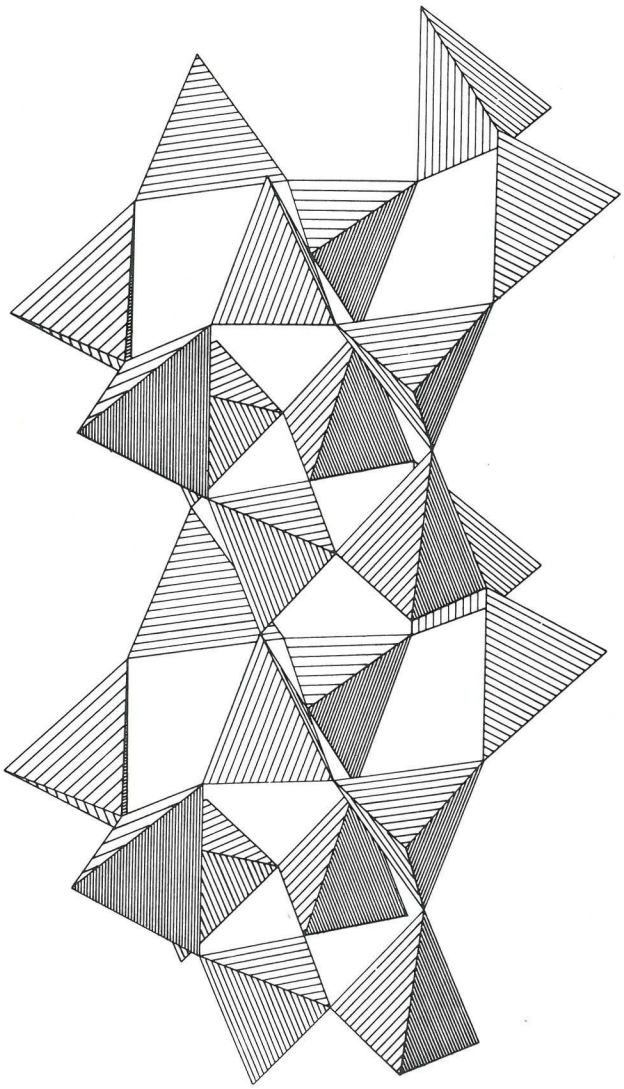

FIG. 2. Mordenite chain.

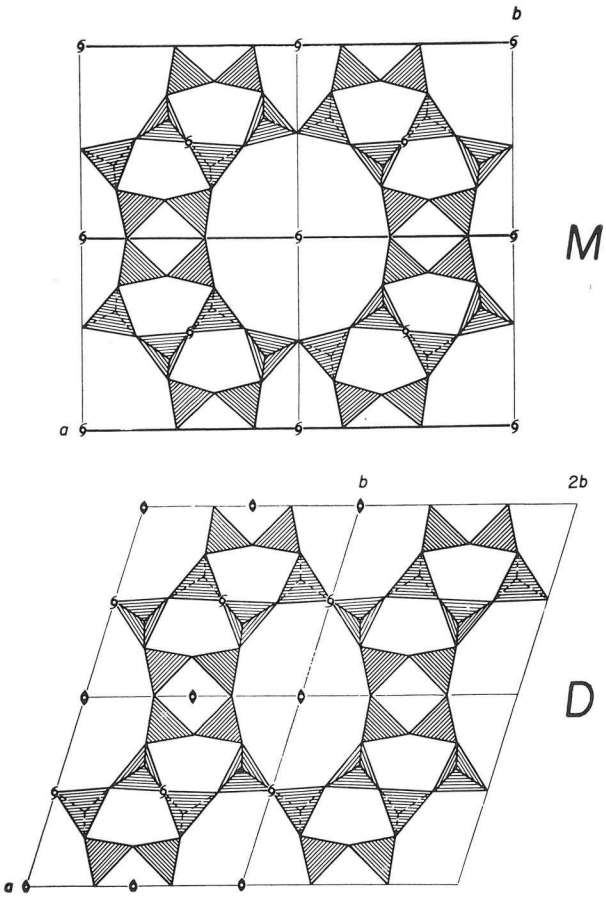


and indicated probable positions for the cations and some of the water molecules. The R-factor for the *hk0* reflections of the structure with cations and water has been reduced to 0.22 in the course of 4 cycles of refinement by means of difference maps. (The R-factor for the aluminosilicate framework alone is 0.30). Fourier projections along [010] and [100] were also computed and helped to confirm the structure.

The structure of D is penetrated by a 2-dimensional system of comparatively wide channels. The main channels run parallel to the *c* axis and are interconnected by channels parallel to the *b* axis. The free openings of these channels are about 4 Å. The observed twinning of D can be readily explained on the basis of the aluminosilicate framework.

Three-dimensional refinement using low-temperature data of the sodium form of D is in progress. A more detailed account of our work will be published in Zeitschrift für Kristallographie.

## References

Gottardi G. (1960) Sul dimorfismo mordenite-dachiardite. *Period. Mineral.* **28,** 183.

Meier W. M. (1961) The crystal structure of mordenite. *Zeit. Krist.* **115,** 439.

Fig. 3. Projections of the framework structures of M and D.

MINERALOGICAL SOCIETY OF AMERICA, SPECIAL PAPER 1, 1963
INTERNATIONAL MINERALOGICAL ASSOCIATION, PAPERS, THIRD GENERAL MEETING

# COMPARISON OF THE CRYSTAL STRUCTURES OF WOLLASTONITE AND PECTOLITE

C. T. PREWITT AND M. J. BUERGER
*Cyrstallographic Laboratory, Massachusetts Institute of Technology, Cambridge, Mass.*

ABSTRACT

Wollastonite, $CaSiO_3$, and pectolite, $CaNaHSi_3O_9$, have similar triclinic cells; because of this and their analogous chemical compositions they have long been regarded as belonging to the same mineral family. An examination of the results of least-squares refinement reveals that although the structures contain similar metasilicate chains, they are not as closely isotypic as had been supposed. The principal differences are in the location of the large cations between layers of oxygen atoms parallel to (101) and in the relative orientations of the metasilicate chains.

The structures of both wollastonite and pectolite contain pseudomonoclinic subcells which are joined together on (100) to give an overall symmetry different from that of the subcell. The geometries of these subcells and the possibility of their being joined in different ways are important in explaining the types of twinning which occur in wollastonite and pectolite.

## INTRODUCTION

Pectolite and wollastonite belong to the same mineral family and have distinct but related crystal structures. Buerger and Prewitt (1961) have shown that the crystal structures proposed by Buerger (1956) for pectolite and by Mamedov and Belov (1956) for wollastonite are correct. The present paper describes in detail the similarities and differences between the two structures and attempts to explain some of the puzzling features of these minerals which have been observed in the past.

## CONFIRMATION OF THE STRUCTURES

Unit cell information for pectolite, wollastonite, and $NaAsO_3$ is given in Table 1. The similarity of the triclinic cells (space group $P\bar{1}$) and the analogous chemical compositions indicate that these substances might have the same structure. A comparison of the results given by Mamedov and Belov (1956) for wollastonite and Liebau (1956) for $NaAsO_3$ shows that these two structures are identical. If either of these is compared to the pectolite structure given by Buerger (1956) certain discrepancies are noted. For example, while in both structures the silicate chains have repeat units of three tetrahedra, they do not have the same orientation in the two structures, and the large cations all lie in a sheet parallel to (101), but do not have the same distribution in the sheet.

TABLE 1. UNIT CELLS OF WOLLASTONITE, $NaAsO_3$, AND PECTOLITE

| | Wollastonite $Ca_3Si_3O_9$ | $Na_3As_3O_9$ | Pectolite $Ca_2NaHSi_3O_9$ |
|---|---|---|---|
| $a$ | 7.94 Å | 8.07 Å | 7.99 Å |
| $b$ | 7.32 Å | 7.44 Å | 7.04 Å |
| $c$ | 7.70 Å | 7.32 Å | 7.02 Å |
| $\alpha$ | 90°02′ | 90° | 90°31′ |
| $\beta$ | 95°22′ | 91°30′ | 95°11′ |
| $\gamma$ | 103°26′ | 104° | 102°28′ |

In order to determine whether these differences were real, Buerger and Prewitt (1961) collected three-dimensional $x$-ray intensities for wollastonite and refined the structure by least-squares. In addition, they refined pectolite using relatively crude intensity data originally obtained by Buerger (1956). The final $R$ factors for wollastonite and pectolite, respectively, were 8.9% and 17%. When the structures and $x$-ray data were interchanged, the wollastonite data could not be refined below 26% and the pectolite data not below 52%. Therefore, the structures as proposed must be correct but different.

## COMPARISON OF STRUCTURES

Figures 1 and 2 are projections along $b$ of the wollastonite and pectolite structures, respectively. Coordinates for the figures in this paper were given originally by Buerger and Prewitt (1961) and are reproduced in Table 2 with a few changes so that all coordinates refer to atoms in or near the same silicate chain. Unless otherwise noted, the origin for the figures is that of the coordinates of Table 2.

Figures 1 and 2 reveal that the structures are topologically different. For example, the bends between the superposed $Si_1$ and $Si_2$ tetrahedra and the $Si_3$ tetrahedron are reversed. The large cations, however, occupy approximately the same positions in the two structures. One immediately wonders whether the misfit is merely a result of identical structures being oriented in different ways. The authors spent some time in considering this possibility and found that the structures can be oriented so that the silicate

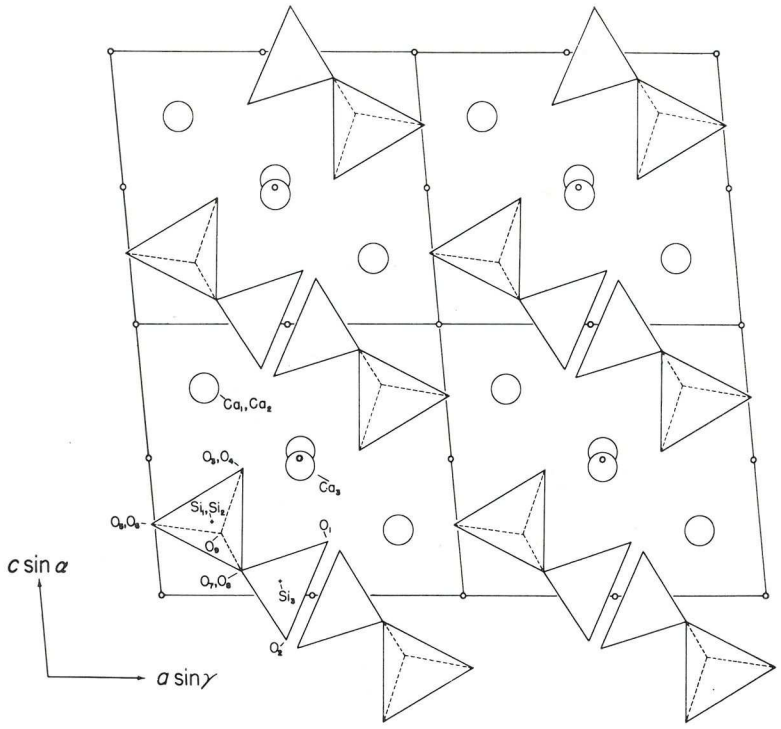


FIG. 1. Projection of the wollastonite structure along *b*.

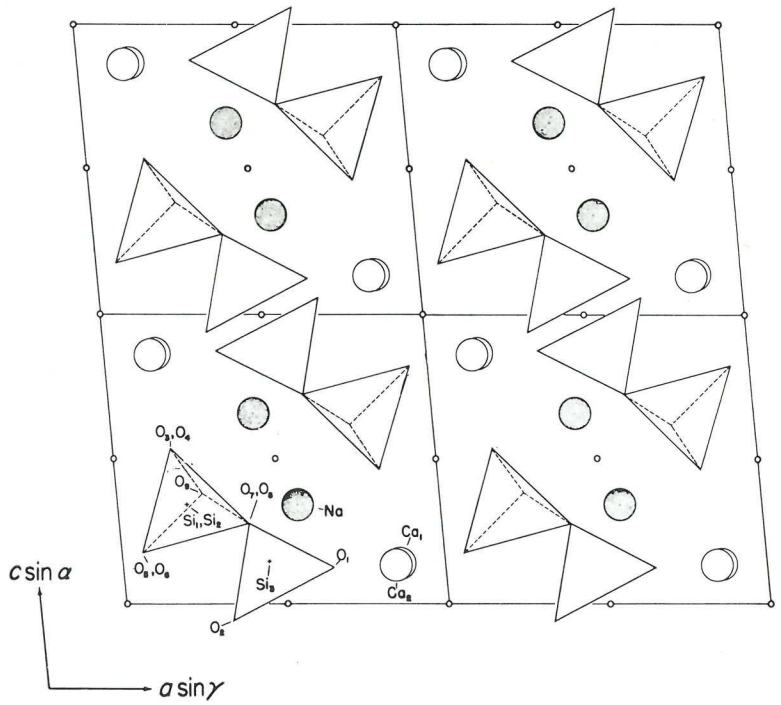


FIG. 2. Projection of the pectolite structure along *b*. Although the $Si_1$ and $Si_2$ tetrahedra should not be exactly superimposed, they are presented this way to simplify the drawing.

TABLE 2. ATOM COORDINATES FOR WOLLASTONITE AND PECTOLITE

| Atom | Wollastonite | | | Pectolite | | | |
|---|---|---|---|---|---|---|---|
| | $x$ | $y$ | $z$ | Atom | $x$ | $y$ | $z$ |
| $Ca_1$ | .1985 | .4228 | .7608 | $Ca_1$ | .857 | .596 | .146 |
| $Ca_2$ | .2027 | .9293 | .7640 | $Ca_2$ | .843 | .074 | .139 |
| $Ca_3$ | .5034 | .7505 | .5280 | Na | .552 | .265 | .344 |
| $Si_1$ | .1852 | .3870 | .2687 | $Si_1$ | .221 | .402 | .337 |
| $Si_2$ | .1849 | .9545 | .2692 | $Si_2$ | .210 | .954 | .344 |
| $Si_3$ | .3970 | .7235 | .0560 | $Si_3$ | .451 | .735 | .148 |
| $O_1$ | .5709 | .7686 | .1981 | $O_1$ | .652 | .788 | .125 |
| $O_2$ | .4008 | .7259 | −.1698 | $O_2$ | .322 | .702 | −.057 |
| $O_3$ | .3037 | .4635 | .4641 | $O_3$ | .185 | .496 | .538 |
| $O_4$ | .3017 | .9374 | .4655 | $O_4$ | .171 | .839 | .541 |
| $O_5$ | −.0154 | .3746 | .2657 | $O_5$ | .070 | .393 | .171 |
| $O_6$ | −.0175 | .8681 | .2647 | $O_6$ | .053 | .896 | .179 |
| $O_7$ | .2732 | .5118 | .0919 | $O_7$ | .396 | .533 | .275 |
| $O_8$ | .2713 | .8717 | .0940 | $O_8$ | .402 | .906 | .275 |
| $O_9$ | .2188 | .1784 | .2228 | $O_9$ | .260 | .182 | .381 |

chains are nearly superposed. This is accomplished by interchanging the $a$ and $c$ axes and shifting the origin of one of the structures. Figure 3 shows projections along $b$ of wollastonite and pectolite in which the silicate chains are oriented to correspond with one another. The $y$ coordinates of the atoms in the respective chains are about as close to each other as are the $x$ and $z$ coordinates. The locations of the large cations, however, are not similar. In fact, the large cations occupy completely different interstices between oxygens when the structures are oriented in this way. The structures must then be different even though the packing of oxygens is roughly similar. The authors originally thought that this kind of comparison might be more useful than the conventional one, but further investigation as reported below showed that the conventional orientations should be retained.

## PSEUDOMONOCLINIC SYMMETRY

A number of investigators have commented on the unusual features which are observed in $x$-ray diffraction photographs of wollastonite and pectolite. Among these features are a mirror symmetry between relative even-numbered reciprocal lattice levels normal to $b^*$, and the presence of a substructure along $b$ with a period of b/2 as indicated by the average spot intensity in even-numbered reciprocal-lattice levels normal to $b^*$ being greater than in the odd-numbered levels. Ito (1950) discussed these effects and proposed that triclinic wollastonite could be constructed by starting with a hypothetical monoclinic cell and shifting successive cells along (100) in increments of $\pm\frac{1}{4}b$. To this pseudomonoclinic cell he attributed a symmetry of $P2/m$ or $P2_1/m$. Figures 4 and 5 show that both wollastonite and pectolite can indeed be so regarded, and that the space group of this unit, which is infinite in the $b$ and $c$ directions and one unit cell thick along $a$, is $P2_1/m$. Liebau (1956) also noticed that $NaAsO_3$ can be so regarded.

This shift between successive pseudomonoclinic units not only determines the triclinic symmetry in

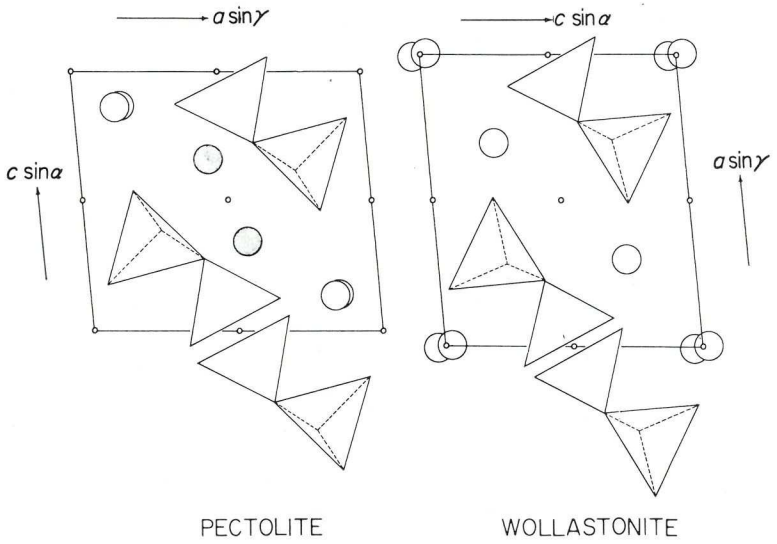


FIG. 3. Projections of the pectolite and wollastonite structures along $b$. The origin and orientation of wollastonite has been changed from that of Fig. 1 so that the silicate chains in wollastonite have the same orientation as in pectolite.

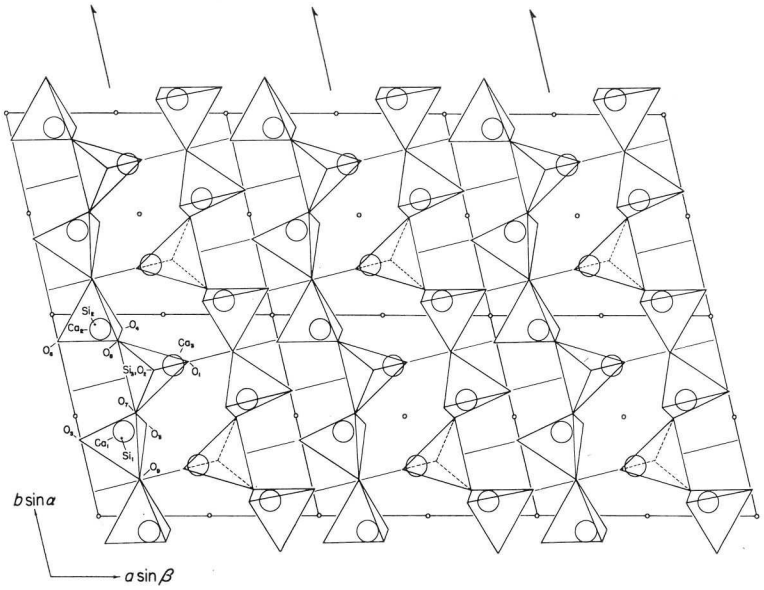


FIG. 4. Projection of the wollastonite structure along $c$. The mirror planes and screw axes are elements of the pseudomonoclinic unit.

pectolite and wollastonite, but also is the key to twinning in these minerals and probably will be found to be significant in other triclinic metasilicates as well. The results of the different shifts which can be made are discussed in another section of this paper.

It is interesting to note how closely the refined atom coordinates conform to the monoclinic symmetry. The coordinates were refined in the space group $P\bar{1}$ so that all atoms were in the general position with no restrictions on $x$, $y$ or $z$. Table 3 gives the wollastonite and pectolite coordinates transformed to the pseudomonoclinic cell using the cell transformation[1]

$$\begin{array}{rc} & \text{Pseudomonoclinic} \\ \text{Triclinic} & \begin{pmatrix} 1 & -\frac{1}{4} & 0 \\ 0 & 1 & 0 \\ 0 & 0 & 1 \end{pmatrix} \end{array}$$

and adding 0.125 to the transformed $y$ coordinates.

For the atoms $Ca_3$, $Si_3$, $O_1$, $O_2$ and $O_9$ in wollastonite, which would be on the mirror plane in $P2_1/m$, the $y$ coordinates should be .250 or .750. The very small deviations of about .001 (or .007 Å) are within the expected accuracy of the measurements. The other atoms which are related by the mirror planes also show little deviation from the positions they would occupy if the monoclinic symmetry held. If the space group $P2_1/m$ is assumed, then the following paired atoms are equivalent and occupy the general position:

$$Ca_1, Ca_2 \quad Si_1, Si_2 \quad O_3, O_4 \quad O_5, O_6 \quad O_7, O_8$$

$Ca_3$, $Si_3$, $O_1$, $O_2$ and $O_9$ are each in the special positions $m$.

Although the atoms in pectolite have the same pseudoequipoint distributions as do those in wollastonite, the refined coordinates for the pectolite atoms do not conform as closely to the monoclinic symmetry. For example, the $y$ coordinate of $O_9$ is .242 as compared with .250 if $O_9$ were on the mirror plane. This is a deviation of about 0.06 Å. A detailed refinement of pectolite now being carried out in this laboratory has shown that these deviations in the pectolite coordinates are real.

The pseudosymmetry gives rise to the strong substructure along $b$, since all the atoms except $O_7$ and $O_8$ in both wollastonite and pectolite and Na in pectolite have $x$ and $z$ coordinates similar to another atom of the same type located $\frac{1}{2}b$ away. It is interesting that $Ca_3$ and its inversion equivalent in wollastonite have similar $x$ and $z$ coordinates and are approximately $\frac{1}{2}b$ apart, while Na and its inversion equivalent in pectolite do not have similar $x$ and $z$ coordinates even though they are separated by $\frac{1}{2}b$. This is one of the major differences between these minerals.

The similarities and differences between wollstonite and pectolite brought out in this section seem to be more useful in describing the structures than do those in the last section where a special orientation of one of the structures was used to show how the sili-

[1] This transformation is not exact when there is a departure of $\alpha$ (triclinic) from 90°; $\alpha$ in wollastonite is nearly 90° and departs from 90° by only 31′ in pectolite.

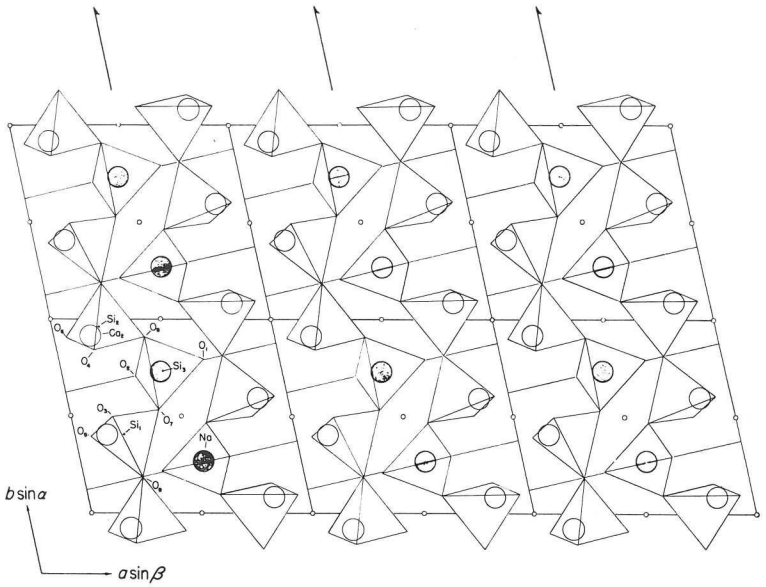


FIG. 5. Projection of pectolite along $c$ corresponding to that of wollastonite of Fig. 4. Note that the orientations of the silicate chains are different in the two structures.

cate chains could be superposed. Because of this, the authors feel that the conventional orientation should be retained and that while the other aspect is interesting, it will not be useful except, for example, in a classification of metasilicates based on oxygen packing.

TABLE 3. ATOM COORDINATES OF WOLLASTONITE AND PECTOLITE REFERRED TO A PSEUDOMONOCLINIC CELL $P2_1/m$ (ORIGIN AT $\bar{1}$)

| Pseudo-equipoint | Wollastonite | | | | Pectolite | | | |
|---|---|---|---|---|---|---|---|---|
| | Atom | $x$ | $y$ | $z$ | Atom | $x$ | $y$ | $z$ |
| 4*f* | $2Ca_1$ | .1985 | .4982 | .7608 | $2Ca_1$ | .857 | .507 | .146 |
| | $2Ca_2$ | .2027 | .0038 | .7440 | $2Ca_2$ | .843 | −.002 | .139 |
| 2*e* | $2Ca_3$ | .5034 | .7496 | .5280 | 2Na | .552 | .252 | .344 |
| 4*f* | $2Si_1$ | .1852 | .4657 | .2687 | $2Si_1$ | .221 | .472 | .337 |
| | $2Si_2$ | .1849 | .0333 | .2692 | $2Si_2$ | .210 | 1.026 | .344 |
| 2*c* | $2Si_3$ | .3970 | .7492 | .0560 | $2Si_3$ | .451 | .747 | .148 |
| 2*e* | $2O_1$ | .5709 | .7509 | .1981 | $2O_1$ | .652 | .750 | .125 |
| 2*e* | $2O_2$ | .4008 | .7507 | −.1698 | $2O_2$ | .322 | .746 | −.057 |
| 4*f* | $2O_3$ | .3037 | .5126 | .4641 | $2O_3$ | .185 | .575 | .538 |
| | $2O_4$ | .3017 | .4870 | .4655 | $2O_4$ | .171 | .921 | .541 |
| 4*f* | $2O_5$ | −.0039 | .5035 | .2657 | $2O_5$ | .070 | .500 | .175 |
| | $2O_6$ | −.0044 | .9975 | .2647 | $2O_6$ | .053 | 1.008 | .179 |
| 4*f* | $2O_7$ | .2732 | .5685 | .0919 | $2O_7$ | .396 | .559 | .275 |
| | $2O_8$ | .2713 | .9287 | .0940 | $2O_8$ | .402 | .930 | .275 |
| 2*e* | $2O_9$ | .2188 | .2487 | .2228 | $2O_9$ | .260 | .242 | .381 |

## DISTRIBUTION OF Ca AND Na

The main difference in the wollastonite and pectolite structures is in the way the large cations are distributed in the sheet parallel to (101). Figures 6 and 7 show parts of the wollastonite and pectolite structures projected onto (101) of the pseudomonoclinic cell. Only the silicate chains on the upper side of (101) are shown.

The Ca in wollastonite are arranged in a nearly planar hexagonal pattern which is separated into bands 3 Ca columns wide running in the $b$ direction and parallel to the silicate chains. The Na and Ca in pectolite are also arranged in a hexagonal pattern with bands consisting of 2 Ca columns bounded on either side by a half-filled Na column. Because each of these bands is translated by $\frac{1}{4}b$ with respect to neighboring bands, every other Na in a particular Na column is missing. This is necessary because otherwise the Na-Na distances between neighboring Na columns would be much too small.

## INTERATOMIC DISTANCES AND INTERBOND ANGLES

Interatomic distances and angles given in Table 4 were calculated for wollastonite and pectolite using a computer program written by Busing and Levy (1959). The Si-O distances in both wollastonite and pectolite show a considerable variation, the lengths apparently being determined by the coordinations of the oxygens. Table 5 gives the coordination and dis-

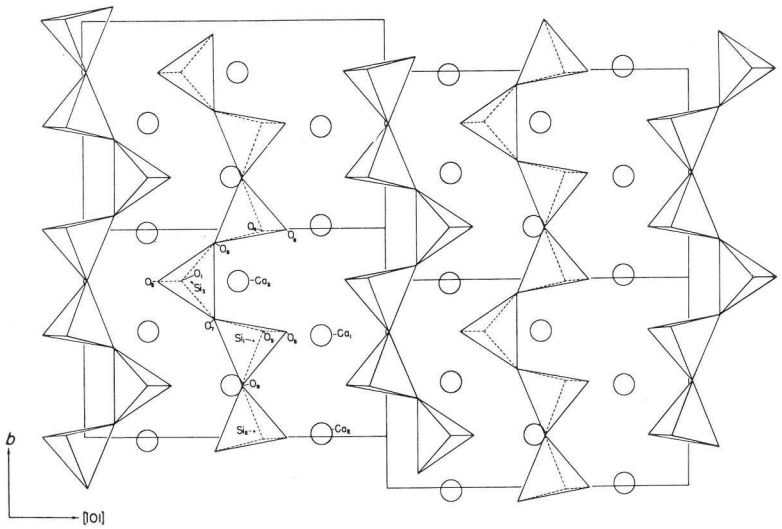


FIG. 6. Structure of wollastonite projected onto (101) of four adjacent pseudomonoclinic cells. Only the silicate chains on the near side of (101) are shown. The axial directions are for the pseudomonoclinic cell.

tances of cations around the oxygens. It can be seen that, for $O_1$ through $O_6$ in wollastonite, the Si-O distances are longer when an oxygen is coordinated by 3 Ca than when coordinated by 2 Ca. The situation is different for $O_7$ through $O_9$ because these oxygens are coordinated by 2 Si as well as Ca, showing that Pauling's electrostatic valence rule does not hold. The Si-O distances here are larger than in either of the examples above. The coordination of oxygens in wollastonite can thus be divided into three classes:

1. Oxygen ($O_1$, $O_2$, $O_3$, $O_4$) coordinated by 1 Si and 3 Ca;
2. Oxygen ($O_5$, $O_6$) coordinated by 1 Si and 2 Ca;
3. Oxygen ($O_7$, $O_8$, $O_9$) coordinated by 2 Si and 1 Ca.

It is felt that an analysis of the pectolite interatomic distances before a detailed refinement is completed would be premature, particularly since the range in Si-O distances is so great, varying from 1.58 Å for $Si_2$-$O_9$ to 1.75 Å for $Si_2$-$O_8$. This may be a real variation, however, since Morimoto *et al.* (1960) reported a range of 1.58–1.74 Å for Si-O in clinoenstatite.

$Ca_1$ and $Ca_2$ in wollastonite are octahedrally coordinated by six oxygen atoms at average distances of $2.38_3$Å for $Ca_1$ and $2.38_8$Å for $Ca_2$. $Ca_3$ is surrounded by six oxygen atoms at an average distance of $2.39_0$Å and by an additional oxygen ($O_9$) at $2.64_2$Å. The

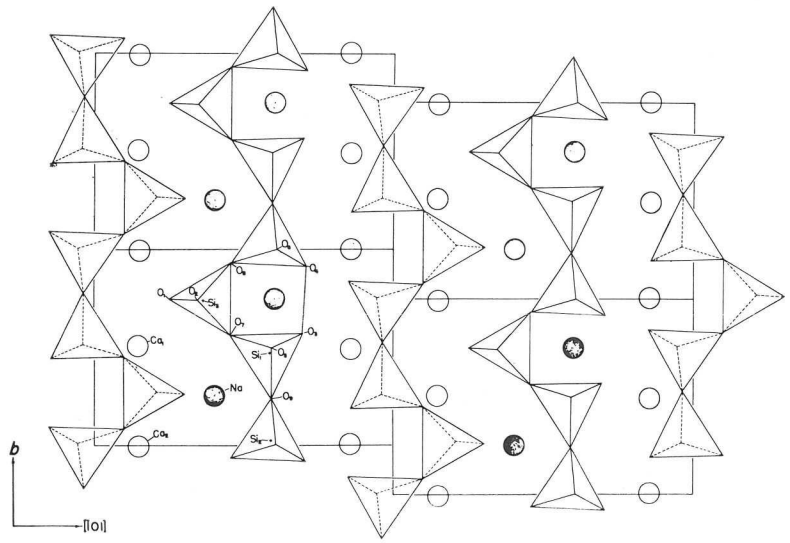


FIG. 7. Structure of pectolite projected onto (101) of the four adjacent pseudomonoclinic cells. Only the silicate chains on the near side of (101) are shown. The most likely location for the hydrogen bond is indicated by the line between the labeled $O_3$ and $O_4$.

TABLE 4. INTERATOMIC DISTANCES AND INTERBOND ANGLES IN WOLLASTONITE AND PECTOLITE

| Interatomic Distances | | | |
|---|---|---|---|
| Atoms | | Wollastonite | Pectolite |
| $Si_1$ | $O_3$ | $1.61_8$ Å | 1.63 Å |
| | $O_5$ | $1.57_2$ | 1.59 |
| | $O_7$ | $1.65_9$ | 1.60 |
| | $O_9$ | $1.64_7$ | 1.67 |
| | $O_{av}$ | $1.62_4$ | 1.62 |
| $Si_2$ | $O_4$ | $1.61_7$ | 1.63 |
| | $O_6$ | $1.58_1$ | 1.61 |
| | $O_8$ | $1.65_0$ | 1.75 |
| | $O_9$ | $1.63_7$ | 1.58 |
| | $O_{av}$ | $1.62_1$ | 1.64 |
| $Si_3$ | $O_1$ | $1.59_9$ | 1.59 |
| | $O_2$ | $1.59_9$ | 1.68 |
| | $O_7$ | $1.66_5$ | 1.68 |
| | $O_8$ | $1.67_3$ | 1.63 |
| | $O_{av}$ | $1.63_4$ | 1.65 |
| $Ca_1$ | $O_1$ | $2.54_8$ | 2.33 |
| | $O_2$ | $2.43_7$ | 2.31 |
| | $O_3$ | $2.32_4$ | 2.35 |
| | $O_5$ | $2.30_2$ | 2.35 |
| | $O_5'$ | — | 2.44 |
| | $O_6$ | $2.27_2$ | 2.34 |
| | $O_7$ | $2.41_2$ | — |
| | $O_{av}$ | $2.38_3$ | 2.35 |
| $Ca_2$ | $O_1$ | $2.50_1$ | 2.30 |
| | $O_2$ | $2.42_1$ | 2.25 |
| | $O_4$ | $2.31_6$ | 2.32 |
| | $O_5$ | $2.36_8$ | 2.51 |
| | $O_6$ | $2.31_6$ | 2.35 |
| | $O_6'$ | — | 2.45 |
| | $O_8$ | $2.40_6$ | — |
| | $O_{av}$ | $2.38_8$ | 2.36 |
| $Ca_3$ | $O_1$ | $2.43_9$ | |
| | $O_2$ | $2.34_9$ | |
| | $O_3$ | $2.42_9$ | |
| | $O_3'$ | $2.33_5$ | |
| | $O_4$ | $2.44_1$ | |
| | $O_4'$ | $2.34_9$ | |
| | $O_9$ | $2.64_2$ | |
| | $O_{av}$ | $2.39_0$ (excluding $Ca_3$-$O_9$) | |
| Na | $O_2$ | | 2.32 |
| | $O_3$ | | 2.46 |
| | $O_4$ | | 2.54 |
| | $O_7$ | | 2.50 |
| | $O_7'$ | | 2.97 |
| | $O_8$ | | 2.57 |
| | $O_8'$ | | 2.97 |
| | $O_9$ | | 2.32 |
| | $O_{av}$ | | 2.45 (excluding Na-$O_7'$, Na-$O_8'$) |

| Interatomic Distances | | | |
|---|---|---|---|
| Atoms | | Wollastonite | Pectolite |
| $Si_1$ | $Si_2$ | $3.16_5$ | 3.10 |
| | $Si_3$ | $3.11_6$ | 3.04 |
| $Si_2$ | $Si_3$ | $3.12_5$ | 3.11 |

| Interbond Angles | | |
|---|---|---|
| | Wollastonite | Pectolite |
| $Si_1$-$O_9$-$Si_2$ | 149° | 150° |
| $Si_2$-$O_8$-$Si_3$ | 140° | 135° |
| $Si_3$-$O_7$-$Si_1$ | 139° | 136° |

Ca-O sheet is similar to a brucite sheet separated into slabs running along *b* and distorted by the presence of $O_9$.

The coordination of $Ca_1$ and $Ca_2$ in pectolite is similar to that of $Ca_1$ and $Ca_2$ in wollastonite with an average $Ca_1$-O distance of 2.35 Å and an average $Ca_2$-O distance of 2.36 Å. Na is surrounded by 6 oxygen atoms at an average distance of 2.45 Å and two further oxygen atoms, both at 2.97 Å.

The most probable location for the hydrogen bond in pectolite is between $O_3$ and $O_4$. These atoms are separated by 2.44 Å which is short even for a hydrogen bond. This is represented by a line between the labelled $O_3$ and $O_4$ in Fig. 7. This separation is much less than that between similar atoms in the wollastonite chain as seen in Fig. 6. Buerger (1956) attributed the presence of a shorter *b* axis in pectolite than in wollastonite to the hydrogen bond.

In both structures, the silicon-oxygen-silicon angles have the same distribution, with $Si_1$-$O_9$-$Si_2$ being larger than $Si_2$-$O_8$-$Si_3$ and $Si_3$-$O_7$-$Si_1$, which are approximately equal. This difference results from the somewhat abnormal location of $O_9$ in the oxygen sheet.

## TWINNING

One of the most interesting aspects of the pectolite and wollastonite structures is the way in which twinning can occur. Mention has already been made of the way in which pseudomonoclinic subcells are fitted together to give a triclinic structure. This is shown schematically in Fig. 8b. It is also possible to reverse the shift between successive pseudomonoclinic subcells to give the sequence shown in Fig. 8a, which corresponds to a twinned structure. If, however, the shift is reversed in each successive cell, the effect is as shown in Fig. 8c. This latter sequence was

TABLE 5. COORDINATION OF OXYGENS IN WOLLASTONITE AND PECTOLITE

| Wollastonite | | Pectolite | |
|---|---|---|---|
| Atoms | Interatomic Distances | Atoms | Interatomic Distances |
| $O_1$ $Si_3$ | $1.59_9$ Å | $O_1$ $Si_3$ | 1.59 Å |
| $Ca_1$ | $2.54_8$ | $Ca_1$ | 2.33 |
| $Ca_2$ | $2.31_6$ | $Ca_2$ | 2.30 |
| $Ca_3$ | $2.43_9$ | | |
| $O_2$ $Si_3$ | $1.59_9$ | $O_2$ $Si_3$ | 1.68 |
| $Ca_1$ | $2.43_7$ | $Ca_1$ | 2.31 |
| $Ca_2$ | $2.36_9$ | $Ca_2$ | 2.25 |
| $Ca_3$ | $2.34_9$ | Na | 2.32 |
| $O_3$ $Si_1$ | $1.61_8$ | $O_3$ $Si_1$ | 1.63 |
| $Ca_1$ | $2.32_4$ | $Ca_1$ | 2.35 |
| $Ca_3$ | $2.42_9$ | Na | 2.46 |
| $Ca_3'$ | $2.33_5$ | | |
| $O_4$ $Si_2$ | $1.61_7$ | $O_4$ $Si_2$ | 1.63 |
| $Ca_2$ | $2.42_1$ | $Ca_2$ | 2.32 |
| $Ca_3$ | $2.44_1$ | Na | 2.54 |
| $Ca_3'$ | $2.34_9$ | | |
| $O_5$ $Si_1$ | $1.57_2$ | $O_5$ $Si_1$ | 1.59 |
| $Ca_1$ | $2.30_2$ | $Ca_1$ | 2.35 |
| $Ca_2$ | $2.50_1$ | $Ca_1'$ | 2.44 |
| | | $Ca_2$ | 2.51 |
| $O_6$ $Si_2$ | $1.58_1$ | $O_6$ $Si_2$ | 1.61 |
| $Ca_1$ | $2.27_2$ | $Ca_1$ | 2.34 |
| $Ca_2$ | $2.50_1$ | $Ca_2$ | 2.35 |
| | | $Ca_2'$ | 2.45 |
| $O_7$ $Si_1$ | $1.65_9$ | $O_7$ $Si_1$ | 1.60 |
| $Si_3$ | $1.66_5$ | $Si_3$ | 1.68 |
| $Ca_1$ | $2.41_2$ | Na | 2.50 |
| | | Na′ | |
| $O_8$ $Si_2$ | $1.65_0$ | $O_8$ $Si_2$ | 1.75 |
| $Si_3$ | $1.67_3$ | $Si_3$ | 1.63 |
| $Ca_2$ | $2.40_6$ | Na | 2.57 |
| | | Na′ | |
| $O_9$ $Si_1$ | $1.64_7$ | $O_9$ $Si_1$ | 1.67 |
| $Si_2$ | $1.63_7$ | $Si_2$ | 1.58 |
| $Ca_3$ | $2.64_2$ | $O_9$ | 2.39 |

suggested by Ito (1950) for parawollastonite[1] which was originally distinguished from wollastonite by Peacock (1935a).

[1] The Commission on Mineral Data recommended at the meeting of the International Mineralogical Association in Washington, D. C., April 17–20, 1962, that wollastonite and parawollastonite be redesignated wollastonite-1T and wollastonite-2M, respectively.

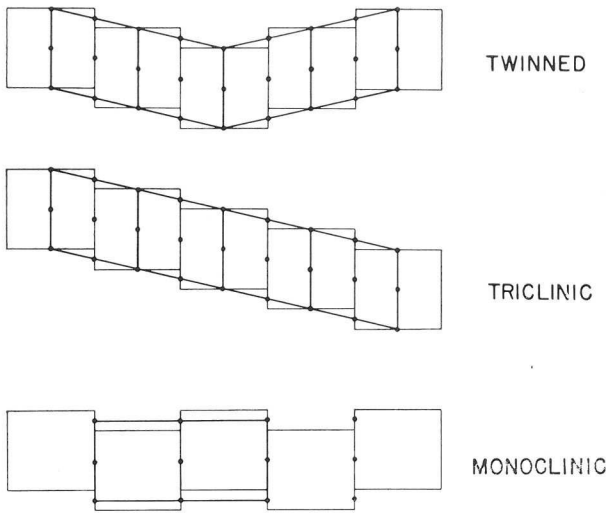


FIG. 8a (top), b (middle) and c (bottom). Three ways in which the pseudomonoclinic unit can be stacked on (100) to produce different overall diffraction effects.

Peacock (1935b) found that the twin law in pectolite is such that $b$ is the twin axis with (100) as the composition plane. This is consistent with Fig. 8a since a rotation of 180° around $b$ of one of the pseudomonoclinic units would be approximately equivalent to translating it by $\frac{1}{2}b$ along a neighboring cell. This is not exactly true unless the cell is actually monoclinic, thus making $\alpha$ (triclinic) equal to 90°. The authors have taken $x$-ray photographs of several twinned pectolite crystals from various localities and have found that the diffraction effects substantiate the above ideas. Fig. 9a represents part of the composite reciprocal lattice of twinned pectolite. When the members of the twin are present in equal amount, oscillating-crystal photographs around $b$, as well as $c$-axis precession photographs, show an apparent mirror plane normal to $b$. Close examination of the films reveals, however, that the registry of superposed spots is not perfect and that the registry is slightly different in different specimens.

If the pseudomonoclinic cells are joined as in Fig. 8c, the parawollastonite structure is formed having an overall monoclinic symmetry with a doubling of the cell along $a$. The symmetry of this monoclinic cell should be $P2_1/a$ with extra centers of symmetry, not required by the space group,[2] being present. In an attempt to refine the structure of parawollastonite,

[2] Tolliday (1958) gives the systematic absences in the parawollastonite diffraction pattern as: for $hkl$, $2h+k=4n+2$, and for $0k0$ as $k=2n+1$.

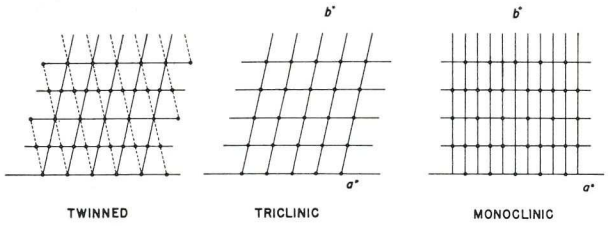


FIG. 9a (left), 9b (middle) and 9c (right). Reciprocal lattices corresponding to the geometries shown in Figs. 8a, 8b and 8c.

however, Tolliday (1958) found that the structure could not be refined using the centrosymmetric space group $P2_1/a$ and that when the non-centrosymmetric space group $P2_1$ was assumed, the refinement proceeded satisfactorily. Since no coordinates, structure factors or $R$ factors were published, the validity of this assumption cannot be evaluated. This is an extremely important point in the crystal chemistry of $CaSiO_3$ and one which should be resolved.

One of the interesting features of Figs. 9a, 9b and 9c is that the reciprocal-lattice levels with $k$ even are identical (when $\alpha = 90°$) and that the differences between triclinic, monoclinic and twinned composite reciprocal lattices occur in only the odd levels. It is simpler for wollastonite than for pectolite to alternate to form the parawollastonite type because $\alpha$ in wollastonite is 90° (within experimental error) and because the symmetry of the repeating unit in wollastonite is nearly monoclinic, *i.e.*, the $Si_1$ and $Si_2$ tetrahedra, as well as $Ca_1$ and $Ca_2$, are symmetrically equivalent. The authors examined several wollastonite specimens from the Monte Somma, Italy, Csiklova, Romania, and Crestmore, California, localities before finding one which gave a parawollastonite diffraction pattern.[3] Continuous radiation streaks along reciprocal lattice rows parallel to $a^*$ were observed in the $b$-axis Weissenberg photographs with $k$ odd for the monoclinic as well as several triclinic specimens. This effect was interpreted by Jeffrey (1953) as a type of disorder due to the presence of regions of wollastonite and parawollastonite, but it could also be thought of as an irregular sequence of pseudomonoclinic subcells.

Peacock (1935a) was unable to find any twinned triclinic wollastonite in the material available to him. Spencer (1903), however, reported a twinned wollastonite crystal from Chiapas, Mexico, which would presumably give a diffraction pattern similar to our twinned pectolite. It is possible that some of the material reported in the literature as ordered parawollastonite is actually twinned wollastonite. One could be misled by diffraction photographs if the members of the twin were present in equal amounts.

One point which should be brought out here is that the way in which these pseudomonoclinic units fit together results in what Ito (1950) called "space-group twinning" and "structure twinning." The "space-group twinning" is seen in the joining of pseudomonoclinic cells to give an overall triclinic or a different monoclinic symmetry, while "structure twinning" corresponds to our twinned pectolite. Dornberger-Schiff (1956) has developed a general classification of order-disorder structures which includes the "space-group twinning" concept.

## CONCLUSIONS

It has been established that wollastonite and pectolite have many structural similarities but yet must be classified as having different structures. Whether the pseudomonoclinic unit found in both wollastonite and pectolite will be of significance in an overall classification of the triclinic metasilicates will depend on the results of structural investigation of such minerals as bustamite, rhodonite and pyroxmangite. This pseudomonoclinic unit at present appears to be important in determining the relations between different modifications of a particular mineral in the wollastonite series. Its departure from actual monoclinic symmetry may also be a controlling factor in determining what forms of a particular triclinic metasilicate can occur. Certainly, any study of the stability relations of wollastonite and parawollastonite would have to be concerned with the details of the structures to a greater extent than is usual in such investigations, because the difference in energy between the two structures must be quite small.

## ACKNOWLEDGMENTS

The authors wish to express thanks to Professor Clifford Frondel and Dr. Alden Carpenter of Harvard University, Professor Adolf Pabst of the University of California, and Dr. George Switzer of the U. S. National Museum for supplying much of the material used in this investigation, and to Donald R. Peacor for many helpful discussions. This work was supported by the National Science Foundation. The computations were carried out at the M.I.T. Computation Center.

[3] The parawollastonite crystal (locality: Crestmore, California) was supplied by Professor A. Pabst from a specimen, 138–80, in the University of California collection.

References

Buerger, M. J. (1956) The determination of the crystal structure of pectolite, $Ca_2NaHSi_3O_9$. *Zeit. Krist.* **108,** 248–261.

——— and C. T. Prewitt (1961) The crystal structures of wollastonite and pectolite. *Proc. Nat. Acad. Sci.* **47,** 1884–1888.

Busing, William R. and Henri A. Levy (1959) A crystallographic function and error program for the IBM 704. *Oak Ridge Natl. Lab. Central Files No.* **59-12-3.** Oak Ridge, Tenn. 1–95.

Collins, H. F. (1903) Notes on the wollastonite rock-mass and it associated minerals, of the Santa Fe Mine, State of Chiapas, Mexico. *Mineral. Mag.* **13,** 356–362.

Dornberger-Schiff, K. (1956) On order-disorder structures (OD-structures). *Acta Cryst.* **9,** 593–601.

Ito, T. (1950) *X-ray Studies on Polymorphism.* Maruzen, Tokyo, 93–110.

Jeffery, J. W. (1953) Unusual diffraction effects from a crystal of wollastonite, *Acta Cryst.* **6,** 821–825.

Liebau, Friedrich (1956) Über die Kristallstruktur des Natriumpolyarsenats, $(NaAsO_3)_x$. *Acta Cryst.* **9,** 811–817.

Mamedov, K. S. and N. V. Belov (1956) Crystal structure of wollastonite. *Dokl. Akad. Nauk. SSSR,* **107,** 463–466.

Morimoto, N., D. E. Appleman and H. T. Evans (1960) The crystal structures of clinoenstatite and pigeonite. *Zeit. Krist.* **114,** 120–147.

Peacock, M. A. (1935a) On wollastonite and parawollastonite. *Am. Jour. Sci.* **30,** 495–529.

——— (1935b) On pectolite. *Zeit. Krist.* **90,** 97–111.

Spencer, L. J. (1903) see paper by Collins, H. F.

Tolliday, Joan (1958) Crystal structure of β-wollastonite. *Nature,* **182,** 1012–1013.

## Discussion

Hans Adler (Washington, D. C.): Why do you think the hydrogen bonding occurs within the chains rather than between the chains in pectolite?

Authors' reply: The unusually short oxygen-oxygen distance of 2.44 Å is taken as evidence of the location of hydrogen between $O_3$ and $O_4$. In recent work with new data, we found an anomaly in three-dimensional difference maps which would correspond to this hydrogen location.

J. D. H. Donnay: (Baltimore, Md.): Does the wollastonite structure satisfactorily account for the cleavages parallel to the *b* axis? The cleavages were redetermined by Peacock.

Authors' reply: Certainly the nature of the silicate chains does account for the fact that the good cleavages are parallel to the *b* axis in both wollastonite and pectolite. Peacock lists five cleavages for wollastonite, (100), ($\bar{1}$02), (001), (101), and ($\bar{1}$01), with the first three being perfect cleavages. While these can be qualitatively justified in an examination of the structure, no work has been done with regard to proving that these are the most likely cleavages.

MINERALOGICAL SOCIETY OF AMERICA, SPECIAL PAPER 1, 1963
INTERNATIONAL MINERALOGICAL ASSOCIATION, PAPERS, THIRD GENERAL MEETING

# INTERPRETATION OF SYSTEMATIC EXTRA-EXTINCTIONS

N. MORIMOTO, F. MARUMO AND R. SADANAGA
*Mineralogical Institute, University of Tokyo, Tokyo, Japan*

ABSTRACT

Systematic absences other than space group absences in the reciprocal lattice (=systematic extra-extinctions) can be divided into two categories depending on their origin: (1) structural extinctions and (2) twinning extinctions. To obtain the characteristics of patterns in direct space from the structural extra-extinctions, a new method based on the Fourier transform of convolution has been developed. This approach through the convolution principle is very useful in interpreting not only the extra-extinctions but also the extra-symmetries in reciprocal space.

## INTRODUCTION

In the study of crystal structures by $x$-rays, it is not rare to observe some systematic extinctions or symmetries in reciprocal space which cannot be interpreted simply by the space group criteria. These systematic extinctions or symmetries are called extra-extinctions or extra-symmetries.

In the studies of sulfides or sulfosalts the extra-extinctions and symmetries were found to be extremely common. It was, therefore, strongly desired to establish some systematic way to obtain characteristics of patterns in direct space which cause the extra-extinctions or symmetries in reciprocal space. This problem is expressed in the following way: What is the maximum information we can expect from extra-extinctions or symmetries in reciprocal space without using any information on reflection intensities?

All the extra-extinction and symmetry rules in reciprocal space have been described to belong to the following two groups:

(a) Rules caused by twinning. In this case, each crystallite in twinning is assumed to be large enough so that the diffracted $x$-rays from one crystallite are incoherent to those from other crystallites. Buerger (1960) explained some possible cases of this kind of extinctions and symmetries.

(b) Rules caused by special arrangements of atoms in crystal structures. Ito (1950) has found in many examples that the extra-extinctions or symmetries in reciprocal space take place by some local symmetries in direct space. The local symmetry is only effective within part of the structure and is different from the space group symmetry, which is effective over the whole structure.

In most cases it is possible to determine whether extra-extinction or symmetry rules are caused by twinning or by single crystals by examining many specimens of the material by $x$-rays and microscope (Buerger, 1960). Extra-extinction or symmetry rules caused by single crystals are, therefore, discussed in this paper.

## GENERAL PRINCIPLE

For simplicity, only the extra-extinction rules will be discussed. When some extra-extinctions are observed in reciprocal space, it is always possible to find a larger reciprocal lattice or a *basic reciprocal lattice*, the extinction rules of which obey the usual space group extinction criteria. We call the reflections belonging to the basic reciprocal lattice *basic reflections*. The reflections which appear inside the basic lattice are called *additional reflections*. The space group derived from the weighted basic reciprocal lattice is generally different from the true space group for the crystal.

Any weighted reciprocal lattice A(s), including the basic and additional reflections, is expressed by a product of two functions—the lattice function, $\Sigma\delta(s-s_{hkl})$, and the function $F_0(s)$, which is the Fourier transform of the electron density in a unit cell of direct space, $\rho_0(r)$—as equation (1) in Fig. 1:

$$A(s) = \sum \delta(s - s_{hkl}) \cdot F_0(s) \qquad (1)$$

The drawings on the right-hand side are schematic representation of the formulas for a one-dimensional case. The electron density $\rho(r)$ in direct space is the

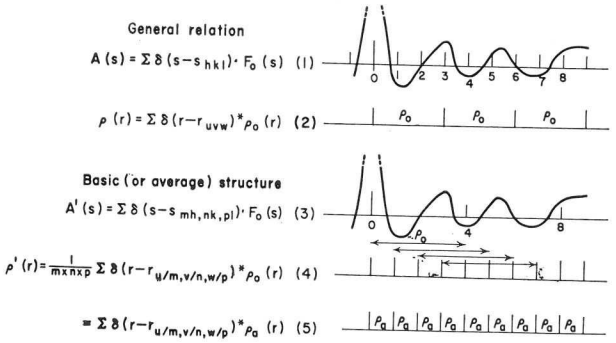


FIG. 1. General relations between A(s) and $\rho(r)$, and their schematic representations for a one-dimensional case.

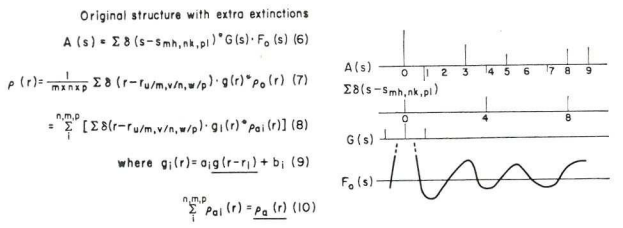


FIG. 2. The relations between A(s) and $\rho(r)$ for structures with extra-extinctions. The function used in formulas are schematically represented for a one-dimensional case.

Fourier transform of A(s), given by equation (2).

$$\rho(r) = \sum \delta(r - r_{u,v,w})^* \rho_0(r) \qquad (2)$$

In this formula $\Sigma\delta(r-r_{u,v,w})$ represents a lattice in direct space, and the asterisk represents convolution of two functions.

Assuming that the basic reflections have indices mh, nk, and pl, we will first consider a structure which only gives the basic reflections. This structure is called *basic structure* or *average structure*, which is different from the original structure with all observed reflections.

The weighted basic reciprocal lattice, A'(s), is expressed as equation (3) by using $F_0(s)$ of the original structure:

$$A'(s) = \sum \delta(s - s_{mh,nk,pl}) \cdot F_0(s) \qquad (3)$$

The electron density $\rho'(r)$ is given as equation (4):

$$\rho'(r) = \frac{1}{m \times n \times p} [\sum \delta(r - r_{u/m,v/p,w/p})]^* \rho_0(r) \qquad (4)$$

The basic lattice in direct space has a sub-cell, the unit translations of which are obtained by dividing those of the original lattice into m, n, and p parts along x, y, and z directions, respectively; $\rho_0$ represents, however, the electron density in the original cell. The electron density of the basic structure is, therefore, obtained by displacing $\rho_0(r)$ by the unit translation of the sub-cell and superposing all the $\rho_0(r)$'s. Thus the basic structure is a kind of average structure represented by using an average unit cell $\rho_a(r)$ as follows:

$$\rho'(r) = \sum \delta(r - r_{u/m,v/p,w/p})^* \rho_a(r) \qquad (5)$$

In order to find characteristic patterns of the original structure with extra-extinction rules, we can use two sources of information: (a) the average structure and (b) the special extinction rules. This can be done as follows.

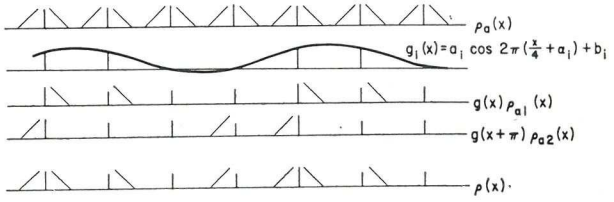


FIG. 3. The derivation of an original structure by means of g(r) and $p_a(r)$ for a simple one-dimensional case.

The weighted reciprocal lattice of the original structure is interpreted to consist of three functions as in equation (6) in Fig. 2. G(s) is a *satellite function* which connects each additional reflection to an appropriate basic reflection. The extra-extinction rules are implicitly expressed by this satellite function. The drawings on the right-hand side in Fig. 2 are schematic representation of the functions for a one-dimensional case. Then the original structure $\rho(r)$ is obtained as equation (7), using a modulation function g(r), the Fourier transform of G(s). If we define $g_i(r)$ and $\rho_{ai}(r)$ as in equations (9) and (10), respectively, by the known g(r) and $\rho_a(r)$, the original structure $\rho(r)$ is expressed as equation (8). The meaning of equation (8) is illustrated for the simple one-dimensional case in Fig. 3.

The average structure $\rho_a(x)$ is obtained by using only the basic reflections. The modulation function g(x) is obtained from G(s). After dividing $\rho_a(x)$ into two parts, $\rho_{a1}(x)$ and $\rho_{a2}(x)$, we apply to them g(x) and $g(x+\pi)$, respectively. The superposition of two patterns makes the final $\rho(r)$, which gives the extra-extinction.

In order to find the final $g_i(r)$ and $\rho_{ai}(r)$ from the known g(r) and $\rho_a(r)$, the intensity data of reflections become necessary. However, the consideration of the space group of the average structure and the original structure can usually limit the possible ways to derive $g_i(r)$ and $\rho_{ai}(r)$ from g(r) and $\rho_a(r)$, without any information on intensity data.

Extra-symmetries, instead of extra-extinctions, are sometimes observed in reciprocal space. The method, explained for the extra-extinctions, is also applicable on extra-symmetries.

## REFERENCES

BUERGER, M. J. (1960) *Crystal-Structure Analysis*. John Wiley & Sons N. Y., pp. 53–76.

ITO, T. (1950) *X-ray Studies on Polymorphism*. Maruzen, Tokyo.

MINERALOGICAL SOCIETY OF AMERICA, SPECIAL PAPER 1, 1963
INTERNATIONAL MINERALOGICAL ASSOCIATION, PAPERS, THIRD GENERAL MEETING

# SPIROFFITE,[1] A NEW TELLURITE MINERAL FROM MOCTEZUMA, SONORA, MEXICO

J. A. MANDARINO, S. J. WILLIAMS AND R. S. MITCHELL
*Royal Ontario Museum, University of Toronto, Toronto, Canada; S. J. Williams Mineral Company, Scottsdale, Arizona; and University of Virginia, Charlottesville, Virginia*

ABSTRACT

Spiroffite, $(Mn,Zn,Ca)_2Te_3O_8$, occurs in small cleavable masses which range in color from red to purple. The luster is adamantine, hardness is $3\frac{1}{2}$, and specific gravity is 5.01. The mineral is biaxial positive, $2V=55°$, $\alpha=1.85$, $\beta=1.91$, $\gamma>2.10$. No euhedral crystals have been found. *X*-ray study shows that spiroffite is monoclinic with a space group of *Cc* or *C2/c*. Unit cell values are: $a=13.00$ Å, $b=5.38$ Å, $c=12.12$ Å, $a:b:c=2.416:1:2.253$, $\beta=98°$. Associated minerals are: tellurite paratellurite, native tellurium, and several other new tellurites. Spiroffite is named in honor of Kiril Spiroff, Professor of Mineralogy at the Michigan College of Mining and Technology, Houghton, Michigan.

## INTRODUCTION AND OCCURRENCE

During the summer of 1960, one of the writers (S.J.W.) obtained a number of specimens from Mina Moctezuma (formerly known as La Bomboya), a gold-tellurium mine near the town of Moctezuma, Sonora, Mexico (Lat. 29° 47.5′N, Long. 109° 41′W). Recognizing that some of the minerals might be new, he sent them to the Royal Ontario Museum for further study. A preliminary investigation revealed five new species and a note on these was published by Mandarino and Williams (1961a). A progress report by the same writers (1961b) was presented at the 1961 Annual Meetings of the Geological Society of America in Cincinnati. In both papers, spiroffite was called "a manganese-zinc tellurite or tellurate."

Because the writers have been unable to visit the locality, this description must be restricted to laboratory findings. Spiroffite is associated with native tellurium, tellurite, paratellurite, a new calcium tellurite (or tellurate), and denningite. Denningite, (Mn, Ca, Zn)$Te_2O_5$, was described recently by the writers (1962). Spiroffite is apparently later than tellurite and native tellurium. The genetic relationships between spiroffite and the other tellurium minerals are not clearly shown in the specimens.

## GENERAL FEATURES AND APPEARANCE

Spiroffite occurs as small cleavage masses ranging in size from 2×2×2 mm to 5×10×20 mm. The color varies from red to purple corresponding to RS-10-2° and RS-9-6° respectively, in the color classification of Villalobos (1947). The streak is colorless and the luster is adamantine. Spiroffite is translucent to transparent.

[1] Pronounced, SPĬR·AWFAIT according to the Royal Geographical Society (R.G.S.II) system as given in Hey (1955); or spĭr·off-īte according to the Oxford Dictionary System.

## CRYSTALLOGRAPHIC CHARACTERISTICS

The entire crystallographic study had to be carried out by means of *x*-rays because no euhedral crystals were found.

*X-ray data.* As neither crystal faces nor good cleavage planes were present, a fragment was oriented by a series of transmission Laue photographs. Fortunately, one of the first films revealed a mirror plane. The crystal was then turned, a few degrees at a time, around the axis perpendicular to this plane. Laue films made at each position showed no additional symmetry. Rotation and Weissenberg (0−l, 1−l, and 2−l) films were made with unfiltered Cu radiation in a camera of 5.73 cm. diameter, using the axis perpendicular to the mirror plane. They confirmed the assumption that this was the monoclinic *b*-axis. Additional orientation work enabled *a*-axis rotation as well as 0−l, and 1−l Weissenberg films to be made. A space group of either *Cc* or *C2/c* is indicated by the characteristic missing reflections: hkl (missing with h+k odd); h0l (missing with l odd, and h odd); 0k0 (missing with k odd).

The measured *x*-ray powder data listed in Table 1 are the average values obtained from a total of five films made in two cameras with CuK$\alpha$ radiation. The two cameras had diameters of 11.46 cm. With some idea of the unit cell values determined from the Weissenberg films, it was possible to partially index the powder films. Procedures similar to those of the Hesse-Lipson method outlined by Azároff and Buerger (1958) were used. Unit cell values, determined from the partially indexed powder data, are: $a=13.00$ Å; $b=5.38$ Å; $c=12.12$ Å; $a:b:c=2.416:1:2.253$; $\beta=98°$.

Since no euhedral crystals were available, an accurate value of $\beta$ could not be determined on the goniometer. Therefore, the reported value of $\beta$ may be in

TABLE 1. X-RAY POWDER DATA FOR SPIROFFITE. CuK$_\alpha$ RADIATION, d VALUES ARE AVERAGES OBTAINED FROM MEASUREMENTS OF FIVE FILMS MADE IN TWO CAMERAS OF 11.46 CM DIAMETER

| hkl | d (calc.) Å | d (meas.) Å | I (obs.) |
|---|---|---|---|
| 200 | 6.44 | 6.44 | vw |
| 002 | 6.00 | | |
| 110 | 4.96 | 4.98 | s+ |
| $\bar{2}02$ | 4.73 | | |
| $\bar{1}11$ | 4.68 | 4.68 | mw |
| 111 | 4.50 | 4.48 | vw |
| 202 | 4.11 | 4.06 | s |
| $\bar{1}12$ | 3.93 | | |
| 112 | 3.73 | 3.69 | vvw |
| 310 | 3.35 | | |
| $\bar{3}11$ | 3.33 | 3.31 | s |
| 400 | 3.22 | | |
| 311 | 3.14 | | |
| $\bar{3}12$ | 3.07 | | |
| 113 | 3.04 | | |
| $\bar{4}02$ | 3.02 | | |
| 004 | 3.00 | 3.00 | s+ |
| $\bar{2}04$ | 2.88 | 2.84 | mw |
| 312 | 2.80 | 2.77 | w |
| $\bar{3}13$ | 2.72 | | |
| 020 | 2.69 | 2.69 | w |
| 402 | 2.68 | 2.65 | vw |
| 021, $\bar{1}14$ | 2.63 | | |
| 204 | 2.58 | 2.60 | w |
| 114 | 2.51 | | |
| 220 | 2.48 | | |
| $\bar{2}21$ | 2.46 | 2.46 | mw |
| 022 | 2.45 | | |
| 313 | 2.44 | | |
| 221 | 2.41 | | |
| $\bar{3}14$ | 2.37 | | |
| $\bar{4}04$ | 2.36 | | |
| $\bar{2}22$, $\bar{5}11$ | 2.34 | 2.33 | w+ |
| 510 | 2.32 | | |
| $\bar{5}12$ | 2.26 | | |
| 222 | 2.25 | 2.24 | vw |
| | | 2.22 | mw |
| | | 2.10 | vw |
| | | 2.04 | w |
| | | 2.00 | vw |
| | | 1.95 | w |
| | | 1.89 | vw |
| | | 1.83 | vw |
| | | 1.80 | vw |
| | | 1.77 | w |
| | | 1.72 | vvw |
| | | 1.67 | mw |
| | | 1.63 | ms |
| | | 1.60 | vvw |
| | | 1.57 | mw |

error. Also, the accuracy of the unit cell dimensions were necessarily affected. However, interplanar spacings calculated from these values reasonably match the observed data, and permit the observed d-spacings to be indexed. In Table 1, all calculated spacings allowed by space groups *Cc* and *C2/c* are listed for $d_{hkl} \geq 2.25$ Å. All spacings down to 1.57 Å were calculated, but so many different values match each of the measured reflections in this range that the inclusion of these data seems pointless. Using a molecular weight of 627.92 for $(Mn_{1.26}Zn_{0.72}Ca_{0.02})Te_3O_8$, and a measured specific gravity of 5.01, the value determined for Z is 4 (4.03 calculated).

## PHYSICAL AND OPTICAL PROPERTIES

The specific gravity of several grains of spiroffite, weighing about 20 mg each, was measured with the Berman balance and found to be $5.01 \pm 0.02$ at 25° C. The calculated value is 4.97. The hardness is about $3\frac{1}{2}$. Spiroffite has a conchoidal fracture and at least two directions of cleavage. It has not been possible to determine the crystallographic orientation of the cleavages.

The optical properties of spiroffite are given in Table 2. The determination of the optical constants was complicated by the high refractive indices and the tendency of cleavage grains to assume a preferred orientation. Although most grains yielded obtuse bisectrix interference figures, a few grains showed centered or nearly-centered acute bisectrix interference figures. Since $\gamma$ was higher than the highest index liquid available (2.10), it could not be measured. The value of $\gamma$ calculated from $\alpha$, $\beta$ and 2V is also given in Table 2. The "average" index of refraction ($\sqrt[3]{\alpha\beta\gamma}$) is 1.98, which agrees with the average index calculated from the Gladstone-Dale relationship, 1.97. The axial angle was estimated at 60 degrees during the immersion work. Later, 2V was measured with a three-axis universal stage equipped with hemispheres of n = 1.699. The value of 2V, after the usual corrections for refraction differences, is 55 degrees. The universal stage work confirmed the fact that $\gamma$ is the acute bisectrix. It was not possible to obtain good readings on the cleavages. Consequently, the orientation of the optical indicatrix in spiroffite is still unknown.

TABLE 2. OPTICAL PROPERTIES OF SPIROFFITE

| | |
|---|---|
| $\alpha = 1.85 \pm 0.01$ | |
| $\beta = 1.91 \pm 0.01$ | Biaxial positive |
| $\gamma > 2.10$ (2.20 calculated) | $2V = 55° \pm 5°$ |
| $\gamma - \alpha$ (calculated) $= 0.35$ | |

## Chemical Characteristics

*Preliminary spectrographic analysis.* A small sample of spiroffite from R.O.M. specimen No. M24880 was submitted to the Ontario Department of Mines for spectrographic analysis. The following results were obtained:

Major Constituents—Mn, Zn, Te
Minor Constituents—Pb, Bi, Al, Si
Trace Constituents—Sb, Cd, Mo, Fe, Cu, Co, Ca, Mg

Only the major constituents could be estimated with any certainty because of the sample's size.

*Quantitative analysis.* Several small masses of the mineral were removed from a specimen (R.O.M. No. M24879) and crushed. A clean concentrate of 500 mg was obtained by hand-picking under a binocular microscope. No other phases were observed in this concentrate under a magnification of 40×. *X*-ray powder patterns of several samples taken from the analysis lot showed no extraneous lines. Additional clean material from the same masses was used for *x*-ray, optical, and specific gravity determinations.

The 500 mg sample was submitted to Mr. C. O. Ingamells, Mineral Constitution Laboratories, Pennsylvania State University. In addition, a small impure sample was provided for exploratory analysis.

Preparatory to the wet chemical analysis, a quantitative spectrographic analysis was carried out by Mr. Norman H. Suhr of Pennsylvania State University. The results of this analysis are given in Table 3. Also included are flame photometer determinations of $Na_2O$ and $K_2O$. No attempt was made to determine the precise amounts of $TeO_2$, ZnO, MnO, and CaO as this would be done later by wet chemical methods.

The results of Mr. Ingamells' quantitative analysis are shown in Table 4. The procedures used in the analysis are given in the appendix. The empirical formula derived from the data of Table 4 is:

$$(Mn_{1.26}Zn_{0.72}Ca_{0.02})Te_{3.01}O_{8.02}$$

or, simplified:

$$(Mn, Zn, Ca)_2Te_3O_8.$$

The natural hypothetical end-members have not yet been found. Attempts are being made to synthesize these compounds and the results will be reported later. Mellor (1931) lists no compounds of this type, although tritellurites of single divalent cations with the formulae of the type $RTe_3O_7$ have been synthesized.

(a) Degree of precision. According to Mr. Ingamells, the $TeO_2$ content is probably accurate to one

Table 3. Emission Spectrographic Analysis of Spiroffite. Royal Ontario Museum No. M24879, Pennsylvania State No. 61-1430. Norman H. Suhr, Spectrographer. Flame Photometer Determinations of $Na_2O$ and $K_2O$ Are Included

| Constituent | Weight % |
|---|---|
| $TeO_2$ | major[1] |
| ZnO | 8.5[1] |
| CdO | 0.07 |
| PbO | 0.05 |
| MnO | 18[1] |
| CaO | 0.02?[1] |
| MgO | 0.02 |
| $Bi_2O_3$ | 0.08 |
| $Sb_2O_3$ | 0.02 |
| $Al_2O_3$ | 0.02 |
| $MoO_3$ | 0.00 |
| FeO | 0.00 |
| CoO | 0.02 |
| NiO | 0.00 |
| $V_2O_5$ | 0.00 |
| $TiO_2$ | 0.00 |
| $Na_2O$ | 0.0 (by flame photometer) |
| $K_2O$ | 0.0 (by flame photometer) |
| Total (less $TeO_2$, ZnO, MnO, and CaO) | 0.28 |

[1] See Table 4 for chemical determinations of these constituents.

Table 4. Quantitative Chemical Analysis of Spiroffite (ROM No. M24879, Penn. State No. 61-1430). C. O. Ingamells, Analyst, Mineral Constitution Laboratories, Pennsylvania State University. See Appendix for Analytical Procedures

| (1) | (2) | (3) | (4) | (5) |
|---|---|---|---|---|
| $TeO_2$ | 75.93 | 76.29 | .478 | 3.01 |
| ZnO | 9.32 | 9.36 | .115 | |
| MnO | 14.13 | 14.20 | .200 .318 | 2.00 { 0.72, 1.26 |
| CaO | 0.15[1] | 0.15 | .003 | 0.02 |
| excess $O_2$ | 0.00 | | | |
| $H_2O$ | 0.03 | | | |
| insoluble | 0.22[2] | | | |
| remainder | 0.28[3] | | | |
| total | 100.06 | 100.00 | | |

[1] Includes SrO (less than 0.1%) if present.
[2] Material insoluble in 1:1 HCl—probably silica or silicate.
[3] Consists of minor constituents determined spectrographically (see Table 3).
(1) Constituent
(2) Weight %
(3) Major constituents recalculated to total 100.00%
(4) Molecular proportions
(5) Ratio of $TeO_2$ to divalent oxides

part in a thousand. The values for MnO, ZnO, and CaO (including SrO) are accurate to about ±0.05% absolute. The excess oxygen determination is true to ±0.01%. Because of the small sample used, the $H_2O$ determination may well be inaccurate. The value of 0.03% is only included to show that the mineral is not a hydrate. The emission spectrographic determinations are within 10% of the amounts present. The alkalies were run by flame photometry on extremely small samples and it is possible that as much as 0.1% of either $Na_2O$ or $K_2O$ may be present.

*Chemical Tests.* Spiroffite darkens and fuses easily in a gas flame. In both open and closed tubes it fuses quietly to a reddish-brown, glass-like substance. It is easily soluble in cold HCl and the resulting solution is yellow. No significant solution was noted in either hot $HNO_3$ or hot $H_2SO_4$.

## Nomenclature and Classification

Spiroffite is an anhydrous tellurite of divalent manganese, zinc, and calcium. Of the known natural tellurites, only one other mineral has this same qualitative chemical composition. This mineral is denningite, (Mn, Ca, Zn)$Te_2O_5$. A comparison of the properties of spiroffite and denningite is given in Table 5. There can be no doubt that these two species are distinct from each other. Spiroffite (as well as denningite) is a so-called "basic" tellurite. That is, the ratio of tellurium (IV) to oxygen is *not* one to three.

Table 5. Comparison of Spiroffite and Denningite

| | Spiroffite | Denningite |
|---|---|---|
| Chemical Formula | (Mn, Zn, Ca)$Te_3O_8$ | (Mn, Ca, Zn)$Te_2O_5$ |
| Crystallography<br>Space group | Monoclinic<br>*Cc* or *C2/c* | Tetragonal<br>$P4_2/n\ b\ c$ |
| Unit cell parameters | $a$=13.00 Å<br>$b$= 5.38 Å<br>$c$=12.12 Å<br>$\beta$=98° | $a$= 8.82 Å<br>$c$=13.04 Å |
| Z | 4 | 8 |
| H | 3½ | 4 |
| Sp. gr. | 5.01 | 5.05 |
| Optical properties | Biaxial (+)<br>$\alpha$=1.85<br>$\beta$=1.91<br>$\gamma$=2.20 (calc.)<br>2V=55° | Uniaxial (+)<br>$\omega$=1.89<br>$\epsilon$=2.00 |
| Strongest $x$-ray powder spacings | 4.98 Å (S+)<br>3.00 Å (S+)<br>4.06 Å (S)<br>3.31 Å (S)<br>1.63 Å (MS) | 4.42 Å (VS)<br>3.38 Å (S+)<br>3.12 Å (S)<br>2.62 Å (S)<br>2.03 Å (S) |

The name spiroffite should be restricted to the high manganese portion of the hypothetical system $Mn_2Te_3O_8$-$Zn_2Te_3O_8$-$Ca_2Te_3O_8$. Consequently, the material described here is properly termed a zincian spiroffite. The amount of CaO (0.15%) is not considered sufficiently high to warrant the use of the additional prefix, calcian.

Spiroffite is named in honor of Kiril Spiroff (1901–), Professor of Mineralogy and Geology, Department of Geology and Geological Engineering, Michigan College of Mining and Technology, Houghton, Michigan.

## Preservation of Specimens

The following specimens of spiroffite have been preserved in the mineral collections of the Royal Ontario Museum: M24879 (analyzed specimen), M24880, M24999, and M25001 (with denningite). Approximately six grams of spiroffite exist in these specimens.

Requests for loan of specimens should be addressed to:

Curator of Mineralogy,
Earth Sciences Division,
Royal Ontario Museum,
University of Toronto,
100 Queen's Park,
Toronto 5, Ontario,
Canada.

## Acknowledgements

The writers take pleasure in acknowledging the assistance of the following people. Messrs. D. A. Moddle and W. O. Taylor of the Ontario Department of Mines kindly ran the original spectrographic analysis of spiroffite. Messrs. L. I. Cowan and C. M. Spooner of the Royal Ontario Museum assisted in various phases of the laboratory work. Dr. V. B. Meen, Royal Ontario Museum, was a constant source of encouragement during this study and contributed several helpful suggestions.

## Appendix—Method of Analysis

The following procedures were used in the analysis of spiroffite. The writers are indebted to Mr. Ingamells for making this information available.

1. Grind all but a few mg. to pass 100 mesh. Pack powder in

glass and lucite holder and take $x$-ray fluorescence spectrum. Prepare synthetic mixtures of pure oxides to approximate composition of unknown, but with an excess of all the minor elements, and a deficiency of $TeO_2$. Make a preliminary estimate of sample composition.

2. Make several successive dilutions of the known mixtures with $TeO_2$, and prepare spectrograms of these as well as the unknown, using about 30 mg of sample. Obtain quantitative values for the trace elements and approximations for the majors, using emission spectrograph.
3. Determine total water on 100 mg in a closed tube.
4. Determine excess oxygen on 20 mg, running known salts of Te (IV) and Te (VI) as controls. Method: C. O. Ingamells (1960).
5. Using small impure sample provided, carry out exploratory analysis to determine behavior of material. Look for the alkali metals with the flame photometer.
6. Carry out main part of the analysis as follows, using 300 mg sample. Dry at 105°, weigh; dry at 160°, weigh. Dissolve in HCl, filter off insolubles, weigh. Precipitate Se with hydroxylamine, weigh; precipitate Te with $SO_2$, hydrazine, weigh. Examine precipitate for Bi, etc. Neither Se nor Bi were found in amounts sufficiently large to determine by these methods. Precipitate sulphide group, precipitate $NH_3$ group, examine precipitates. Triple oxalate precipitation, weigh CaO+Mn, Zn. Determine Mn, Zn contamination and correct. Double $PO_4^{3-}$ precipitation, weigh $Mn_2P_2O_7$: determine Mg, Ca contamination and correct. Destroy $NH_4^+$ salts with $HNO_3$, determine Zn by weighing as pyrophosphate. Determine Mn contamination and correct.

## References


Azároff, L. V. and M. J. Buerger (1958) *The Powder Method in X-ray Crystallography*, McGraw-Hill Book Company, Inc., New York.

Ingamells, C. O. (1960) A new method for "ferrous iron" and "excess oxygen" in rocks, minerals, and oxides. *Talanta*, **4**, 268–273.

Mandarino, J. A. and S. J. Williams (1961a) Five new minerals from Moctezuma, Sonora, Mexico. *Science*, **133**, (3469) 2017.

Mandarino, J. A. and S. J. Williams, (1961b) The tellurium minerals of Moctezuma, Sonora, Mexico. *Abs. Program 1961 Ann. Meet. Geol. Soc. Am.* 99A.

——— S. J. Williams and R. S. Mitchell (1962) Denningite, a new tellurite mineral from Moctezuma, Sonora, Mexico, *Canadian Mineral.* (in press). Presented at the 1962 meetings of the Mineralogical Association of Canada, April 25, 1962.

Mellor, J. W. (1931) *A Comprehensive Treatise on Inorganic and Theoretical Chemistry, Volume XI (Te, Cr, Mo. W)*, Longmans, Green and Company, London.

Villalobos-Domínguez, C. and Julios Villalobos, (1947) *Atlas de los Colores*. Liberia El Ateneo Editorial, Buenos Aires.

MINERALOGICAL SOCIETY OF AMERICA, SPECIAL PAPER 1, 1963
INTERNATIONAL MINERALOGICAL ASSOCIATION, PAPERS, THIRD GENERAL MEETING

## THE CRYSTAL STRUCTURE OF PSEUDOMALACHITE

SUBRATA GHOSE
*Crystallography Laboratory, University of Pittsburgh, Pittsburgh, Pennsylvania*[1]

ABSTRACT

Pseudomalachite, $Cu_5(PO_4)_2(OH)_4$, is monoclinic with $a=4.49$, $b=5.76$, $c=17.06$ Å, $\beta=91°02'$; space group $P2_1/c$, $Z=2$. The interpretation of sharpened Patterson projections on (100) and (010) yielded the three independent copper and one phosphorus positions. Successive structure factor calculations and Fourier summations brought out the six oxygen atoms.

The structure consists of the two types of Cu-octahedrel chains running parallel to *b*. The first type of chain is composed of one $Cu_1$- and two $Cu_2$-octahedra and is similar to the chain found in lindgrenite and azurite. The second chain is composed of $Cu_3$-octahedra sharing square edges. These two types of chains are bonded together to form sheets parallel to *bc*; these sheets again are tightly bonded to each other by means of isolated ($PO_4$) groups. As a result there is no distinct cleavage in the mineral. Erinite is isostructural with pseudomalachite.

[1] Present Address: Mineralogical Institute, University of Bern, Bern, Switzerland.

## LIGHT EXTINCTION AND SCATTERING BY SUSPENSIONS OF FINELY-DIVIDED MINERALS

J. R. HODKINSON
*Safety-in-Mines Research Establishment, Sheffield 1, England*

ABSTRACT

The true total extinction and the absolute angular distribution of scattered intensity from 0 to 90 degrees have been measured for aqueous suspensions of quartz, flint, diamond, ilmenite and coal as size-graded fractions in the diameter-range $\frac{1}{2}$ to 15 microns. Due to the irregular shape and spread in size of the particles, their behavior differs from that of mono-disperse spheres on the Mie theory. The extinction coefficient shows a constant value 2 down to 1 or 2 microns particle-size, the precise lower limit depending on refractive index and absorption coefficient. The angular scattering coefficient is more or less independent of particle-size within the same size-range, for angles outside the forward diffraction lobe, and agrees well with the scattering calculated from geometrical optics. The measurements were made to ascertain the conditions under which extinction and scattering could be used to estimate the surface-area concentration and composition of airborne dust causing pneumoconiosis, but the results are of general application.

## ACCURATE DETERMINATION OF OLIVINE COMPOSITION USING STANDARD SMALL-DIAMETER *X*-RAY POWDER CAMERAS[1]

J. L. JAMBOR AND CHARLES H. SMITH
*Geological Survey of Canada, Ottawa, Ontario, Canada*

ABSTRACT

Olivine composition can be rapidly and accurately obtained by using standard (Straumanis mounting) 57.3 mm *x*-ray powder cameras. A determinative curve based on analyzed natural olivines has been constructed by plotting the mol per cent Fo against the spacing of a $K\alpha_1$ back-reflection line which has been variously indexed as (0.10.0) and (450). The new graph deviates from the generally accepted straight line relationship of d-spacing versus composition, but corresponds instead to the slightly curved graphs derived from specific gravity measurements by Bloss and from *x*-ray powder measurements by Eliseev.

[1] Published by permission of the Director, Geological Survey of Canada.

The powder camera technique was developed for use with the small amounts of olivine normally found in thin sections of altered ultramaffic rocks, thereby avoiding the task of preparing concentrates as is generally required in the diffractometer method. Olivine composition determinations can be made where only one or two grains are present in a thin section, and the method can therefore be applied to rocks that are almost completely serpentinized, to olivine-bearing gabbros, meteorites and other rocks with a low olivine content.

The camera method has been successfully utilized in outlining the pattern of olivine variation in the Mount Albert ultramafic pluton, Gaspé, Quebec, and is now being applied to the study of olivines from the Muskox intrusion, Northwest Territories, by Smith. On the basis of 125 determinations, a range in composition of approximately $Fo_{60}$ to $Fo_{90}$ has been established. All determinations were made on material removed from thin sections.

## INFRARED STUDY OF SULFATE MINERALS

KEIICHI OMORI AND PAUL F. KERR
*Tohoku University, Sendai, Japan and Columbia University, N. Y.*

ABSTRACT

The cations Na, K, $NH_4$, Ca, Mg, Mn and at times, Ba, Sr and Pb combine with the anion $SO_4$ to form some 58 mineral species, which may be considered as belonging to six groups, as follows:

Group I. Anhydrous sulfates with Na, K, $NH_4$, Ca, Pb, Sr or Ba—thenardite aphthitalite, mascagnite, glauberite, langbeinite, palmierite, anhydrite, celestite and barite.

Group II. Alkali hydrous sulfates with Na, K, $NH_4$, Ca, Mg, Cu or Fe—kroenkite, bloedite, ferrinatrite, syngenite, picromerite, polyhalite, kalinite, valtite and tschermigite.

Group III. Hydrous sulfates with Ca, Cu, Fe, Co, Mg, Zn or Al—gypsum, epsomite, goslarite, siderotil, melanterite, coquimbite, pisanite, chalcanthite, bieberite, alunogen, halotrichite and pickeringite.

Group IV. Sulfates with (OH) or (F, Cl) and oxysulfates—natroalunite, alunite, natrojarosite, zincalunite, jarosite, raimondite, plumbojarosite, beaverite, sulfohalite, antlerite, brochantite, linarite and dolerophanite.

Group V. Hydrous sulfates with (OH) or (F, Cl)—sideronatrite, natrochalcite, metavoltine, kainite, botryogen, copiapite, fibroferrite, langite, ettringite, aluminite, johannite, zippeite and uranopilite.

Group VI. Alkali sulfates to carbonates—burkeite, hanksite, leadhillite and calcite.

Infrared adsorption spectra of most of these species have been obtained with a split beam infrared spectrophotometer. The identity of each species examined has been verified optically and by means of $x$-ray diffraction for further confirmation.

Examination of the spectra indicates that the sulfates yield infrared curves that fall naturally into several groups. These groups have been outlined, and the relative ranges in absorption characteristics are given for each.

## STUDY OF TRANSLUCENT TINY GRAINS USING THE INTERFERENCE MICROSCOPE

HORST PILLER
*Carl Zeiss, Oberkochen, West Germany*

ABSTRACT

Special measures have to be taken to carry out microscopic examination of fine-grained material in order to make the particles visible with sufficient contrast. For that purpose the author proposed the phase contrast method, and he found that by combining this method with the well-known embedding methods the accuracy of the determination of refractive indices is increased. Furthermore, this showed that by using suitable embedding media with very high dispersion properties, transparent particles of a certain refractive index could be imaged with characteristic colors and were thus differentiated from other particles of different refractive index. On the basis of a newly developed supplementary device for the polarizing microscope it

it now possible to examine transparent particles by means of interference microscopy. As in the case of phase contrast microscopy, here too contrast is increased; however with the difference that it can be adjusted to an optimum extent depending on the optical thickness of the particle. The simple relation between the image contrast and the difference of the optical thickness of the object to that of its surrounding can be used to ascertain refractive indices and thicknesses in the microscopic specimen. The following possibilities are observed:

1. Determination of the refractive indices of smallest particles by means of compensator and using but one (in some cases a second) embedding liquid. Therefore, repeated embedding, as is necessary in the case of conventional immersion methods, is not needed. 2. Determination of refractive indices exceeding that of the embedding media; this is of special importance when examining heavy minerals. 3. Ascertainment of the thickness of each individual particle present in the embedding media. 4. Possibility of application of interference phenomena combined with dispersion staining methods for routine identification of individual components in mineral complexes.

A big advantage of interference microscopy is that continuously changing optical thicknesses, as for instance with a change in concentration or in the cross section of a crystal "weathering" from its external surfaces, can be made visible and the corresponding refractive indices measured at any position.

## STUDIES OF ROCK-FORMING MICAS[1]

J. Rimsaite
*Geological Survey of Canada, Ottawa, Ontario, Canada*

Abstract

An extensive age determination program by isotopic dating of micas at the Geological Survey of Canada has made available for mineralogical study several hundred concentrates of micas from rocks of diverse age, origin and history. The present study is concerned with determining the homogeneity of each mica concentrate, establishing the type or types of micas present, and correlating physical and chemical properties of the micas with their mode of occurrence in rocks. The study is confined largely to unaltered micas.

Spectrochemical and $x$-ray spectrographic analyses and complete chemical analyses have been made on about 20 selected samples of micas. Chemical formulas, negative and positive charges of tetrahedral and octahedral layers, and occupancy of the octahedral layer have been calculated. These data are discussed in relation to the following experimental data: (1) intensities of (00l) reflections in $x$-ray diffractometer patterns; (2) optical properties—color, refractive indices, 2V; (3) specific gravity; (4) behavior on heating from 20° C. to 1200° C. in air, in argon and in vacuum; (5) loss of weight on heating to 1400° C.; (6) trace element content.

As a result of these studies, interesting relationships have been found between the varieties of micas and the types of their host rocks. Furthermore, in rocks containing two or more generations of trioctahedral micas, the difference in composition between an early and a late mica has been established and confirmed by different content of trace elements in these micas.

[1] Published by permission of the Director, Geological Survey of Canada.

## THE COMPOSITION OF QUARTZ-FORMING FLUIDS IN NATURE

Edwin Roedder
*U. S. Geological Survey, Washington, D. C.*

Abstract

A microscope freezing stage has been developed with which qualitative and semi-quantitative data may be obtained on the composition of individual fluid inclusions as small as ten microns. Although the technique can be used to obtain a variety of geologically useful data, the major application has been in the determination, under equilibrium conditions, of the depression of the freezing point of the fluid; in ordinary water solutions, this depression varies directly with the total concentration of salts. Both primary and secondary inclusions in quartz crystals that formed in a variety of geological environments have been examined. The freezing temperatures obtained range from $-20°$ to 0° C., although most samples from alpine-type veins, and from

pegmatites, range only from −8.5° to −2.5° C. Large and consistent differences are found between different genetic groups of inclusions in single samples, indicating gross chnnges in the composition of the fluids that have bathed the samples during their growth and at subsequent stages in their history.

## THE CRYSTAL STRUCTURES AND CRYSTAL CHEMISTRY OF VARIOUS MEMBERS OF THE METATORBERNITE GROUP

MALCOLM ROSS AND HOWARD T. EVANS, JR.
*Harvard University, Cambridge, Mass. and the U. S. Geological Survey, Washington, D. C.*

ABSTRACT

A large number of minerals and synthetic compounds belonging to the torbernite and metatorbernite mineral group can be represented by the formula $A^{+z}(UO_2XO_4)_z \cdot nH_2O$, where A may be almost any monovalent or divalent cation and X = P or As. In order to learn more of the crystal chemistry of these phases, detailed crystal-structure studies of (I), $K(UO_2AsO_4) \cdot 3H_2O$ (abernathyite); (II), $NH_4(UO_2AsO_4) \cdot 3H_2O$; (III), $K(H_3O)(UO_2AsO_4)_2 \cdot 6H_2O$; and (IV), $Cu(UO_2PO_4)_2 \cdot 8H_2O$ (metatorbernite) have been carried out. The structures were refined by two- and three-dimensional least-squares analysis of intentity data measured on Buerger precession photographs made with MoK$\alpha$ radiation. The well-known waffle-like $(UO_2XO_4)_n^{-n}$ sheet structure proposed by Beintema is confirmed, and details of the interlayer structure are also revealed through a complete resolution of all except the hydrogen atoms in the electron density maps. In all four structures studied, the positions of the interlayer water molecules are based on an ideal arrangement in which four molecules are hydrogen-bonded together to form squares about the four-fold rotation axes, lying between the uranyl ions of successive layers. On Phases I and II, $K^+$ and $NH_4^+$ substitute randomly for one out of four water molecules and in Phase III, $K^+$ and $H_3O^+$ substitute randomly for two out of eight water molecules. An isomorphous series probably exists between the end members $K(UO_2AsO_4) \cdot 3H_2O$ (abernathyite) and $H_3O(UO_2AsO_4) \cdot 3H_2O$ (troegerite) and also between $NH_4(UO_2AsO_4) \cdot 3H_2O$ and troegerite. The ratio of cation (including hydronium) to water of 1:3, required by the cation replacement of water found in these structures, has been confirmed by careful chemical analysis.

In metatorbernite (IV) cation substitution of water does not occur, but rather $Cu_2^+$ occupies special positions at the center of half of the square groups of water molecules, thus giving a cation-water ratio of 1:8.

In all four structures each water molecule of a square group is also hydrogen-bonded in a nearly tetrahedral manner to a water molecule in an adjacent square and to an arsenate or phosphate oxygen atom. The latter bond causes a slight distortion of the $(UO_2XO_4)_n^{-n}$ sheet from ideal symmetry and accounts for the doubling of the ideal one-layer *c* axis.

## THE SIGNIFICANCE OF SAPPHIRINE IN THE GRANULITE TERRAINS OF WESTERN AUSTRALIA

ALLAN F. WILSON
*Department of Geology and Mineralogy, University of Queensland, Brisbane, Australia*

ABSTRACT

Several new analyses of sapphirine (Mg, Fe)$_4Al_{10}Si_2O_{23}$, spinel, bronzite, and phlogopite have been made from a restricted Archean area 10 miles south of Quairading which is 100 miles east of Perth, Western Australia. A normal "parent rock" is phlogopite-spinel-bronzite. Spinel (and also phlogopite and bronzite) is replaced by sapphirine. In rocks rich in cordierite, spinel is always separated from cordierite by a reaction rim of sapphirine. Chemical analyses indicate that the formation of sapphirine is favored by replacement (in reducing conditions) of Al, Fe, Mg and Ca by Si, K, P and rare earths. The spinel-bronzitites and associated cordierite gneisses and pyroxene-plagioclase granulites form mappable bands and boudins in a biotite-microcline gneissose granite. The sapphirine, cordierite and phlogopite have no preferred orientation, and in many rocks the "parent" spinel and bronzite are likewise in random orientation, thus suggesting growth in a

non-shear environment. A survey of the regional geology suggests that these sapphirine-bearing rocks form a zone ($2620 \times 10^6$ years old) in an immense area which is dominated by rocks of granulite facies and of granites. These granulites show preferred orientation of the two pyroxenes and plagioclase and are the result of regional metamorphism in which shearing was important.

It appears that sapphirine can form only in areas of granulite facies and as the result of release of pressure and granitization of massive rocks rich in Mg and Al and deficient in Si. However, "granulite facies-granitization" of such rocks is common yet in most cases without the formation of the rare mineral sapphirine. A granitzation process in which there is an abnormally low partial pressure of oxygen together with a plentiful supply of rare earths may be necessary for its formation.

## IRON-FELDSPAR POLYMORPHS IN THE SYSTEM $K_2O$-FeO-$Fe_2O_3$-$SiO_2$-$H_2O$

DAVID R. WONES AND DANIEL E. APPLEMAN
*U. S. Geological Survey, Washington, D. C.*

ABSTRACT

Potassium-iron feldspar, $KFe^{3+}Si_3O_8$, has been synthesized hydrothermally in two distinct polymorphs. The form stable at low temperatures, analogous to microcline, was synthesized directly from a mixture of crystallized $K_2O \cdot 6SiO_2$ glass and $Fe_2O_3$ at gas pressures of 1000 to 2000 bars and temperatures below 690° C.; above 710° C., a form analogous to high-sanidine was synthesized. At 600° C. and 2000 bars gas pressure iron-sanidine was completely converted to iron-microcline, whereas at 770° C. and 1000 bars gas pressure iron-microcline was completely converted to iron-sanidine. No "intermediate" states were observed in hydrothermal experiments.

Iron-microcline is triclinic, $C\bar{1}$; $a = 8 \cdot 69$ Å, $b = 13.11$, $c = 7.33$ (all $\pm 0.15\%$); $\alpha = 90°36'$, $\beta = 116°02'$, $\gamma = 86°30'$ (all $\pm 10'$); optical orientation $X \approx b$, $Z \wedge c = 20° \pm 5°$. Iron-sanidine is monoclinic, $C2/m$; $a = 8.69$ Å, $b = 13.12$, $c = 7.32$ (all $\pm 0.15\%$); $\beta = 116°06' \pm 05'$, optical orientation $Y = b$, $Z \wedge c = 16° \pm 4°$.

The relationship between the $KFeSi_3O_8$ polymorphs is strikingly similar to that between the $KAlSi_3O_8$ polymorphs. This increases the probability that crystal-structure studies of the Fe-Si distribution in $KFeSi_3O_8$ will elucidate the crystal-chemical and phase-equilibria behavior related to Al-Si distribution in the natural potassium feldspars.

# PROCEEDINGS OF THE INTERNATIONAL MINERALOGICAL ASSOCIATION

## Third General Business Meeting of Delegates

Washington, D. C., April 18 and 20, 1962

JOSÉ L. AMORÓS, *Secretary*

CONTENTS

First Session

Opening ..... 315
Reports of Officers ..... 315
President's Report ..... 315
Report of the Treasurer ..... 316
Reports of Committee Chairmen ..... 317
Liaison Committee to the I.U.G.S. Committee on Meteorites ..... 317
Other Committees ..... 318
Other Matters ..... 319
Changes in the Constitution ..... 319
New Commission on Ore Microscopy ..... 319
Next Meeting ..... 319
Miscellaneous ..... 319

Second Session

Report by the Auditors ..... 319
New Commissions ..... 319
Commission Reports ..... 320
New Business ..... 320
Reports of the Commissions ..... 320
Commission on Abstracts ..... 320
Commission on Mineral Data ..... 321
Museums Commission ..... 322
Commission on New Minerals and Mineral Names ..... 322
Commission on Teaching ..... 324

## FIRST SESSION

### OPENING

The first session of the III General Business Meeting of Delegates of the 22 Member Societies of the International Mineralogical Association was held in the Auditorium of the Natural History Building of the U. S. National Museum of the Smithsonian Institution in Washington, D. C. on April 18, 1962. Of the possible 43 voting delegates, 37 were present, representing Mineralogical Societies of Austria, Belgium, Canada, Denmark, Egypt, Finland, France, Germany, India, Italy, Japan, Netherlands, New Zealand, Spain, Sweden, Switzerland, United Kingdom, U.S.A., and U.S.S.R. The member Societies of Bulgaria, Czechoslovakia, and Norway were not represented. In addition there were registrants from Australia, Chile, Ghana and Kenya.

After the welcome of the Delegates by President D. Jerome Fisher, by Dr. Leonard Carmichael, Secretary of the Smithsonian Institution, and by Dr. Thomas B. Nolan, Director of the U. S. Geological Survey, the session continued according ot the agenda (Constitution 4A*a*). The Proceedings of the previous meeting at Copenhagen in August 1960 were approved as already published in the *Cursillos y Conferencias, Instituto Lucas Mallada, C.S.I.C. (España), Fasc.* III, pp. 169–182, 1961, with the addition of the minor change that they neglected to call attention to the I.M.A. dinner held on August 25, 1960 in the beautiful Sopavillonen.

### REPORTS OF OFFICERS

#### PRESIDENT'S REPORT

The current affairs of the Association seem to be running along well; however, there are two items which should be stressed; both of these were mentioned in President Parker's report given at Copenhagen.

1. More activity is needed on the part of some of our Representatives. Now the Representative is the laison officer functioning between the Executive Committee of the I.M.A. and the individual National Society or similar organization (see Constitution, Art. 3*b*). It is his duty to publicize the I.M.A. to the individual members of the Society, and to transmit from these to the Secretary of the I.M.A. any suggestions or recommendations. Not less than once a year the Representative should report on the doings of the I.M.A. to his Society assembled at its meeting, and the gist of these remarks should be published in the Society's journal. Or if his group is a small informal one that holds no regular meetings, then at least once a year he should circularize it with a written (duplicated) notice that covers this same ground. Representatives are asked to send a copy to the Secretary of the I.M.A., or to send him a reference to where this appears in the Society's journal. It must be stressed that nothing is accomplished unless some *individual* does some thinking and work, and makes these known to others in the I.M.A.

2. Careful thought should be given to the election of a new Council and new Commission officers to become effective at the Madras meeting in December, 1964. It is particularly important that the Executive committee (President, Secretary, Treasurer) of the I.M.A. and the officers (Chairman, Secretary) of the various Commissions be people with zeal and ideas who can afford to expend the time that must necessarily be devoted to the affairs of the Association if it is to be successful. Of course it is desirable that these be as well distributed among the various Societies as is possible (see Constitution 4B*a* and 12*b*), but it is far more important that these people be willing to put in the necessary effort to see that the Association continues to progress. The rules for electing a new Council appear in Article 11; the present Executive Committee asks that anyone who knows the name of a person who would make a good officer and who would presumably be willing to serve, transmit this to the secretary before June, 1964.

REPORT OF THE TREASURER

Covering July 1, 1960 to March 31, 1962

Receipts

| | | | |
|---|---|---|---|
| Cash on hand July 1, 1960 | | $1,269.44 | |
| Dues for July 1, 1960 to June 30, 1961 | | | |
| Mineralogical Societies of Austria (15), Belgium (30), Bulgaria (30), Canada (60), Egypt (14.25), France (90), Japan (60), Netherlands (15), New Zealand (15), Sweden (57.80), United Kingdom (90), U.S.S.R. (130+20) | $ 627.05 | | |
| Dues for July 1, 1961 to Dec. 31, 1962 | | | |
| Mineralogical Societies of Austria (15), Belgium (30), Czechoslovakia (30), Denmark (30), Egypt (30.40), France (90), Germany (120), India (30), Italy (90), Japan (60), Netherlands (15), New Zealand (15), Switzerland (60), United Kingdom (90), U.S.A. (150), U.S.S.R. (150) | 1,005.40 | | |
| Dues for 1963 | | | |
| Mineralogical Society of Austria (15) | 15.00 | | |
| Total receipts July 1, 1960—March 31, 1962 | $1,647.45 | 1,647.45 | |
| Grand total | | $2,916.89 | $2,916.89 |

Disbursements

| | | | |
|---|---|---|---|
| President's office | | | |
| Stationery—5000 letterheads | $ 73.32 | | |
| R. L. Parker—badges, postage | 32.27 | | |
| D. J. Fisher—postage and telephone | 100.32 | | |
| | $ 205.91 | $ 205.91 | |
| Secretary's office | | | |
| Author's reprints, Zürich meeting | 16.43 | | |
| | $ 16.43 | 16.43 | |
| Treasurer's office | | | |
| Rubber stamp | 2.25 | | |
| Receipt book & envelopes | 1.95 | | |
| Stamps | 25.80 | | |
| | $ 30.00 | 30.00 | |
| Publication of World Directory | | | |
| Advance to M. Font-Altaba | 200.00 | | |
| | $ 200.00 | 200.00 | |
| Total Disbursements | | $ 452.34 | |
| Bank balance March 31, 1962 | 2,293.64 | | |
| Extra check to M. Font-Altaba (to be collected) | 200.00 | | |
| Check not yet credited at bank (Egypt) | 30.40 | | |
| | $2,524.04 | | |
| Check for postage not cashed at bank | 59.49 | | |
| | $2,464.55 | 2,464.55 | |
| Grand Total | | $2,916.89 | $2,916.89 |

Note: the dues from Egypt were paid by UNESCO coupons which are subject to 5% clearance fees. Thus the first payment realized only $14.25, the deficit was made up by a larger payment ($30.40) the following year.

The dues for Sweden were paid by Postal Order payable in Canadian Dollars. The amount shown is the U. S dollar equivalent allowed by the Chicago bank.

*Supplementary Treasurer's Report*
April 1 to June 30, 1962

Receipts

| | | | |
|---|---|---|---|
| Bank balance April 1, 1962 | | $2,293.64 | |
| Dues July 1, 1961 to December 31, 1962 | | | |
| Canada (60), Spain (30) | 90.00 | | |
| Dues 1963 | | | |
| Netherlands (15) | 15.00 | | |
| Dues for Egypt received in March credited at bank in April | 30.40 | | |
| Credit for lost check | 200.00 | | |
| Total receipt April 1, to June 30 | $ 335.40 | 335.40 | |
| Total | | $2,629.04 | $2,629.04 |

Disbursements

| | | | |
|---|---|---|---|
| Secretary's Office | | | |
| Postage, duplicating, typing | | 240.00 | |
| Publication of World Directory | | 680.00 | |
| Check written in March, debited at bank in April | | 59.49 | |
| Total disbursements April 1 to June 30 | | $ 979.49 | |
| Bank balance June 30, 1962 | $1,619.55 | | |
| Check not yet credited at bank | 30.00 | | |
| Total | $1,649.55 | 1,649.55 | |
| | | $2,629.04 | $2,629.04 |

Respectfully submitted, L. G. BERRY

## REPORTS OF COMMITTEE CHAIRMEN

After the Delegates had approved the appointment of Professors W. F. von Engelhardt and M. Font-Altaba as auditors and scrutineers for this meeting of the Association, the following Committee reports were presented.

### LIASON COMMITTEE TO THE I.U.G.S. COMMITTEE ON METEORITES

In the absence of the chairman, Professor D. P. Grigoriev of Leningrad, the following report prepared by him was presented by Dr. E. P. Henderson.

*A. Members of the Committee*

Prof. D. P. Grigoriev, Chairman, Mineralogical Society of USSR. Prof. F. Heide, Deutsche Mineralogische Gesellschaft, Dr. E. P. Henderson, Mineralogical Society of America, Prof. M. N. Viswanathiah, Mineralogical Society of India.

*B. Object of the Committee*

The Committee according to the decision at the Copenhagen meeting of the I.M.A. has the problem to decide in detail what should be the objectives of an I.M.A. Commission on Meteorites (if one is set up), and to find out what the I.U.G.S. Commission is doing in the matter. Moreover, if the latter has objectives substantially the same as those that an I.M.A. Commission on Meteorites should have, it is suggested that the Committee explore ways and means in which the two groups can possibly work together effectively.

*C. Contacts with the Commission on Meteorites of the I.U.G.S.*

The Committee has carried out the necessary discussion with the Commission of the I.U.G.S. and became acquainted with the plan of its work. As a result the rationality of the establishment of the Commission in the I.M.A. that shall organize the international work on meteoritic mineralogy was established. The opinion of the Commission of the I.U.G.S. on this problem is expressed in the letter of Dr. E. L. Krinov, President, Sept. 18, 1961: "In addition to the preliminary discussion concerning the problem of the establishment of a Meteoritic Commission of the I.M.A. I think it is appropriate to convey the following: The modern progress of science which has shown the importance of meteorites especially in our days in relation to the direct study of the Cosmos requires a considerable extension of our knowledge of meteorites from all possible points of view, and the importance of international collaboration in this aspect is obvious. For this purpose in 1948 the Permanent Commission of the International Geological Congress was organized and in 1955 a Subcommission (NO. 22-a-) on Meteorites of the International Astronomical Union was formed. The development of these organizations on Meteorites ensures international collaboration as regards conditions of meteorite fall and their substantial composition. But if the existence of the first organization entirely secures this object, the same could not be said about the second because of the large scope of the problems concerning meteoritic composition. Accordingly, I consider that it is very timely for the establishment of

a Meteoritic Commission in the International Mineralogical Association. The object of this Commission should be the organization of international collaboration on meteoritic mineralogy and the coordination of programs for both Commissions."

*D. Recommendation of the Liaison Committee on Meteorites to the I.M.A. Congress, Washington,* 1962

The Committee favors the establishment not of a Commission on Meteorites but of a Commission on Cosmic Mineralogy with a wider scope of problems the fulfilment of which will become necessary in the near future.

1. *Preamble*

For the advancement of science it is necessary to recognize a new branch in mineralogy—cosmic mineralogy. Up to now we have had the opportunity to get the information about cosmic minerals from meteorites alone. But the time approaches when investigators will have to deal directly with cosmic minerals collected from other planets. Considering the foundation of this branch of science as an important step for the future and making attempts to intensify the study of the mineralogy of meteorities already at hand, it is recommended that the I.M.A. establishes the new Commission which will have for its object the development of international collaboration in cosmic mineralogy.

2. *Name*

The Commission on Cosmic Mineralogy, I.M.A.

3. *Members*

The members of the Commission shall be specialists in cosmic minerals and in meteorite minerals in particular or specialists in methods of mineralogical study who are nominated by the Member-Societies of the I.M.A.

4. *Objects*

Increase of knowledge regarding cosmic minerals: at first—meteorite minerals and then—minerals collected on the other planets. This includes chemical composition (both elements and isotopes); crystal structure or amorphous nature; chemical and physical properties; morphology; genetic history including crystallization processes, chemical reactions of formation, and physicochemical equilibrium conditions; processes of chemical and physical alterations; absolute age of minerals; distribution and possible practical importance of cosmic minerals.

5. *Methods*

The Commission may arrange for international symposia; for exhibitions of cosmic minerals; and for programs of international cooperation in their study; it will assist in the realization of these programs; it may propogandize in scientific and popular publications the achievements of cosmic mineralogy; it will collaborate with other international organizations studying the cosmos.

Dr. Henderson then recommended the formation of a new Commission of the I.M.A. on Cosmic Mineralogy. This was moved and seconded and then opened for discussion. Dr. B. Mason stressed that the new Commission should be distinct from the already existing Commission on Meteorites of the International Union of Geological Sciences, although the two had somewhat similar goals. Prof. Fisher summarized the feeling of the Council, which agreed in general with the desirability of establishing the new Commission, and read a letter from Dr. E. L. Krinov to Prof. Grigoriev. E. P. Henderson stressed the name of Cosmic Mineralogy and E. Ingerson pointed out the need for the new Commission. The President postponed the voting on the possible creation of the Commission to the second session of the Business Meeting, but in order to avoid legal trouble in voting for its officers, suggested that candidates be nominated for Chairman and Secretary of the Commission, to be voted on in case the creation of such a Commission was approved. Dr. E. P. Henderson proposed Prof. D. P. Grigoriev as Chairman; and Professor J. L. Amorós proposed E. P. Henderson as Secretary.

## OTHER COMMITTEES

Dr. E. Wm. Heinrich reported on the work done by the Liason Committee to the Geochemical Society:

1. The Geochemical Society does not have a commission on teaching; however, it does have an education committee. Its chairman for 1961 is Kurt E. Lowe. The chairman for 1962 has not yet been appointed.

2. The Geochemical Society has a book translation program under way. These books are selected from Russian publications which are translated into English and are either published or in the process of being published. The following books will be of interest to the mineralogists:

a. *Beryllium* by A. A. Beus (1956 ed.). To be published by Freeman and Company, San Francisco. (Ed. Note: Published, August, 1962).
b. *Geochemistry of Beryllium* by A. A. Beus (1960 ed.)
c. *Types of Dolomite Rocks and their Genesis*, edited by M. N. Strakhov. To be published by the Ronald Press Company.
d. A book by N. P. Ermakov dealing with liquid inclusions and ore forming solutions.
e. "Deposits, Mineralogy, and Geochemistry of Selenium and Tellurium" by Sindeeva.
f. "Dikes and Mineralization" by Abdulaev.
g. The Geochemistry of Thallium. A short publication.
h. The Geochemistry of Gallium. Also a short publication.
i. *Rare and Dispersed Elements in Soils* by A. P. Vinogradov, available from Consultants Bureau, New York.
j. *Physical-Chemical Principles of Mineral Paragenesis* by Korzhinsky, also published by the Consultants Bureau.

3. The Standards Committee, under the chairmanship of A. A. Van Valkenburg, has been doing an outstanding job on the selection and preparation of mineral and rock standards. Its reports have been published from time to time in *The Geochemical News:* see, for example, the October 1960 number, the June 1961 number, and the forthcoming February 1962 number.

4. Since there seems to be no further need for the existence of this Committee, I request it be abolished.

As there was no opposition from the Delegates, the President declared the Committee discharged, with thanks to Dr. Heinrich.

Dr. L. G. Berry reported for the Liaison Committee to the International Union of Geological Sciences noting that friendly contact had been established.

The President pointed out that through the efforts of Professor Fritz Laves, Chairman of the Liaison Committee to the International Union of Crystallography, and himself, arrangements were being made for a joint session with the latter during its Rome meeting September 9–14, 1963 on Topic 17(2) Crystal Morphology in its relation to Crystal Structure with Professor J. D. H. Donnay as Convenor.

No report was presented by Chairman Conrad Burri of the Liaison Committee to the I.U.G.S. Committee on Petrographic Nomenclature. However, Professor Burri wrote the President July 28, 1962 stating that he had no success in trying to effect the desired liaison between the two committees, and requesting that his resignation as chairman be accepted.

Since several Commissions were holding meetings the next day, the President suggested delaying the reports of the Chairmen of the Commissions until the second session of the Business Meeting.

## OTHER MATTERS

### Changes in the Constitution

The following changes in the Constitution were moved and seconded and then adopted by the delegates:

Add to 3*b*); One of his (the Representative's) major tasks is to make sure that the members of his Society are informed about current I.M.A. affairs; this may be done through notices in his *Mineralogical Journal*, through distribution of mimeographed material to the individual members of his Society, and by announcements at the meetings of his Society.

Add to 4 A*a*): vi New Business

Art. 5b): In last line replace *or* by *and*

Art. 5c): change June 30 to read Dec. 31

Art. 5d): Change July 1 to read Jan. 1

Art. 12f): change the last half of the second sentence to read: not over four weeks after the Business Meeting. Change the final eight words to read: along with the minutes of the Business Meeting.

Art 12g): delete this.

Time Table at the end: alter this so it agrees with the above changes.

NOTE: The Constitution as adopted at the first general meeting of the I.M.A. in Zürich, September 1959, is printed with the report of that meeting on pages 104–106 of Cursillos y Conferencias Instituto Lucas Mallada, C.S.I.C. (España), Fasc. VII, 1960. Minor changes were also effected at the Copenhagen meeting (*ibid.*, Fasc. VIII, p. 173, 1960).

### New Commission

The desireability of having a Commission on Ore Microscopy was stressed by Professor E. N. Cameron. He stated that the objectives of such a Commission would be:

1. To discuss methods of standardizing quantitative techniques of ore microscopy, especially measurements of microhardness, reflectivity, and rotation properties of ore minerals.

2. To provide for the accumulation and distribution of standard data on the above and other properties of ore minerals.

His proposal for creating the new Commission was moved and seconded. In the following discussion R. M. Thompson pointed out the convenience of having a symposium on the subject rather than a new Commission. C. Guillemin expressed the thought of the French Mineralogical Society that there was no need for such a Commission as much of the work to be done is already included in the existing Commission on Mineral Data. Dr. H. Strunz, Chairman of the latter Commission was not of the same opinion. It was voted to create the new Commission (three negative votes were cast).

E. N. Cameron and W. Uytenbogaardt were proposed for Chairman of the Commission and S. H. U. Bowie as Secretary. However, Dr. E. N. Cameron refused to be a candidate.

### Next Meeting

The President told the Assembly that an invitation had been received from the Indian Mineralogical Society to hold the next meeting in Madras in 1964 in connection with the International Union of Geological Sciences. He asked Prof. P. R. J. Naidu to explain the situation. The latter described in some detail the preliminary plans for the proposed meeting to be held the first half of December 1964 in Madras; these include a six day field trip in South India. The invitation was accepted by acclamation. Professor C. E. Tilley was appointed Program Chairman for this meeting.

### Miscellaneous

There was a brief discussion of a possible field trip before the Rome meeting of the International Union of Crystallography, September 1963. President H. Winkler of the German Mineralogical Society called attention to the fact that its meeting is scheduled for Vienna in September 1963 and stated that this would be a fine opportunity for a gathering of mineralogists in advance of the Rome meeting.

The President reported on his informal canvas of mineralogists as to the possible desireability of establishing a new journal, the International Mineralogist. While there was much divergence of opinion, in general it was favored by the smaller member Societies which lacked their own journal, and was opposed by the others. While a majority of the Societies in the I.M.A. might favor the founding of such a journal, it seems clear that the opposition is strong enough so that the present time is not ripe for such a project.

Attention was called to the available publications of the I.M.A. as follows:

First meeting (Zürich)—Symposia on Twinning and on Alpine Fissure Minerals

Second Meeting (Copenhagen)—Feldspar Symposium

Third Meeting (Washington)—Three guidebooks are available. Also the World Directory of Mineralogists. See the advertisement on p. viii of the May-June 1962 number of *The American Mineralogist* (vol. 47) and on p. 325 of this volume.

## SECOND SESSION

The second session of the Business Meeting of the Delegates was held on April 20th at 4:00 P.M. at the same place. The President opened the Session by calling the roll of Delegates, after which business proceeded according to the agenda.

### REPORT BY THE AUDITORS

The auditors stated that they had examined the bank statements of the International Mineralogical Association for the period July 1, 1960 to March 30, 1962 and found them to be in agreement with the financial statement presented by the treasurer. Therefore they moved the acceptance of the Treasurer's Report as presented. The motion was seconded and accepted unanimously.

### NEW COMMISSIONS

E. P. Henderson recommended a favorable vote on the motion to establish a Commission on Cosmic Mineralogy in accordance with the report of the Liaison Committee on Meteorites of the I.M.A. as written by Prof. Grigoriev. He also recommended that the I.M.A. instruct Prof. Grigoriev to explore the possibility of holding an International Symposium on meteorites within the

immediate future. The purpose of this symposium would be to bring together representatives of all the various scientific disciplines interested in research on meteorites.

Both recommendations were moved, seconded and carried, and the Commission on Cosmic Mineralogy was established. As there were no new candidates for officers of the Commission, Prof. D. P. Grigoriev and Dr. E. P. Henderson were automatically elected as Chairman and Secretary, respectively.

Then the election of the officers of the Commission on Ore Microscopy was held. Besides W. Uytenbogaardt, Prof. P. Ramdohr was also proposed as Chairman of the new Commission. Before the voting, Prof. Ramdohr refused to be a candidate, and therefore W. Uytenbogaardt and S. H. U. Bowie were automatically elected as Chairman and Secretary respectively of the Commission on Ore Microscopy.

### COMMISSION REPORTS

The Chairmen of the five Commissions reported on the work done by their Commissions. All the reports were followed by discussion and accepted (See Reports).

### NEW BUSINESS

E. F. Osborn moved a vote of thanks to the local Committee; this was approved by acclamation.

Having no more business to transact the third Business Meeting of the Association was adjourned.

Note that a general account of the meeting including pictures of about 70 of the over 300 participants appeared in *GeoTimes* (American Geological Institute) July–August, 1962.

## REPORTS OF THE COMMISSIONS

### COMMISSION ON ABSTRACTS

PROF. M. FORNASERI, *Chairman*

The work of this commission up to the time of the Copenhagen meeting (August 1960) is described in the report on that meeting; this includes a Draft Plan worked out by a sub-committee of the Commission.

The Abstracts Commission held a meeting on August 20, 1960 at Copenhagen where the organization of an International Abstracting Journal as well as the Draft Plan proposed by the Subcommittee were again examined. After discussion the members present voted eight in favor and one against acceptance of the Draft Plan. The result of this voting was rather embarrassing since the lack of unanimity makes any further development of the Draft Plan very difficult if not impossible.

At the following general meeting of the I.M.A. on Aug. 24, 1960 new officers of the Abstracts Commission were elected and a second meeting of all available members of the Commission was held. After a careful re-examination of the Draft Plan it was decided that it would serve for the future organization of Abstracts on an International basis but that it would probably be too difficult, particularly for financial reasons, to start with it in the immediate future.

Furthermore, although the Chairman of the earlier Commission Prof. E. Onorato, clearly stated that the new project must be careful not to destroy any good established organization, the delegates felt there was no such danger. In the following discussion the Commission was informed unofficially that several National Societies are taking steps to start direct cooperation with the publication, *Mineralogical Abstracts*. In this situation it appeared that the best way to overcome all present difficulties would be just to follow this procedure and to stimulate direct contacts between the National Societies and the Anglo-American organization. Therefore all present members agreed that, after approval of their own councils the British and American Societies will circulate to all National Societies a formal invitation to cooperate with *Mineralogical Abstracts*. Should the procedure be successful, the existing *Mineralogical Abstracts* would gradually evolve into an international journal without any change of structure and ownership at first. On the other hand the whole operation might eventually be taken over by the International Mineralogical Association after enough National Societies become part-owners through private arrangements.

Following the suggestion formulated at the meeting of Aug. 24th the Councils of the Mineralogical Society of America and of the Mineralogical Society of Great Britain approved the following statement:

"During the Copenhagen meeting of the International Mineralogical Association the new Commission on Abstracts discussed the organization of a comprehensive journal of mineralogical abstracts.

"The most promising plan envisages the extension of *Mineralogical Abstracts*, at present owned jointly by the Mineralogical Society of Great Britain and the Mineralogical Society of America. With the approval of the Councils of both these Societies, the Commission is sending this letter to all known national mineralogical societies in an effort to obtain their cooperation.

"I. *Mineralogical Abstracts* could be readily enlarged if more abstracts covering different countries were available. Regional or national societies can secure for all their members a 50% reduction in the cost of *Mineralogical Abstracts* by agreeing to contribute free of charge English abstracts comprising a comprehensive coverage of papers appearing in their region; they need undertake no other responsibility. Members of such societies would pay $4.50 (U.S.) for a personal annual subscription. National mineralogical societies in Canada, Japan, Norway, and Switzerland are already partaking in this scheme.

"II. The question of a wider ownership of *Mineralogical Abstracts* is being considered, but the British and American Societies feel that it would be premature to extend ownership prior to 1963. They feel that more experience with the present financial arrangement would be essential to devise an equitable scheme. Both the British and American Societies put up appreciable capital sums in order to start *Mineralogical Abstracts* (as from vol. 14); moreover they have agreed to stand losses that *Mineralogical Abstracts* might incur. Members of the British Society pay an annual subscription of the equivalent of $3.00 for *Mineralogical Abstracts* and this is included in their subscription on the *Mineralogical Magazine*, *i.e.*, they cannot contract out of buying *Mineralogical Abstracts*. Members of the American Society can purchase *Mineralogical Abstracts* for $3.00 which may be included in their dues at their discretion. The subscription appropriate to wider ownership would depend considerably on the number of participating countries."

The above statement has to be interpreted as a formal invitation to all Mineralogical Societies to contribute to the *Mineralogical Abstracts*. This document has been circulated by the Abstracts Commission to all members of the Commission and all

National Delegates in order to be submitted for discussion to the Councils of each National Society.

The Commission on Abstracts held meetings in Washington on April 17, 18, and 19, 1962 and noticed with satisfaction that following the invitation of the British and American Mineralogical Societies, the Mineralogical Societies of Austria, Bulgaria, Germany, and Italy decided to cooperate with Mineralogical Abstracts. The same is likely to be true for the Netherlands. Belgium, Canada, Denmark, Finland, New Zealand, Norway, Spain and Switzerland confirmed their cooperation and Australia, Czechoslovakia, Egypt, India, Israel, Japan, Pakistan, South Africa and Sweden are already listed as contributors to the "Mineralogical Abstracts." More recently mineralogists in Mexico, Brazil and Argentina have agreed to assist by abstracting literature published in their countries.

As the result of the work of the Commission on Abstracts during the Washington meeting, the Commission submitted to the General Assembly of the I.M.A. the following proposal.

"There is a definite feeling among the members of the Commission that in the years to come an International Abstracting Journal should be established and that *Mineralogical Abstracts* might well become the nucleus of such an International Journal. At present the Commission proposes to the Council of I.M.A. to request *Mineralogical Abstracts* to print the names of all the National Mineralogical Societies that cooperate in Abstracting. This, we feel, would indicate the international scope of Abstracting."

This proposal was accepted by the delegates of all the countries present at the meeting of the Commission on Abstracts, with the exception of France and the U.S.S.R.

## COMMISSION ON MINERAL DATA

Dr. H. Strunz, *Chairman*

Mineralogy is the Science of Crystals-minerals-rocks. In this widespread field the Mineral Data Commission first had to approve and recommend on an internationally acceptable basis a Crystallographic Nomenclature and a Mineralogical Classification. Furthermore it was necessary to find a way to present the known mineral data either in the form of a book or a punch card file or a Wyckoff loose leaf system, etc. Finally, every two years, we will try to classify the new minerals and collect their data, as far as these minerals are accepted by the Commission on New Minerals and Mineral Names.

### Crystallographic nomenclature

(Full publication in *Cursillos y Conferencias, "Lucas Mallada," Madrid.* VIII, 176–181, 1961.)

*Cell dimensions* $a_0$, $b_0$, $c_0$ (in metric Å; 1 Å=1 kX:1.002; "Internationale Tabellen zur Kristallstrukturbestimmung" (1936) give kX, and all up to about 1945 published "Å"-values are to be multiplied by 1.002); $a_0:b_0:c_0$, axial ratio derived from cell dimensions; a:b:c, derived from morphological measurements; $\alpha$, $\beta$, $\gamma$, interaxial angles.

*Orientation* 1) *Triclinic:* reduced cell (shortest three translations) with $c_0<a_0<b_0$; with $\alpha$ and $\beta$ obtuse (stumpf), $\gamma$ cannot be chosen obtuse or acute at will, its character follows from the preceding conditions (see exceptions below); *Monoclinic:* shortest two translations in plane (010), $c_0<a_0$ (see exceptions), $\beta$ obtuse (stumpf); *Orthorhombic:* axes along symmetry directions, with $c_0<a_0<b_0$ (see exceptions); *Tetragonal:* smallest cell; *Hexagonal-P:* smallest hexagonal cell; *Hexagonal-R:* smallest hexagonal cell with extra nodes at $\frac{1}{3}\frac{2}{3}\frac{1}{3}$ and $\frac{2}{3}\frac{1}{3}\frac{2}{3}$; *Cubic:* no recommendations necessary.—2) *Exceptions:* For one-face-centered translation lattices a C-face centered orientation is to be prefered (*C2/m*, not *A2/m*, not *I2/m; Cmmm*, not *Ammm*, not *Bmmm;* etc.).—3) *Further Exceptions* from these rules shall be allowed: (1) in such well established families as the mica family, (2) in order to show the close relationship of a given mineral to other minerals, and (3) for species with a higher pseudosymmetry.

*Symmetry.* To avoid confusion of "rhombisch" and "rhomboedrisch" the first one is named "orthorhombisch" (orthorhombic), so we have the orthorhombic system with the classes "rhombic-disphenoidal," "rhombic-pyramidal" and "rhombic-dipyramidal." The cubic classes are named: "tetartoidal" (tetartoidisch), "gyroidal" (gyroidisch), "disdodecahedral" (disdodekaedrisch), "hextetrahedral" (hex'tetraedrisch) and "hexoctahedral" (hex'-oktaedrisch).

In *"Internationale Tabellen zur Kristallstrukturbestimmung"* (1936) and *"International Tables for X-ray Crystallography"* (1952) the meaning of the old morphological symbol ⏢ unfortunately was changed; since it now has two meanings, it should be dropped; IMA recommends Figs. 1 and 2 to the IUC.

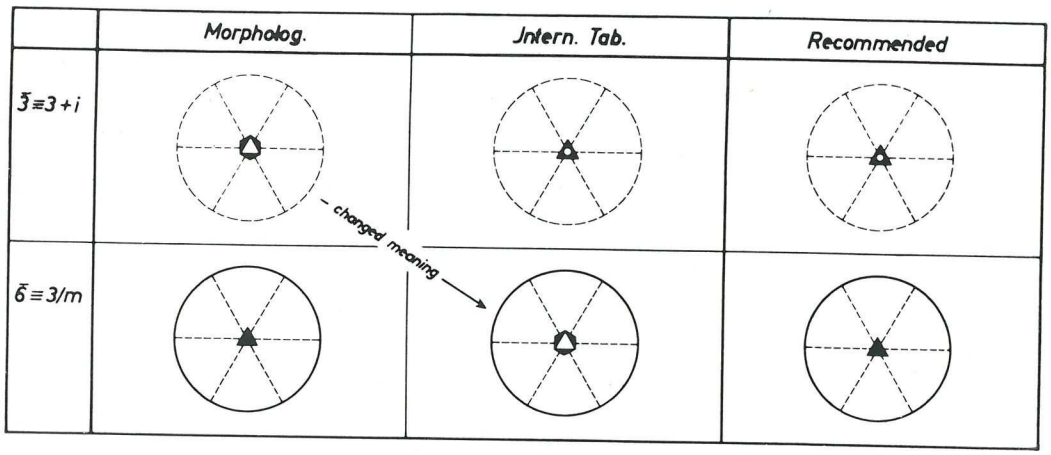


Fig. 1

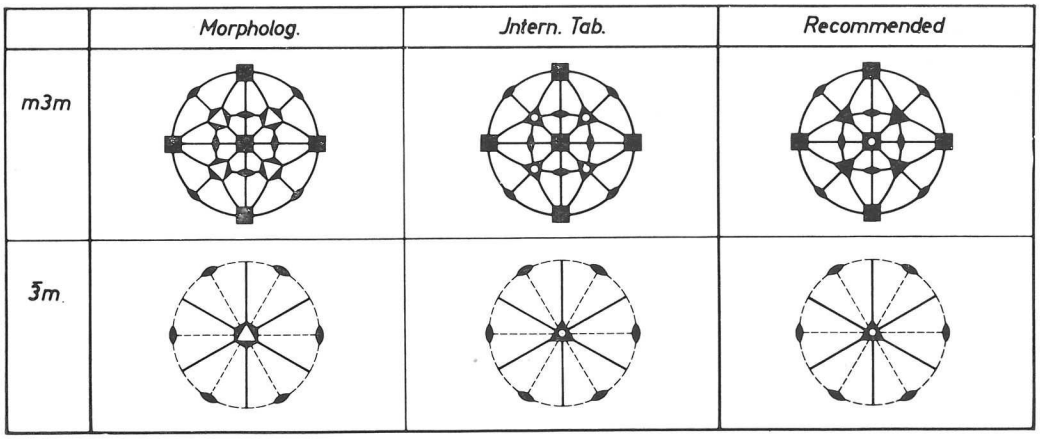


FIG. 2

*Chemical formulae.* As in malachite $Cu_2[(OH)_2|CO_3]$, dolerophanite $Cu_2[O|SO_4]$, apatite $Ca_5[(OH, F, Cl)|(PO_4)_3]$, titanite $CaTi[O|SiO_4]$ etc. the oxygen of the complex groups is partially bound to C, S, P, Si and partially to the cations Cu, Ca etc., where the adjacent O, OH, F, Cl are only bound to the cations, the latter O, OH etc. should be written *before* the complexes, as done above. For vacant sites a square, □, should be used, for instance for coffinite $U[(SiO_4)_{1-x}, (□(OH)_4)_x]$. Concerning H, OH, $H_2O$ in the formulae, sepiolite $(Mg, Fe)_3Mg[(OH)_2|Si_6O_{15}]\cdot 2H_2O+4H_2O$ may be chosen as the prototype, where OH means hydroxyl water (800° C.), $\cdot 2H_2O$ means coordination water (450° C.) and $+4H_2O$ means zeolitic water (250° C.); in opal $SiO_2+n$ aqu. we have absorption water.—Sequence of cations according to decreasing ionic radii; in diadochic substitution according to abundance.

### MINERALOGICAL CLASSIFICATION

(Open for further discussion). There are nine classes, I. Elements (A. Metals, B. Semimetals and Nonmetals), II. Sulfides, III. Halogenides, IV. Oxides etc. (the oxides come after the halogenides, so leading over to the complex oxides). II, III and IV are divided by decreasing formulae factor and subdivided by increasing radii of the cations or increasing coordination number. Class V contains all the complex oxides with planar complexes $NO_3$, $CO_3$, $BO_3$, where the borates already show partial tetrahedral $BO_4$-complexes and condensed ($BO_3$–, $BO_4$–) complexes similar to the silicates. VI. Sulfates (selenates, tellurates, chromates, molybdates, wolframates), VII. Phosphates (arsenates, vanadates) and VIII. Silicates have tetrahedral complexes $RO_4$. V, VI, VII have the Divisions A. Simple compounds, B. With mixed anions, C. Simple compounds with water, D. With mixed anions and water; the nitrates and borates are excluded as V.A′ and V.E, F, G. The silicates have the known Divisions VIII.A. Nesosilicates, VIII.B. Sorosilicates, VIII.C. Cyclosilicates etc.—IX.A. contains the salts of organic acids, IX.B. the Hydrocarbons, IX.C. the Resins and other organic compounds (Table 1.)

### MINERAL DATA

The suggestion of the Mineral Data Commission (made in Washington 1962) was to consider the form of a possible publication of "Mineral Data"—either a book or a punch card file or the Wyckoff loose leaf system etc.—; this should be discussed by the members and representatives of the national societies with their colleagues in their countries and recommendations should be made at the meeting in Madras, India, in 1964.

### CLASSIFICATION OF NEW MINERALS

The Mineral Data Commission collected new mineral data from 1957 till 1961. This was reduced to a brief form, and published in a 29 page mimeographed manuscript, and distributed to the members and representatives of the national societies at the meeting in Washington 1962. Absent members got their copies by mail. The chairman of the Commission on New Minerals and Mineral Names was consulted. The members and representatives were requested to send in comments to these data, with corrections and additions, before July 31, 1962. In the future a publication every two years is intended, the next at the Madras Meeting 1964.

## MUSEUMS COMMISSION

The chairman of this commission, Professor C. Frondel, submitted no written report, but it is known that plans for publishing a list of museums are being matured. The compilation of a list of type specimens is also being actively pushed.

## COMMISSION ON NEW MINERALS AND MINERAL NAMES

DR. MICHAEL FLEISCHER, *Chairman*

The aim of the Commission is to act as a central group to coordinate the study of problems of mineralogical nomenclature, to call attention to problems whose resolution would aid the science, and to initiate discussions leading to as much uniformity in nomenclature as possible.

The discussions held at Copenhagen in 1960 have been published in *Bull. Soc. Franc. Mineral. Crist.*, **84**, 96–105, 1961, in particular a report by F. Permingeat (p. 98–104) on what should be given in the description of a new mineral. It is to be hoped that this will be read and re-read by mineralogists the world over.

Specific actions taken by the Commission include the following:

### REVIEW OF PROPOSED CHANGES IN NOMENCLATURE BEFORE PUBLICATION

The Commission has undertaken to distribute to its members summaries of data on which new names or changes in old ones are based. The members are allowed 45 days to record their votes.

TABLE 1. MINERALOGICAL CLASSIFICATION

| Classes I–IX | Divisions A, B, C etc. | | | | | | | | |
|---|---|---|---|---|---|---|---|---|---|
| I. Elements | A. Metals Cu, Ag, Au . . . | | B. Semimetals and Nonmetals As, Sb, Bi; C, S | | | | | | |
| | M:N ⩾ 2 | <2>1 | 1 | <1>½ | ½ | <½ | With $H_2O$, OH | Complex Compounds | |
| II. Sulfides (Selenides, Arsenides . . . ) | A. $Ni_3Pb_2S_2$, $Cu_2S$, $Ag_2S$ | B. $Ni_3S_2$, $Cu_3Se_2$ | C. ZnS, PbS | D. $Co_3S_4$, $Sb_2S_3$ | E. $FeS_2$, FeAsS | F. $CoAs_3$, $VS_4$ | ——— | G. $5Ag_2S \cdot Sb_2S_3$, $5PbS \cdot 2Sb_2S_3$ | ——— |
| III. Halogenides | ——— | ——— | A. NaCl, KCl | ——— | B. $MgF_2$, $CaF_2$ | C. $FeCl_3$ | D. $MgCl_2 \cdot 6H_2O$ $AlF_3 \cdot H_2O$ | E. $Na_3[AlF_6]$, $K_3Na[FeCl_6]$ | F. Oxihalogenides |
| IV. Oxides | A. $Cu_2O$ | ——— | B. BeO, MgO | C. $Fe_3O_4$, $Fe_2O_3$ | D. $SiO_2$, $TiO_2$ | E. $V_2O_5$, $MoO_3$ | F. $Mg(OH)_2$, FeOOH, $Al(OH)_3$ | G. Arsenites, Selenites, Iodates (and V–VIII) | ——— |
| | A′ | A. Simple Compounds | B. With mixed anions | C. Simple Compounds with $H_2O$ | D. With mixed anions and $H_2O$ | | E. F. G. | | |
| V. Carbonates (Nitrates, Borates) | Nitrates | $MgCO_3$ | $Cu_3[OH \mid CO_3]_2$ | $MgCO_3 \cdot 3H_2O$ | $Mg_3[(OH)_2 \mid CO_3] \cdot 3H_2O$ | | Borates | | |
| VI. Sulfates (Selenates, Tellurates, Chromates, Molybdates, Wolframates) | ——— | $CuSo_4$ | $Cu_2[O \mid SO_4]$ | $CuSO_4 \cdot 5H_2O$ | $Cu_4[(OH)]_6 \mid SO_4] \cdot H_2O$ | | ——— | | |
| VII. Phosphates (Arsenates, Vanadates) | ——— | $LiFePO_4$ | $Mn_2[OH \mid PO_4]$ | $Fe_3[PO_4]_2 \cdot 8H_2O$ | $Cu_2[OH \mid PO_4] \cdot H_2O$ | | ——— | | |
| VIII. Silicates | A. Neosilicates<br>A′. Neso-Subsilicates | B. Sorosilicates | C. Cyclosilicates | D. Inosilicates | E. Phyllosilicates | F. Tectosilicates | | | |
| IX. Organic Compounds | A. Salts of organic acids | B. Hydrocarbons | C. Resins and other organic compounds | | | | | | |

New names or changes approved will carry the designation, "Name approved by the Commission on New Minerals and Mineral Names, I.M.A." The first such name, roquesite, was approved in June, 1962. The Mineralogical Society of Great Britain has voted that all such proposals will be submitted to the Commission in the future.

### Annual Review of New Names and Changes in Nomenclature

The Commission voted in 1960 to prepare annually a summary of new names and changes in nomenclature and to vote approval or disapproval. Lists for 1959 and 1960 have been voted on and the results sent to the members; it is hoped that these will be published in the journals of the member societies and will have the effect of discouraging the proposal of names based on inadequate data.

In these two years 97 new names were considered; 53 were accepted by more than 60% of those voting (29 unanimously), 36 were rejected by more than 60% of those voting (13 unanimously), and opinion was sharply divided on 8. Some of these were rejected because of inadequate data; these will be reconsidered when more data are published.

### Uniformity in Mineral Names

The use of different names for the same mineral causes confusion and difficulty in indexing. The Commission has tried to bring about some measure of agreement and, with considerable tolerance and good will displayed, has been able to reach agreement on some. The following have been unanimously agreed to:

Analcime, not analcite
Anatase, not octahedrite
Bornite, not erubescite
Devilline, not devillite or herrengrundite
Digenite, not neodigenite
Feldspar or Feldspath, not felspar
Grossular, not grossularite
Hematite, not oligiste
Hemimorphite, not calamine
Magnesite, not giobertite
Nontronite, not chloropal
Piemontite, not piedmontite
Rutherfordine, not rutherdordite
Spessartine, not spessartite
Spodumene, not triphane
Tenorite, not melaconite
Tetrahedrite, not fahlerz, fahlore, or panabase
Torbernite, not chalcolite
Valentinite, not exitele
Wernerite for the species, Scapolite to be a group name.

The Commission recommends by large majorities:

Arsenopyrite, rather than mispickel
Bromargyrite rather than bromyrite
Chlorargyrite rather than cerargyrite
Gibbsite rather than hydrargillite
Iodargyrite rather than iodyrite
Natron rather than soda
Orthoclase rather than orthose
Rhodochrosite rather than dialogite
Siderite rather than chalybite or siderose
Sphalerite rather than blende
Spherocobaltite rather than cobaltocalcite
Stilbite rather than desmine
Szaibelyite rather than ascharite

It is hoped that mineralogists will abide by these recommendations.

The names wollastonite (low-temperature form) and pseudowollastonite (high-temperature form) were agreed upon, and it was recommended that parawollastonite be dropped. The use of suffixes (−Tc, −2M, etc.) was recommended to distinguish stacking polymorphs of $CaSiO_3$.

No agreement could be reached for many pairs of names, including allanite-orthite, idocrase-vesuvian-vesuvianite, kyanite-cyanite-disthene, sphene-titanite, stibnite-stibine-antimonite, and others. Discussion of these will be continued in the future.

In addition, the Commission has discussed, *What is a Mineral?*, with no clear agreement evident on any definition. It has also tried to encourage attempts at systematizing the nomenclature of the clay minerals and the feldspars, both now badly confused, and hopes that the future will bring some improvement. A proposal for rationalizing the nomenclature of rare-earth minerals is now under consideration.

It is evident that much remains to be done and that we need the good will and help of all mineralogists. We hope that they will continue to make suggestions and comments on our work.

### COMMISSION ON TEACHING

Neither the Chairman, Professor J. Orcel, nor the Secretary, Professor H. J. deWijs, was able to attend the Washington meeting of this commission which was newly formed in Copenhagen in August, 1960. When the group of ten commission members gathered at Washington on April 17 were informed by Professor Hocart that the officers would not be present, and that no agenda had been prepared, Professor C. S. Hurlbut, Jr. was requested to serve as acting chairman and Professor D. H. Gorman as acting secretary. After some discussion those present agreed to limit their remarks to the questions dealing with the teaching of the beginning mineralogy course, but later they also discussed the domain of modern mineralogy. The commission members were urged to develop these ideas further before the Madras meeting; also to give particular attention to the question of desireable teaching aids.

## INTERNATIONAL MINERALOGICAL ASSOCIATION

REPRESENTATIVES OF THE MEMBER NATIONAL MINERALOGICAL SOCIETIES

Austria: Dr. Alfred Schiener, Vienna
Belgium: Dr. R. Van Tassel, Brussels
Bulgaria: Prof. Ivan Kostov, Sofia
Canada: Prof. L. G. Berry, Kingston
Czechoslovakia: Prof. J. Sekanina, Brno
Denmark: Dr. Hans Clausen, Copenhagen
Egypt: Dr. E. M. El Shazly, Cairo
Finland: Prof. Th. G. Sahama, Helsinki
France: Dr. C. Guillemin, Paris
Germany: Prof. W. von Engelhardt, Tübingen
India: Mr. K. Rajagopalaswamy, Bombay
Italy: Prof. M. Fenoglio, Turin
Japan: Prof. N. Katayama, Tokyo
Netherlands: Prof. H. J. deWijs, Delft
New Zealand: Prof. D. S. Coombs, Dunedin
Norway: Dr. Henrich Neumann, Oslo
Spain: Prof. M. Font-Altaba, Barcelona
Sweden: Prof. Otto Mellis, Stockholm
Switzerland: Prof. E. Wenk, Basel
United Kingdom: Dr. J. R. Butler, London
U.S.A.: Dr. E. F. Osborn, University Park, Pa.
U.S.S.R.: Dr. G. P. Barsanov, Moscow

## AVAILABLE PUBLICATIONS OF THE INTERNATIONAL MINERALOGICAL ASSOCIATION

| | | |
|---|---|---|
| 1959 | First General Meeting, Zürich<br>Symposia on Twinning and Alpine Fissure Minerals | $2.00 |
| 1960 | Second General Meeting, Copenhagen<br>Symposium on Feldspars | 2.00 |
| 1962 | Third General Meeting, Washington<br>Northern Field Trip Guidebook | 1.00 |
| | Southern Field Trip Guidebook | 1.00 |
| | Visitor's Guide to the Geology of the National Capital Area | 0.75 |
| 1962 | World Directory of Mineralogists | 1.50 |
| 1963 | Third General Meeting, Papers and Proceedings, Mineral. Soc. Am. Spec. Paper 1 (this volume) | |

The *World Directory of Mineralogists*, compiled by Prof. M. Font-Altaba, Mineralogy Department, University of Barcelona, is a 156-page octavo volume prepared from typewritten copy with paper covers. It lists more than 4000 individuals specializing in the mineralogical sciences from over 50 countries. It supplies much useful information, such as year of birth, title, highest degree (with field of specialization), conferring institution and date, present position, address, telephone number (including extension), and a listing of areas of major scientific interest. Mineralogists are urged to order a copy for their individual use. **Such support is necessary if the I.M.A. is to publish a revised directory every few years.**

Send orders, with remittances, to

Mineralogical Society of America
Marjorie Hooker, Treasurer
U. S. Geological Survey
Washington 25, D. C.

Orders will be shipped postpaid.

# INDEX

The names of **authors** of complete articles are set in **bold-face type.**


Accurate determination of olivine composition using standard small-diameter x-ray powder cameras (Jambor, J. L., and Smith, Charles H. )(abs.) ..... 310
Adcumulus growth ..... 1, 2
Adler, H. (discussion) ..... 302
Agpaitic magma ..... 17
Alaska, ultramafic complex, Duke Island ..... 36
Albite-diopside-anorthite system ..... 204
Alpine peridotite-gabbro complexes ..... 55
Amorós, J. L., Business meeting of I.M.A. ..... 315
Amphiboles ..... 121
——— Optical properties ..... 121
——— (Clino) regression series ..... 267
**Amstutz, G. C.,** with **El Baz, Farouk,** A statistical study of bravoite zoning ..... 190
Analcime group ..... 282
Anorthite-diopside-albite system ..... 204
Antarctica, Ferrar dolerites ..... 124
Antimony trisulfide, properties of ..... 144
Apatite, chemical analyses ..... 223
Appleman, D. E., with Wones, D. R., Iron-feldspar polymorphs in the system $K_2O$-FeO-$Fe_2O_3$-$SiO_2$-$H_2O$ (abs.) ..... 314
Australia
——— Broken Hill, Nairne, pyrite deposit ..... 177
——— (western) sapphirine plus granulite (abs.) ..... 313

**Barton, Paul B., Jr., Bethke, Philip M.,** and **Toulmin, Priestley, 3rd,** Equilibrium in ore deposits ..... 171
Barton, Paul B., Jr., with Toulmin, Priestley, 3rd, Thermodynamic study of pyrrhotite and pyrite (abs.) ..... 198
Basaltic magmas and pyroxenes as illustrated on the diopside-olivine-silica diagram, trends and affinities of ..... 227
Basalts, primary ..... 210
Basaltic suites, averaged chemical compositions ..... 235, 236
Basic potassic rocks, chemical analyses ..... 255
Baumhauerite, $Pb_5As_9S_{18}$, crystal structure of ..... 149
Berry, L. G., Treasurer's report—I.M.A. ..... 316
**Bethke, Philip M.,** with **Barton, Paul B., Jr.** and **Toulmin, Priestley, 3rd,** Equilibrium in ore deposits 171
Bikitaite ..... 287
Binn, sulfides of lead and arsenic ..... 149
Black Jack sill, pyroxenes ..... 242
Bornite
——— on the transition of ..... 153
——— transformations in ..... 145
Bravoite zoning, a statistical study of ..... 190
Brazil, Morro Velho ..... 158
Brett, P. R., discussion on chalcocite ..... 170
**Buerger, M. J.,** with **Prewitt, C. T.,** Comparison of the crystal structure of wollastonite and pectolite ..... 293
**Buerger, M. J.,** with **Wuensch, Bernhardt, J.,** The crystal structure of chalcocite, $Cu_2S$ ..... 164
Bushveld, structure in eastern complex ..... 93

**Caillère, S.** and **Kraut, F.** Sur les constituants phosphatés des minerais de fer oolithiques de France ..... 223
**Cameron, Eugene N.,** Structure and rock sequences of the critical zone of the eastern Bushveld Complex. 93
Canada
——— Coppermine River area ..... 30
——— Northwest Territories (Muskox) ..... 30
Cell parameters of orthopyroxenes **(Howie, R. A.)** ..... 213
Chabazite group ..... 283
Chalcocite, the crystal structure of ..... 164
Chalcopyrite, diffusion in ..... 146
Chemical analyses, minerals
——— Leucite ..... 255
——— Nepheline ..... 255
——— Orthopyroxenes ..... 215–219
——— Pseudoleucite ..... 255
Chemical analyses, rocks
——— Chilled phases of layered intrusions, Muskox, Skaergaard, Stillwater ..... 33
——— Ferrar dolerites ..... 127, 129
——— Garnetiferous rocks (Sittampundi) ..... 122
——— Noritic anorthosites (Sierra Nevada) ..... 63
——— Picrite-anorthositic gabbro sheet (Nevada) ..... 72
——— Ultramafic rock (Duke Island) ..... 45
Chromite composition (Stillwater Complex) ..... 46
Clinoamphibole regression studies **(Winchell, Horace)** .. 267
Clinopyroxenes
——— Chemical composition ..... 42
——— Optical Properties ..... 39, 41, 130
Coexisting pyroxenes, gabbro, Duke Island ..... 38
Colorado, Creede ..... 178, 180–181, 183
Commission reports, I.M.A. ..... 320
Committee reports, I.M.A. ..... 317
Comparison of the crystal structures of wollastonite and pectolite (**Prewitt, C. T.,** and **Buerger, M. J.**) ..... 293
Composition of quartz-forming fluids in nature (Roedder, E.) (abs.) ..... 312
Concretions, phosphate ..... 223
Connecticut, Bristol ..... 166
Contrasted styles of igneous layering in the Gardar Province of south Greenland (**Ferguson, J.,** and **Pulvertaft, T. C. R.**) ..... 10
Contribution to the study of the fluorite deposit "Mina Berta" in San Cugat del Valles (Barcelona, Spain) **(Pous, J. Montoriol, San Miguel, A.,** and **Font-Altaba, M.)** ..... 278
Convective circulation ..... 5, 41
**Coombs, D. S.,** Trends and affinities of basaltic magmas and pyroxenes as illustrated on the diopside-olivine-silica diagram ..... 227
Coppermine River area, Canada ..... 30
Critical zone, eastern Bushveld Complex ..... 93
Cryptic layering ..... 45, 110, 126
Crystal structure.
——— of chalcocite, $Cu_2S$ **(Wuensch, B. J.,** and **Buerger, M. J.)** ..... 164
——— dachiardite **(Gottardi, G.,** and **Meier, W. M.)** ... 291
——— metatorbernites (Ross, M., and Evans, H. T., Jr.) (abs.) ..... 313
——— pectolite ..... 293
——— pseudomalachite (Ghose, Subrata) (abs.) ..... 310
——— wollastonite ..... 293

Crystal surfaces, studies of ..... 258
Crystallization of leucite-nepheline-sanidine in basic differentiates from a periodtite-dunite mass in Salem, Madras State, India **(Naidu, P. R. J.)** ..... 251

Dachiardite, crystal structure of ..... 291
Defects, in crystals ..... 136
Deicha, G., Discussion on sulfide equilibrium ..... 185
**Dent Glasser, L. S., Glasser, F. P.,** and **Taylor, H. F. W.,** The role of oriented transformations in mineralogy 200
Diffusion, in chalcopyrite ..... 146
Digenite ..... 164
Diopside-anorthite-albite, effects of the change in slope occurring on liquidus and solidus paths in the system 204
Diopside-olivine-silica diagram, trends and affinities of basaltic magnas and pyroxenes as illustrated on 227
Diopsides, chromian, norms ..... 244
Dolerites (Antarctica) ..... 124
Donnay, J. D. H. (discussion)
——— on pyrrhotite ..... 163
——— on wollastonite and pectolite ..... 302
Duke Island, southeastern Alaska ..... 36

Effects of the changes in slope occurring on liquidus and solidus paths in the system diopside-anorthite-albite **(Wyllie, Peter J.)** ..... 204
**El Baz, Farouk,** and **Amstutz, G. C.,** A statistical study of bravoite zoning ..... 190
Electrical properties, in sulfides ..... 139
**Emeleus, C. H.,** Structural and petrographic observations on layered granites from southern Greenland 22
Equilibrium in ore deposits **(Barton, Paul B., Jr., Bethke, Philip M.,** and **Toulmin, Priestley, 3rd,)** ..... 171
Étude structurale de quelques sulfures de plomb et d' arsenic naturels du gisement de Binn **(Le Bihan, M.-Th.)** ..... 149
Evans, H. T., with Ross, M., The crystal structures and crystal chemistry of various members of the metatorbernite group (abs.) ..... 313
Extra-extinctions, systematic, interpretation of ..... 303, 304

Fault, stacking
——— in hematite ..... 262
—— in silicon carbide ..... 262
Feldspar, iron, polymorphs in the system $K_2O$-FeO-$Fe_2O_3$-$SiO_2$-$H_2O$ (abs.) ..... 314
**Ferguson, J.,** and **Pulvertaft, T. C. R.,** Contrasted styles of igneous layering in the Gardar Province of South Greenland ..... 10
Fer oolithiques de France, sur les constituants phosphatés des minerais de ..... 223
Ferrar dolerites (Antarctica) ..... 124
Fisher, D. J., President's report, I.M.A. ..... 315
Flow layering in alpine peridotite-gabbro complexes **(Thayer, T. P.)** ..... 55
Fluorite deposit "Mina Berta" in San Cugat Del Valles (Barcelona, Spain) ..... 278
Fluorite, spectroscopic analysis ..... 279
**Font-Altaba, M.,** with **Pous, J. Montoriol,** and **San Miguel, A.,** Contributions to the study of the fluorite deposit "Mina Berta" in San Cugat Del Valles (Barcelona, Spain) ..... 278
**Font-Altaba, M.,** A study of distorted pyrite crystals from Spain ..... 186
France, phosphates in iron oolites ..... 223

Galena, semiconducting properties of ..... 135
Garbh Eilean sill, pyroxenes ..... 242
Gardar Province, south Greenland ..... 10
Ghose, S., The crystal structure of pseudomalachite (abs.) ..... 310
**Glasser, F. P.,** with **Dent Glasser, L. S.,** and **Taylor, H. F. W.,** The role of oriented transformations in mineralogy ..... 200
**Gottardi, G.,** and **Meier, W. M.,** The crystal structure of dachiardite ..... 291
Granulite terrain, sapphirine in (abs.) ..... 313
Greenland
——— Central complex of Tugtutôq ..... 11
——— Eqadloqarfia dike ..... 12
——— Gardar Province ..... 10
——— Grønnedal-Ika Complex ..... 11
——— Igaliko batholith ..... 11
——— Ilimaussaq intrusion ..... 11
——— Klokken intrusion ..... 11
——— Kûngnât Complex ..... 11
——— Narssaq intrusion ..... 11
——— Nunarssuit Complex ..... 11
——— Puklen intrusion ..... 11
——— Skaergaard intrusion ..... 1
——— Tigssaluk Complex ..... 22
Growth spirals in crystals ..... 259
**Gunn, Bernard M.,** Layered intrusions in the Ferrar dolerites, Antarctica ..... 124

Haplo—magmas
——— basaltic ..... 207
——— diortic ..... 207
——— granitic ..... 207
Harrisitic textures ..... 4
Hawaii, pyroxene norms ..... 243
Hematite twinning ..... 262
Hodkinson, J. R., Light extinction and scattering by suspension of finely-divided minerals (abs.) ..... 310
**Howie, R. A.,** Cell parameters of orthopyroxenes ..... 213
Hunter, H. E., Layered basic intrusive rocks of the Wichita Mountains, southwest Oklahoma (abs.) ..... 134
Hybridization ..... 210

Igneous rock series, liquidus slopes for ..... 208
India, Madras State
——— Salem, leucite-nepheline-sanidine in basic differentiates ..... 251
——— Sittampundi, layered complex ..... 116
Infrared study of sulfate minerals (Omori, K. and Kerr, P. F.) (abs.) ..... 311
Intercumulus liquid ..... 1
Interference microscope, study of translucent tiny grains using (abs.) ..... 311
Internal structure of a differentiated teschenite intrusion, Prospect Hill, New South Wales (Wilshire, H. G.) (abs.) ..... 134
International Mineralogical Association
——— Changes in the Constitution ..... 319
——— Commission reports ..... 320
——— Committee reports ..... 317
——— Proceedings ..... 315
——— Publications ..... 325
——— Representatives ..... 325

Interpretation of systematic extra-extinctions **(Morimoto, N., Marumo, F.,** and **Sadanaga, R.)** ..... 303
Iron-feldspar polymorphs in the system $K_2O$-FeO-$Fe_2O_3$-$SiO_2$-$H_2O$ (Wones, D. R., and Appleman, D. E.) (abs.) ..... 314
**Irvine, T. N.,** Origin of the ultramafic complex at Duke Island, southeastern Alaska ..... 36
Isotope mineralogy of sulfides (Jensen, M. L.) (abs.) ... 198

**Jackson, Everett D.,** Stratigraphic and lateral variation of chromite composition in the Stillwater Complex. 46
**Jahns, Richard H.,** and **Tuttle, O. Frank,** Layered pegmatite-aplite intrusives ..... 78
Jambor, J. L., and Smith, C. H., Accurate determination of olivine composition using standard small-diameter x-ray powder cameras (abs.) ..... 310
Japan,
——— hematite growth layers ..... 263, 264
——— pyroxene norms ..... 243
Jensen, Mead Leroy, Sulfur isotope mineralogy of sulfides (abs.) ..... 198

Kakortokite, South Greenland ..... 16
Kapalagulu layered intrusion of Western Tanganyika **(Wadsworth, W. J.)** ..... 108
**Kapp, H. E.,** with **Smith, C. H.,** The Muskox intrusion, a recently discovered intrusion in the Coppermine River area, Northwest Territories, Canada ..... 30
Kerr, P. F., with Omori, K., Infrared study of sulfate minerals (abs.) ..... 311
**Kraut, F.,** with **Caillère, S.,** Sur les constituants phosphatés des minerais de fer colithiques de France... 223

Layered
——— basic intrusive rocks of the Wichita Mts., southwest Oklahoma (Hunter, H. E.) (abs.) ..... 134
——— complex in Sittampundi, Madras State, India **(Naidu, P. R. J.)** ..... 116
——— granites, southern Greenland ..... 22
——— intrusions in the Ferrar dolerites, Antarctica **(Gunn, Bernard M.)** ..... 124
——— pegmatite-aplite intrusives **(Jahns, Richard H.** and **Tuttle, O. Frank)** ..... 78
——— picrite-anorthositic gabbro sheet, West Humboldt Range, Nevada **(Speed, Robert C.)** ..... 69
Layering in igneous rocks (S. Greenland) ..... 11
Leake, B. (discussion) ..... 277
**Le Bihan, T.-Th.,** Étude structurale de quelques sulfures de plomb et d'arsenic naturels du gisement de Binn 149
Leo, G. W., Discussion on sulfide equilibrium ..... 185
Leucite, chemical analysis ..... 255
Leucite-nepheline-sanidine in basic differentiates from a peridotite-dunite mass in Salem, Madras State, India, crystallization of ..... 251
Light extinction and scattering by suspension of finely-divided minerals (Hodkinson, J. R.) (abs.) ..... 310
Loomis, Alden A., Noritic anorthosite bodies in the Sierra Nevada batholith ..... 62
Lujavrites, southern Greenland ..... 19

Madras
——— Salem basic differentiates ..... 251
——— Sittampundi Complex ..... 116
**Mandarino, J. A., Williams, S. J.,** and **Mitchell, R. S.,** Spiroffite, a new tellurite mineral from Moctezuma, Sonora, Mexico ..... 305
**Marumo, F.** with **Morimoto, N.,** and **Sadanga, R.,** Interpretation of systematic extra-extinctions ..... 303
Mechanism of adcumulus growth in the layered series of the Skaergaard intrusion **(Wager, L. R.)** ..... 1
Megaw, H. D. (discussion) ..... 212
**Meier, W. M.** with **Gottardi, G.,** The crystal structure of dachiardite ..... 291
Metatorbernite group, the crystal structure and crystal chemistry of various members of (abs.) ..... 313
Mexico, spiroffite, Moctezuma, Sonora ..... 305
Micas, rock-forming, studies of (abs.) ..... 312
Miscellaneous papers ..... 200–314
Missouri, Fredericktown ..... 190
**Mitchell, R. S.** with **Mandarino, J. A.,** and **Williams, S. J.,** Spiroffite, a new tellurite mineral from Moctezuma, Sonora, Mexico ..... 305
Modal analyses, minerals, nepheline and sanidine ..... 256
Modal analyses, rocks
——— Ferrar dolerites ..... 125, 128, 131
——— kakortokites ..... 16
——— layered granites ..... 23, 26
——— noritic anorthosites ..... 63
——— picrite-anorthositic gabbros ..... 72
——— ultramafic rocks ..... 40
Montana, Stillwater Complex ..... 46
Mordenite ..... 291
Mordenite group ..... 287
Morimoti, N., Discussion on chalcocite ..... 170
**Morimoto, N., Marumo, F.,** and **Sadanaga, R.,** Interpretation of systematic extra-extinctions ..... 303
**Morimoto, Nobuo,** On the transition of bornite ..... 153
Muskox intrusion, a recently discovered layered intrusion in the Coppermine River area, Northwest Territories, Canada **(Smith, Charles H.,** and **Kapp, H. E.)** ..... 30

**Naidu, P. R. J.,** A layered complex in Sittampundi, Madras State, India ..... 116
**Naidu, P. R. J.,** Crystallization of leucite-nepheline-sanidine in basic differentiates from a peridotite-dunite mass in Salem, Madras State, India ..... 251
Natrolite group ..... 285
Naujaite, southern Greenland ..... 18
Nepheline, chemical analysis ..... 255
Nevada, layered picrite-anorthositic gabbro sheet ..... 69
——— West Humboldt Range gabbro ..... 69
New South Wales, teschenite intrusion (abs.) ..... 134
Noritic anorthosite bodies in the Sierra Nevada batholith **(Loomis, Alden A.)** ..... 62
Norms
——— basaltic suites ..... 235, 236
——— diopsides (chromian) ..... 244
——— pyroxenes, Japan and Hawaii ..... 243
——— Skaergaard ..... 239
——— Stillwater Complex ..... 240

Oklahoma, layered basic intrusive rocks of the Wichita Mountains (abs.) ..... 134

Olivine composition using standard small-diameter x-ray powder cameras, accurate determination of (abs.). 310
——— variations in the Muskox intrusion. . . . . 34
Olivine-diopside-silica diagram. . . . . 227
Olivines, optical properties. . . . . 41
Omori, K., and Kerr, P. F., Infrared study of sulfate minerals (abs.). . . . . 311
Oolites, iron, phosphate content. . . . . 223
Ore deposits, equilibrium in. . . . . 171
Oriented transformations in mineralogy, the role of. . . . 200
Origin of ultramafic complex at Duke Island, southeastern Alaska **(Irvine, T. N.)**. . . . . 36
Orthocumulates. . . . . 2
Orthopyroxenes, cell parameters of. . . . . 213
——— chemical analyses. . . . . 215–219
——— optical properties. . . . . 110, 130

Pectolite and wollastonite, comparison of the crystal structures of. . . . . 293
Pectolite, twinning. . . . . 299
Pegmatite-aplite intrusives. . . . . 78
Phillipsite group. . . . . 286
Phosphates in iron oolites. . . . . 223
Photoconductivity, in sulfides. . . . . 141
Photomicrographs
——— bornite. . . . . 146
——— bravoite. . . . . 192, 193
——— chalcopyrite. . . . . 147
——— Ferrar dolerites. . . . . 127, 130, 131
——— gneisses (Sittampundi). . . . . 118–120
——— hexagonal spiral. . . . . 259, 260
——— layered granites (Greenland). . . . . 26, 27
——— leucite. . . . . 253
——— nepheline. . . . . 254
——— noritic anorthosite (Sierra Nevada). . . . . 64, 66
——— olivine. . . . . 253
——— phlogopite. . . . . 253
——— positive phase contrast. . . . . 260
——— pyrite. . . . . 187–189
——— pyroxene. . . . . 253
——— sanidine. . . . . 253, 254
——— Skaergaard gabbro. . . . . 6
——— stacking fault, silicon carbide. . . . . 262
——— triangular spiral. . . . . 259
——— twin domains. . . . . 261
Physical properties of semiconducting sulfides, selenides, and tellurides **(Scanlon, Wayne W.)**. . . . . 135
Piller, H., Study of translucent tiny grains using the interference microscope (abs.). . . . . 311
Polymorphs, iron-feldspar (abs.). . . . . 314
**Pous, J. Montoriol, San Miguel, A.,** and **Font-Altaba, M.,** Contributions to the study of the fluorite deposit "Mina Berta" in San Cugat Del Valles (Barcelona, Spain). . . . . 278
**Prewitt, C. T.,** and **Buerger, M. J.,** Comparison of the crystal structure of wollastonite and pectolite. . . . . 293
**Prouvost, Jean,** Various aspects of atomic displacements in metallic sulfides. . . . . 144
Pseudoleucite, chemical analysis. . . . . 255
Pseudomalachite, the crystal structure of (Ghose, Subrata) (abs.). . . . . 310
**Pulvertaft, T. C. R.,** with **Ferguson, J.,** Contrasted styles of igneous layering in the Gardar Province of south Greenland. . . . . 10
Pyrite crystals from Spain, a study of distorted. . . . . 186
Pyrite, thermodynamic study of pyrrhotite and (abs.). . 198
Pyroxenes, and basaltic magmas, trends and affinities of, as illustrated on the diopside-olivine-silica diagram 227
Pyroxene norms, alkaline basaltic rocks. . . . . 241
——— Japan and Hawaii. . . . . 243
——— Skaergaard. . . . . 239
——— Stillwater complex. . . . . 240
Pyrrhotite and pyrite, thermodynamic study of (abs.). . . 198
Pyrrhotite, superstructure and twinning of. . . . . 157

Quartz-forming fluids in nature, the composition of (abs.) 312

Rathite, crystal structure of. . . . . 149
Regression studies, clinoamphibole. . . . . 267
Regressions of optical properties and density on composition (clinoamphiboles). . . . . 267
Rhythmic layering. . . . . 13, 37, 111, 114
Rimsaite, J., Studies of rock-forming micas (abs.). . . . . 312
Roedder, E., The composition of quartz-forming fluids in nature (abs.). . . . . 312
Role of oriented transformations in mineralogy **(Dent Glasser, L. S., Glasser, F. P.,** and **Taylor, H. F. W.)** 200
Roseboom, E. H. (discussion). . . . . 212
Ross, M., and Evans, H. T., The crystal structures and crystal chemistry of various members of the metatorbernite group (abs.). . . . . 313

**Sadanaga, R.,** with **Morimoto, N.,** and **Marumo, F.,** Interpretation of systematic extra-extinctions. . . . . 303
Sanidine, chemical analysis. . . . . 255
**San Miguel, A.,** with **Pous, J. Montoriol,** and **Font-Altaba, M.,** Contributions to the study of the fluorite deposit "Mina Berta" in San Cugat Del Valles (Barcelona, Spain). . . . . 278
Sapphirine in the granulite terrains of Western Australia, the significance of (abs.). . . . . 313
Sartorite, $PbAs_2S_4$, structure of. . . . . 149
**Scanlon, Wayne W.,** The physical properties of semiconducting sulfides, selenides and tellurides. . . . . 135
Selenides, as semiconductors. . . . . 135
Semiconductors, sulfides, etc. . . . . 135
Sierra Nevada batholith. . . . . 62
Significance of sapphirine in the granulite terrains of Western Australia (Wilson, A. F.) (abs.). . . . . 313
Silica-diopside-olivine diagram. . . . . 227
Silicon carbide, polytypes. . . . . 259
——— twinning. . . . . 261
Skaergaard intrusion. . . . . 1
——— pyroxene norms. . . . . 239
Skinner, B., Discussion on chalcopyrite. . . . . 148
**Smith, C. H.,** and **Kapp, H. E.,** The Muskox intrusion, a recently discovered intrusion in the Coppermine River area, Northwest Territories, Canada. . . . . 30
Smith, C. H., with Jambor, J. L., Accurate determination of olivine composition using standard small-diameter x-ray powder cameras (abs.). . . . . 310
**Smith, J. V.,** Structural classification of zeolites. . . . . 281
Space group, spiroffite. . . . . 305

Spain, distorted pyrite crystals from Fuente Valoria... 186
——— study of fluorite deposit..... 278
**Speed, Robert C.,** Layered picrite-anorthositic gabbro sheet, West Humboldt Range, Nevada..... 69
Spiroffite, a new tellurite mineral from Moctezuma, Sonora, Mexico **(Mandarino, J. A., Williams, S. J., and Mitchell, R. S.)**..... 305
Statistical study of bravoite zoning **(El Baz, Farouk,** and **Amstutz, G. C.)**..... 190
Stillwater Complex..... 46
——— pyroxene norms..... 240
Stratigraphic and lateral variation of chromite composition in the Stillwater Complex **(Jackson, Everett, D.)** 46
Stromeyerite, structure compared with chalcocite..... 169
Structural and petrographic observations on layered granites from southern Greenland **(Emeleus, C. H.)** 22
Structural classification of zeolites **(Smith, J. V.)**..... 281
Structural studies of some natural sulfides of lead and arsenic from the deposits of Binn..... 149
Structure and rock sequences of the critical zone of the eastern Bushveld Complex **(Cameron, Eugene N.)**. 93
Studies of crystal surfaces **(Sunagawa, Ichiro)**..... 258
Studies of rock-forming micas (Rimsaite, J.) (abs.)..... 312
Study of distorted pyrite crystals from Spain **(Font-Altaba, M.)**..... 186
Study of translucent tiny grains using the interference microscope (Piller, Horst) (abs.)..... 311
Sulfate minerals, infrared study of (abs.)..... 311
Sulfides, as semiconductors..... 135
——— atomic displacements in..... 144
——— isotope mineralogy (abs.)..... 198
——— of lead and arsenic from Binn..... 149
——— symposium, on the mineralogy of the.....135–199
Sulfur isotope mineralogy of sulfides (Jensen, M. L.) (abs.)..... 198
**Sunagawa, Ichiro,** Studies of crystal surfaces..... 258
Supercooling of magma..... 4
Superstructure and twinning of pyrrhotite, on the **(Wuensch, B. J.)**..... 157
Sur les constituants phosphatés des minerais de fer oolithiques de France **(Caillère, S.** and **Kraut, F.)**. 223
Switzerland, Binn..... 149
Symposium on the mineralogy of the sulfides.....135–199
——— layered intrusions.....1–134
Systematic extra-extinctions, interpretation of..... 303
Systems
——— diopside-anorthite-albite..... 204
——— diopside-olivine-silica..... 227
——— $K_2O$-FeO-$Fe_2O_3$-$SiO_2$-$H_2O$ (abs.)..... 314
——— leucite-nepheline-sanidine..... 251

Tanganyika (western intrusion)..... 108
**Taylor, H. F. W.,** with **Dent Glasser, L. S.,** and **Glasser, F. P.,** The role of oriented transformations in mineralogy..... 200
Tellurides, as semiconductors..... 135
Tellurite mineral (spiroffite)..... 305
Teschenite intrusion, New South Wales..... 134
**Thayer, T. P.,** Flow layering in Alpine peridotite-gabbro complexes..... 55
Thermodynamic study of pyrrhotite and pyrite (Toulmin, P., and Barton, P. B.) (abs.)..... 198
Tholeiitic magmas, origin of..... 248
Tigssaluk Complex, southern Greenland..... 22
Topotactic reactions..... 200
Toulmin, Priestley, 3rd, and Barton, Paul B., Jr., Thermodynamic study of pyrrhotite and pyrite (abs.).. 198
**Toulmin, Priestley, 3rd,** with **Barton, Paul B., Jr.,** and **Bethke, Philip M.,** Equilibrium in ore deposits.... 171
Transformations, oriented, in mineralogy..... 200
Transition of bornite, on the **(Morimoto, Nobuo)**..... 153
Trends and affinities of basaltic magmas and pyroxenes as illustrated on the diopside-olivine-silica diagram **(Coombs, D. S.)**..... 227
**Tuttle, O. Frank,** with **Jahns, Richard H.,** Layered pegmatite-aplite intrusives..... 78
Twinning and superstructure of pyrrhotite..... 157
Twinning, hematite..... 262
——— pectolite..... 299
——— pyrrhotite..... 157
——— silicon carbide..... 261
——— wollastonite..... 299

Ultramafic complex, Duke Island, southeastern Alaska. 36
Unit cell, dachiardite..... 291
——— mordenite..... 291
——— orthopyroxenes..... 215
——— spiroffite..... 305

Variation of chromite composition, Stillwater Complex. 46
Various aspects of atomic displacements in metallic sulfides **(Prouvost, Jean)**..... 144

**Wadsworth, W. J.,** The Kapalagulu layered intrusion of western Tanganyika..... 108
**Wager, L. R.,** The mechanism of adcumulus growth in the layered series of the Skaergaard intrusion..... 1
Water vapor, role in genesis of pegmatites and aplites.. 91
Western Tanganyika, Kapalagulu layered intrusion.... 108
West Humboldt (Nevada) layered sheet..... 69
**Williams, S. J.,** with **Mandarino, J. A.,** and **Mitchell, R. S.,** Spiroffite, a new tellurite mineral from Moctezuma, Sonora, Mexico..... 305
Willow Lake type layering..... 65
Wilshire, H. G., Internal structure of a differentiated teschenite intrusion, Prospect Hill, New South Wales (abs.)..... 134
Wilson, A. F., The significance of sapphirine in the granulite terrains of Western Australia (abs.)..... 313
Wilson, A. (discussion)..... 277
Wimmenauer, W. (discussion)..... 226
**Winchell, Horace,** Clinoamphibole regression studies... 267
Wollastonite and pectolite, comparison of the crystal structures of..... 293
Wollastonite, twinning..... 299
Wones, D. R., and Appleman, D. E., Iron-feldspar polymorphs in the system $K_2O$-FeO-$Fe_2O_3$-$SiO_2$-$H_2O$ (abs.)..... 314
Wones, D. R. (discussion)..... 202
**Wuensch, Bernhardt J.,** and **Buerger, M. J.,** The crystal structure of chalcocite, $Cu_2S$..... 164
**Wuensch, Bernhardt J.,** On the superstructure and twinning of pyrrhotite..... 157

**Wyllie, Peter J.,** Effects of the change in slope occurring on liquidus and solidus paths in the system diopside-anorthite-albite ..... 204

X-ray diffraction data, orthopyroxenes ..... 215

Zeolites, structural classification of ..... 281
——— Analcime group ..... 282
——— Bikitaite ..... 287
——— Chabazite group ..... 283
——— Dachiardite ..... 291
——— Leucite ..... 253, 255
——— Mordenite ..... 291
——— Mordenite group ..... 287
——— Natrolite group ..... 285
——— Phillipsite group ..... 286
——— Pseudoleucite ..... 255
Zoning in bravoite (statistical study) ..... 190
——— oscillatory, in plagioclase ..... 210